Morphological modelling of an artificial sand ridge near Hoek van Holland, The Netherlands

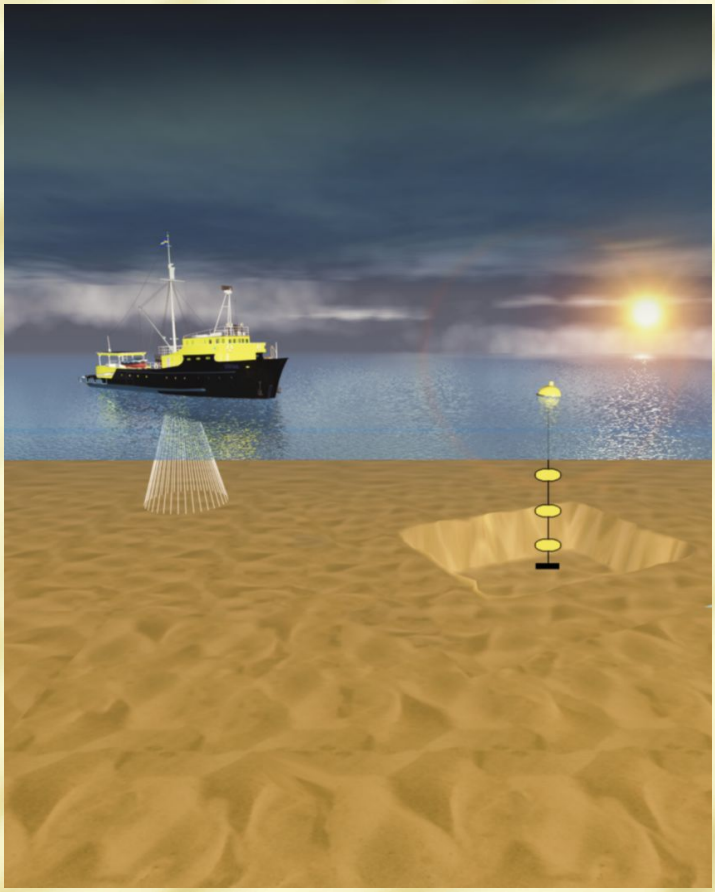

P.K. Tonnon

Supervisors:
prof. dr. ir. M.J.F. Stive
prof. dr. ir. L.C. van Rijn
dr. ir. J. van de Graaff
ir. D.J.R. Walstra
ir. G.J. de Boer

TU Delft
Delft University of Technology

WL | delft hydraulics

Report Z3079.40; May 2005

SAND PIT Fifth Framework Project No. EVK3-CT-2001-00056

Prepared for:

TU Delft

Morphological modelling of an artificial sand ridge near Hoek van Holland, The Netherlands.

P.K. Tonnon

Report

May, 2005

Preface

This is the report for my MSc. thesis, which forms the completion of my study Civil Engineering at Delft University of Technology, Faculty of Civil Engineering and Geosciences, Division of Hydraulic and Offshore Engineering. The study was carried out at WL | Delft Hydraulics.

This study is part of the SANDPIT project, an European research project which aims to develop reliable prediction techniques and guidelines to better understand, simulate and predict the morphological behavior of sand mining areas and associated sand transport processes at the middle and lower shoreface and surrounding coastal zone. This particular study aims to assess the predictive capabilities of the process based morphodynamic model Delft3D on the morphological development of an artificial sand ridge near Hoek van Holland, The Netherlands. Herein, the recently implemented TRANSPOR2004 sand transport model (van Rijn et al., 2004) was used.

I would like to thank my supervisors at WL | Delft Hydraulics and Delft University of Technology, Prof. dr. ir. M.J.F. Stive, Prof. dr. ir. L.C. van Rijn, dr. ir. J. van de Graaff, ir. D.J.R. Walstra and ir. G.J. de Boer for sharing their knowledge and giving support during this study. I further would like to thank ir. M van Ormondt for his co-operation and support with the modelling software Delft3D.

I am grateful for the opportunity given by WL | Delft Hydraulics to perform my MSc. thesis at their institute and would like to thank my temporary colleagues and my fellow graduate students for showing their interest and making my stay a very pleasant one.

Delft, May 2005
Pieter Koen Tonnon

Contents

List of Figures

List of Tables

Summary

This study entitled “morphological modelling of an artificial sand ridge near Hoek van Holland, The Netherlands” is part of the European SANDPIT project and was carried out at WL | Delft Hydraulics.

Introduction
The European SANDPIT project was set-up to develop reliable prediction techniques and guidelines to better understand, simulate and predict the morphological behavior of large-scale sand mining areas and associated sand transport processes at the middle and lower shoreface and surrounding coastal zone. Sand mining may take place by dredging in pits, channels and trenches or by removal (dredging) of existing large-scale sand banks or shoals in the offshore zone.

This study aims to verify the predictive capabilities of the morphodynamic model Delft3D on the morphological development of an artificial sand ridge near Hoek van Holland, The Netherlands on a time scale of about ten years. Herein, a research version of Delft3D was used including the engineering sand transport model TRANSPOR2004 (Van Rijn et al., 2004) which features a bed roughness predictor.

The artificial sand ridge Hoek van Holland was created between 1982 and 1986 by dumping approximately 3.500.000 m3 sand (Woudenberg, 1996) in an area with depths between -15 m and -23 m on the northern side of the approach channel to the port of Rotterdam, see Figure I.

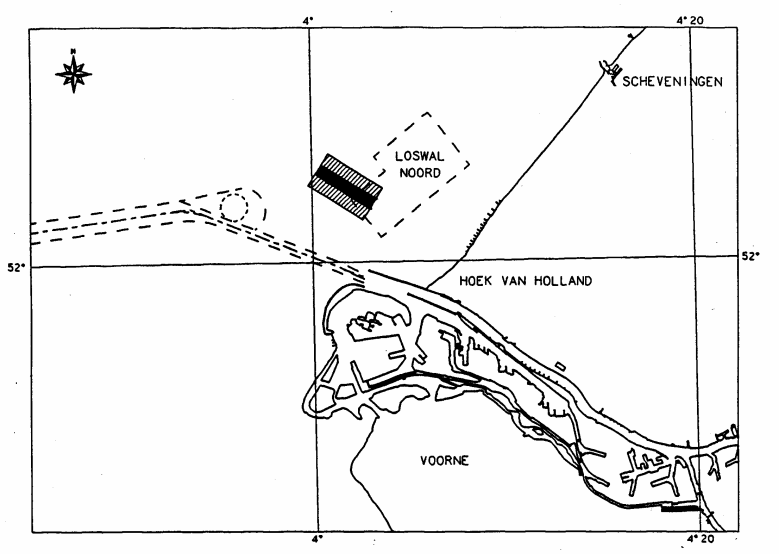

Figure I Location artificial sand ridge Hoek van Holland, The Netherlands

The sand ridge is more or less perpendicular to the coast. The ridge dimensions just after creation were: length of about 3600 m; toe width between 250 and 370 m; height between 1.3 and 4 m; slopes between 1:50 and 1:100 on the south flank and between 1:20 and 1:50 on the north flank; D50 between 0.15 and 0.45 mm. The landward end of the ridge is about 6300 m from the shoreline. Tidal flow is parallel to the coast and thus normal to the ridge.

The sand ridge is located close to Loswal Noord, which is a dumping site for little-poluted silt from the Rotterdam harbour mouth. Primary goals upon creation of the ridge were to study the stability of sand ridges normal to the tidal flow and the effect on shoreface sand transport. Also the possibility to use sand ridges as silt trap for backflow of silt to the Rotterdam harbour mouth was to be investigated.

Morphology data

Bathymetric surveys of the sand ridge Hoek van Holland for the period 1982 – 2000 showed a clear reduction in ridge height and a net migration in flood direction that reduces with depth and leads to a slight rotation of the ridge with respect to the original axis. The average rate of migration in flood direction is about 5.50 m per year and the average decrease in height of the ridge is about 0.1 m per year. Between 1992 and 1993 a southward migration of the ridge and increase in height was observed. The bathymetric surveys are comparable to those of the NOURTEC study (Westlake, S.J., 1996); the vertical accuracy is therefore in the order of 0.1 to 0.2 m and the horizontal accuracy is in the order of 1 to 5 m.

Basic ridge morphology (idealized sand ridge model)

An idealized sand ridge model was set up to gain insight in the physical processes at the sand ridge and investigate the effect of tides, waves and basic model settings on the morphological development of a symmetric ridge at a depth comparable to that of the sand ridge Hoek van Holland.

It was shown that:

- With symmetric and weak-asymmetric tides (propagating tidal wave) the sand ridge increases in height due to the deformation of velocity profiles over the ridge; the time-averaged near-bed velocities are in direction of the top of the ridge and so is the bed-load transport. With increasing tidal velocities or net currents the suspended-load transport dominates the bed-load transport; sediments are moved outside the region where they can be brought back to the top with bed-load transport and thus the ridge decreases in height.
- With symmetric and weak-asymmetric tides the migration of the ridge is in ebb-direction due to the dominant ebb transports caused by the higher bed-shear stresses with shallower water during ebb. With increasing net current in flood direction, the effect of the shallower water during ebb is cancelled out and the ridge migrates in flood direction.
- Waves stir up sediments and lead to larger suspended-load transports and a reduction in height of the ridge. Waves also affect the shape of the ridge; with waves the ridge develops more asymmetrically. The effect of waves increases with diminishing water depth and therefore suspended-transports during ebb (shallower water) are increased more than suspended-load transports during flood. With symmetric tides (no net current) the migration in ebb direction therefore increases with waves. The migration for tides with a net current is in flood direction and reduces with waves.

Modelling of the sand ridge Hoek van Holland

Both transect models (1DH and 2DV) and area models (2DH, 3D) were set-up for simulating the morphological development of the sand ridge Hoek van Holland for the periods 1986–1991 and 1991–2000. Model settings were derived from a basic calibration and sensitivity analysis using the 2DV model. The hydronamic boundary conditions for the simulations were generated from the well-calibrated Holland Coastal Zone (HCZ) model

(Roelvink et al., 2001) using a automated nesting procedure. To reduce computational time a morphological tide was derived using the method of Latteux (1995) that gives an optimal representation of the residual (e.g. yearly averaged) sediment transports. A single representative wave height was used herein.

Conclusions and recommendations

The morphological development of the sand ridge near Hoek van Holland, The Netherlands over a period of about 10 years was modelled with reasonable accuracy. The accuracy is strongly affected by the accuracy of the morphological tide, when waves are present. This morphological tide should be carefully determined based on data points outside the ridge location and on top of the ridge where the water depth is much smaller and waves are more important. This implies that the wave schematization is of significant importance with morphological simulations of sand ridges. Here, a single representative wave was used, which was found to lead to a morphological development being in good agreement with the long-term average development of the sand ridge Hoek van Holland. It was also was found that large wave heights lead to significant morphological changes. Therefore it is recommended to investigate whether modelling of large wave conditions is vital to the morphological development of sand ridges.

Further conclusions are:

- Depth-averaged models should not be used to model the morphological development of sand ridges as these models use fixed, logarithmic velocity profiles and therefore cannot model the effect of deformation of velocity profiles over the ridge. Deformation of velocity profiles may lead to a net transport to the top of the ridge and may cause the ridge to increase in height.
- It was found that the mean sediment diameter D50 needs to be determined rather accurately as it affects the distribution of sediments in the water column and thereby determines the morphological behaviour of the sand ridge; with larger sediments and subsequent dominant bed-load transports, the ridge increases in height.

Due to this study improvements were realized within the Delft3D software and TRANSPOR2004 formulations. The main improvement involved the bottom layer sub-grid model in Delft3D; it is recommended to investigate the restrictions on the relative thickness of the bottom layer in Delft3D with respect to the accurate determination of concentrations in the bottom layer at deeper water.

1 Introduction

1.1 General introduction

Large-scale mining of sand from the Dutch sector of the North Sea is being discussed for several years now. Various studies of the morphological consequences of sea sand mining have been performed, but most focus on the technical evaluation of mining from pits. Within the European SANDPIT project, both mining from pits and from large-scale sandbanks is subject of discussion. This report aims to verify the morphological predictive capabilities of Delft3D on the morphological development of an artificial sand ridge close to Hoek van Holland, The Netherlands.

In Section 1.2 an introduction is given to the EU-SANDPIT project, which is the framework of this study. The problem definition and main objectives of this study are given in Section 1.3. In Section 1.4 the study approach is discussed and in Section 1.5 the report outline is given.

1.2 Introduction to EU-SANDPIT project

Massive mining of sand from the middle and lower shoreface (depths of 10 to 30 m) will be required in future in many European countries for shoreface, beach and dune nourishments and large-scale engineering works at sea (Maasvlakte extension, airport at sea). The volume of sand required in the near future (10 to 20 years) will be in the order of 100 to 1000 million m^3 per country surrounding the North Sea (Van Rijn et al., 2002).

To meet these demands, the existing areas for mining of sand need to be extended considerably and new areas should be exploited. Moreover, the ‘traditional’ method of sand mining over relative shallow depths of a few meters (e.g. for The Netherlands the presently maximum allowable depth of sandpits is 2 m) is considered to be insufficient to cover future sand needs. Increasing costs of sand dredging operations related to transport distances, induce questions on the possibilities of mining from local sources of sand. Sand mining from local sources may take place by dredging in pits, channels and trenches or by removal (dredging) of existing large-scale sand banks or shoals in the offshore zone.

The technical evaluation of sand mining activities requires fundamental knowledge of morphological processes, sand transport processes, sand budgets and ecology in the offshore coastal zones. At present stage of research our understanding of these processes is not sufficient to assess the impact of massive sand mining.

The accurate determination of sand budgets for the sand mining area considered requires rather accurate information of sand transport rates at the boundaries. Often, the accuracy of the computed sand transport rates is not sufficient, because of the application of relatively simple sand transport models. Furthermore, model verification and validation based on detailed field data is lacking in most cases. The main reason for this is that detailed field data sets of sand transport in offshore (deep water) conditions are scarcely available.

The European SANDPIT project was set up to develop reliable prediction techniques and guidelines to better understand, simulate and predict the morphological behavior of large-scale sand mining pits and the associated sand transport processes at the middle and lower (offshore) shoreface and surrounding coastal zone. The potential use of large-scale sand banks and shoals for sand mining will also be studied. Research on sand transport focusing on the middle and lower shoreface will be a key topic within the SANDPIT project. Existing research models of sand transport will be improved based on field and laboratory data. Practical sand transport models will be improved for use in 2-dimensional horizontal and 3-dimensional morphodynamic models, such as Delft3D.

1.3 Problem definition and objectives

This study aims to verify the predictive capabilities of Delft3D on the morphological development of an artificial sand ridge near Hoek van Holland, The Netherlands on a time scale of about ten years. The ridge is about 5 m high and a few hundred meters wide and is more or less perpendicular to the coast, see Figure 1-1. Tidal flow is parallel to the coast and thus normal to the ridge. The ridge has migrated northward during a period of about 10 years, and is a rather well-defined case of migration and reduction in height of an isolated body of sand. At present no verification exists of Delft3D on the morphological development of such shore-perpendicular ridge.

The main objectives of this study are:

- To derive the ridge characteristics from available morphology data.
- To derive basic physical insight in ridge morphology by means of numerical modelling
- To assess the predictive capabilities of Delft3D regarding the morphological development of the sand ridge near Hoek van Holland.
- To evaluate the predictive capabilities of different model approaches (1DH, 2DV, 2DH, 3D)

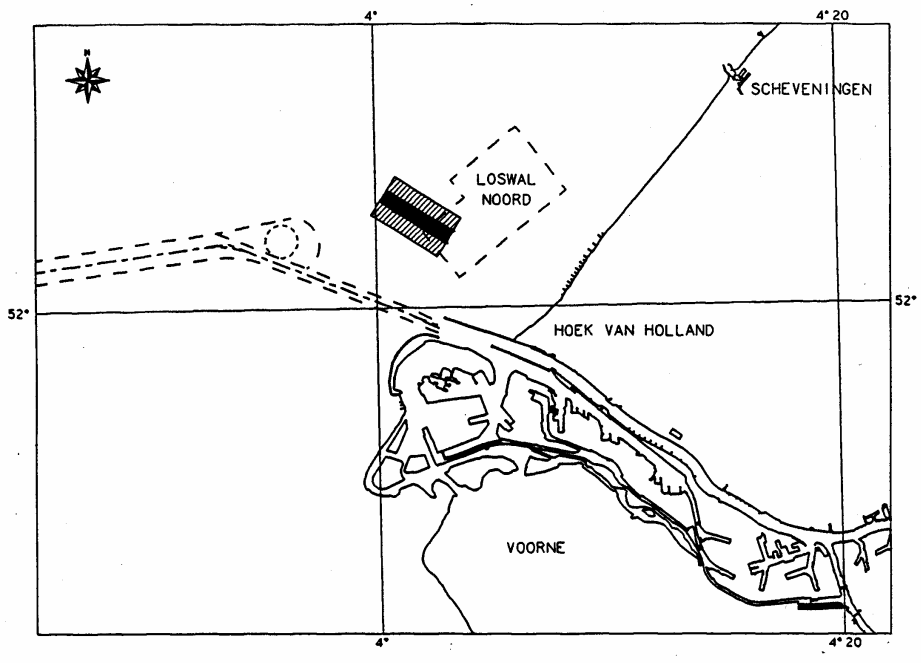

Figure 1-1 Location of artificial sand ridge near Hoek van Holland.

This study was carried out using the most recent version of the Delft3D modelling system, which includes the new TRANSPOR2004 sediment model and the new bed roughness predictor; a constant wave height was applied within the Sediment Online module.

1.4 Study approach

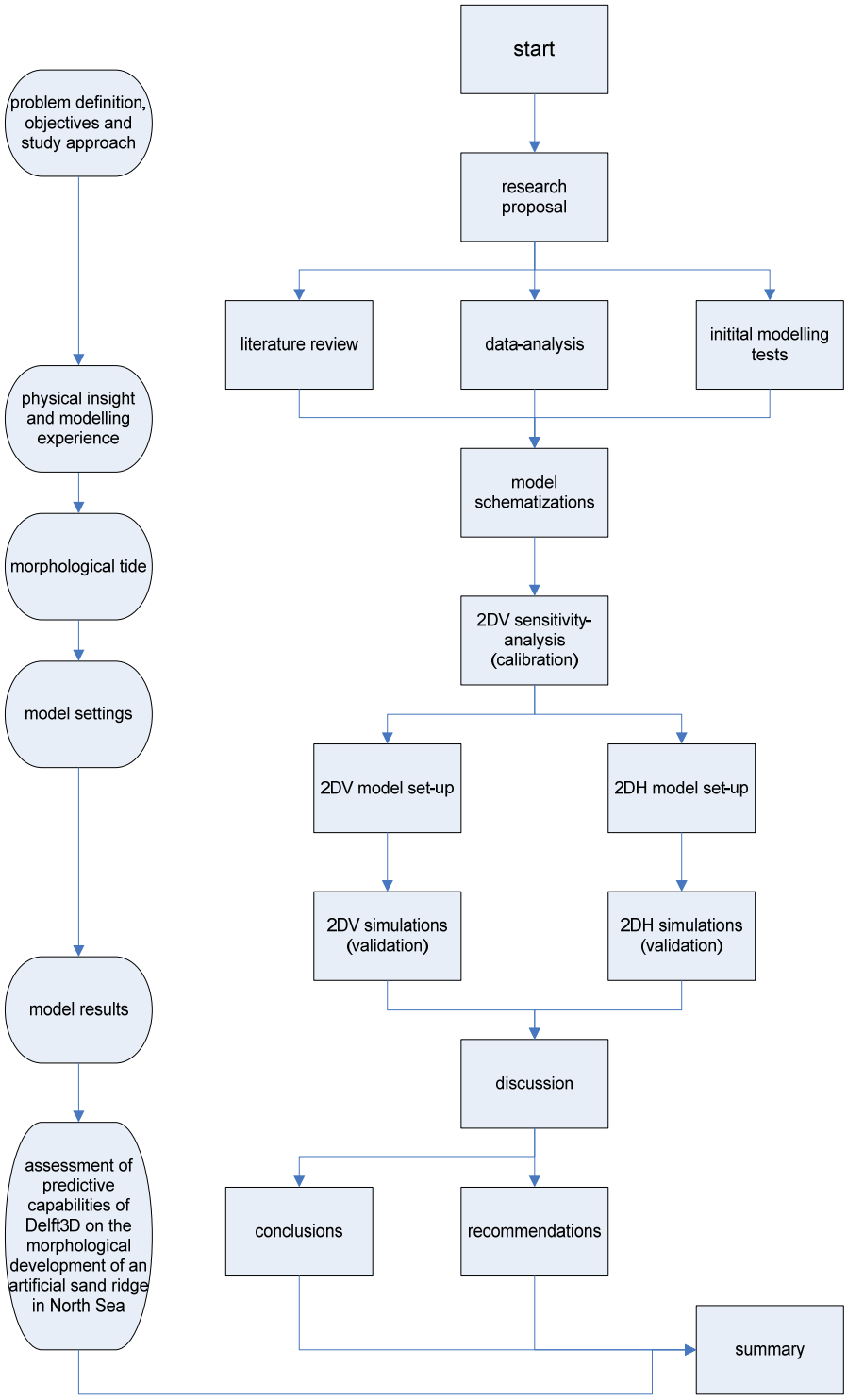

Figure 1-2 Study approach

First the problem definition, objectives and study approach were defined in the study proposal. Next, a literature review, data-analysis and simulations of an idealized sand ridge were carried out to derive ridge characteristics and basic physical insight in sand ridge morphology. After that, a well-calibrated model was used to provide boundary conditions for the models used in this study. Next, input reduction techniques were applied for tidal- and wave-input and a 2DV sensitivity analysis was carried out. After that, 2DV and 2DH models were set-up and run for 2 periods. Model results and physical insight were discussed and conclusions were drawn. Finally, recommendations were made and a summary was written. The study approach is visualized in Figure 1-2.

The simulations of an idealized sand ridge in Chapter 4 were carried out with a more recent version of Delft3D than the simulations in Chapter 5 and 6. In Section 2.3.3.3 the differences in bottom layer sub-grid model between both versions are discussed.

1.5 Report outline

In Chapter 2 earlier studies involving the sand dump Hoek van Holland are discussed and the concept of morphological modelling, process-based modelling and Delft3D is dealt with. Chapter 3 discusses the available morphology data and includes a basic data-analysis of the data used in this study. In Chapter 4 modelling tests with an idealized sand ridge were carried out to provide physical insight in sand ridge morphology. Chapter 5 discusses the model schematizations used in this study and deals with nesting and input reduction techniques. This chapter also includes a 2DV sensitivity analysis. In chapter 6, the 2DH and 3D model set-up is discussed and modelling results are presented. Finally, the overall most important conclusions and recommendations are given in Chapter 7.

2 Literature review and modelling principles

2.1 Introduction

In this chapter a brief literature review on the sand dump Hoek van Holland is given in Section 2.2. Three reports regarding the sand ridge Hoek van Holland will be discussed herein; the results and findings of those earlier studies will be summarized and provide insight in the sand ridge morphology. In Section 2.3 a general introduction to modelling principles is given, including a brief description of the Delft3D modelling package and the TRANSPOR2004 sediment transport model which were used in this study.

2.2 Literature review

2.2.1 Redeker and Kollen (1983)

Shortly after the dumpings which first created the sand ridge Hoek van Holland, Redeker and Kollen (1983) investigated the efficiency of dumpings and the erosion rates of the ridge. One of their main concerns was to investigate the effects of bed-gradients and waves on sediment transport, which the existing sediment transport formula's at that time did not include. The sediment transport rates at the specific location were not known; a comparison was made between three sediment transport formulas; Kalinske-Frijlink (K.F.), Engelund-Hansen (E.H.) and Meyer-Peter-Muller (M.P.M.) for adaptation possibilities. They found that the M.P.M formula was most suited to be adjusted for bed-gradient and wave effects. They adjusted the M.P.M formula to allow for bed-gradient and wave effects. The M.P.M formula is a bed-load transport formula only. Suspended-load transport is not taken into account. Large waves usually stir up sediments and contribute to suspended-load transport, therefore the modified M.P.M. formula is valid only with limited wave influence.

From analytical and numerical computations they concluded that:

- The erosion rate at the top of the ridge is strongly related to the steepness of the slopes.
- Wave effects at the toe of the ridge are not negligible, and will even be of greater importance when suspended-load transports are taken into account.
- The erosion rate at the top of the ridge at MSL -16m without waves is about 0.3 m per year; the reduction rate is expected to increase about 20 - 40% when waves are taken into account.
- The migration rate, without waves, of the top of the ridge is approximately 4.5 m per year and is in southwestern direction, opposite to the residual current.
- The wave influence determines the migration rate to a large extent. The migration rate therefore increases with diminishing depth.

2.2.2 Van Woudenberg (1996)

Van Woudenberg (1996) studied the behavior and stability of the artificial sand ridge Hoek van Holland. The ridge behavior was compared to that of sand waves and to numerical predictions for the artificial sand ridge from Redeker and Kollen (1983). Furthermore, yearly sediment transport rates were computed using a bed-load transport model from Ribberink (Koelewijn and Ribberink, 1994). Herein a basic summary of the study is given, including the most relevant findings with respect to morphodynamic modelling of the sand ridge.

A comparison of the ridge behavior with that of sand waves was made based on Tobias (1989). The main findings of that study of sand waves in the area of the Euromaas-channel were that sand waves are found at depths between 20 and 35 m and typically are between 2.8 and 6.3 m high with lengths between 195 and 387 m. At the flanks of the sand waves mega ripples occur with a height between 0.25 m and 0.7 m and a length between 12.8 m and 23 m. Sand waves closer to the shore migrate in north-eastern direction while sand waves at more than 75 km offshore migrate in southwestern direction. Seasonal fluctuations in height of the sand waves between 0.5 to 1.2 m were observed; in the summer an increase in height of the sand waves was observed, while in winter a decrease in height was observed.

behaviour of sand ridge

A detailed analysis of morphology data between 1982 and 1995 showed that:

- The migration of the top of the ridge is in north-eastern direction, except for the periods 1985-1986 and 1992-1993 where a south-western migration of the top was observed. No correlation between wind data and this south-western migration in those periods was found.
- The migration of the top varied with depth; the maximum migration rate was found at the shallower part of the ridge. The migration rate decreases with increasing depth, but increases again in the deepest parts of the ridge.
- The observed migration rates between 1986 and 1991 are in the order of 10 m per year, while between 1991 and 1995 the observed migration rates where in the order of 4 m per year.
- The migration rates of the centre of gravity of the ridge are smaller than the migration rates of the top of the ridge. The observed migration rates of the centre of gravity between 1986 and 1991 are in the order of 5 m per year and in the order of 3 m per year between 1991 and 1995.
- At the deeper, seaward part of the ridge no migration of the toes of the ridge was observed, while in the shallower part a linear increasing migration with diminishing depths of the toes in north-eastern direction was observed. It was suggested that this linear increasing migration at depths smaller than MSL -19 m is due to wave action.
- The height of the top decreases in time with about 0.072 m per year, except for the periods 1990-1991 and 1992-1993 where the height of the top increases.

Furthermore it was found that the asymmetric development of the ridge was more pronounced in the deeper parts of the ridge, where wave action is of less importance. Also, mega ripples were observed at the southern flank of the ridge, which can influence the

development in time of the height of the ridge. Furthermore, it was shown that structural erosion of the sounding area takes place; the area itself is not a closed system in terms of sediment transport.

The main findings of this study were:

- The sand ridge is stable for depths greater than 19 m; a reduction in height was observed, but the overall migration is small. This part of the ridge develops asymmetrically.
- The shallower part of the ridge is not stable; a migration of about 150 m in 12.5 years was observed. Furthermore, a reduction in height was observed, however the asymmetric development is smaller than at the deeper part of the ridge.
- Mega ripples can be found at depths greater than 18 m, these can also be found at natural sand waves which can be found at depths greater than 20 m.
- The observed height increase of the ridge in two sounding intervals was thought to be caused by mega ripples at the southern flank of the ridge; with sand waves this phenomena is seasonal.
- The backward (southward) migration of the ridge which was found in two sounding intervals can also be found with sand waves.
- The migration in the deeper part is negligible and therefore corresponds with sand waves.

Yearly transport rates

Yearly sand transport at the location of the sand ridge rates were computed with a bed load transport model from Ribberink (Koelewijn and Ribberink, 1994) which was calibrated with an approximation of the yearly sand transport rates derived from the soundings. A roughness length k_s of 0.05 m was found to yield accurate results. The computed longshore bed-load transport rates (without ridge) at depths between 15 m to 23 m were between 7 and 26 m^3 /m/yr (excl. pores). The computed transport rates comply with values from van Rijn (1995) and from Verhagen and Wiersma (1992).

2.2.3 Klein (2003)

Klein (2003) carried out numerical simulations of the sand ridge Hoek van Holland with SUTRENCH as part of a verification study of morphodynamic models on sand mining areas.

A single section located about 6800 m offshore was simulated over the period 1982 to 1995 using SUTRENCH with the TRANSPOR1993 and TRANSPOR2000 sediment transport models. The simulations were carried using a horizontal grid resolution of 4.0 m and 10 vertical layers, a schematic tide of 12 hours was used with an average flood velocity of 0.6 m/s and an average ebb velocity of -0.5 m/s. The water level was NAP +0.5 m during flood and NAP -0.5 m during ebb. The average wave height during the simulation period was assumed to be between 1.0 and 1.5 m. Calibration showed that a wave height of 1.0 m and a peak period (Tp) of 5.0 s gave optimal results. The dominant wave direction was assumed to be perpendicular to the ridge and thus parallel to the shore.

Sediment characteristics used were:

- Median grain size d_{50} of 0.2 mm
- 90% grain size d_{90} of 0.3 mm
- sediment fall velocity w_s of 0.02 m/s
- reference level z_a 0.03 m

The wave-related roughness height r_w and current-related roughness height r_c were estimated at 0.03 m; assuming small-scale ripples at the bed.

Measurements of the ridge were available for the years 1982, 1986, 1991 and 1995 and showed a migration in flood direction between 1982 and 1986, whereby the height of the ridge remained equal. Between 1986 and 1991 migration was in flood direction and the ridge increased in height, which was credited to either inaccurate measurements or dumpings. Between 1991 and 1995 migration was in flood direction once more, while the ridge decreased in height. It was found that between 1982 and 1986 erosion south of the ridge equalled sedimentation north of the ridge, while between 1986 and 1995 erosion was larger than sedimentation.

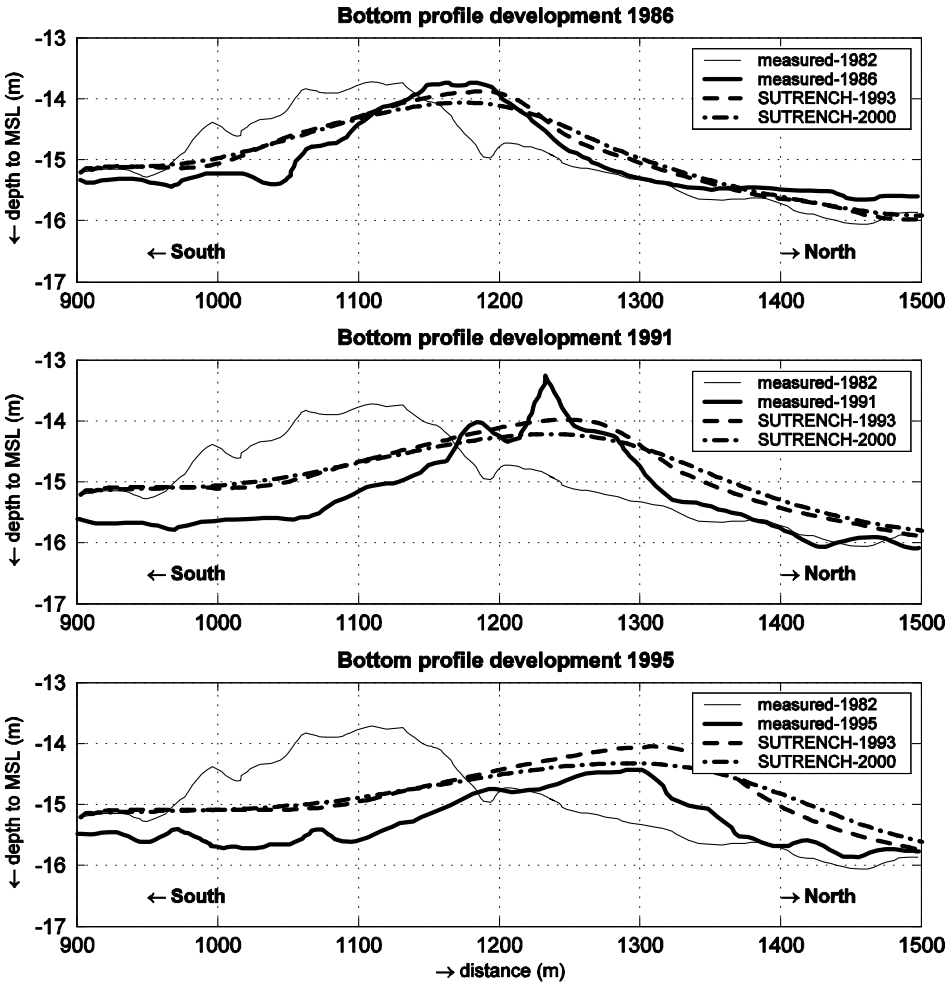

Figure 2-1 Results SUTRENCH simulations Klein (2003)

Both SUTRENCH computations with TRANSPOR1993 and TRANSPOR2000 showed migration in northern direction and a decrease in height comparable to that of the measurements, see Figure 2-1. The computation with TRANSPOR1993 also showed the asymmetric development of the ridge with a steeper northern slope as found from the measurements. The computation with TRANSPOR2000 predicted a much more symmetric shape of the ridge. Both models underestimate the erosion near the southward boundary and overestimate sedimentation at the northward boundary.

The main findings were that both models predicted the migration and decrease in height of the ridge reasonably well and that with TRANSPOR1993 the course of the northern slope was predicted somewhat better than with TRANSPOR2000.

2.2.4 Synthesis

Previous studies of the sand ridge include Redeker and Kollen (1983), Woudenberg (1996) and Klein (2003). Redeker and Kollen (1983) carried out numerical computations using bed-load transport only. They applied the Meyer-Peter-Muller formula and predicted a migration of about 4.5 m in southern direction, opposite to the residual current and a reduction in height without waves of about 0.3 m per year. Woudenberg (1996) found similarities with sand waves that show seasonal fluctuations in height and migration in north-eastern direction and computed yearly averaged transport rates between 7 and 26 m^3/m/yr excl. pores at depths between -15 to -23 m using a bed-load transport model. Klein (2003) carried out SUTRENCH computations of the ridge using the TRANSPOR1993 and TRANSPOR2000 sediment transport models and showed that the development of the ridge can be predicted reasonably well.

2.3 Modelling principles

This Section discusses the concept of morphological modelling in general. Subsequently, process-based modelling and the Delft3D model software package are dealt with. Furthermore, the TRANSPOR2004 sediment transport model and bed roughness predictor are discussed briefly. Next, the bottom layer sub-grid model used in Delft3D Sediment-Online is discussed, which was subject of a recent update of Delft3D.

2.3.1 Morphological modelling

The morphological development of coastal regions is subject to complex interaction between currents, waves, sediment transport and bed level variations. Furthermore, most coastal areas are liable to human interference such as structures, dredging and nourishments. During the past decades, different mathematical-physical models have been developed to simulate these processes and their interactions and to predict the morphological development. This Section gives a short introduction in mathematical-physical modelling of coastal regions. The scales, approaches and concepts in morphodynamic modelling are discussed.

Scales, concepts and approaches

In morphostatic models the bottom is assumed to be fixed under the assumption that significant changes in the bottom morphology occur on much larger time-scales than the time-scales involved with the adaptation of the flow and transports. In morphodynamic models the bottom morphology is dynamically coupled into the system; bottom changes are taken into account and influence flow and transports.

An important problem in morphodynamic modelling is that of non-linear multiple-scale dynamics; most of the physical understanding and corresponding models concern scales which are significantly smaller than the scale of phenomena in which we are interested. One can distinguish between coastal evolution concepts and models on a range of scales.

- Micro-scale (process-scale) concerns primarily the constituent processes (waves, currents, sediment transport). Phenomena take place at an essentially smaller scale than the corresponding morphodynamic behaviour
- Meso-scale (dynamic-scale) concerns the primary morphodynamic behaviour, due to the interaction of the constituent processes and the bed topography. Principal forcings are seasonal, interannual variations in tide, waves and currents and human activities such as sand-mining can be taken into account.
- Macro-scale (trend-scale) phenomena concern slow trends at scales much larger than those of the primary morphodynamic behaviour.

In accordance with the range of scales on which processes and behaviour take place, three basic concepts of morphological models can be distinguished:

- Initial Sedimentation/Erosion (ISE) models describe micro-scale phenomena such as the sedimentation/erosion rate on a given bed topography, these models don’t take the interaction with the topographic changes into account.
- Medium-Term Morphodynamic (MTM) models take the interaction with the topographic changes into account. They are able to describe the meso-scale dynamic behaviour of a system.
- Long-Term Morphodynamic (LTM) models, in which the constituent equations are not describing the individual physical processes, but integrated processes at a higher level of aggregation.

Model concepts can be classified according to the type of information they are based on: process knowledge, data knowledge or a mixture of both. On one side of the spectrum models are found describing systems of which processes are well understood, on the other side of the spectrum models are found describing systems of which the behaviour is understood from measured data. Figure 2-2 shows the classification of models with respect to process knowledge and available data.

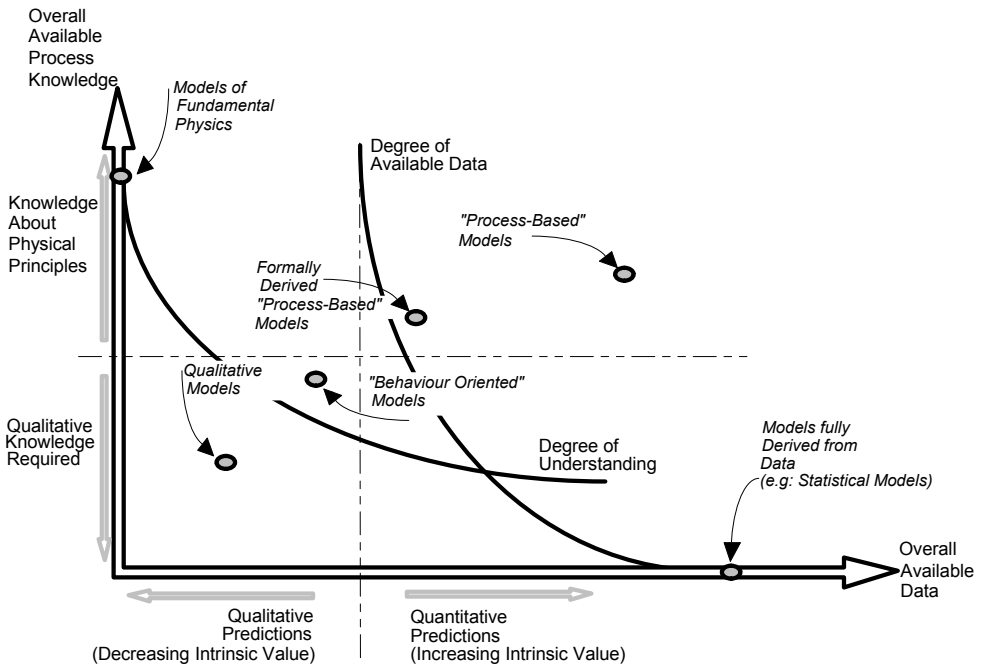

Figure 2-2 Classification of models with respect to knowledge and data (Capobianco, M., 1998)

Present-day morphodynamic models are based on three different modelling approaches:

- Process-based models aim at describing the physical processes as well as possible. Data sets are only used for calibration and validation purposes. At larger time-scales, errors can accumulate and computational effort increases substantially.
- Parametric models can be considered as reduced process-based models, where the dominant processes are modelled by means of parameterization. This approach reduces computational time but allows for more inaccuracy at the same time.
- Behaviour-orientated models assume that a system evolves towards an equilibrium state, a priori known from long-term data sets. Basic knowledge of the dominant processes is applied to describe intermediate states.

2.3.2 Process-based morphodynamic modelling

During the past decades, so-called process-based morphodynamic models have been developed to simulate the complex interaction between currents, waves, sediment transport and bed level variations and their interactions and to predict the morphological development. Process-based modelling is relevant to the meso-scale, which concerns the primary morphodynamic behaviour due to the interaction of the constituent processes and the bed topography. The appropriate morphodynamic length scale is about 1 km with a time-scale of years. Principal forcings are seasonal and interannual variations in tide, waves and currents and human activities such as sand-mining can be taken into account. Process-based modelling aims at describing the physical processes as well as possible. Data sets are only used for calibration and validation purposes.

Figure 2-3 shows the concept of a process-based morphodynamic model. The essence of such a model is the simulation of physical processes, based on primary physical principles, such as conservation of mass, momentum and energy.

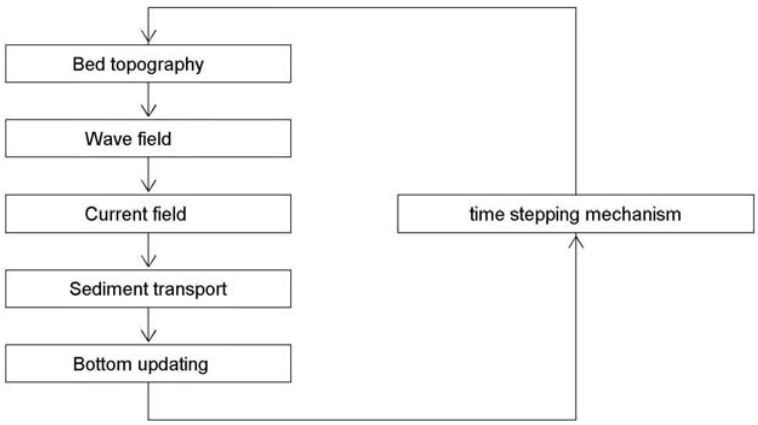

Figure 2-3 Principles of morphodynamic process-based modelling

2.3.3 Delft3D

In this Section, a short description of the software packet Delft3D is given, a detailed description can be found in the Delft3D-FLOW user manual (WL | Delft Hydraulics, 2003) and in Lesser et al. (2004).

2.3.3.1 General introduction to Delft3D

The Delft3D modelling system is developed by WL | Delft Hydraulics to simulate two-dimensional or three-dimensional simulations of coastal, river and estuarine areas. It can simulate flows, sediment transport, waves, water quality, morphological developments and ecology. The modelling system consist of several modules, herein, a short description is given of FLOW and WAVE. In addition to these modules two smaller modules are used to create and modify grids and bathymetry. RGFGRID handles model grids for Delft3D modules. QUICKIN can be used to create, manipulate and visualise the bathymetry of a model area and to interpolate sample points onto model grids.

WAVE
With the Delft3D-WAVE module, the evolution of wind-generated waves can be simulated. The WAVE module is either based on HISWA or SWAN; herein SWAN will be used. SWAN, an acronym for Simulating Waves Near shore, is a third generation, spectral wave model that computes the non-steady propagation of short crested waves over an uneven bottom, considering wind action, dissipation due to bottom friction, wave-breaking, refraction, shoaling and directional spreading.

The SWAN model takes into account the following physics:

- Wave propagation in time and space, shoaling due to current and depth, refraction and frequency shifting.
- Propagation from laboratory up to global scales
- Wave generation by wind
- Dissipation by white-capping, depth-induced breaking and bottom friction
- Non-linear wave-wave interactions
- Wave-induced set-up
- Wave-blocking by flow
- Transmission through and reflection from obstacles

The SWAN model does not account for:

- diffraction
- scattering reflections

The wave conditions (i.e. wave forces based on the energy dissipation rate or the radiation stresses, orbital velocities) calculated in Delft3D-WAVE module are used as input for the Delft3D-FLOW module, to compute wave-driven currents, enhanced turbulence, bed-shear stress and stirring up by wave breaking.

FLOW

The FLOW-module is a hydrodynamic simulation program, which calculates non-steady flow and transport phenomena resulting from tidal and/or meteorological forcing on a curvilinear, boundary fitted grid. The numerical system of the program solves the unsteady shallow water equations in two or three dimensions. Typical applications of Delft3D-FLOW includes simulations of tide and wind driven flows, stratified and density driven flows, river flow, transport of dissolved material and pollutants.

The shallow water equations can be derived from the three-dimensional Navier-Stokes equations for incompressible free surface flow, under the assumption of shallow water and Bousinesq. In the vertical momentum equation the vertical accelerations are neglected, which lead to the hydrostatic pressure equation. The system of partial differential equations for conservation of mass and momentum is solved with a finite difference method on the model grids. The principal variables, such as water level, bottom level and velocities, are arranged in a special way that is known as the staggered grid.

Sediment Online

Sediment Online is an add-on with the Delft3D-FLOW module which concerns simultaneous computation of flows and transports and simultaneous feedback to bottom changes. Therefore, hydronamic flow calculations are always carried out using the correct bathymetry. The Sediment Online transport sub-module accounts for:

- Cohesive sediment transport, including the effect of salinity on flocculation
- Non-cohesive suspended (sand)transport
- Bed-load transport
- Influence of waves and hindered settling
- Updating the bed level and feedback to hydronamics
- Up to 5 fractions of sand or combination of sand and mud.

The effects of density currents, stratification, and spiral flow are automatically taken into account without requiring any special parametric formulations. The time-scale and length scale of the applications are similar as for the hydronamic applications of Delft3D-FLOW.

Morphological time scale factor
Morphodynamic developments take place on time scale several times longer than typical flow changes, which would lead to long simulation times in case of morphological predictions. To shorten the simulation time a morphological time scale factor can be used, whereby the speed of the changes in the morphology is scaled up to a rate where it begins to have a significant impact on the hydrodynamic flows.

2.3.3.2 The TRANSPOR2004 sand transport model and bed roughness predictor

TRANSPOR2004 (Van Rijn et al., 2004) is a new version of the engineering sand transport model TRANSPOR and was developed within the EU-SANDPIT project. The most important improvements involve a bed-roughness predictor for the previously user-specified current-related and wave-related bed roughness parameters and a refined predictor for the suspended sediment size. The reference concentration of the suspended sediment concentration profile was recalibrated for use with the predictors.

The implementation of TRANSPOR2004 in Delft3D-ONLINE itself is part of an update of Delft3D which involves among others: the extension of the model to be run in profile mode, the synchronization of the roughness formulations and inclusion of two breaker delay concepts.

The bed roughness predictor is implemented separately, via a add-on called trachytopes and predicts the bed roughness based on hydronamic conditions and sediment characteristics and is to be used in combination with the TRANSPOR2004 sediment transport model.

2.3.3.3 Bottom layer sub-grid model

A recent update of the Delft3D software involved the bottom layer sub-grid model and a correction vector to the suspended-load transport in the bottom layer(s). This Section describes the approach and a recent update to this approach that was used in Chapter 4.

In Delft3D Sediment-Online the transfer of sediment between the bed and the water column is modelled using sink and source terms acting on the near-bottom layer that is entirely above van Rijn's reference height; (this layer is referred to as *kmx* layer for brevity). Each half time step the source and sink terms for the *kmx* layer are computed, which represent the quantity of sediment entering and dropping out of the flow. In order to determine the required sink and source terms, the concentration and concentration gradient at the bottom of the *kmx* layer need to be specified.

The concentration and concentration gradient at the bottom of the kmx layer are determined after assuming a standard Rouse profile between the reference concentration and the concentration at the centre of the *kmx* layer, see Figure 2-4. This approach of fitting a Rouse profile for determination of the concentration and concentration gradient at the bottom of the *kmx* layer is discussed in the most recent draft version of the FLOW user manual (WL | Delft Hydraulics, 2005).

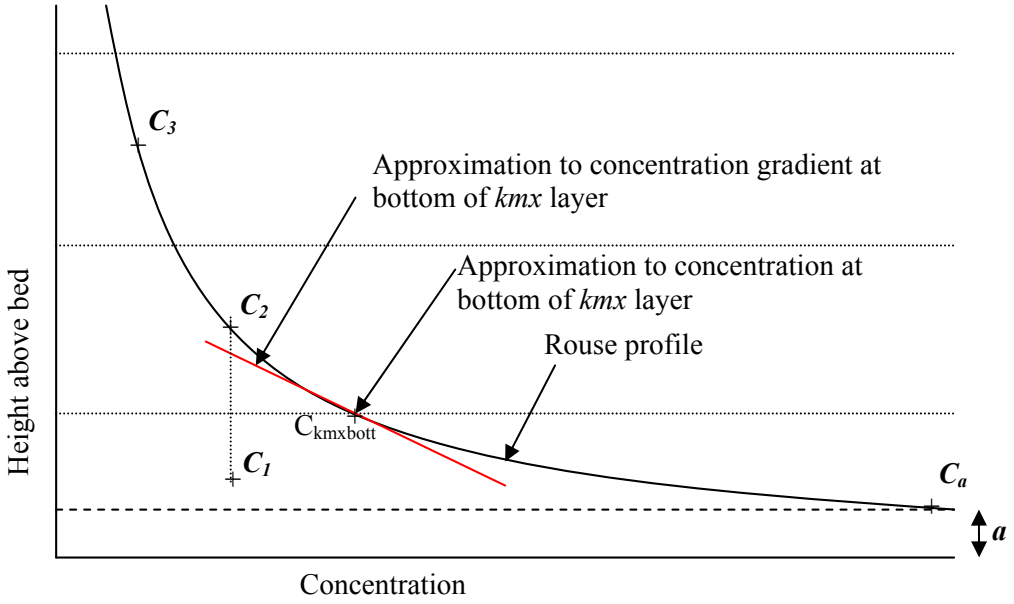

Figure 2-4 Improved version of Delft3D bottom layer sub-grid model

Where

a	van Rijns reference height
C_a	reference concentration
$C_{kmxbott}$	concentration at bottom of *kmx* layer
C_1, C_2, C_3	Delft3D computed concentrations in centre of layers 1, 2 and 3

For reasons of numerical stability, the sediment settling velocity w_s is set to zero ($w_s = 0$) beneath the *kmx* layer and the vertical diffusion coefficient ε beneath the *kmx* layers is set very high ($\varepsilon >> 1$). This causes the concentration in the layer(s) beneath the *kmx* layer to be equal to the concentration of the *kmx* layer ($C_1 = C_2$) and thus leads to under prediction of suspended-load transport.

To this end a correction vector to the suspended-load transport for the layer(s) beneath the *kmx* layer is introduced.

$$\vec{u} \cdot (C_{estimated} - C_1) \tag{1.1}$$

$C_{estimated}$ is the analytically determined average concentration between the bottom of the *kmx* layer and the reference concentration. With this correction vector the suspended-load transport in the layer(s) beneath the *kmx* layer can be determined accurately.

Criterion

With very wide concentration profiles the fitting of Rouse profiles can be troublesome, therefore a criterion was built-in so that when the reference concentration is 100 times the concentration of the kmx layer ($C_a > 0.01C_2$) the correction vector is not included in the transport scheme. Due to the use of relatively coarse sediments in this study and a relatively large (mandatory) bottom layer it was found that the criteria was mostly not met and the correction vector was not included, which resulted in significantly smaller suspended-load transport rates. However, during max. flood and max. ebb the criteria was regularly met in the top region of the ridge, which caused a stepwise increase in suspended-load transport rates at the top of the ridge resulting in artificial bathymetric features.

Very recently, at the end of the study, a Delft3D update became available in which the criterion for applying the correction vector was omitted so this correction vector is continuously used and suspended-load transport is determined accurately. Due to the limited time available in this study it was not possible to redo all of the simulations that were already carried out with a Delft3D version using the criterion for the accurate determination of concentrations in the bottom layer. It was decided to redo the simulations in chapter 4 and investigate the effect of the updated Delft3D version in Section 6.4.

3 Data description and analysis

3.1 Introduction

This chapter discusses the morphology data used in this study. First, an introduction is given to the sand ridge Hoek van Holland. Next, the accuracy of bathymetric surveys is discussed in Section 3.3. The exact location, dimensions and some background information on the sand ridge are discussed. Furthermore, in Section 3.4 the available morphology data is discussed and a specific study area is selected, based upon characteristics of available soundings. Next, a data-analysis is carried on the morphology data in Section 3.5.

3.2 Introduction to the sand ridge Hoek van Holland

From 1982 to 1986 dumpings at Hoek van Holland created an artificial sand ridge, known as sand ridge Hoek van Holland, of about 3600 m normal to the peak tidal current and the shore, (location Hoek van Holland, see Figure 3-1) in an area with depths between 15 m. and 23 m. on the northern side of the approach channel. In all, 3.5 million m^3 sand was dumped over the period 1981 to 1986 (Van Woudenberg, 1996)

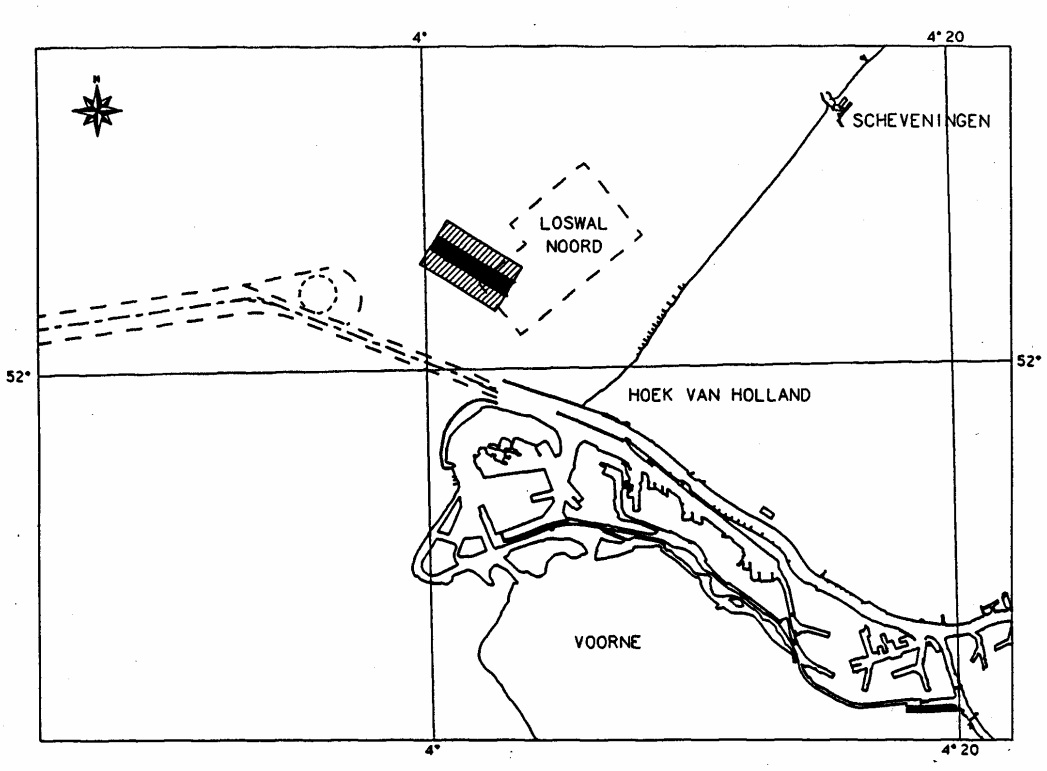

Figure 3-1. Location sand ridge Hoek van Holland.

The ridge dimensions just after creation of the ridge were: length of about 3600 m; toe width between 250 m and 370 m; height between 1.3 and 4 m; slopes between 1:50 and 1:100 on

the south flank and between 1:20 and 1:50 on the north flank; d50 between 0.15 mm and 0.45 mm. The landward end of the ridge is about 6300 m from the shoreline.

The sand ridge Hoek van Holland is located close to Loswal Noord, which is a dumping site for class I and II silt from the Rotterdam harbour mouth. The ridge is perpendicular to the coast and thus normal to the tidal flow. Primary goals were to study the stability of a submerged ridge, normal to the tidal flow and to study the effect of the ridge on shoreface sand transport. Also the possible use of submerged ridges as silt traps for backflow of silt from Loswal Noord to the port of Rotterdam was an issue. Furthermore similarities with sand waves were to be investigated.

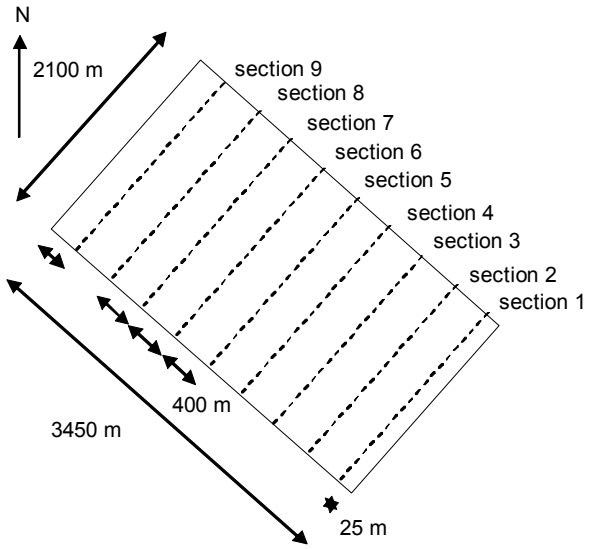

Figure 3-2 Schematic plan view of the sounding area and sections (section 1 is about 6 km from the coast)

Figure 3-2 shows a schematic plan view of the sounding area and sections, sections are 400 m apart and run over the entire length of the sounding area, which is about 2200 m. Section 1 is about 6 km from the coast. In this study sections 3, 4, 5 and 6 will be modelled with the line-models (1DH and 2DV).

3.3 Accuracy of bathymetric surveys

This Section discusses the accuracy of bathymetric studies, and is based upon evaluation of bathymetric surveys and research on systematic surveying errors within the NOURTEC project on shoreface nourishments at Terschelling, The Netherlands and shoreface and beach nourishments at Torsminde Tange, Denmark and Norderney, Germany (Westlake et al., 1996). The bathymetric surveys of the sand dump at Hoek van Holland are comparable to the bathymetric surveys carried out within the NOURTEC project and surveying errors therefore will be much alike.

Survey errors may have a large effect on the results; they can be described as two types: systematic errors that have a cumulative effect on the results and stochastic errors that are ‘random’ errors. Definitions are not always clear and often depend on the time-frame of analysis; errors systematically over one survey lane may be stochastic over the whole survey. The influence of stochastic errors on bathymetry plots is considered negligible as the

main interest is the mean depth of certain areas and stochastic errors are averaged out when finding the mean depth in those areas.

In the NOURTEC surveys, the following systematic errors sources were considered:

1. Error in determination of the water level

The water level is the height difference between the ordnance level and the sea bottom which is calculated by transferring the height of a NAP mark of the primary network to a water post near the coast and then to the gauges at sea. The water level at the gauge is assumed to be equal to the level at the ships position. A further aspect of this error is that it depends on the position of the ship in relation to the gauge and if the ship is measuring during a rising or falling tide.

2. Error from setting of the zero line

The zero value is the depth of the transducer, measured from the water surface. Depth of the transducer is determined by reading the water level from marks on the hull when the ship is stationary. The depth of the echo sounder below the marks is known. Setting the zero is the main error source, variations in the ship' weight and in water density (salinity) will affect the zero line setting.

3. Error caused by squat

Squat is the phenomenon of falling water level around a moving ship and occurs only in shallow or very narrow waters. The amount of squat is proportional to the square of the ship's speed through the water divided by the gravitational acceleration multiplied by the water depth. If the water depth exceeds six times the ship's draught, the bottom is not felt by the ship so no squat occurs. Thus for a draught of approximately one meter a limiting depth of six meters may be defined.

4. Echo sounding distance

The echo sounder distance is the distance between the transducer and the sea bottom. The transducer produces a sound pulse which is reflected by the sea bottom, by measuring the delay between emitting and receiving, the distance to the bottom can be determined. From various error sources, the error resulting from the variation of the sound velocity in water is thought to be the most important; also the calibration error may have some effect.

5. Error caused by waves and swell

Waves and swell cause vertical rolling movements, resulting in an error described by the vertical movement, the surf rider effect and the rolling effect. The surf riders effect is caused by the displacement of the ship in the direction of the waves as the ship spends more time on the top of the wave than in the trough and thus a greater depth is registered.

6. Error resulting from incorrect positioning

The DGPS system, which is used in the surveys has an horizontal positioning accuracy of 2 m. Assuming a maximum bottom slope of 1:50, the worst error case is then 4 cm. This results in an rms error of approximately 3 cm.

Summary of possible systematic errors at Terschelling
For survey measurements at Terschelling, systematic errors are considered a major problem. From this investigation, the main errors that may cause problems with survey accuracy are: (with s the root-mean-square error and od the one-directional root-mean-square error)

- Error in determination of the water level (s = 3 cm)
- Error from squat (od = 10 – 20 cm), or with squat differences (s = 2 cm)
- Error from systematic differences between ships (s = 4 – 8 cm)
- Error from setting of the zero line (s = 5 cm)
- Error from variation in the ship's weight (s = 3 cm)
- Error from the surf riders effect (od = 0 – 5 cm)
- Error from the accuracy of the positioning system (s = 0 – 5 cm)

Within the NOURTEC project, main sources of systematic error in surveying are defined and quantified. Systematic errors are considered the main problem in obtaining accurate survey results. From analysis of surveys of the NOURTEC site at Terschelling, the survey accuracy was obtained, which should be used with the results as an indication of the reliability of the measurement.

- The total effect of the systematic errors in the bathymetric measurements of each survey at Terschelling ranges from -1 to -24 cm in water shallower than about 6 m, or -4 to +9 cm in water deeper than about 6 m.
- The error in differences between surveys at Terschelling is estimated at -5 to +10 cm, where the negative notation indicates that the water depth is underestimated.

3.4 Morphology data

This Section describes which morphology data is available for the evaluation of the Delft3D-model. First a general description is given of the available data. Next, the selected measurements are discussed and the study area is precisely defined.

3.4.1 Soundings

The Sand dump Hoek van Holland was created between 1982 and 1986. Since 1982 yearly bathymetric surveys were carried out by Directorate North Sea (DNZ), with some years missing, see Table 3-1. A sounding in 1999 was not processed by DNZ due to errors. Soundings before 1991 were not available on tape and were digitized from maps or microfilm, and thus are less reliable. Data collection before 1991 was carried out with the less-accurate single beam method, while data collection after 1991 was carried out with the more accurate multi-beam method. Soundings were carried out with fixed gauges at Hoek van Holland, amplitude correction was carried out.

sounding	date	year	method	ship
1	8 and 9th of September	1982	single-beam	unknown
2	16, 17 and 18th of February	1983	single-beam	unknown
3	4, 5, 10, 11 and 14th of June	1985	single-beam	unknown
4	12 and 23rd of Dec. 25, 26th of Jan.	1985/86	single-beam	unknown
5	14, 15 and 18th of March	1991	multi-beam	Octans
6	9, 10,16 and 17th of April	1992	multi-beam	Octans
7	5, 8 and 9th of March	1993	multi-beam	Octans
8	22, 29 of April 2nd of May	1994	multi-beam	Octans
9	1, 2, 3 and 4th of May	1995	multi-beam	Octans
10	22 March, 16 and 17 April	1996	multi-beam	Octans
11	20, 21 and 22 of August	1997	multi-beam	Octans
12	5, 13, 16, 17 and 19 October	2000	multi-beam	Octans

Table 3-1 Sounding dates.

From the national Institute for Coastal and Marine Management (RIKZ) two datasets were obtained, the first spanning the period 1982 to 1997, the second covering the period 1991 to 2000. The dataset with soundings from 1982 to 1997 originates from research by Van Woudenberg (1996), while the second dataset, including the sounding in 2000, was directly obtained from the “lodingen” database of RIKZ. The sounding in 2000 includes several large pits that were dredged within the framework of the PUTMOR project; fortunately these are located in the seaward part of the sounding area so as to ensure the usability of the sounding.

In the first dataset, the single beam soundings before 1991 previously were corrected for differences between single and multi beam sounding by increasing the height values (z) with 0.2 m (Van Woudenberg, 1996).

Comparison of the two datasets shows that the second dataset (1991 to 2000) is somewhat out of line with the first (1982 to 1997), as the z-values are about 10 to 15 cm lower. The first dataset will be used herein, along with the sounding in 2000 from the second dataset, which will be corrected based upon analysis of average height in a small inactive compartment of the sounding area.

Soundings for 1994 and later cover a slightly larger area, which exceeds earlier soundings to the shallower part for about 200 m. This shallower part is of less importance and for compatibility reasons it was decided not to use this extra area in analysis.

Dumpings

From 1981 to 1986 sand was being dumped on the ridge on regular basis, exact locations of the dumpings cannot be found. Data on the quantities and dates involved are listed in Table 3-2.

	dumping date	**quantity**
1	original dumping, before September 1982	1,644,000 m^3
2	between September 1982 and February 1983	234,750 m^3
3	between February 1983 and June 1985	537,500 m^3
4	between June 1985 and February 1986	457,000 m^3
5	in 1986	496,500 m^3
	in total :	approx. 3.500.000 m^3

Table 3-2 Dumping dates.

Research on diffusion of dredging material (silt) at the nearby location Loswal Noord showed a maximum displacement of 600 m from dumping location (van den Heuvel, 1988). Sand is heavier and will settle even faster and displacement will be smaller. The sounding area is 2200 m wide, loss of sand from dumpings will therefore be set to zero.

Correction of sounding of 2000

The first dataset will be used for the morphological computations, however the second dataset will be used for the sounding of 2000 as the first dataset lacks a sounding in that year. The z-values of the second dataset are about 10 to 15 cm lower than z-values from the first dataset. The sounding of 2000 from the second dataset therefore needs to be corrected for proper use in combination with data from the first dataset. To this end the average depth in the inactive south-western corner (500 x 500 m^2) of the sounding area for both the first and second dataset were compared, see Figure 3-3 and Table 3-3.

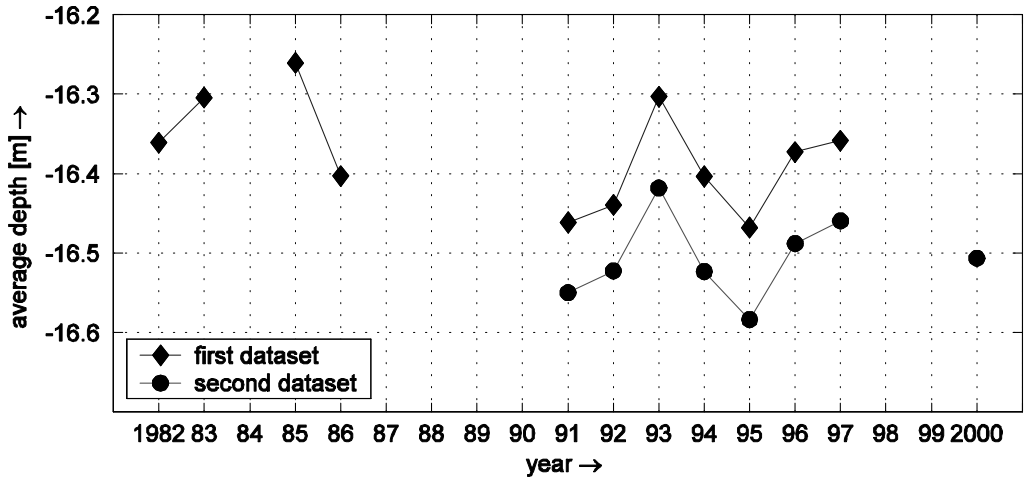

Figure 3-3. Average depth in south-western corner (500 x 500 m) for both datasets.

year	first dataset	second dataset	difference
1991	-16.4615	-16.5499	0.0884
1992	-16.4395	-16.5226	0.0831
1993	-16.3032	-16.4182	0.1150
1994	-16.4036	-16.5235	0.1199
1995	-16.4681	-16.5837	0.1156
1996	-16.3729	-16.4882	0.1154
1997	-16.3586	-16.4597	0.1011
2000	-	-16.5068	-

Table 3-3 Average depth (m) in south-western corner (500 x 500m) for both datasets.

Furthermore, the volumes above a reference level at -50 m to MSL were compared for both datasets, see Figure 3-4 and Table 3-4. Given the total surface of the sounding area, the differences herein represent a difference in height, which is given in the last column of Table 3-4.

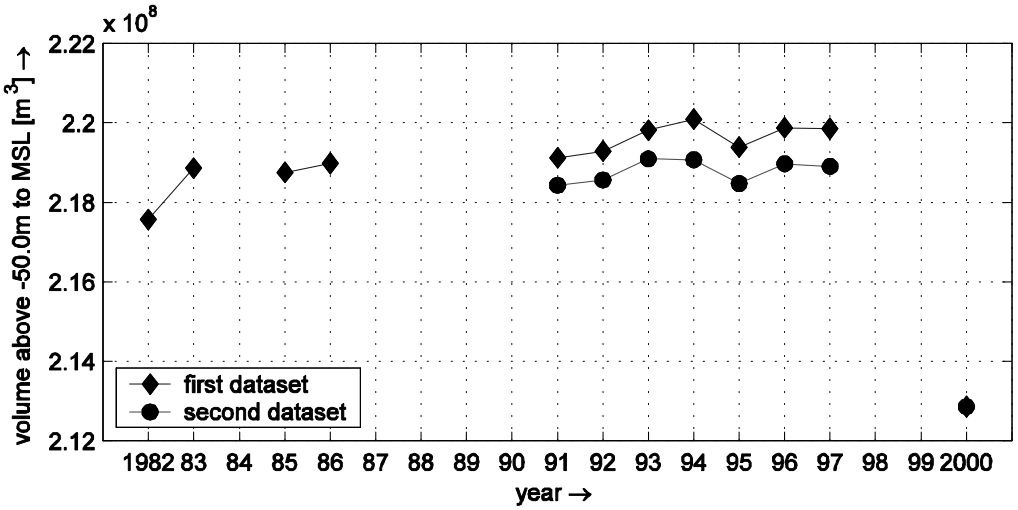

Figure 3-4 Volume above -50.0 m to MSL for both datasets.

year	first dataset	second dataset	difference (m^3)	difference (m)
1991	219,428,750	218,428,750	696,500	0.096
1992	219,288,750	218,565,750	723,000	0.099
1993	219,817,500	219,096,500	721,000	0.099
1994	220,096,750	219,073,000	1,023,750	0.141
1995	219,389,000	218,471,500	917,500	0.126
1996	219,879,500	218,972,750	906,750	0.121
1997	219,583,000	218,903,750	949,000	0.131
2000	-	212,860,000	-	-

Table 3-4 Volume (m^3) above -50.0 m to MSL and accompanying difference in depths.

From Figure 3-3, Figure 3-4 and Table 3-4 it can be seen that soundings from the first and second dataset differ significantly. For proper use of the sounding of 2000 from the second dataset in combination with sounding from the first dataset (which contains more soundings) this sounding from 2000 needs to be corrected. From computations it can be seen that the correction is to be somewhere between +0.09 and +0.13 m. As the total effect of errors in the bathymetric measurements is estimated at -0.09 to +0.19 m, the correction needs not to be very exact; herein a value of +0.12 m is chosen.

3.4.2 Cross-sections

Although more data is available, the morphological development of the ridge is shown well from data of 1982, 1991, 1995 and 2000. Herein measured bed levels for cross-sections 1-9 are discussed, see Figure 3-5.

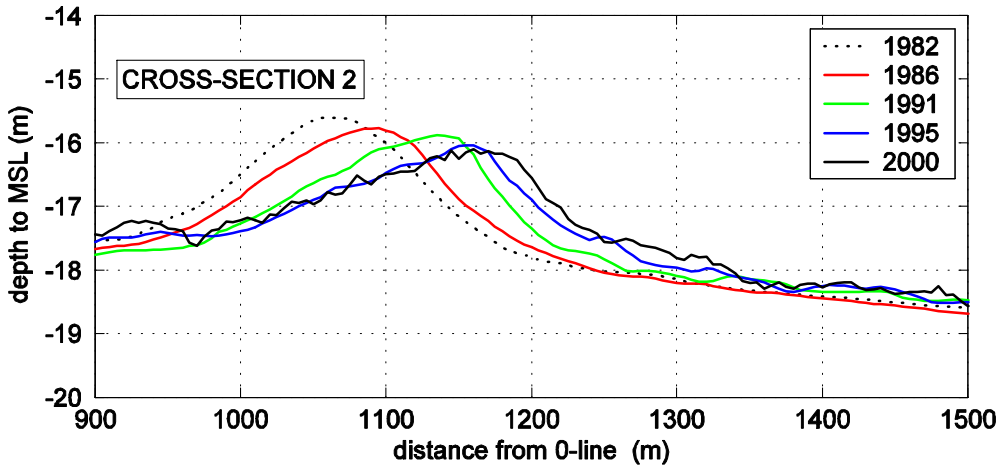

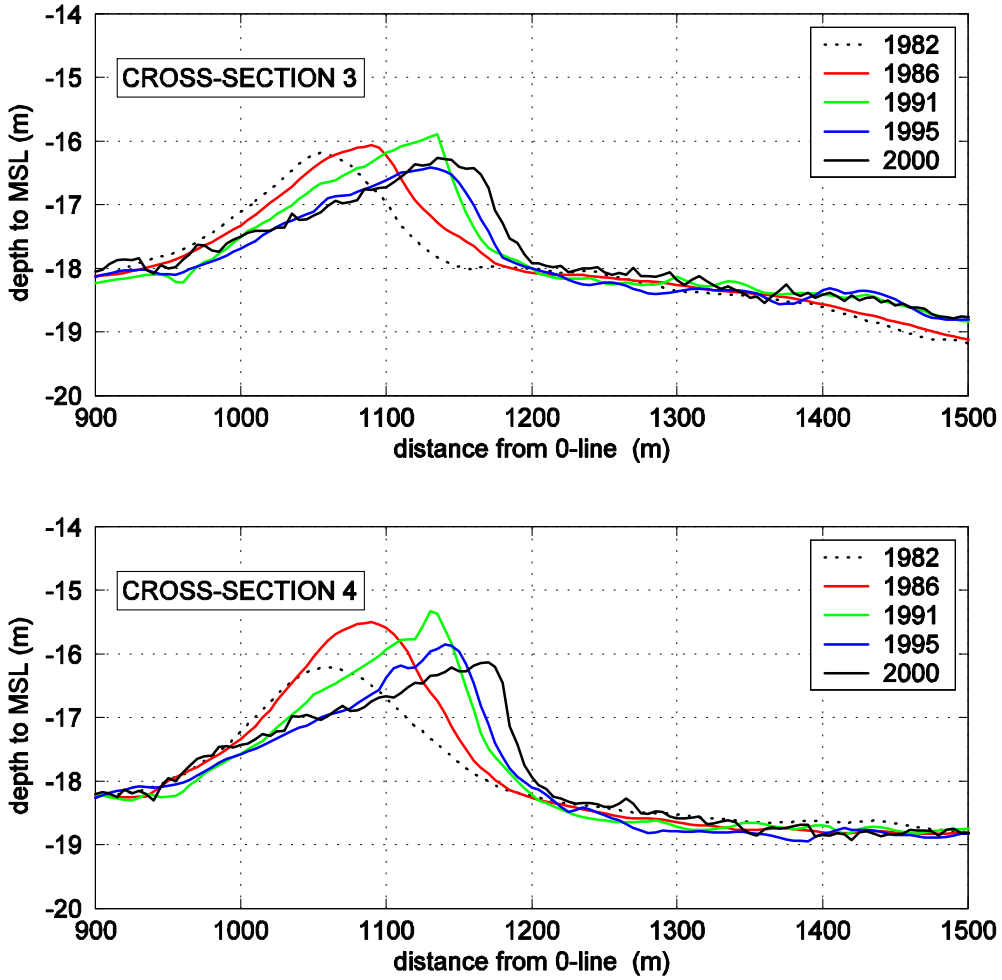

Figure 3-5 Measured bed level developments for section 2, 3 and 4.

Figure 3-5 shows measured bed levels for 1982, 1986, 1991, 1995 and 2000 at three cross-sections in the sounding area. Measured bed levels for sections 1 to 9 are shown in figures B.03a-c in appendix B. The data of 1982 to 1991 was originally digitized from plots, which is why the bed levels of those years seem smoother than bed levels in later years.

The cross-sections clearly show a reduction in height of the ridge and a migration in north-eastern direction; in the direction of the net tidal flow. The rate of migration changes with depth. This reduction of migration with increasing depth induces a rotation of the ridge with respect to the original axis of the ridge. The average migration of the ridge in northern direction is about 5.50 m per year and the average decrease in height is about 0.1 m per year.

Between 1992 and 1993 a migration in south-western direction and increase in height of the ridge was observed. This behaviour was also observed with sand waves (Woudenburg, 1996). Between 1992 and 1993 more storms were observed, but as in other years these were from dominant wind directions (south western – north western); no relationship between wind data over that period and the backward migration can be found (Van Woudenberg, 1996). The backward migration may also be the result of inaccuracies in the soundings,

therefore it was decided not to use the intermediate years for calibration and validation as the present intervals provide enough information on migration of the sand dump on a longer timescale.

3.4.3 Study area

As dredging was carried out in the seaward side of the sounding area between 1997 and 2000, it was decided to focus on the shallower part of the Sand dump Hoek van Holland for analysis and verification. Also the width of the area was chosen somewhat smaller than the width of the sounding area. Sedimentation and erosion volumes were computed, varying the spatial domain. The chosen study area whereby erosion and sedimentation are more or less in balance and the ridge is approximately in the centre of the area, is 1600 m long and 700 m wide, Figure 3-6.

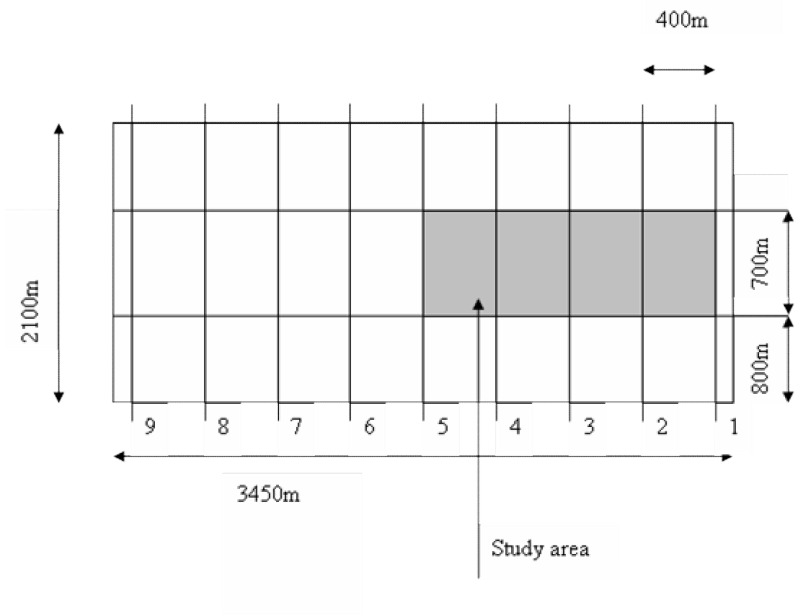

Figure 3-6 Smaller study area.

3.5 Data-analysis

In this Section the available morphologic data will be analysed, sedimentation / erosion plots will be discussed and sedimentation / erosion volumes will be computed. Also, the sounding area was divided into 56 sections, for these sections the development of the average depth in time is discussed. Finally the position of the crest of the ridge in time is dealt with.

3.5.1 Introduction and background information

Sedimentation / erosion plots have been made for all successive years and also for the period 1991 to 2000 and are given in Appendix B. These plots show sedimentation / erosion patterns in the sounding area and reveal yearly rates of erosion or sedimentation. All plots have been scaled back to one year; periods between soundings have been taken from Table 3-1. In all but two plots the crest of the ridge is clearly visible, as there is considerable

erosion at the crest of the ridge and sedimentation direct behind the crest. The two plots that don't show the crest of the ridge are for the period 1994-1995 and 1995-1996.

3.5.2 Description of sedimentation / erosion plots

- Figure B.04 shows sedimentation / erosion for 1982 - 1983 and shows the second dumping that was carried out in the sounding area; the dumping was carried out in the deeper part of the area, just north of the study area. In the shallower part of the sounding area erosion marks the contours of the ridge.
- From figure B.05 it was found that between 1983 and 1985 no strong erosion occurred, the sedimentation along the crest of the ridge indicates a small dumping was carried out. This dumping was carefully placed at the location of the crest to enlarge the top of the artificial ridge thus created.
- Figure B.06 shows sedimentation / erosion for 1985 – 1986; another dumping can be seen in the plot, partly located at the crest of the ridge, partly in the north-eastern corner of the area.
- The sedimentation / erosion plot for 1986 – 1991, see figure B.07, shows a neat pattern, with erosion in front of the ridge and sedimentation just behind the ridge. In the area surrounding the ridge, minor erosion takes place. Sedimentation is not found in this plot except for the small strip just behind the crest of the ridge.
- Figure B.08 shows sedimentation / erosion for 1991-1992 and shows an alternating pattern of sedimentation and erosion over the sounding area, with strong erosion in front of the crest and sedimentation just behind the crest. In the period 1992-1993 there's more sedimentation then in most other periods, erosion only occurs in front of the crest and in the uppermost northern boundary of the sounding area.
- Between 1993 and 1994 a predictable pattern of erosion and sedimentation was found, see figure B.09, with erosion in front of the ridge, some sedimentation on the ridge and strong erosion just before the crest of the ridge. Behind the crest strong sedimentation occurred followed by some erosion and finally, sedimentation to the northern boundary of the sounding area.
- Sedimentation / erosion plots for 1994-1995 and 1995-1996 (see figure B.10 and B.11) don't show the crest of the ridge very well, in these plots no specific area's of erosion or sedimentation can be seen. In the plot for 1994-1995 mostly erosion occurs and between 1995 and 1996 mostly sedimentation occurs, the cause of this odd behaviour is not clear.
- Figure B.12 shows sedimentation / erosion between 1995 and 1996, sedimentation and erosion lanes alternate, on the overall more sedimentation occurs.

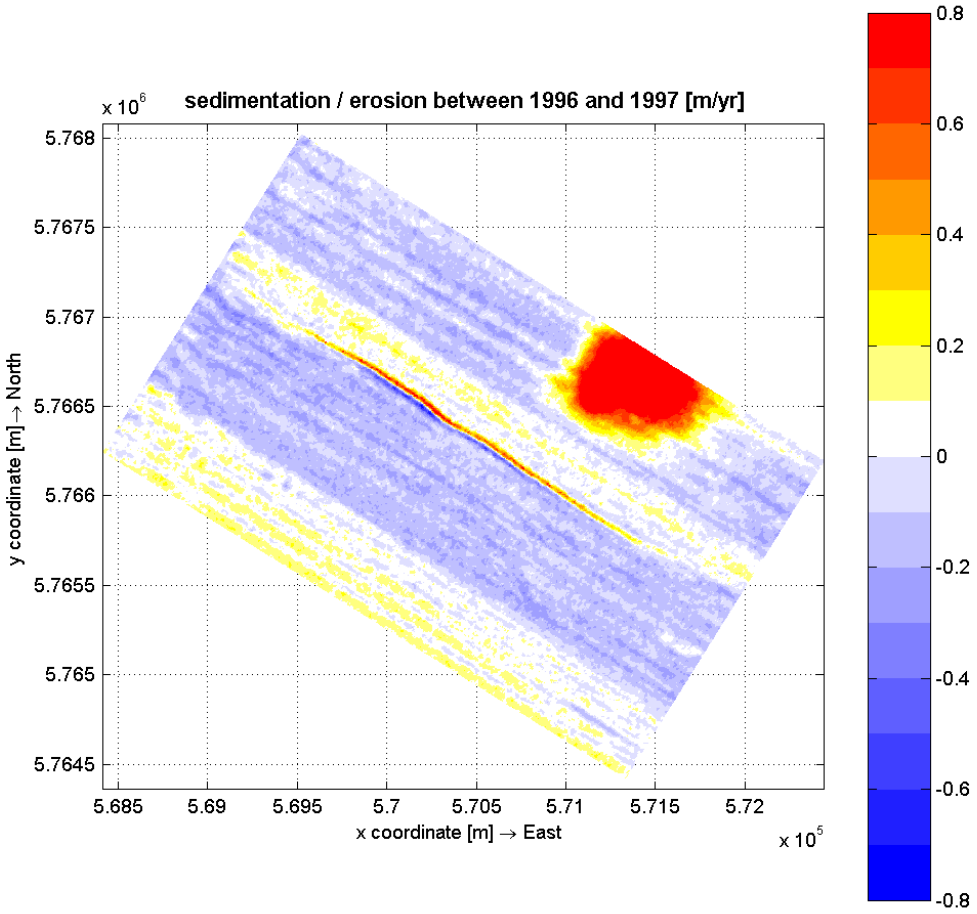

Figure 3-7 Sedimentation / erosion between 1996 and 1997 [m/yr]

- The sedimentation / erosion plot for 1996-1997 is shown in Figure 3-7 and figure B.13 and reveals an abnormal increase in height in a specific area, indicating a dumping has been carried out at the northern boundary of the sounding area The dumping didn't affect the ridge directly, but the effect on the flow and transport in the area can affect the ridge.
- The sedimentation / erosion plot for 1997-2000 is shown in figure B.14 and clearly shows the dredging activities that took place in that period, as the deeper part of the ridge was partly removed and three pits can bee seen in the plot. The plot was scaled to show yearly erosion or sedimentation up to a maximum of 0.8 m per year, for comparison with other plots, but the pits that can be seen in the plot are much deeper.

- The sedimentation / erosion over the period 1982-2000 is shown in figure B.15; both the dumping at the northern boundary and the dredging activities between 1997 and 2000 are shown, furthermore sedimentation directly north of the ridge was observed.
- The sedimentation / erosion plot over the period 1986-1991 is shown in figure B.16; overall erosion occurred, only directly north of the top sedimentation was found.

- The sedimentation / erosion plot over the period 1991-2000 is shown in figure B.17 and shows the dumping at the northern boundary and the dredging activities in the deeper part of the area. The plot also shows the erosion in front of the crest and sedimentation direct behind the crest of the ridge.

3.5.3 Sedimentation / erosion volumes

The total sedimentation / erosion over the period 1982 - 2000 was computed for this study area, possible inaccuracies herein were taken into consideration. Careful analysis of computations of sedimentation / erosion volumes in the study area showed that all dumpings between 1982 and 2000 were carried out outside the study area. Also the dredging activities between 1997 and 2000 were carried out outside the study area, in fact this area was chosen so as to exclude any dredging pits to allow for proper analysis. Therefore the computed sedimentation / erosion volumes in the study area don't need to be corrected for dumpings or dredging.

First the sedimentation / erosion in the study area (see Figure 3-6) was computed over the period 1982 – 2000, next the sedimentation / erosion for 1986 – 1991 and 1991 - 2000 was computed. It was found that between 1982 and 2000 in total 300,900 m^3 eroded from the southern side of the ridge and 201,900 m^3 accreted at the northern side, thus resulting in a net loss of sediment from the study area of 99,000 m^3. Between 1986 and 1991 129.900 m^3 eroded, mostly from the southern side of the ridge and 156,300 m^3 accreted at the northern side. In this period 26.286,1 m^3 of sediment was imported in the study area. In the period 1991 – 2000, total erosion in the study area was 169,600 m^3 and sedimentation was 116,400 m^3, thus resulting in a net loss of 53,200 m^3. Sedimentation / erosion volumes for the three period s are given in Table 3-5. it can be seen that overall, between 1982 and 2000, sediment is lost from the study area. However in the period 1986-1991 sediment was gained. Between 1991 and 2000 a net loss of sediment from the study area was observed.

period	erosion	sedimentation	net change
1982-2000	300,900	201,900	-99,000
1986-1991	129,900	156,300	26,400
1991-2000	169,600	116,400	-53,200

Table 3-5 Sedimentation / erosion volumes study area

3.5.4 Volume of top of the ridge

For all available soundings, the volume of the top of the ridge was determined by computing the volume of the ridge above a reference level at -17.5 m to MSL and between 800 m and 1500 m from the 0-line, see Figure 3-8.

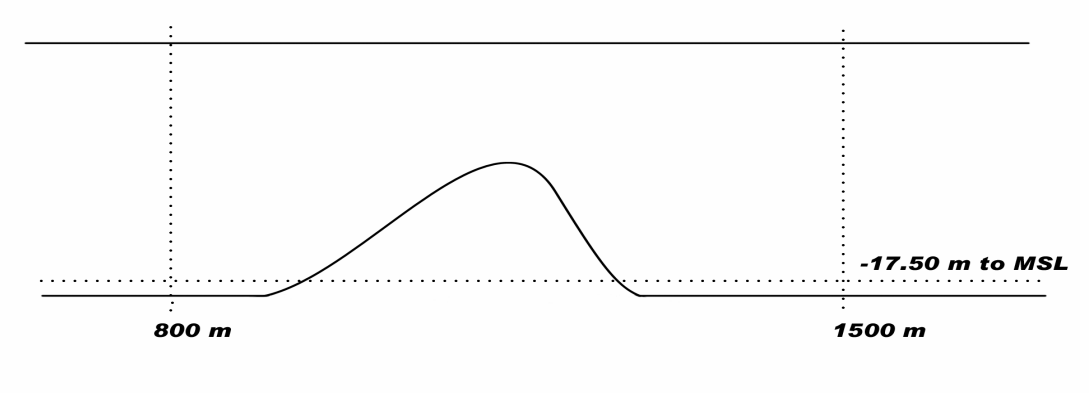

Figure 3-8 Definition sketch; volume study area above -17.50m to MSL

The volume of the top of the ridge for all available years and the change in volume of the top for successive years are listed in Table 3-6.

year	volume of top (m^3)	change in volume (m^3
1982	546,750	
1983	569,500	22,750
1985	624,750	55,250
1986	614,750	-10,000
1991	598,250	-16,500
1992	591,750	-6,250
1993	665,500	73,500
1994	620,000	-45,250
1995	513,500	-106,500
1996	569,750	56,250
1997	526,500	-43,500
2000	502,750	23,750

Table 3-6 Volume and change in volume of the top of the ridge (above -17.5 m to MSL and between 800m and 1500m from 0-line)

Figure 3-9 shows the volume of the top of the ridge (above -17.5m to MSL and between 800 m and 1500 m from the 0-line) for all available years. Figure B.18 presented in Appendix B shows the same data as ridge chart with separate plot that shows the changes in volume of the top for successive years . A decrease of volume of the top of the dam can be seen, but it must be stated that the volume of the top increases between 1992 and 1993 and also between 1995 and 1996.

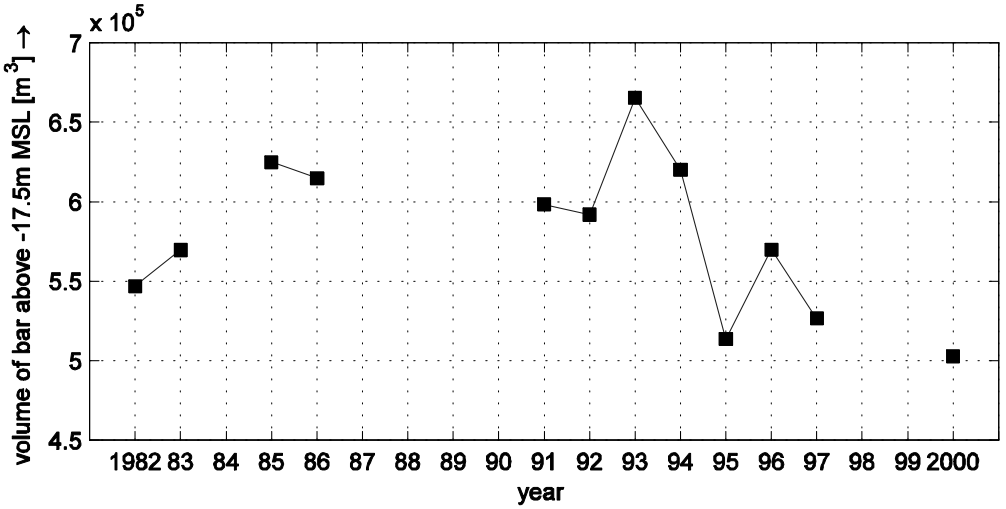

Figure 3-9 Volume of the top of the ridge (above -17.5m to MSL and between 800m and 1500m from the 0-line)

3.5.5 Total volume of the ridge

For all available soundings, the total volume of the ridge was determined by computing the volume of the ridge above a reference level at -40.0 m to MSL for the entire sounding area., see Figure 3-10. The pits that were dredged between 1997 and 2000 reach levels of about -33 m to MSL, therefore computing the volumes above -40.0 m to MSL allows for an honest comparison.

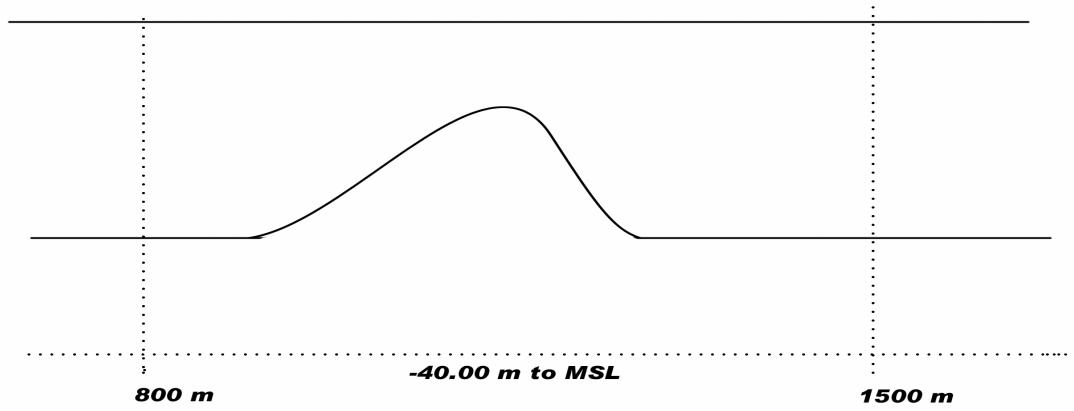

Figure 3-10 Definition sketch: volume study area above -40.00 m to MSL.

Volumes of the ridge for all available years are listed in Table 3-7, also the change in volume for successive soundings are given. The volume that was dredged is determined from this data.

year	volume of the ridge (m^3)	change in volume (m^3)
1982	145,114.995,9	-
1983	146,407,000	1,292,000
1985	146,302,250	-104,000
1986	146,535,000	232,250
1991	146,675,000	139,750
1992	146,838,750	163,750
1993	147,367,500	528,750
1994	147,646,750	279,500
1995	146,939,000	-707,500
1996	147,429,500	490,500
1997	147,403,000	-26,500
2000	141,279,500	-6,123,750

Table 3-7 Volume and changes in volume of the ridge (above -40m to MSL and over the entire sounding area).

Figure 3-11 shows the volume of the ridge above -40.0 m to MSL over the entire sounding area for all available soundings. Figure B.19, presented in Appendix B shows the same data as ridge chart with a separate plot that shows the changes in the volume for successive years.

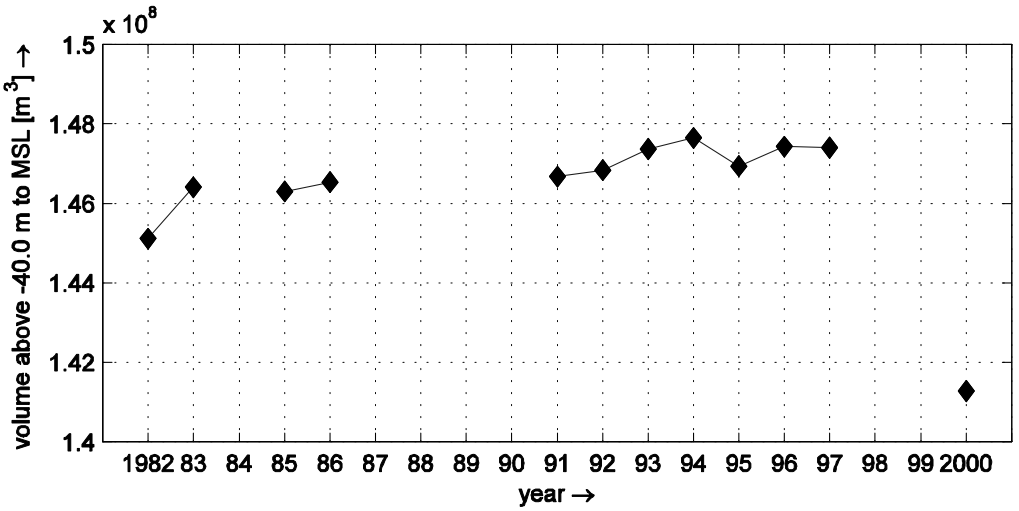

Figure 3-11 Volume of the ridge above -40m to MSL.

The dumping between 1996 and 1997 cannot be distinguished; it doesn't show on the scale of the total volume of the ridge. Dredging activities between 1997 and 2000 are clearly shown in both figures. From Figure 3-11 and B.19 it can be seen that changes in volume are between 0.1 and 0.6 million m^3 per year.

3.5.6 Dredged volume between 1997 and 2000

The volume above -40.0 m to MSL was computed for the entire area and for all years. The loss in volume between 1997 and 2000 is thought to be caused by the dredging activities only. The volume above -40.0 m to MSL in 1997 is 147,403,000 m^3 and in 2000 141,279,500 m^3, thus the dredged volume is 6,123,750 m^3.

3.5.7 Volume of dumping between 1996 and 1997

From the sedimentation / erosion plot over 1996-1997 it was concluded that a dumping has been carried out in that period. The dumping area is about 900 m long (perpendicular to the coast) and 600m wide (alongshore direction) and is located along the northern boundary of the sounding area. In Table 3-8 the volume above -25m to MSL for the dumping area is given from 1994 to 1997. This data is also shown in Figure 3-12. The average volume over 1994, 1995 and 1996 is 3.068.449,5 m^3, while the volume in 1997 is 3.429.163,9 m3. Therefore the dumping between 1996 and 1997 is about 375.000 m^3.

year	volume dumping area above -25m (MSL)
1994	3,070,000 m^3
1995	3,063,750 m^3
1996	3,071,750 m^3
1997	3,429,000 m^3

Table 3-8 Volume of dumping area above -25m to MSL.

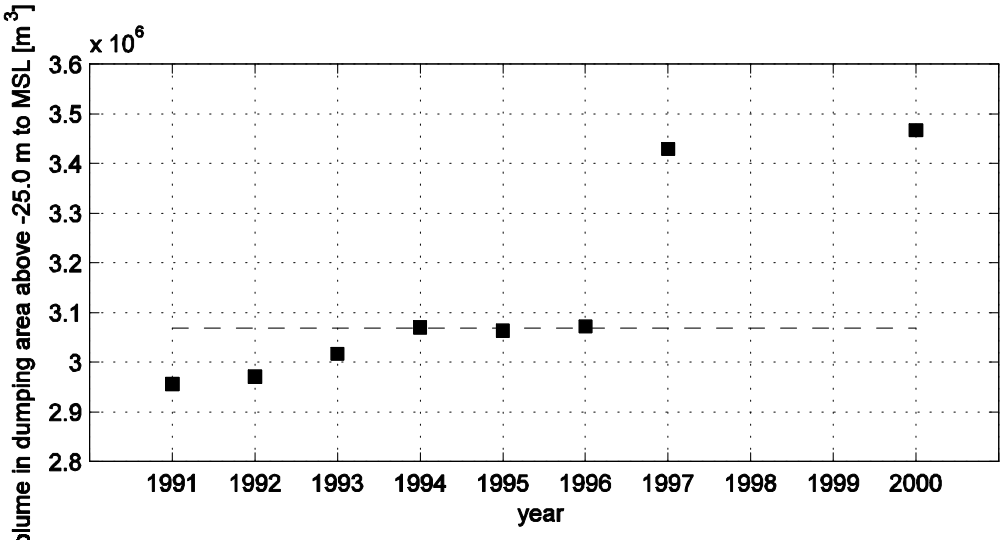

Figure 3-12 Volume of dumping area above -25m to MSL.

3.5.8 Subdivision of sounding area

The sounding area (3450 m x 2100 m) was divided into 56 compartments to study local deviations from the overall sedimentation / erosion trends. The compartmentalisation of the

sounding area was based upon sedimentation / erosion plots of the area for successive years, the dimensions of the compartments in alongshore direction were chosen such as to represent areas of either sedimentation or erosion over all years as closely as possible. As these areas differ somewhat from year to year, the chosen compartments don't always exactly cover areas of only sedimentation or only erosion, but on the average the compartments coincide with those areas.

The sounding area was divided into 8 compartments in alongshore direction, 4 of which are in front of the ridge with respect to the average tide driven current in northward direction and 4 of which are behind the ridge, see Figure B.20. The first compartment is 300m wide, successive compartments in front of the ridge are 500, 150 and 50 m wide. Compartments behind the ridge in consecutive order are 50, 275, 225 and 400m wide. In seaward direction, from the origin of the sounding area in the southern corner, the first compartment is 450 m long and the next six compartments are 500 m long.

For all 56 compartments the average height of the compartment for all years was computed and plotted, see figure B.21, as was the change in average height, see figure B.22. From Figure B.21 and B.22 it can be seen that

- The general trend of sedimentation just north of the ridge, was not met between 1994 and 1995 in compartments 1-5 to 7-5 and 1-6 to 6-6, which are compartments just north of the ridge.
- Between 1993 and 1995 there was erosion in the first two alongshore compartments (most southern compartments) whereas in general sedimentation takes place in those compartments.
- An increase of the average height in compartments 5-7, 5-8 and 6-8 between 1996 and 1997 suggest dumpings have been carried out.
- Compartments in the uppermost northern corner of the sounding area between 1997 and 2000 show the dredging activities that have been carried out.

From inspection of the sedimentation / erosion plots and from the change in height of the all compartments in figure B.22 the following conclusions can be drawn.

- Between 1993 and 1995 significantly more erosion took place in almost all compartments.
- Between 1996 and 1997, a dumping has been carried out, about 600 m perpendicular to the ridge in north-eastern direction.
- Between 1997 and 2000 dredging activities have been carried out, creating pits in the deeper parts of the sounding area.

3.5.9 Positions of the crest of the ridge

The position of the crest of the ridge was computed every 5m, by determination of the minimum depth in the cross-section. For better representation of the displacement in time, the ridge was again divided into 7 compartments over the length of the sounding area. For these compartments the average position of the crest of the ridge was computed for all years.

As the peculiar phenomenon of smaller displacement of the crest in the centre of the sounding area was found for all years but 2000, and considering the dredging activities that were carried out between 1997 and 2000 it was decided not to use the data from 2000 for

determining the average displacement of the crest. The average displacement per year was computed for the periods 1982 – 1986, 1986 – 1991 and 1991 and 1997 and are shown in Figure 3-13.

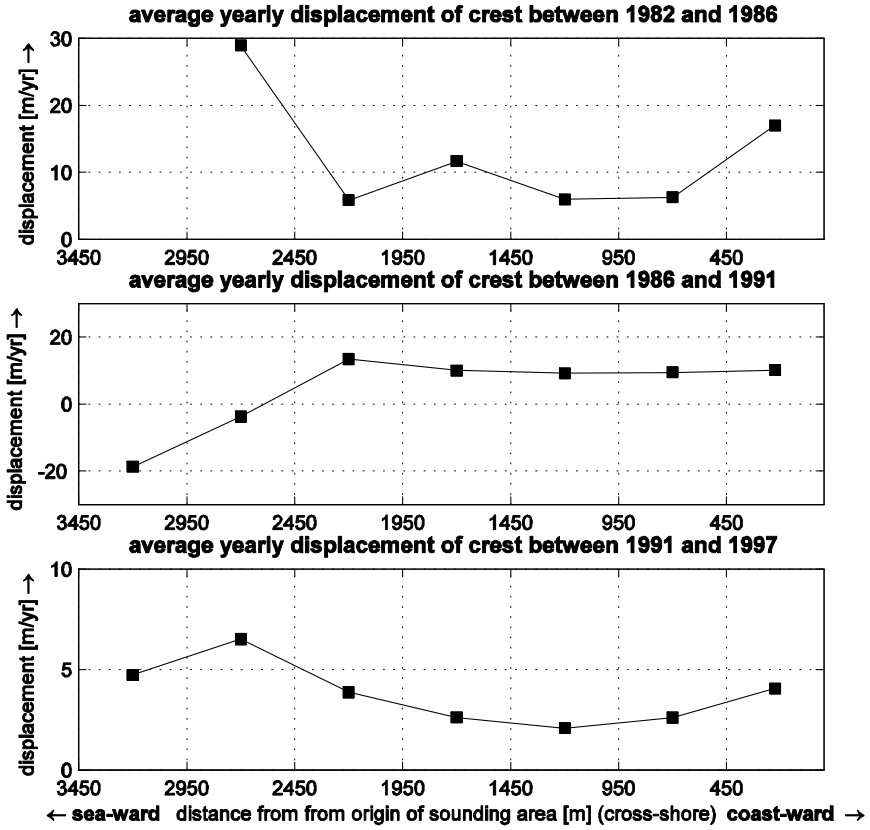

Figure 3-13 Average yearly displacement of crest for 3 periods over the length of the sounding area.

Considerable differences over the length of the ridge occur in the displacement of the crest in all periods. Overall, the displacement is particularly evident in the first, landward part of the ridge and in the seaward end of the ridge, while the displacement in the middle is considerable smaller. Displacement in the most seaward part of the sounding area between 1982 – 1986 and 1986 – 1991 is completely different from the general trend in those periods and are therefore considered inaccurate.

3.6 Synthesis

Herein a brief recapitalization of chapter 3 is given.

From 1982 to 1986 dumpings created an artificial sand ridge at Hoek van Holland normal to the peak tidal current and the shore; the ridge is about 5 m high and a few hundreds meters wide and about 3600 m in length and the landward end of the ridge is about 6300 m from the shoreline. Tidal flow is parallel to the coast and thus normal to the ridge.

The bathymetric surveys of the artificial sand ridge Hoek van Holland are comparable the surveys carried out within the NOURTEC project; the vertical accuracy of soundings is in the order of 0.1 to 0.2 m and the horizontal accuracy of soundings is in the order of 1 to 5 m.

Regular soundings between 1982 and 2000 show a clear reduction of the ridge height in time and a net migration of the ridge in flood direction. The rate of migration reduces with increasing depth. The average migration of crest of the ridge in northern direction is about 5.50 m per year and the average decrease in height is about 0.1 m per year. Between 1992 and 1993 a southward migration of the ridge and increase in height was observed.

As dredging was carried out in the seaward part of the sounding area between 1997 and 2000, it was decided to focus on the shallower part of the ridge; a study area was defined whereby erosion and sedimentation are more or less in balance.

From computed sedimentation and erosion volumes it was found that overall, between 1982 and 2000 more sediment eroded at the southern side of the ridge than accreted at the northern side of the ridge; sediment was lost from the study area. However, between 1986 and 1999 a net gain of sediment was observed in the study area. Between 1991 and 2000 sediment was lost from the study area. Sedimentation / erosion plots showed annually changing patterns per year; no characteristic erosion pattern could be derived, except for the notion that erosion takes place at the top of the ridge and sedimentation directly north of the ridge. Furthermore it was found that between 1996 and 1997 a dumping of approximately 375.000 m^3 was carried out.

4 Idealized sand ridge

4.1 Introduction

In this chapter 2DV simulations for an idealized sand ridge are discussed. The simulations were carried out using a recent version of Delft3D (Section 2.3.3.3). The idealized sand ridge consists of a symmetric ridge at a depth comparable to the sand ridge near Hoek van Holland. The tidal flow is represented by a sinusoidal function ($U=U_0+U_1\cos(\omega t)$) with and without a net current (drift), thus representing a propagating tidal wave as in the Dutch coastal zone. A small phase difference between horizontal and vertical tides is not taken into account. These simulations were carried out to gain insight in the physical processes at the sand ridge and to investigate the effect of tides, waves and basic model settings on the morphological development of an idealized sand ridge. The investigated process- and model parameters are given in Table 4-1.

Section	investigated effect	variation
4.4	tides	tides without drift, with a drift of 0.05 m/s and 0.10 m/s
4.5	waves	Hs = 0.00 / 1.50 / 2.00 / 2.50 / 3.00 m
4.6	layers	10 / 20 / 30
4.7	turbulence model	algebraic / k-L / k-epsilon
4.8	bed roughness	constant / variable (predictor)
4.9	model approach	1DH (1 layer) / 2DV (20 layers)

Table 4-1 Investigated process- and model parameters.

First, in Section 4.2, basic characteristics of flow and transport over sand ridges normal to the flow are discussed. In Section 4.3 the model set-up is discussed. Next, in Section 4.4 the effect of tides with and without a net current is investigated. In Section 4.5 the effect of waves was investigated and in Section 4.6 the number of vertical layers was varied. Next, the effect of three different turbulence models was investigated in Section 4.7 and in Section 4.8, simulations were carried out with a constant- and variable bed roughness (with and without the bed roughness predictor). In Section 4.9 a comparison is made between the 1DH and 2DV model approach. Finally in Section 4.10 the most important findings are discussed once more.

4.2 Basic analysis of flow, transport and morphology over a schematized sand ridge normal to the flow

4.2.1 Unidirectional flow

Herein, unidirectional flow over a sand ridge is discussed; First the velocity profiles at the upsloping and downsloping flanks of the ridge are given. Next the implications for transport and morphology are discussed.

4.2.1.1 Velocity profiles at upsloping and downsloping flank

With unidirectional flow over a sand ridge the velocity profiles at both sides of the top of the ridge are differently-shaped; the velocity profiles upstream of the top of the ridge are logarithmic (decreasing water depth), while downstream the velocity profiles are characterized by reduced velocities in the near-bed zone (due to increasing water depth and deceleration processes), see Figure 4-1.

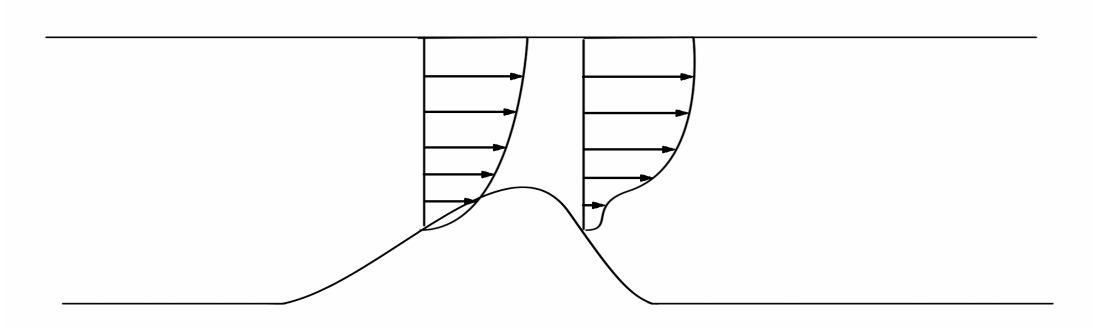

Figure 4-1 Velocity profiles over sand ridge

4.2.1.2 Implications for transport and morphology

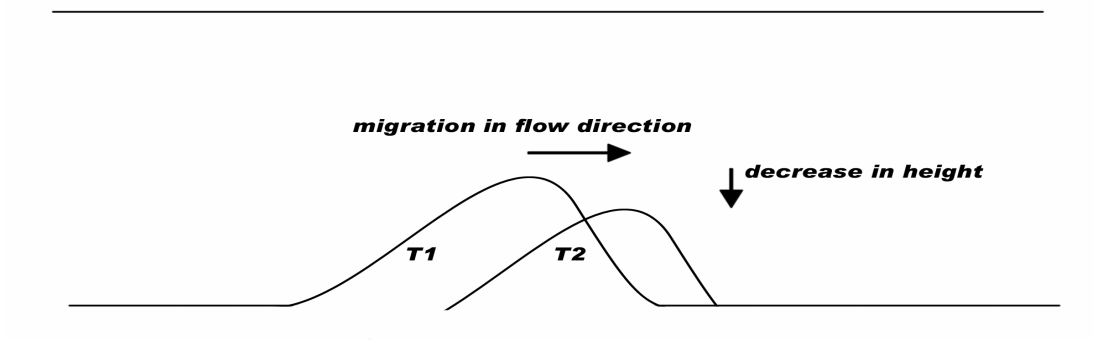

Figure 4-2 Morphological development with unidirectional flow

Figure 4-2 shows the morphological development of the sand ridge with unidirectional flow; both bed-load and suspended-load transport is in flow direction. The ridge migrates in flow direction and reduces in height when suspended-load transport is dominant. It may grow in height when bed-load transport is dominant.

4.2.2 Tidal flow

Herein, the effect of symmetric tidal flow (without a net current) over a sand ridge is discussed. With tidal flow the direction of the flow reverses periodically and the water level varies; the water depth at ebb is shallower than at flood. Both the reversing flow and the varying water level affect velocities, transports and morphology and are discussed herein.

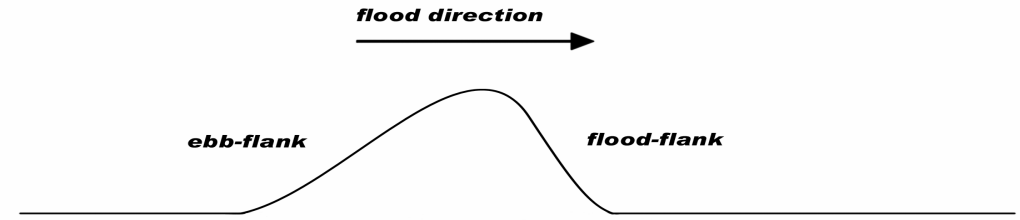

Figure 4-3 Definition ebb- and flood flank of sand ridge

Figure 4-3 shows the definition of the ebb- and flood flank of the ridge. The artificial sand ridge which is subject of this study is about perpendicular to the Dutch coast. Tidal flow is parallel to the coast and thus normal to the ridge; flood is in north-eastern direction and ebb in south-western direction.

4.2.2.1 Effect of reversing flow

With tidal flow, the direction of the flow changes with the turning of the tide which has its consequences on the time-averaged velocity profiles at both sides of the ridge. At maximum flood and maximum ebb, the velocity profiles are as described in Section 4.2.1.1; the velocity profiles are logarithmic upstream of the top and show reduced near-bed velocities downstream of the top. As the flow during flood and ebb is in opposite direction, the upstream and downstream locations are at opposite sides of the top; the logarithmic upstream velocity profile at one side of the top changes to the velocity with reduced near-bed velocities when the flow reverses and the location is downstream of the top, see Figure 4-4.

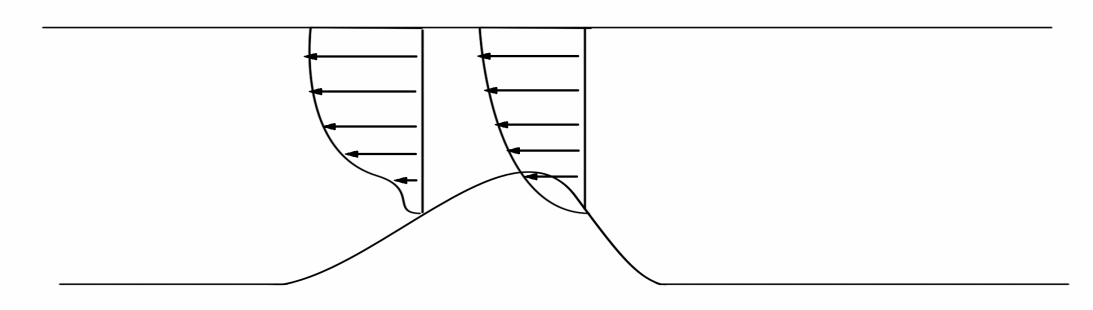

Figure 4-4 Ebb velocity profiles over ridge

The velocity profiles during ebb and flood are dissimilar, the net effect can be seen from the time-averaged velocity profiles. The time-averaged velocity profiles at both sides of the top show near-bed velocities in top direction; this is due to the dip in the downstream velocity profiles. Figure 4-5 shows the time-averaged velocity profile at the flood flank of the ridge; the time-averaged near-bed velocities are in the direction of the top of the ridge.

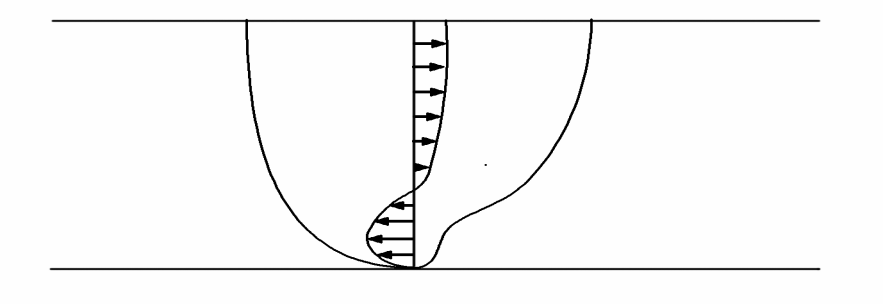

Figure 4-5 Time-averaged velocity profile at flood flank of the ridge

4.2.2.2 Effect of water level variation

The tidal range with shallower water depths during ebb affects velocities, transports and morphology. Herein two important mechanisms, related to the shallower water depth during ebb, are discussed.

The bed shear stress depends on water depth. During ebb, the bed shear stress will be larger due to the shallower water, see Equation 1.2 and 1.3; with shallower water (smaller h), C will be smaller and subsequently τ_b will be larger. Thus with equal depth-averaged ebb- and flood-velocities, transports will be larger during ebb than during flood.

$$\vec{\tau}_b = \frac{g\rho\vec{U}\left|\vec{U}\right|}{C^2} \tag{1.2}$$

and

$$C = 18\log(\frac{12h}{k_s}) \tag{1.3}$$

with

τ_b the bed shear stress [N/m^2]
g the gravitational acceralation [m/s^2]
ρ the water density [kg/m^3]
U the velocity [m/s]
C the Chézy coefficient [m$^{1/2}$/s]
k_s the equivalent geometrical roughness of Nikuradse [m]

The effect of waves also depends on the water depth. Waves intensify the stirring action of the fluid motion in the near-bed region and lead to larger sediment concentrations and larger transports; with shallower water the effect will be greater and transports will be larger. Thus with equal depth-averaged ebb- and flood-velocities, transports in ebb direction are larger than transports in flood direction due to wave action.

4.2.2.3 Implications for transport and morphology

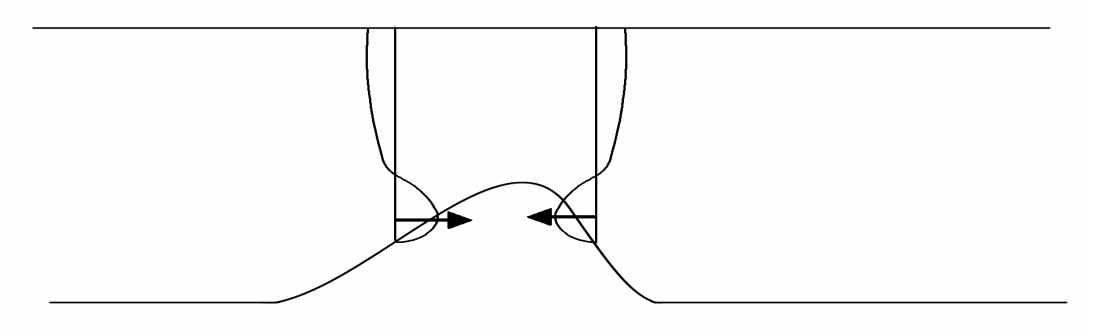

Figure 4-6 time-averaged near-bed velocities directed to the top

Figure 4-6 shows the time-averaged velocities with tidal flow at both sides of the top; it can be seen that the time-averaged near-bed velocities at both sides of the top are in top direction. This mechanism results in vertical growth of the ridge when bed-load transport is dominant and (particles remain in top region of the ridge). When suspended-load transport is dominant the particles may be transported beyond the top region resulting in flattening of the ridge.

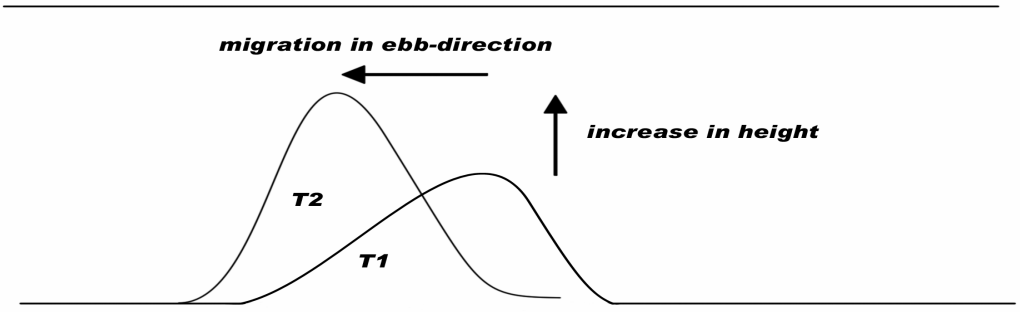

Figure 4-7 Morphological development with tidal flow (without net current)

Figure 4-7 shows the morphological development of the sand ridge for tidal flow without a net current (drift). The ridge increases in height when bed-load transport is dominant and migrates in ebb-direction. The increase in height is due to bed-load transport; the time averaged bed-load transports at both flanks of the ridge are in direction of the top of the ridge due to the time-averaged near-bed velocities in top direction. The migration in ebb-direction is caused by the time-averaged transports in ebb-direction due to the greater bed shear stresses with shallower water during ebb than during flood.

4.3 Model set-up idealized sand ridge

This Section describes the idealized sand ridge model set-up. Not all possible input parameters of the Delft3D software are mentioned herein. Only the relevant parameters are discussed, which include the model grid and -bathymetry, boundaries, time parameters, processes, wind, waves and transport settings. This Section also discusses the sensitivity of the model to the horizontal grid size, the computational time step and the morphological scale factor used.

4.3.1 Model grid

The model grid used herein is 20 m wide and 2000 m long. The grid is a single cell wide to allow for true 2DV simulations without 3D effects.

horizontal grid

Herein, the effect of using horizontal grid sizes of 5, 10 and 30 m was investigated. Five-year morphological simulations with waves (Hs = 1.50m, Tp = 5.0s) were carried out using peak-ebb velocities of 0.55 m/s and peak-flood velocities of 0.65 m/s, which are representative for Hoek van Holland (van Rijn, 1995). The computational time step was 3 s.

Figure C.01 in appendix C shows the bottom profile development and time-averaged bed-load and suspended-load transports from simulations using a horizontal grid size of 5, 10 and 20 m. Figure C.02 shows bed-load and suspended-load transport rates at max. flood and max. ebb over the initial bottom profile. It can be seen that the computation using a horizontal grid size of 20m shows a sharp-edged course of transport rates over the main axis of the grid as a result of which the morphological development is affected and therefore computed less accurately, with increasing horizontal resolution the course of the transport rates along the main axis of the grid is computed more accurately and converges for horizontal grid sizes of 5 and 10m. A horizontal grid size of 10m was chosen as it provides enough resolution and is computationally more efficient than a horizontal grid size of 5m.

vertical grid

Delft3D uses a sigma-coordinate system for the vertical grid, whereby the vertical grid consists of layers bounded by two sigma planes, which are not strictly horizontal but follow the bottom topography and the free surface. As a result a smooth representation of the topography is obtained. For a sigma coordinate grid the number of layers is constant over the entire horizontal computational area, irrespective of the water depth. The distribution of

the relative layer thickness is usually non-uniform. This allows for more resolution in the zones of interest such as the near surface area (important for e.g. wind-driven flows, heat exchange with the atmosphere) and the near bed area (sediment transport). Due to the use of a sigma coordinate grid, only the number of layers and relative thickness of each layer has to be specified.

In this chapter, a vertical grid of 20 computational layers with a logarithmic layer distribution and a relative bottom layer thickness of 2% of the water depth was used. The layer distribution, i.e. the thickness of the individual layers is given in Figure 4-8 It can be seen that the variation-factor for each layer is 1.087, which complies with the criteria specified in the Delft3D manual that states the vertical grid must have a smooth distribution; i.e. the variation-factor for each layer should not exceed 0.7 – 1.4. The effect of using 10, 20 and 30 logarithmically distributed layers is investigated in Section 4.6.

layer	relative thickness %	layer	relative thickness %
1 (water surface)	9.92	11	4.27
2	9.12	12	3.93
3	8.38	13	3.61
4	7.71	14	3.32
5	7.08	15	3.05
6	6.51	16	2.80
7	5.98	17	2.58
8	5.50	18	2.37
9	5.06	19	2.18
10	4.65	20 (bed)	2.00

Figure 4-8 Vertical grid

4.3.2 Model bathymetry

A symmetric Gaussian-shaped sand ridge was created for the simulations, which roughly resembles the ridge characteristics at section 4 in 1991, i.e. a mean depth outside the ridge of about -17.8 m to MSL, a ridge height of about 3 m and a ridge width of about 400 m. The formula which was used to create the Gaussian shape reads:

$$z_b = H \cdot \exp(-x^2 / L^2) \tag{1.4}$$

with L the e-folding distance in x-direction in which the height decreases with a factor 1/e, and H the height of the ridge.

Here, L was taken 100m and H was taken 3 m, the top of the ridge is located at 1150 m from the first boundary, the resulting model bathymetry is shown in Figure 4-9

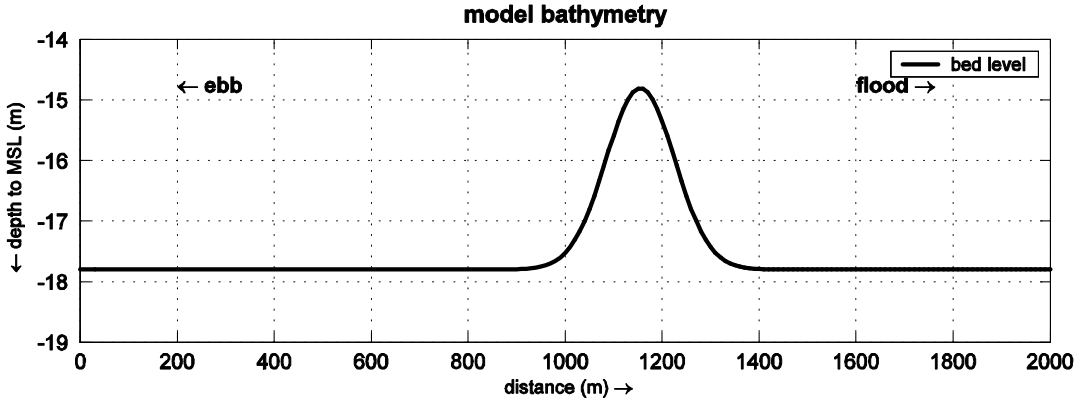

Figure 4-9 Model bathymetry initial tests.

4.3.3 Open boundary conditions

Two open boundaries were defined; at the downstream boundary (x = 0 m) velocities need to be specified and at the upstream boundary (x = 2000 m) water levels need to be specified. The initial water level was set at 0.00 m. The harmonic forcing type with flow conditions from user-defined frequencies, amplitudes and phases was applied at both the velocity and water level boundary. Basically, the flow system will be represented by:

$$\begin{aligned} U &= U_0 + U_1 \cos(\omega t) \\ h &= h_0 + h_1 \cos(\omega t) \end{aligned} \tag{1.5}$$

with $\omega = 2\pi/T$ and T = 12 hours. The velocity amplitude (U_1) was set to either 0.50, 0.75 or 1.00 m/s with a average (U_0) of either 0.00, 0.05 or 0.10 m/s. The water level amplitude was set to 1.0 m. The velocities used are given in Figure 4-10, Figure 4-12 and Figure 4-12.

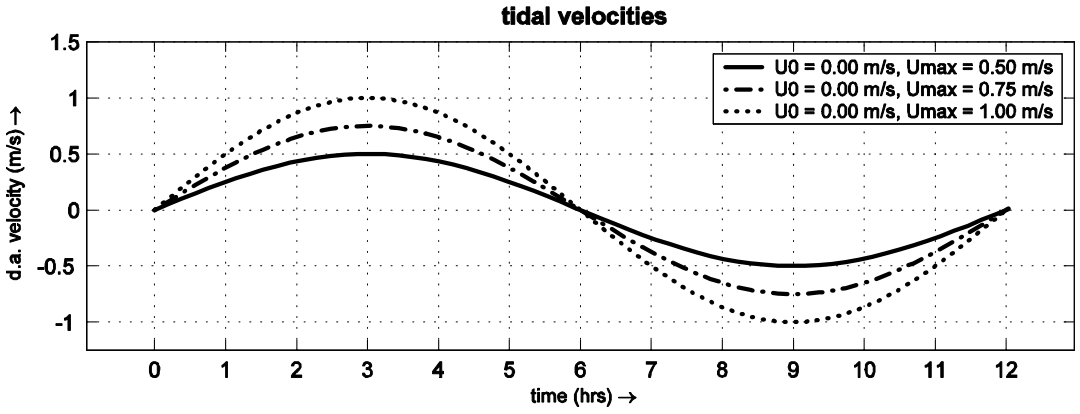

Figure 4-10 Tidal velocities with U0 = 0.00 m/s

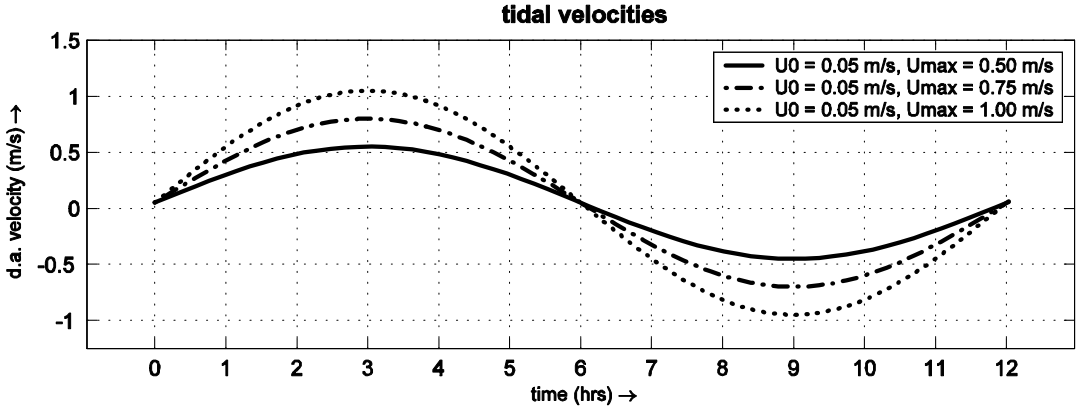

Figure 4-11 Tidal velocities with U0 = 0.05 m/s

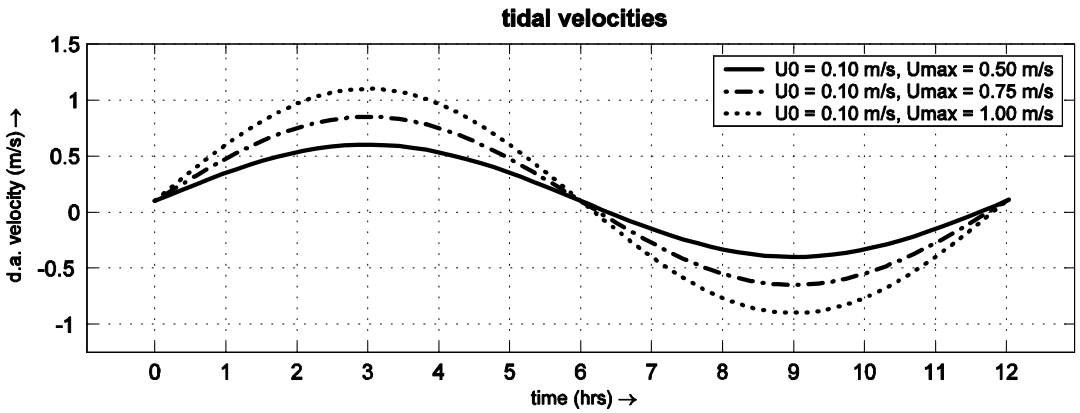

Figure 4-12 Tidal velocities with U0 = 0.10 m/s

4.3.4 Time scale parameters

A period of 5 years was chosen to assess the effect of tides, waves and basic model settings on the morphological development of the ridge. To reduce computational time, the numerical simulations are run over a much shorter period of 273 hours; the morphological changes are speed up to that of the 5 year period using a morphological scale factor, see Section 4.3.7.

The simulation period of 273 hours includes a spin-up period of 33 hours to allow the model to adapt itself to the boundary conditions. During the spin-up period no bed level updating takes place; the effective simulation time is therefore 240 hours, in this period 20 complete tidal cycles of 12 hours are simulated.

Time step

Time step limitations in Delft3D depend on several parameters, such as required accuracy, stability, grid size and water depth. An indication of the magnitude of the time step is the Courant number for wave propagation, it gives the relation between wave propagation, time step and the smallest grid size in either x- or y-direction. The formula reads:

$$CFL = \frac{\sqrt{gh} * \Delta t}{\{\Delta x', \Delta y'\}} \leq 10 \qquad (1.6)$$

In which :

g = acceleration due to gravity [m/s^2]
h = local water depth [m]
Δt = times step [s]
Δx', Δy' = smallest grid size in x- or y-direction [m]

In practical situations the Courant number should not exceed a value of 10, which in this case yields a computational time step of about 8 seconds. However the Courant criterion is a rough estimate and it was investigated whether a larger time step was allowed, which would significantly reduce computational time and is not unlikely as Delft3D uses a numerical scheme that is unconditionally stable.

The sensitivity of the model to the computational time step was investigated with five-year morphological simulations with waves (Hs = 1.50m, Tp = 5.0s) using peak-ebb velocities of 0.55 m/s and peak-flood velocities of 0.65 m/s, which are representative for Hoek van Holland (van Rijn, 1998). The computational time step was set to 3, 6, 12, 15 and 30s. Figure C.03 in appendix C shows the bottom profile development and time-averaged bed-load and suspended-load transports from simulations using a computational time step of 3, 6, 12, 15 and 30s. Figure C.03 shows bed-load and suspended-load transport rates at max. flood and max. ebb over the initial bottom profile. It can be seen that both transport rates and morphological development are independent of the time step. A computational time step of 15s was chosen, which yields a Courant number of about 19

4.3.5 Processes and physical parameters

The initial model was set-up to include waves and sediments, which will be discussed separately hereafter. Wind, salinity and temperature were not activated herein.

The physical parameters used were:

- Coriolis acceleration was set up for 52 °N,
- Acceleration of gravity was set to 9.8100 m/s^2
- Air density was 1.000 kg/m^3
- Water density was set to 1025 kg/m^3
- Salinity was 31.00 p.p.t
- Water temperature was 15 °C

turbulence model

In a Delft3D model, the grid is usually too coarse and the time step too large to resolve the turbulent scales of motion; the turbulent processes are “sub-grid” The space- and time-averaged turbulent mixing and diffusion can be computed with horizontal and vertical eddy viscosity and diffusivity. The vertical turbulent eddy viscosity and the vertical turbulent eddy diffusivity in a multi-layer Delft3D model are determined by means of a turbulence model, while the horizontal eddy viscosity and horizontal eddy diffusivity are specified dependent on the grid size.

The turbulence models differ in their prescription of the turbulent kinetic energy κ, the dissipation rate of turbulent kinetic energy ε, and /or the mixing length L. With the algebraic turbulence model the coefficients are determined by algebraic equations for the turbulent energy and mixing length. The k-L turbulence model uses a transport equation to determine the turbulent kinetic energy and mixing length. With the k-epsilon turbulence model, the coefficients are determined by transport equations for both the turbulent kinetic energy and the kinetic energy dissipation. Here, the algebraic turbulence model was used. The effect of using the k-L and k-epsilon turbulence model is investigated in Section 4.7.

4.3.6 Waves

In the simulations with waves, the recently implemented constant wave height version of Sediment Online was used, which accounts for a spationally constant wave height. Four different wave conditions were evaluated:

- Hs = 1.50 m, Tp 5.0 s, direction 315 °N
- Hs = 2.00 m, Tp 5.5 s, direction 315 °N
- Hs = 2.50 m, Tp 5.7 s, direction 315 °N
- Hs = 3.00 m, Tp 6.0 s, direction 315 °N

4.3.7 Transport settings

The Sediment-Online add-on of Delft3D was used for simultaneous computation of flows and transports and simultaneous feedback to bottom changes; the elevation of the bed is dynamically updated each time step. The advantage of this over an offline morphological computation is that the hydronamic flow computations are always carried out using the correct bathymetry. The Sediment Online add-on was used in combination with the TRANSPOR2004 sediment transport model and the bed roughness predictor, sediment characteristics and Online-Sediment parameters used are given in Table 4-2.

sediment characteristics	
sediment density	2650 kg/m^3
dry bed density	1600 kg/m^3
mean sediment diameter D_{50}	300 μm
Online-Sediment parameters	
morphological scale factor	182.50
spin-up time	1980 minutes
equilibrium concentrations at inflow boundaries	true
effect sediment on density gradient	true
updating bed at inflow boundaries	false

Table 4-2 Sediment characteristics and Online-Sediment parameters

Morphological scale factor

Morphodynamic developments take place on scales several times larger than typical flow changes, which would lead to long simulation times in case of morphological computations. To shorten the simulation time a morphological time scale factor (MORFAC) can be applied, which scales up the speed of morphological changes by simply multiplying the erosion and sedimentation fluxes from the bed to the flow and vice-versa by the MORFAC-factor, it thereby reduces computational time. The MORFAC factor may be scaled up to such a rate that it begins to have a significant impact on the hydrodynamic flows. Fortunately at deep water the MORFAC factor can be set quite high.

To investigate the sensitivity of the model to the morphological scale factor (MORFAC), the model was run with 5 different MORFAC numbers, see Table 4-3. Basically, the simulation time was varied and for each simulation the MORFAC number was set so as to result in the morphological changes in 5 years. The required MORFAC number per simulation can be determined by dividing the 5 year period by the simulation time. For example, when using 32 tidal cycles for simulating the five-year morphological changes , the MORFAC number for scaling 32 * 12 hr to the required 5 * 365 *24 hr can easily be determined by division: (5*365*24) / (32*12) = 114.06. The simulation time needs to be an integer number of tidal cycles (12 hrs) for accurate comparison, this is why the MORFAC numbers used here are not round numbers.

simulation time (exc. spin-up time)	MORFAC
32 * 12 hr = 384 hr	114.06
20 * 12 hr = 240 hr	182.50
16 * 12 hr = 192 hr	228.12
12 * 12 hr = 144 hr	304.17
10 * 12 hr = 120 hr	365.00

Table 4-3 Morphological scale factors

Figure C.05 in appendix C shows the bottom profile development and time-averaged bed-load and suspended-load transports from simulations using the 5 different MORFAC numbers. Figure C.06 shows bed-load and suspended-load transport rates at max. flood and max. ebb over the initial bottom profile. It was found that even the relatively high MORFAC number of 365 yields the same computational results as lower MORFAC numbers and thus it is allowed to apply a high MORFAC number. Here, a morphological scale factor of 182.50 was applied, in this way the simulation period of 240 hours gives the morphological development of 240 x 182.50 = 43800 hours (5 years).

4.4 Effect of tides

Herein, the effect of tides on the morphological development of the ridge was investigated, no waves were applied. The effect of the following tides was investigated:

- tides without a net current (U_0 = 0.00m/s, U_1 = 0.50/0.75/1.00m/s, see Figure 4-10).
- tides with a net current of 0.05 m/s (U_0 = 0.05m/s, U_1 = 0.50/0.75/1.00m/s)
- tides with a net current of 0.10 m/s (U_0 = 0.10m/s, U_1 = 0.50/0.75/1.00m/s)

Most relevant figures are given here, further figures are given appendix C.

4.4.1 Tides without net current

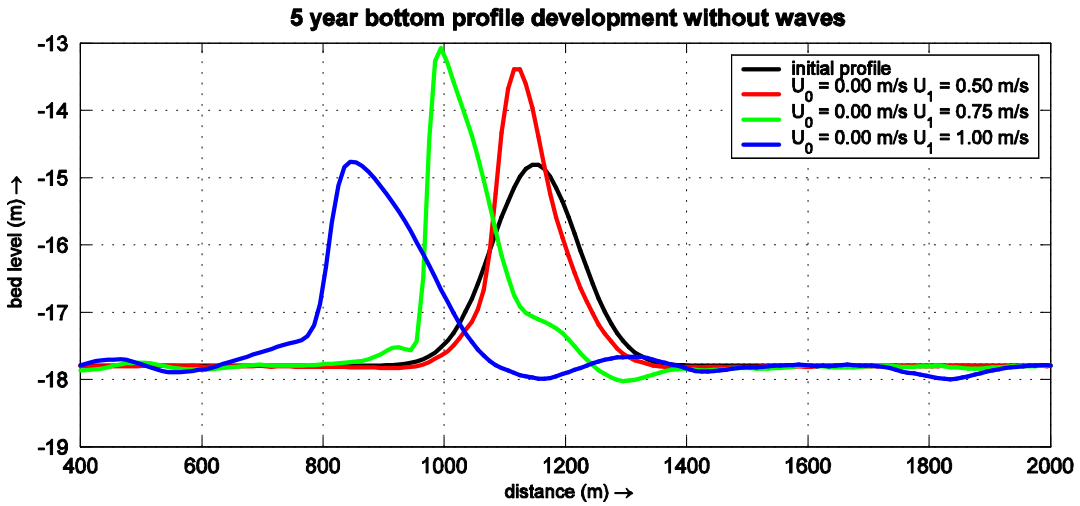

Figure 4-13 Five-year bottom profile development with symmetric tides.

Figure 4-13 shows the 5 year bottom profile development from simulations without waves using symmetric tides with velocity amplitudes of 0.50, 0.75 and 1.00 m/s. It can be seen that the ridge migrates in ebb-direction, furthermore it was found that the ridge increases in height for simulations with velocity amplitudes of 0.50 and 0.75 m/s and that the height is approximately unchanged with a velocity amplitude of 1.00 m/s. The latter simulation shows small boundary-related disturbances in morphology, which were not found from simulations with smaller velocity amplitudes. From this figure it was found that when suspended transport rates become significantly larger than the bed-load transport rates or when the suspended-load transport is not confined to the ridge vicinity only, the suspended-load transport dominates the effects of bed-load transport and no increase in height of the ridge was found.

In figure C.07 the bottom profile development and time-averaged bed-load and suspend-load transport rates are given and in figure C.08 the bed-load and suspended-load transport rates at max. flood and max. ebb are given. Figure C.09 and C.10 show the bed shear stresses and depth-averaged velocities at max. flood and max ebb. In figure C.11 till C.16 time-averaged velocity profiles at several locations before and after the top of the ridge are given for simulations with velocity amplitudes of 0.50/0.75/1.00 m/s.

It was found that close to the top of the ridge the time-averaged bed-load transport rates at both sides of the top are directed to the top of the ridge, while the time-averaged suspended-load transport rates are directed away from the top of the ridge. It can be seen that both the bed-load and suspended-load transport rates in ebb direction are somewhat larger than the transport rates in flood direction due to larger bed-shear stresses during ebb, see figure C.09; this complies with the observed migration of the ridge in ebb-direction. Figure C.07and C.08 show that increasing the velocity amplitude leads to larger transports rates; the suspended-load transport rates are effected more than bed-load transport rates.

4.4.1.1 Increasing ridge height

The increase in ridge height, which was observed from simulations with velocity amplitudes of 0.50 and 0.75 m/s, can be credited to the bed-load transport. The time-averaged bed-load transports are in top-direction at both flanks of the ridge. The process behind this particular phenomena was discussed in Section 4.2.

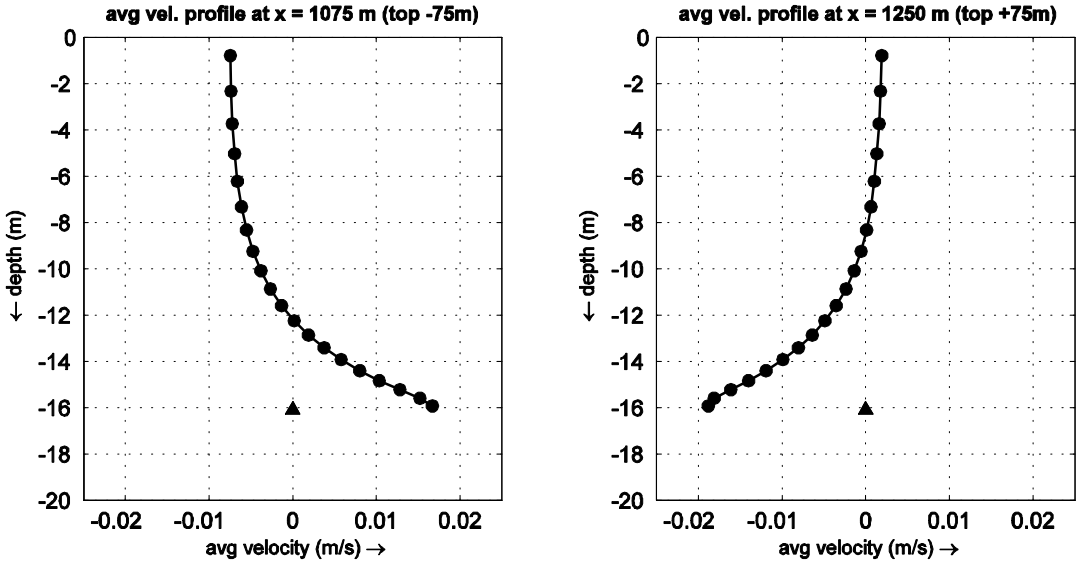

Figure 4-14 Time-averaged velocity profiles at 75 m before and after the top of the ridge

Figure 4-14 shows the time-averaged velocity profiles at 75 m before and after the top of the ridge for the simulation with a velocity amplitude of 0.75 m/s. It can be seen that the time-averaged near-bed velocities at both flanks of the ridge are in direction of the top of the ridge. This is due to the differently-shaped velocity profiles during flood and ebb and lead to the observed bed-load transport in top-direction which causes the ridge to increase in height, see Section 4.2.2.1.

4.4.1.2 Migration in ebb-direction

The observed migration in ebb-direction for simulations without a net current in flood direction is due to shallower water depth during ebb and is discussed in Section 4.2.2.2.

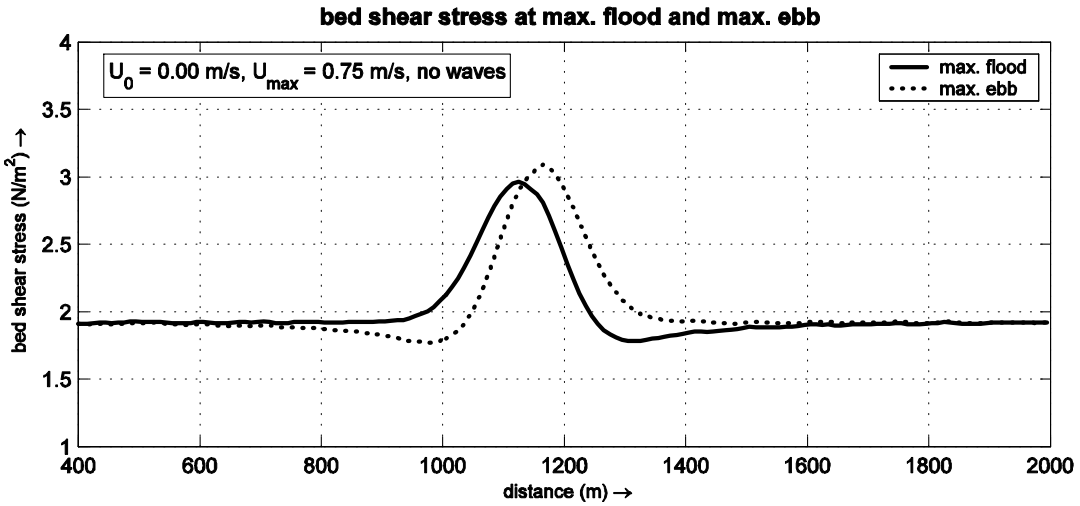

Figure 4-15 Bed shear stress at max. flood and max ebb with U0 = 0.00 m/s, Umax = 0.75 m/s without waves.

Figure C.09 and C.10 in appendix C show bed–shear stresses and depth-averaged velocities at maximum flood and maximum ebb for simulations with velocity amplitudes of 0.50/0.75

and 1.00 m/s. Figure 4-15 shows bed-shear stresses at maximum flood and maximum ebb for the simulation with a velocity amplitude of 0.75 m/s. It can be seen that that at maximum ebb the bed shear stresses at the top of the ridge and at the north-eastern (flood side) flank of the ridge are larger than at maximum flood, which is due to the shallower depth at max ebb, see Section 4.2.2.2. Due to the higher bed shear stresses during ebb, the bed-load transports during ebb are larger than bed-load transports in flood direction during flood, which causes the ridge to migrate in ebb direction. It can be seen that at max flood and max ebb, the bed-shear stress at the downstream toe of the ridge is smaller than at the upstream toe, this is due to the deformation of the velocity profile over the ridge with reduced near-bed velocities at the downstream flank and toe.

4.4.1.3 Effect of suspended-load transport

From figure C.07 it can be seen that the time-averaged suspended-load transport without a net current and without waves is in ebb direction, which is due to the shallower water depth during ebb, see Section 4.2.2.2. The time-averaged bed-load transport at both flanks is in top-direction and causes the ridge to increase in height, this is due to the differently-shaped velocity profiles during flood and ebb, see Section 4.2.2.1.

The magnitude and spatial extent over the ridge of the suspended-load transport determines whether the ridge increases in height. This is due to the spatially confined area where time-averaged bed-load transports are in top direction. If sediments are transported from the top region to area's where it cannot be brought back to the top, the ridge will decrease in height.

The distribution of the time-averaged bed-load transports over the ridge shows the region of influence of the growth mechanism; it's only at both flanks of the ridge that the time-averaged bed-load transports are in top-direction. Whether or not sediments are moved from the region where bed-load transports can bring them back to the top can be seen from the gradients in time-averaged suspended-load and time-averaged bed-load transports; If the gradients in suspended-load transports change direction outside of the region of interest of the bed-load transport, sediments are deposited outside this regions and cannot be brought back to the top of the ridge.

In short: there's only a limited region at both sides of the ridge where time-averaged bed-load transports are in top-direction and sediments are moved to the top of the ridge. When sediments are moved from this region to area's outside of this region due to larger suspended-transports over the entire area, it cannot be brought back to the top and the ridge decreases in height. If the suspended-load transport is limited to the top area only, sediments stay within the region and the top will increase in height.

4.4.2 Tide with net current of 0.05 m/s

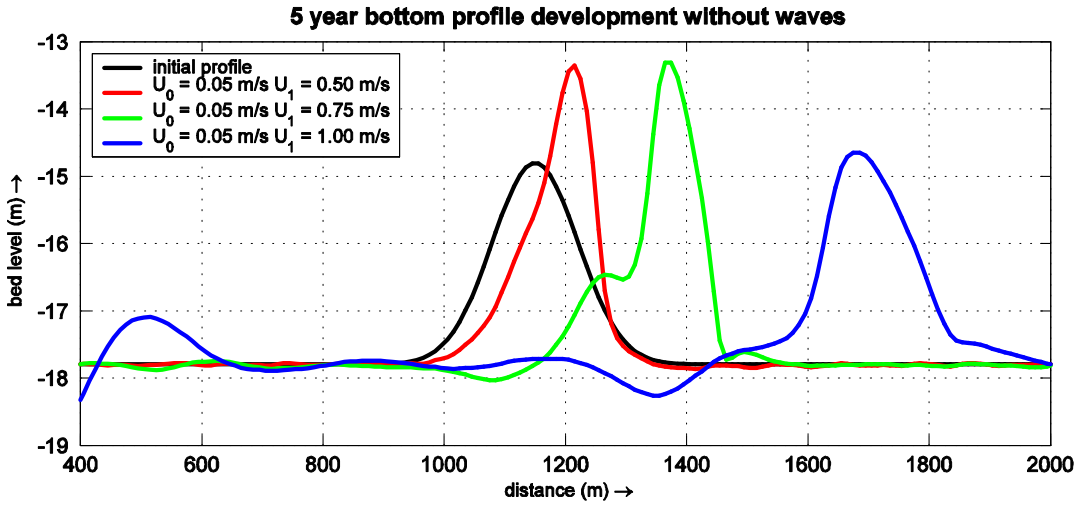

Figure 4-16 Five-year bottom profile development with tides with a net current of 0.05 m/s.

Figure 4-16 shows the 5 year bottom profile development from simulations using tides with velocity amplitudes of 0.50, 0.75 and 1.00 m/s and a net current of 0.05 m/s. It can be seen that the ridge migrates in flood-direction and that the ridge increases in height with velocity amplitudes of 0.50 and 0.75 m/s, while the height is approximately unchanged with a velocity amplitude of 1.00 m/s. The latter simulation shows relatively large boundary-related disturbances in morphology, which were not found from simulations with smaller velocity amplitudes.

In figure C.17 the bottom profile development and time-averaged bed-load and suspend-load transport rates are given and in figure C.18 the bed-load and suspended-load transport rates at max. flood and max. ebb are given. Figure C.19 and C.20 show the bed shear stresses and depth-averaged velocities at max. flood and max. ebb. From figure C.17, it can be seen that both time-averaged bed-load and time-averaged suspended-load transport is in flood direction at both sides of the ridge. Figure C.18 shows that the bed-load and suspended-load transport rates during flood are larger than during ebb. Furthermore from figure C.19 it was found that the bed shear stresses during max. flood are larger than during ebb; the effect of the shallower water during ebb is therefore cancelled out completely with a drift of 0.05 m/s. All of this complies with the observed migration in flood direction

With velocity amplitudes of 0.50 and 0.75 m/s the ridge increases in height, which is due to the strong gradients in bed-load transport just north of the top of the ridge; sediments are picked up at the flanks of the ridge and are moved in downstream, over the top of the ridge, but immediately settle and therefore stay within the top region.

4.4.3 Tides with net current of 0.10 m/s

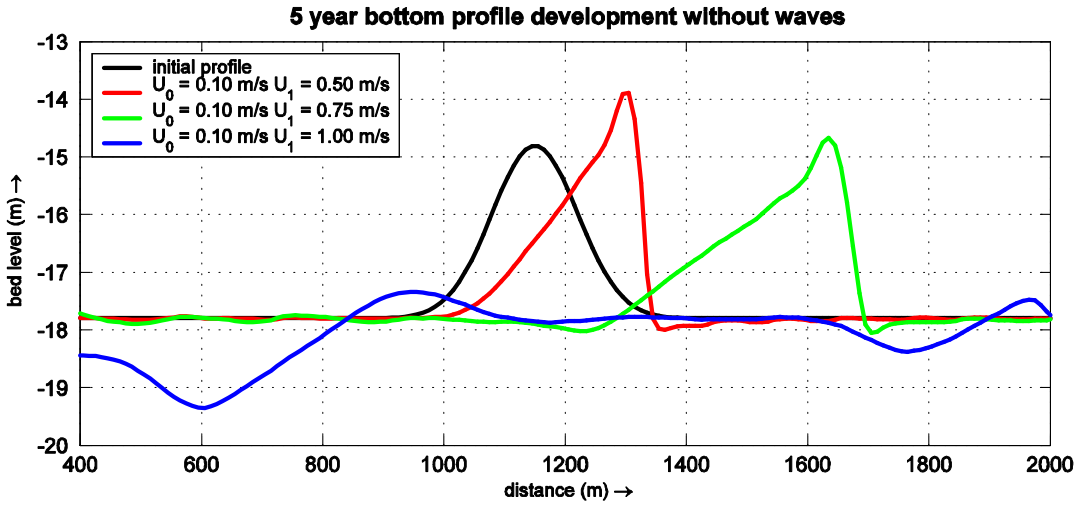

Figure 4-17 Five-year bottom profile development from tides with a net current of 0.10 m/s.

Figure 4-17 shows the 5 year bottom profile development from simulations using tides with velocity amplitudes of 0.50, 0.75 and 1.00 m/s and a net current of 0.10 m/s. It was found that ridge completely erodes using a velocity amplitude of 1.00 m/s, which is due to boundary effects; the result of this particular simulation will therefore not be taken along in the conclusions. From the simulations with velocity amplitudes of 0.50 and 0.75 m/s it was found that the ridge migrates in flood-direction and that the shape of the ridge is affected strongly; a rather sharp-edged forward-leaning ridge was found with a steep flood flank. The ridge increases in height with velocity amplitudes of 0.50, while the height is approximately unchanged with a velocity amplitude of 0.75 m/s.

In figure C.21 the bottom profile development and time-averaged bed-load and suspend-load transport rates are given and in figure C.22 the bed-load and suspended-load transport rates at max. flood and max. ebb are given. Figure C.23 and C.24 show the bed shear stresses and depth-averaged velocities at max. flood and max. ebb. From figure C.21, it can be seen that both time-averaged bed-load and time-averaged suspended-load transport is in flood direction at both sides of the ridge. Figure C.22 shows that the bed-load and suspended-load transport rates during flood are much larger than during ebb. Furthermore from figure C.23 it was found that the bed shear stresses during max. flood are much larger than during ebb. All of this complies with the observed migration in flood direction

4.4.4 Synthesis effect of tides

With symmetric and weak asymmetric tides (drift < 0.10 m/s) with velocity amplitudes up to 0.75 m/s the ridge increases in height. This is due to the differently-shaped velocity profiles during flood and ebb at both sides of the top (logarithmic profile upstream and reduced near-bed velocities downstream of the top). The result of which is that the time-averaged bed-load transport at both sides of the top of the ridge is directed to the top, which causes the top to increase in height. This bed-load transport related effect can be found with tidal amplitudes up to 0.75 m/s, above which the suspended-load transport dominates the bed-load transport and no increase in height was found.

The observed migration in ebb direction with symmetric tides (no net current) is due to the shallower water depth during ebb, which causes higher velocities and transports in ebb direction. Also the bed shear stress during ebb is higher as it is related to water depth. With increasing drift (0.05 – 0.10 m/s) the effect of the shallower water during ebb is cancelled out and no migration in ebb direction was be found.

The magnitude of the northward drift determines in large extent the time-averaged suspended-load transport over the ridge and thereby determines the migration of the ridge; with a small drift the ridge migrates in ebb-direction due to the shallower water depth during ebb. With increasing drift (0.05 – 0.10 m/s) the effect of the shallower water is cancelled out and the ridge migrates in flood-direction.

The suspended-load transport also affects the height of the ridge; with increasing suspended-load transports over the ridge and smaller gradients therein, sediments are picked up from the top region and are moved outside of the region where they can be moved back to the top with the bed-load mechanism; the ridge decreases in height.

4.5 Effect of waves

Herein, the effect of waves on the morphological development of the ridge was investigated. Waves are perpendicular to the section and therefore do not influence the velocity profile, except for the near-bed zone. The following simulations were carried out:

- U_0=0.00 U_1 = 0.50 m/s, with Hs = 0.00 / 1.50 / 2.00 / 2.50 / 3.00 m
- U_0=0.00 U_1 = 0.75 m/s, with Hs = 0.00 / 1.50 / 2.00 / 2.50 / 3.00 m
- U_0=0.00 U_1 = 1.00 m/s, with Hs = 0.00 / 1.50 / 2.00 / 2.50 / 3.00 m
- U_0=0.05 U_1 = 0.75 m/s, with Hs = 0.00 / 1.50 / 2.00 / 2.50 / 3.00 m
- U_0=0.10 U_1 = 0.75 m/s, with Hs = 0.00 / 1.50 / 2.00 / 2.50 / 3.00 m

Most relevant figures are given here, further figures are given appendix C.

4.5.1 U_0 = 0.00 m/s, U_1 = 0.50 m/s with waves

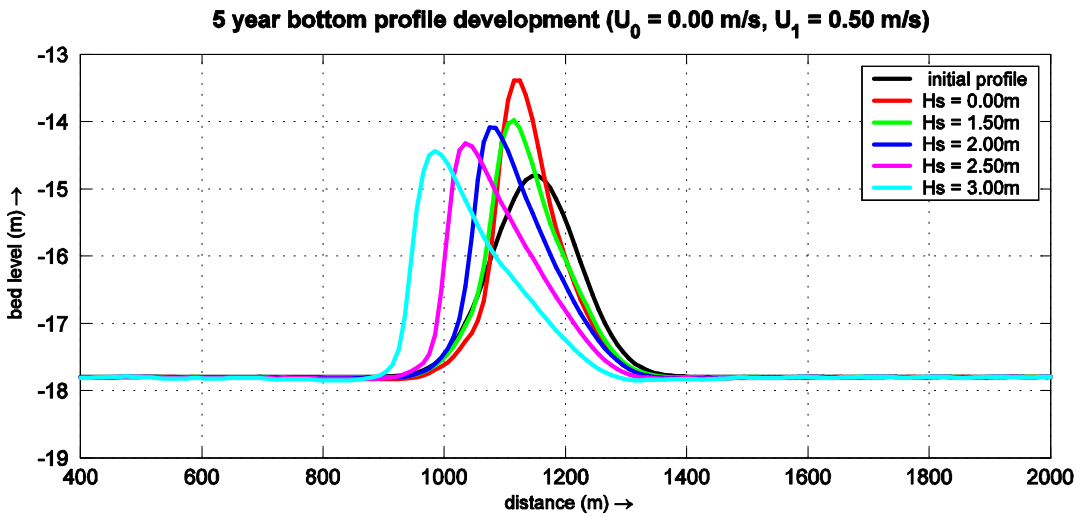

Figure 4-18 Five-year bottom profile development with different waves (U_0 = 0.00 m/s U_1 = 0.50 m/s)

Figure 4-18 shows the 5 year bottom profile development from simulations with a symmetric tide with a velocity amplitude of 0.50 m/s and Hs = 0.00 / 1.50 / 2.00 / 2.50 / 3.00 m. It can be seen that with increasing wave heights the migration in ebb-direction is larger due to the increased stirring action and subsequent increased transports with increasing waves. This wave effect is particularly effective with shallower water depth during ebb. The increase in height of the ridge is smaller with increasing wave height, which is due to the increased suspended-load transport rates with increasing waves. Furthermore it was found that with increasing wave height the flood flank of the ridge becomes steeper and the ridge therefore becomes more asymmetric.

In figure C.25 the bottom profile development and time-averaged bed-load and suspend-load transport rates are given and in figure C.26 the bed-load and suspended-load transport rates at max. flood and max. ebb are given. Due to the larger migration of the ridge with waves, the time-averaged bed-load transport with waves is not in top direction at both flanks of the ridge, while the time-averaged bed-load transport without waves is in top direction. From figure C.26 it shows that both bed-load and suspended-load transport rates increase with increasing wave height, but that the bed-load transport without waves is significantly higher than with relatively small waves. The cause of this difference in bed-load transport rates with and without waves could not be found and requires further investigation.

4.5.2 U_0 = 0.00 m/s, U_1 = 0.75 m/s with waves

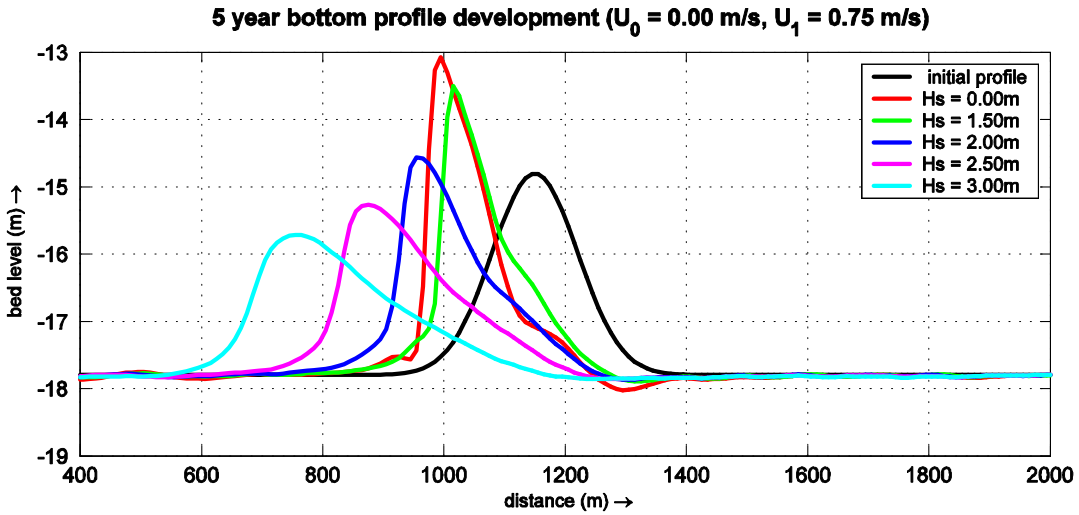

Figure 4-19 Five-year bottom profile development with different waves (U_0 = 0.00 m/s U_1 = 0.75 m/s)

Figure 4-19 shows the 5 year bottom profile development from simulations with a symmetric tide with a velocity amplitude of 0.75 m/s and Hs = 0.00 / 1.50 / 2.00 / 2.50 / 3.00 m. Besides the increased migration in ebb-direction and larger asymmetric development of the ridge with increasing wave height it was found that the ridge increases in height with wave height smaller than 2.50 m and decreases in height with wave heights greater than 2.50 m.

In figure C.27 the bottom profile development and time-averaged bed-load and suspend-load transport rates are given and in figure C.28 the bed-load and suspended-load transport

rates at max. flood and max. ebb are given. The migration without waves is about equal to that of the migration with a wave of 1.50 m, which is due higher suspended-load transport rates at the top of the ridge without waves; which requires further investigation. Bed-load transport rates without waves are higher than with waves, which also requires further investigation

4.5.3 U_0 = 0.00 m/s, U_1 = 1.00 m/s with waves

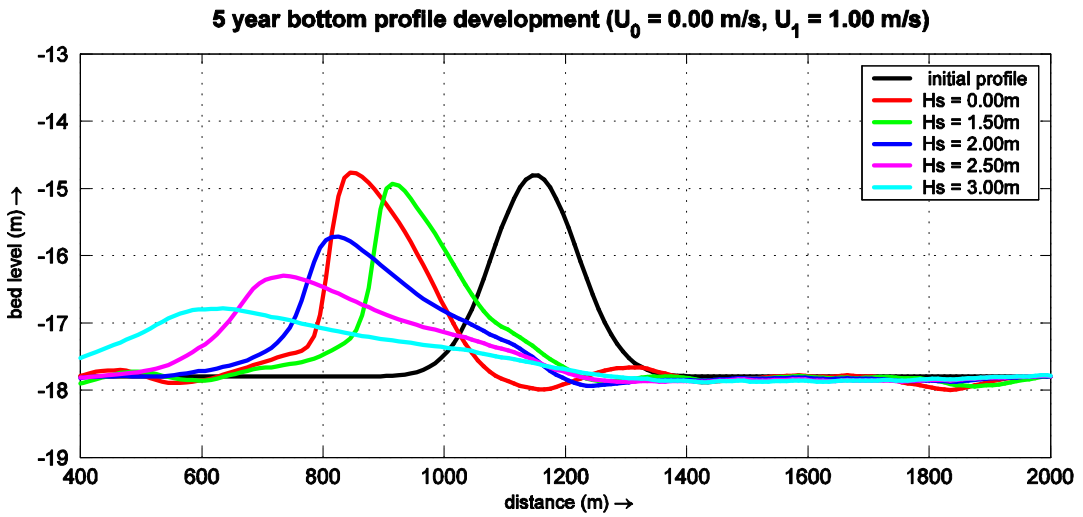

Figure 4-20 Five-year bottom profile development with different waves (U_0 = 0.00 m/s U_1 = 1.00 m/s)

Figure 4-20 shows the 5 year bottom profile development from simulations with a symmetric tide with a velocity amplitude of 1.00 m/s and Hs = 0.00 / 1.50 / 2.00 / 2.50 / 3.00 m. Here, the height of the ridge is approximately unchanged with wave smaller than 1.50 m and decreases with waves larger than 1.50 m. Migration without waves is significantly larger without waves than with waves of 1.50 m, which is due to the much larger bed-load transport rates and larger suspended-load transport rates without waves.

In figure C.29 the bottom profile development and time-averaged bed-load and suspend-load transport rates are given and in figure C.30 the bed-load and suspended-load transport rates at max. flood and max. ebb are given. It can be seen that the bed-load transport rates without waves are much larger than with waves; this was mentioned in the previous two Sections and should be looked after by the model developers. Furthermore the suspended-load transport rates at the top of the ridge without waves are higher than with waves of 1.50 m.

4.5.4 U_0 = 0.05 m/s, U_1 = 0.75 m/s with waves

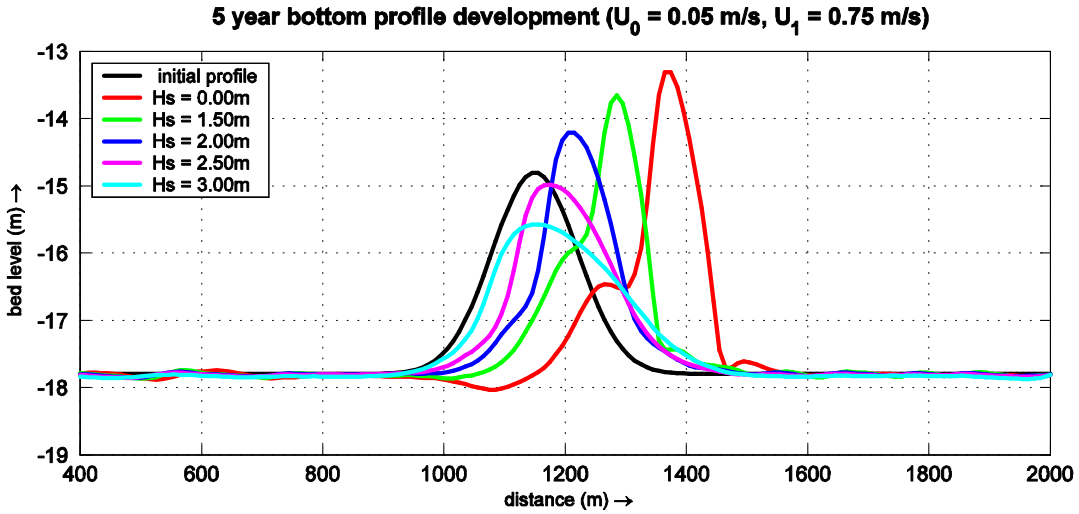

Figure 4-21 Five-year bottom profile development with different waves (U_0 = 0.05 m/s U_1 = 0.75 m/s)

Figure 4-21 shows the 5 year bottom profile development from simulations with a tide with a velocity amplitude of 0.75 m/s and a net current of 0.05 m/s, with Hs = 0.00 / 1.50 / 2.00 / 2.50 / 3.00 m. It can be seen that the northward migration decreases to almost no migration with increasing waves, which is due to the increased stirring effect with increasing waves (especially during ebb) and the subsequent effect on transports. The ridge also becomes more asymmetric with increasing waves. The simulation without waves and with relatively small waves shows a small kink in the ebb flank, which requires further investigation as the cause is unclear.

In figure C.31 the bottom profile development and time-averaged bed-load and suspend-load transport rates are given and in figure C.32 the bed-load and suspended-load transport rates at max. flood and max. ebb are given. Both bed-load and suspended-load transport rates show the behaviour that was described in the previous Sections.

4.5.5 U_0 = 0.10 m/s, U_1 = 0.75 m/s with waves

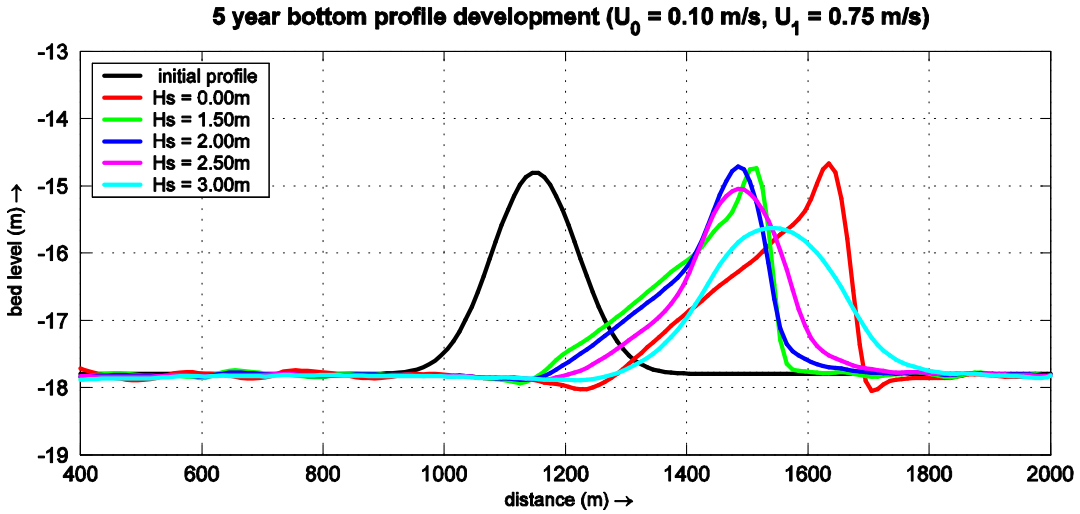

Figure 4-22 Five-year bottom profile development with different waves (U_0 = 0.10 m/s U_1 = 0.75 m/s)

Figure 4-22 shows the 5 year bottom profile development from simulations with a tide with a velocity amplitude of 0.75 m/s and a net current of 0.10 m/s, with Hs = 0.00 / 1.50 / 2.00 / 2.50 / 3.00 m. It can be seen that both the shape of the ridge and the migration are affected with higher waves. The height is approximately unchanged with increasing waves, but decreases significantly with waves of 3.00 m. Without waves the ridge becomes relatively sharp-edged, with a steep flood flank. With increasing waves the ridge develops more gradually with approximately equally steep flood and ebb flanks. Interestingly the migration of the ridge with waves of 1.50, 2.00 and 2.50 m is smaller than without waves or with waves of 3.00 m.

In figure C.33 the bottom profile development and time-averaged bed-load and suspend-load transport rates are given and in figure C.34 the bed-load and suspended-load transport rates at max. flood and max. ebb are given. The bed-load transport rates without waves are much larger than with waves, which was also found in the previous Sections and needs to be looked after. Here, with a net current of 0.10 m/s the suspended-load transport rates at the top of the ridge without waves is larger than with waves of 1.50m and about equal to that with waves of 2.00m.

synthesis effect of waves

From the simulations discussed in this Section it was found that waves strengthen the suspended-load transport and affect the migration, height and shape of the ridge. Herein the most important finding of this Section are recapitulated.

Waves intensify the stirring action of the fluid motion in the near-bed region and lead to larger sediment concentrations and larger suspended-load transports. The effect of waves increases with diminishing water depth and therefore the suspended-transports during ebb (shallower water) are increased more than suspended-load transports during flood.

The effect of waves is amplified with increasing wave heights, for tides without a net current the migration in ebb direction therefore increases with increasing wave height. The migration for tides with a net current is in flood direction as the shallow water effect is cancelled out due to the dominant suspended-load transports in flood direction. With a net current the migration in flood direction is reduced significantly with increasing wave height due to the increased suspended-load transports during ebb.

Sediments from both flanks of the ridge are moved to the top as the net bed-load transport is directed to the top; when sediments are moved to areas outside of the ridge due to larger suspended-load transports over the ridge, they cannot be brought back to the top and the ridge decreases in height. Waves strengthen the suspended-load transports and therefore lead to reduced ridge height in comparison to results without waves, also the range of velocity amplitudes whereby the ridge increases in height is limited with increasing wave height.

Waves affect the shape of the ridge: with waves the top of the ridge becomes less peaked, than without waves due to the increased suspended-load transports; with increasing wave height and subsequent increasing suspended-load transports, the ridge develops asymmetrically.

From the simulations in this chapter it was found that the bed-load transports with waves was significantly smaller than without waves and it was advised to investigate this behaviour. Detailed study of the TRANSPOR2004 formulations by the developers revealed that this was due to the transition between current -and wave-related roughness. This is done by means of a weighting procedure based upon current- and wave-related velocities. This weighting procedure is currently being adjusted to guarantee a smooth transition between transports without and with waves.

The suspended-load transport rates at the top of the ridge without waves were higher than with modest waves; this requires further investigation.

4.6 Number of vertical layers in 2DV mode

In this Section the sensitivity of the model to the number of vertical layers used was investigated. Ideally the number of layers should be such that there is no effect on the computed net transport and morphology. The sensitivity of the model was investigated from simulations with 10, 20 and 30 vertical layers with and without waves, using a velocity amplitude of 0.75 m/s without a net current (U_0=0.00, U_1 = 0.75 m/s). In all simulations, the relative thickness of the bottom layer was 2% of the water depth.

The following simulations were carried out using 10, 20 and 30 vertical layers:

- U_0=0.00, U_1 = 0.75 m/s, with Hs = 0.00 / 1.50 / 2.00 / 2.50 / 3.00 m

4.6.1 Sensitivity to vertical resolution without waves

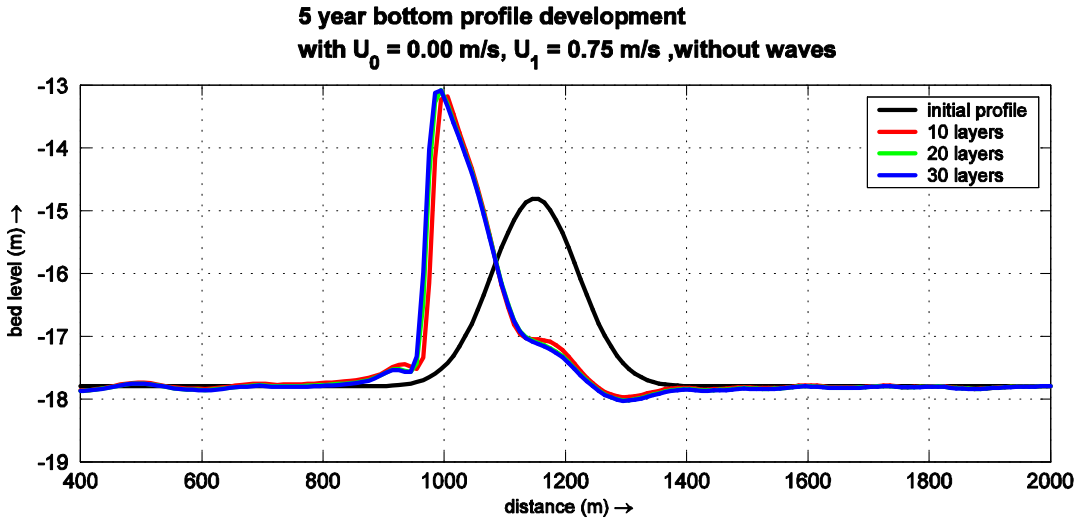

Figure 4-23 Five-year bottom profile development without waves for 10, 20 and 30 layers.

Figure 4-23 shows the 5 year bottom profile development from simulations with a velocity amplitude of 0.75 m/s without a net current and without waves for 10, 20 and 30 logarithmically distributed layers. It was found that results from simulations using 10, 20 and 30 layers are similar; both the migration and increase in height are very close to identical.

Figure C.35 shows the bottom profile development and time-averaged bed-load and suspended-load transports, while figure C.36 shows the bed-load and suspended-load transport rates at max. flood and max. ebb. The velocity- and concentration profiles at max flood and max ebb for 10, 20 and 30 layers are shown in figure C.37 and C.38 No differences between 10, 20 and 30 layers were found except for the concentrations profiles; with 10 layers the concentrations in the upper part of the water column are slightly larger and the concentrations at the bottom are slightly smaller than with 20 and 30 layers.

4.6.2 Sensitivity to vertical resolution with waves

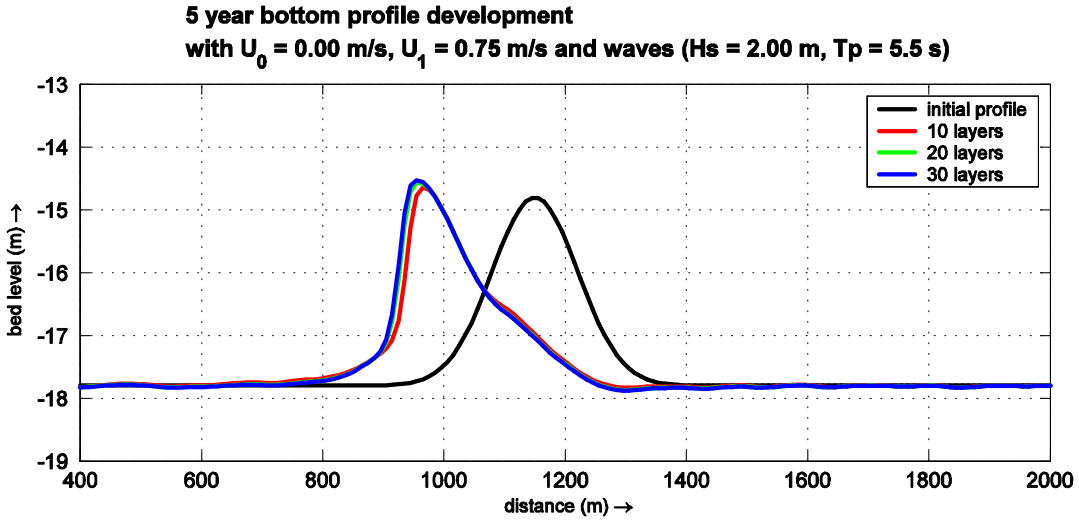

Figure 4-24 Five-year bottom profile development with waves (Hs = 2.00m, Tp = 5.5s)

Figure 4-24 shows the 5 year bottom profile development from simulations using 10, 20 and 30 layers with waves (Hs = 2.00 m, Tp = 5.5 s). It can be seen that results from simulations using 10, 20 and 30 layers are similar; both the migration and increase in height are very close to identical.

Figure C.39 shows the bottom profile development and time-averaged bed-load and suspended-load transports, while figure C.40 shows the bed-load and suspended-load transport rates at max. flood and max. ebb. The velocity- and concentration profiles at max flood and max ebb for 10, 20 and 30 layers are shown in figure C.41 and C.42. It was found that with 10 vertical layers the bed-load and suspended-load transport rates at max. flood and max. ebb were slightly smaller than with 20 and 30 layers.

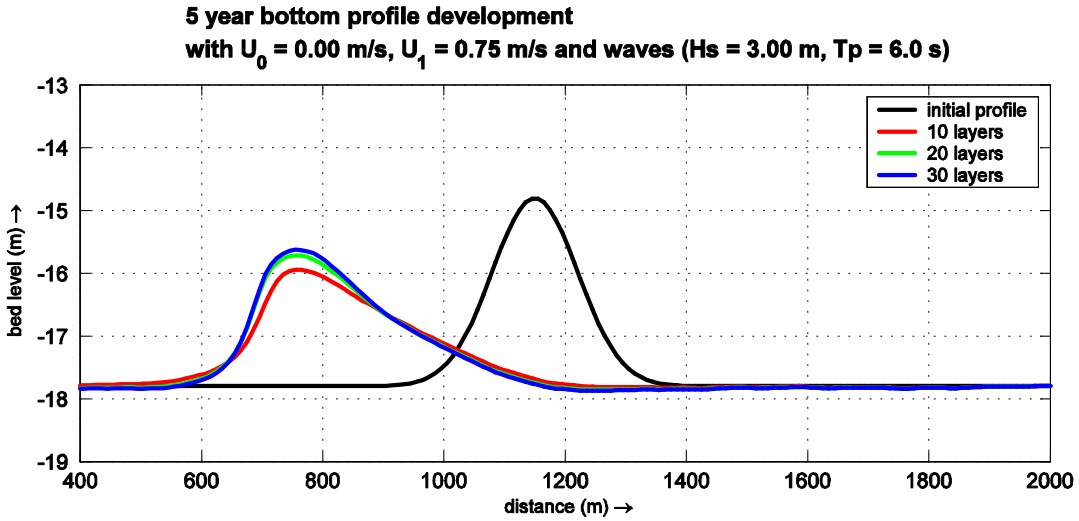

Figure 4-25 Five-year bottom profile development with waves (Hs = 3.00 m, Tp = 6.0s)

Figure 4-25 shows the 5 year bottom profile development from simulations using 10, 20 and 30 layers with waves (Hs = 3.00 m, Tp = 6.0 s). It can be seen that results from simulations using 10 layers deviate from results using 20 and 30 layers are similar; the decrease in height is larger using 10 layers.

Figure C.43 shows the bottom profile development and time-averaged bed-load and suspended-load transports, while figure C.44 shows the bed-load and suspended-load transport rates at max. flood and max. ebb. The velocity- and concentration profiles at max flood and max ebb for 10, 20 and 30 layers are shown in figure C.45 and C.46. It was found that with 10 vertical layers the bed-load and suspended-load transport rates at max. flood and max. ebb were slightly smaller than with 20 and 30 layers, which is due to the reduced vertical resolution. Concentration profiles from 10 vertical layers show slightly larger concentrations in the upper part of the water column and smaller concentrations at the bottom than concentration profiles from 20 and 30 layers. The smaller near-bed concentrations with 10 layers lead to smaller bed-load transport rates in top-direction and a larger decrease in height.

Synthesis effect of number of vertical layers in 2DV mode

An assessment of the sensitivity of the idealized sand ridge model to the number of layers showed that with higher waves, the number of layers used affected the computations and lead to slightly different morphological development of the ridge. It was shown that with large waves (Hs > 3.00 m), the decrease in height was over-estimated using 10 layers in comparison with results using 20 and 30 layers. The general conclusion is that with large waves greater vertical resolution is necessary.

4.7 Effect of the turbulence model used

In this Section, the effect of the turbulence model used was investigated. Simulations were made using the algebraic, the k-L and the k-epsilon turbulence model, whereby the latter was run with either the parabolic-linear sediment mixing coefficient of van Rijn or with vertical sediment mixing coefficients from the k-epsilon turbulence model itself. It should be noted that the TRANSPOR2004 sediment transport model was not designed for use with vertical sediment mixing values from the turbulence model itself.

The following simulations were carried out using the different turbulence models.

- U_0=0.10 U_1 = 0.75 m/s, without waves
- U_0=0.10 U_1 = 0.75 m/s, with waves (Hs = 2.50m, Tp = 5.75s)

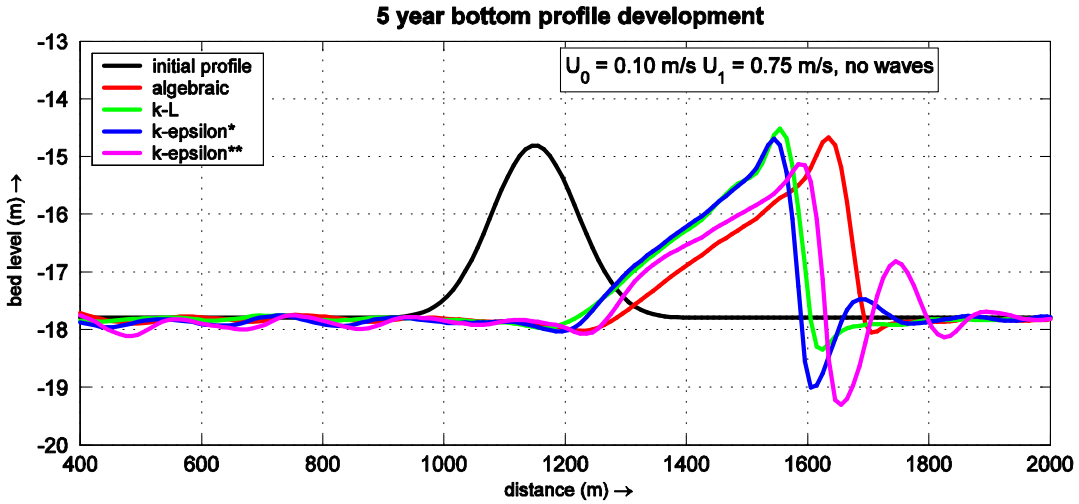

Figure 4-26 Five-year bottom profile development with different turbulence models without waves

* parabolic-linear sediment mixing
** vertical sediment mixing values from the k-epsilon turbulence model

Figure 4-26 shows the 5 year bottom profile development from simulations using the algebraic, k-L and k-epsilon turbulence model. The k-epsilon turbulence model was ran with either the parabolic linear sediment mixing of van Rijn or with vertical sediment mixing values from the k-epsilon turbulence model itself. It can be seen that the migration of the ridge with the algebraic turbulence model is larger than with the k-L and k-epsilon turbulence models. Furthermore, it was found that with the k-L and k-epsilon turbulence models a dip at the flood ward toe of the ridge develops. The increase in height is much alike, although it was found that with vertical sediment mixing values from the k-epsilon model itself, the increase in height was somewhat smaller than with the algebraic, k-L and k-epsilon turbulence model with parabolic linear mixing.

In figure C.47 the bottom profile development and time-averaged bed-load and suspended-load transports are given. In figure C.48 the bed-load and suspended-load transport rates at max flood and max. ebb are given. It can be seen that, at the top of the ridge, both the bed-load and suspended-load transports rates at max flood and max ebb using the algebraic turbulence model are greater than using the k-l and k-epsilon turbulence model. The k-epsilon turbulence model with vertical sediment mixing values from the model itself leads to significant higher suspended-load transports.

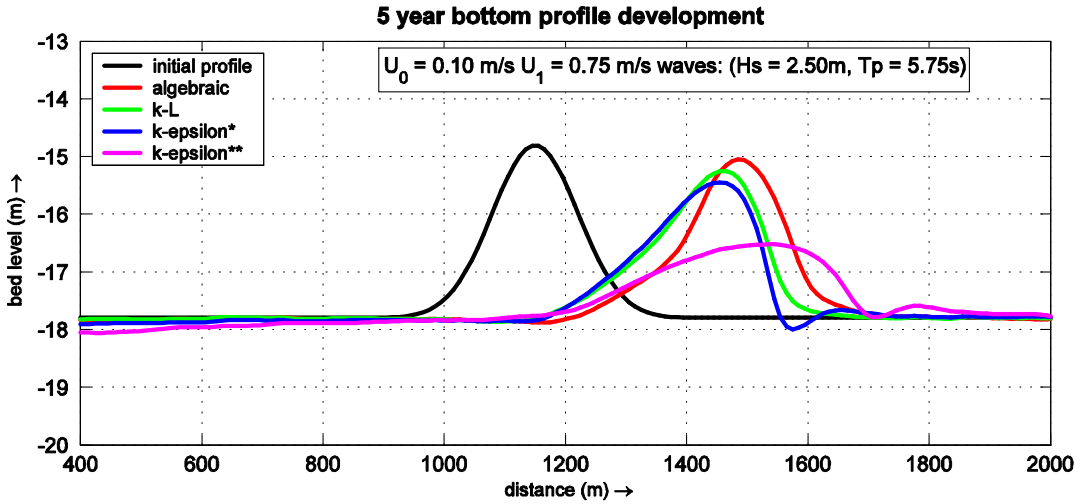

Figure 4-27 Five-year bottom profile development with different turbulence models with waves

* parabolic-linear sediment mixing
** vertical sediment mixing values from the k-epsilon turbulence model

Figure 4-27 shows the 5 year bottom profile development from simulations with waves using the algebraic, k-L and k-epsilon turbulence model. The k-epsilon turbulence model was ran with either the parabolic linear sediment mixing of van Rijn or with vertical sediment mixing values from the k-epsilon turbulence model itself. It can be seen that the migration of the ridge using the algebraic turbulence model is slightly larger than with the k-L and k-epsilon turbulence model and that shape of the ridge is less asymmetric than with the k-L and k-epsilon turbulence models. The morphological development using the k-epsilon with the parabolic-linear mixing distribution shows a dip at the flood side toe of the ridge. The ridge erodes significantly using the k-epsilon turbulence model with vertical sediment mixing values from the k-epsilon turbulence model itself.

In figure C.49 the bottom profile development and time-averaged bed-load and suspended-load transports are given. In figure C.50 the bed-load and suspended-load transport rates at m,ax flood and max. ebb are given. It can be seen that both the bed-load and suspended-load transport rates at the top of the ridge at max flood and max ebb using the algebraic turbulence model are significantly larger than with the k-L and k-epsilon turbulence models. The suspended-load transport from the k-epsilon turbulence model with vertical sediment mixing values from the k-epsilon turbulence model itself are much larger than from the other turbulence models, especially at max flood.

synthesis of effect of turbulence model

In this Section it was found that the turbulence model is of significant influence on the morphological development of the ridge. In this Chapter the algebraic turbulence model was used which was found to lead to slightly larger migration of the ridge and a less asymmetric development of the ridge with waves than with the k-L or k-epsilon turbulence model.

4.8 Effect of the bed roughness predictor

Herein, results from simulations using a constant bed roughness (Chézy coefficient of 65 $m^{1/2}/s$) were compared to results from simulations using a variable bed roughness (updated every 10 minutes by means of a bed roughness predictor) to investigate the effect of the bed roughness predictor.

The following simulations were carried out with both a constant and variable bed roughness:

- U_0=0.10 U_1 = 0.75 m/s, without waves
- U_0=0.10 U_1 = 0.75 m/s, with waves (Hs = 2.50m, Tp = 5.75s)

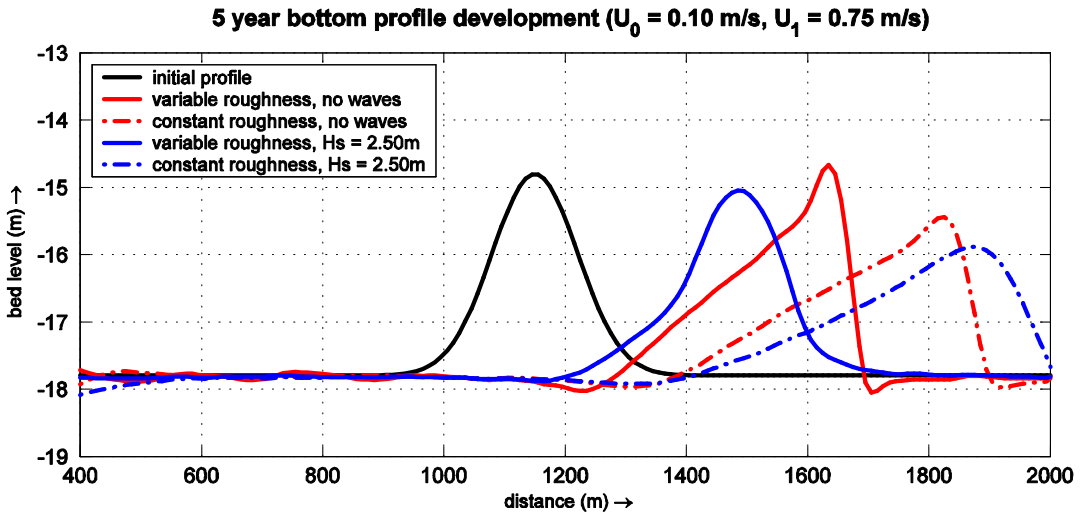

Figure 4-28 Five-year bottom profile development with constant and variable bed roughness

Figure 4-28 shows the 5 year bottom profile development from simulations with constant and variable bed roughness, with and without waves, simulations with the constant bed roughness were ran with a Chézy coefficient of 65 $m^{1/2}/s$. It can be seen that the morphological development is affected in large extent by the bed roughness. Without waves the migration is smaller with a variable bed roughness than with the constant bed roughness. With waves the migration is much smaller with a variable roughness than with a constant bed roughness. Both without and with waves the decrease in height is larger with a variable bed roughness than with a constant bed roughness. With waves the shape of the ridge develops more asymmetrically with a constant bed roughness than with a variable bed roughness.

In figure C.51 the bottom profile development and time-averaged bed-load and suspended-load transports are given, while in figure C.52 the bed-load and suspended-load transport rates at max flood and max ebb are given. It can be seen that the bed-load transport rates at max flood are significantly larger with a constant bed roughness, which complies with the observed increased migration. The increase in bed-load transport rates at max flood is larger with waves than without waves.

Figure C.53 shows bed shear stresses and depth-averaged velocities at max flood and max ebb without waves and figure C.54 shows bed shear stresses and depth-averaged velocities

at max flood with waves. It was found that the bed shear stresses at both max flood and max ebb with the variable bed roughness were higher than with the constant bed roughness of 65 $m^{1/2}/s$.

synthesis of effect of bed roughness predictor

With a variable bed roughness (bed roughness predictor) the migration of the ridge is smaller than with a constant bed roughness of 65 $m^{1/2}/s$ due to the smaller transport rates at max flood. The reduction in height of the ridge is larger with a variable bed roughness, but the shape develops less asymmetrically than with a constant bed roughness, especially with waves

4.9 Comparison of 1DH and 2DV model approach

Herein, a comparison was made between simulations in 1DH and 2DV mode. In both simulations the TRANSPOR2004 sediment transport model was used. Simulations in 2DV mode were carried out using 20 vertical layers.

The following simulations were carried out in 1DH and 2DV mode:

- $U_0 = 0.00$ m/s; $U_1 = 0.75$ m/s, without waves
- $U_0 = 0.10$ m/s; $U_1 = 0.75$ m/s, with waves (Hs = 2.50m, Tp = 5.75s)

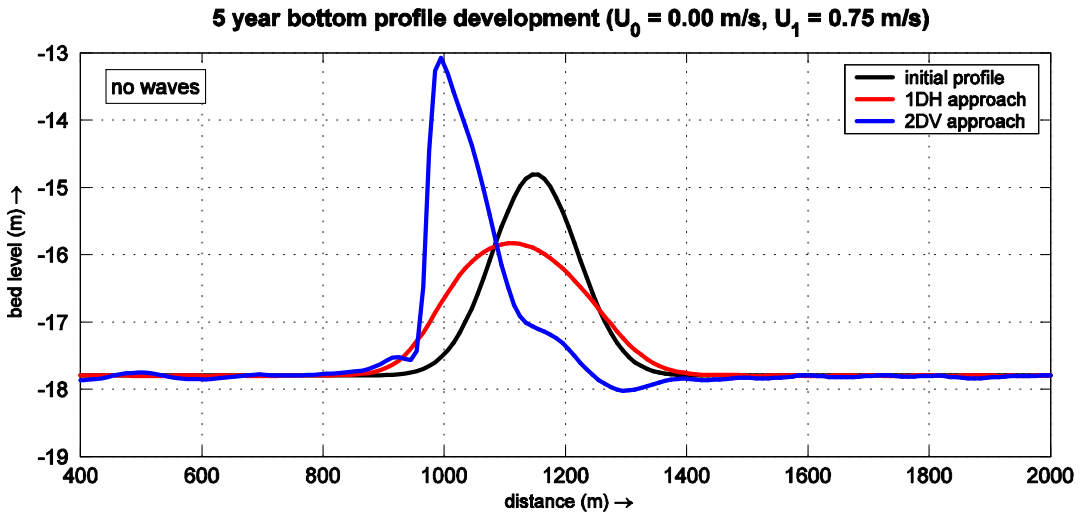

Figure 4-29 Five-year bottom profile development using 1DH and 2DV approach, without waves

Figure 4-29 shows the 5 year bottom profile development for simulations in 1DH and 2DV mode. Both simulations show the migration in ebb-direction, but the 1DH simulation doesn't show the increase in height as found with the 2DV simulation with 20 layers, this is due to the fixed velocity profiles used in the 1DH simulation; velocity profiles downstream of the top don't show the reduced near-bed velocities due to deceleration processes, see Section 4.2.

Figure C.55 shows the bottom profile development and time-averaged bed-load and suspended-load transports and figure C.56 shows the bed shear stress and depth-averaged

velocities at max flood and max ebb. It can be seen that the both the bed-load and suspended-load transport rates are larger with the 2DV model approach, especially at the location of the top of the ridge.

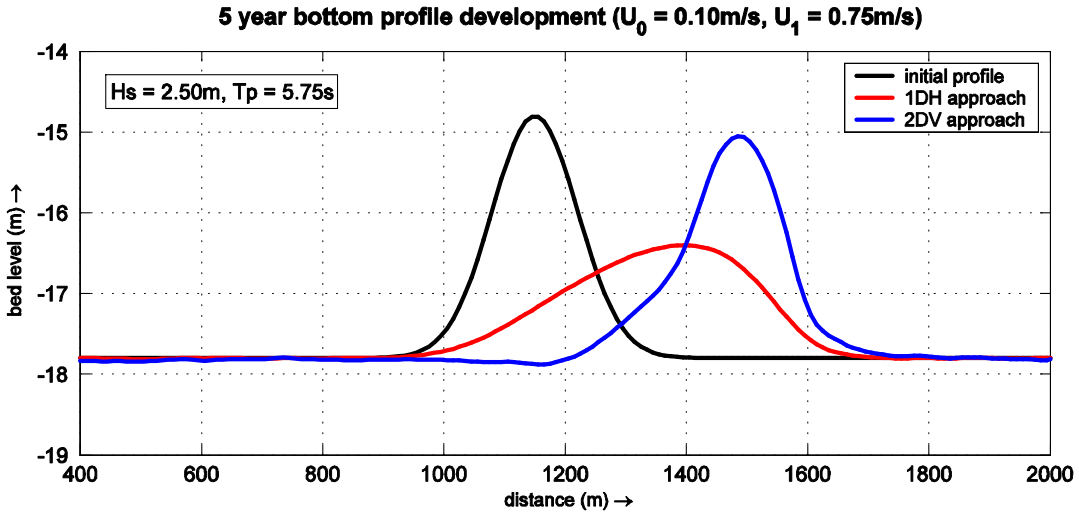

Figure 4-30 Five-year bottom profile development using 1DH and 2DV approach with waves (Hs = 2.50m, Tp = 5.75 s)

Figure 4-30 shows the 5 year bottom profile development for simulations in 1DH and 2DV mode with a net current of 0.10 m/s and waves (Hs = 2.50 m, Tp = 5.75 s). Both simulations show the migration in flood-direction, and while both simulations show a reduction in height of the ridge, the 1DH simulation over-estimates the reduction due to the fixed velocity profiles used as a result of which time-averaged bed-load transports at both flanks of the ridge are in flood direction, see Section 4.2. Furthermore it was found that the migration using the 1DH model approach is significantly smaller than using the 2DV model approach and that the ridge develops much more asymmetrically using the 1DH model approach than using the 2DV model approach.

Figure C.57 shows bottom profile development and time-averaged bed-load and suspended-load transports and figure C.58 shows the bed-load and suspended-load transport rates at max flood and max ebb. It can be seen that the 2DV simulations shows higher bed-load and suspended-load transport rates at the location of the ridge, especially at max flood.

synthesis comparison of 1DH and 2DV model approach

In this section it was shown that with a 1DH (depth-averaged) model approach the ridge cannot increase in height due to the fixed logarithmic velocity profiles and therefore cannot model the effect of deformation of velocity profiles. As a result depth-averaged models cannot model the net near-bed velocities in the direction of the top of the ridge that may lead to an increase in height of the ridge. Furthermore, it was found that a 2DV model approach leads to higher transports rates over the ridge and a subsequent larger migration of the ridge.

4.10 Synthesis

Herein the main findings of this chapter are listed once again, this Section serves as a brief recapitulation of the entire chapter and offers valuable physical insight which come of just in the next chapters.

With symmetric and weak asymmetric tides (drift < 0.10 m/s) the ridge increases in height due to the net effect of the deformation of velocity profiles over the ridge; the time-averaged near-bed velocities at both sides of the top are in the direction of the top and so is the net bed-load transport which causes the ridge to increase in height. This bed-load transport related effect can be found with tidal amplitudes up to 0.75 m/s, above which the ridge will decrease in height as the suspended-load transport dominates the bed-load transport and sediments are moved outside of the region where they can be brought back to the top with the bed-load transport.

The observed migration in ebb direction with symmetric tides (no net current) is due to the shallower water depth during ebb, which causes higher velocities and transports in ebb direction. Also the bed shear stress during ebb is higher as it is related to water depth. The magnitude of the northward drift determines the average suspended-load transport over the ridge and thereby determines the migration of the ridge; with a small drift the ridge migrates in ebb-direction due to the shallower water depth during ebb. With increasing net current (0.05 – 0.10 m/s) the effect of the shallower water is cancelled out and the ridge migrates in flood-direction.

Waves stir up sediments and lead to larger suspended-load transports. The effect of waves increases with diminishing water depth and therefore suspended-transports during ebb (shallower water) are increased more than suspended-load transports during flood. The effect of waves is amplified with increasing wave heights, for tides without a net current the migration (in ebb direction) therefore increases with increasing wave height. The migration for tides with a net current is in flood direction as the shallow water effect is cancelled out due to the dominant suspended-load transports in flood direction. With a net current the migration in flood direction is reduced significantly with increasing wave height due to the increased suspended-load transports during ebb. Waves furthermore affect the shape of the ridge; with increasing wave height the ridge becomes less peaked and more asymmetric.

It was found that with larger waves (Hs > 3.00m) the decrease in height was larger using 10 vertical layers in comparison with results from simulations using 20 and 30 layers; with large waves greater vertical resolution is required

The turbulence model proved to be of significant influence on the morphological development of the ridge; the algebraic turbulence model was found to lead to slightly larger migration of the ridge and a less asymmetric development of the ridge with waves than with the k-L or k-epsilon turbulence model.

With a variable bed roughness (bed roughness predictor) the migration of the ridge was found to be smaller than with a constant bed roughness of C = 65 $m^{1/2}/s$ due to the smaller transport rates at max flood. The reduction in height of the ridge is larger with a variable bed roughness, but the shape develops less asymmetrically than with a constant bed roughness, especially with waves

It was shown that with a 1DH (depth-averaged) model approach the ridge cannot increase in height due to the fixed logarithmic velocity profiles and therefore cannot model the effect of deformation of velocity profiles. As a result depth-averaged models cannot model the net near-bed velocities in the direction of the top of the ridge that may lead to an increase in height of the ridge. Furthermore, it was found that a 2DV model approach leads to higher transports rates over the

From the simulations in this chapter it was found that the bed-load transports with waves was significantly smaller than without waves; detailed study of the TRANSPOR2004 formulations by the developers revealed that this was due to the transition between current - and wave-related roughness. This is done by means of a weighting procedure based upon current- and wave-related velocities. This weighting procedure is currently being adjusted to guarantee a smooth transition between transports without and with waves and will be included in the next update of the morphological kernel of Delft3D.

5 Model schematizations of sand ridge near Hoek van Holland

5.1 Introduction

In this chapter, the modelling approach of this study and the model schematizations used are discussed. First, the modelling approach is given in Section 5.2. Both transect model applications (1DH, 2DV) and area models (2DH, 3D) are used in this study, with boundary conditions from nesting in the overall Holland Coastal Zone (HCZ) model, which is discussed in chapter 5.3. The nesting procedure itself is discussed in Section 5.4. Two input reduction techniques are applied in this study, viz. tidal schematisation and wave schematisation. Tidal schematisation by means of a morphological tide is discussed in Section 5.4. In Section 5.5 two wave schematizations are discussed.

The simulations in this chapter were carried out an older version of Delft3D. In Section 2.3.3.3 the main difference in bottom layer sub-grid model between this version and a recently improved version of Delft3D are discussed.

5.2 Modelling approach

Herein, the model approach is discussed. The basis for the model verification using the morphological development of the artificial sand ridge close to Hoek van Holland is a Delft3D model of the Dutch coast developed in the Flyland project (WL | Delft Hydraulics, 2001) called the Holland Coastal Zone model, abbreviated as HCZ-model. The HCZ-model, obtains its boundary conditions from a well calibrated model called the large scale fine grid model covering the entire North-Sea (see WL | Delft Hydraulics, 2001). In the Flyland study it was shown that the HCZ-model showed reasonable agreement with available field data. Boundary conditions for the 2DV and 2DH models used in this study were derived from the HCZ-model using an automated nesting procedure. Next, input reduction techniques were applied for tidal- and wave-input; to reduce computation time, a representative, morphological tide was derived which gives an optimal representation of the neapspring-averaged sediment transports if a complete neap-spring tidal cycle would be simulated. The morphological tide was derived using a weighting procedure with data points distributed over the area including the ridge. After that a wave schematization was selected. Next a sensitivity analysis was carried out to investigate several process and model parameters with respect to accurate simulation of the morphological development of the sand ridge Hoek van Holland. This sensitivity analysis was carried out with the Delft3D Sediment-Online add-on in 2DV mode for the period 1986-1991. The obtained optimal model- and process parameters were used to set-up transect model applications (1DH, 2DV) and area models (2DH, 3D), after which a validation of the models was carried out for the periods 1986-1991 and 1991-2000. The modelling approach is visualized in Figure 5-1.

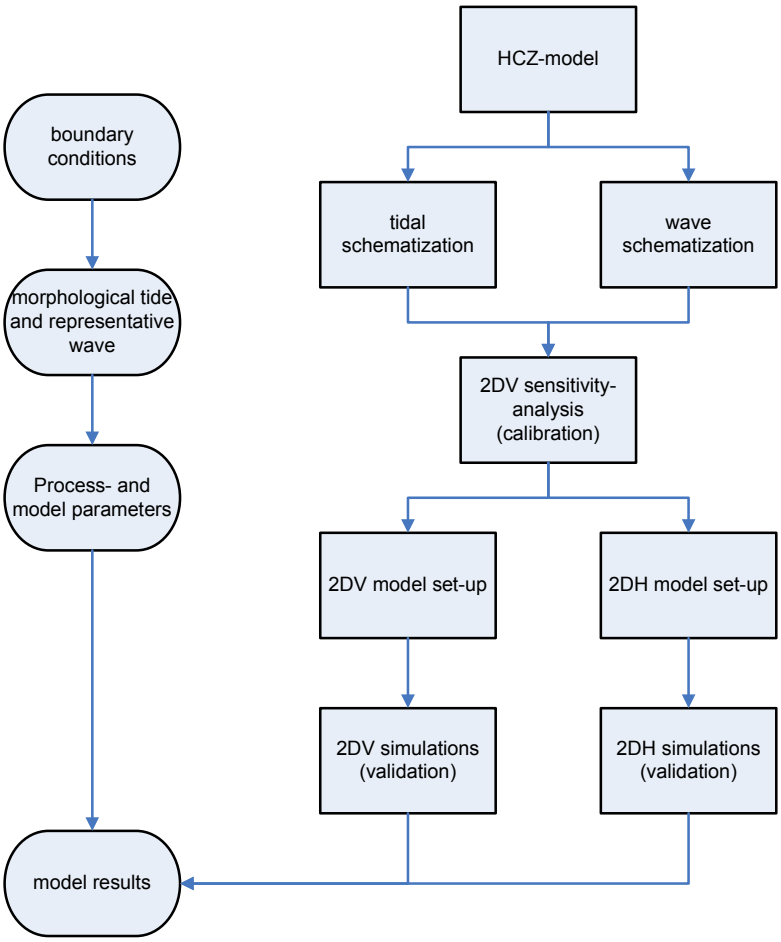

Figure 5-1 Modelling approach

5.3 Holland Coastal Zone (HCZ) model

The boundary conditions for the detailed models used in this study are derived from nesting in the Holland Coastal Zone (HCZ) model (Roelvink et al., 2001), a 2DV hydronamic model which includes salinity. In order to achieve optimal agreement between the overall model and nested models, the HCZ-model was modified and run with Sediment Online, TRANSPOR2004, trachytopes and a constant wave height, which will also be used in the nested models. In this Section the basic model set-up of the HCZ-model is discussed.

Model grid HCZ model

The model grid of the HCZ model was derived from a well-calibrated model called the fine grid large scale model covering the entire North Sea. A coastal stretch, reaching from “Schouwen Duiveland” to “Terschelling”, with an offshore extent of 70 km was taken from the large scale model. In the vicinity of the “Marsdiep” the orientation of the grid lines was modified to allow for a better representation of the “Texelstroom”.

By refinement of the grid mesh the required resolution, especially in the near shore zone, was obtained. This results in grid distances in cross-shore direction varying between 50 m at the beach to 5 km at open sea. Alongshore grid distances equal approximately 1 km. In total

the computational grid contains approximately 20,000 computational elements. The model computations aim at predicting the morphological development of the shoreline, to allow for a retrieving coastline, the computational grid also covers some 200 m of the beach/dune area. Figure 5-2 shows the computational grid of the HCZ-model (left).

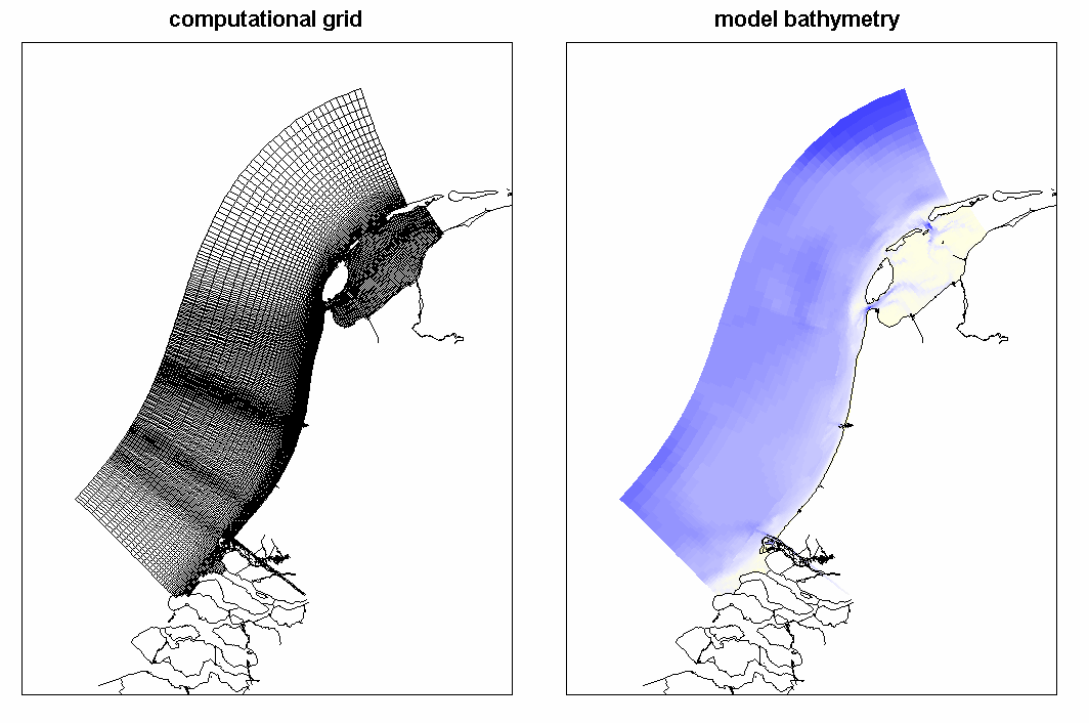

Figure 5-2 Computational grid (left) and model bathymetry (right) of the HCZ-model.

Bathymetry HCZ model

To represent the present situation, an initial bathymetry using depth data originating from the “Kuststrook” model bathymetry has been used. This data covers the area of specific interest for the present study in greatest detail. However, comparison of the depths generated using the Kuststrook data with the model bathymetry of the fine grid large scale model set-up previously (Roelvink et al., 2001) revealed large depth differences, up to 5m, most pronounced near the open sea boundary of the HCZ model. Therefore, depths in the deeper areas, outside the areas covered by the yearly bathymetric surveys carried out within the JARKUS program, were regenerated using recent Dutch Continental Shelf Data supplied by TNO-NITG. This data also served to generate, a part of, the bathymetry of the fine grid large scale model set-up previously. Figure 5-2 shows the model bathymetry of the HCZ-model (right).

Open boundary conditions HCZ model

The open boundary conditions of the HCZ model were derived from 3-dimensional computations with the large scale fine grid model covering the entire North-Sea. Since the HCZ model was set-up to represent average conditions, the model computation of the fine grid large scale model used for the generation of boundary conditions also represents the average conditions, i.e. a south-westerly wind of 7 m/s and long term average river

discharges. At the cross-shore open sea boundary near "Schouwen-Duiveland" a velocity boundary is defined. All of the other open boundaries are defined as water level boundaries.

The boundary conditions as generated by the fine grid large scale model are specified as time series of water levels or velocities. Hence, they relate to the simulation period of the fine grid large scale model. To allow for the simulation of any calendar period in time, the original time-series boundary conditions were converted into astronomical boundary conditions by means of a tidal analysis on the time series. In the present study the constant, representative, discharge values for all discharge locations were used. In Table 5-1 an overview is given of the applied discharge rates.

Location:	**Discharge rate:**
Haringvliet	660 m^3/s
Nieuwe Waterweg	1540 m^3/s
Sluices of IJmuiden	80 m^3/s
Sluices of Den Helder	250 m^3/s
Sluices of Kornwerderzand	200 m^3/s

Table 5-1 Discharge rates HCZ model

Other model parameters

- Computational time step: Previous modelling exercises with the fine model revealed that the flow rates through the "Marsdiep" appeared to determine the maximum computational time step allowed. From this analysis it was found that a time step of 5 minutes is allowed for the HCZ-model. Here a computational time step of 3 minutes is used.
- Salinity; a constant salinity of 31 ppt was imposed at the open sea boundaries. At the discharge locations the salinity value was set to zero.
- Wind; a constant representative wind was applied: wind speed 7 m/s from 240° N (Southwest).
- Waves; the single representative wave condition from Walstra et al. (1997) was applied: significant wave height of 2.25 m, period of 6.6 s, direction 315 °N

In order to achieve the best agreement between overall and nested models, the original HCZ model was modified and run with Sediment Online, TRANSPOR2004, trachytopes and a constant wave height, which will also be used in the nested models.

5.4 Nesting procedure

The boundary conditions for all simulations were derived from nesting in the HCZ model, using an automated nesting procedure, which guarantees an optimal transition between the overall HCZ model and the 2DV model. The nesting procedure, and therefore the HCZ model itself was run for 75 days, from 1 September 1991 to 15 November 1991 and covers 5 complete neap-spring tidal cycles.

Figure 5-3 shows water levels, alongshore and cross-shore velocities at the Southern boundary at section 4 for the HCZ-model, the 2DV and the 2DH model. The HCZ-model was run with astronomical boundary conditions, while the 2DV and the 2DH models were run with the morphological tide mt2, which runs from 21 October 1991, 03hrs57m to 22 October 1991, 04hrs42m, see Section 5.5.3. It can be seen that the nesting procedure was accurate and that both the 2DV and the 2DH model give identical results for water levels and velocities. In appendix D, water levels and velocities at section 3, 4, 5 and 6 are given for the HCZ-model, the 2DV and the 2DH models.

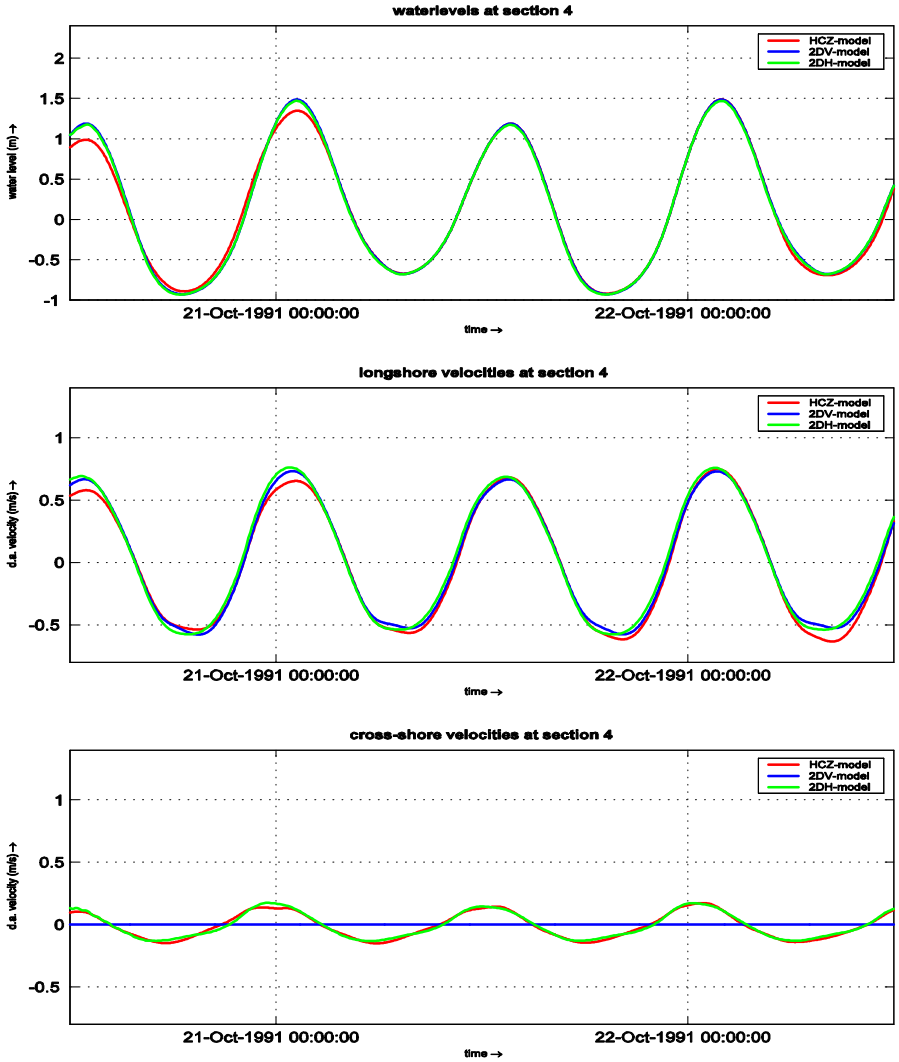

Figure 5-3 Water levels, alongshore and cross-shore velocities in HCZ, 2DV and 2DH model.

The boundary conditions obtained from the nesting procedure were used to derive a representative, morphological tide. The boundary conditions from the nesting procedure are specified as time-series of water levels and velocities. Hence, they relate to the simulation period of the HCZ model, this can be adjusted for by converting a morphological tide into harmonical components. The procedure of determining the morphological tide and converting it into harmonical components is discussed in Section 5.5.

5.5 Tidal schematization

5.5.1 Input reduction techniques

Reduction of information is one of the key elements in medium and long term modelling. This involves essentially four levels, which concern the input, the physical system or its model, the output and the interpretation or generalisation (cf. De Vriend et al., 1993). Therefore various approaches to medium and long term modelling exist, viz. input reduction, model reduction and behaviour orientated modelling.
Input reduction techniques are based on the idea of finding the representative input that drives long term residual effects (e.g. water or sediment transport). In this study this approach was followed for both tidal and wave input. This Section deals with tidal schematisation only; wave schematization is discussed in Section 5.6.

5.5.2 Derivation of basic morphological tide

Simulating complete tidal cycles is time-inefficient, especially when, for a number of wave conditions, the wave-induced currents have to be taken into account. To reduce computation time, a representative, morphological, tide can be selected which gives an optimal representation of the residual (e.g. yearly averaged) sediment transports of a complete neap-spring tidal cycle.

For practical applications two methods can be used to derive a morphological tide. The first method is described in Van Rijn (Van Rijn, 1993), and involves a correction factor ζ to the velocities of the mean tidal cycle, to account for the higher transport rates during spring tide conditions. This correction factor is of order ζ=1.1 along the Dutch Coast, but measurements should be analysed to derive the exact values for each specific location. The method of Latteux (Latteux, 1995) is based on a statistical description of the performance of a tidal schematisation with respect to the optimal representation of the derived or measured residual sediment transports.

Herein, a simplification of the method of Latteux (Latteux, 1995) was used to determine the morphological tide. At a single location, the residual transports were determined from preliminary simulations using a flat bottom at -17.80 m to MSL.

A 2DV simulation for section 4, using boundary conditions from a nesting procedure in the HCZ model, was run from 14 October 1991 00hrs00m00s. to 3 November 1991 00hrs00m00s. The neap-spring tidal cycle used herein runs from 18 October 1991 01hrs03m00s. to 1 November 1991 07hrs06m00s and thus covers a period of 20520 minutes. This simulation period of 20 days covers the neap-spring tidal cycle and includes a spin-up period of about 4 days. The Sediment Online add-on of Delft3D FLOW with both TRANSPOR2004 and trachytopes was used for simultaneous computation of transports and flows, bed level updating was not accounted for. The model was set up with a flat bottom at -17.80m to MSL and the median sediment diameter d_{50} was 0.300 mm. The single representative wave from Walstra et al. (1997) was used and a constant representative wind of 7 m/s from 240° N (Southwest) was applied. The computational time step used in the HCZ model was 3.0 minutes.

The neapspring-averaged transport rate over the neap-spring tidal cycle was computed and was evaluated against tide-averaged transport rates over 1488 minutes (two semi-diurnal tides). Often a period of 1490 minutes is chosen as average tidal period, herein a period of 1488 was chosen because the period needed to be an integer number of computational time steps.

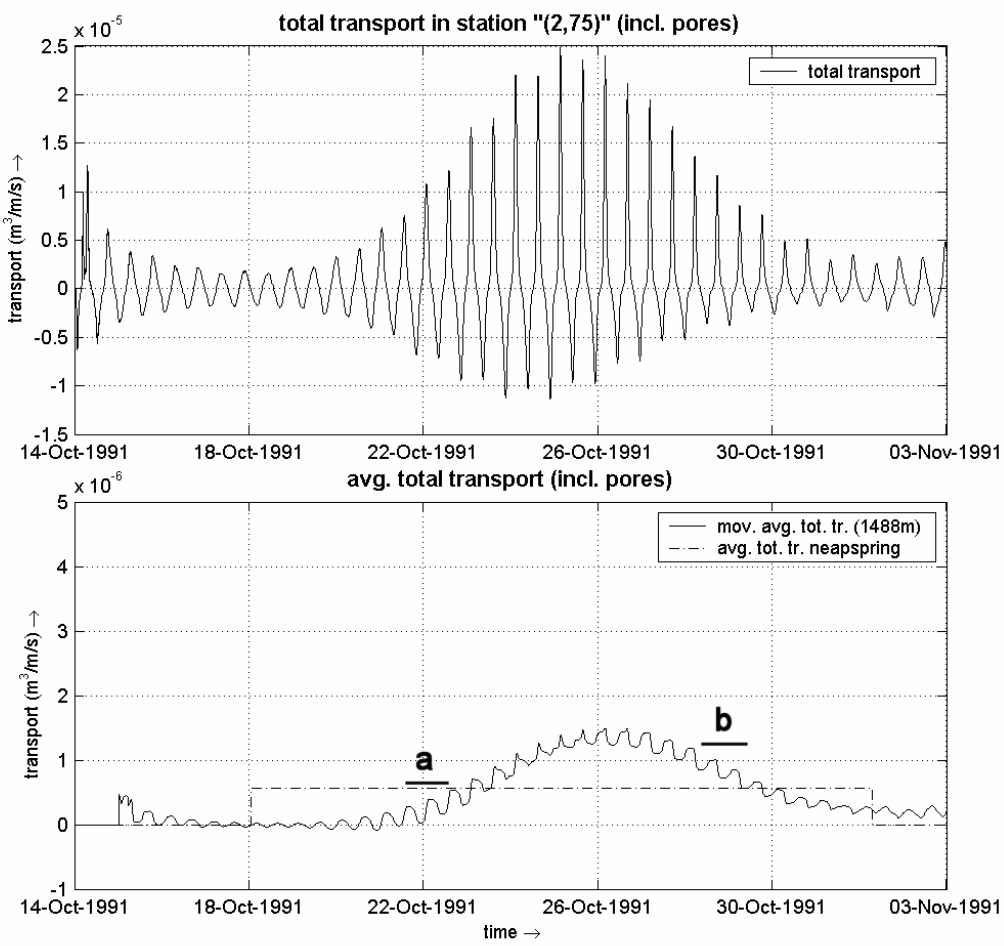

Figure 5-4 Total transport over neap-spring tidal cycle, flat bottom at -17.80 m.

In Figure 5-4, the total transport over a neap-spring tidal cycle and the moving average of this total transport is given with the average total transport over the neap-spring tidal cycle. From this figure it shows that two periods qualify as morphological tide. The first period runs from 21 October 1991, 16hrs27m to 22 October 1991, 17hrs15m and thus covers a period of 1488 minutes. This morphological tide is referred to as “basic a”. The second period lies somewhat after spring tide and runs from 28 October 1991, 08hrs27m to 29 October 09hrs15m and is referred to as morphological tide “basic b” Both periods are given in Table 5-2. As morphological tide “basic b” includes agger, it was decided to use the first period as morphological tide

morphological tide	from	to
“basic a”	21 October 1991, 16hrs27m	22 October 1991, 17hrs30m
“basic b”	28 October 1991, 08hrs27m	28 October 1991, 09hrs15m

Table 5-2 Morphological tides "basic a" and "basic b"

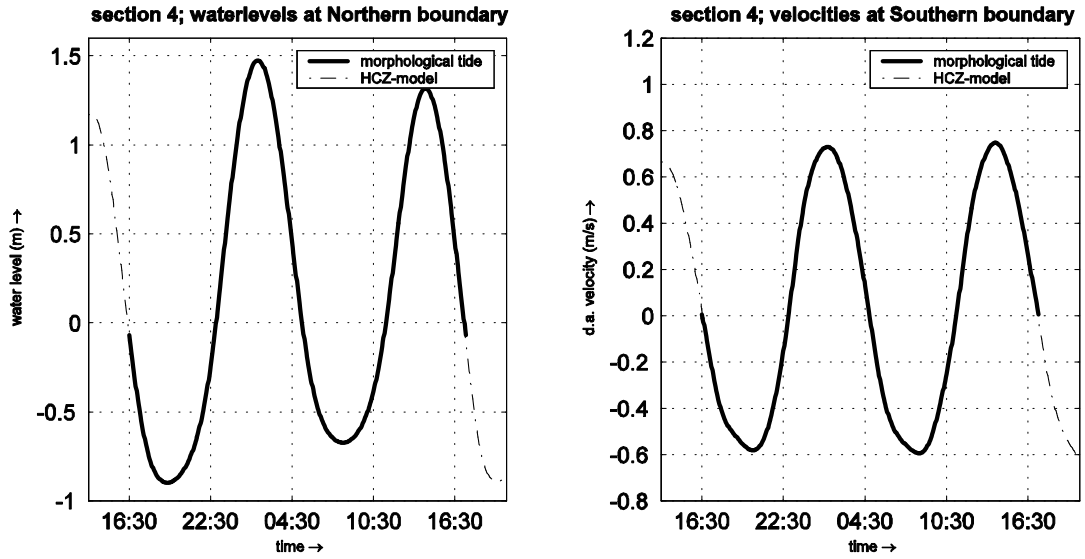

Figure 5-5 Boundary conditions for section 4; morphological tide "basic a"

Figure 5-5 shows the boundary conditions at section 4 for morphological tide “basic a” which runs from 21 October 1991, 16hrs27m to 22 October 1991, 17hrs15m, The boundary conditions were derived from nesting in the HCZ-model, both the original conditions from the HCZ-model and the morphological tide in harmonic components are plotted, it can be seen that 16 harmonic components are sufficient for accurate representation. In Figure E.01 and E.02 boundary conditions for morphological tide “basic a” at sections 3, 4 5 and 6 are given.

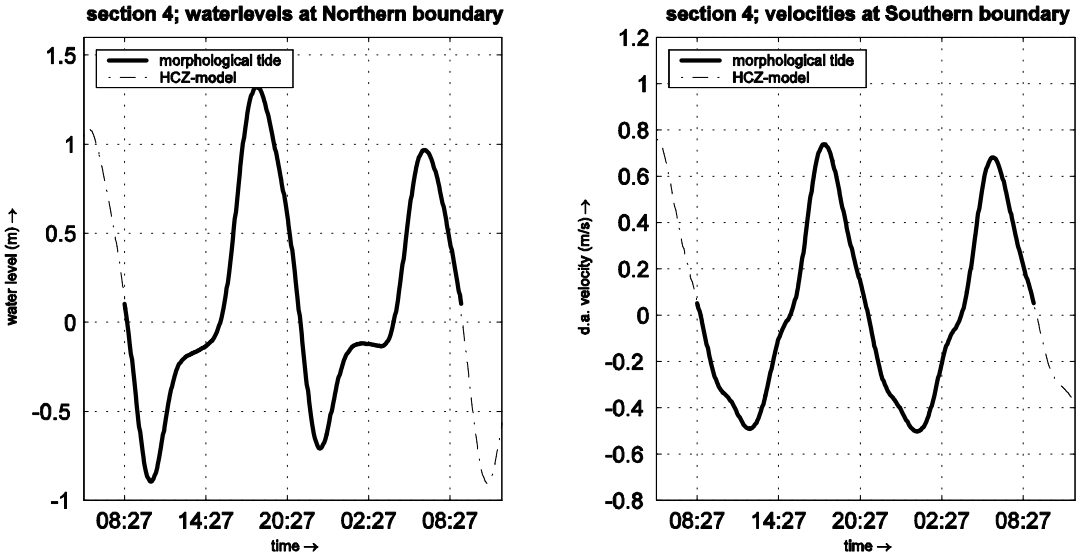

Figure 5-6 Boundary conditions at section 4: morphological tide "basic b".

Figure 5-6 shows the boundary conditions at section 4 for morphological tide “basic b”, these boundary conditions were derived from nesting in the HCZ-model, both the original conditions from the HCZ-model and the morphological tide in harmonical components are plotted, it can be seen that 16 harmonical components are sufficient for accurate representation. It can be seen that the water levels of this morphological tide includes agger and that velocities are much more peaked than in morphological “tide a”. In Figure E.03 and E.04 boundary conditions for morphological tide “basic b” at sections 3, 4 5 and 6 are given.

The method used in this Section is a simplification of the method of Latteux, as the neapspring-averaged transports were computed in one station only and therefore no standard deviation over the differences between the transports in several points and the neappring-averaged transports needed to be determined. Here, the neapspring-averaged transport rate was computed and was matched to the moving average of the transport rates over a period of 2 complete tides (two semi-diurnal tides) In this way, a representative tidal schematisation with respect to the neapspring-averaged transport rates was obtained.

5.5.2.1 Harmonic components

The morphological tide is derived as a time series and therefore relates to a specific period of time. To allow for the simulation of any calendar period in time the morphological tide was converted into harmonic components. The conversion of the time series into harmonic components was checked by converting the harmonic components back to time series and plotting the initial and final time series, the conversion was found to be good. The conversion into harmonic components could also affect the transport rates in the model and this needs to be checked for. The transport rates from a run using time series were compared to that of a run using the morphological tide given in 16 harmonic components, see Figure 5-7. It was found that by using harmonic components the average total transport rates were underestimated less than 1% with regard to the time-series from the nesting procedure. This underestimating was found to be in an acceptable range and does not need to be accounted for.

Using harmonic components the morphological tide can be run repeatedly, but as it represents the neapspring-averaged transports (over a complete neap-spring tidal cycle), the simulation period always needs to be an integer number of morphological tides for valid morphological computations.

5.5.2.2 Evaluation of morphological tide "basic a"

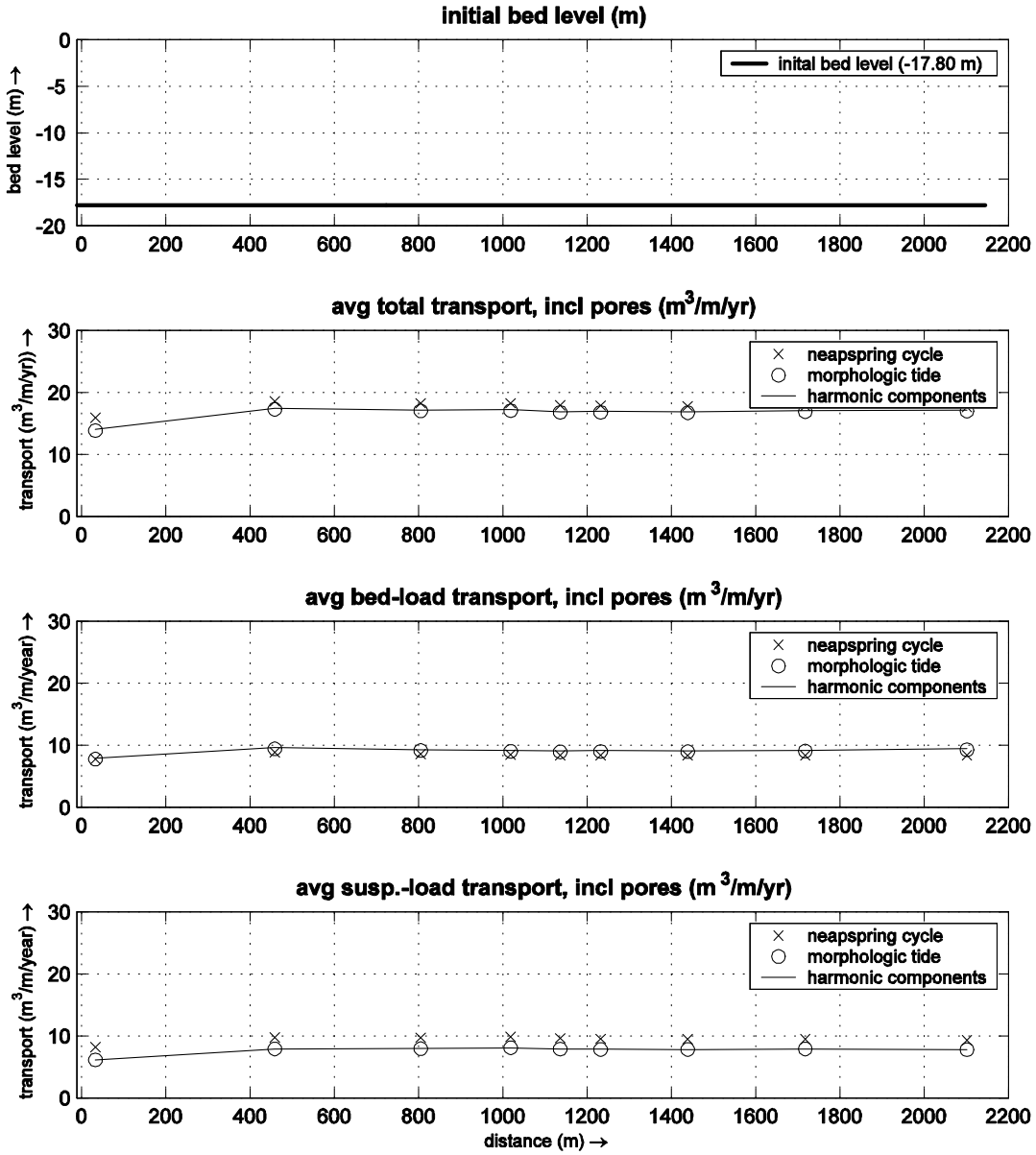

Figure 5-7 Average transport over neap-spring cycle and morphological tide "basic a", flat bottom at -17.80 m.

Figure 5-7 shows the average total transport, the average suspended-load transport and the average bed-load transport for a neap-spring tidal cycle and the morphological tide "basic a" in observation points at section 4, using a flat bottom at -17.80 m and including waves. Furthermore the average transports using harmonic components are given. From this figure it was found that the average total transports over the morphological tide represent the average total transports over the neap-spring tidal cycle very well. Bed-load transports are

represented slightly better than the suspended-load transport, but the overall conclusion is that the morphological tide is representative for the neap-spring tidal cycle. The average transports using 16 harmonic components are almost in perfect agreement with the average transports using time series, it can be concluded that the conversion to harmonic components does not affect the transports and that 16 harmonic components do adequately represent the time series.

Next, the morphological tide "basic a" derived using a flat bottom at -17.80m to MSL will be tested for use with the 1986 bathymetry. All other parameters were identical to the run with the bottom at -17.80 m to MSL.

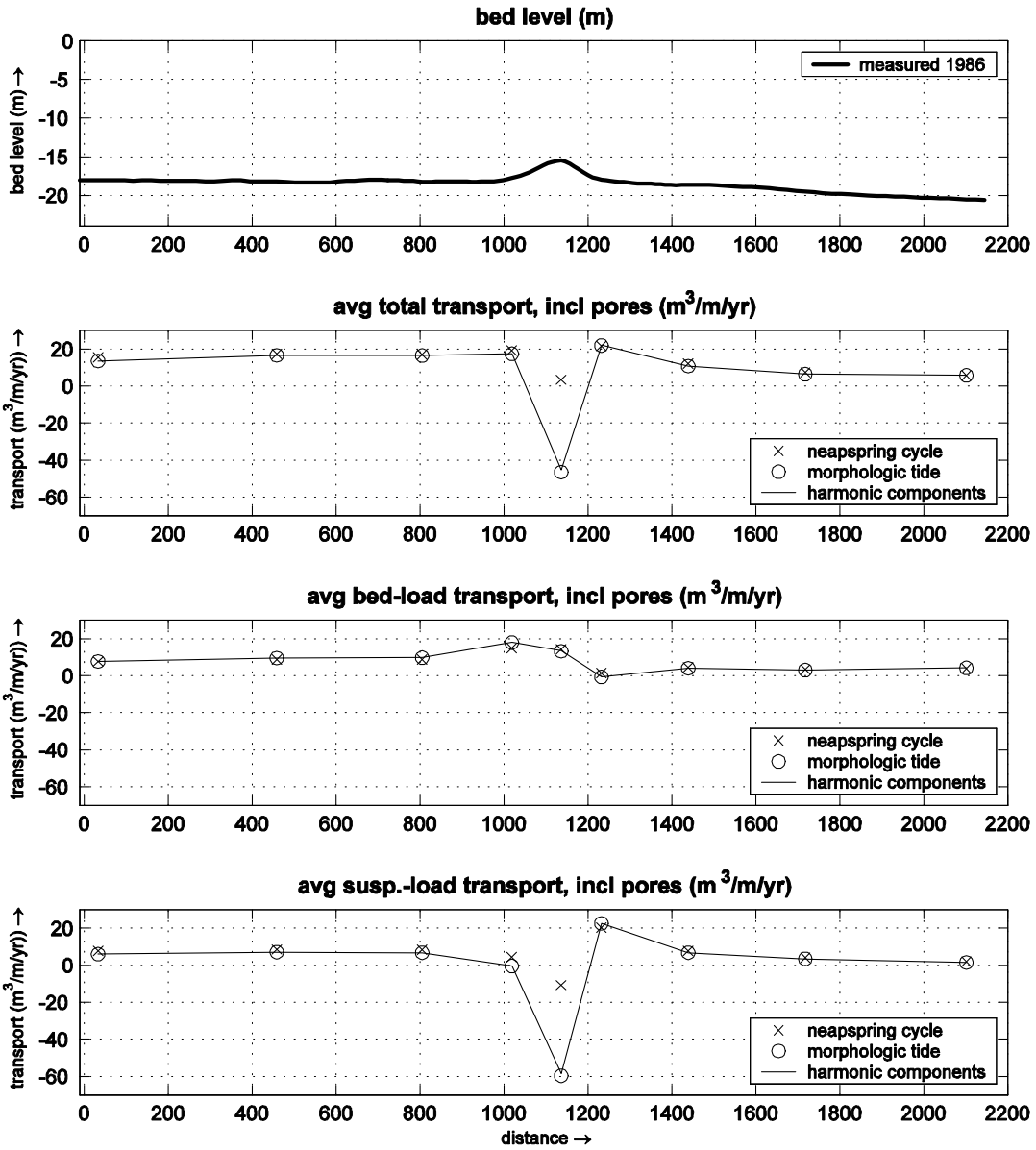

Figure 5-8 Average transports from morphological tide "basic a" using the 1986 bathymetry at section 4.

Figure 5-8 shows the average total, bed-load and suspended-load transports over the neap-spring tidal cycle and the morphological tide using the 1986 bathymetry, also the average transports using 16 harmonic components were plotted. All simulations used were including waves. From this figure it was found that using the 1986 bathymetry the average total transports over the neap-spring tidal cycle, which are in northern direction, show a local decrease and are negative (i.e. in southern direction) at the southern flank of the ridge.

The average total transports over the neap-spring tidal cycle locally drop to almost zero. The bed-load transport does not show any decrease in transport at the specific location, therefore the negative (i.e. in southern direction) transports are due to the suspended-load transport only. This peculiar phenomenon is investigated later on. The average total transports using the derived morphological tide overestimate the negative transport at the southern flank of the ridge considerably compared to the neapspring-averaged transports. The average bed-load transport over the ridge is represented well; the deviation is due to the suspended-load transport only. The overestimation of the decrease in suspended-load transport at the southern flank of the ridge makes the morphological tide unsuitable for use in medium-term morphological simulation; due to the negative transports, the ridge would erode much quicker than supposed to be.

From Figure 5-8 it was found that the morphological tide “basic a” was unsuitable for use with the 1986 bathymetry at section 4, it was investigated whether the morphological tide resulted in similar residual transports for other sections as well. For section 3, 5 and 6, separate simulations were made using the local 1986 bathymetry and local boundary conditions. Both simulations covering a complete neap-spring tidal cycle and using the morphological tide with harmonic components were made. The boundary conditions at each section were derived separately from nesting in the HCZ model, and for each section a morphological tide in harmonic components was computed, using the morphological period of 21 October 1991, 16hrs27m to 22 October 1991, 17hrs15m (“basic a”). Extra observation points were added for better insight in the development of the transports over the ridge.

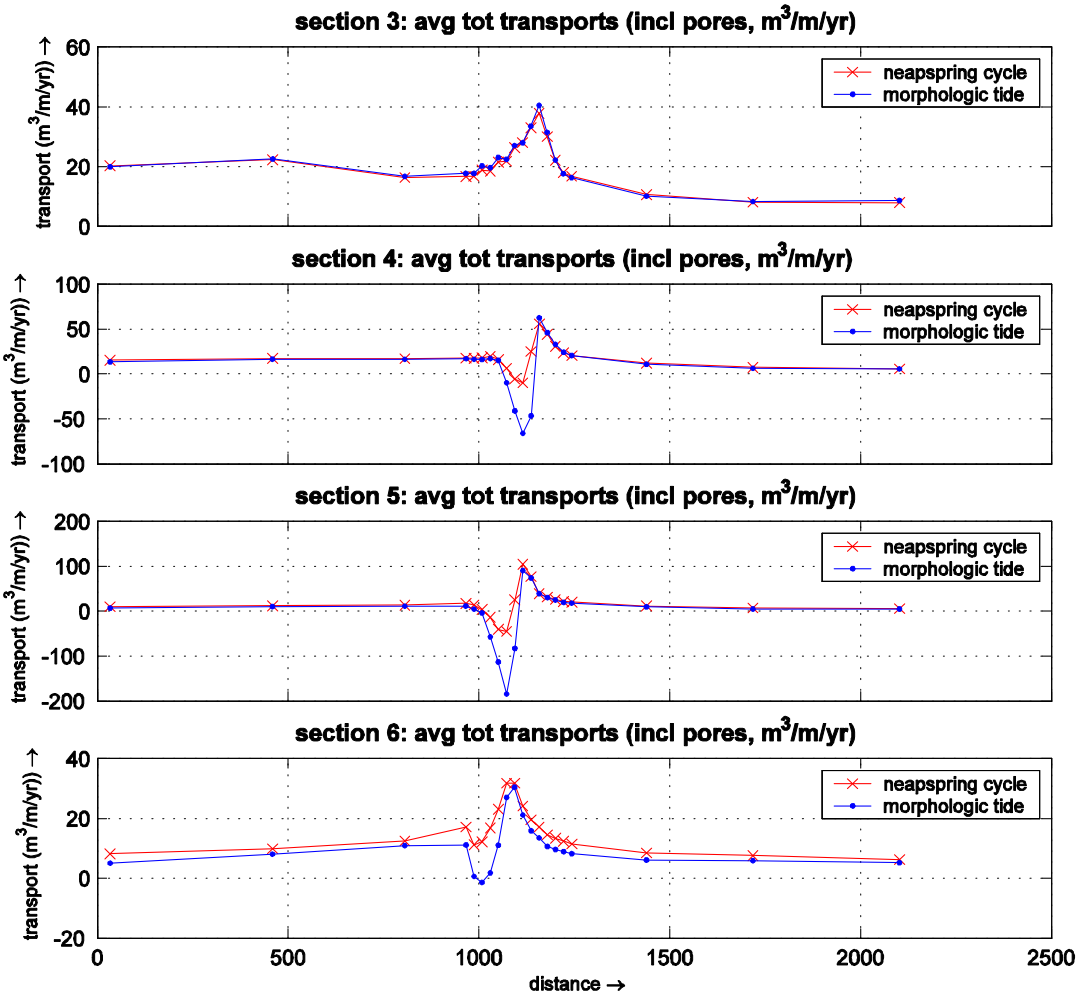

Figure 5-9 Average total transports from morphological tide "basic a" for sections 3,4,5 and 6 with 1986 bathymetry.

Figure 5-9 shows the average total transports over the neap-spring tidal cycle and the morphological tide for sections 3, 4, 5 and 6 with the 1986 bathymetry. Section 6 is the most seaward section. In Appendix E the average total transports and average bed-load and suspended-load transports for each section are given. From this Figure it was found that the average total transports over the neap-spring tidal cycle vary between each section; The average total transport at the depth outside the ridge crest decreases from about 22 m^3/m/year at section 3 to about 10 m^3/m/year at section 6.

The figure also shows that the average total transports over the ridge from the morphological tide represent those from a neap-spring tidal cycle well in section 3, but overestimate the dip in transport just in front of the top in section 4 and 5. The average transports in section 6 are somewhat better represented by the morphological tide. The conclusion to be drawn is that the derived morphological tide represents the transports from a neap-spring tidal cycle at the undisturbed depth only; it overestimates the dip in suspended-load transport at the ridge itself and therefore is not suitable for use with a medium-term morphological simulation.

5.5.2.3 Evaluation of morphological tide "basic b"

The morphological tide "basic a" was found to be unsuitable for use in medium-term morphological simulations due to the overestimation of the local decrease in average suspended-load transports at the southern flank of the ridge and the subsequent morphological consequences. Therefore the performance of the morphological tide "basic b" was investigated hereafter.

The morphological tide "basic b" (see Figure 5-6) was converted into 16 harmonic components and was evaluated using the 1986 bathymetry. Simulations were carried out using a single representative wave condition, TRANSPOR2004 and trachytopes; bed level updating was switched off for accurate representation of the transports at the 1986 bathymetry.

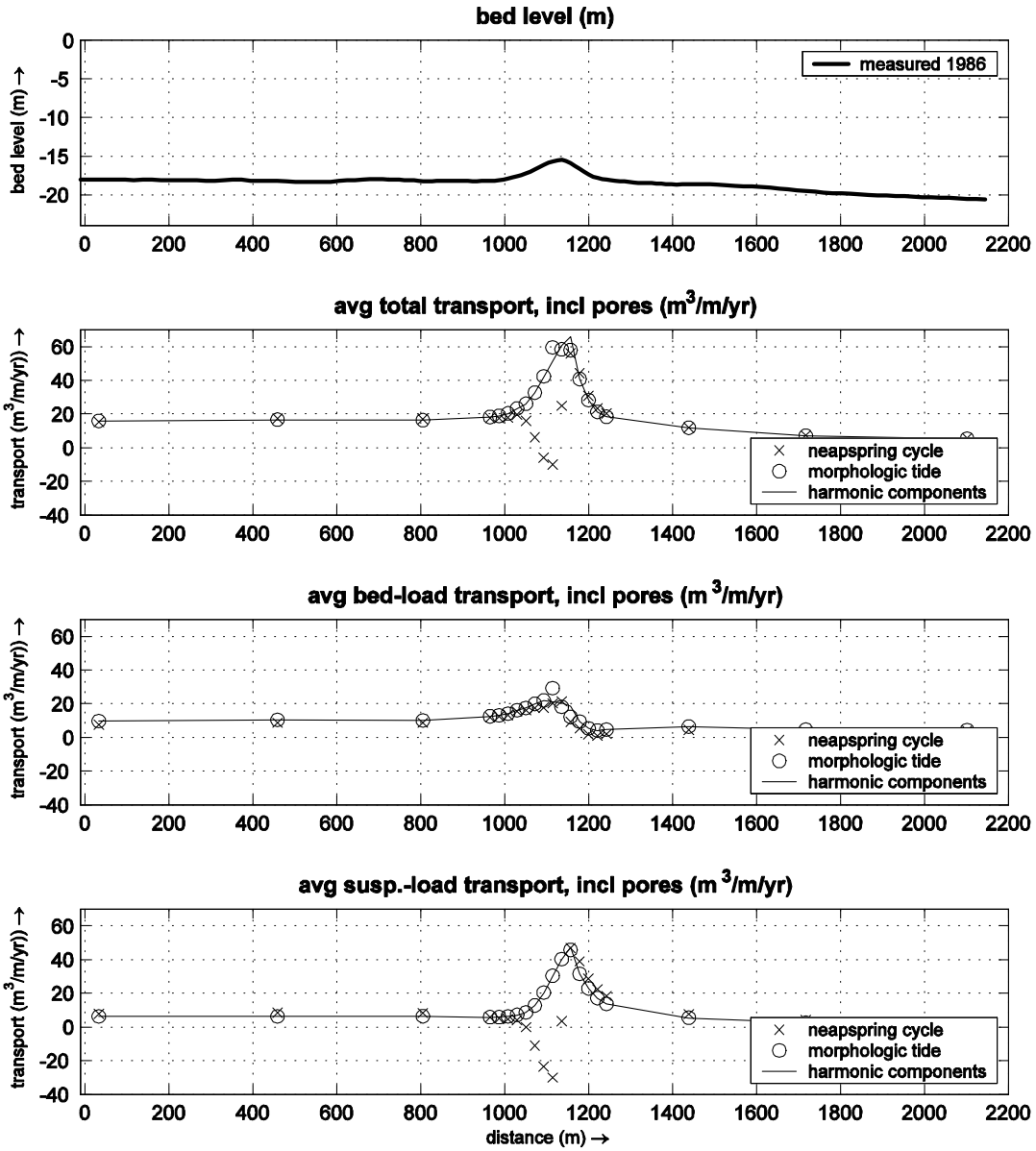

Figure 5-10 Average transports from morphological tide "basic b" using the 1986 bathymetry (section 4).

Figure 5-10 shows the tide-averaged total, bed-load and suspended-load transports over the neap-spring tidal cycle and the morphological tide “basic b” using the 1986 bathymetry, also the tide-averaged transports using 16 harmonic components were plotted. All simulations used were including waves. The average total transports over the neap-spring tidal cycle, which are in northern direction, show the local decrease and are negative (i.e. in southern direction) at the southern flank of the ridge which was observed earlier. The average total transports using the derived morphological tide “basic b” do not show the negative neapspring-averaged transport at the southern flank of the ridge. The average bed-load transport from the morphological tide “basic b” over the ridge is therefore not in agreement with the neapspring-averaged transports and is unsuited for use in medium-term morphological simulations.

In figures E.11 –E14 shows the average total, bed-load and suspended-load transports over the neapspring cycle and the morphological tide “basic b” for section 3,4,5 and 6. It can be seen that both bed-load and suspended-load transports at the southern flank of the ridge are represented badly using morphological tide “basic b”.

Further analysis of transport time series for the complete neap spring tidal cycle showed that at the southern flank of the ridge, ebb transports in the second half of the neap spring cycle are significantly smaller than over the first half. Apparently, tidal asymmetry at the southern flank is larger in the second half of the neap spring cycle. Therefore, any morphological tide that is to represent the averaged transports over the entire ridge cannot be from the second half of the neap spring tidal cycle.

5.5.3 Derivation of optimal morphological tide

The morphological tides (“basic a” and “basic b”) do not represent the average transports near the top of the ridge very well. They were derived from a single observation point at section 4 using a flat bottom. The morphological tide therefore does not account for different conditions at section 3,5 and 6 and is not suitable for use in those sections. From analysis of simulations using morphologic tide “basic b” it was found that any morphological tide which is to represent the neapspring-averaged transports at the location of the decrease in suspended-load transport will have to lie in the first half of the neapspring tidal cycle; transports from individual tides in the second half of the neapspring tidal cycle at that location are much more asymmetric and do not coincide with the neapspring averaged transports.

5.5.3.1 Weighting procedure

In this Section a better morphological tide will be derived which will be able to reproduce the average transports over a neap-spring tidal cycle at all four sections. The selected morphological tide will be based upon simulations and computations at section 3, 4, 5, and 6. For each section a morphological tide will be derived at three different observation points; the first at the relatively flat section between the southern boundary and the ridge, the second at the location of the previously observed decrease in average suspended-load transport at the southern flank of the ridge and the third at the top of the ridge, these locations are labelled “flat”, “dip” and “top”. These three points represent the different

conditions over the ridge. From these points at all four sections, an overall valid morphological tide will be selected.

Improvements in the method of derivation of the morphological tide include the use of the 1986 bathymetry instead of the flat bottom at -17.80 m to MSL. Also, as tidal periods vary over the neap-spring tidal cycle they will be determined exactly for accurate computation of the average total transport over two tides. Simulations were carried out using a single representative wave condition, TRANSPOR2004 and trachytopes; bed level updating was switched off for accurate representation of the transports at the 1986 bathymetry.

In the simulations a set of 20 observation points was used at fixed positions to the southern boundary. As the ridge bends in southern direction with increasing depth, the observation points used in different section vary to ensure correct locations with respect to the top of the ridge. Observation points used in each section with corresponding distances from the southern boundary are given in Table 5-3.

section	**location "flat"**	**location "dip"**	**location "top"**
section 3	obs 2 at x = 460 m	obs 11 at x = 1115 m	obs 13 at x = 1158 m
section 4	obs 2 at x = 460 m	obs 11 at x =1115 m	obs 13 at x = 1158 m
section 5	obs 2 at x = 460 m	obs 9 at x = 1072 m	obs 11 at x = 1115 m
section 6	obs 2 at x = 460 m	obs 5 at x = 987 m	obs 10 at x = 1093 m

Table 5-3 Observation points and corresponding distance from southern boundary used in each section.

Per section and per observation point a morphological tide has been derived with the improved method (using exact tidal periods for tide-averaging) Hence 12 morphological tides were derived. From those 12 morphological tides, three will be selected for testing at all sections. The three tides selected for testing were found in multiple points at different sections and therefore are more likely to be valid at all four sections and at all observation points.

The computed morphological tides from observation points at location "dip" only are very different from the computed morphological tides at location "flat" and location "top". The morphological tide from location "dip" does not represent the transports in the other locations very well, and therefore cannot be used in morphological computations. The final overall morphological tide will lie between the morphological tides from location "dip" and the morphological tide at location "flat" and "top", and overestimation of the decrease in suspended-load transports at the southern flank of the ridge is therefore inevitable. An overall valid morphological tide will be selected from testing the three individually selected morphological tides.

Improvements in the method of derivation of the morphological tide include:
1. use of the 1986 bathymetry instead of a flat bottom at -17.80m to MSL.
2. computations of the morphological tide for all four sections instead of section 4 only.
3. use of three observation points per section, at characteristic locations.
4. computation of exact tidal periods for determining the accurate tide-averaged transports.

5.5.3.2 Exact tidal periods for accurate computation of tide-average transports

The HCZ overall-model, which was used to generate boundary conditions for the 2DV models, was run with astronomical boundary conditions; the tidal period therefore is not fixed, it varies over a neap-spring tidal cycle. Here, instead of using a moving average over the neap-spring cycle with a fixed tidal period for averaging, the average transport over each individual tide was computed using the exact tidal period. First the zero-crossings of total transport were determined, from this the exact tidal periods over the neap-spring tidal cycle can be found. Using these tidal periods for averaging the exact average over two tides was computed and was matched with the neapspring-averaged transports.

Results

The method described above was carried out at three locations per section; in total 12 computations were made. Results of computations for section 4 are discussed and results of computations at other sections are summarized hereafter. Next, several morphological tides were selected for testing in all four sections.

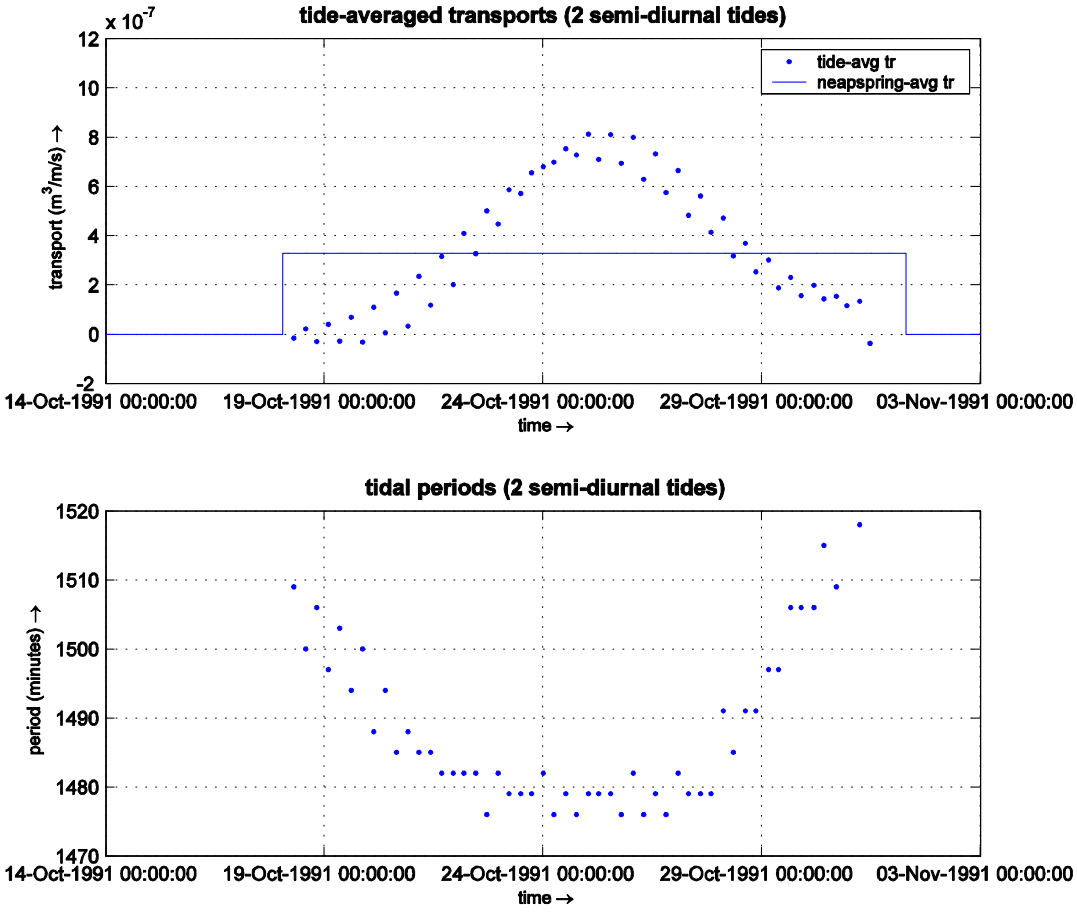

Figure 5-11 Average total transport using exact tidal periods, section 4.

Figure 5-11 shows the tide-averaged total transports (two semi-diurnal tides) and the neapspring-averaged total transports at observation point 2 of section 4 using exact tidal periods, which are also shown. From this figure a morphological period can be selected which is valid for observation point 2 of section 4. From the lower figure, it can be seen that the tidal period varies over the neap-spring tidal cycle; the average tidal period around spring tide is about 1476 minutes and up to 1509 minutes around neap tide. From the upper figure, it can be seen that two morphological tides can be selected which both represent the neapspring-averaged transports at location "top" at section 4 very well. The first morphological tide runs from 22 October 1991, 11hr03 to 23 October 1991, 11hr45 and covers a period of 1482 minutes. The second morphological tide runs from 21 October 1991, 03hrs57m to 22 October 1991, 04hrs42m and covers a period of 1485 minutes.

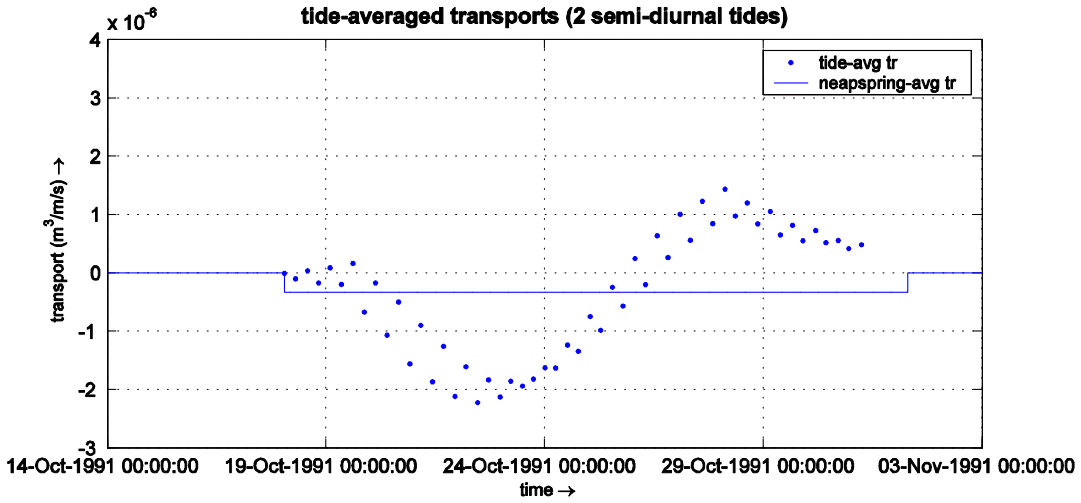

Figure 5-12 Tide-averaged transports at observation point 11 (location "dip") for section 4.

Figure 5-12 shows the tide-averaged total transports (two semi-diurnal tides) and the neapspring-averaged total transports at observation point 11 at section 4. Interestingly, it can now be seen that the tide-averaged transports at the second part of the neap-spring tidal cycle are in northward direction, while tide-averaged transports in the first part of the neap-spring tidal cycle are in southward direction. The neapspring-averaged transport is in southward direction, therefore any morphological tide that is to represent the average transports at location "dip" should be in the first part of the neap-spring tidal cycle. The morphological tide selected from location "dip" at section 4 runs from 20 October 1991, 03hr09 to 21 October 1991, 03hr57 and covers a period of 1488 minutes.

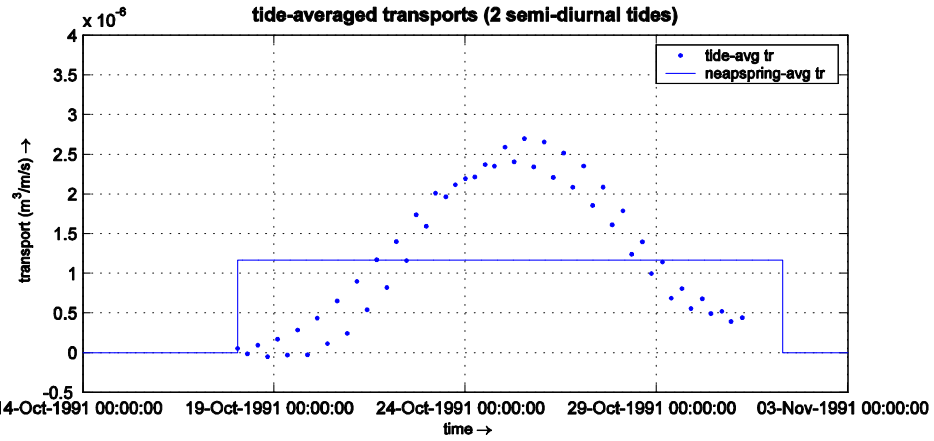

Figure 5-13 Tide-averaged transports at observation point 13 (location "top") for section 4.

Figure 5-13 shows the tide-averaged total transports (two semi-diurnal tides) and the neapspring-averaged total transports at observation point 13 (location "top") at section 4. Tide-averaged transport is in northward direction only. It can be seen that two morphological tides can be selected which both represent the neapspring-averaged transports at location "top" at section 4 very well , the first morphological tide runs from 22 October 1991, 11hr03 to 23 October 1991, 11hr45 and covers a period of 1482 minutes. The second morphological tide runs from 21 October 1991, 03hrs57m to 22 October 1991, 04hrs42m and covers a period of 1485 minutes. This procedure followed for sections 3, 4, 5 and 6, see Table 5-4.

section	obs	from	to	period
3	2	21 October 1991, 16hr21	22 October 1991, 17hr06	1485m
	11	21 October 1991, 16hr21	22 October 1991, 17hr06	1485m
	13	21 October 1991, 16hr21	22 October 1991, 17hr06	1485 m
4	2 1st	22 October 1991, 11hrs03	23 October 1991, 11hrs45	1482 m
	2 2nd	21 October 1991, 03hr57	22 October 1991, 04hr42	1485 m
	11	20 October 1991 03hr09	21 October 1991, 03hr57	1488 m
	13 1st	22 October 1991, 11hrs03	23 October 1991, 11hrs45	1482 m
	13 2nd	21 October 1991, 03hr57	22 October 1991, 04hr42	1485 m
5	2	22 October 1991, 04hr39	23 October 1991, 05hr21	1482 m
	9	20 October 1991, 03hr09	21 October 1991, 03hr57	1488m
	11	22 October 1991, 11hrs03	23 October 1991, 11hrs45	1482 m
6	2	22 October 1991, 04hr39	23 October 1991, 05hr21	1482 m
	5	24 October 1991, 00hr15	25 October 1991, 00hr57	1482 m
	10	21 October 1991, 16hr21	22 October 1991, 17hr06	1485m

Table 5-4 Morphological tides selected from three observation points at all four sections.

5.5.3.3 Selection of optimal morphological tide

The individually selected morphological tides which where found at several observation points at different sections are given in Table 5-5.

nr	section	from	to	period
1	4	21 October 1991, 03hr57	22 October 1991, 04hr42	1485 m
2	3	21 October 1991, 16hr21	22 October 1991, 17hr06	1485 m
3	5,6	22 October 1991, 04hr39	23 October 1991, 05hr21	1482 m
4	4	22 October 1991, 11hrs03	23 October 1991, 11hrs45	1482 m

Table 5-5 Morphological tides selected for evaluation.

These morphological tides were evaluated by comparing the average transports from simulations with the morphological tide for each section against simulations with a complete neap-spring tidal cycle. It was found that morphological tides 3 and 4 heavily overestimate the average southwards transports at the southern flank in section 4 and 5. Also the average transports over the southern flank of the ridge at section 6 are not represented very well. Morphological tides 1 and 2 both overestimate the average southward transports, but not as heavily as morphological tide 3 and 4. Although morphological tide 2 represents the neapspring-averaged transports at section 3 better than morphological tide 1, the latter is chosen as overall valid morphological tide as it performs slightly better at section 5, where the southward transports at the southern flank are represented better than with morphological tide 2.

The selected overall morphological tide runs from 21 October 1991, 03hrs57m to 22 October 1991, 04hrs42m and thus covers a period of 1485 minutes, see Table 5-6. This period was selected as it represents the neapspring-averaged transports at location “flat” and “top” in all four sections reasonably well and does represent the southward transports in location “dip” in all sections better than the other morphological periods.

overall morph.tide	from	to	period
“mt2”	21 October 1991, 03hr57	22 October 1991, 04hr42	1485 m

Table 5-6 Selected overall morphological tide "mt2".

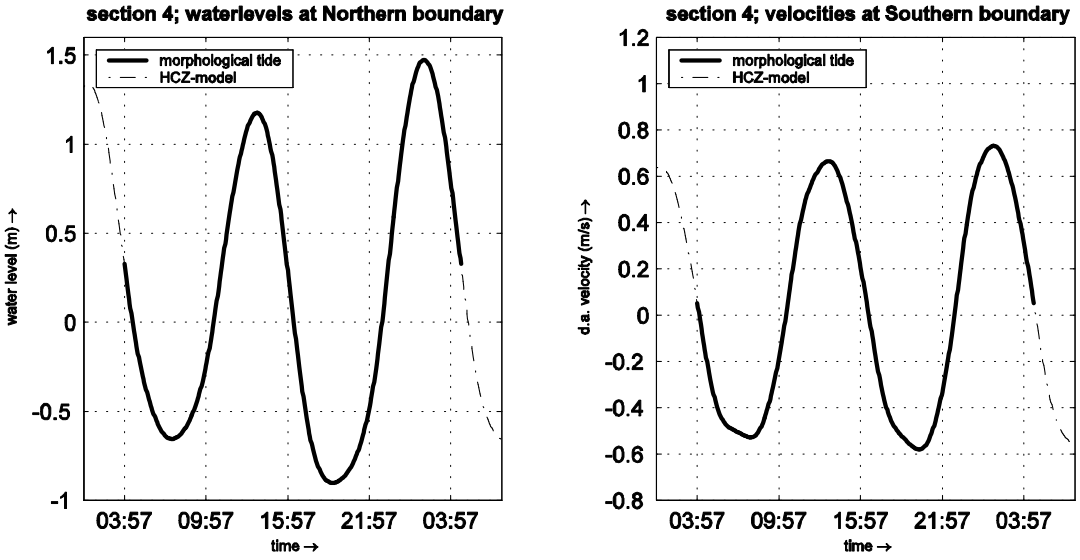

Figure 5-14 Boundary conditions for section 4; morphological tide "mt2".

Figure 5-14 shows the boundary conditions at section 4 for morphological tide “mt2”, these boundary conditions were derived from nesting in the HCZ-model, both the original conditions from the HCZ-model and the morphological tide in harmonic components are plotted, it can be seen that 16 harmonic components are sufficient for accurate representation. In Figure E.05 and E.06 boundary conditions for morphological tide “mt2” at sections 3, 4 5 and 6 are given.

Comparison to first morphological tide

The morphological tide derived in the previous Section is not very different from the one derived here, there’s time difference of only 753 minutes between both periods. The morphological tide derived with the second method starts somewhat earlier and is just a little further from springtide and ebb velocities are therefore a little smaller. In general, the residual transport (in Northern direction) is somewhat underestimated, the advantage of this is a better representation of the average transports at the southern flank of the ridge. The decrease itself is still overestimated compared to the neapspring-averaged transports, but not as much as with the morphological tide “basic a”.

It must be noted that the morphological tide “basic a” represents the neapspring-averaged transports very well, except for the southern flank of the ridge. The morphological tide “mt2” derived in this Section performs slightly better, but does still overestimate the southward transports at the southern flank of the ridge at section 4 and 5.

Morphological tide “mt2” in harmonic components

The morphological tide was converted into harmonic components to allow for simulation of any calendar period in time. This conversion was checked and was found to be good. Also, the average transport rates from a run using the morphological tide given in 16 harmonic components were compared to the average transport using the time series from the nesting procedure over the exact same morphological period; the agreement was found to be good. The morphological tide can be run repeatedly, but as it represents tide-averaged transports

over a complete neap-spring tidal cycle, the simulation period always needs to be an integer number of morphological tides.

5.5.3.4 Evaluation of morphological tide "mt2"

The morphological tide derived in this Section was tested by comparing the average transports from simulations with the morphological tide for each section against simulations with a complete neap-spring tidal cycle.

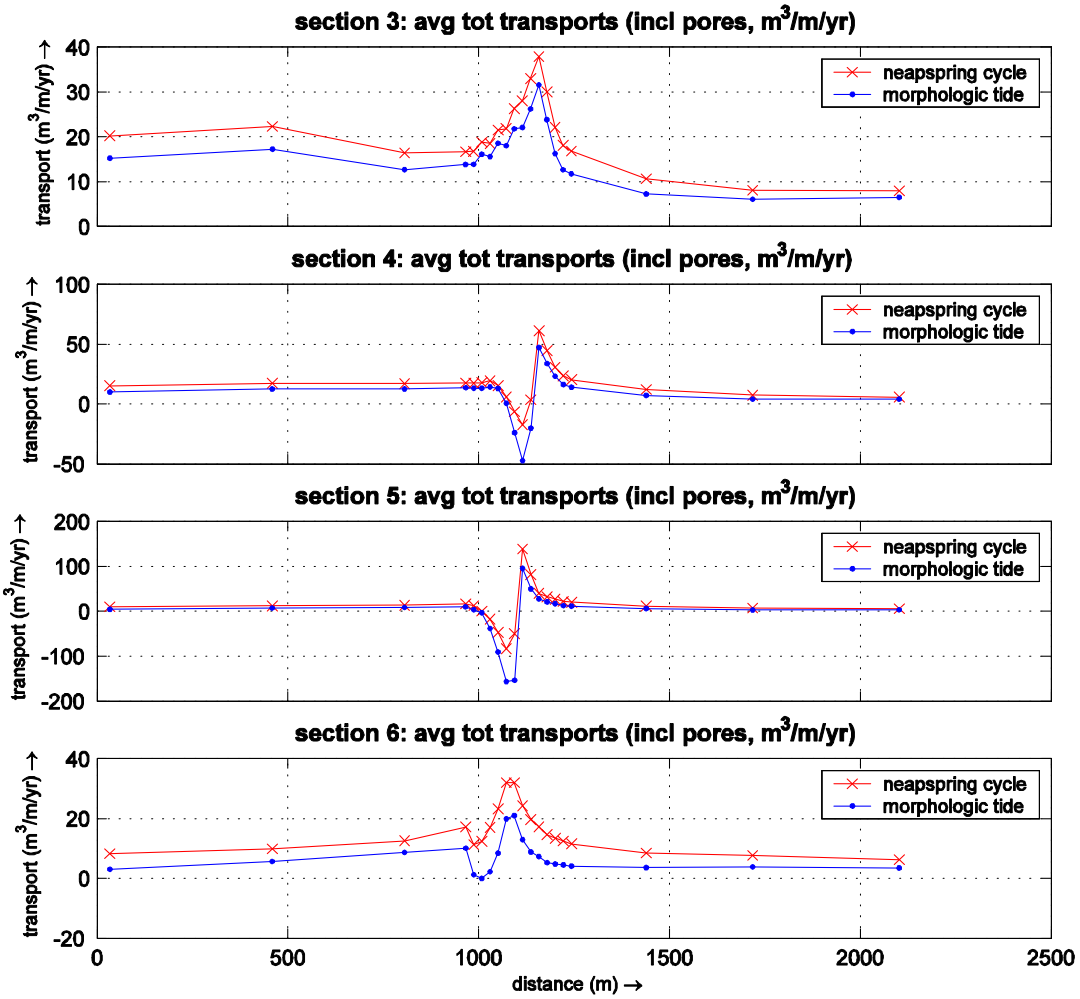

Figure 5-15 Average total transports from morphological tide "mt2" for sections 3, 4, 5 and 6.

Figure 5-15 shows the time-averaged total transports for both the neap-spring tidal cycle and the morphological tide from 21 October 1991, 03hrs57m to 22 October 1991, 04hrs42m for each section using the 1986 bathymetry. From this figure it can be seen that the morphological tide "mt2" underestimates the transports in section 3 and 6 with nearly 10 m^3/m/year (incl. pores), transports in section 4 and 5 are represented well. Furthermore, the morphological tide still overestimates the average southern transports at the southern flank of the ridge, though not as strongly as the previous derived morphological tide "basic a".

In Figures E.15 to E.18 both results from simulations using the full neap-spring tidal cycle and using the morphological tide “mt2” are given. It was found that the morphological tide showed a somewhat greater decrease in height of the ridge than the full neap-spring simulations and that, especially at shallower water (section 3 and 4) the migration was underestimated compared to the full neap-spring simulation. At deeper water the migration was accurately represented with the morphological tide.

The tide-averaged transports in southern direction at the top of the ridge is overestimated using the morphological tide “mt2” (see Figure 5-15), but has limited effect. Analysis of transport rates showed that the top of the ridge initially erodes at a considerable rate, but that after some time, as the height of the ridge is altered, the time tide-averaged transports over the ridge are in northern direction only and the ridge erodes at a much slower rate, comparable to that of the full neap-spring cycle
Results from morphological simulations with the selected morphological tide are encouraging irrespective of the temporal, initial erosion at the top of the ridge that it entails. Considering the encouraging results and the computational efficiency it was decided to use the morphological tide “mt2” for all simulations

5.6 Wave schematisation

In order to simulate the effect of waves on the morphological changes, either the WAVE module of Delft3D or the constant wave height setting in Sediment Online can been used. Herein, the constant wave setting of Sediment Online was used, which accounts for a spationally constant wave height. The wave model provides wave forces to the flow model and therefore enables the flow model to simulate wave driven currents. Also, the wave parameters are provided to the Sediment-Online add-on to account for the stirring effect of the waves on the sediment transport. Two wave schematizations are available for the area, model results using both wave schematizations will be evaluated against measurements in the next Section.

In Walstra et al. (1997) a single representative wave condition (long term average wave condition) was derived to give the best representation of the overall, yearly wave climate at location Euro-Maas channel by applying the Latteux method to evaluate residual transports, see Table 5-7.

Study	H_s (m)	T_p (s)	Direction (° N)	Period (%)
Walstra et al. (1997)	2.25	6.6	315	84

Table 5-7 Applied single representative wave condition.

Also a representative wave climate from Roelvink et al. (1998) was used in this study. The wave climate consists of 11 wave conditions and was selected from wave data close to the Port of Rotterdam over the period June 1990 – July 1991. The wave climate is given in Table 5-8.

Condition	H_s (m)	T_p (s)	Direction (° N)	days per year	Period (%)
W00	0.10	5.0	310	136.5	37.123
Z01	1.05	5.0	255	46.0	12.603
N10	2.35	7.1	355	19.7	5.397
Z02	2.75	7.2	245	15.7	4.301
W06	2.35	6.8	295	5.1	1.397
N08	2.35	7.2	345	8.8	2.411
W05	1.05	5.0	295	10.6	2.904
Z04	2.15	6.5	275	6.9	1.890
N09	1.05	6.0	5	65.7	18.000
Z03	1.25	5.3	285	15.0	4.109
N07	1.25	6.3	345	35.0	9.589

Table 5-8 Applied wave climate.

5.7 2DV sensitivity analysis of sand ridge near Hoek van Holland

Herein the 2DV sensitivity-analysis is discussed that was carried out to investigate the sensitivity of the 2DV model to several process and model parameters with respect to fair simulation of the morphological development of the sand ridge near Hoek van Holland. The sensitivity-analysis thus also serves as a basic calibration of the 2DV model. Simulations were carried out with the Delft3D Sediment-Online add-on in 2DV mode. First the basic 2DV model set-up is discussed, next the sensitivity simulations per model or process parameter are discussed. The settings found from the 2DV calibration and sensitivity runs will be used in chapter 6 for the validation of both the line model (1DH, 2DV) and area model (2DH, 3D).

For the sensitivity analysis and calibration of the model, the period Jan 26th 1986 to March 18th 1991 was selected. This period allows for comparison of the computational results with the measurements. The validation in chapter 6 is also carried out for this period and also for the period March 18th 1991 to October 19th 2000.

5.7.1 Model set-up

In this Section the overall approach to the 2DV sensitivity-analysis is given. First the basic model set-up is discussed, which includes the model grid and bathymetry, boundaries, time-parameters, processes, wind, waves and transport settings.

5.7.1.1 Computational grid

To allow for a true 2DV simulation of the sand dump a small, detailed grid was constructed by taking a selection of the HCZ model which was locally refined in the area of the sand dump to have an accurate representation. The model grid used herein is 20 m wide and 2134 m long, with a minimal horizontal grid size of about 10 m over the ridge and about 30 m at both boundaries. This horizontal grid size of 10 m was found provide enough resolution and is computationally efficient, see Section 4.3.1. The constructed grid is one cell wide and because of the staggered grid concept used in Delft3D it really is just a single line of water level points. The grid is a one-dimensional flume so to speak, with open boundaries at both ends of the grid and no slip at walls.

A vertical grid of 10 layers with logarithmic layer distribution was used herein as it was found that 10 vertical layers suffice with waves smaller than 3.00m, see Section 4.3.1.

5.7.1.2 Bathymetry

The bathymetry was generated using the data described in Chapter 3. The original sample points from the measurements were interpolated onto a 5 x 5m grid that was used for data analysis. Next the depth points were used as sample points for generating the bathymetry of the 2DV model by triangular interpolation onto the model grid. The bathymetry of Jan 26th 1986 for section 4 was used herein.

5.7.1.3 Open boundary conditions

Two open boundaries were defined; at the south-western boundary (x = 0 m) velocities need to be specified and at the north-eastern boundary (x = 2134 m) water levels need to be specified. The harmonic forcing type was applied at both the velocity and water level boundary; the morphological tide “mt2” for section 4 was used herein, see Figure 5-14.

5.7.1.4 Time parameters

The period of Jan 26th 1986 to March 18th 1991 was chosen for calibration and sensitivity purposes. To reduce computational time simulations were run over a much shorter time; the morphological changes were sped up to that of the calibration period using a morphological scale factor, see Section 4.3.7. Here, a simulation period of 7425 minutes was used, including a spin-up time of 1485 minutes to allow the model to adapt itself to the boundary conditions. The effective simulation time is therefore 5940 minutes; in this period 4 complete morphological cycles of 1485 minutes are simulated. In Section 4.3.7 different simulation periods and morphological scale factors were investigated.

A computational time step of 30 seconds was used, which is computationally efficient and was verified to lead to accurate results, see Section 4.3.4.

5.7.1.5 Processes and physical parameters

The 2DV sensitivity model was set-up to include wind, waves and sediments, salinity and temperature were not activated. The physical parameters used were:

- Coriolis acceleration was set up for 52 °N
- Acceleration of gravity was set to 9.8100 m/s^2
- Air density was 1.000 kg/m^3
- Water temperature was 15 °C

The algebraic turbulence model was used, see Section 4.3.5.

5.7.1.6 Wind

Wind driven currents play an important role in determining tide-averaged residual currents and transports. Here, the wind-field was simplified into a single representative speed and direction which yields the same alongshore and cross-shore wind stress is averaged over the entire wind-field. This representative speed and direction were taken as 7 m/s and 240 °N, the validity of these values was recently tested and confirmed against long-term wind records at 5 stations within the FLYLAND project (Roelvink et al., 2001b)

5.7.1.7 Waves

The recently implemented constant wave height version of Sediment Online was used, which accounts for a spationally constant wave height. In Section 5.7.2.1 simulations using a single representative wave condition and using a representative wave climate were compared to a simulation without waves.

5.7.1.8 Transport settings

The Sediment-Online add-on of Delft3D was used for simultaneous computation of flows and transports and simultaneous feedback to bottom changes; the elevation of the bed is dynamically updated each time step. The advantage of this over an offline morphological computation is that the hydronamic flow computations are always carried out using the correct bathymetry. The Sediment Online add-on was used in combination with the TRANSPOR2004 sediment transport model and a bed roughness predictor, sediment characteristics and Online-Sediment parameters used are given in Table 5-9.

sediment characteristics	
sediment density	2650 kg/m^3
dry bed density	1600 kg/m^3
mean sediment diameter D_{50}	300 μm
Online-Sediment parameters	
morphological scale factor	382.225
spin-up time	1485 minutes
equilibrium concentrations at inflow boundaries	true
effect sediment on density gradient	true
updating bed at inflow boundaries	false

Table 5-9 Sediment characteristics and Online-Sediment parameters

A morphological scale factor of 382.225 was applied in the simulations using the single representative wave of Walstra et al. (1997) , in this way the simulation gives the morphological development the period Jan 26th 1986 to March 18th 1991 (1877 days). The use of high morphological scale factors was verified in Section 4.3.7.

5.7.2 Sensitivity simulations

In this Section, the sensitivity simulations will be discussed which show the sensitivity of the 2DV model to several process and model parameters with respect to accurate simulation of the morphological development and serve as a basic calibration to ensure an optimal set-up of the model. For the sensitivity analysis and calibration of the model, the period Jan. 26th 1986 to March 18th 1991was selected. Several settings or parameters are investigated, for each setting or parameter a value or setting is selected for use in the sensitivity and validation runs.

The process and model parameters that have been investigated are listed in Table 5-10.

Input parameter(s)	**Values**
wave schematization	no waves, representative wave and wave climate
horizontal eddy diffusivity	0.10, 1.00, 10 and 25 m^2/s
mean sediment diameter	225, 300 and 420 μm
multiplication factor for bed-load transport	0.25, 0.50, 1.00 and 1.50
multiplication factor for susp.-load transport	0.25, 0.50, 1.00 and 1.50
longitudinal bed-gradient factor	0.50, 1.00, 1.50 and 5.00

Table 5-10 Overview of investigated process and model input parameters

For each setting a morphodynamic Delft3D simulation for section 4 was carried out using the algebraic turbulence model in combination with TRANSPOR2004 and the bed roughness predictor. The single representative wave from Walstra et al. (1997) was used.

5.7.2.1 Wave schematization

The recently implemented constant wave height version of Sediment Online was used, which accounts for a spationally constant wave height. Both a single representative wave and a wave climate are available (see Section 5.6) and will be evaluated herein.

The eleven wave conditions from the wave climate each have a different probability of occurrence (duration in % of time), therefore each wave condition needs to be simulated for a corresponding period of time. Because of the use of a morphological tide, this simulation period needs to be an integer number of tidal periods (1485 minutes). By applying different MORFAC numbers for all simulations, the different probability of occurrence of the wave conditions are taken into account. The MORFAC numbers are chosen so as to give the morphological effect over the period that a wave condition would occur in the total simulation period 1986 – 1991. All wave conditions have been simulated consecutively, the result of the simulation of the last wave condition therefore is the final result of simulating the entire wave climate. The total simulation period Jan 26th 1986 to March 18th 1991 takes up 1877 days (2702880 minutes). MORFAC numbers for scaling 4x1485 minutes to the required 2702880 minutes can easily be determined by division: 2702880 / 5940 = 455.03, this is the total MORFAC number for simulating the entire wave climate. Next, the different wave conditions and their probability of occurrence needs to be accounted for. By simply multiplying the MORFAC numbers with the probability of occurrence of the wave conditions, the MORFAC numbers for the separate runs can be found in Table 5-11.

wave condition	**probability**	**MORFAC**
W00	0.374	170.169
Z01	0.126	57.346
N10	0.054	24.559
Z02	0.043	19.573
W06	0.014	6.358
N08	0.024	10.970
W05	0.029	13.215
Z04	0.019	8.602
N09	0.180	81.905
Z03	0.041	18.700
N07	0.096	43.633
totals	**1.00**	455.03

Table 5-11 MORFAC numbers for eleven wave conditions

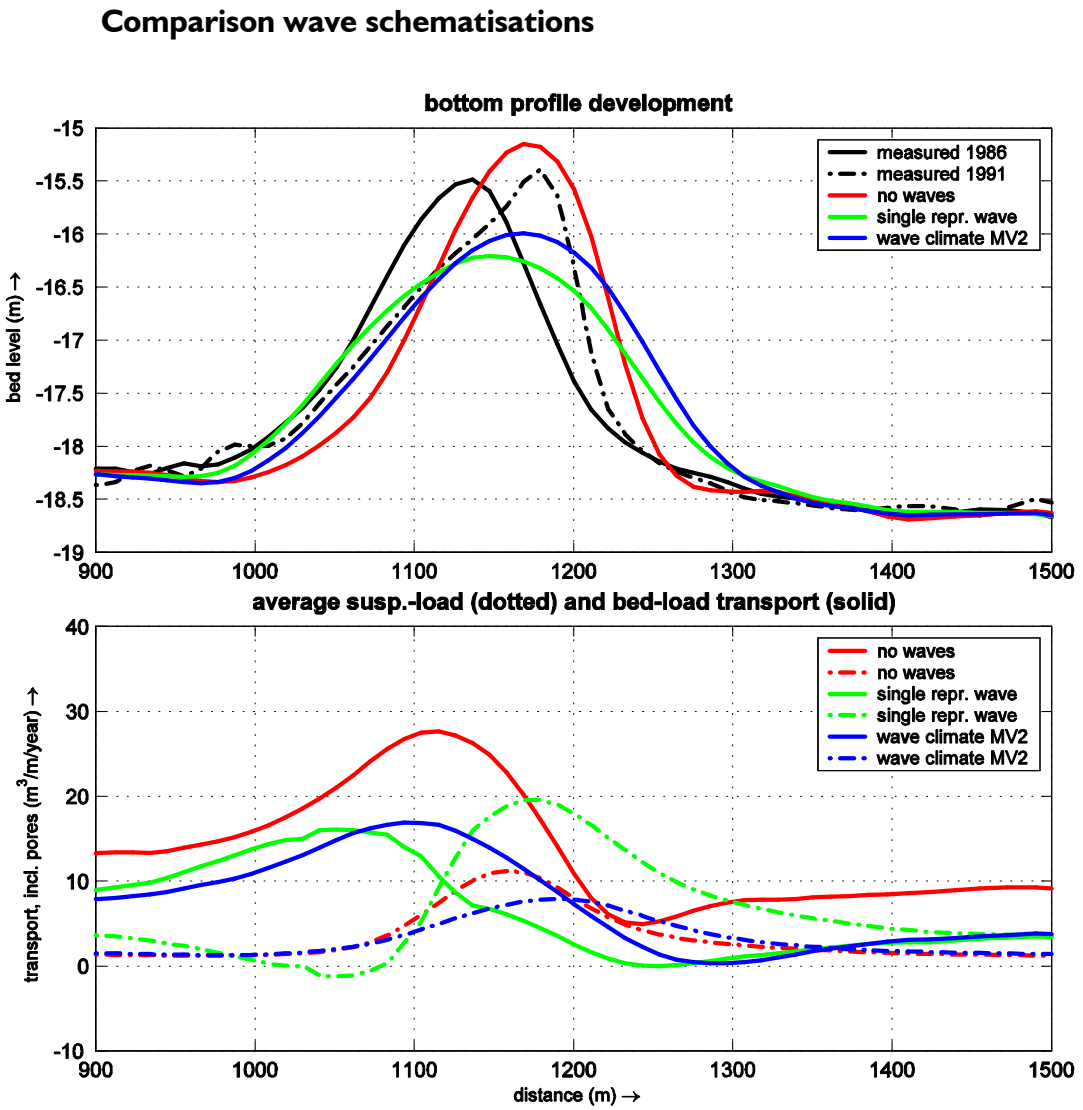

Figure 5-16 Bottom profile development and time-averaged transports using different wave schematizations.

In Figure 5-16, the computed bottom profiles for simulations without waves, with a single representative wave condition and with the wave climate from Roelvink et al. (1998) are given. Also the time-averaged transports are given. It can be seen that the ridge increases in height without waves, which was also found from initial modelling tests in Section 4.5.

The increase in height was also observed from measurements of 1986 and 1991. As the morphological development between 1986 and 1991 is not exemplary and an average decrease in height of about 0.10 m/yr was found over a longer period (see chapter 3), it was thus proved that simulations need to be carried out including waves.

Results from simulations with a single representative wave condition and the wave climate from Roelvink et al. (1998) are in reasonable agreement. Ideally, the single representative wave condition leads to time-averaged transports and morphological development identical to that of a complete wave climate. Here, it was found that the single representative wave

condition overestimates the decrease in height and underestimates the migration in flood direction. From the initial modelling test in Section 4.5 it was shown that with asymmetric tides, larger waves leads to larger decrease in height and larger migration. From this, the conclusion can be drawn that the single representative wave of Walstra et al. (1997) does not represent the wave climate from Roelvink et al. (1998) perfectly; considering the overestimation of the decrease in height is was found that the single representative wave of Walstra et al. (1997) is to large and that a slightly smaller wave condition would represent the wave climate from Roelvink et al. (1998) better.

However, the wave climate from Roelvink et al. (1998) is a schematization also and therefore is not perfect either; no clear assessment can be made on the validity of both wave schematizations. Because simulations using the wave climate are time-inefficient in comparison to simulations using the single representative wave condition and because both the 2DV and 2DH model need to be run with the same wave schematization for consistency and to allow for comparison, the single representative wave was selected for use in both models.

Figure F.01 shows the bottom profile development and time-averaged bed- and suspended-load transports for simulations without waves, with the single representative wave form Walstra et al. (1997) and with the wave climate from Roelvink et al. (1998).

5.7.2.2 Horizontal eddy diffusivity

The horizontal eddy diffusivity is an exchange coefficient for the horizontal diffusion of a conservative property by eddies in a turbulent flow; it exerts influence on the concentration distribution by means of the advection-diffusion (mass-balance) equation, see the Delft3D FLOW manual (WL |Delft Hydraulics, 2003).

The value for the horizontal eddy diffusivity depends on the flow and the grid size used. For detailed models with grid sizes of about ten meters or less, the value for the horizontal eddy diffusivity usually are in the range of 1 to 10 m^2/s, while with large coarse-grid models the value typically lies in the range of 1 to 10 m^2/s. The horizontal eddy diffusivity is a so-called calibration parameter; the value must be determined in the calibration process. Here, values of 0.10, 1.00, 10 and 25 m^2/s were evaluated.

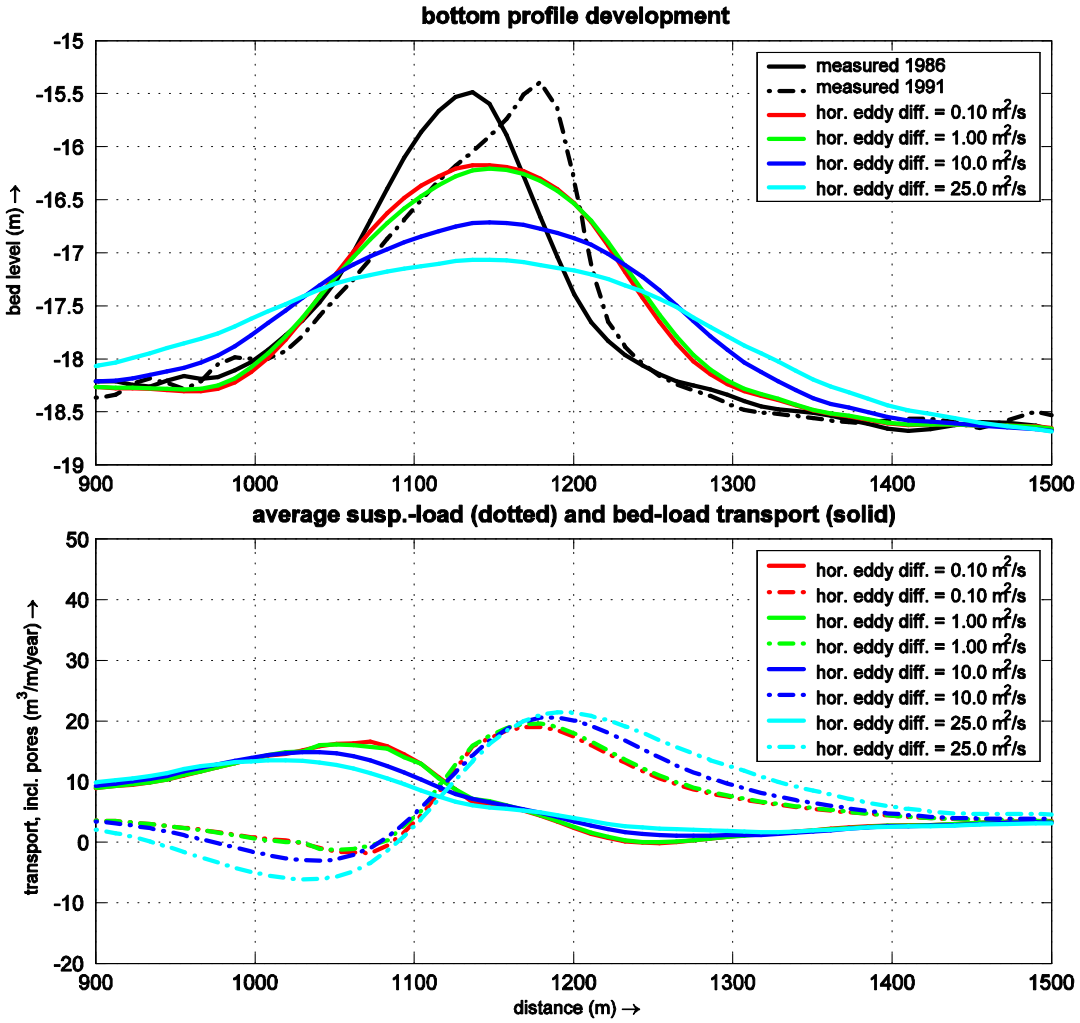

Figure 5-17 Bottom profile development and time-averagd transports using different values for the horizontal eddy difussivity.

Figure 5-17 shows the computed bottom profiles and average suspended and bed-load transport rates using mean a horizontal eddy diffusivity of 0.10, 1.0, 10.0 and 25,0 m^2/s. From this figure it was found that a with horizontal eddy diffusivity of 10 and 25 m^2/s the erosion at the top of the ridge was overestimated due to the greater horizontal distribution of sediment. A horizontal eddy diffusivity of 1.0 m^2/s was selected for use in the validation runs.

Figure F.03 shows the bottom profile development and time-averaged transports for simulations with a horizontal eddy diffusivity of 0.10, 1.0, 10.0 and 25,0 m^2/s.

5.7.2.3 Mean sediment diameter

Herein, the effect of the mean sediment diameter is investigated; simulations using a mean sediment diameter of 225, 300 and 420 µm were carried out and compared. These values were chosen to represent the average mean sediment diameter at a depth of about 20m at Hoek van Holland (225 µm), to represent the average mean sediment diameter at the top of the sand dump Hoek van Holland (420 µm) and to represent a rough average over both values (300 µm).

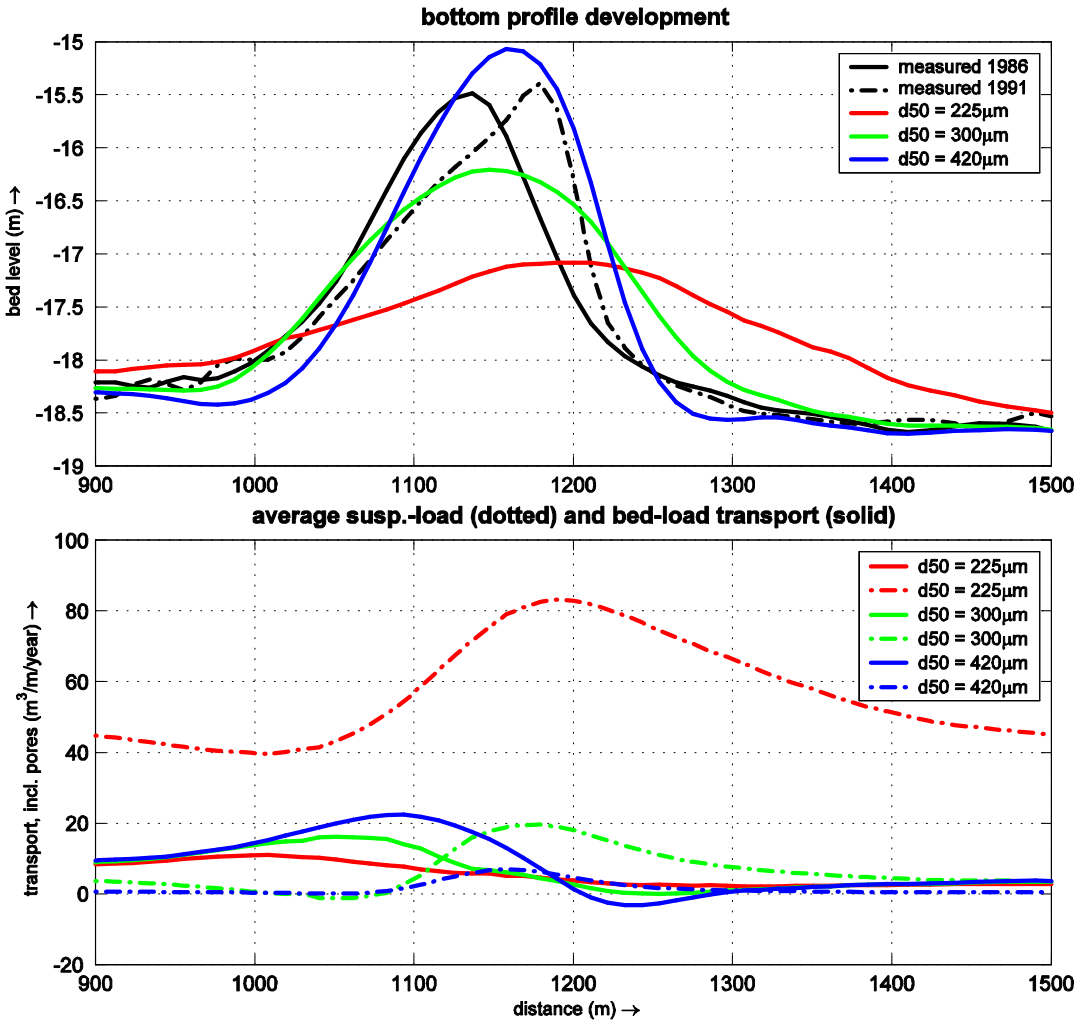

Figure 5-18 Bottom profile development and time-averaged transports using a mean sediment diameter of 225, 300 and 420 µm.

Figure 5-18 shows the computed bottom profiles and average suspended and bed-load transport rates using a mean sediment diameter of 225, 300 and 420 µm. From this figure it was found that using a mean sediment diameter of 420 µm the ridge increases in height, which was also found from initial modelling tests without waves or a net current, see Section 4.5. The time-averaged suspended-load transport using a mean sediment diameter of 420 µm is smaller than using a mean sediment diameter of 300 or 225 µm. The time-average bed-load transport is bigger than using a mean sediment diameter of 300 or 225 µm.

This effect on sediment transport of the mean sediment diameter is opposite proportional to the effect on sediment transport of waves (see Section 4.5); coarse sediment leads, like small waves, to relatively small suspended-load transports as a result of which bed-load transports are dominant and the ridge increases in height. With small sediments or large waves, suspended-load transports dominate bed-load transports and the ridge decreases in height

The increase in height was also observed from measurements of 1986 and 1991. As the morphological development between 1986 and 1991 is not exemplary and an average decrease in height of about 0.10 m/yr was found over a longer period (see chapter 3), it was

decided to use a mean sediment diameter of 300 µm in the morphological computations to provide sediment transports and morphology that represents the long-term behaviour of the ridge.

Figure F.02 shows the bottom profile development and time-averaged bed- and suspended-load transports for simulations using a mean sediment diameter of 225, 300 and 420 µm.

5.7.2.4 Multiplication factor on the bed-load transport (BED)

In Delft3D Sediment-Online a multiplication factor on the bed-load transport can be applied for calibration purposes. Here, the sensitivity of the model to variations of the multiplication factor was investigated, simulations were carried out with multiplication factor on the bed-load transport of 0.25, 0.50, 1.00 and 1.50.

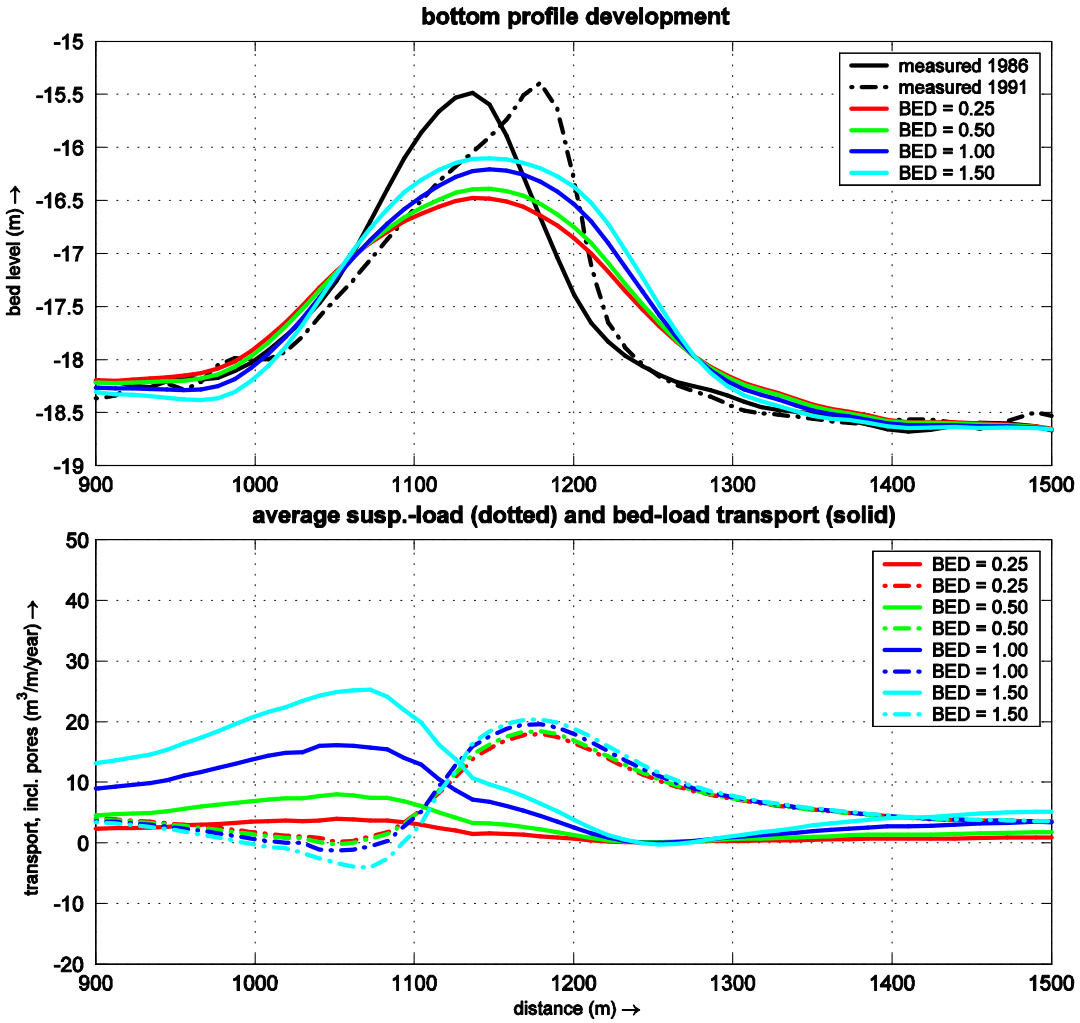

Figure 5-19 Bottom profile development and time-averaged transports using different multiplication factors for the bed-load transport (BED)

Figure 5-19 shows the computed bottom profiles and average suspended and bed-load transport rates using multiplication factors on the bed-load transport (BED) of 0.25, 0.50,

1.00 and 1.50. From this figure it follows that reducing the bed-load transport leads to overestimation of the top-erosion of the ridge due to the increasing dominancy of suspended-load transport, see Section 4.5 and 5.7.2.3. A multiplication factor on the bed-load transport of 1.0 is selected for use in the validation runs.

Figure F.04 shows the bottom profile development and time-averaged bed- and suspended-load transports for simulations using multiplication factors on the bed-load transport (BED) of 0.25, 0.50, 1.00 and 1.50.

5.7.2.5 Multiplication factor on the suspend-load transport (SUS)

In Delft3D Sediment-Online a multiplication factor on the suspended-load transport can be applied for calibration purposes. Here, the sensitivity of the model to variations of the multiplication factor was investigated, simulations were carried out with multiplication factor on the suspended-load transport of 0.25, 0.50, 1.00 and 1.50.

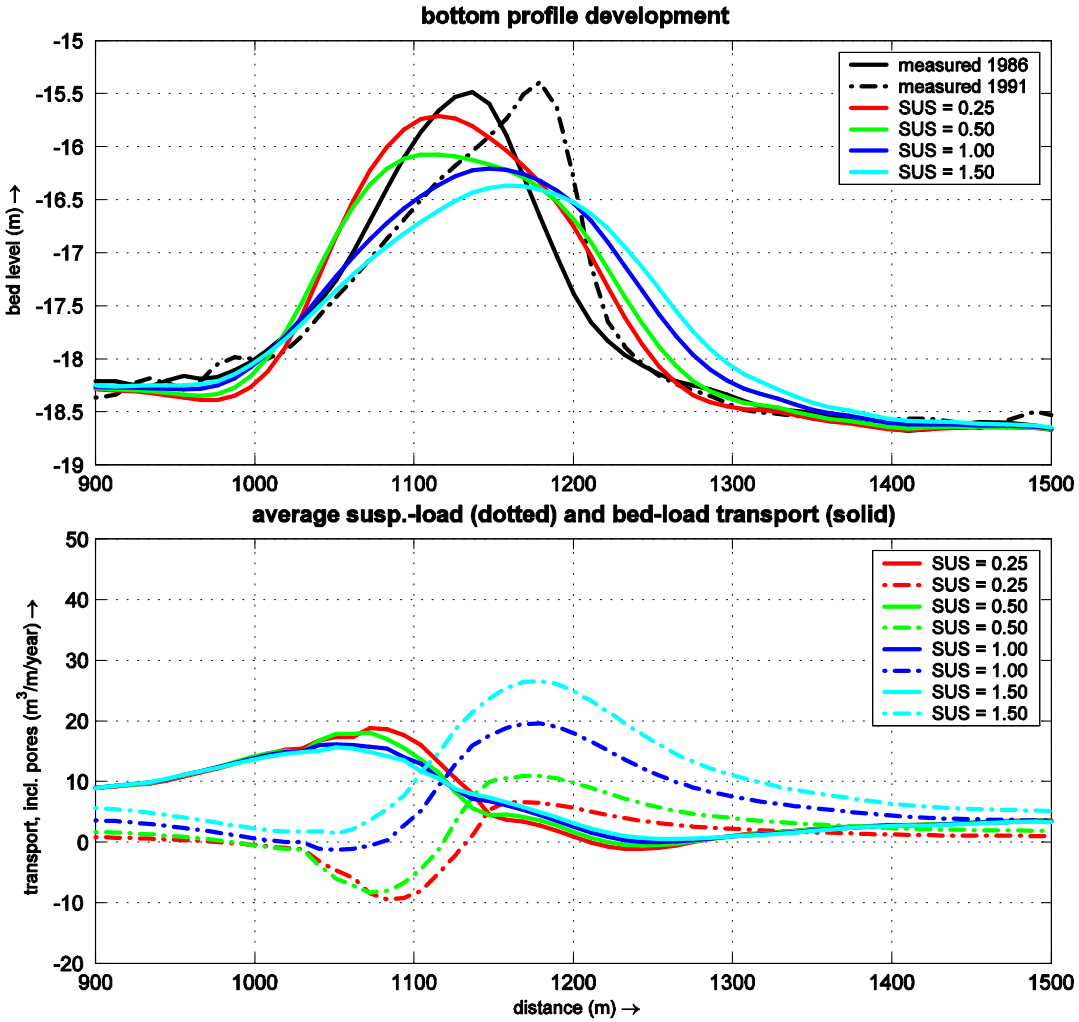

Figure 5-20 Bottom profile development and time-averaged transports using different multiplication factor for the suspended-load transport (SUS)

Figure 5-20 shows the computed bottom profiles and average suspended and bed-load transport rates using multiplication factors on the suspended-load transport (SUS) of 0.25, 0.50, 1.00 and 1.50 . From this figure is was found that with reduced suspended-load transport the ridge migrates in ebb-direction and increases in height, like with small waves or large sediments, see Section 4.5 and 5.7.2.3. A multiplication factor on the suspended-load transport of 1.0 is selected for use in the validation runs.

Figure F.05 shows the bottom profile development and time-averaged transports for simulations using a SUS factor of 0.25, 0.50, 1.00 and 1.50.

5.7.2.6 Longitudinal bed-gradient factor for bed-load transport

Within the Sediment-Online add-on of Delft3D it is possible to adjust the bed-load transport for bed-lope effects using bed-gradient factors for bed-load transport. Both longitudinal and transverse bed-gradient factors can be altered. Here, the effect of the longitudinal bed-gradient factor is discussed, the transverse bed-gradient factor is of no importance in a 2DV simulation. The magnitude of the bed-load transport vector is adjusted if a bed slope exists in the direction of the bed-load transport vector.

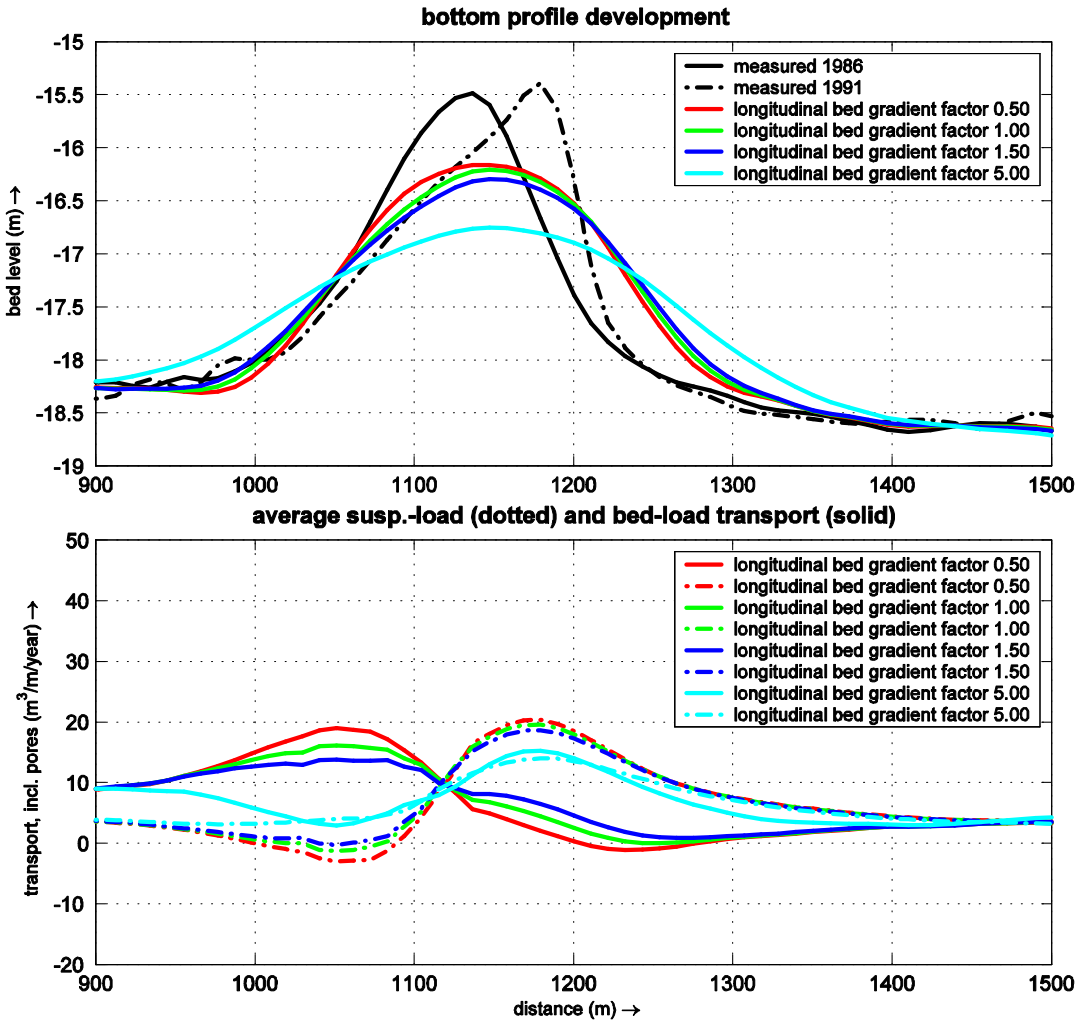

Figure 5-21 Bottom profile development and time-averaged transports using different longitudinal bed gradient factors.

Figure 5-21 shows the computed bottom profiles and average suspended and bed-load transport rates using longitudinal bed-gradient factor of 0.50, 1.00, 1.50 and 5.00. From this figure it can be seen that increasing the longitudinal bed-gradient factor for bed-load transport increases transports from the top of the ridge to the toes, the ridge itself therefore erodes faster, this is also shown from the average bed-load transports. A longitudinal bed-gradient factor of 1.0 is selected for use in the validation runs.

Figure F.06 shows the bottom profile development and time-averaged bed- and suspended-load transports for simulations using longitudinal bed-gradient factor of 0.50, 1.00, 1.50 and 5.00.

5.8 Synthesis

In this study both transect model applications (1DH, 2DV) and area models (2DH, 3D) will be used to simulate the morphological development of the sand ridge Hoek van Holland. Boundary conditions for these models were generated using the well-calibrated Holland Coastal Zone (HCZ) model and were eventually converted into harmonic components to allow for simulation of any calendar period in time.

To reduce computational time, a representative, morphological tide was derived using the method of Latteux (1995). The morphological tide gives an optimal representation of the residual (e.g. yearly averaged) sediment transports. The determination of a morphological tide to schematize the full neap-spring tidal cycle showed that the morphological tide is quite sensitive to the water depth considered when waves are taken into account. It was shown that outside of the ridge location the net transport from a neap-spring tidal cycle is to the north due to the dominant flood velocities. On top of the ridge the net transport from a neap-spring tidal cycle is to the south (ebb-dominated) due to the dominant effect of waves during ebb (shallower water). These effects were taken into account by a weighting procedure using data points distributed over the area including the ridge.

The tide-averaged transports from the derived morphological tide were evaluated against time-averaged transports using a full neap-spring tidal cycle. It was found that the net tide-integrated transport in southern direction at the top of the ridge is overestimated somewhat and that transport rates outside the ridge at section 3 and 6 were underestimated. Transport rates at section 4 and 5 are accurately represented using the morphological tide. Furthermore, morphological simulations using a full neap-spring tidal cycle were compared to simulations using the morphological tide. From this, it was found that using the morphological tide the decrease in height of the ridge was larger and that at section 3 and 4 the migration was underestimated in comparison to the results using a full neap-spring tidal cycle. At deeper water the migration was accurately represented with the morphological tide.

Given the encouraging modelling results and computational efficiency and for consistency and compatibility reasons, it was decided to use the selected morphological tide for both the line (1DH, 2DV) and area models (2DH, 3D).

Two suitable wave schematizations are available. The single representative wave from Walstra et al. (1997) was derived to give the best representation of the overall, yearly wave climate at location Euro-Maas channel by applying the Latteux method to evaluate residual transports. A representative wave climate from Roelvink et al. (1998) was selected from wave data close to the port of Rotterdam over the period June 1990 – July 1991 and consists of 11 wave conditions. Both wave schematizations were evaluated in a 2DV sensitivity analysis.

It was found that the single representative wave of Walstra et al. (1997) leads to a morphological development that is in good agreement with the long-term average development of the sand ridge Hoek van Holland and it was decided to use this representative wave for the simulation of the morphological development of the sand ridge Hoek van Holland with both the line (1DH, 2DV) and area models (2DH, 3D). The representative wave climate leads to a larger decrease in height and smaller migration of the ridge than the single representative wave from Walstra et al (1997), without waves the ridge increased in height, which was also found from the idealized sand ridge modelling in chapter 4.

The 2DV sensitivity analysis further showed that with larger values for the horizontal eddy diffusivity the ridge erodes at a considerable rate; a value of 1.00 m2/s was found to lead to results that are in good agreement with the long-term averaged development of the ridge.

Next, the sensitivity of the model to the mean sediment diameter D_{50} was investigated. A value of 420 μm, which is the mean sediment diameter on top of the ridge, was found to lead to an increase in height of the ridge due to the dominant effect of bed-load transport over suspended-load transport, see chapter 4. A value of 300 μm was found to lead to characteristic morphological development of the ridge and characteristic transport rates.

Within Delft3D multiplication factors on the bed-load and suspended-load transport can be applied for calibration purposes. The sensitivity of the model to variations in these multiplication factors were investigated. It was found that with reduced suspended-load transport the ridge migrates in ebb-direction and increases in height, which complies with the findings of chapter 4. With increasing transport the ridge erodes at a larger rate. No multiplication factors were applied as transport rates were in good agreement with known values and the morphological development was in good agreement with the long-term average development as found from measurements.

6 Model results of sand ridge near Hoek van Holland

6.1 Introduction

In this chapter the set-up of the area model (2DH, 3D) for the validation runs is discussed in Section 6.2. Next, in Section 6.3 the validation runs of both the line model and the area model are discussed. Results of both models are given in single plots for mutual comparison. The simulations in this chapter were carried out using an older version and an improved version of Delft3D. In Section 2.3.3.3 the main difference in bottom layer sub-grid model between both versions is discussed. The results of the older version are presented in Section 6.3. In Section 6.4 modelling results with both versions are compared for simulations at section 4 over a period of 9 and 14 years.

6.2 Model set-up area model (2DH, 3D)

In this Section the model set-up of the area model (both 2DH and 3D) is given. First the FLOW schematizations are given, which include the computational grid, model bathymetry, open boundary conditions and time parameters. The different processes used and physical parameters are also given. Next, the wind- and wave schematizations and transport settings are discussed.

2DH vs 3D

Both the 2DH and the 3D set-up is discussed in this Section, the main difference being the number of vertical layers; the 2DH simulation is a depth-averaged simulation which reduces the computational times involved; no turbulence model and no eddy diffusivity settings need to specified. For the 3D simulation a vertical grid needs to be specified, along with the turbulence and eddy settings mentioned. These 3D settings are clearly stated hereafter.

6.2.2 FLOW schematizations area model (2DH and 3D)

6.2.2.1 Computational grid

The morphological computations aiming at predicting the morphological development of the ridge require a high resolution at the location of the ridge. From simulations with the 2DV model it was found that a horizontal, longshore grid size of about 10 m at the location of the ridge is required for accurate morphological simulation of the ridge development. The computational grid of the area model was constructed by taking a selection of the HCZ-model, which was locally refined for accurate representation at the location of the ridge. Figure 6-1 shows the computational grid of the area model (left).

The constructed grid covers an area of about 40 km alongshore and 27 km in seaward direction and consists of 66 x 180 grid cells. The longshore grid cell size varies from about 1700m at the lateral boundaries to about 12m in the ridge vicinity, the cross-shore grid cell size varies from about 1400m at the coast-parallel seaward boundary to about 100m at the location of the ridge.

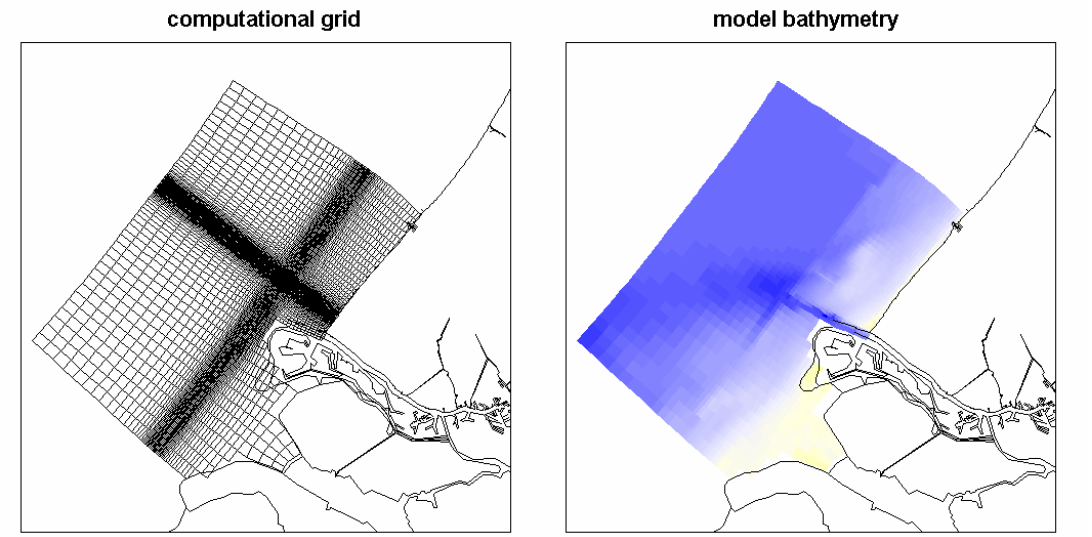

Figure 6-1 Computational grid (left) and model bathymetry (right) of the area model.

Vertical grid (3D)

For 3-dimensional computations with the area model, a so-called sigma-coordinate vertical grid was specified. This means that the total water depth is divided into a number of layers each covering a percentage of the total water depth. Using these sigma layers results in the same vertical resolution in the entire model domain regardless of the local water depth. Here, the distribution of the relative layer thickness is non-uniform to allow for more resolution in the near bed area.

From 2DV simulations it was found that a vertical grid of 10 computational layers with a logarithmic layer distribution and a relative bottom layer thickness of 2% of the water depth ensure accurate representation of the sediment transports, see section 4.3.1. The layer distribution, i.e. the thickness of the individual layers is given in Figure 6-2. It can be seen the variation-factor for each layer is 1.33, which complies with the criteria specified in the Delft3D manual that states the vertical grid must have a smooth distribution; i.e. the variation-factor for each layer should not exceed 0.7 – 1.4.

layer	relative thickness (%)
1 (water surface)	26.439
2	19.846
3	14.897
4	11.182
5	8.393
6	6.300
7	4.729
8	3.550
9	2.665
10 (bed)	2.000

Figure 6-2 Vertical grid resolution of the area model.

6.2.2.2 Model bathymetry

The model bathymetry was generated using morphology data of the ridge from the national institute for Coastal and Marine Management (RIKZ). This data is described in chapter 3 and was converted from UTM coordinates to Paris coordinates for consistency with the HCZ-model. The HCZ-bathymetry was used at the remaining areas. First, the ridge data was interpolated to the grid using triangular interpolation. Then, the remaining area was interpolated from the HCZ-model using triangular interpolation. Following this method bathymetries for 1986, 1991 and 2000 were generated. In the HCZ-model, the "slufter" at the south-western tip of the Maasvlakte and the "van Dixhoorn driehoek" north of the entrance channel to the port of Rotterdam were not included in the land boundary of the model, both were schematized as negative depths, this also applies for the area model. The model bathymetry of 1991 of the area model is shown in the right plot of Figure 6-1.

To allow for a high morphological scale factor a small strip of a few grid cells along the coast was made un-erodable. This non-erodable strip adjacent to the coastline does not affect morphological computations further away from the coastline; the morphological development of the ridge is not affected.

6.2.2.3 Time scale parameters

For the validation of the area model two periods were simulated, the first period runs from January 26th 1986 to March 18th 1991 and the second period runs from March 18th 1991 to October 19th 2000. These periods allow for comparison of computational results with measurements.

The area model was run with cyclic boundary conditions for time-efficient morphological computations. A cyclic period of 1485 minutes was derived based upon the prerequisite that the sediment transport over the cyclic period should equal the long-term average sediment

transport, see Figure 5-14. The simulation time should equal an integer number of morphological cycles; 8 cycles were used for both periods

The time step used in Delft3D depends on several parameters, such as required accuracy, stability, grid size and water depth. An indication of the magnitude of the time step is the Courant number for wave propagation, it gives the relation between wave propagation, time step and the smallest grid size in either x- or y-direction. Delft3D uses a numerical scheme that is unconditionally stable, the Courant number therefore may be as high as 20. The time step used in the area model was 15 s, resulting in a Courant number of about 16.

6.2.2.4 Open boundary conditions and discharges

The model has three open boundaries; two lateral and a coast-parallel seaward boundary. Each open boundary is divided in a number of boundary segments, at the intersection points of the boundary segments open boundary conditions need to be specified. All open boundaries were specified as water level boundaries. Boundary conditions were generated from the HCZ-model, the morphological cycle of October 21 1991, 03hrs57m to 22 October 1991, 04hrs42m was used herein.

Two discharges were included in the model. The discharge from the Nieuwe Waterweg was obtained from the HCZ-model. Furthermore, the long-term average discharge of 660 m^3/s at the Haringvliet sluices was used.

6.2.2.5 Processes and physical parameters

The area model was set-up to include several processes, which will be discussed separately hereafter:

- wind
- waves
- salinity
- sediments

The physical parameters in the area model were:

- Coriolis acceleration was set up for 52 °N,
- Acceleration of gravity was set to 9.8100 m/s^2
- Air density was 1.000 kg/m^3
- Water temperature was 15 °C

6.2.2.6 3D schematizations

For the 3D simulation a vertical grid was specified, see Section 6.2.2.1. Furthermore, the algebraic turbulence model was used as it proved better suited for use with the TRANSPOR2004 equations in the 2DV calibration and is more time-efficient than other turbulence models, which is a big advantage here. The horizontal eddy diffusivity was set to 1.00 m^2/s, which was found accurate for the equivalent grid sizes in the 2DV model.

6.2.3 Wind

The model was set-up to represent average conditions. The wind-field was simplified into a single representative speed and direction which yields the same alongshore and cross-shore wind stress is averaged over the entire wind-field. This representative speed and direction were taken as 7 m/s and 240°, the validity of these values was tested and confirmed against long-term wind records at 5 stations within the FLYLAND project (Roelvink et al., 2001b)

6.2.4 Wave schematization

The single representative wave condition from Walstra et al. (1997) was used, which was derived to give the best representation of the overall, yearly wave climate at location Euro-Maas channel by applying the Latteux method to evaluate residual transports, see Figure 6-3

Study	H_s (m)	T_p (s)	Direction (° N)	Period (%)
Walstra et al. (1997)	2.25	6.6	315	84

Figure 6-3 Single representative wave condition from Walstra et al. (1997).

6.2.5 Transport parameters

The Sediment-Online add-on of Delft3D was used for simultaneous computation of flows and transports and simultaneous feedback to bottom changes; the elevation of the bed is dynamically updated each time step. The advantage of this over an offline morphological computation is that the hydronamic flow computations are always carried out using the correct bathymetry. The Sediment Online add-on was used in combination with the TRANSPOR2004 sediment transport model and the bed roughness predictor. Sediment characteristics and Online-Sediment parameters used are given in Table 6-1.

sediment characteristics	
sediment density	2650 kg/m^3
dry bed density	1600 kg/m^3
mean sediment diameter D_{50}	300 μm
Online-Sediment parameters	
morphological scale factor	382.225
spin-up time	1485 minutes
equilibrium concentrations at inflow boundaries	true
effect sediment on density gradient	true
updating bed at inflow boundaries	false

Table 6-1 Sediment charachteristics and Online-Sediment parameters

The morphological scale factor used to speed up morphological changes to that of the selected periods is:

- 191.12 for the period of January 26th 1986 to March 18th 1991
- 355.75 for the period of March 18th 1991 to October 19th 2000

6.3 Results

Herein the model results are discussed, figures are given in appendix G. Simulations were carried out using different model approaches; 1DH. 2DV, 2DH and 3D simulations were used to compute the morphological development of the ridge over the periods 1986-1991 and 1991-2000 for Section 3-6.

6.3.1 Computed bottom profile development and time-averaged transports

6.3.1.1 Section 3

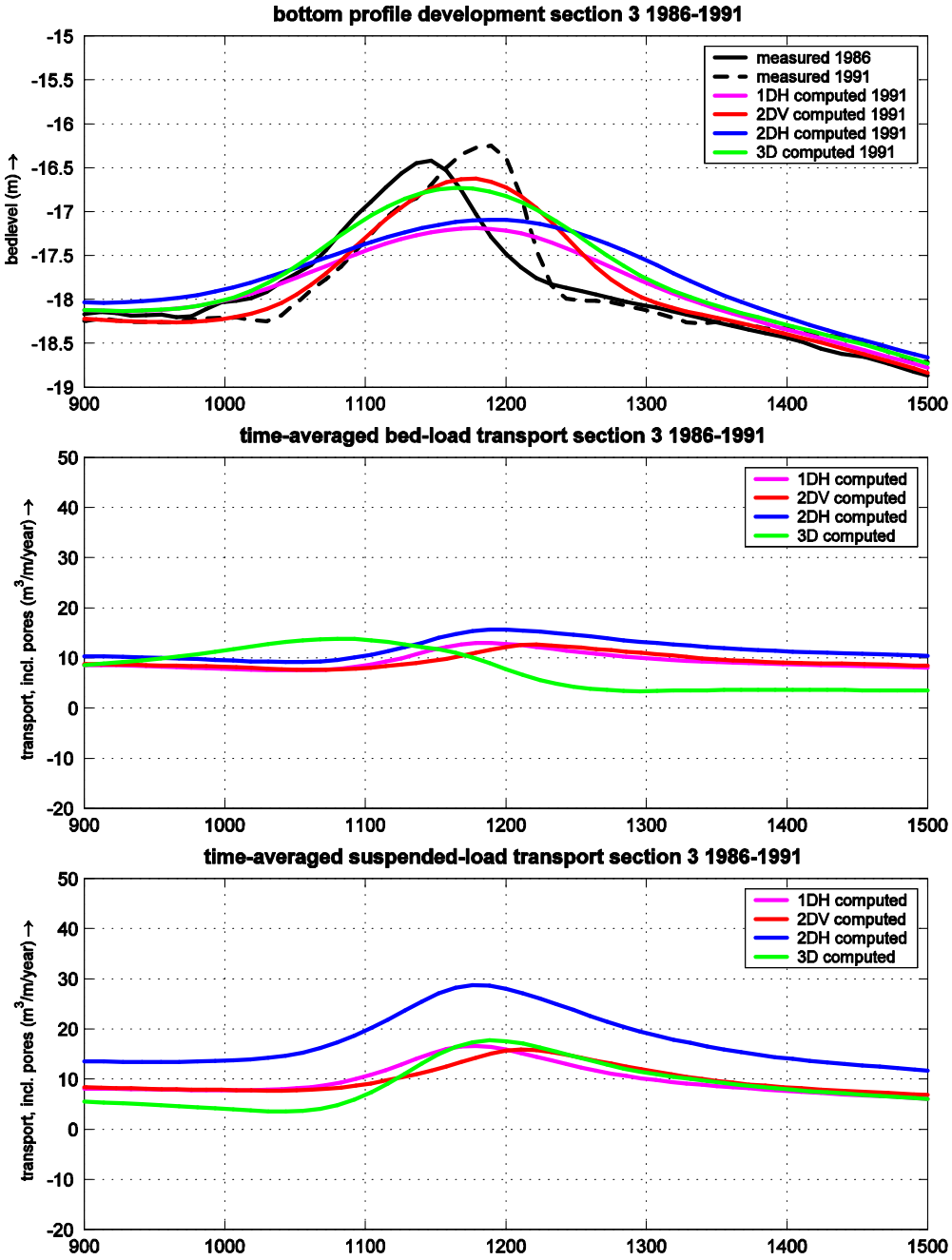

Figure 6-4 Computed bottom profile development and time-averaged bed-load and suspended-load transport between 1986 and 1991 for section 3 using 1DH, 2DV, 2DH and 3D simulations.

1986 - 1991

Figure 6-4 and G.01 show the computed bottom profile development and time-averaged bed-load and suspended-load transports between 1986 and 1991 for section 3 using a 1DH, 2DV, 2DH and 3D model approach. It can be seen that all simulations show a reduction in height of the ridge, while measurements show an increase in ridge-height of about 0.25 m. Both multi-layer simulations (2DV and 3D) show a significantly smaller reduction in height than the 1DH and 2DH simulations. The computed migration of the ridge from all model approaches is in north-western direction and is in good agreement with measurements that showed a migration of about 75 m. It was found that migration is slightly larger using the single-layer model approaches (1DH and 2DH) than with the 2DV and 3D model approach. The migration from the 3D simulation is slightly smaller than the migration from the 2DV simulation, with the single layer simulations it's the other way around; the migration from the area model approach (2DH) is slightly larger than migration from the line model approach (1DH).

Time-averaged bed-load transport from the 1DH, 2DV and 2DH simulation is about 10 m3/m year, incl. pores and increases at the top of the ridge to about 15 m^3/m year, incl. pores after which it decreases to about 10 m^3/m year, incl. pores. The time-averaged bed-load transports from the 3D simulation is about 10 m^3/m year, incl. pores but is at it's maximum at the southern slope of the ridge and decreases at the top and is about 5 m^3/m year, incl. pores north of the ridge. Time-averaged suspended-load transport from the 1DH, 2DV and 3D simulation is about 8 m^3/m/yr, incl. pores south and north of the ridge and is about 15 m3/m/yr at the top of the ridge. Time-averaged suspended-load transport from the 2DH simulation is about 7.5 m^3/m/yr, incl. pores higher than from the 1DH, 2DV and 3D simulations.

1991-2000

Figure G.02 shows the computed bottom profile development and time-averaged bed-load and suspended-load transports between 1991 and 2000 for section 3 using a 1DH, 2DV, 2DH and 3D model approach. Measurements show a decrease in height of about 0.25 m and a northward migration of about 50m. It can be seen that the decrease in height of the ridge from both the 2DV and the 3D simulations are in reasonable agreement with measurements, while the 1DH and 2DH simulations overestimate the decrease in height. The computed migration of the ridge from all model approaches is about 100 m in north-western direction and thus is overestimated in comparison with the measurements.

Time-averaged bed-load transport from the 1DH, 2DV, 2DH and 3D simulation is about 10 m^3/m/yr, incl. pores and gradually increases to 14 m^3/m/yr at the top of the ridge, the 2DV time-averaged bed-load transport shows a sudden increase to about 17.50 m^3/m/yr at the top of the ridge. Time-averaged suspended-load transport from the 1DH, 2DV and 3D simulation is about 10 m^3/m/yr, incl. pores south and north of the ridge, while the time-averaged suspended-load transports from the 2DH simulation are about 7.5 m^3/m/yr, incl. pores higher. Time-averaged suspended-load transports from both the 2DV and 3D simulation increase rapidly at the location of the top , while transports from both the 1DH and 2DH simulation increase gradually.

6.3.1.2 Section 4

1986-1991

Figure G.03 shows the computed bottom profile development and time-averaged bed-load and suspended-load transports between 1986 and 1991 for section 4 using a 1DH, 2DV, 2DH and 3D model approach. It can be seen that all simulations show a reduction in height of the ridge, while measurements show that the top of the ridge stays at approximately MSL – 15.5m. The 2DV simulation shows a significantly smaller reduction in height than the 1DH, 2DH and 3D simulations. The computed migration from all model approaches is in north-western direction; migration of the ridge from the 2DV and 3D simulations is underestimated in comparison with measurements that showed a migration of about 80 m. The migration from the 1DH and 2DH simulations in reasonable agreement with the measurements.

Time-averaged bed-load transport from the 1DH, 2DV and 2DH simulation is about 10 m^3/m year, incl. pores and increases at the top of the ridge to about 15 m^3/m year, incl. pores after which it decreases to about 10 m^3/m year, incl. pores. The time-averaged bed-load transport from the 3D simulations about 10 m^3/m/yr, incl. pores south of the ridge, increases at the southern slope and decreases at the top and is about 5 ^{m3}/m/yr north of the ridge.
Time-averaged suspended-load transport from the 1DH and 2DV simulation is about 7.5 m^3/m/yr, incl. pores south and north of the ridge and is about 17 m^3/m/yr at the top of the ridge. Time-averaged suspended-load transport from the 2DH simulation is about 10 m^3/m/yr, incl. pores higher than from the 1DH, 2DV simulations, while time-averaged suspended-load transport from the 3D simulation is equal to the transports from the 1DH and 2DV simulations north of the ridge, it subsequently tends to the values of the 2DH simulation south of the ridge.

1991-2000

Figure G.04 shows the computed bottom profile development and time-averaged bed-load and suspended-load transports between 1991 and 2000 for section 4 using a 1DH, 2DV, 2DH and 3D model approach. Measurements show a decrease in height of about 0.65 m and a northward migration of about 80 m. It can be seen that the decrease in height of the ridge from both the 2DV and the 3D simulations are in reasonable agreement with measurements, while the 1DH and 2DH simulations overestimate the decrease in height. The computed migration of the ridge from all model approaches is about 70 m in north-western direction and thus is in good agreement with the measurements.

Time-averaged bed-load transport from all simulations is about 10 m^3/m/yr, incl. pores and transports from the 1DH and 2DH simulation gradually increase to 14 m^3/m/yr at the top of the ridge, while the 2DV and 3D time-averaged bed-load transport shows a sudden increase to about 17.50 m^3/m/yr at the top of the ridge. Time-averaged suspended-load transport from the 1DH, 2DV and 3D simulation is about 10 m^3/m/yr, incl. pores south and north of the ridge, while the time-averaged suspended-load transports from the 2DH simulation is about 10 m^3/m/yr, incl. pores higher. Time-averaged suspended-load transports from both the 2DV

and 3D simulation increase rapidly at the location of the top , while transports from both the 1DH and 2DH simulation increase gradually.

6.3.1.3 Section 5

1986-1991

Figure G.05 shows the computed bottom profile development and time-averaged bed-load and suspended-load transports between 1986 and 1991 for section 5 using a 1DH, 2DV, 2DH and 3D model approach. Measurements show a slight increase in height of about 0.15 m, while the 1DH and 2DH simulations show a decrease in height of about 2.00 m and the 2DV and 3D simulations show a decrease in height of about 1.20 m. The computed migration of the ridge from all model approaches is about 25 m in north-western direction and thus is severely underestimated in comparison with the measurements that showed a migration of about 100 m.

Time-averaged bed-load transport from the 1DH, 2DV and 2DH simulations is about 5 m^3/m year, incl. pores south of the ridge and increases at the top of the ridge to about 15 m^3/m/yr, incl. pores after which it decreases to about 5 m^3/m/yr, incl. pores north of the ridge. The time-averaged bed-load transport from the 3D simulation show the shifted pattern with increasing bed-load transport at the southern slope and decrease at the top and is about 15 m^3/m/yr south of the ridge and about 0 m^3/m/yr north of the ridge. Time-averaged suspended-load transport from the 1DH and 2DV simulation is about 2 m^3/m/yr, incl. pores south and north of the ridge and is about 17 m^3/m/yr at the top of the ridge after which it decreases to the original value. While the time-averaged suspended-load transport from the 3D simulation is in southward direction and the 2DH time averaged suspended-load transport is in northern direction south of the ridge, both increase to about 30 m^3/m/yr incl. pores at the top of the ridge after which both decrease to about 7.5 m^3/m/yr ,incl. pores in northern direction north of the ridge.

1991-2000

Figure G.06 shows the computed bottom profile development and time-averaged bed-load and suspended-load transports between 1991 and 2000 for section 5 using a 1DH, 2DV, 2DH and 3D model approach. Measurements show a decrease in height of about 1.25 m and a northward migration of about 80 m. It can be seen that the decrease in height of the ridge from both the 2DV and the 3D simulations are in fair agreement with measurements, while the 1DH and 2DH simulations overestimate the decrease in height. The computed migration of the ridge from the 2DV and 3D simulations is about 10 m in southern direction and is thus inaccurate. The migration from the 1DH and 2DH simulations is about 150 m in northern direction and is thus overestimated

Time-averaged bed-load transport from all simulations is about 5 m^3/m/yr, incl. pores and transports from the 1DH and 2DH simulation gradually increase to 12 m3/m/yr at the top of the ridge, while the 2DV and 3D time-averaged bed-load transport shows a sudden increase to about 17.50 m^3/m/yr at the top of the ridge. Time-averaged suspended-load transport from

the 1DH, 2DV and 3D simulation is about 0 m^3/m/yr, incl. pores south and north of the ridge, while the time-averaged suspended-load transport from the 2DH simulation is about 10 m^3/m/yr, incl. pores higher. Time-averaged suspended-load transports from both the 2DV and 3D simulation increase rapidly at the location of the top, while transports from both the 1DH and 2DH simulation increase gradually.

6.3.1.4 Section 6

1986-1991

Figure G.07 shows the computed bottom profile development and time-averaged bed-load and suspended-load transports between 1986 and 1991 for section 6 using a 1DH, 2DV, 2DH and 3D model approach. Measurements show a decrease in height of about 1.20 m, the 2DV and 3D simulations show a decrease in height of about 1.40 m and are thus in reasonable agreement with measurements. The 1DH and 2DH simulations show a decrease in height of about 2.00 m and thus overestimate the decrease in height. The computed migration of the ridge from all model approaches is about 10 m in north-western direction with the 2DV and 3D simulations and about 50 m from 1DH and 2DH simulations and thus is underestimated in comparison with the measurements that showed a migration of about 100 m.

Time-averaged bed-load transport from the 1DH, 2DV and 2DH simulations is about 0 m^3/m year, incl. pores and increases at the top of the ridge to about 10 m^3/m/yr, incl. pores after which it decreases to about 5 m^3/m/yr, incl. pores. The time-averaged bed-load transport from the 3D simulation show the shifted pattern with increasing bed-load transport at the southern slope and decrease at the top and is about 15 m^3/m/yr south of the ridge and about 0 m^3/m/yr north of the ridge. Time-averaged suspended-load transport from the 1DH and 2DV simulation is about 2.5 m^3/m/yr, incl. pores in southern direction south of the ridge, about 10 m^3/m/yr in northern direction at the top of the ridge after which it decreases to about 0 m^3/m/yr, incl. pores. While the time-averaged suspended-load transport from the 3D simulation is in southward direction and the 2DH time averaged suspended-load transport is in northern direction south of the ridge, both increase to about 30 m^3/m/yr incl. pores at the top of the ridge after which both decrease to about 7.5 m^3/m/yr ,incl. pores north of the ridge.

1991-2000

Figure G.08 shows the computed bottom profile development and time-averaged bed-load and suspended-load transports between 1991 and 2000 for section 6 using a 1DH, 2DV, 2DH and 3D model approach. Measurements show a decrease in height of about 0.80 m and a northward migration of about 100 m. It can be seen that the decrease in height of the ridge from both the 2DV and the 3D simulations are in fair agreement with measurements, but that the migration is in southern direction and thus inaccurate as measurements show a migration of about 100 m in northern direction. The decrease in height from the 1DH and 2DH simulations is about 2.00 m and is thus overestimated. The computed migration of the ridge from the 1DH and 2DH simulations is about 75 m and is thus in good agreement with the measurements.

Time-averaged bed-load transport from all simulations is about 2 m^3/m/yr, incl. pores and transports from the 1DH and 2DH simulation gradually increase to 10 m^3/m/yr at the top of the ridge, while the 2DV and 3D time-averaged bed-load transport shows a sudden increase to about 17.50 m^3/m/yr at the top of the ridge. Time-averaged suspended-load transport from the 1DH, 2DV and 3D simulation is about 2 m^3/m/yr, incl. pores in southern direction south of the ridge and about 0 m3/m/yr, incl. pores north of the ridge. The time-averaged suspended-load transports from the 2DH simulation are about 10 m^3/m/yr, incl. pores higher. Time-averaged suspended-load transports from both the 2DV and 3D simulation increase rapidly at the location of the top, while transports from both the 1DH and 2DH simulation increase gradually.

6.3.1.5 Underestimation of migration at section 5 and 6

From the model results for section 5 and 6 it was found that the migration at deeper water was underestimated. From the evaluation of the morphological tide shown in Figures E.15 to E.18 it can be seen that the migration from simulations using the morphological tide is similar to that of simulations using a fill neap-spring tidal cycle. Therefore it was concluded that the underestimation of the migration at deeper water is not due to the use of a morphological tide.

6.3.2 Sedimentation / erosion

6.3.2.1 2DH sedimentation / erosion

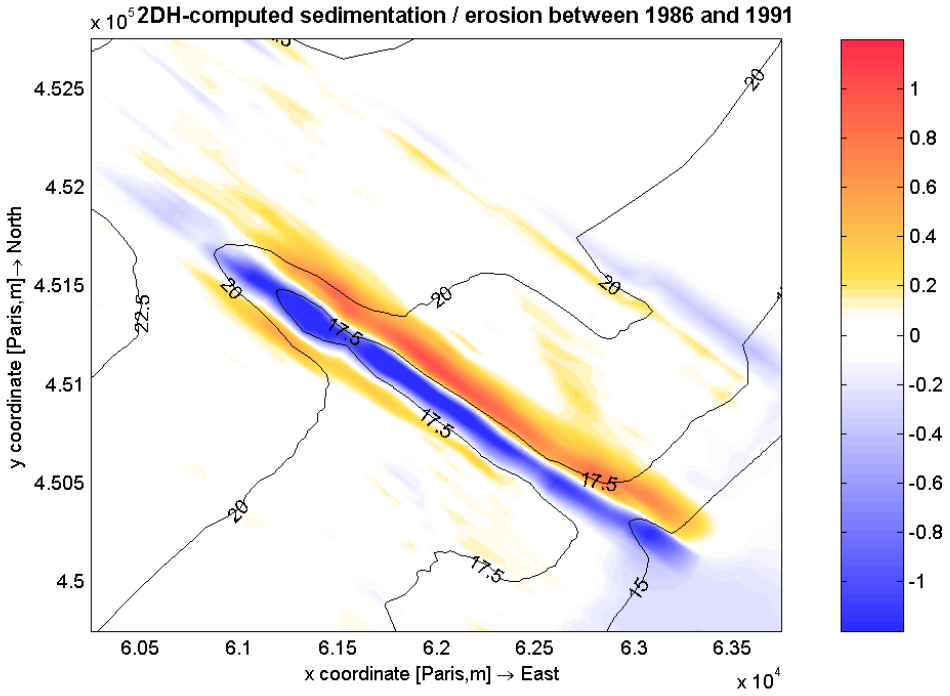

Figure 6-5 2DH-computed sedimentation / erosion between 1986 and 1991 with depth as isolines.

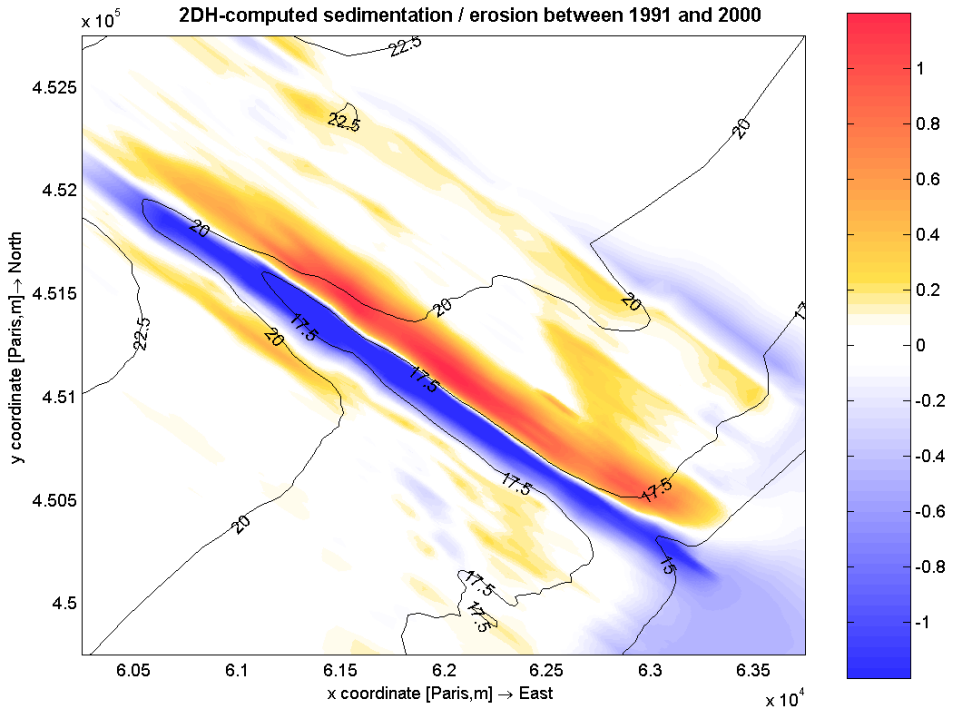

Figure 6-6 2DH-computed sedimentation / erosion between 1991 and 2000 with depth as isolines.

Figure 6-5 shows the 2DH-computed sedimentation and erosion between 1986 and 1991. It can be seen that erosion is limited to the ridge only and that sedimentation occurs over the entire length of the ridge at the north-eastern side and at the deeper part also at the south-western side of the ridge. Figure 6-6 shows the 2DH-computed sedimentation and erosion between 1991 and 2000. It was found that erosion and sedimentation was larger in this period than between 1986 and 1991. It can be seen that sedimentation at the north-eastern side of the ridge is particularly large and takes up a wider area, while sedimentation at the south-western side of the ridge at deeper water is less pronounced.

6.3.2.2 3D sedimentation / erosion

Figure 6-7 shows the 3D-computed sedimentation and erosion between 1986 and 1991. Sedimentation and erosion is clearly smaller than from the 2DH computation, especially at deeper water. Sedimentation was found along the north-eastern side of the ridge and at deeper water, also at the south-western side of the ridge. Figure 6-8 shows the 3D-computed sedimentation and erosion between 1991 and 2000. Again, sedimentation and erosion is smaller than with the 2DH computation, particularly at deeper water. The spatial distribution over the area closely resembles that of the 2DH computation; erosion of the top of the ridge and sedimentation along the entire north-eastern flank of the ridge and at deep water also at the south-western flank.

It was found that both the 2DH and 3D computations lead to an identical spatial pattern of sedimentation and erosion with erosion only of the top of the ridge and sedimentation both along the entire north-eastern flank of the ridge and at deep water also at the south-western

flank of the ridge. It can be seen that sedimentation and erosion from the 2DH computation is larger than from the 3D computation, especially at deep water.

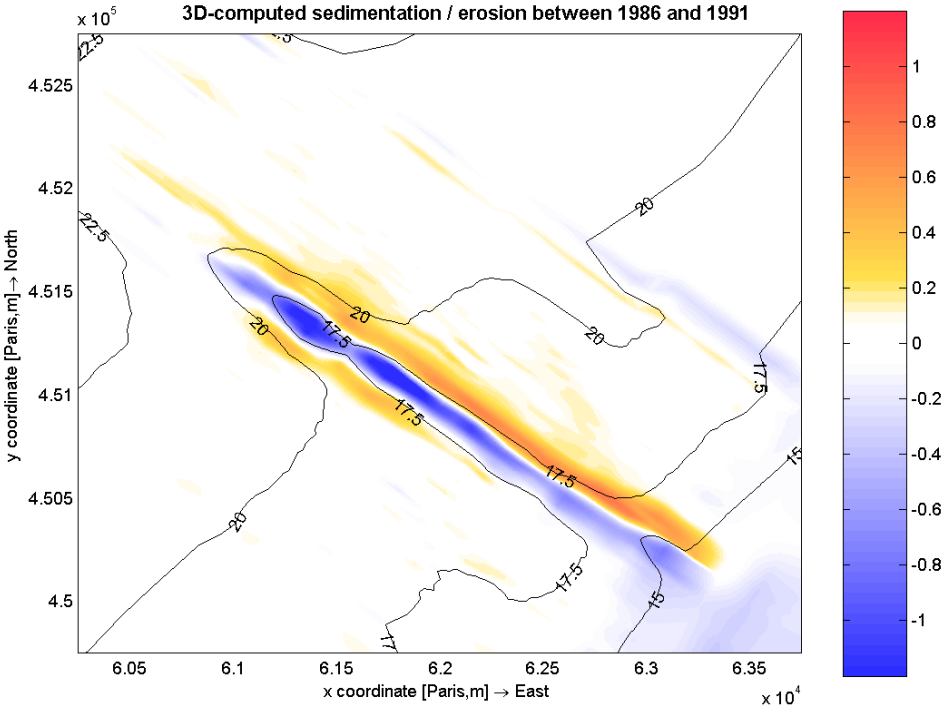

Figure 6-7 3D-computed sedimentation / erosion between 1986 and 1991 with depth as isolines.

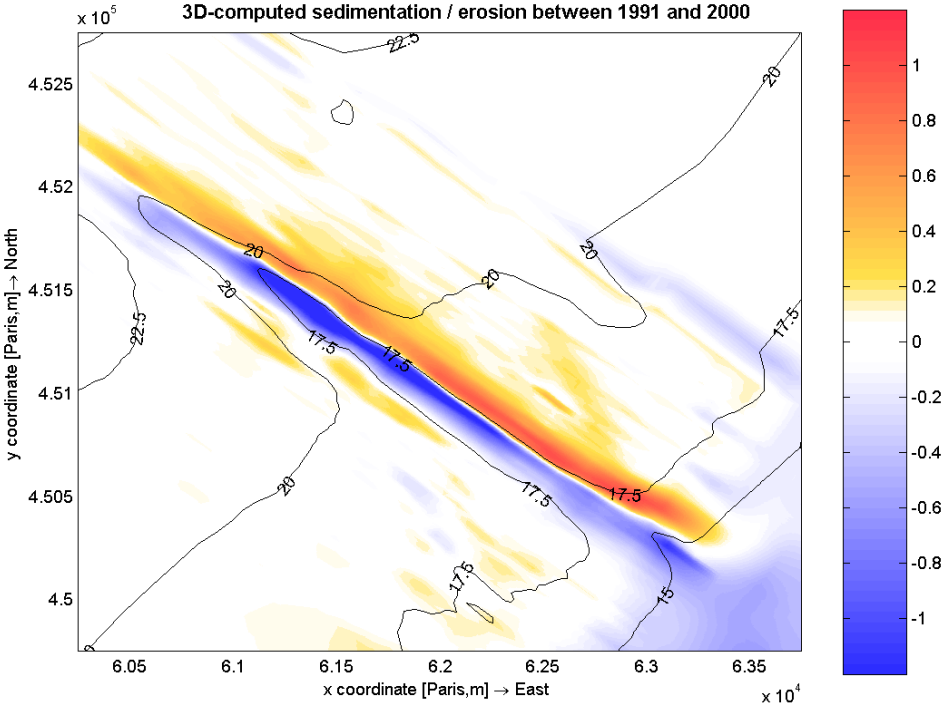

Figure 6-8 3D-computed sedimentation / erosion between 1991 and 2000 with depth as isolines.

6.4 Comparison of modelling results with different Delft3D versions

Herein a comparison is made between the two Delft3D versions used in this study. The Delft3D research version released 11-11-2004 is referred to as the older version and the Delft3D research version released 01-04-2004 is referred to as improved version. The difference in bottom layer sub-grid model between both versions is discussed in Section 2.3.3.3. For simulations using the improved Delft3D version, a new morphological tide was derived. The simulations using the older version are ran with the morphological tide as derived in Section 5.5.3. In all simulations the previously verified model settings as used in section 6.3 were used.

6.4.1 Morphological tide with most recent version.

To guarantee a fair comparison between both versions, a morphological tide was derived using the improved version of Delft3D. The morphological tide was derived for section 4, in similar fashion to the method presented in Section 5.5.2. This morphological tide runs from 21 October 1991, 16hrs27m to 22 October 1991, 17hrs15m and is characterized by tidal velocities between -0.6 and 0.75 m/s and a water level variation between -0.75 and 1.30 m. The morphological tide that was used with the older version was situated only half a day earlier and runs from 21 October 1991, 03hrs57m to 22 October 1991, 04hrs42m and is characterized by tidal velocities between -0.55 and 0.70 m/s and a water level variation between -0.75 and 1.25 m. Both morphological tides are presented in Figure 6-9.

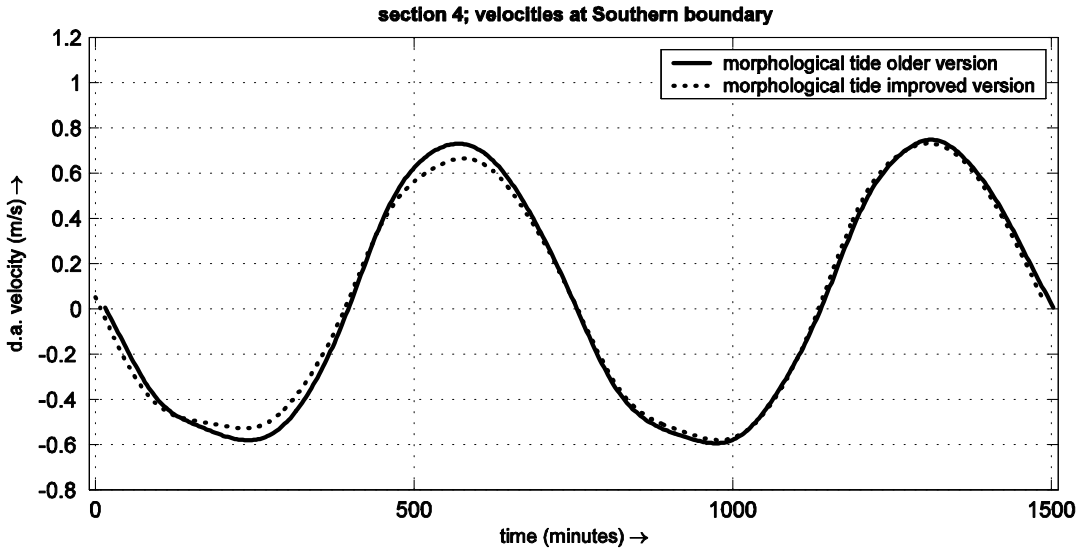

Figure 6-9 Comparison morphological tides

The newly derived morphological tide was evaluated against residual transport rates from a full neap-spring tidal cycle, see Figure G.09 in Appendix G. It was shown that the improved version leads to significantly higher time-averaged suspended-load transport rates than the older version (see Figure Figure 5-8 and E.08.) which is due to the accurate determination of suspended-load transport using the correction vector (see Section 2.3.3.3). Further, the improved version leads to smaller bed-load transports than the older version (see Figure

Figure 5-8 and E.08.) which is due to due to modifications in the combined friction coefficient for waves and currents which is used in the instantaneous grain related bed-shear stress due to both current and wave motion (see Van Rijn et al., 2004).

Also the distribution of the time-averaged suspended-load transport over the ridge has changed; the time-averaged suspended-load transport at the top of the ridge is in flood direction. The time-averaged suspended-load transport using the older version of Delft3D is in ebb-direction at the top of the ridge due to the underestimation of suspended-load transport in the near-bed zone; suspended-load transport therefore reacts much slower to changes in flow regime and especially during ebb, sediments settle further from the top, where they cannot be brought back to the top, resulting in a net transport in ebb direction. Furthermore it was shown that the time-averaged bed-load transport is opposite to the residual current.

From G.09 it can be seen that the morphological tide represents the total transport rates over the ridge rather accurately, although the bed-load transport rates (opposite to the residual current) are over-estimated at the top of the ridge.

6.4.2 Comparison of morphological simulations for section 4

Herein, 2DV simulations using both Delft3D versions were used to compute the morphological development of the ridge over the periods 1986-1991 and 1991-2000 for section 4. In all simulations the exact same model settings were used, except for the morphological tide. Figures G..10, G.11, Figure 6-10 and Figure 6-11 show the computed bottom profile development and time-averaged bed-load and suspended-load transports for both periods for section 4 using the two Delft3D versions used in this study.

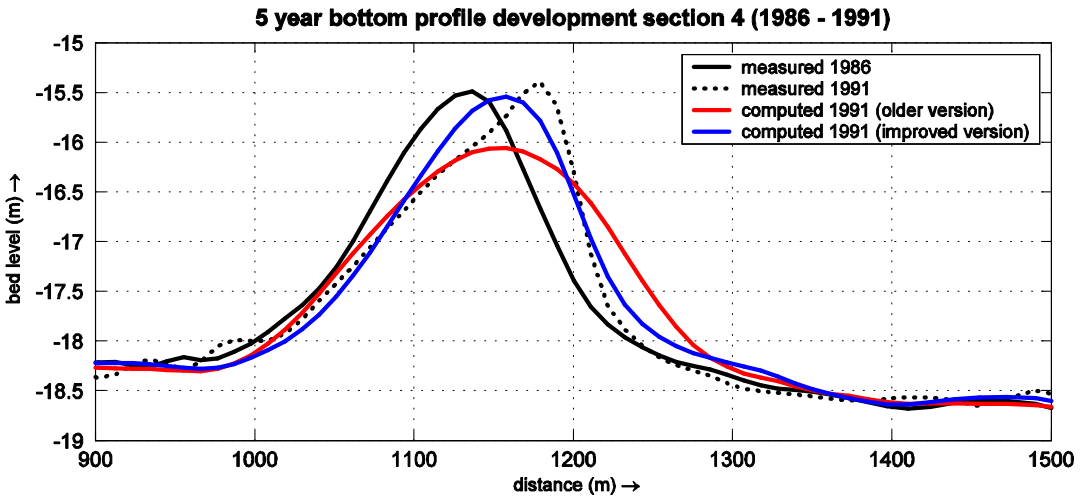

Figure 6-10 Bottom profile development for section 4 between 1986 and 1991 for two Delft3D versions.

Figure 6-10 shows the bottom profile development for section 4 between 1986 and 1991 using the two Delft3D versions used in this study. It can be seen that both versions rather accurately model the migration of the ridge and that the improved version with the new morphological tide leads to a much smaller decrease in height than the older version. The result with the improved version is more in line with measurements. However, the

morphological development between 1986 and 1991 for section 4 is not exemplary and an average decrease in height of about 0.10 m/yr was found over a longer period (see chapter 3), which corresponds with the results using the older Delft3D version.

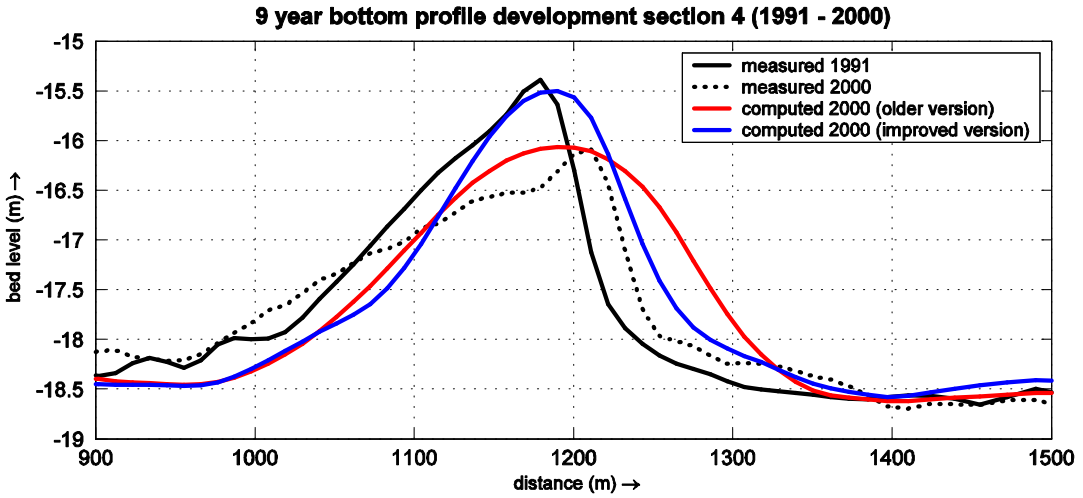

Figure 6-11 Bottom profile development for section 4 between 1991 and 2000 for two Delft3D versions

Figure 6-11 shows the bottom profile development for section 4 between 1991 and 2000 using the two Delft3D versions used in this study. It can be seen that both versions rather accurately model the migration of the ridge and that the improved version with the new morphological tide leads to a much smaller decrease in height than the older version.

Although two different morphological tides were used, both versions lead to similar migration of the ridge, that is in line with measurements. The improved version was ran with the new morphological tide that consists of smaller velocities than the older morphological tide. It can therefore be concluded that the improved versions leads to larger migration of the ridge (equal migration with smaller velocities) which is due to the under prediction of suspended-load transports using the older version, see Section 2.3.3.3. It can be concluded that the morphological development of the sand ridge is very sensitive to the morphological tide used.

It can be seen that the ridge develops rather symmetrically using both versions, which is not in line with the measurements, further the decrease in height using the improved version is under predicted in comparison with measurements, while using the older version the decrease in height was modelled rather accurately. From simulations in Chapter 4 (using the improved Delft3D version) it was found that larger waves lead to a more asymmetric development of the ridge and a larger decrease in height; it therefore is concluded that a larger single representative wave height or a wave climate including storm conditions should be used with the improved version. Further investigation into wave schematization with morphological modelling of sand ridges is required.

6.4.3 14 year morphological simulation

To investigate the validity of the model and model-settings for a time-scales larger than 10 years, a 14 year simulation for section 4 was carried out using two different Delft3D versions.

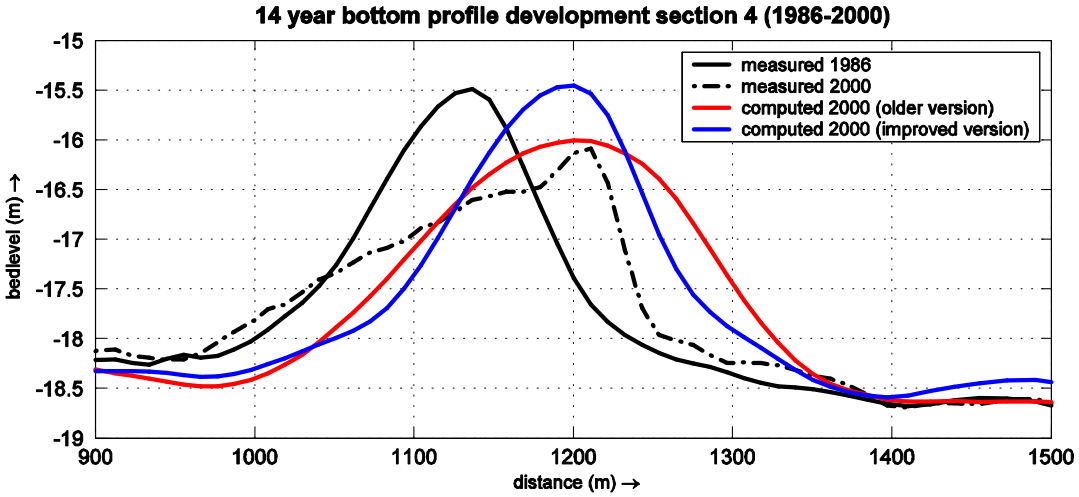

Figure 6-12 Bottom profile development between 1986 and 2000 for two Delft3D versions.

In Figure 6-12 and G.12 the 2DV computed bottom profile development between 1986 and 2000 is given for section 4, it was found that the 2DV model that was setup to simulate the morphological development of the sand ridge can accurately predict the reduction in height on a time-scale of 14 years. Migration of the ridge was slightly over estimated and, compared to the measurements, the ridge develops rather symmetrically. The overall conclusion is that the 2DV Delft3D model can simulated the medium-term sand ridge behaviour with reasonable accuracy.

6.5 Synthesis

Herein, a synthesis of the main findings of this chapter is given. Model results were evaluated against measurements, a distinction was made between results at shallower water depth (section 3 and 4) and deeper water (section 5 and 6).

Morphology

- The computed decrease in height from 2DV and 3D simulations is in good agreement with measurements between 1991 and 2000, which are representative for a longer period. Both the 1DH and 2DH simulation overestimate the decrease in height.
- Measurements show a increasing migration in northern direction with increasing depth. The computed migration from 2DV and 3D simulations is in good agreement at shallower depth but is underestimated with increasing depth and eventually is in southern direction. The computed migration from 1DH and 2DH simulations is overestimated at shallower water depth, but is less sensitive to increasing water depth and therefore in better agreement at deeper water.

Time-averaged bed-load transport

- At shallower water depth, time-averaged bed-load transports from 1DH, 2DV and 2DH simulation are about 10 m3/m/yr, incl. pores and gradually increase to about 15 m3/m/yr, incl. pores at the top of the ridge while time-averaged bed-load transport from the 3D simulations show a different pattern with increasing bed-load transport at the southern slope of the ridge and decreasing transport at the top of the ridge. At deeper water, time-averaged bed-load transports are about 5 m3/m/yr, incl. pores and gradually increase to about 10 m3/m/yr, incl. pores. Just as at shallower depth, transports from the 3D simulation are at it's maximum at the southern slope of the
- Time-averaged bed-load transports from 2DV and 3D simulations for the period 1991-2000 show a rapid increase at the top of the ridge to about 17.50 m3/m/yr, incl. pores, while transports from 1DH and 2DH simulations gradually increase to about 15 m3/m/yr, incl pores at the top at shallower water depth and about 10 m3/m/yr, incl. pores at the top at deeper water.

Time-averaged suspended-load transport

- The time-averaged suspended-load transports from 1DH and 2DV simulations decrease with increasing water depth; south of the ridge typical values are about 10 m3/m/yr, incl. pores at shallower water and about 5 m3/m/yr, incl. pores at deeper water. Time-averaged transports from the 2DH simulation are about 10 m3/m/yr, incl. pores higher.
- Time-averaged suspended-load transport from the 3D simulation increases with increasing depth and approach the values from the 2DH simulation at deeper water.
- While time-averaged suspended-load transports from the 1DH and 2DH simulation increase gradually over the ridge, transports from 2DV en 3D simulation rapidly increase at the top of the ridge

From the sedimentation / erosion plots from both the 2DH and 3D computations it was found that both computations showed an identical spatial pattern of sedimentation and erosion with erosion only of the top of the ridge and sedimentation both along the entire north-eastern flank of the ridge and at deep water also at the south-western flank of the ridge. It was found that sedimentation and erosion from the 2DH computation is larger than from the 3D computation, which was especially pronounced at deep water.

It was found that three-dimensional (3D) models overestimate the reduction in height in comparison with two dimensional-vertical (2DV) models, while migration and deformation of the ridge are approximately identical. It is recommended to investigate in detail the existence of 3-dimensional circulations in the ridge vicinity and it's effects on morphology with a 3D model.

Comparison Delft3D versions

In section 6.4, a comparison between the two Delft3D versions that were used in this study was made by evaluation of model results for section 4. The difference in bottom layer sub-grid model between both versions is discussed in Section 2.3.3.3.

It was found that the improved version of Delft3D leads to larger suspended-load transports due to the continuous use of a correction vector to the suspended-load transport in the bottom layers (see Section 2.3.3.3) and thus leads to a larger migration of the ridge.

Furthermore, it was found that the decrease in height is smaller using the new version. This is due to the larger suspended-load transports in the bottom layers which transport sediment to the top region due to the deformation of velocity profiles over the ridge.

The improved version further leads to smaller bed-load transports than the older version due to small modifications in the combined friction coefficient for waves and currents which is used in the instantaneous grain related bed-shear stress due to both current and wave motion (see Van Rijn et al., 2004).

From the derivation of the morphological tide using the new version it was found that time-averaged suspended-load transport is in flood-direction only and that time-averaged bed-load transport is in ebb-direction. These changes with respect to the results from the previous version are related to the larger suspended-load transports in the bottom layers with the improved version, due to which the suspended-load behaves more like bed-load transport.

From the 14 year simulation it was concluded that the 2DV Delft3D model can simulate the medium-term sand ridge behaviour with reasonable accuracy.

comparison Delft3D versions with respect to the model results using the older version

In section 2.3.3.3 and 6.4 it was shown that the older Delft3D version leads to under prediction of suspended-load transport in the bottom layers. This under prediction increases with depth due to the increased bottom layer thickness when the relative thickness of the bottom layer remains equal (2.0 %). Therefore the under predicted migration at section 5 and 6 (deeper water) (see Section 6.3) is due to the older Delft3D version.

In Section 6.4 it was shown that using the improved version the suspended-load transport rates increase due to the proper functioning correction vector on the suspended-load transport in the bottom layers. Furthermore, bed-load transport rates decrease due to small modifications in the TRANSPOR2004 formulations. Therefore the ration between suspended-load and bed-load transport changes with this improved Delft3D version, which has significant influence on the morphological development of the ridge as this ratio determines in great extend whether the ridge increases or decreases in height.

7 Conclusions and recommendations

Herein, the main findings of this study are presented and recommendations for further investigation are given. In Section 7.2 the overall most important conclusions with respect to the main objectives of this study are presented. Next, in Section 7.2 recommendations for further investigation are given .

7.1 Conclusions

Herein the overall most important conclusions with respect to the main objectives of this study are presented. The conclusions will be given with respect to the following subjects:

- ridge characteristics
- ridge morphology
- model settings
- model results
- model approach

Ridge characteristics

The accuracy of bathymetric surveys of the sand ridge Hoek van Holland is comparable to that bathymetric surveys carried out in the NOURTEC study; the vertical accuracy is therefore in the order of 0.1 to 0.2 m and the horizontal accuracy is in the order of 1 to 5 m.

Bathymetric surveys of the sand ridge Hoek van Holland for the period 1982 – 2000 showed a clear reduction in ridge height and a net migration in flood direction that reduces with depth. The average rate of migration in flood direction is about 5.50 m per year and the average decrease in height of the ridge is about 0.1 m per year. Between 1992 and 1993 a southward migration of the ridge and increase in height was observed.

Ridge morphology

With symmetric and weak-asymmetric tides the sand ridge increases in height due to the deformation of velocity profiles over the ridge; the time-averaged near-bed velocities are in direction of the top of the ridge and so is the bed -load transport. With increasing tidal velocities or net currents the suspended-load transport dominates the bed-load transport; sediments are moved outside the region where they can be brought back to the top with bed-load transport and the ridge decreases in height.

With symmetric and weak-asymmetric tides the migration of the ridge is in ebb-direction due to the dominant ebb transports caused by the higher bed-shear stresses with shallower water during ebb. With increasing net current in flood direction, the effect of the shallower water during ebb is cancelled out and the ridge migrates in flood direction.

Waves stir up sediments and lead to larger suspended-load transports and a reduction in height of the ridge. Waves also affect the shape of the ridge; with waves the ridge develops more asymmetrically. The effect of waves increases with diminishing water depth and therefore suspended-transports during ebb (shallower water) are increased more than suspended-load transports during flood. With symmetric tides (no net current) the migration in ebb direction therefore increases with waves. The migration for tides with a net current is in flood direction and reduces with waves.

Model settings

In this study the effect of variation of several model- and process parameters in Delft3D models was investigated; most important conclusions from this investigations were:

- With large waves, the reduction in height of the ridge using 10 vertical layers was larger comparison to simulations using 20 and 30 vertical layers; with large waves greater vertical resolution is required.

- The turbulence model used is of significant influence on the computed morphological development of the ridge; the algebraic turbulence model leads to slightly larger migration of the ridge and a less asymmetric development with waves than the k-L or k-epsilon turbulence model.

- With a variable bed roughness (bed roughness predictor) the migration of the ridge is significantly smaller than with a constant bed roughness of C = 65 $m^{1/2}/s$. The reduction in height of the ridge is larger with a variable bed roughness, but the shape develops less asymmetrically than with a constant bed roughness, especially with waves

- The mean sediment diameter D_{50} needs to be determined rather accurately as it affects the distribution of sediments in the water column and thereby determines the morphological behaviour of the sand ridge; with larger sediments and subsequent dominant bed-load transports, the ridge increases in height.

Model results

The morphological development of the sand ridge near Hoek van Holland, The Netherlands over a period of about 10 years has been modelled with reasonable accuracy at most sections. The accuracy is strongly affected by the accuracy of the morphological tide, when waves are present. This morphological tide should be carefully determined based on data points outside the ridge location and on top of the ridge where the water depth is much smaller and waves are more important.

This further implies that the wave schematization is of significant importance with morphological simulations of sand ridges. Here, a single representative wave was used, which was found to lead to a morphological development that is in good agreement with the long-term average development of the sand ridge Hoek van Holland.

Model approach

Depth-averaged models should not be used to model the morphological development of sand ridges as these models use fixed, logarithmic velocity profiles and therefore cannot model the effect of deformation of velocity profiles over the ridge. Deformation of velocity profiles may lead to a net transport to the top of the ridge and may cause the ridge to increase in height.

Three-dimensional (3D) models overestimate the reduction in height in comparison with two dimensional-vertical (2DV) models, while migration and deformation of the ridge are approximately identical. It is recommended to investigate in detail the existence of 3-dimensional circulations in the ridge vicinity and it's effects on morphology with a 3D model.

Bottom layer sub-grid

In this study it was discovered that a criterion for the accurate determination of the concentrations in the bottom layer did not function properly (due to relatively large sediments and a mandatory bottom layer thickness), resulting in an under-prediction of suspended-load transports. During the finalization of the study an update of Delft3D was released that put things right and continuously uses an accurate method for determination of the concentrations in the bottom layer. Furthermore, the reference height was recalibrated and a mobility term (critical velocity) on the bed-load transport was added in this updated Delft3D version.

Simulations with an idealized sand ridge were redone using the updated version of Delft3D and a brief comparison between both versions revealed that this update leads to significantly larger suspended-load transport and thus to larger migration rates. As suspended-load transport in the bottom was not under-estimated anymore, the effect of deformation of velocity profiles over the ridge (transport to top of the ridge) was strengthened and the reduction in height was reduced. Furthermore, it was found that bed-load transport rates were smaller due to the smaller reference height and the mobility term for the bed-load transport

From the derivation of a morphological tide using the updated Delft3D version it was found that time-averaged suspended-load transport is in flood-direction and time-averaged bed-load transport is in ebb-direction.

TRANSPOR2004

In this study it was found that using the TRANSPOR2004 sediment transport model bed-load transport rates without waves were significantly larger than with waves. It was recommended to investigate the TRANSPOR2004 formulations for this and recently a study of the TR2004 formulations by the model developers revealed that this was due to the transition between current- and wave-related roughness. The weighting procedure based

upon current- and wave-related velocities was adjusted to guarantee a smooth transition between bed-load transport rates without and with waves and will be included in the next update of the Delft3D modelling software

7.2 Recommendations

Herein, recommendations for further investigation are given. The recommendations are given with respect to the following subjects:

- Model schematizations and –approach
- Delft3D bottom layer sub-grid model and –restrictions
- Transport formulations
- Large-scale sand mining

Model schematizations and -approach

It was found that the mean sediment diameter D_{50} determines the morphological behaviour of the sand ridge in great extent. It is therefore recommended to investigate the effect of the grain size distribution on the morphological development of the ridge in future studies.

It was found that the representative morphological tide needs to be determined carefully, based on data points outside the ridge location and on top of the ridge where the water depth is much smaller and waves are more important. In a continuation of this study it is advised to investigate the validity of a morphological tide in more detail.

The validity of the single representative wave condition was only investigated briefly, but it was found that large wave heights lead to significant morphological changes; it therefore is recommended to investigate in more detail whether modelling of large wave conditions is vital to the morphological development of sand ridges.

It was further shown that three-dimensional (3D) models overestimate the reduction in height in comparison with two dimensional-vertical (2DV) models. It therefore is recommended to investigate in detail the existence of 3-dimensional circulations in the ridge vicinity and it's effects on morphology with a 3D model.

Delft3D bottom layer sub-grid model and -restrictions

It this study it was found that the concentrations in the bottom layer were severely under-predicted due to a criterion for accurate determination of the concentrations in the bottom layer that was not due to relatively large sediments and a mandatory bottom layer thickness of at least 2.0 % of the water depth. A recently released update of Delft3D put things right and continuously uses an accurate method to determine the concentrations in the bottom layer.

Simulations varying the relative bottom layer thickness confirmed the value of 2.0 % of the water depth that was stated in the Delft3D-FLOW user manual as minimum value for the bottom layer thickness. It is recommended to investigate the restrictions on the relative thickness of the bottom layer with respect to the accurate determination of concentrations in the bottom layer at deeper water.

Transport formulations

In this study it was found that using the TRANSPOR2004 sediment transport model bed-load transport rates without waves were significantly larger than with waves. It was recommended to investigate the TRANSPOR2004 formulations for this and recently a study of the TR2004 formulations by the model developers revealed that this was due to the transition between current- and wave-related roughness. The weighting procedure based upon current- and wave-related velocities was adjusted to guarantee a smooth transition between bed-load transport rates without and with waves and will be included in the next update of the Delft3D modelling software.

In this study it was found that the suspended-load rates at the top of the ridge without waves were larger than with modest waves. This was not found from the TRANSPOR2004 sediment transport formulations and it is recommended to investigate the cause of this effect.

Large-scale sand mining

This study was carried out within the SANDPIT project which was set up to develop reliable prediction techniques and guidelines to better understand, simulate and predict the morphological behavior of large-scale sand mining from pits and large-scale sand banks. In this study an artificial sand ridge of limited dimensions was modelled with reasonable accuracy using Delft3D. For the continuation of this study it is recommended to focus on modelling of regeneration of large-scale sand banks after sand extraction.

A Work overview

Herein, an overview is given of the extra work that was carried out during this study but that was not included in the body text of the report due to relevancy with respect to the Delft3D version that was ultimately used . This extra work is related to a series of updates of the Delft3D modelling software that were released during this study. The extra work includes simulations and a tidal schematization using the TRANSPOR1993 sediment transport model and numerous sensitivity simulations using different research versions of Delft3D.

Successively the following topics will be mentioned briefly:

- The estimation of average transports from measurements
- TRANSPOR1993 vs TRANSPOR2004 (incl. trachytopes)
- The sensitivity to the horizontal and vertical grid resolution using TRANSPOR2004

Estimated transports from measurements

A indication of the sediment transport rates over the ridge was derived from measurements and served as a check of time-average sediment transports from the morphological tide. The method used here is described in detail in Woudenberg (1996).

The total sediment transport rates cannot be determined from soundings because of the unknown initial sediment transport at x = 0. Total sediment transport: Stot. = S +Sconst. S can be determined from soundings and the shape of the sediment transport over the ridge can therefore be estimated. The development of S over the ridge is an indication of the sediment rates over the ridge. S can be determined from soundings by subtracting the integrated profiles and correcting the resulting transport rates for difference at both ends (assumption of a closed system). Estimated transports from sounding do not show any decrease in sediment transport at the Southern side of the ridge, but transports from using morphological tides do. Also simulations over a complete neap-spring tidal cycle show the

TRANSPOR1993 vs. TRANSPOR2004 (incl. bed roughness predictor)

At the start of the study, the TRANSPOR2004 sediment transport model and the bed roughness predictor were not yet implemented in the Delft3D modelling package and waves could only be modelled via the WAVE module. Therefore it was decided to use the TRANSPOR1993 sediment transport model and a SWAN computation for the assessment of the predictive capabilities of Delft3D on the morphological development of the sand ridge near Hoek van Holland. Boundary conditions were derived from the HCZ-model using the automated nesting procedure and a morphological tide was derived. Next a sensitivity analysis was carried out using the morphological tide and using the TRANSPOR1993 sediment transport model with and without SWAN wave computations. This sensitivity analysis was carried out in more detail than reported in the report.

Mid-august 2004, a research version of Delft3D was released, which included the TRANSPOR2004 sediment transport model and the trachytopes bed roughness predictor. It was decided to switch to this new version as it is was developed within the SANDPIT project and provides a state-of-the-art morphological modelling system

It was found that the morphological tide derived using the TRANSPOR1993 sediment transport model didn't suffice with this newer version and a new morphological tide needed to be derived.

Also the nesting in the HCZ-model needed to be redone as the bed roughness predictor caused significant deviations in water levels. It was decided to redo the sensitivity analysis using the new version with the TR2004 sediment transport model, the bed roughness predictor and the constant wave height applied from within the Sediment-Online module. From this sensitivity analysis it was found that the model was very sensitive to the number of vertical layers and the relative thickness of the bottom layer.

The sensitivity to the horizontal and vertical grid resolution using TRANSPOR2004
Shortly after the first research version of Delft3D that included the TRANSPOR2004 sand transport model, two updates became available. The sensitivity of these three version to the vertical resolution and the bottom layer thickness was compared. The three research versions of Delft3D that were compared were released at
28-09-2004, 11-11-2004 and 29-11-2004.

Computations were made for each version with TR2004 using 10, 20 and 30 vertical layers, varying the relative thickness of the bottom layer between 0.6, 1.0 and 2.0 %. of the water depth. In this computations the morphological tide "mt2" was used in combination with the single representative wave from Walstra (1997). The horizontal grid size over the bar was about 10 m and the computational time step used was 30 s. The mean sediment diameter used was 300 μm.

It was found that 10 vertical layers suffice for accurate simulation of. Furthermore, a non-equidistant logarithmic spacing of the vertical grid was preferred and a bottom layer thickness of no less than 2% of the water depth was required as smaller bottom layer thickness lead to unrealistic transports

This set of computations was also run with a horizontal grid size of about 32 m using three different turbulence model (algebraic, k-L and k-epsilon). Also, the exact same computations were made using morphological tide "basic a" .

From these computations, it was found that:

- The research version dd 29-11-2004 using a bottom layer thickness of 1% was very sensitive to the horizontal grid resolution, whereby with greater resolution the bar increased in height and became more asymmetric. It was decided not to use this version as it seemed not very trustworthy in comparison with the two previous versions released.
- It was confirmed that a horizontal grid size of about 10 m provided enough resolution for accurate modelling of the ridge behaviour.
- The turbulence model used had only little effect on the morphological development of the ridge and it was decided to use the algebraic turbulence model as it is more time-efficient.

B Morphology data

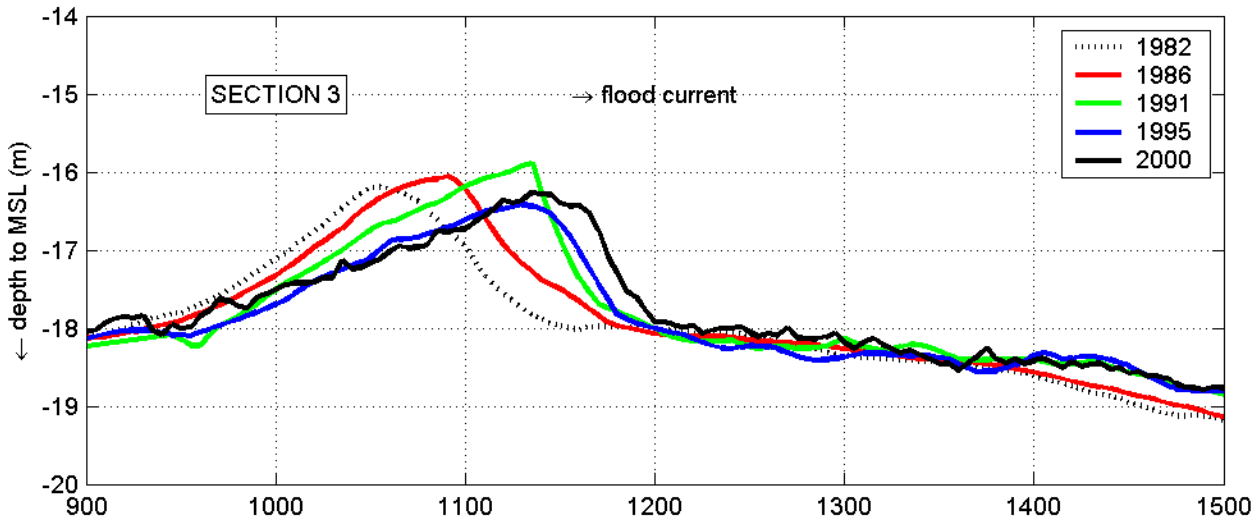

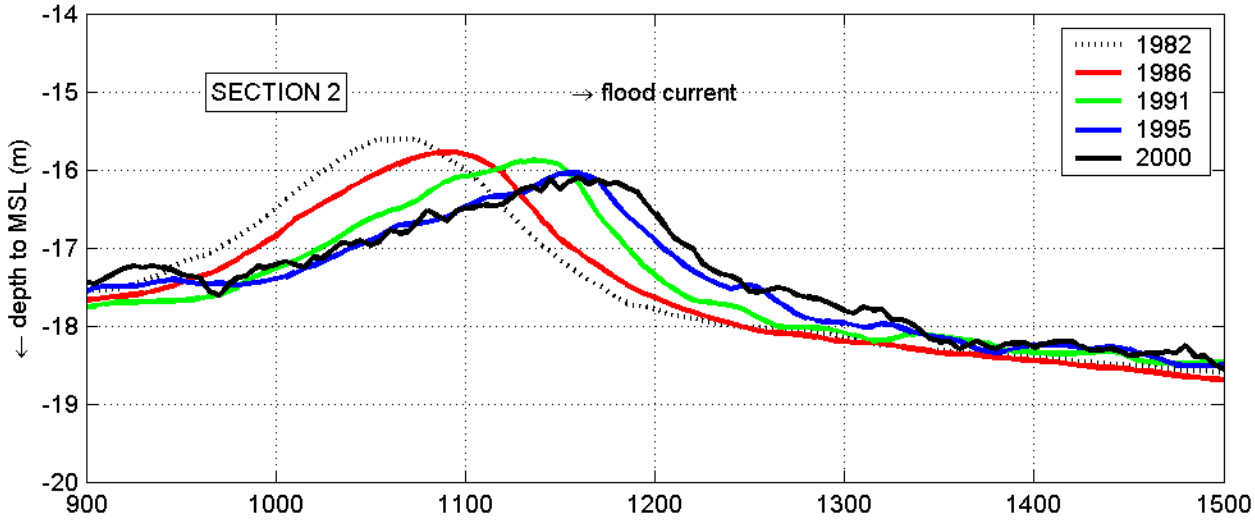

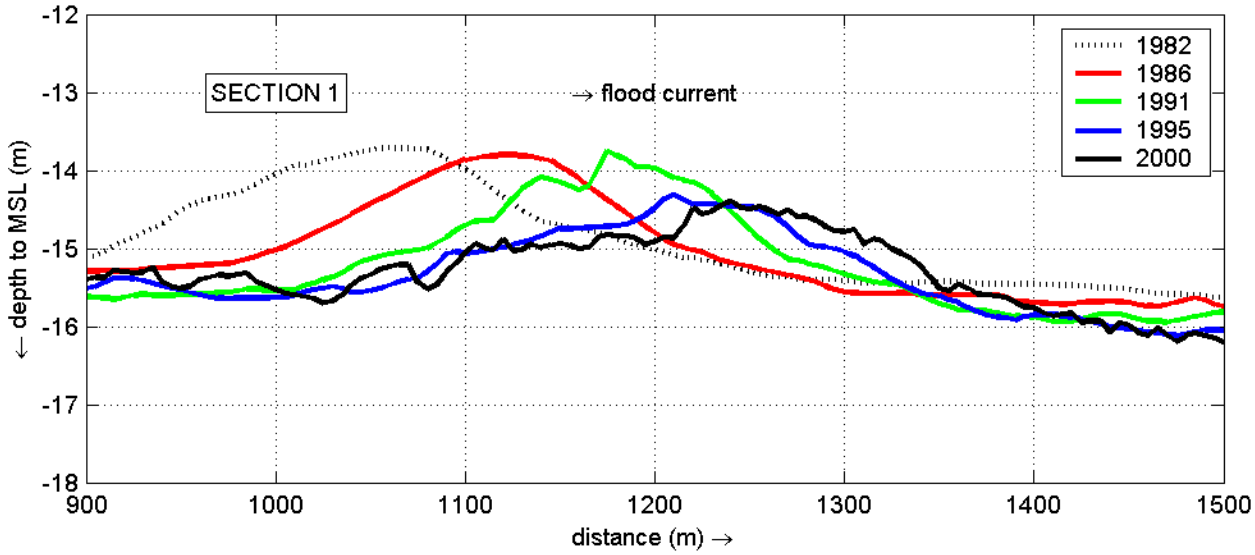

measured bedlevels cross-sections 1-3		2005
WL | Delft Hydraulics	Z3079.40	Figure B.03

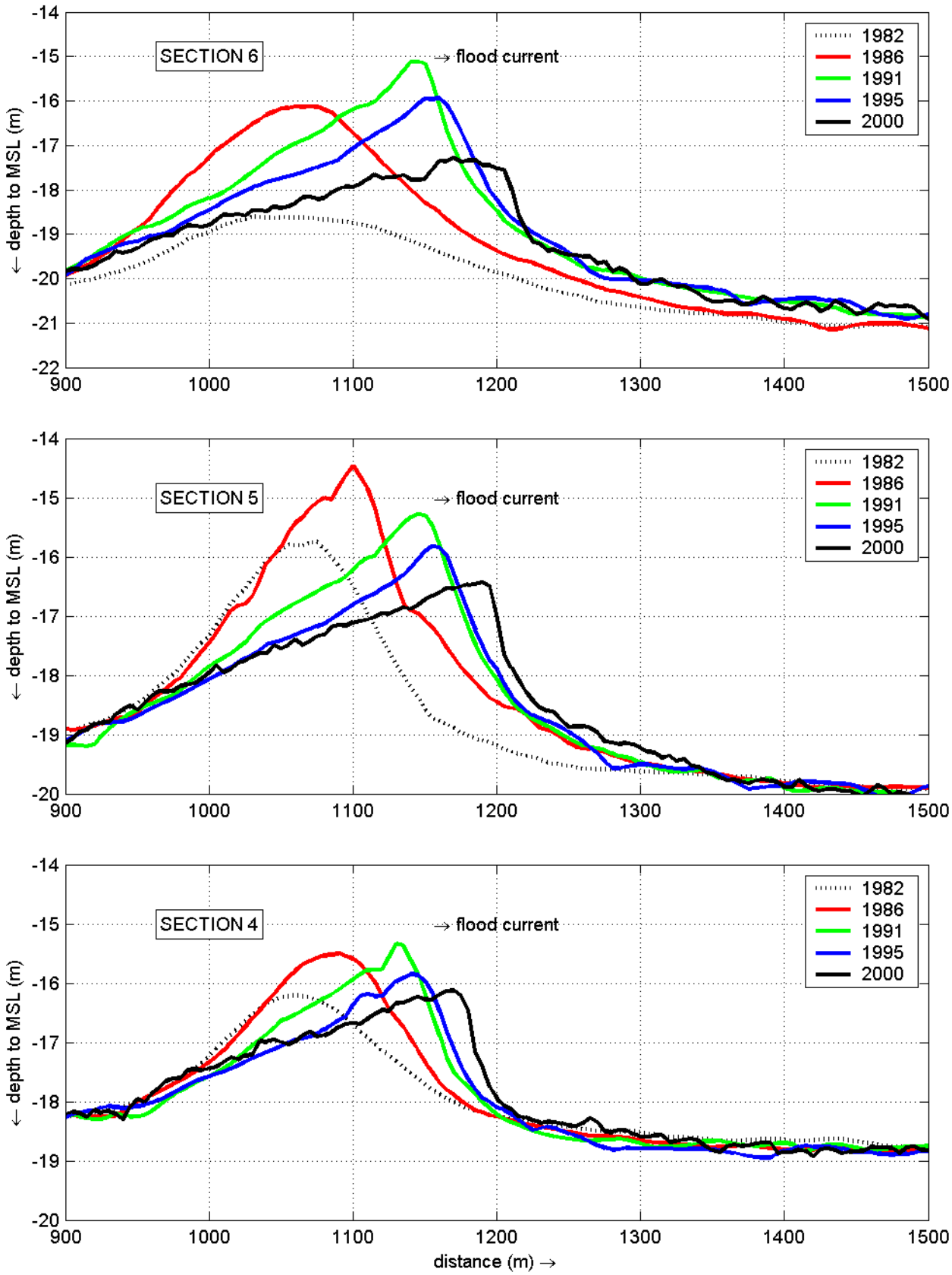

measured bedlevels cross-sections 4-6

2005

WL | Delft Hydraulics

Z3079.40

Figure B.03b

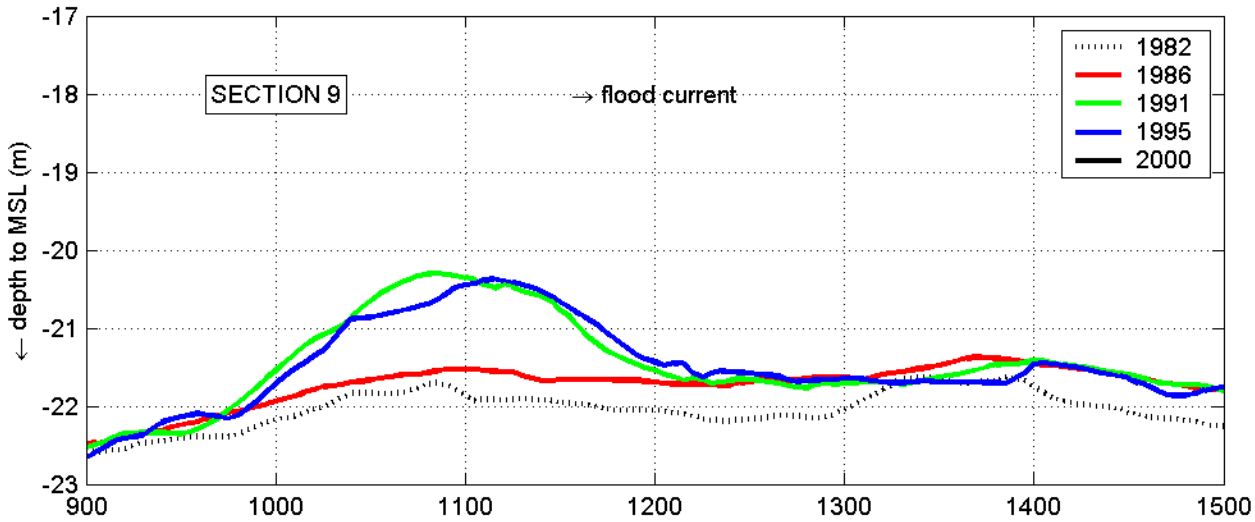

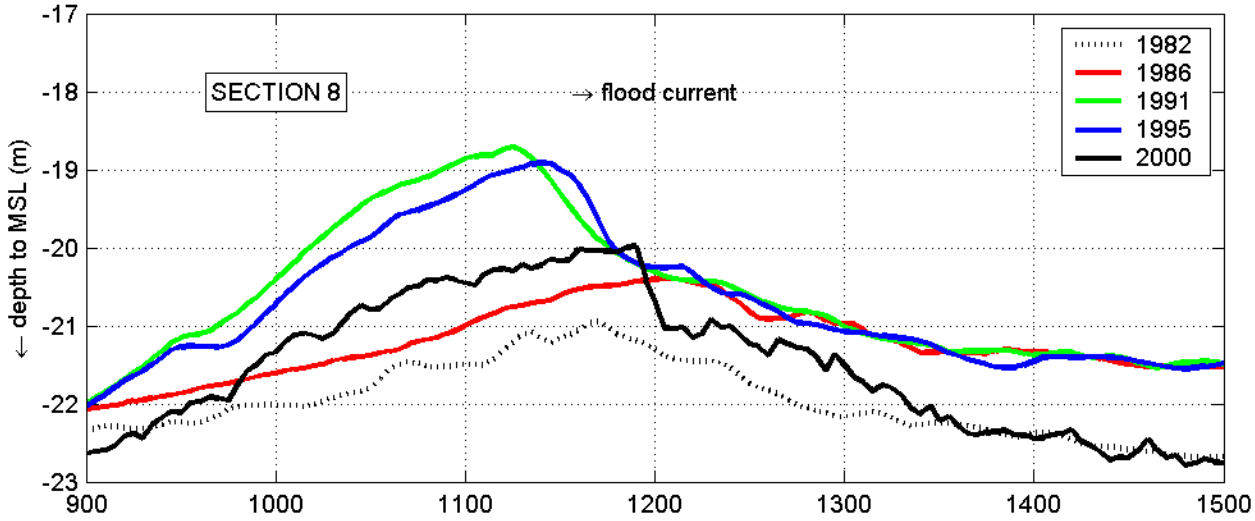

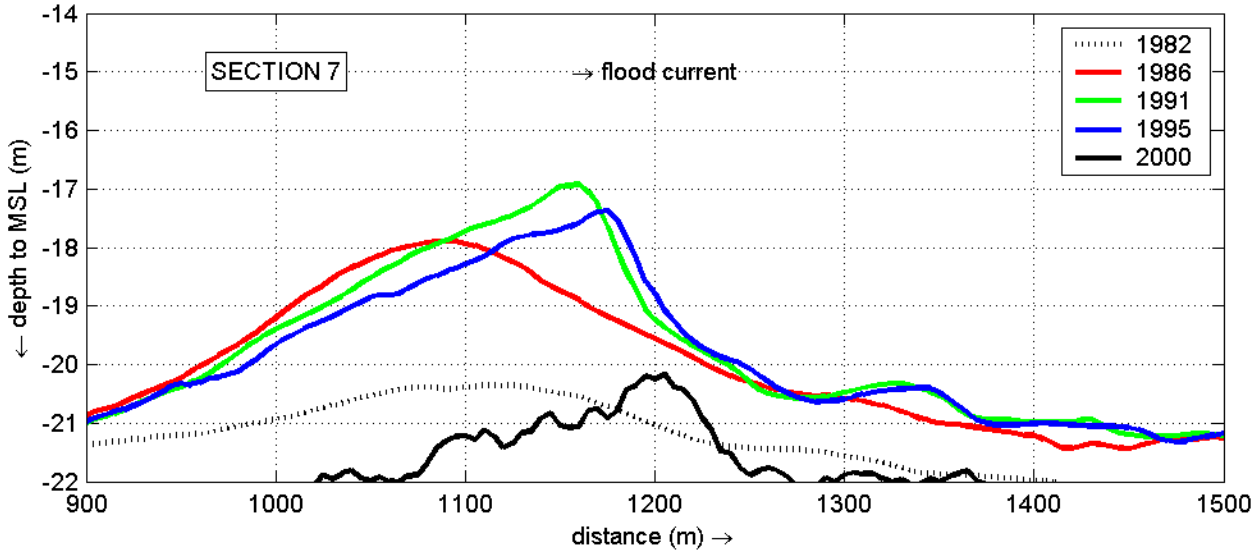

measured bedlevels cross-sections 7-9

2005

WL | Delft Hydraulics

Z3079.40

Figure B.03c

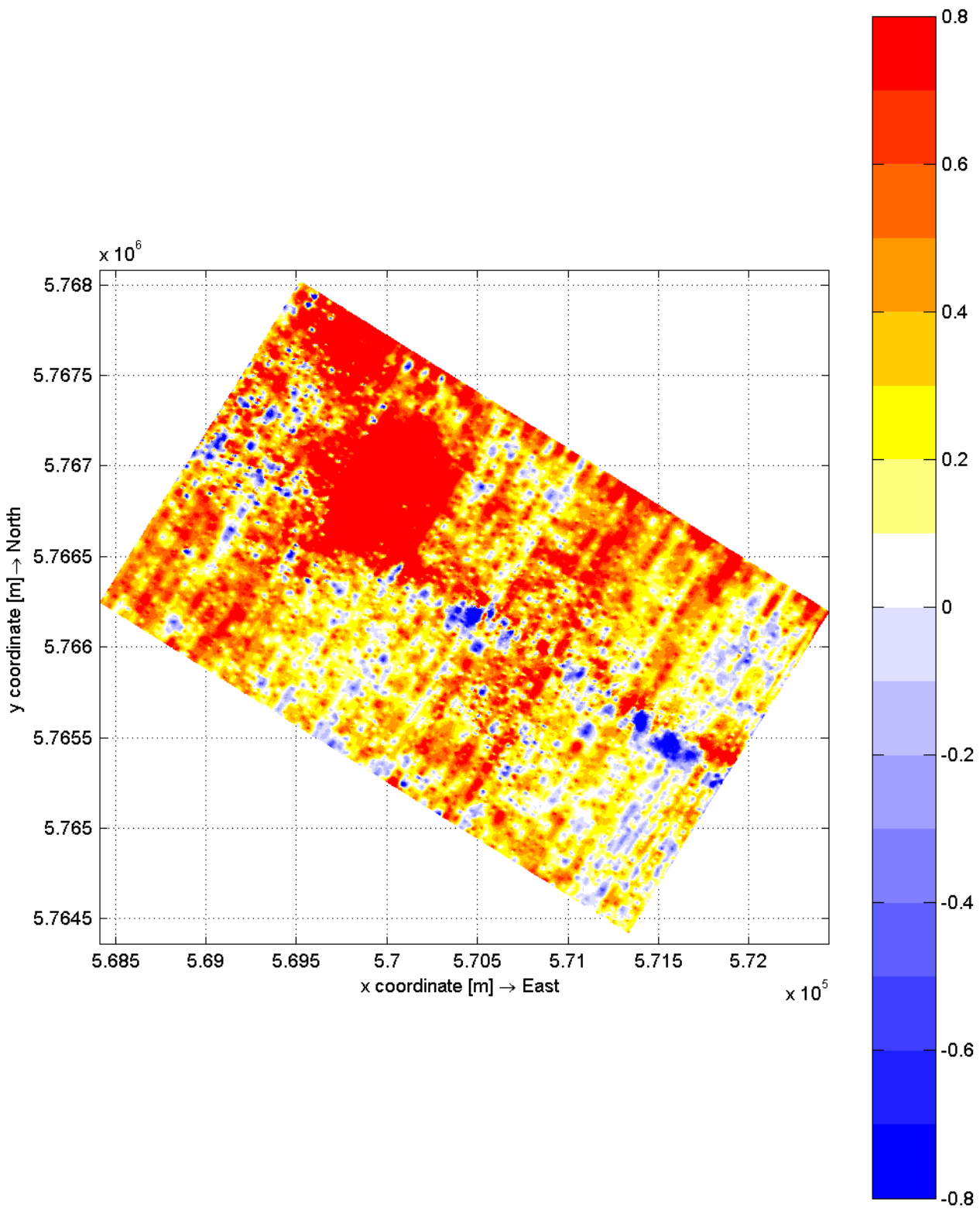

data-analysis: sedimentation / erosion between 1982 and 1983 [m/yr]
sand dump Hoek van Holland, The Netherlands (UTM coordinates, zone 31

2005

data-analysis

WL | Delft Hydraulics

Z3079.40

Figure B.04

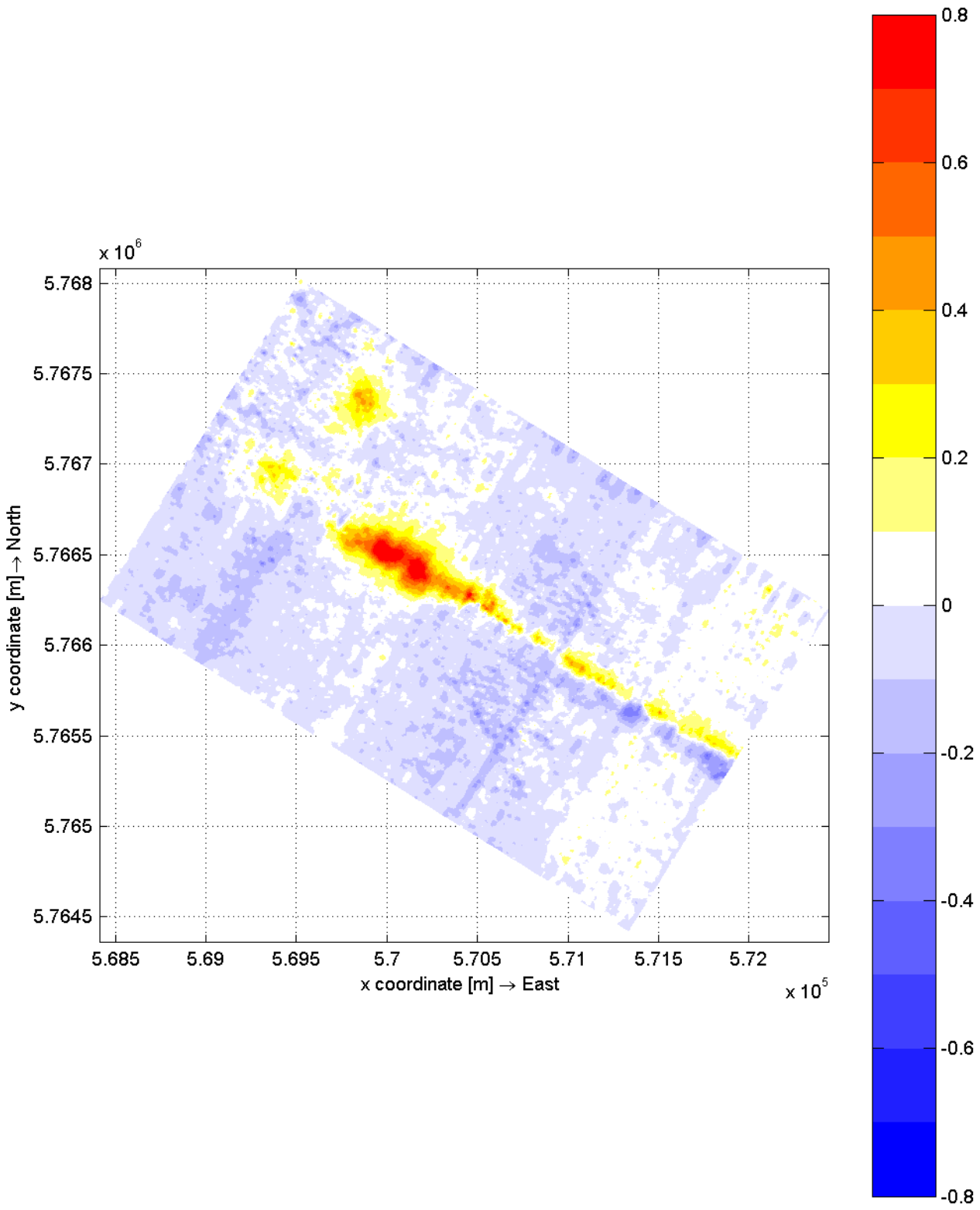

data-analysis: sedimentation / erosion between 1983 and 1985 [m/yr]
sand dump Hoek van Holland, The Netherlands (UTM coordinates, zone 31

2005

data-analysis

WL | Delft Hydraulics

Z3079.40

Figure B.05

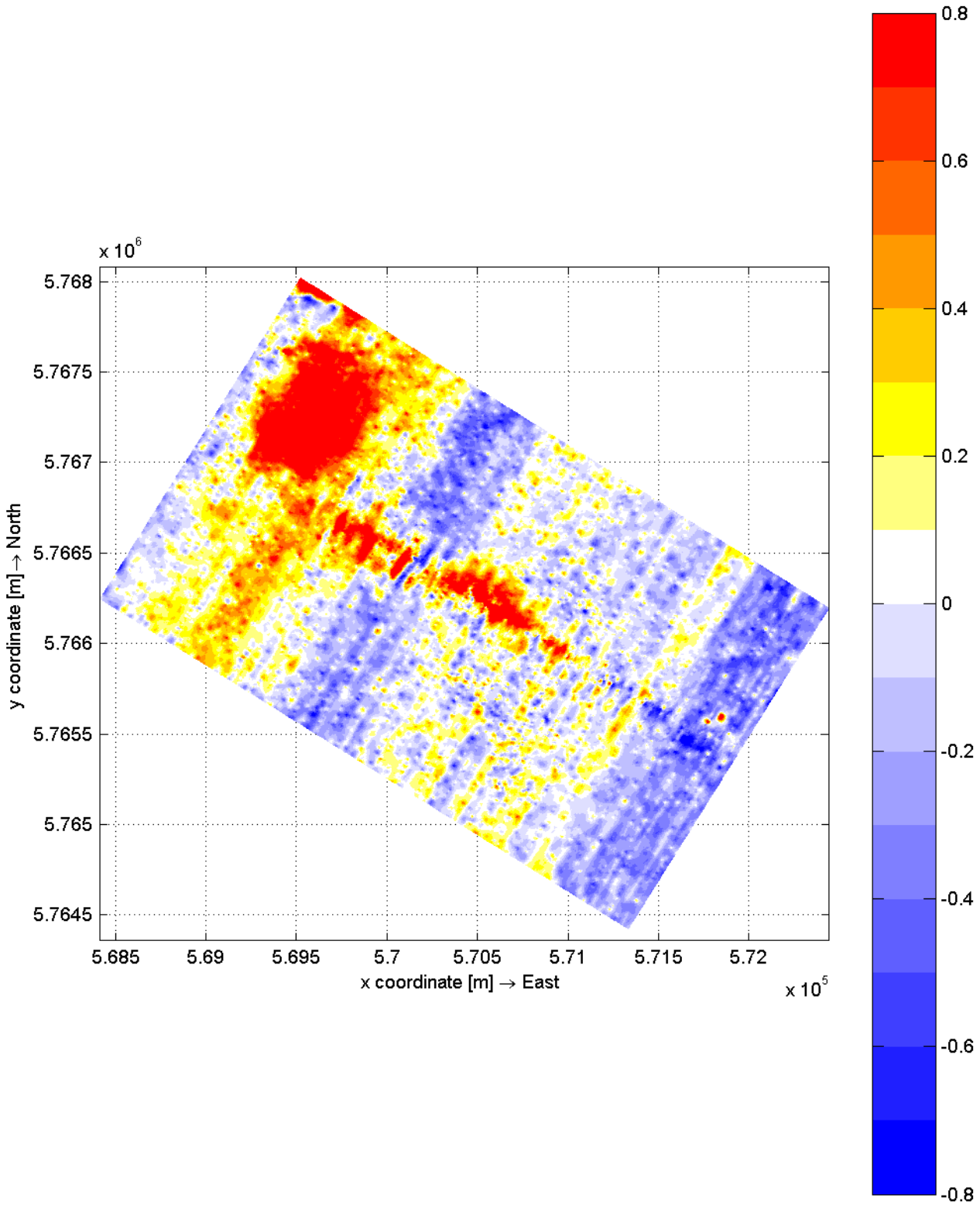

data-analysis: sedimentation / erosion between 1985 and 1986 [m/yr]
sand dump Hoek van Holland, The Netherlands (UTM coordinates, zone 31

2005

data-analysis

WL | Delft Hydraulics

Z3079.40

Figure B.06

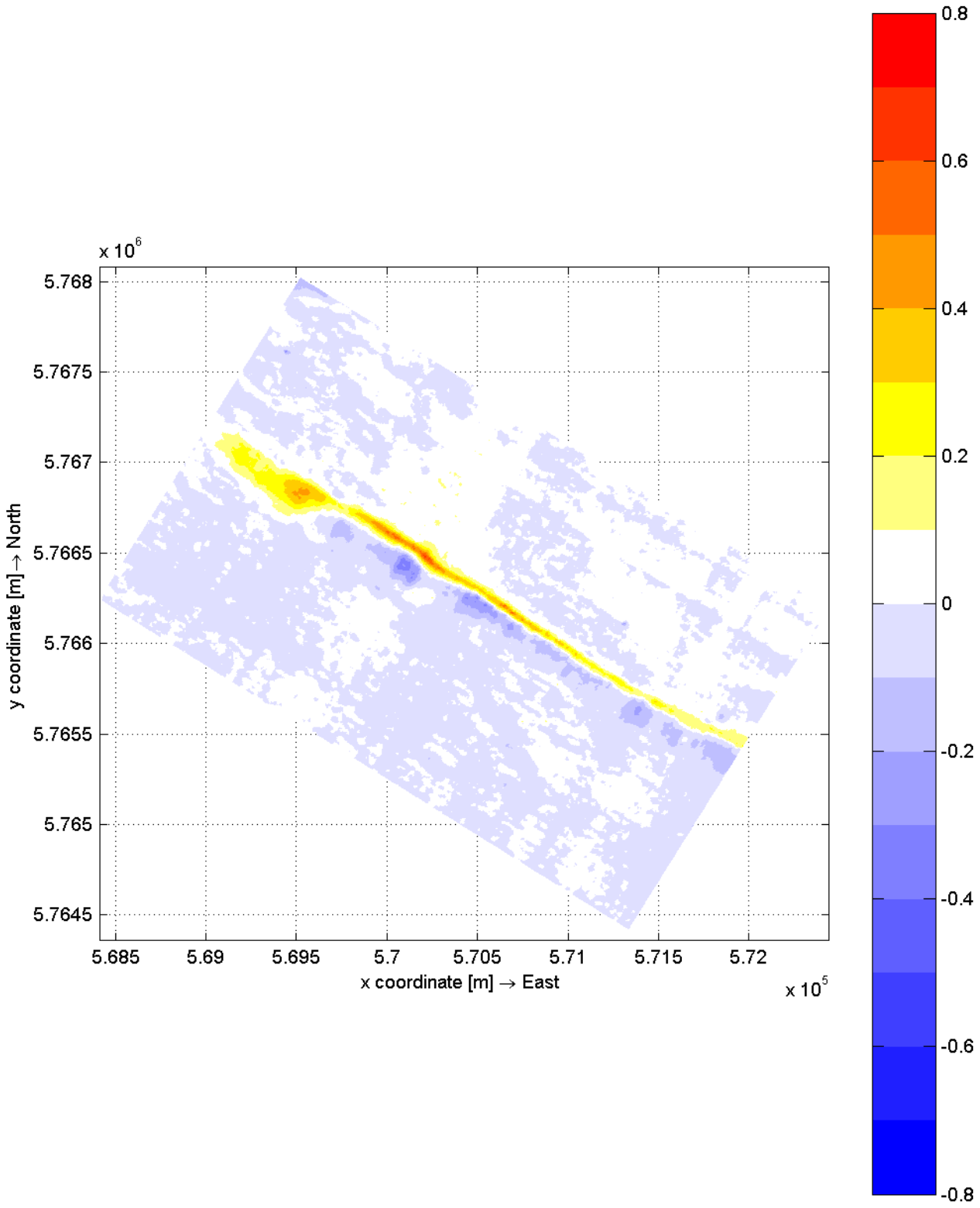

data-analysis: sedimentation / erosion between 1986 and 1991 [m/yr] sand dump Hoek van Holland, The Netherlands (UTM coordinates, zone 31		2005
	data-analysis	
WL | Delft Hydraulics	Z3079.40	Figure B.07

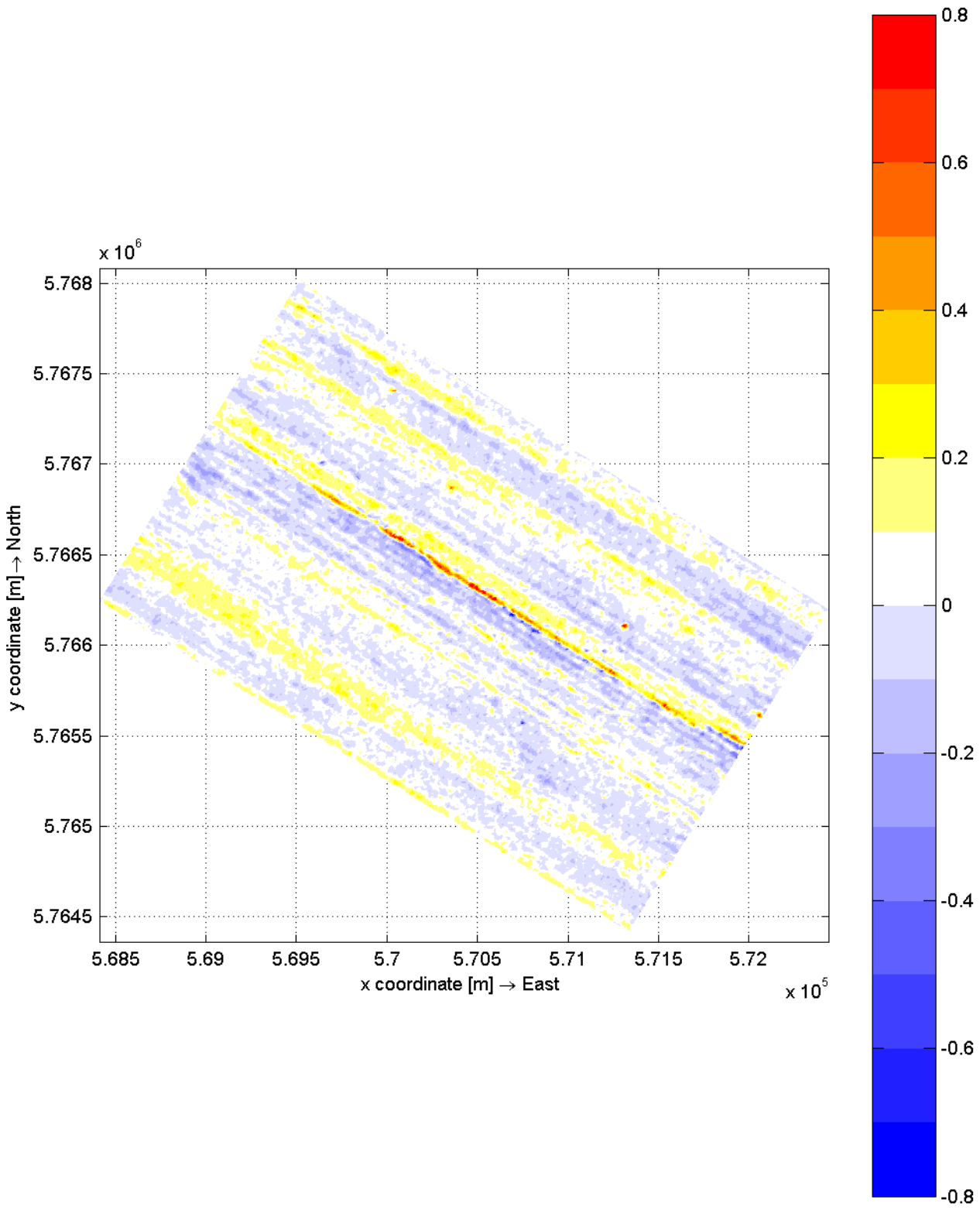

data-analysis: sedimentation / erosion between 1991 and 1992 [m/yr]
sand dump Hoek van Holland, The Netherlands (UTM coordinates, zone 31

2005

data-analysis

WL | Delft Hydraulics

Z3079.40

Figure B.08

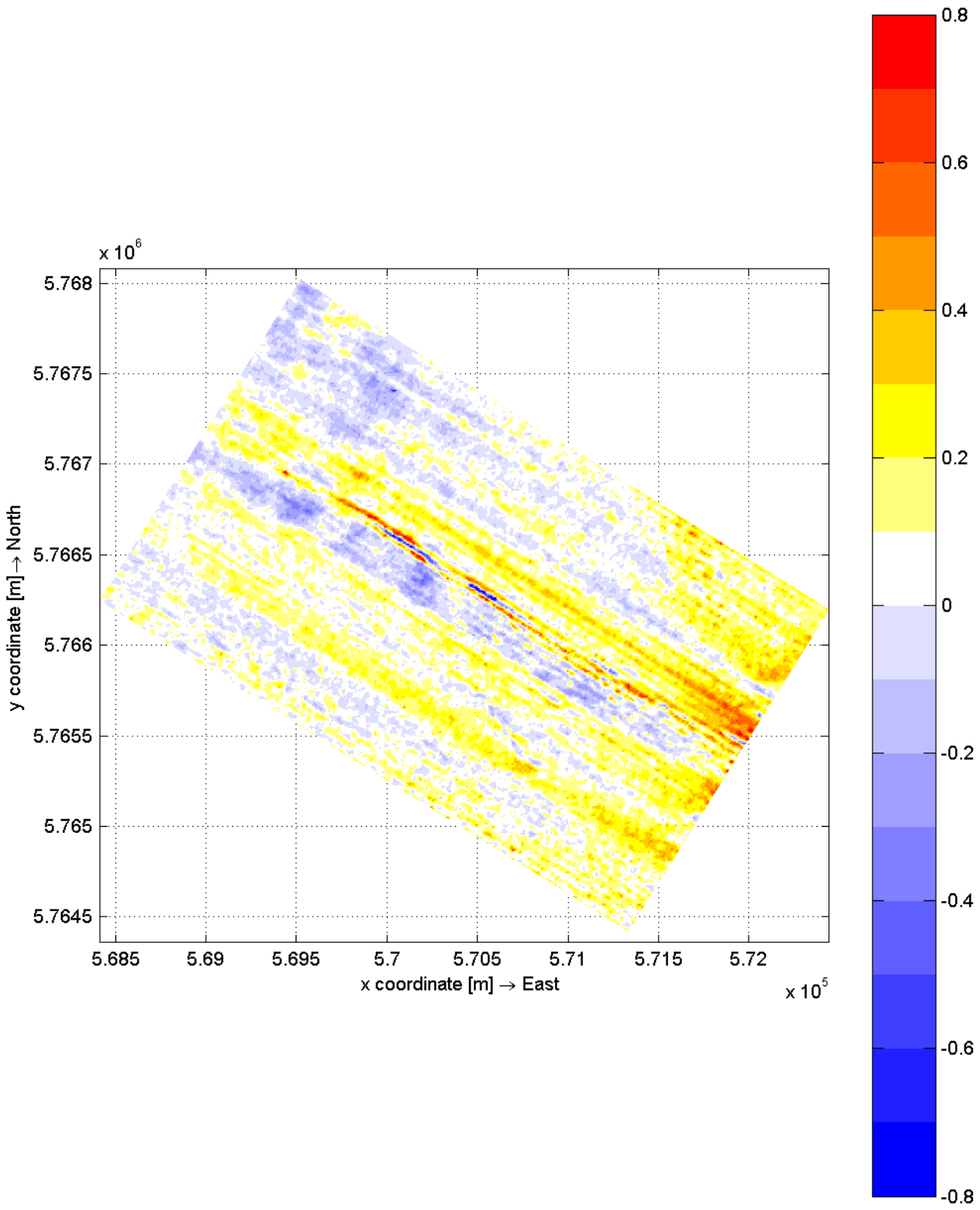

data-analysis: sedimentation / erosion between 1992 and 1993 [m/yr]
sand dump Hoek van Holland, The Netherlands (UTM coordinates, zone 31

2005

data-analysis

WL | Delft Hydraulics

Z3079.40

Figure B.09

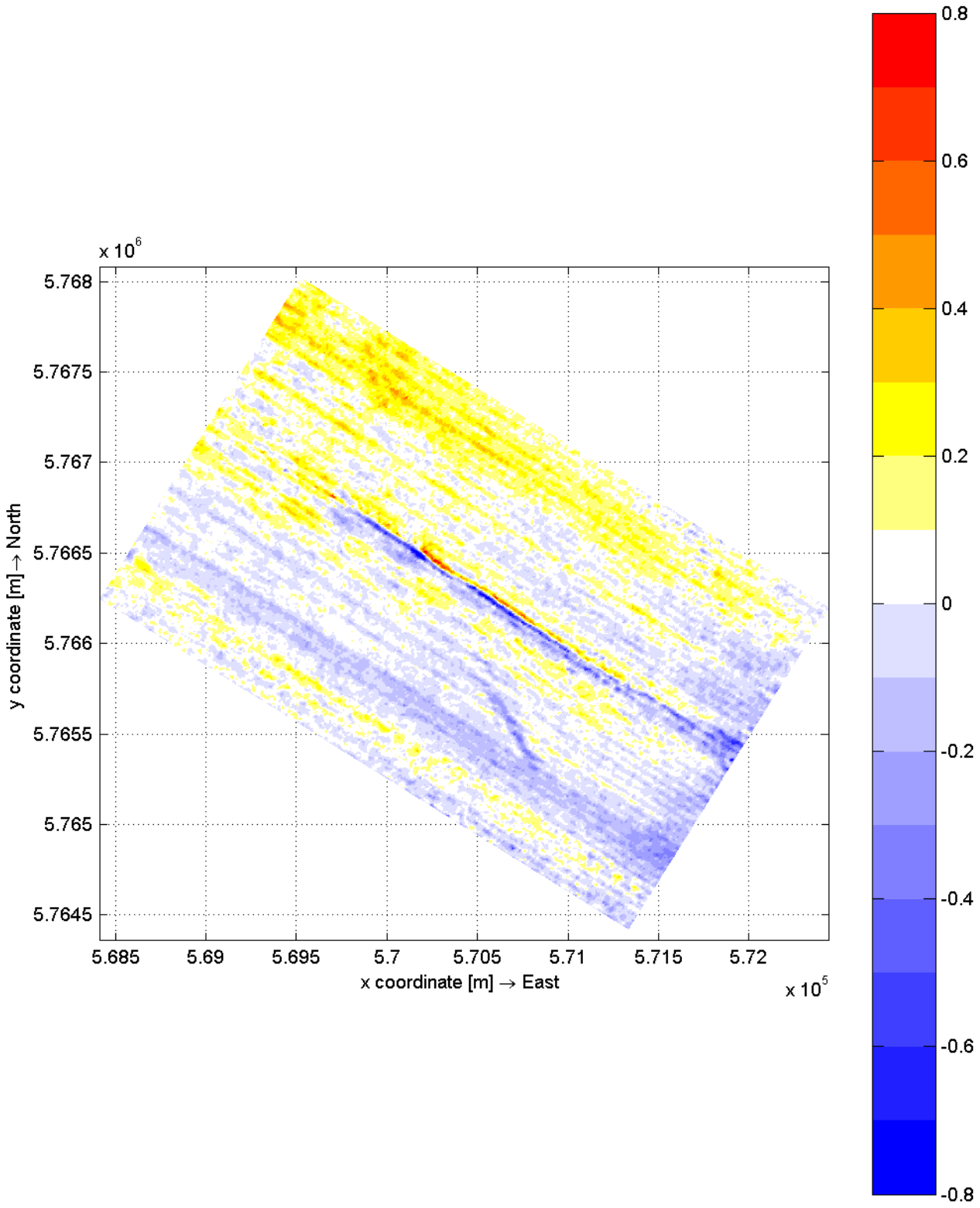

data-analysis: sedimentation / erosion between 1993 and 1994 [m/yr]
sand dump Hoek van Holland, The Netherlands (UTM coordinates, zone 31

2005

data-analysis

WL | Delft Hydraulics

Z3079.40

Figure B.10

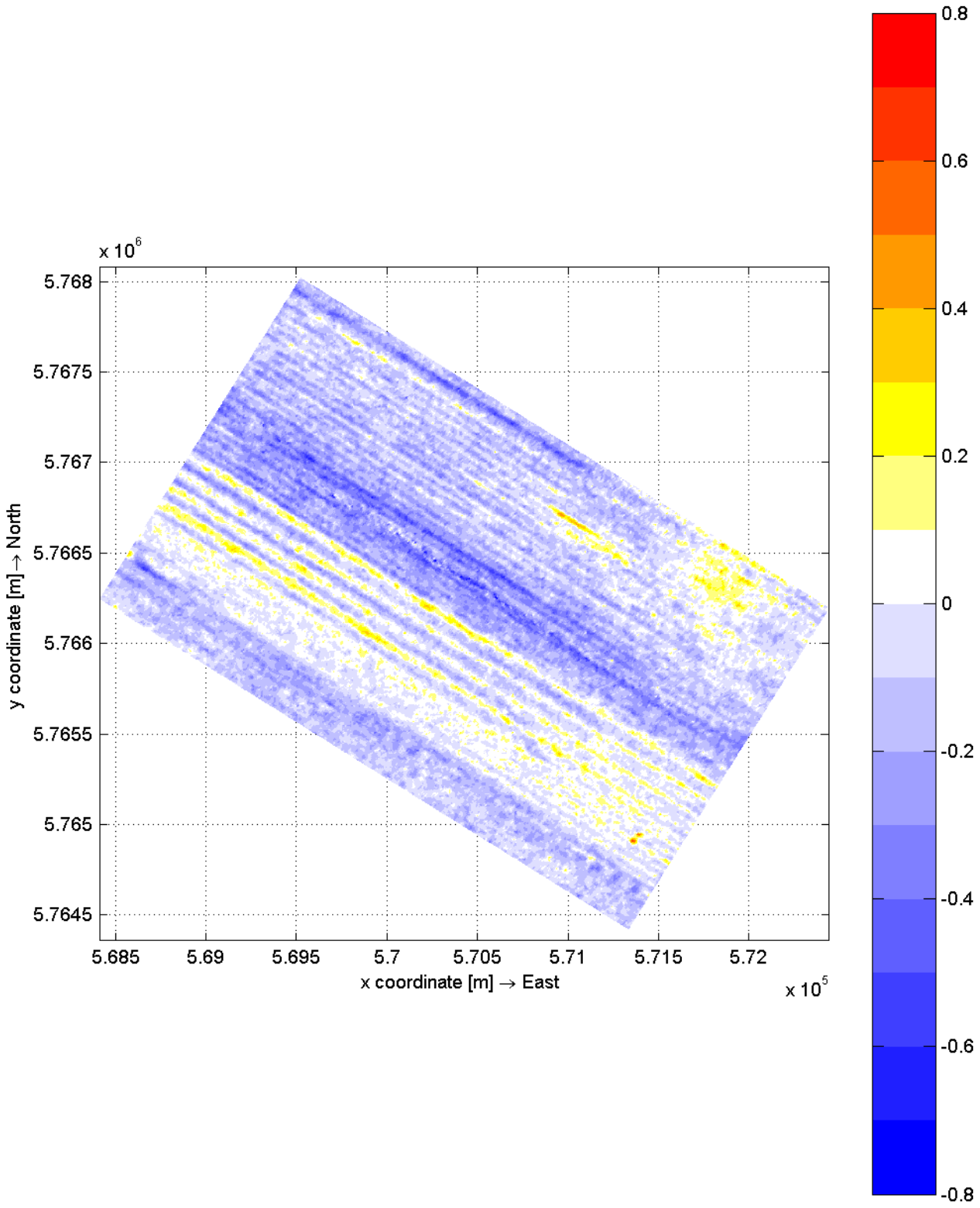

data-analysis: sedimentation / erosion between 1994 and 1995 [m/yr] sand dump Hoek van Holland, The Netherlands (UTM coordinates, zone 31		2005
	data-analysis	
WL | Delft Hydraulics	Z3079.40	Figure B.11

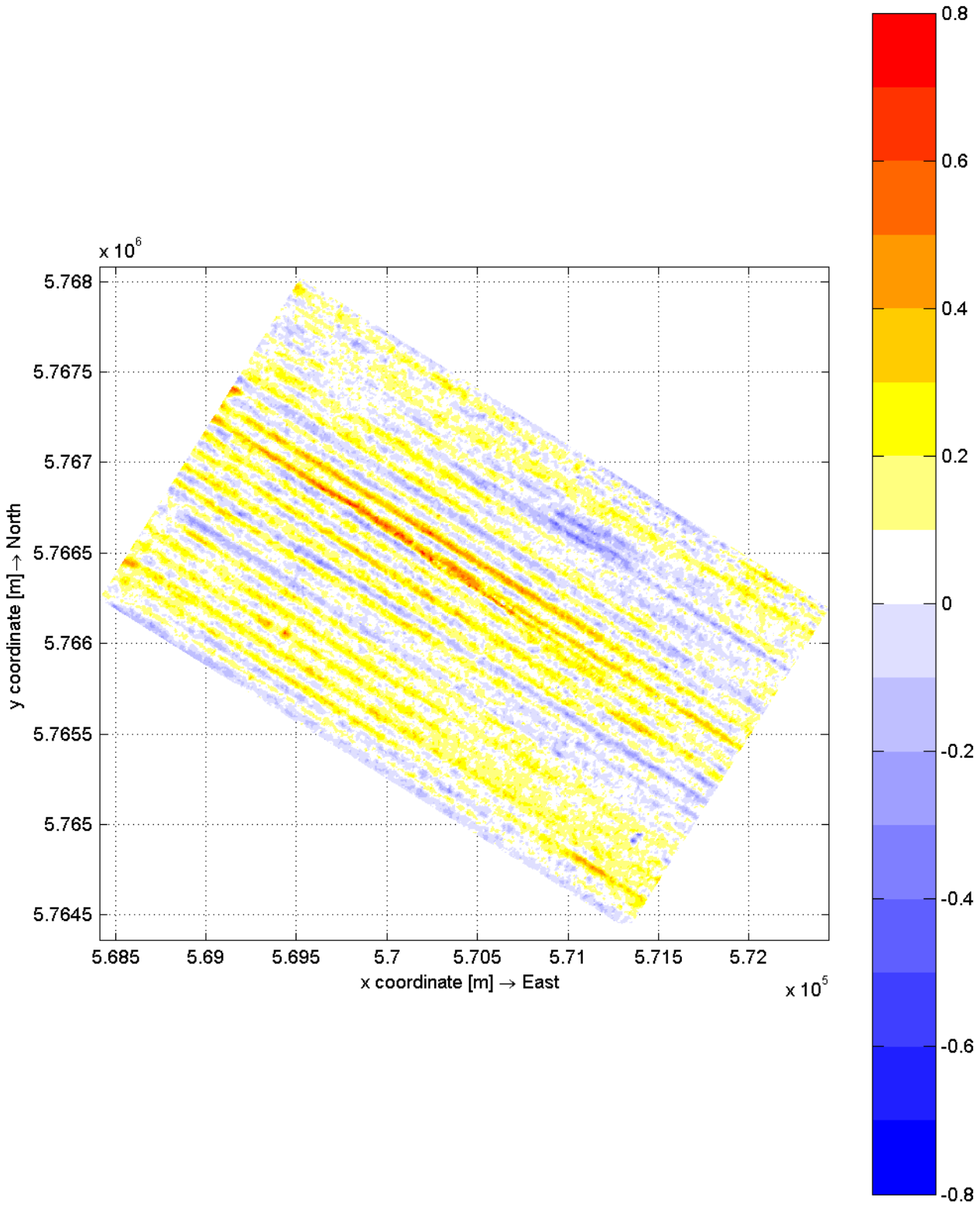

data-analysis: sedimentation / erosion between 1995 and 1996 [m/yr]
sand dump Hoek van Holland, The Netherlands (UTM coordinates, zone 31

2005

data-analysis

WL | Delft Hydraulics

Z3079.40

Figure B.12

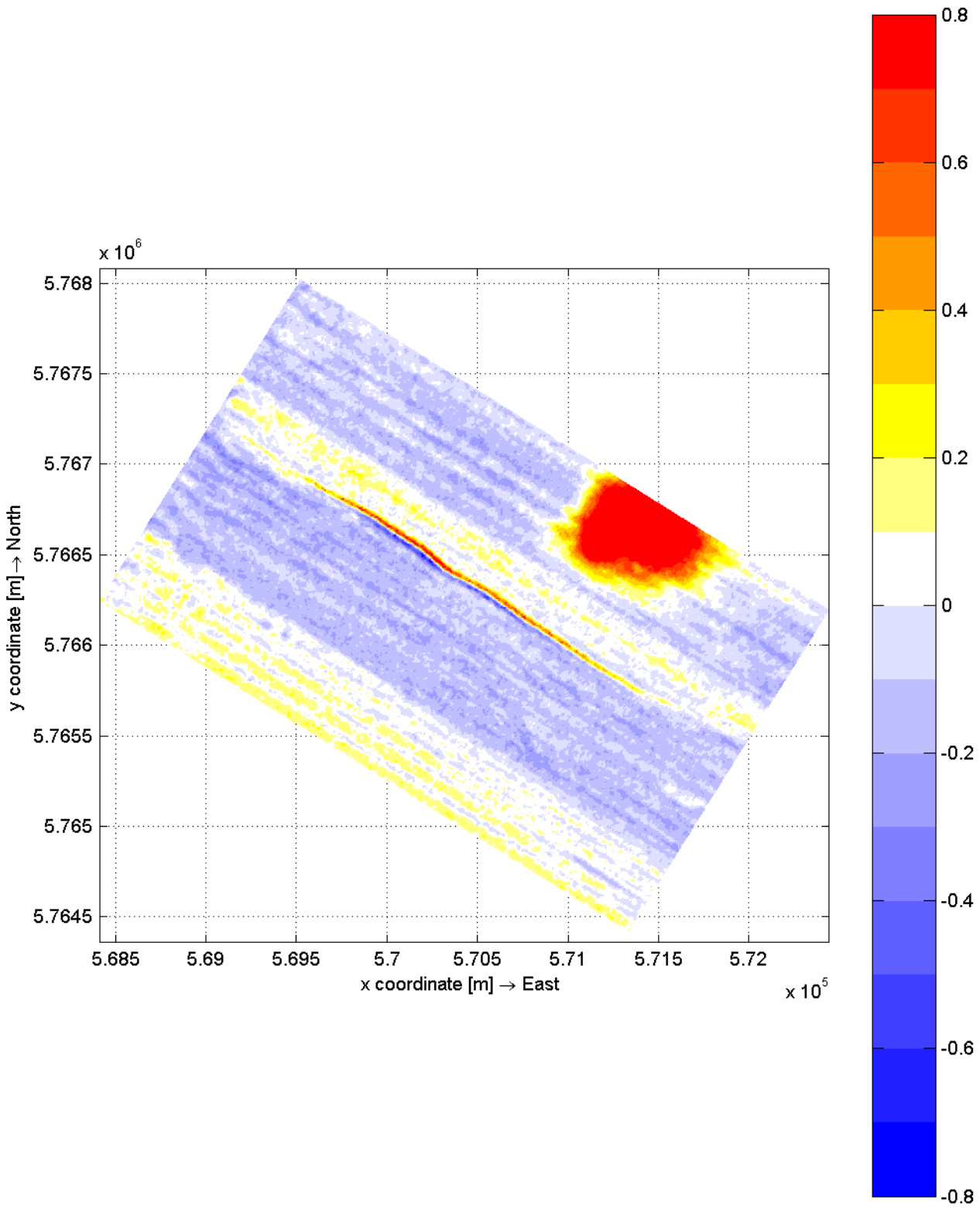

data-analysis: sedimentation / erosion between 1996 and 1997 [m/yr]
sand dump Hoek van Holland, The Netherlands (UTM coordinates, zone 31

2005

data-analysis

WL | Delft Hydraulics

Z3079.40

Figure B.13

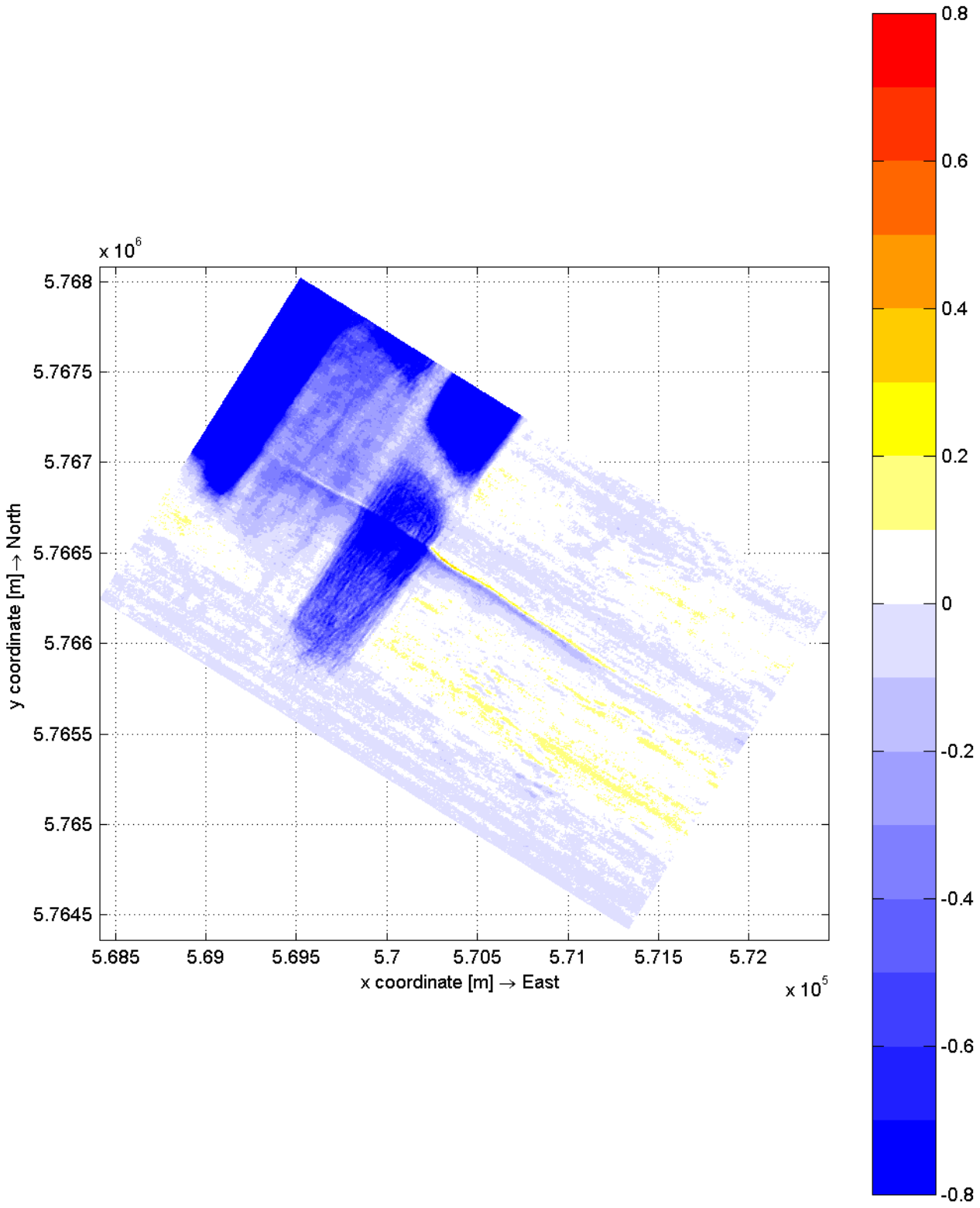

data-analysis: sedimentation / erosion between 1997 and 2000 [m/yr]
sand dump Hoek van Holland, The Netherlands (UTM coordinates, zone 31

2005

data-analysis

WL | Delft Hydraulics

Z3079.40

Figure B.14

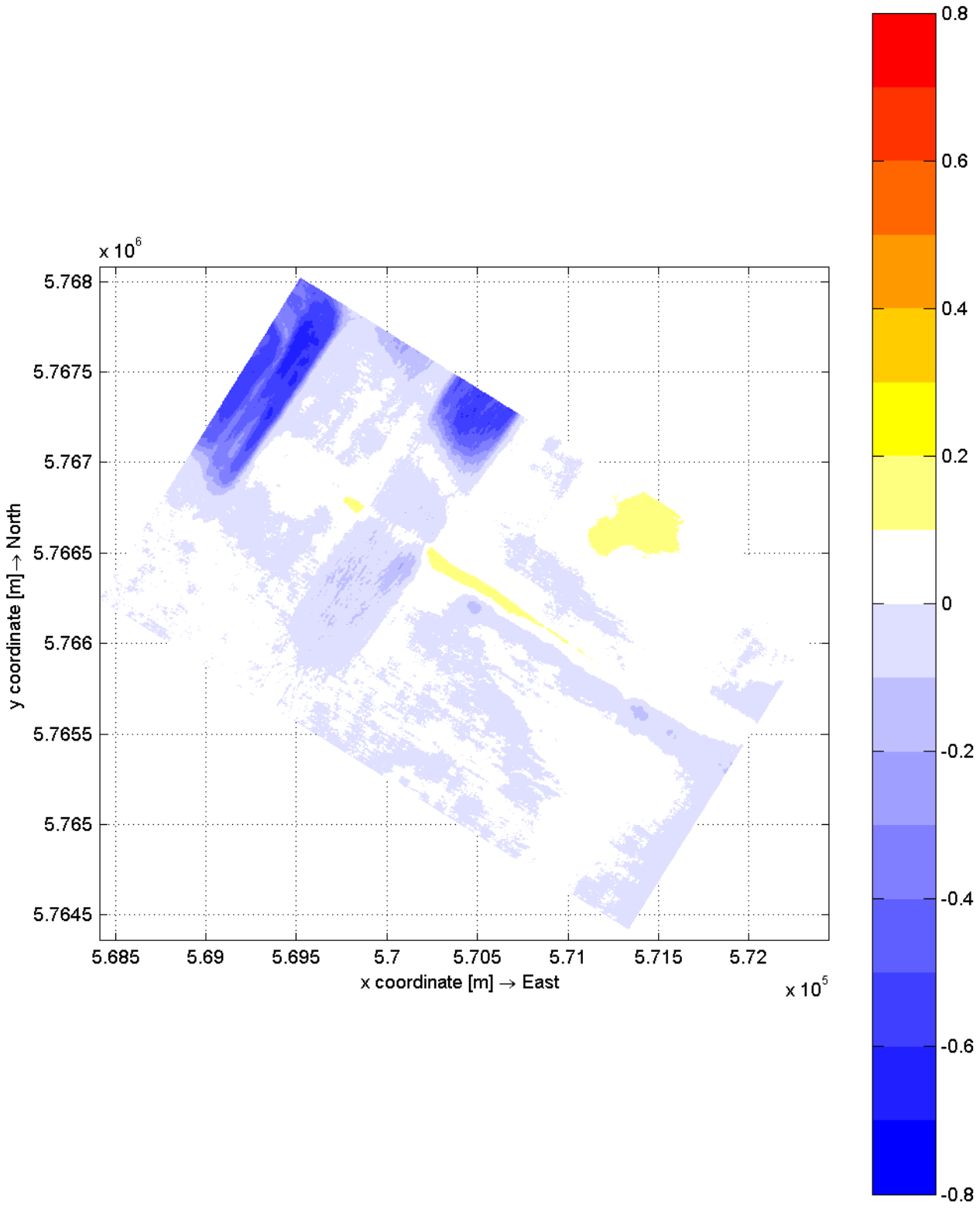

data-analysis: sedimentation / erosion between 1982 and 2000 [m/yr] sand dump Hoek van Holland, The Netherlands (UTM coordinates, zone 31		2005
	data-analysis	
WL | Delft Hydraulics	Z3079.40	Figure B.15

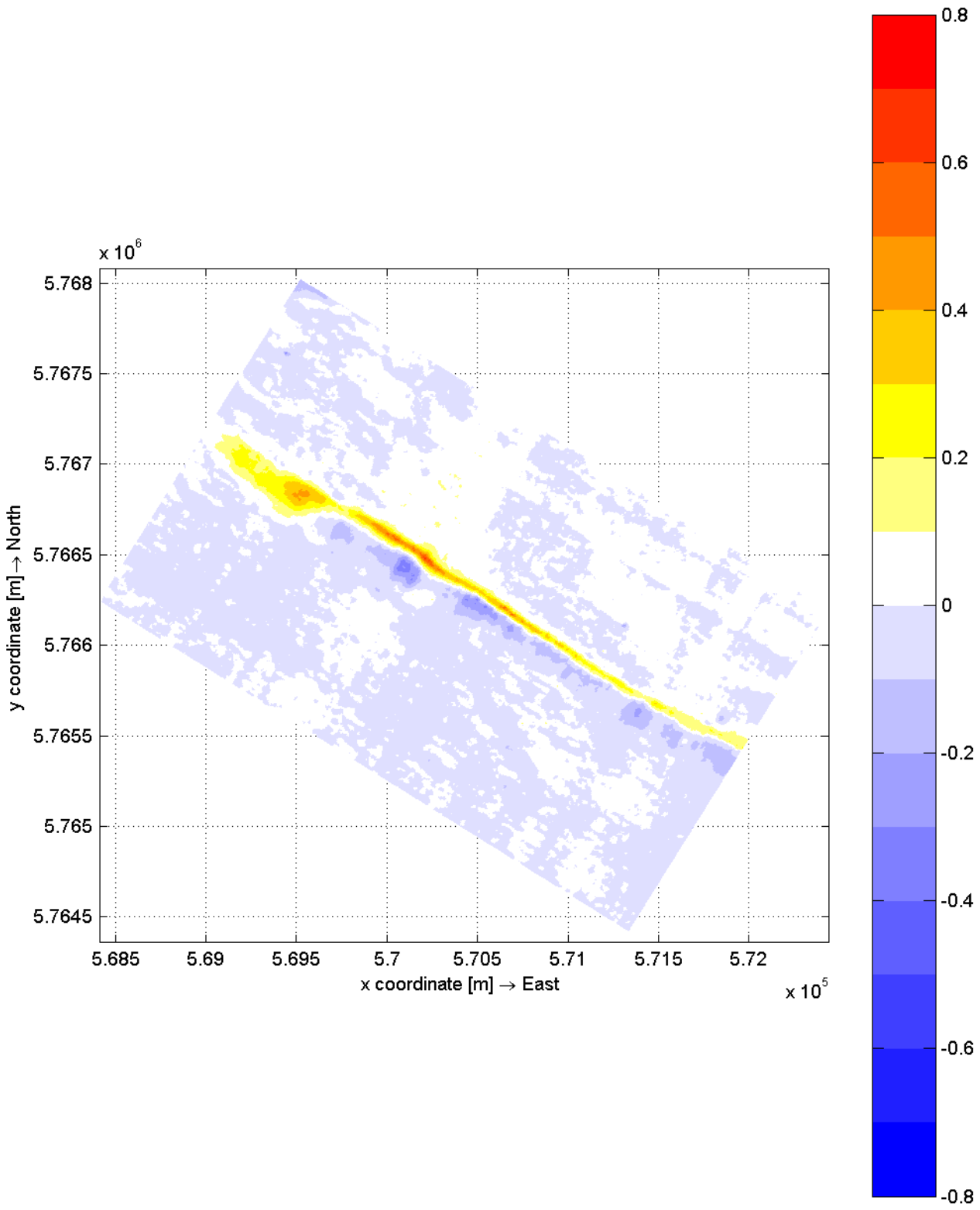

data-analysis: sedimentation / erosion between 1986 and 1991 [m/yr]
sand dump Hoek van Holland, The Netherlands (UTM coordinates, zone 31

2005

data-analysis

WL | Delft Hydraulics

Z3079.40

Figure B.16

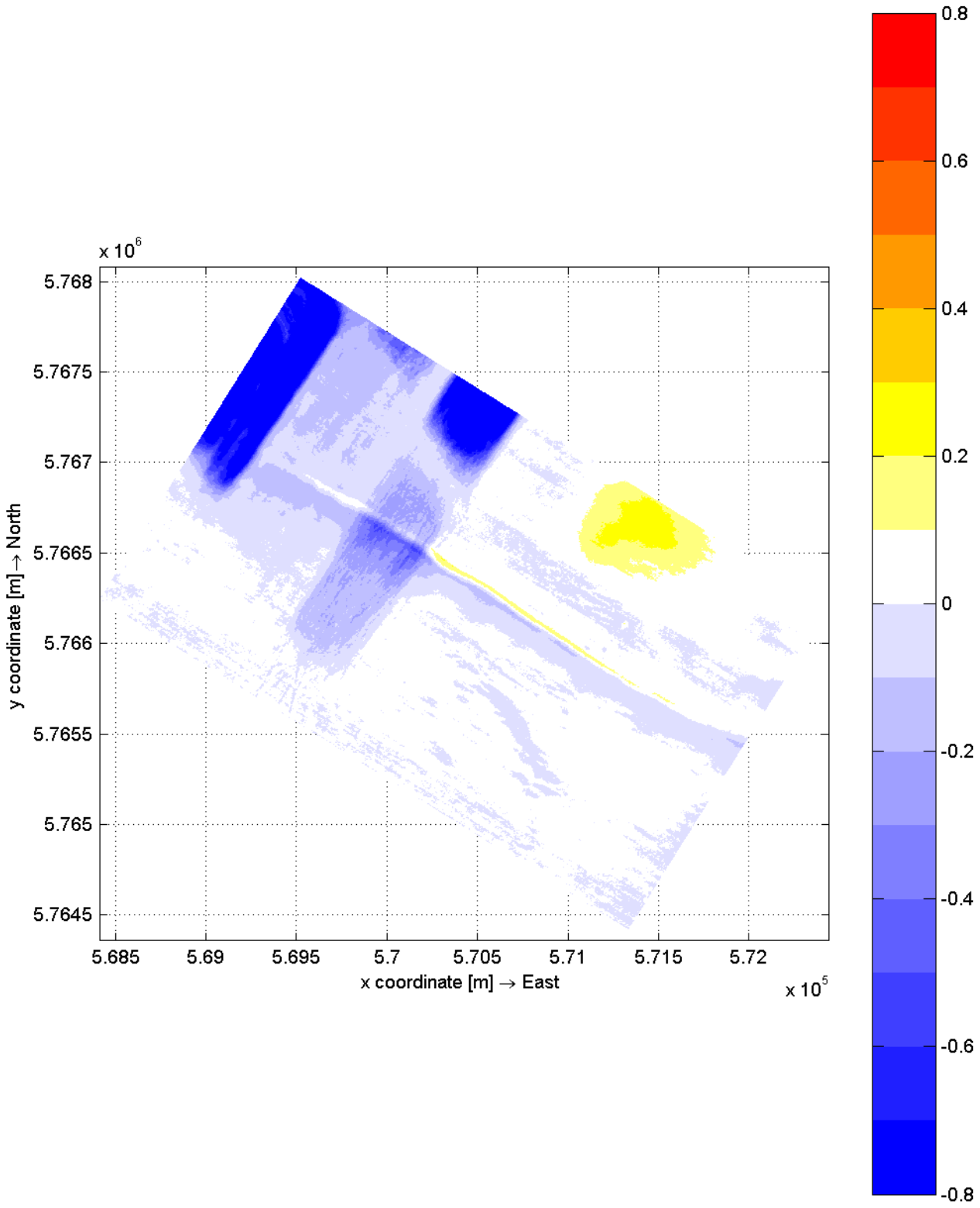

data-analysis: sedimentation / erosion between 1991 and 2000 [m/yr]
sand dump Hoek van Holland, The Netherlands (UTM coordinates, zone 31

2005

data-analysis

WL | Delft Hydraulics

Z3079.40

Figure B.17

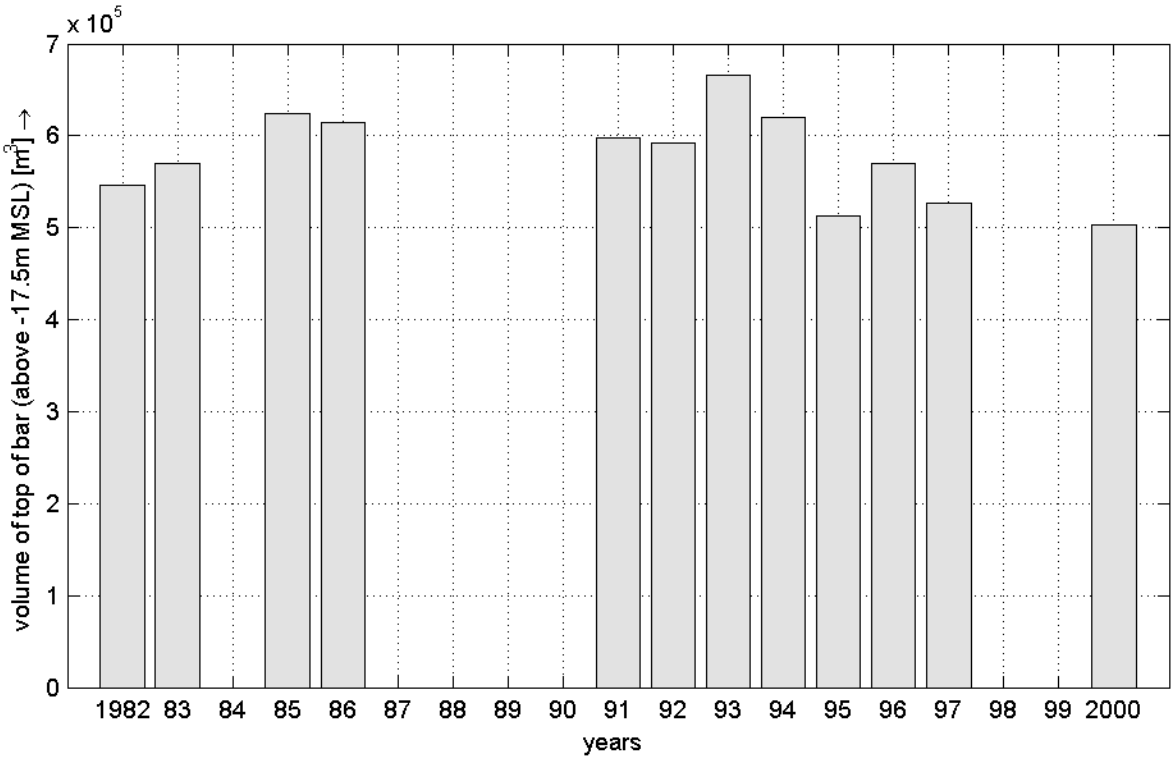

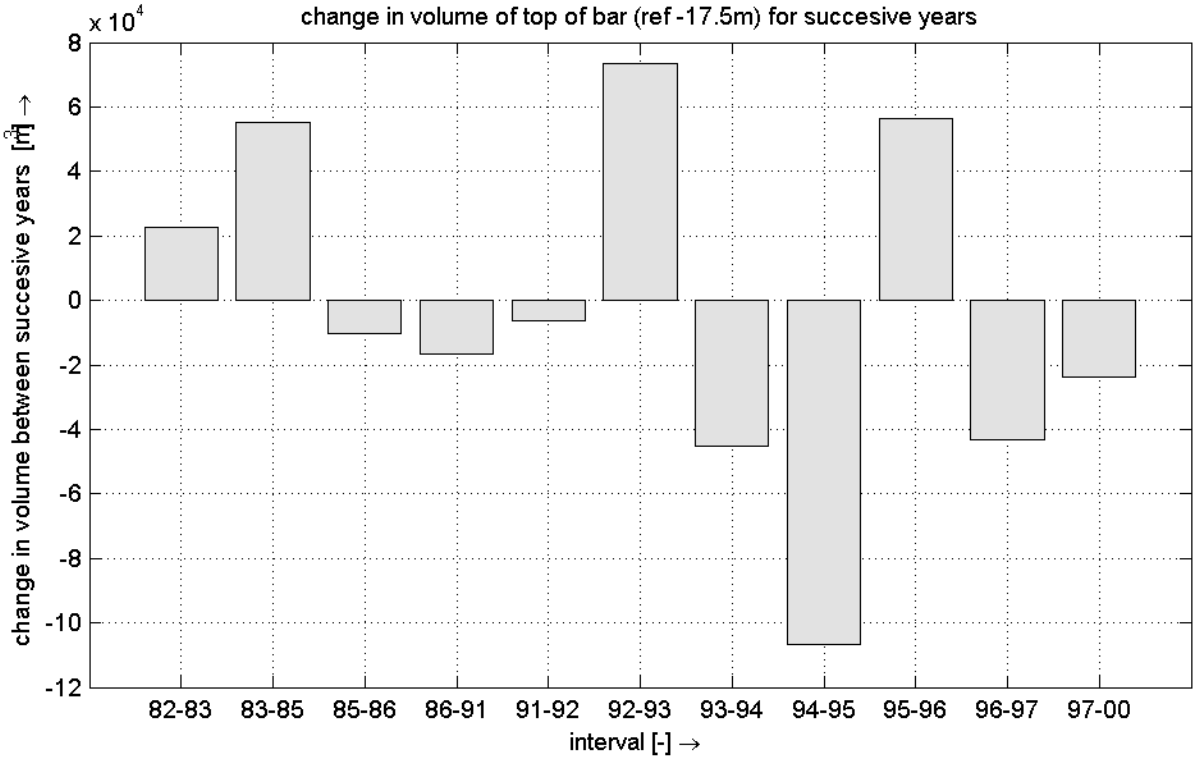

WL | Delft Hydraulics (11:14:05 on Fri 25th Mar 2005)

data-analysis volume of bar above -17.5 m to MSL. considered area: 800 to 1500m from 0-line sand dump Hoek van Holland, The Netherlands		2005
	data-analysis	
WL | Delft Hydraulics	Z3079.40	Figure B.18

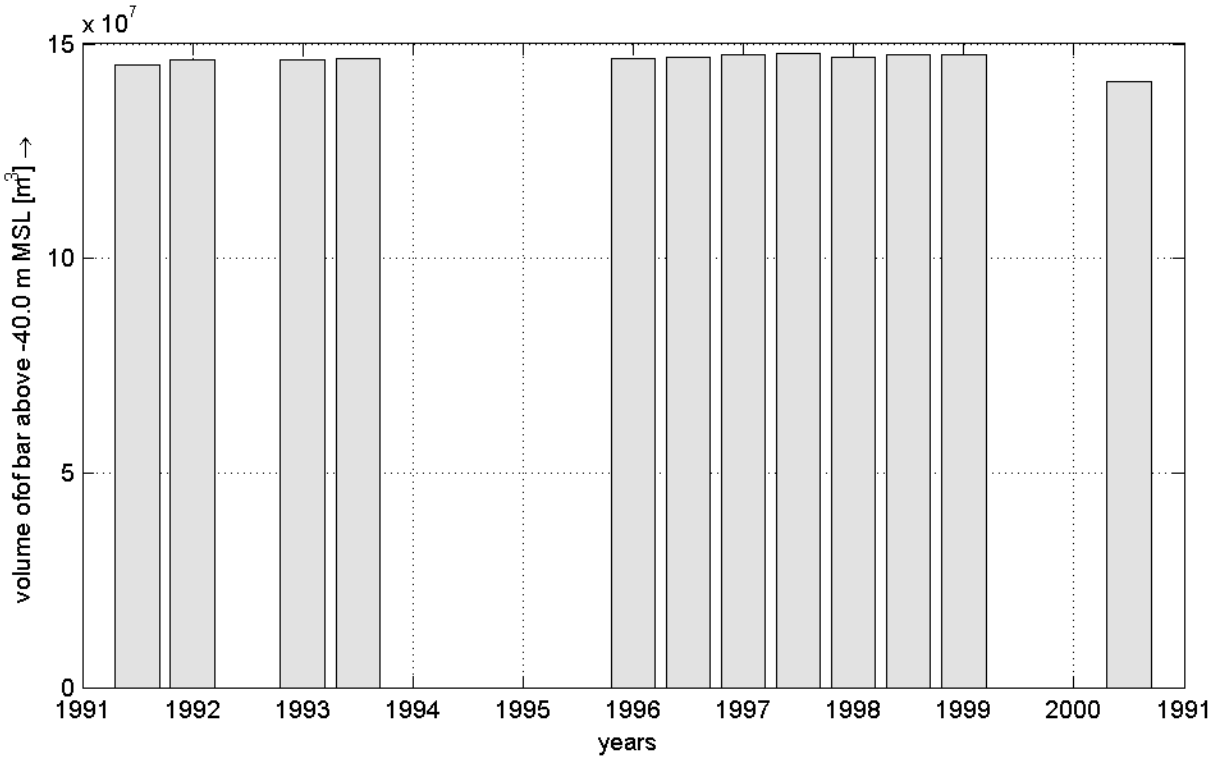

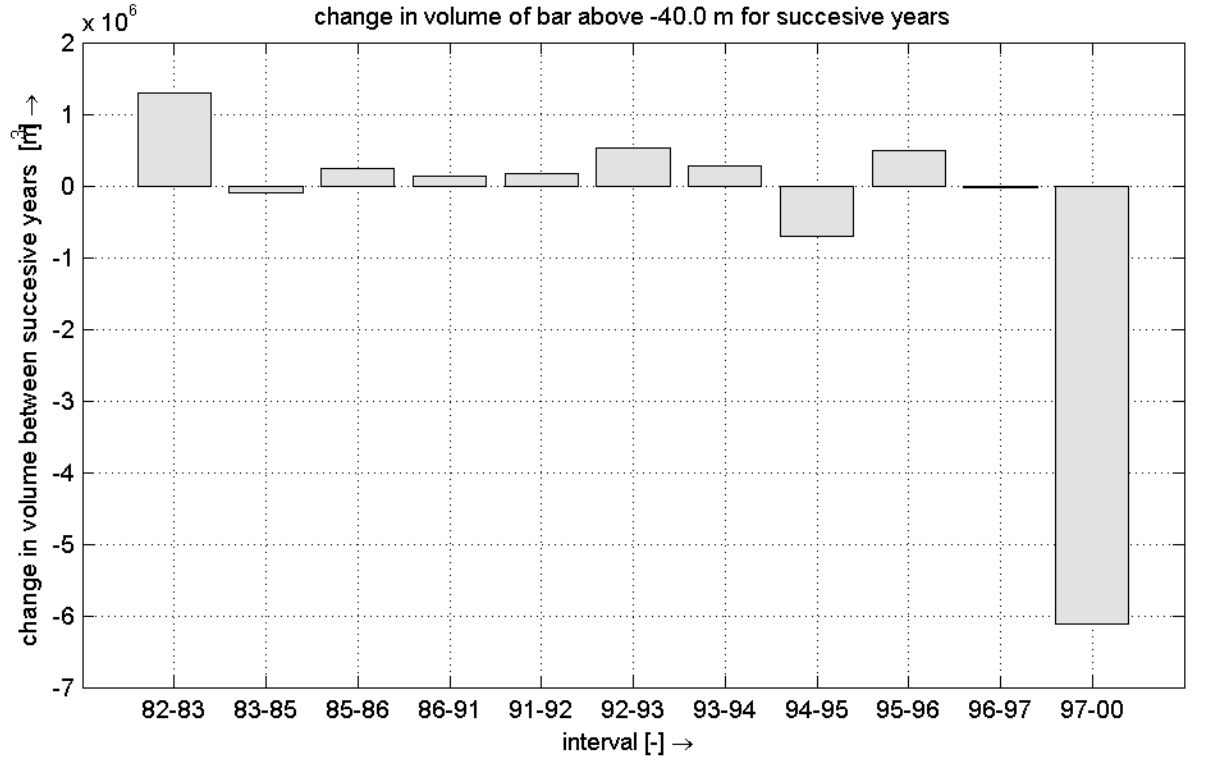

WL | Delft Hydraulics (11:11:19 on Fri 25th Mar 2005)

data-analysis: volume of bar above -40.0 m to MSL. considered area: 800 to 1500m from 0-line sand dump Hoek van Holland, The Netherlands		2005
	data-analysis	
WL | Delft Hydraulics	Z3079.40	Figure B.19

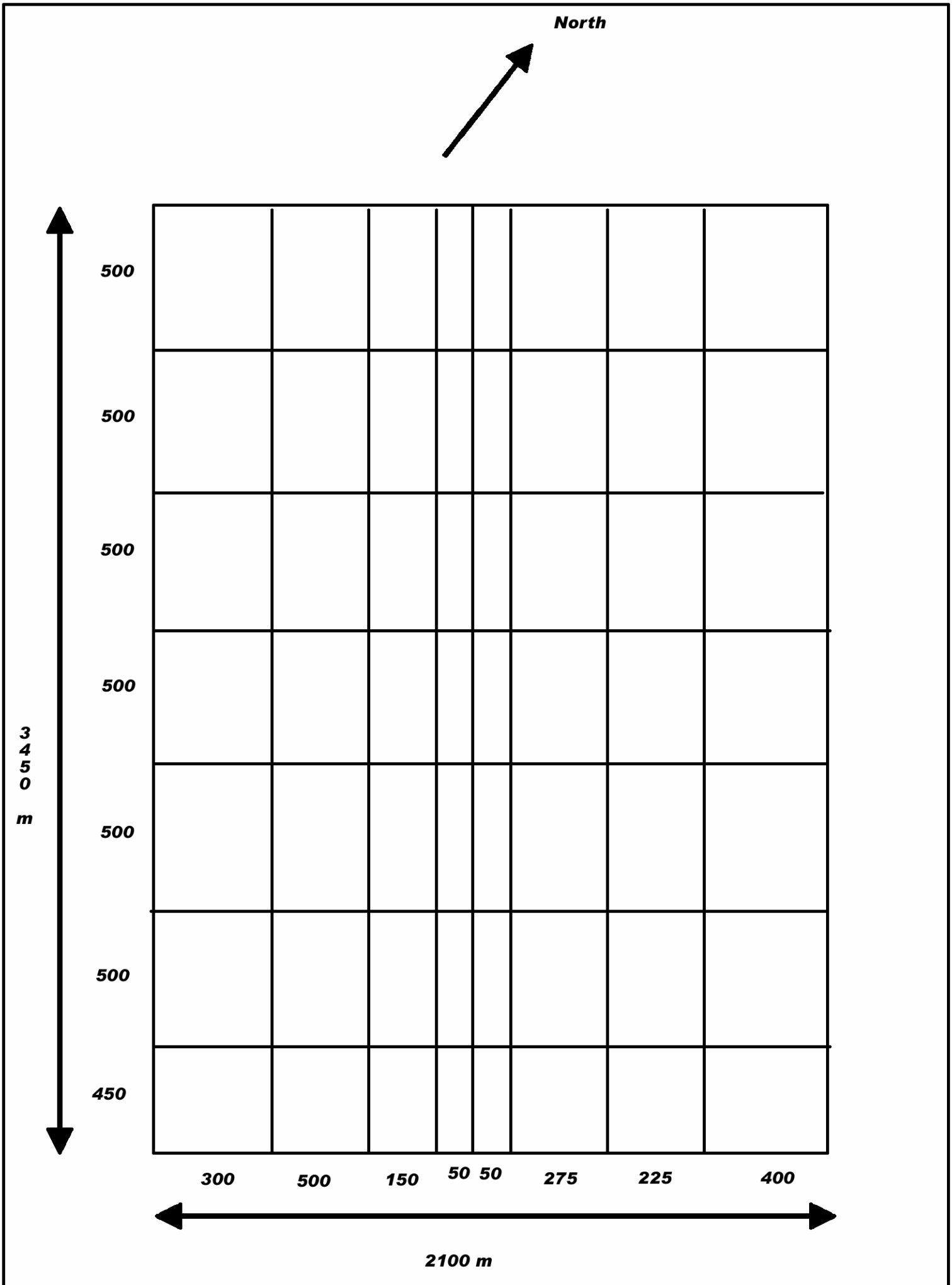
North
500
500
500
500
500
450
3450 m
300
500
150
50
50
275
225
400
2100 m

Figure B.20

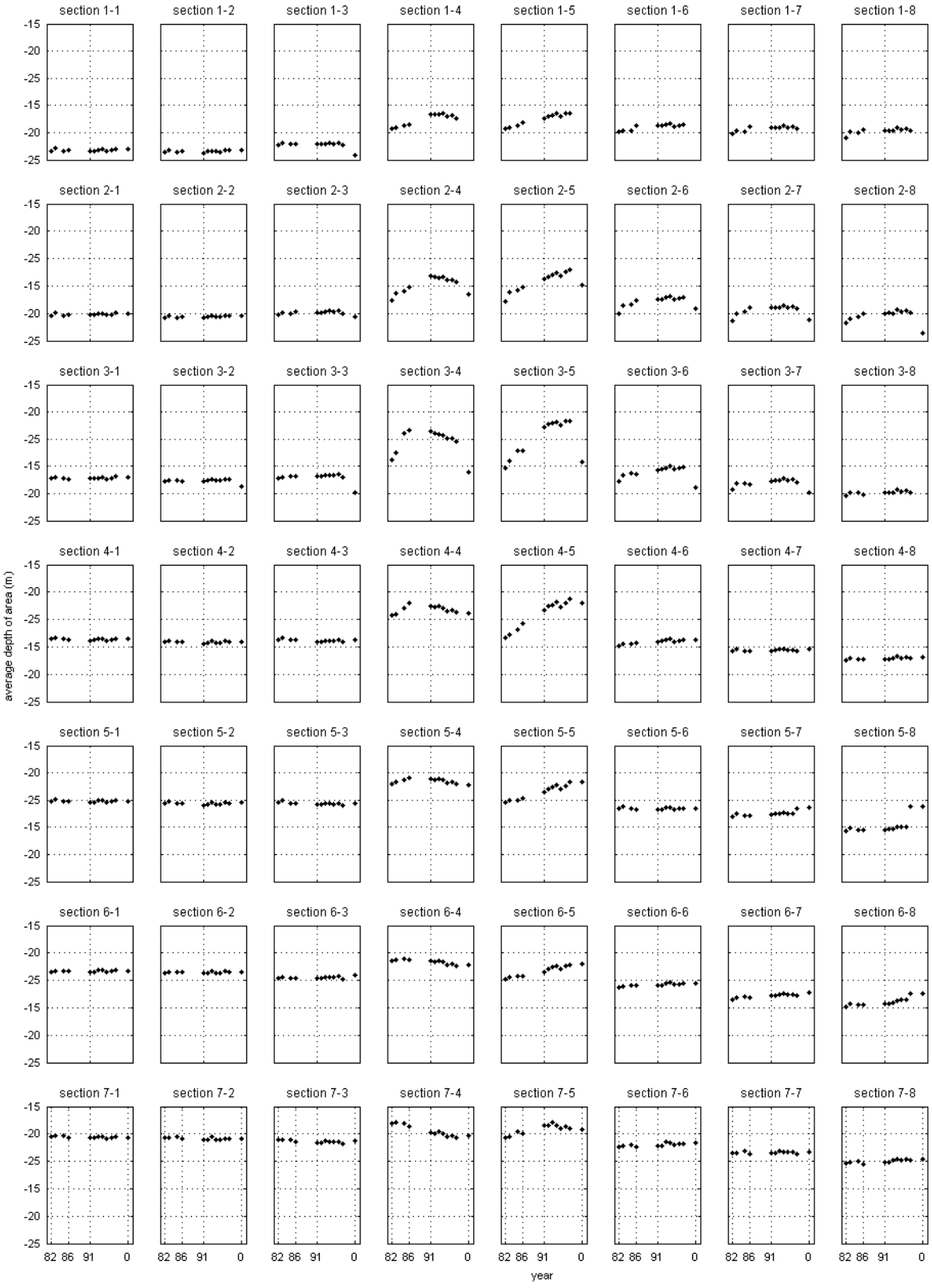

data-analysis: average depth per section for all available years
sand dump Hoek van Holland, The Netherlands

2005

data-analysis

WL | Delft Hydraulics

Z3079.40

Figure B.21

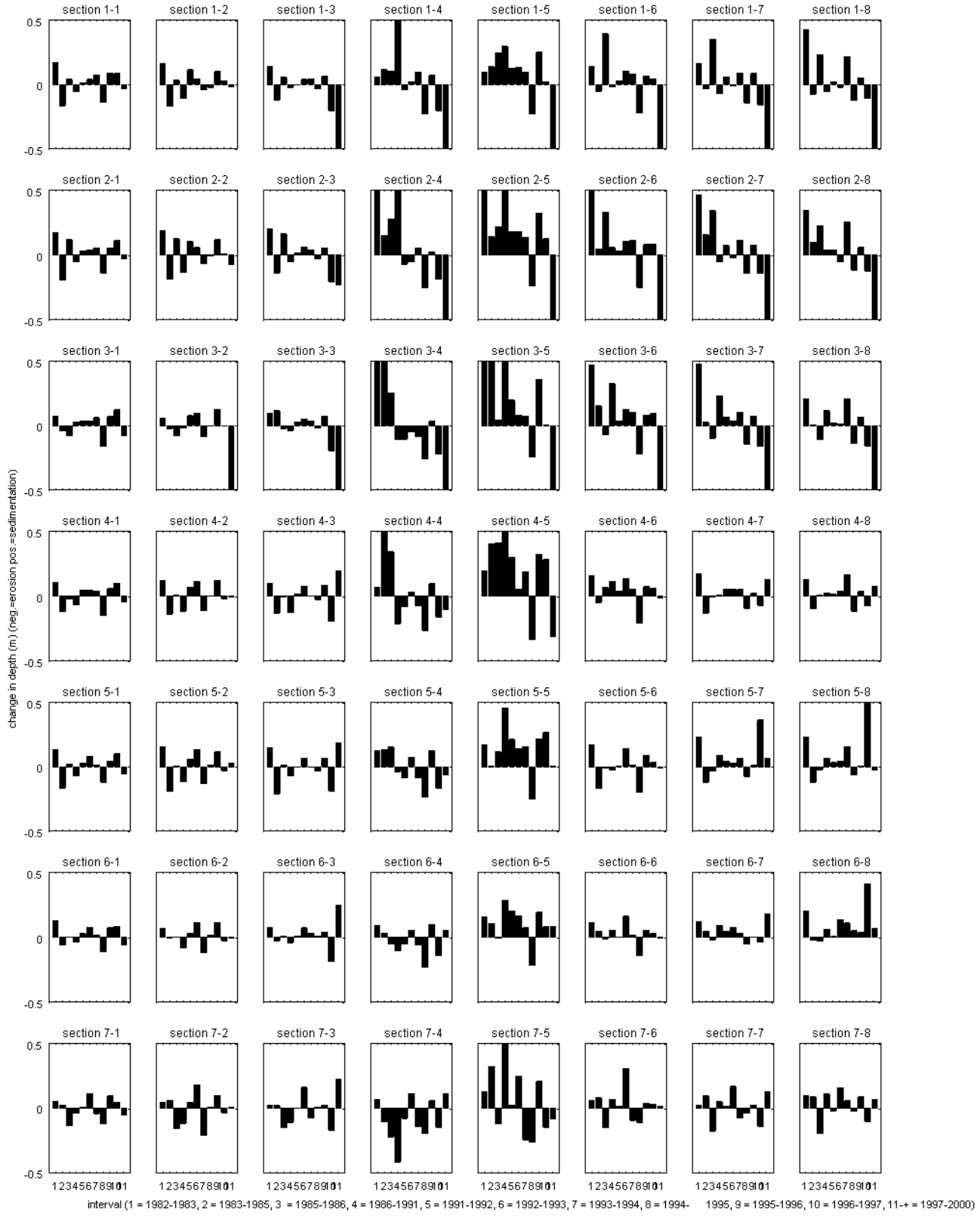

data-analysis: change in depth per section for succesive years
sand dump Hoek van Holland, The Netherlands

2005

data-analysis

WL | Delft Hydraulics

Z3079.XX

Figure B.22

C Idealized sand ridge modelling

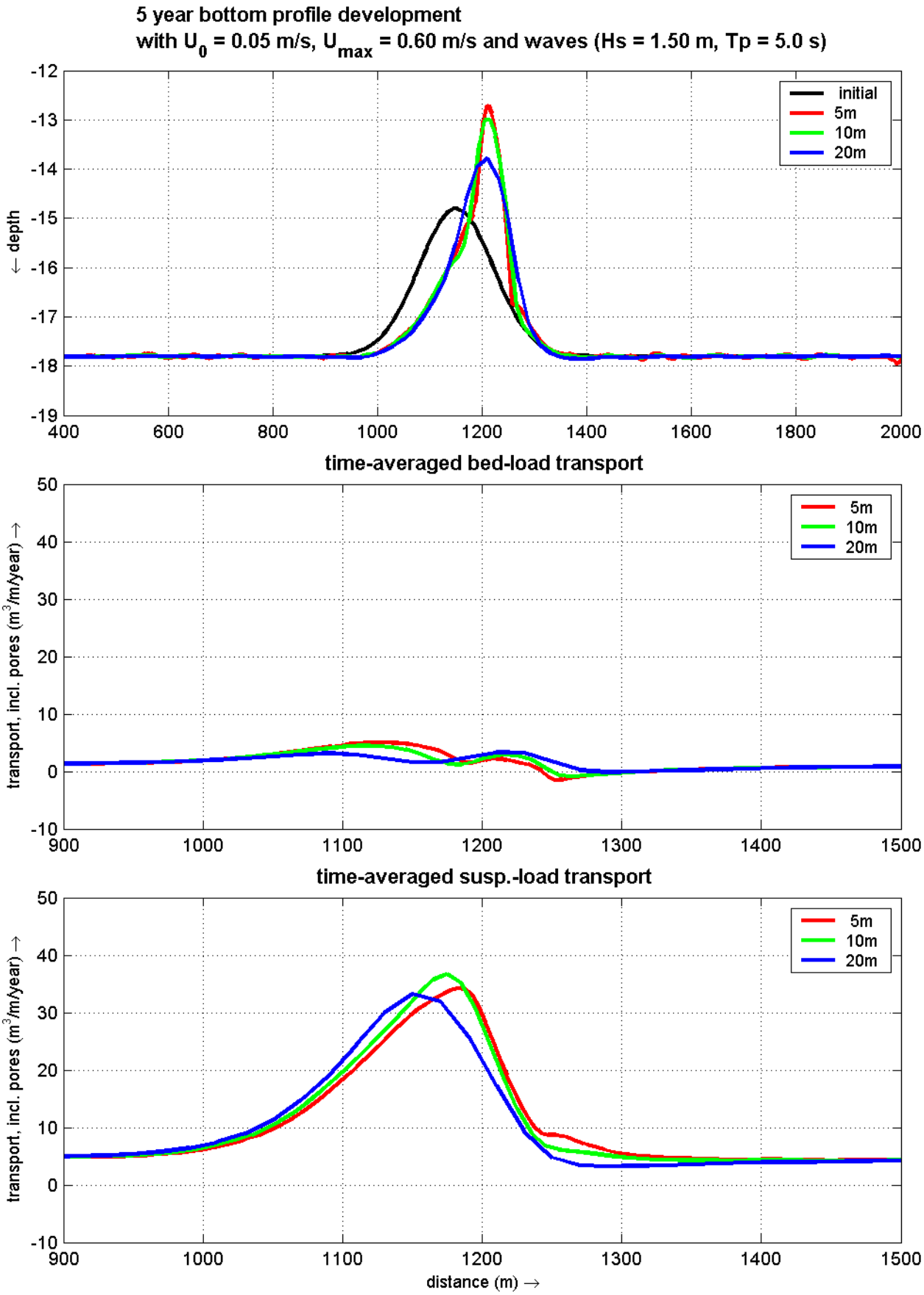

idealized sand ridge, model set-up: horizontal gridsize 5 year bottom profile development, time-averaged bed-l. and susp.-l transport rates algebraic turb. model, TR2004 with variable roughness, waves (Hs = 1.50 m, Tp = 5.0 s)		2005
	idealized sand ridge	
WL | Delft Hydraulics	Z3079.40	Figure C.01

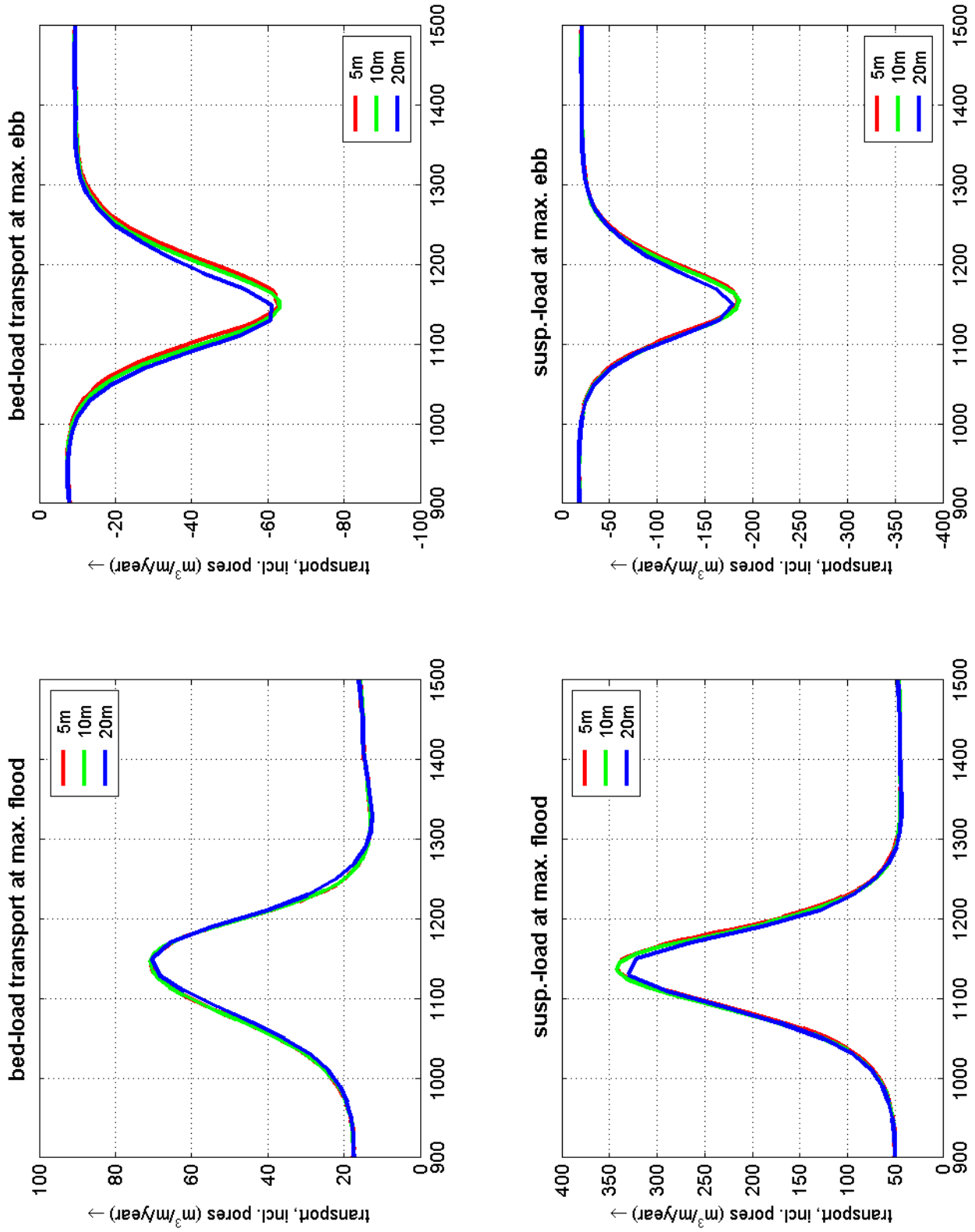

idealized sand ridge model set-up: horizontal gridsize
transport rates at max. flood and max. ebb over initial bottom profile
tide: (U_0 = 0.05m/s, U_1 = 0.60m/s) waves: (Hs = 1.50m, Tp = 5.0s)

2005

idealized sand ridge

WL | Delft Hydraulics

Z3079.40

Figure C.02

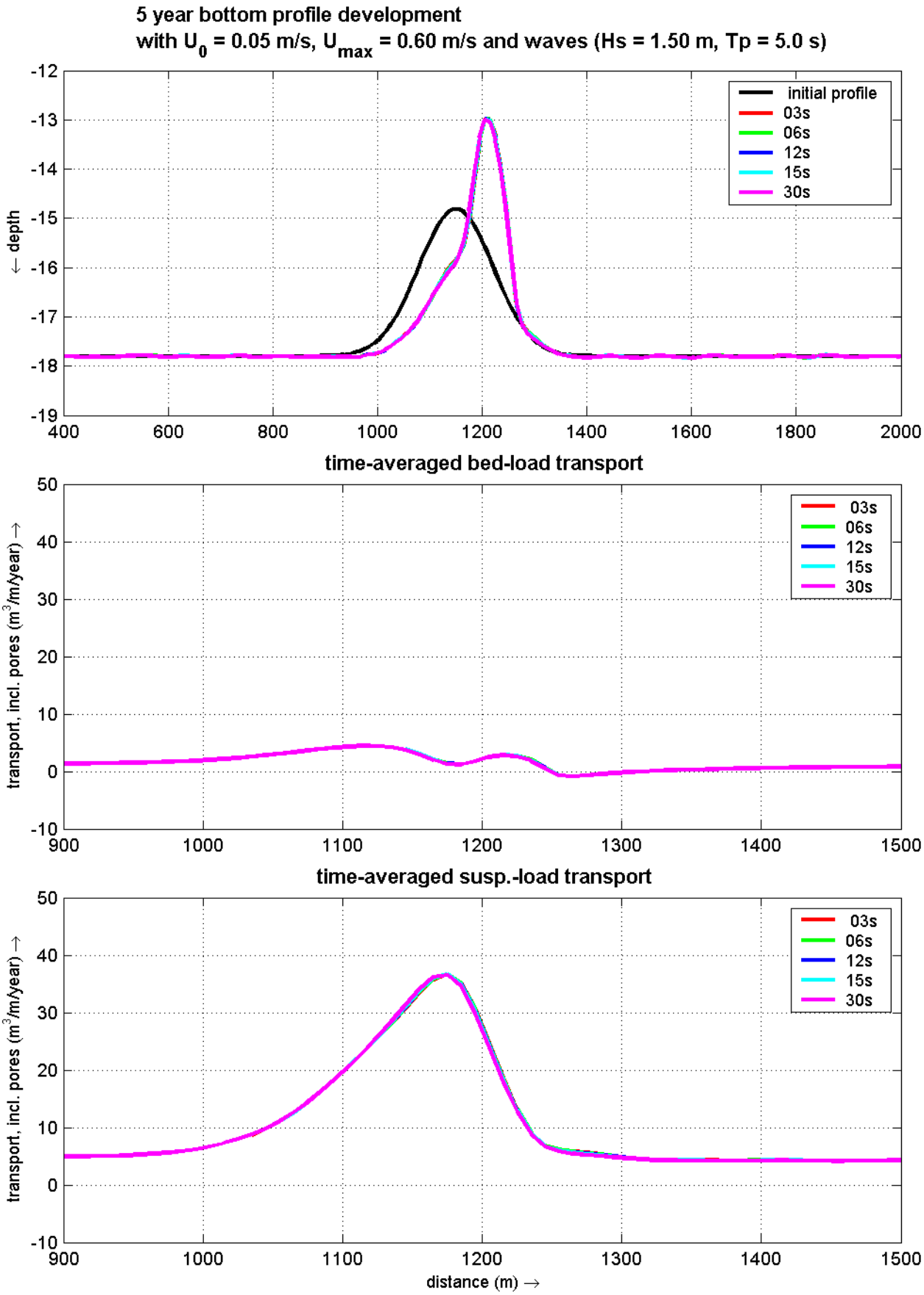

idealized sand ridge, model set-up: computational time step time-averaged bed-l. and suspended-l transport rates over initial bottom profile algebraic turb. model, TR2004 with variable roughness, waves (Hs = 1.50 m, Tp = 5.0 s)		2005
	idealized sand ridge	
WL | Delft Hydraulics	Z3079.40	Figure C.03

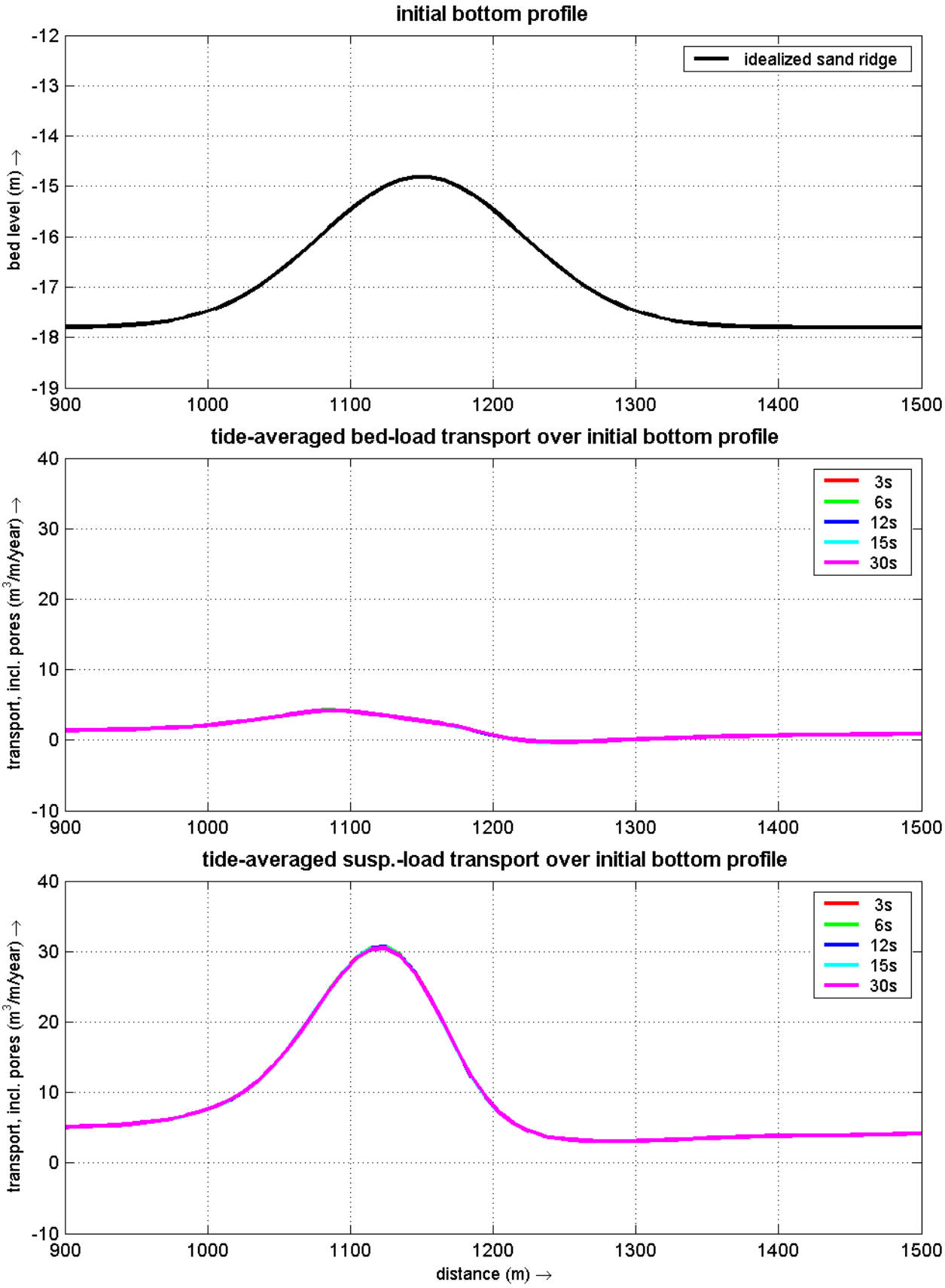

idealized sand ridge model: timestep
tide-averaged bed-l. and suspended-l transport rates over initial bottom profile
tide: (U_0 = 0.05, U_1 = 0.60 m/s) waves: (Hs = 1.5m, Tp = 5.0s)

2005

idealized sand ridge

WL | Delft Hydraulics

Z3079.40

Figure C.04

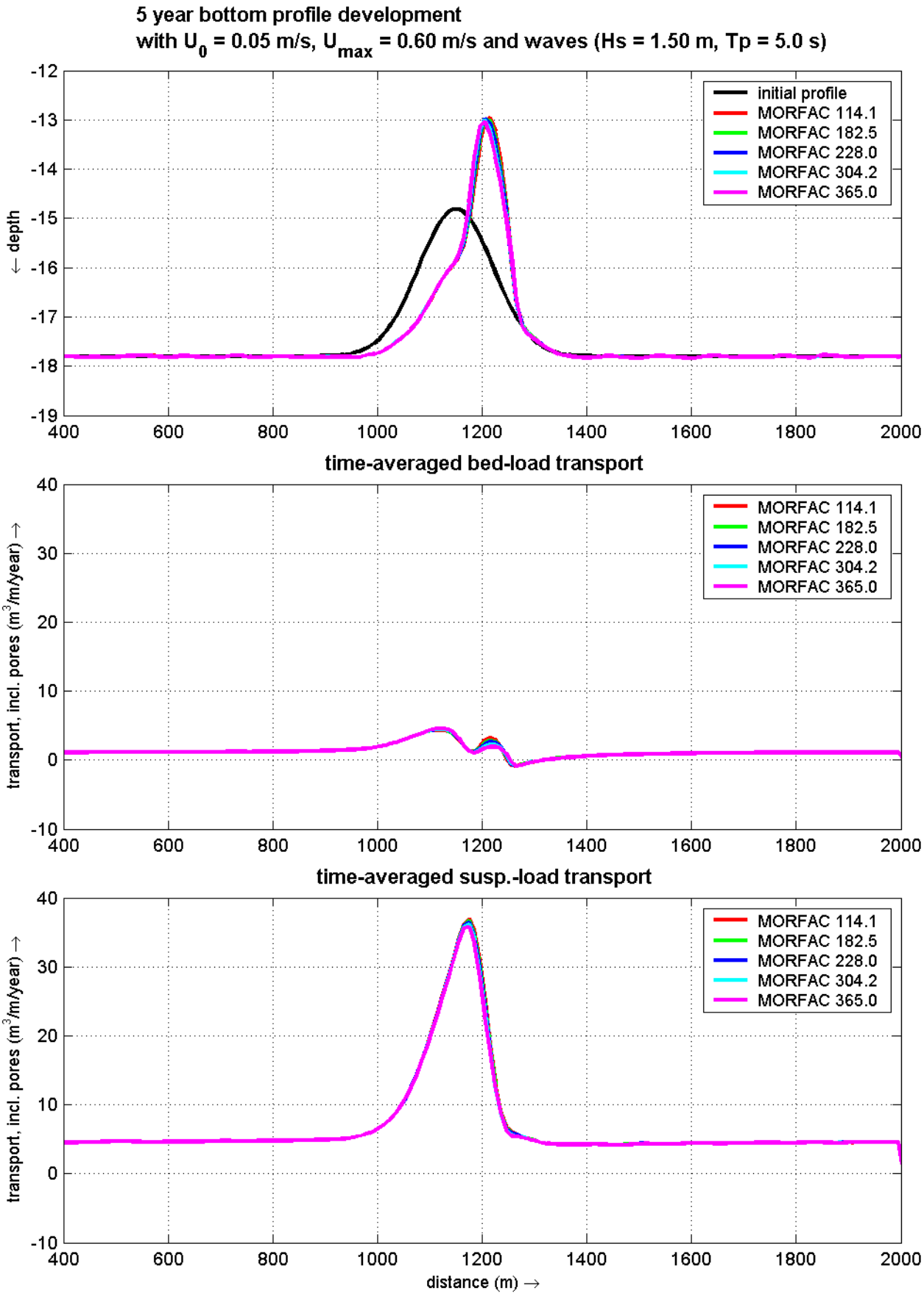

idealized sand ridge model set-up: morphological scale factor time-averaged bed-l. and suspended-l transport rates over initial bottom profile algebraic turb. model, TR2004 with variable roughness, waves (Hs = 1.50 m, Tp = 5.0 s)		2005
	idealized sand ridge	
WL | Delft Hydraulics	Z3079.40	Figure C.05

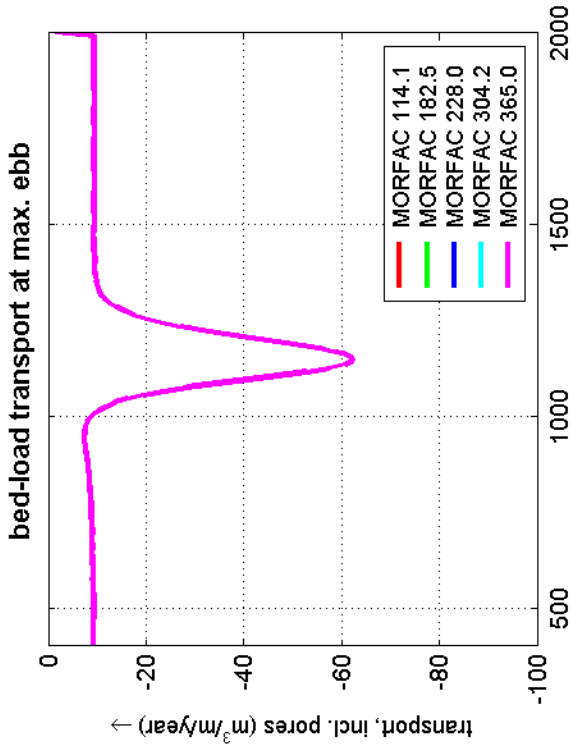

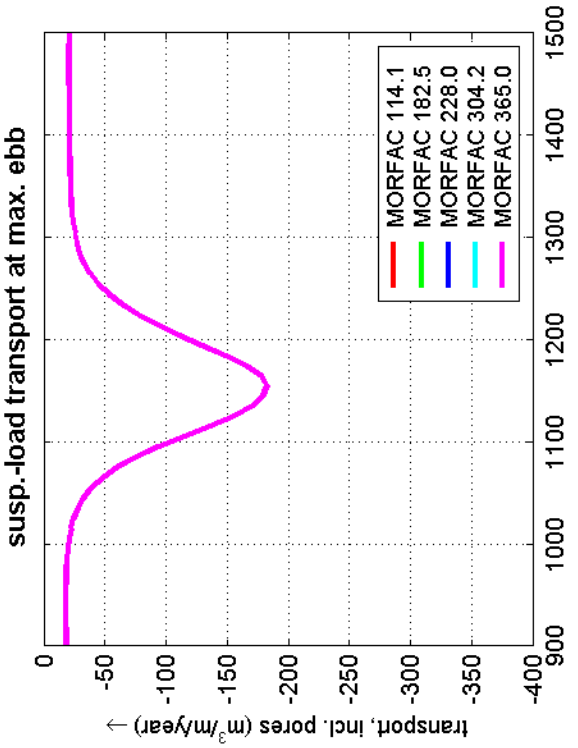

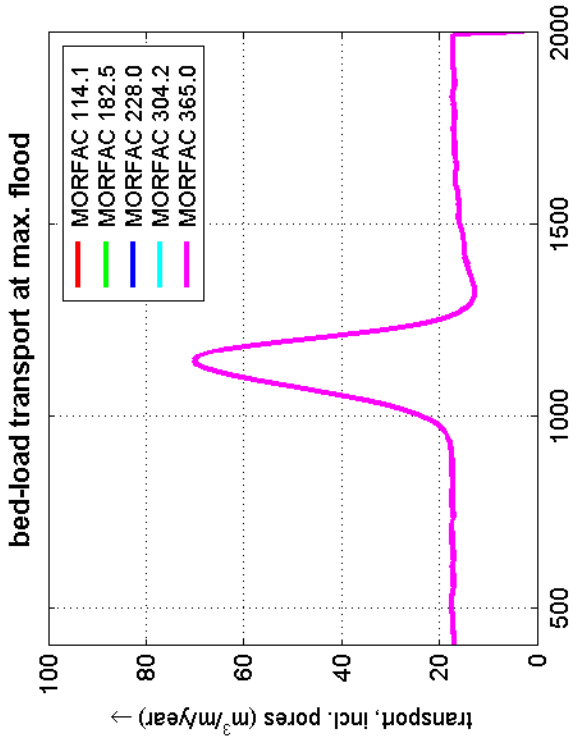

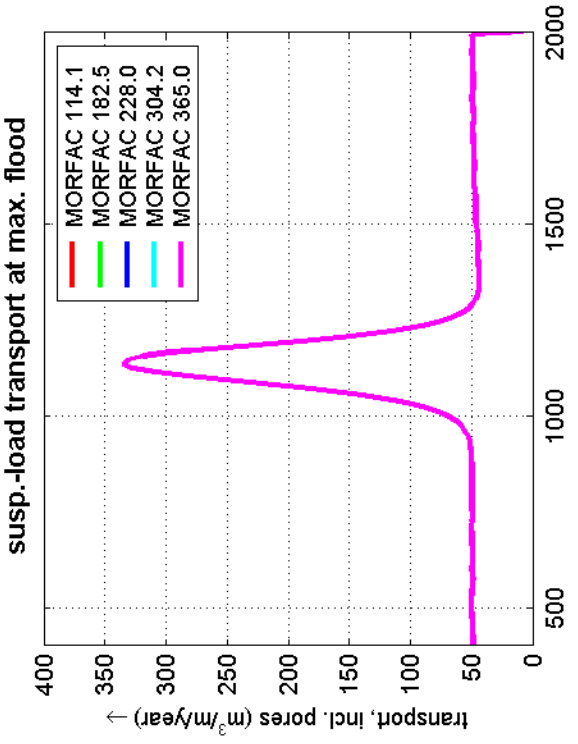

idealized sand ridge model set-up: morphological scale factor
transport rates at max. flood and max. ebb over initial bottom

2005

idealized sand ridge

WL | Delft Hydraulics

Z3079.40

Figure C.06

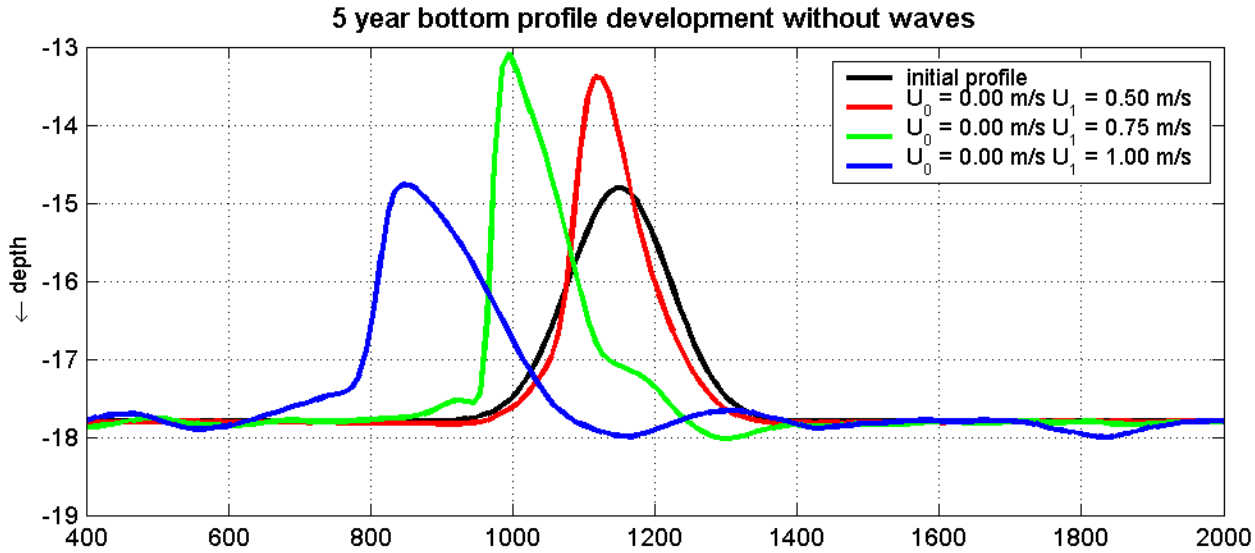

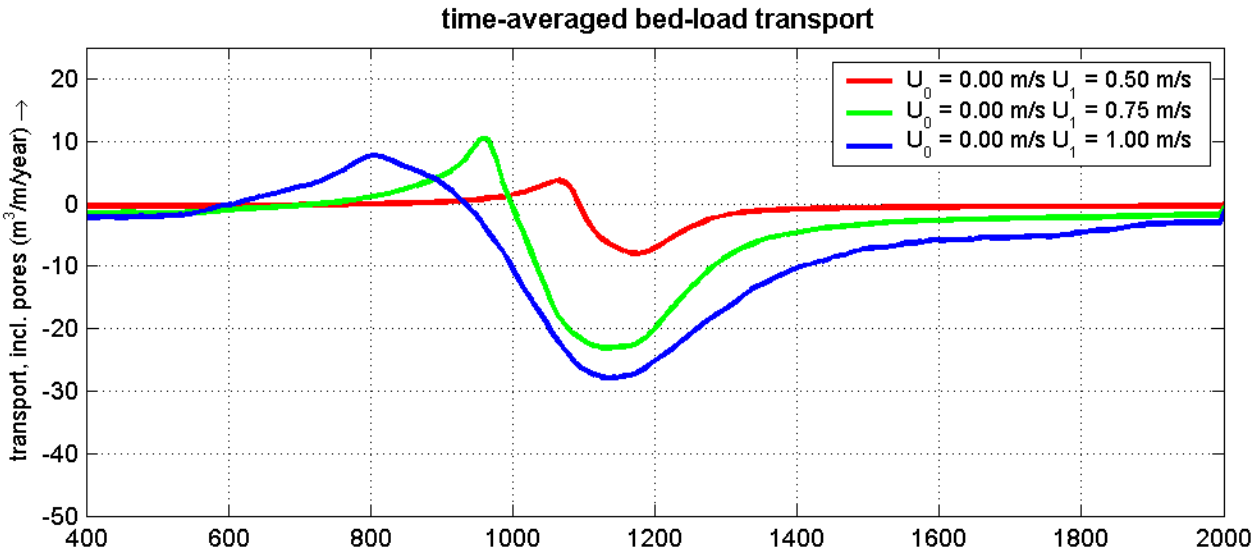

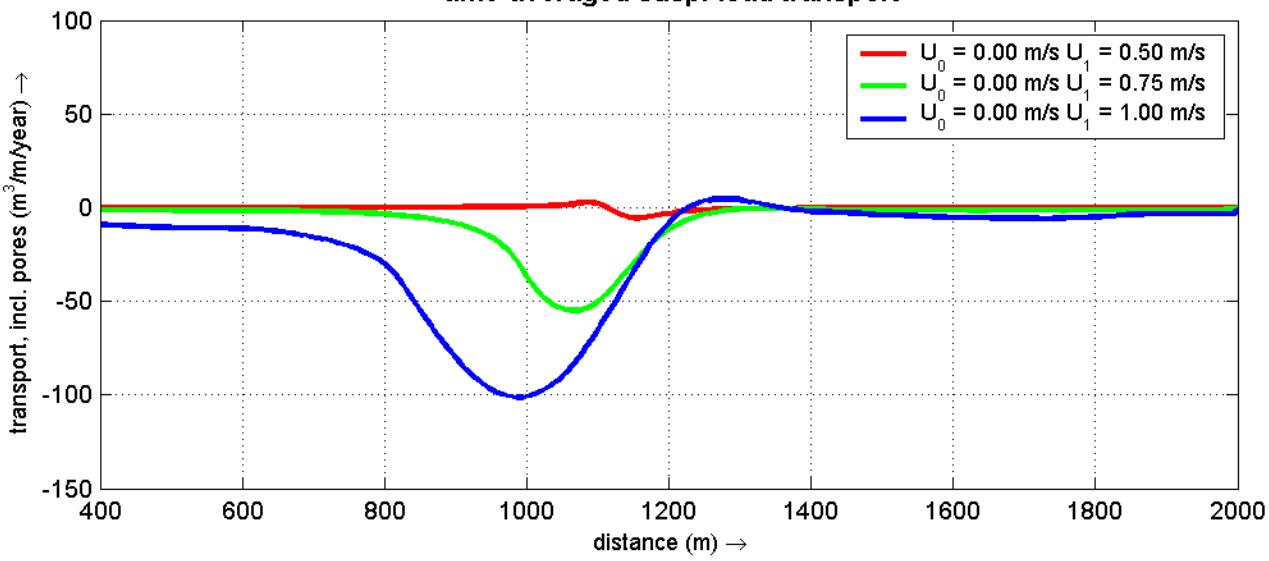

idealized sand ridge model: effect of tides without drift
bottom profile development, time-averaged bed-l. and suspended-l. transport rates
U_0 = 0.00 m/s and U_1 = 0.50/0.75/1.00 m/s without waves

2005

idealized sand ridge

WL | Delft Hydraulics

Z3079.40

Figure C.07

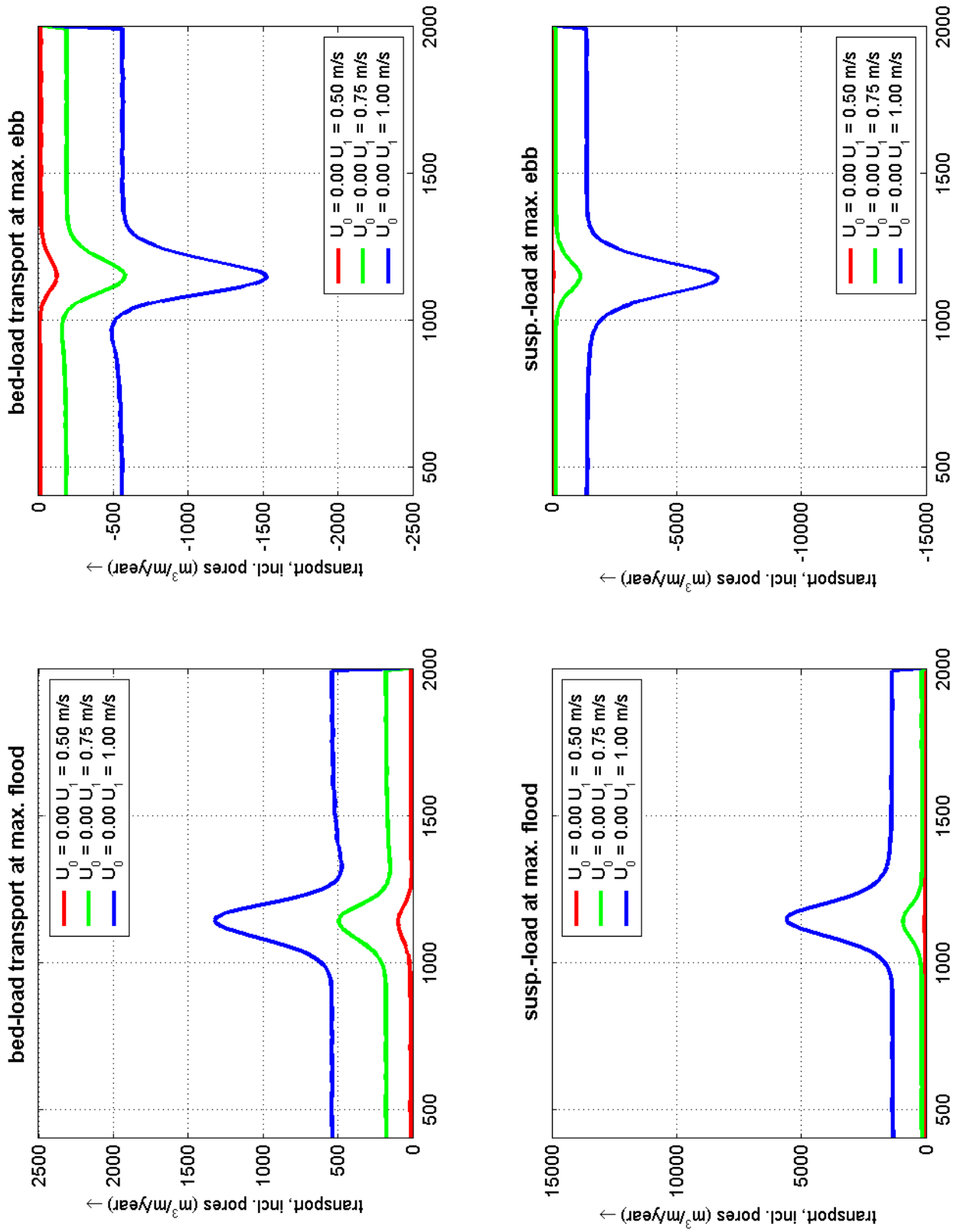

idealized sand ridge model: effect of tides without drift
transport rates at max. flood and max. ebb over initial bottom profile
tide: (U_0 = 0.00m/s, U_1 = 0.50/0.75/1.00 m/s) without waves

2005

idealized sand ridge

WL | Delft Hydraulics

Z3079.40

Figure C.08

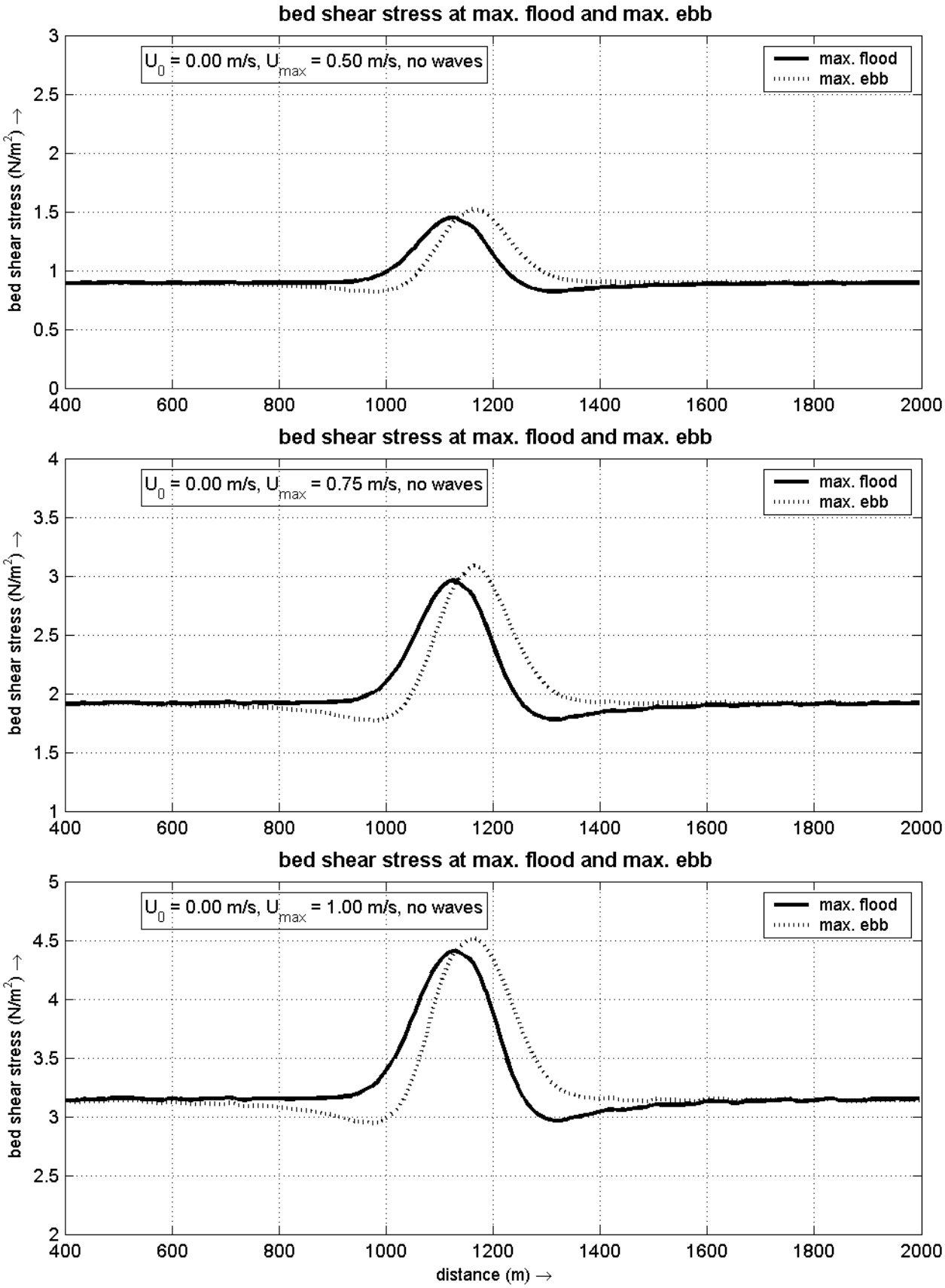

idealized sand ridge model: effect of tides without net current (drift)
bed shear stress at max. flood and max. ebb
U_0 = 0.00m/s, U_1 = 0.50/0.75/1.00m/s, no waves

2005

idealized sand ridge

WL | Delft Hydraulics

Z3079.40

Figure C.09

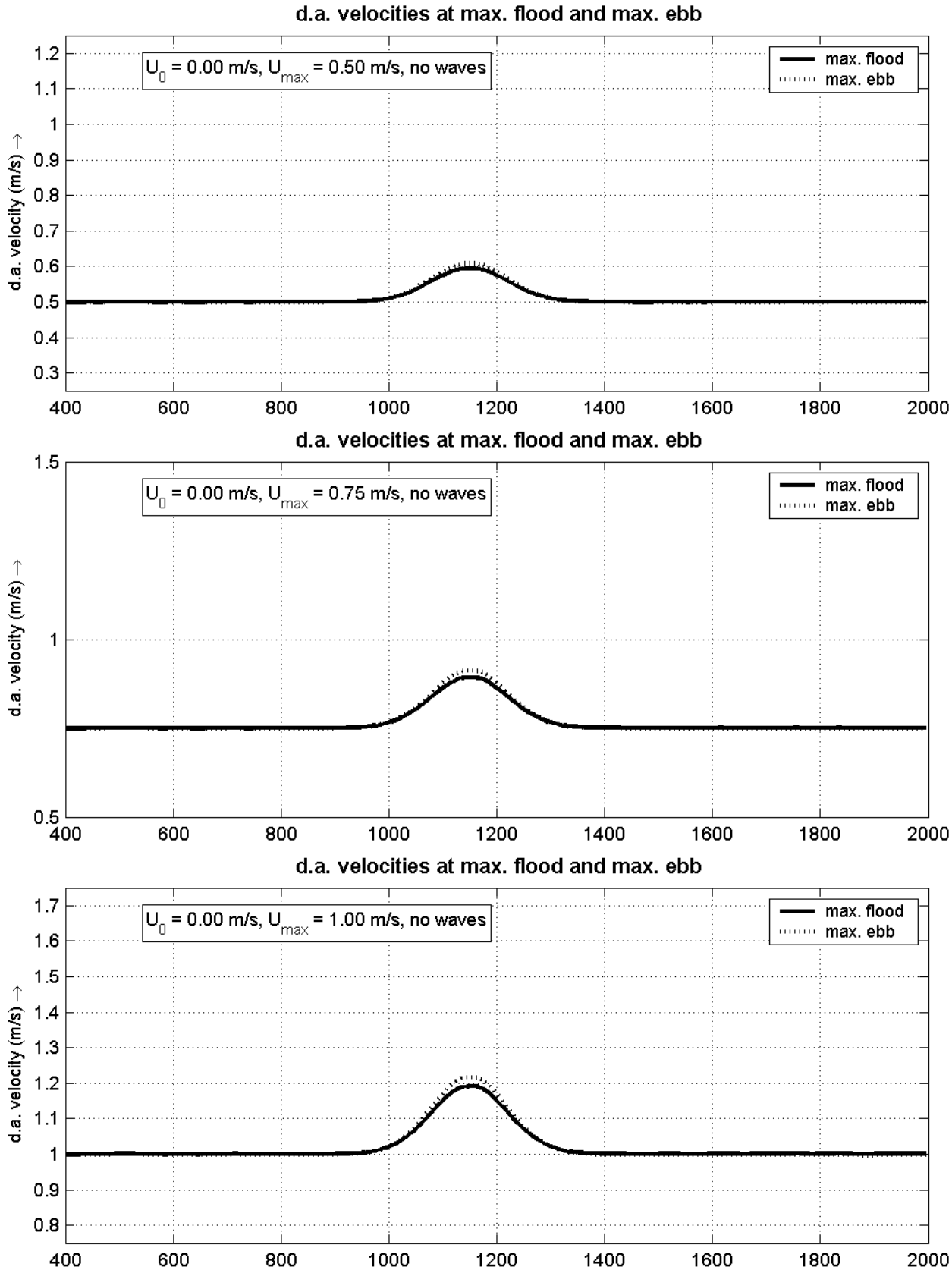

idealized sand ridge model effect of tides without net current (drift) d.a. velocities at max. flood and max. ebb U_0 = 0.00m/s, U_1 = 0.50/0.75/1.00m/s. no waves		2005
	idealized sand ridge	
WL | Delft Hydraulics	Z3079.40	Figure C.10

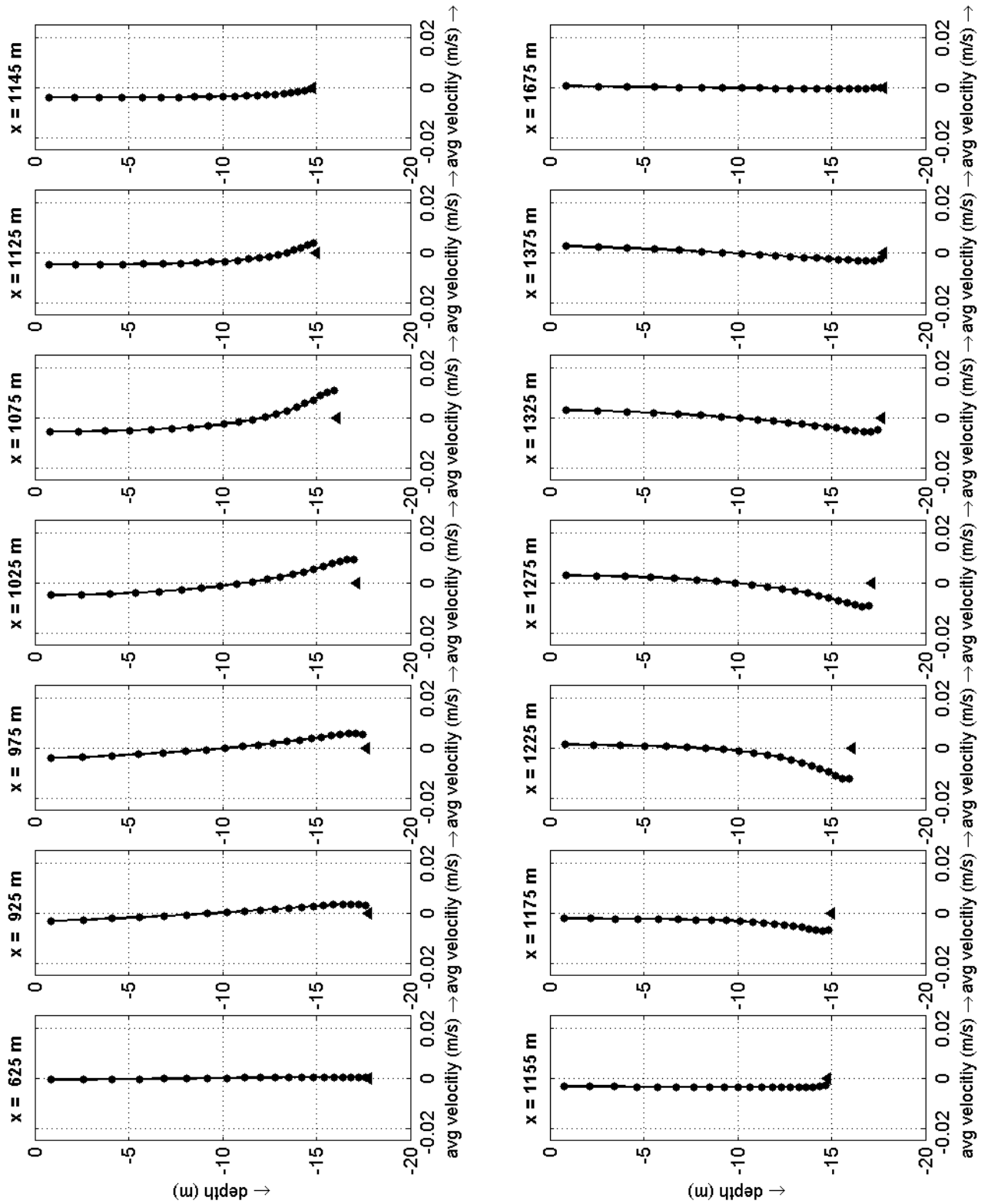

idealized sand ridge model: effect of tides without net current (drift)
tide-averaged velocity profiles at observation points
U_0 = 0.00 m/s U_1 = 0.50 m/s, no waves

2005

idealized sand ridge

WL | Delft Hydraulics

Z3079.40

Figure C.11

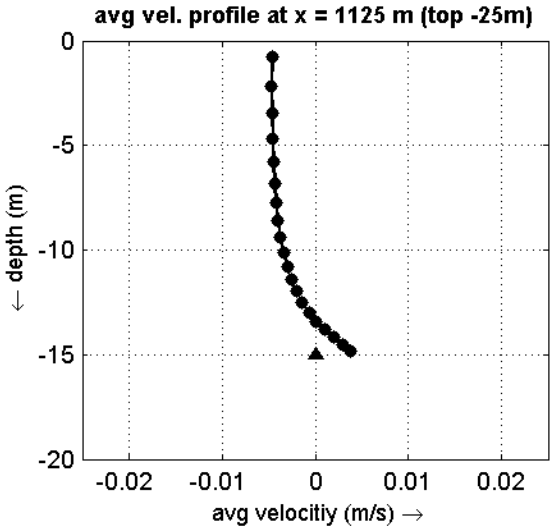

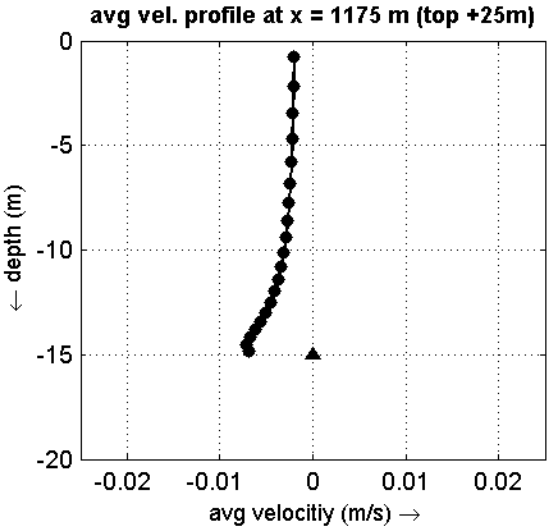

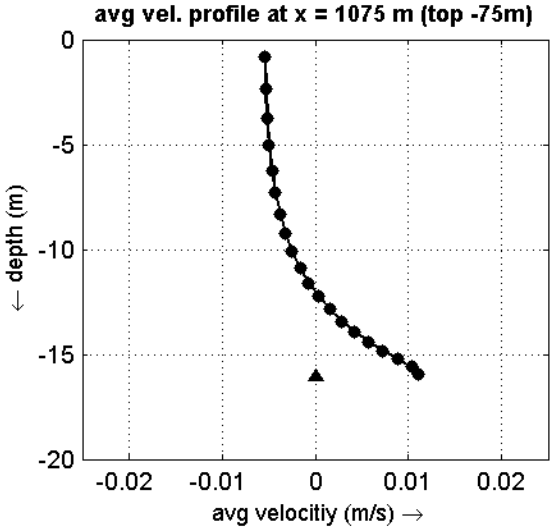

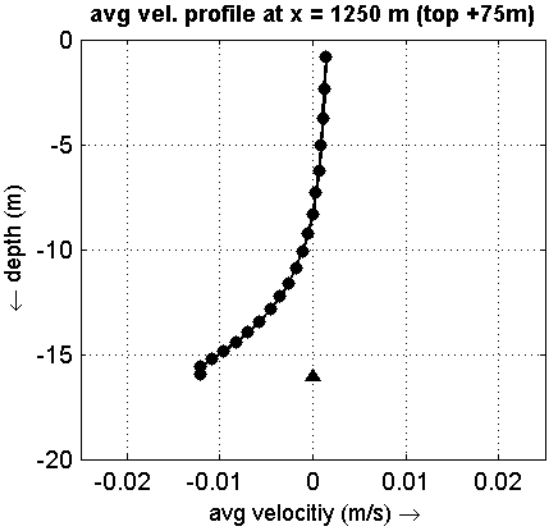

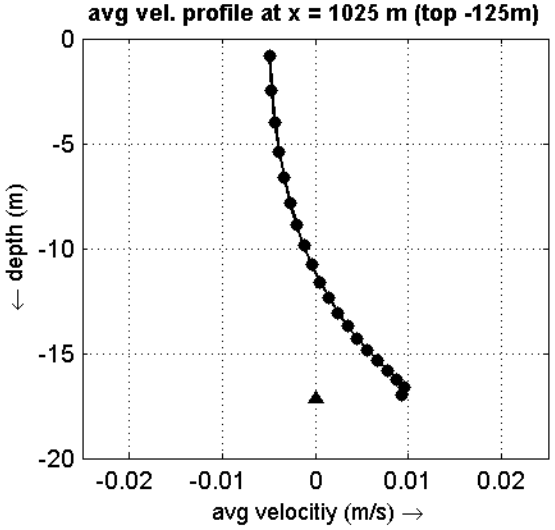

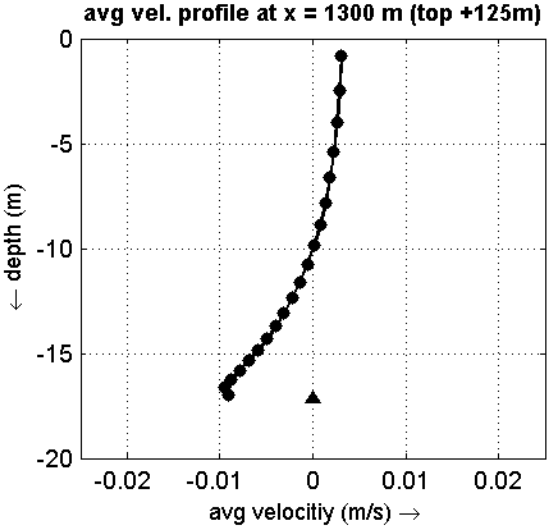

idealized sand ridge model: effect of tides without net current (drift)
tide-averaged velocity profiles at +/- 25, 75 and 125 m from the top
U_0 = 0.00 m/s U_1 = 0.50 m/s, no waves

2005

idealized sand ridge

WL | Delft Hydraulics

Z3079.40

Figure C.12

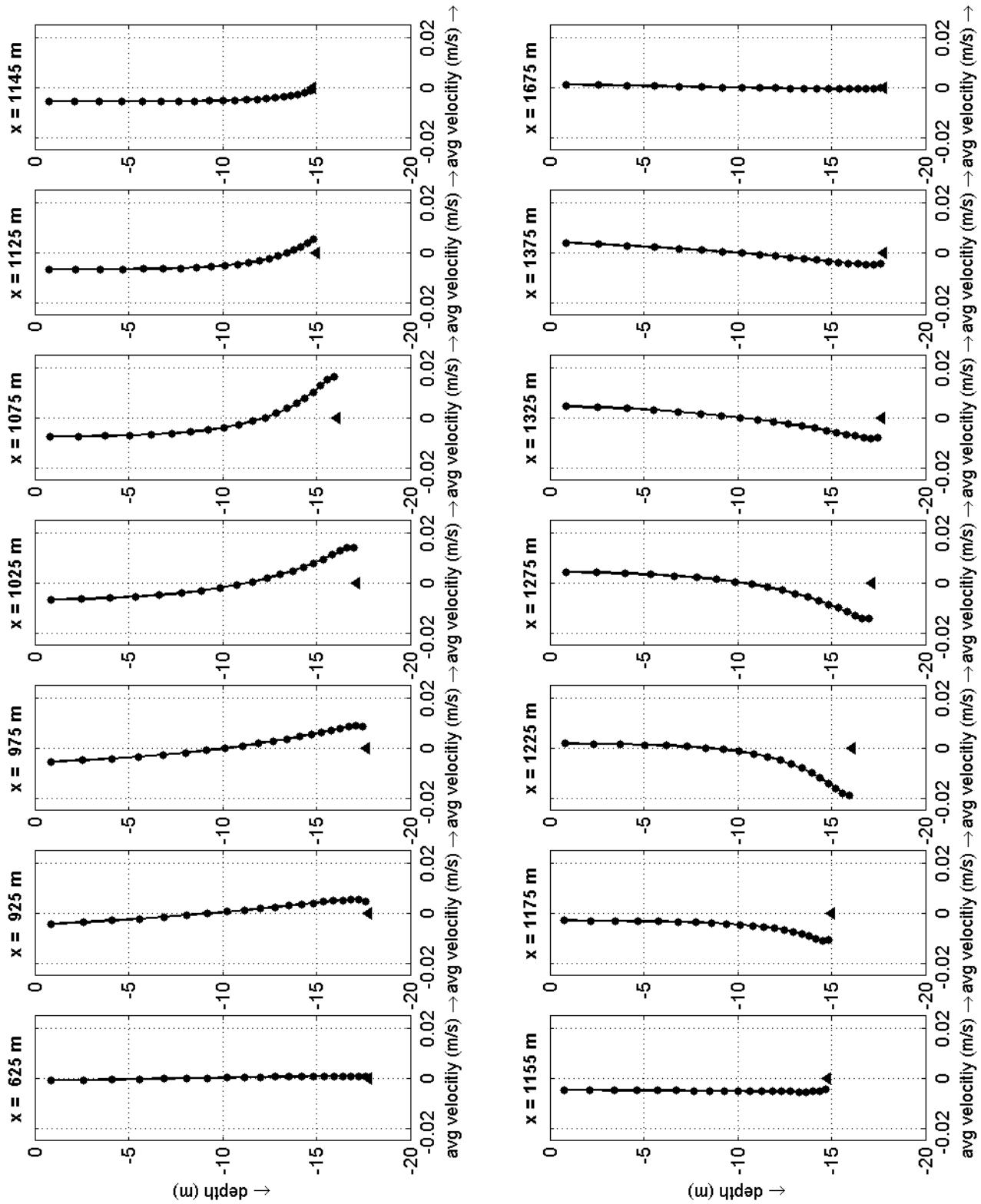

idealized sand ridge model: effect of tides without net current (drift)
tide-averaged velocity profiles at observation points
U_0 = 0.00 m/s U_1 = 0.75 m/s, no waves

2005

idealized sand ridge

WL | Delft Hydraulics

Z3079.40

Figure C.13

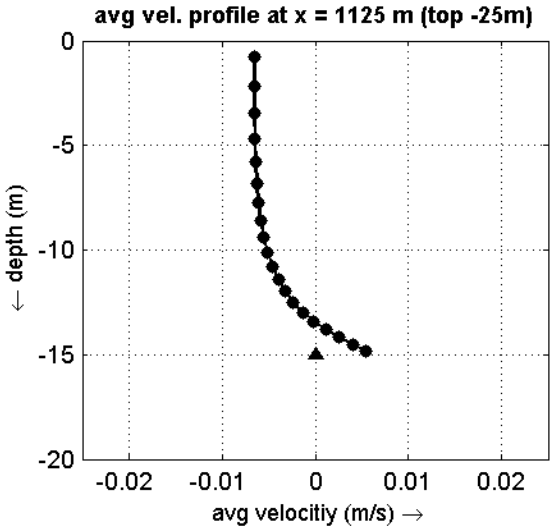

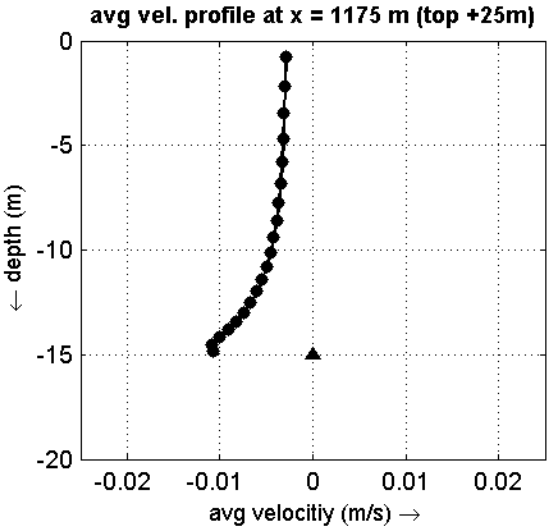

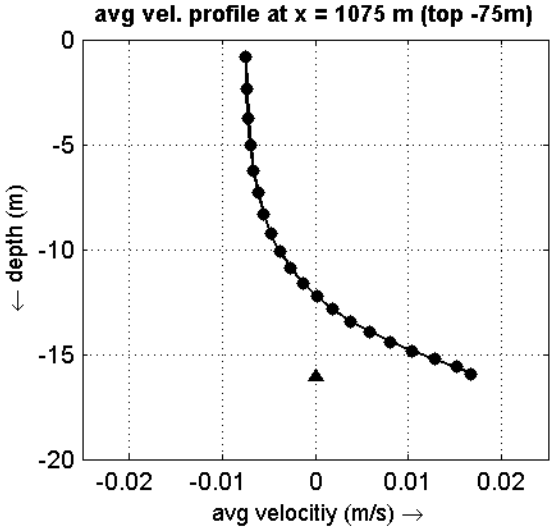

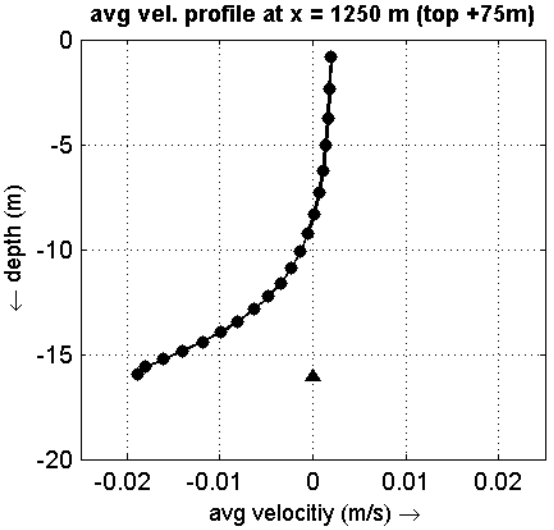

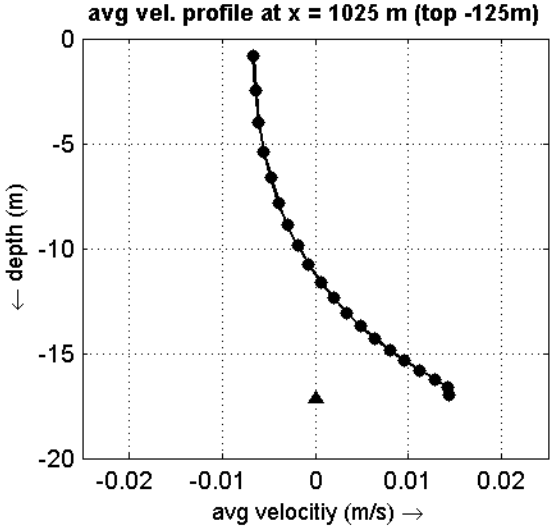

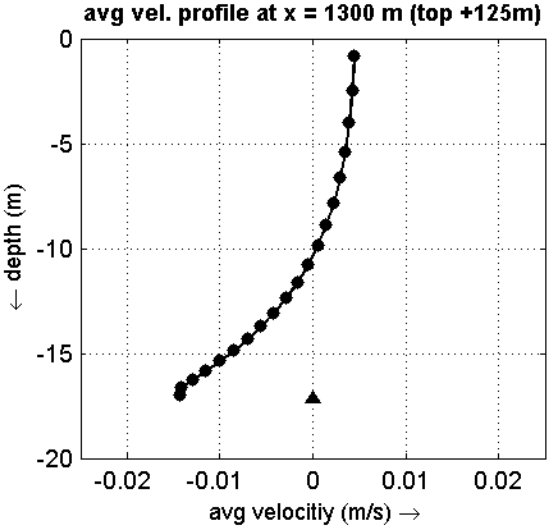

idealized sand ridge model: effect of tides without net current (drift)
tide-averaged velocity profiles at +/- 25, 75 and 125 m from the top
U_0 = 0.00 m/s U_1 = 0.75 m/s, no waves

2005

idealized sand ridge

WL | Delft Hydraulics

Z3079.40

Figure C.14

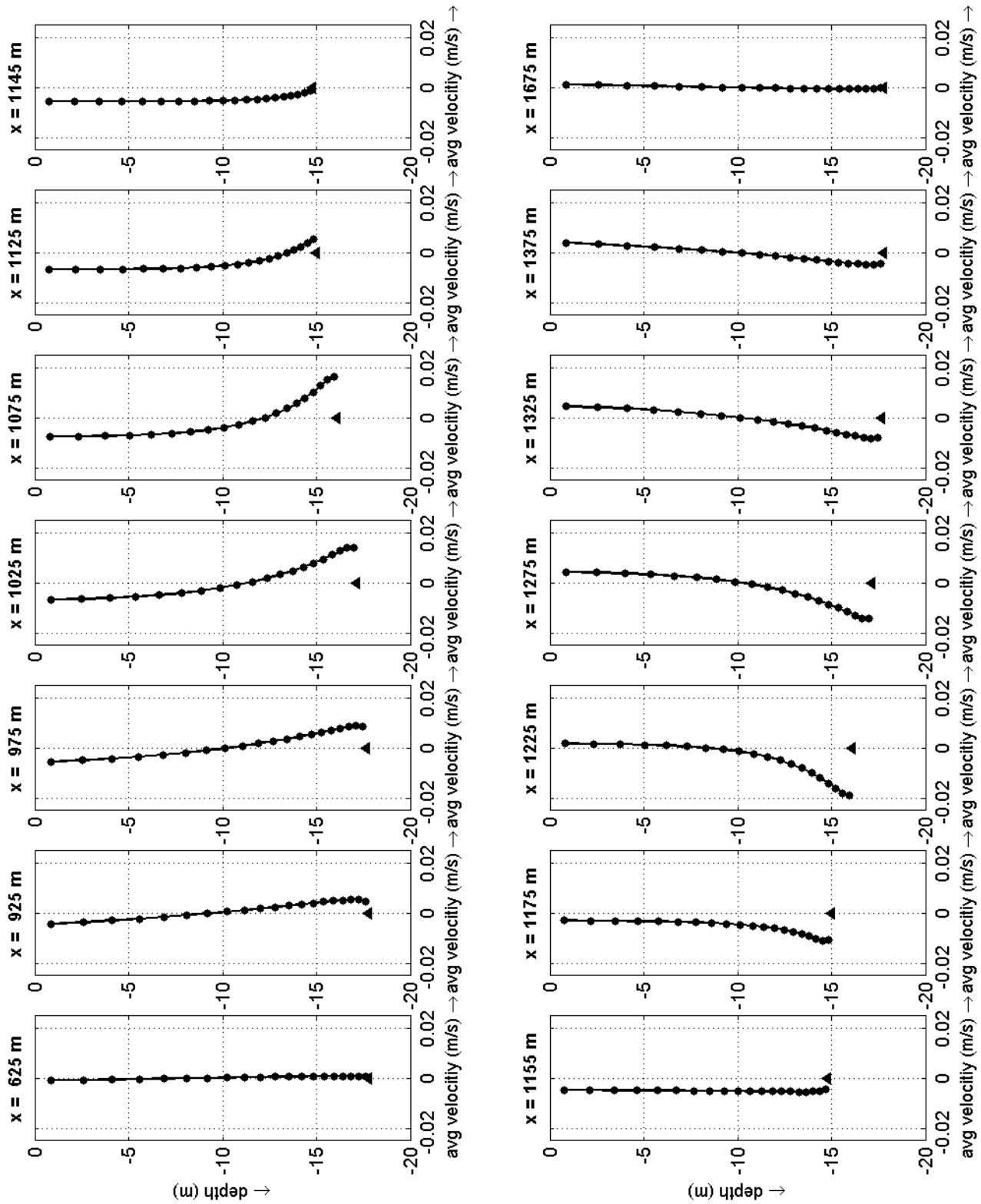

idealized sand ridge model: effect of tides without net current (drift) tide-averaged velocity profiles at observation points U_0 = 0.00 m/s U_1 = 1.00 m/s, no waves		2005
	idealized sand ridge	
WL | Delft Hydraulics	Z3079.40	Figure C.15

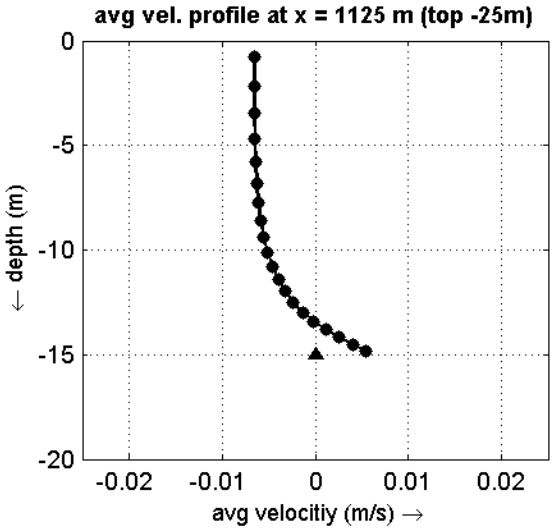

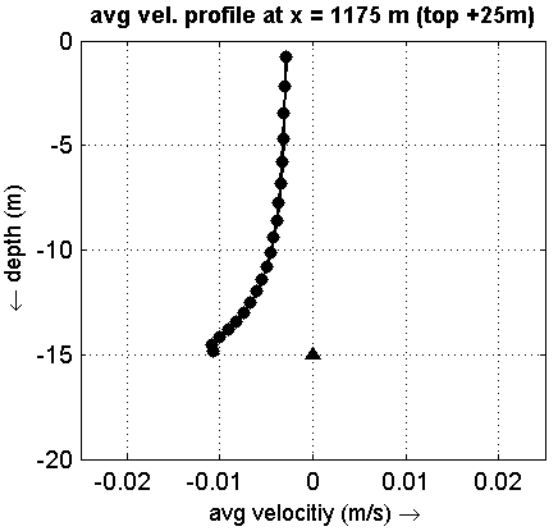

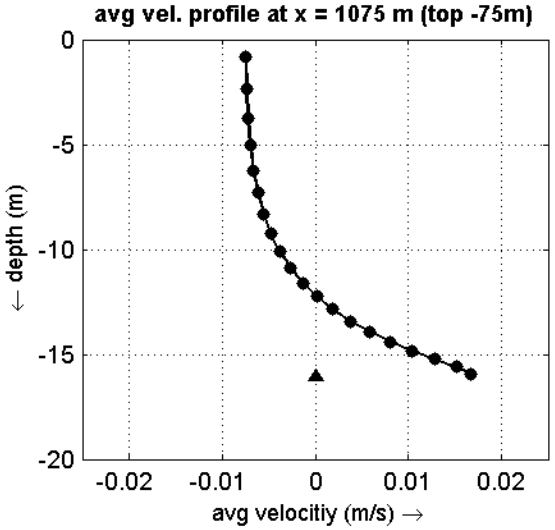

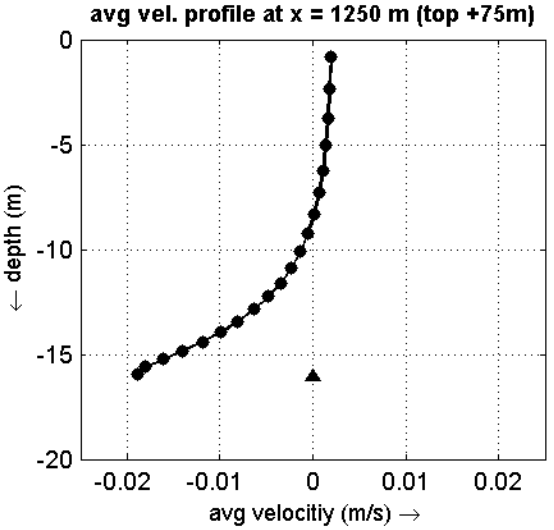

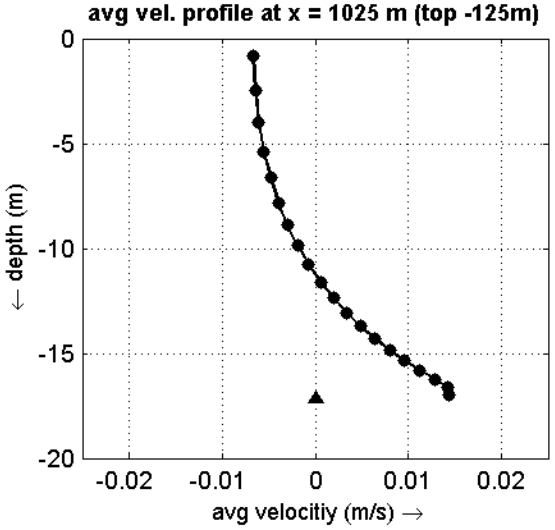

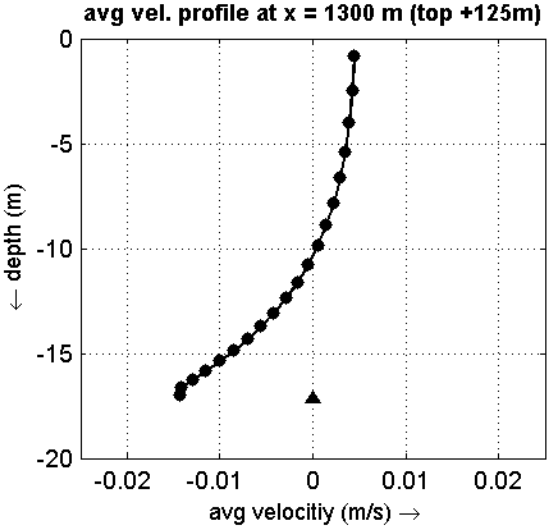

idealized sand ridge model: effect of tides without net current (drift)
tide-averaged velocity profiles at +/- 25, 75 and 125 m from the top
U_0 = 0.00 m/s U_1 = 1.00 m/s, no waves

2005

idealized sand ridge

WL | Delft Hydraulics

Z3079.40

Figure C.16

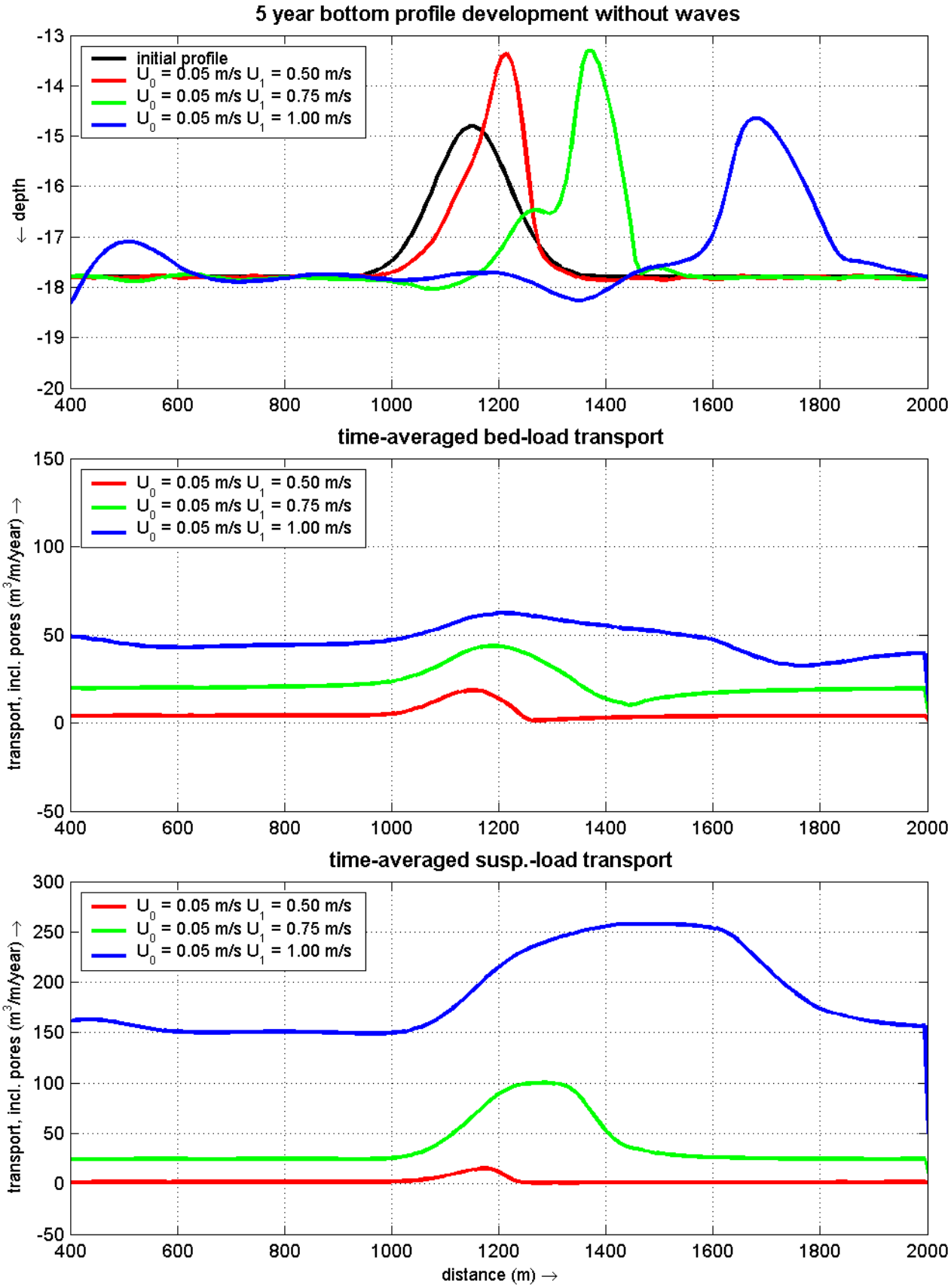

idealized sand ridge model: effect of tides with drift
bottom profile development, time-averaged bed-l. and suspended-l. transport rates
U_0 = 0.05 m/s and U_1 = 0.50/0.75/1.00 m/s without waves

2005

idealized sand ridge

WL | Delft Hydraulics

Z3079.40

Figure C.17

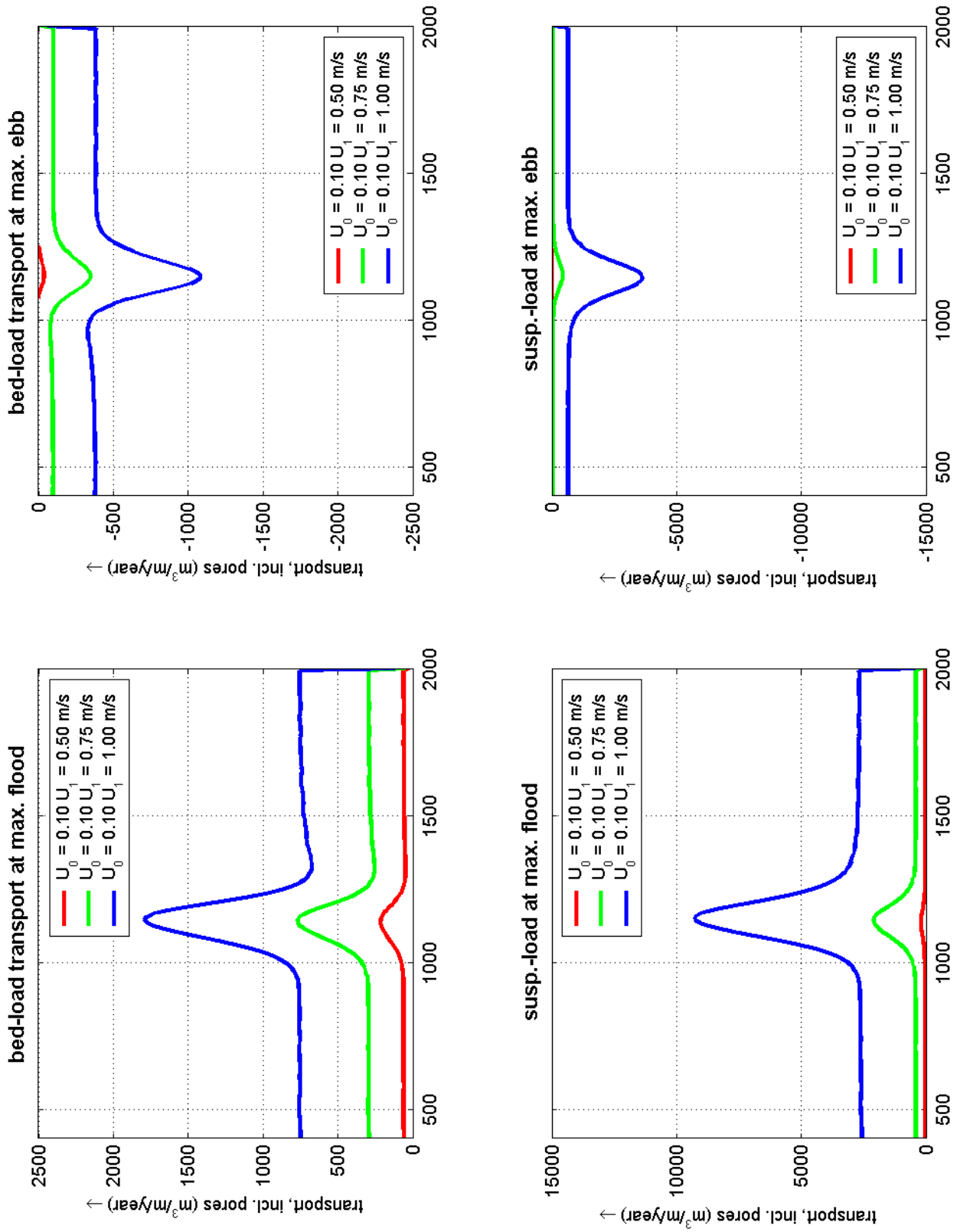

idealized sand ridge model: effect of tides with drift
transport rates at max. flood and max. ebb over initial bottom profile
tide: (U_0 = 0.10m/s, U_1 = 0.50/0.75/1.00 m/s) without waves

2005

idealized sand ridge

WL | Delft Hydraulics

Z3079.40

Figure C.18

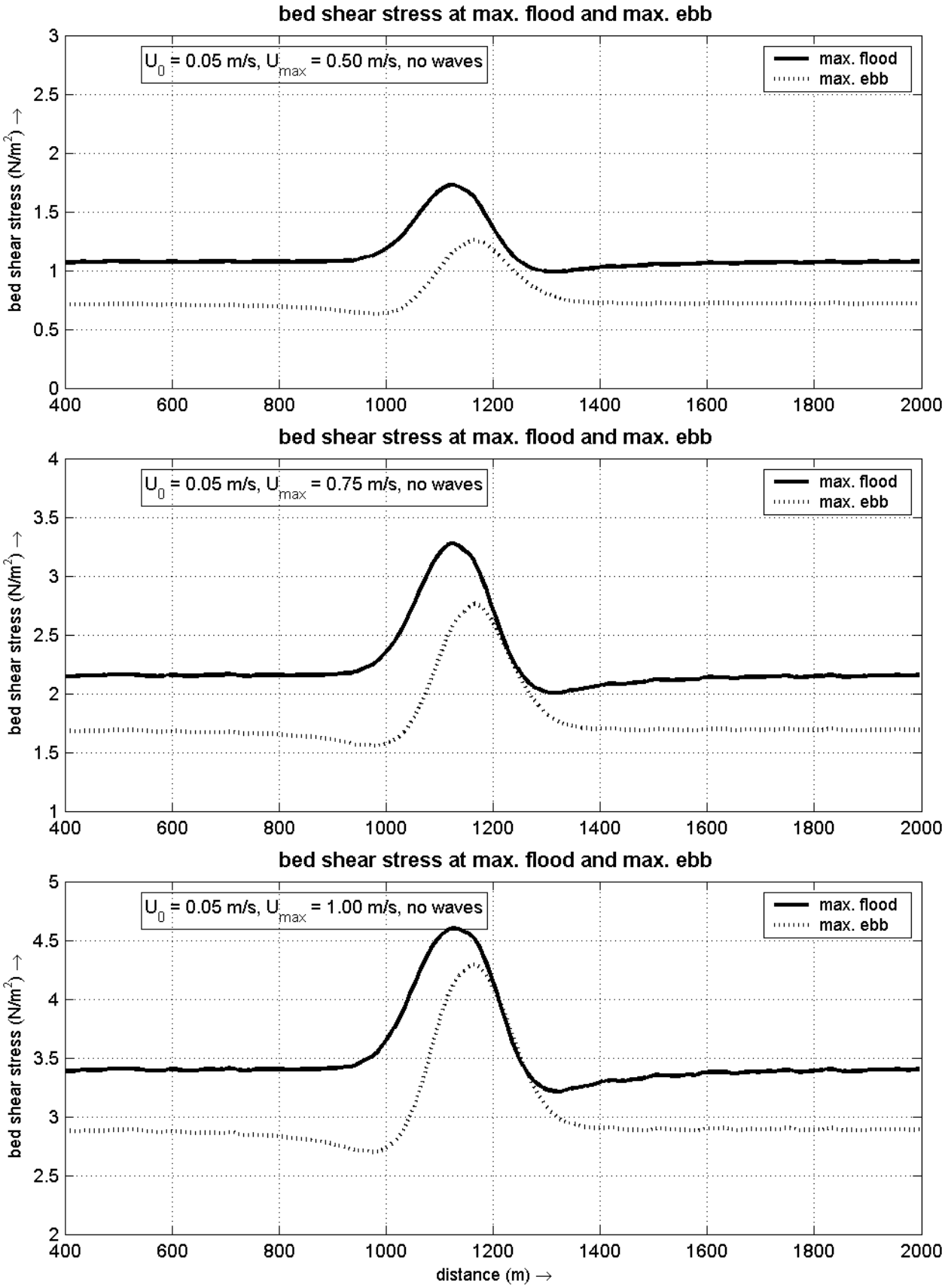

idealized sand ridge model: effect of tides with net current (drift)
bed shear stress at max. flood and max. ebb
U_0 = 0.05m/s, U_1 = 0.50/0.75/1.00m/s, no waves

2005

idealized sand ridge

WL | Delft Hydraulics

Z3079.40

Figure C.19

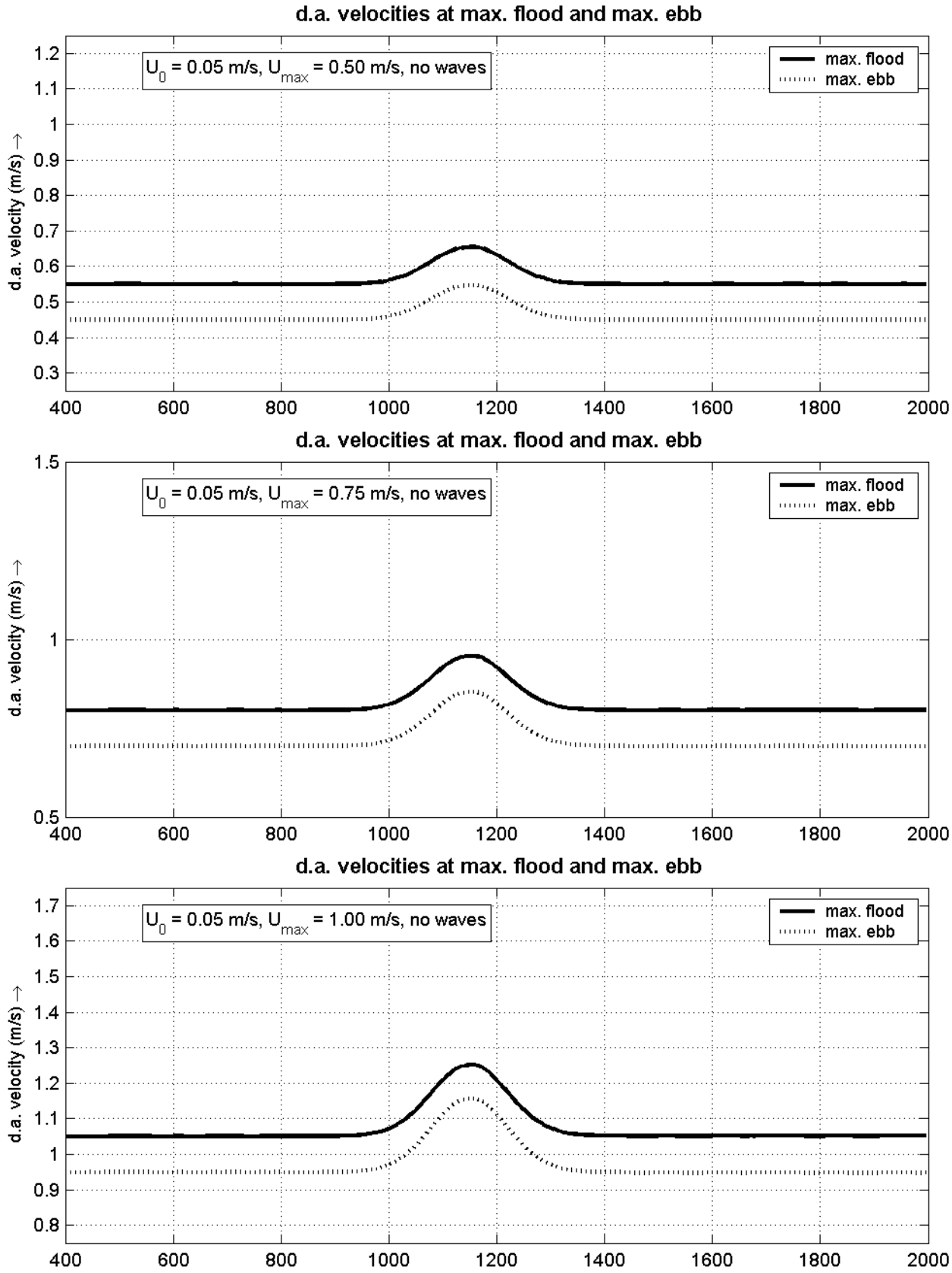

idealized sand ridge model effect of tides with net current (drift)
d.a. velocities at max. flood and max. ebb
U_0 = 0.05m/s, U_1 = 0.50/0.75/1.00m/s. no waves

2005

idealized sand ridge

WL | Delft Hydraulics

Z3079.40

Figure C.20

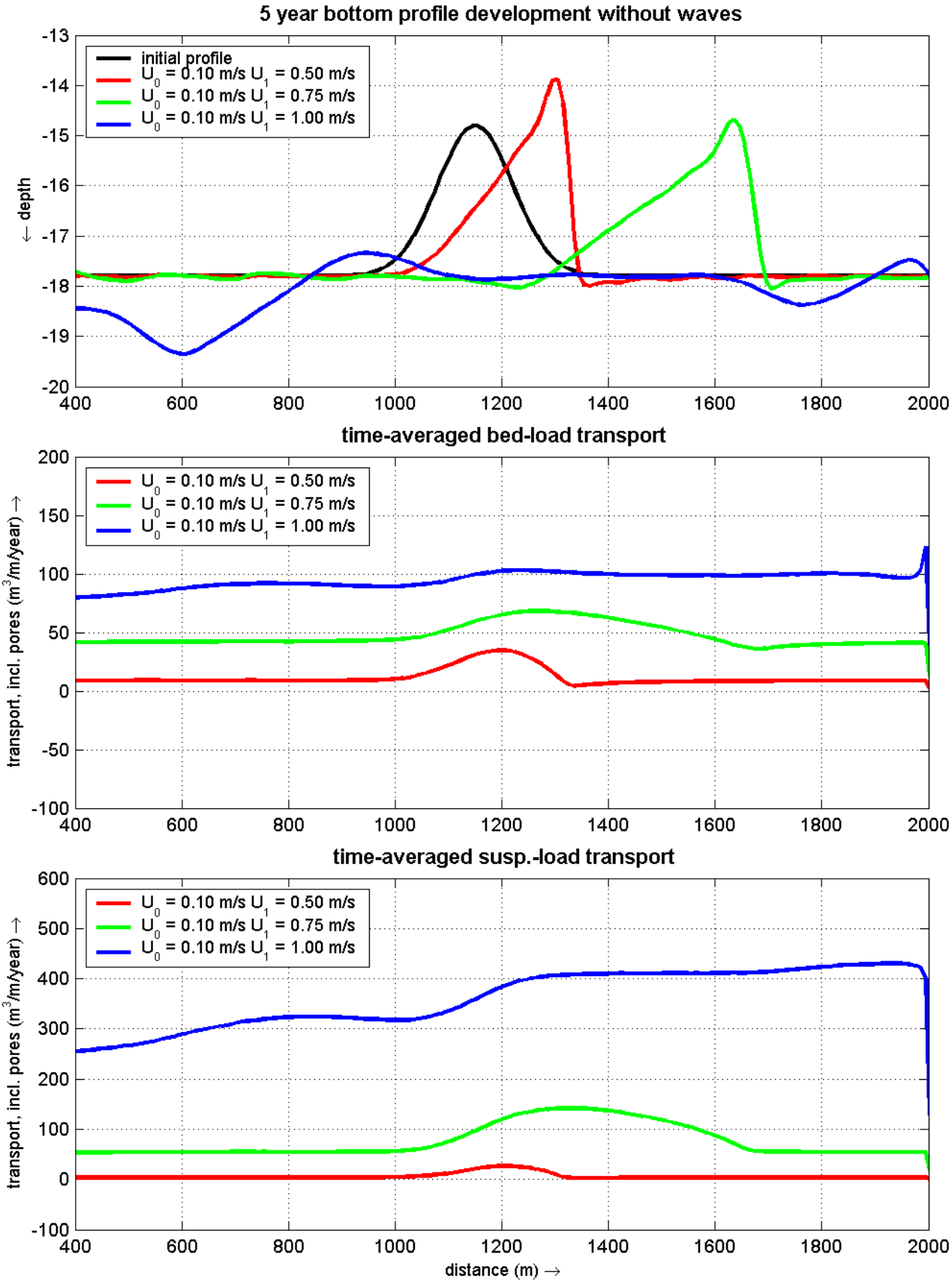

idealized sand ridge model: effect of tides with drift
bottom profile development, time-averaged bed-l. and suspended-l. transport rates
U_0 = 0.10 m/s and U_1 = 0.50/0.75/1.00 m/s without waves

2005

idealized sand ridge

WL | Delft Hydraulics

Z3079.40

Figure C.21

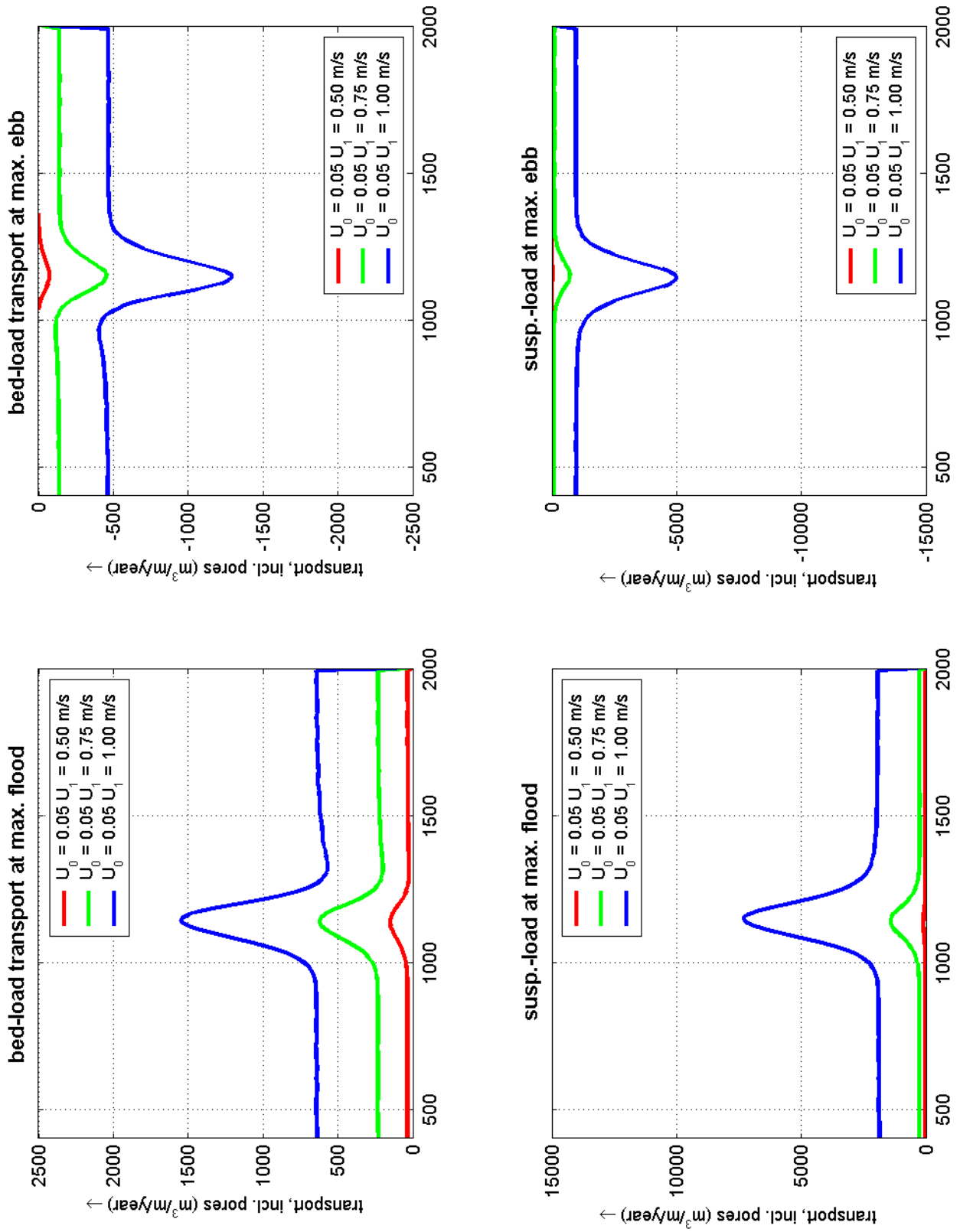

idealized sand ridge model: effect of tides with drift
transport rates at max. flood and max. ebb over initial bottom profile
tide: (U_0 = 0.05m/s, U_1 = 0.50/0.75/1.00 m/s) without waves

2005

idealized sand ridge

WL | Delft Hydraulics

Z3079.40

Figure C.22

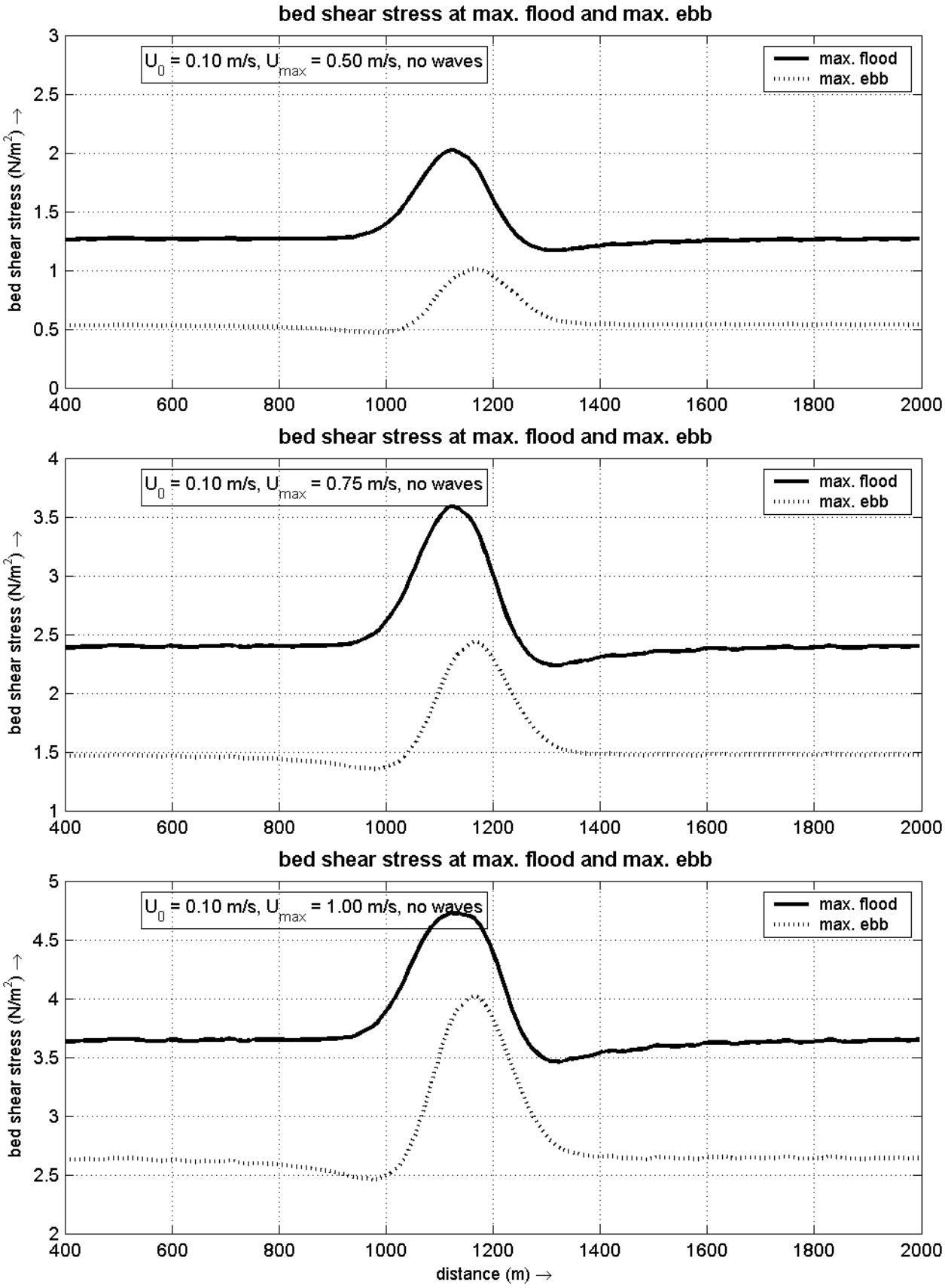

idealized sand ridge model: effect of tides with net current (drift)
bed shear stress at max. flood and max. ebb
U_0 = 0.10m/s, U_1 = 0.50/0.75/1.00m/s, no waves

2005

idealized sand ridge

WL | Delft Hydraulics

Z3079.40

Figure C.23

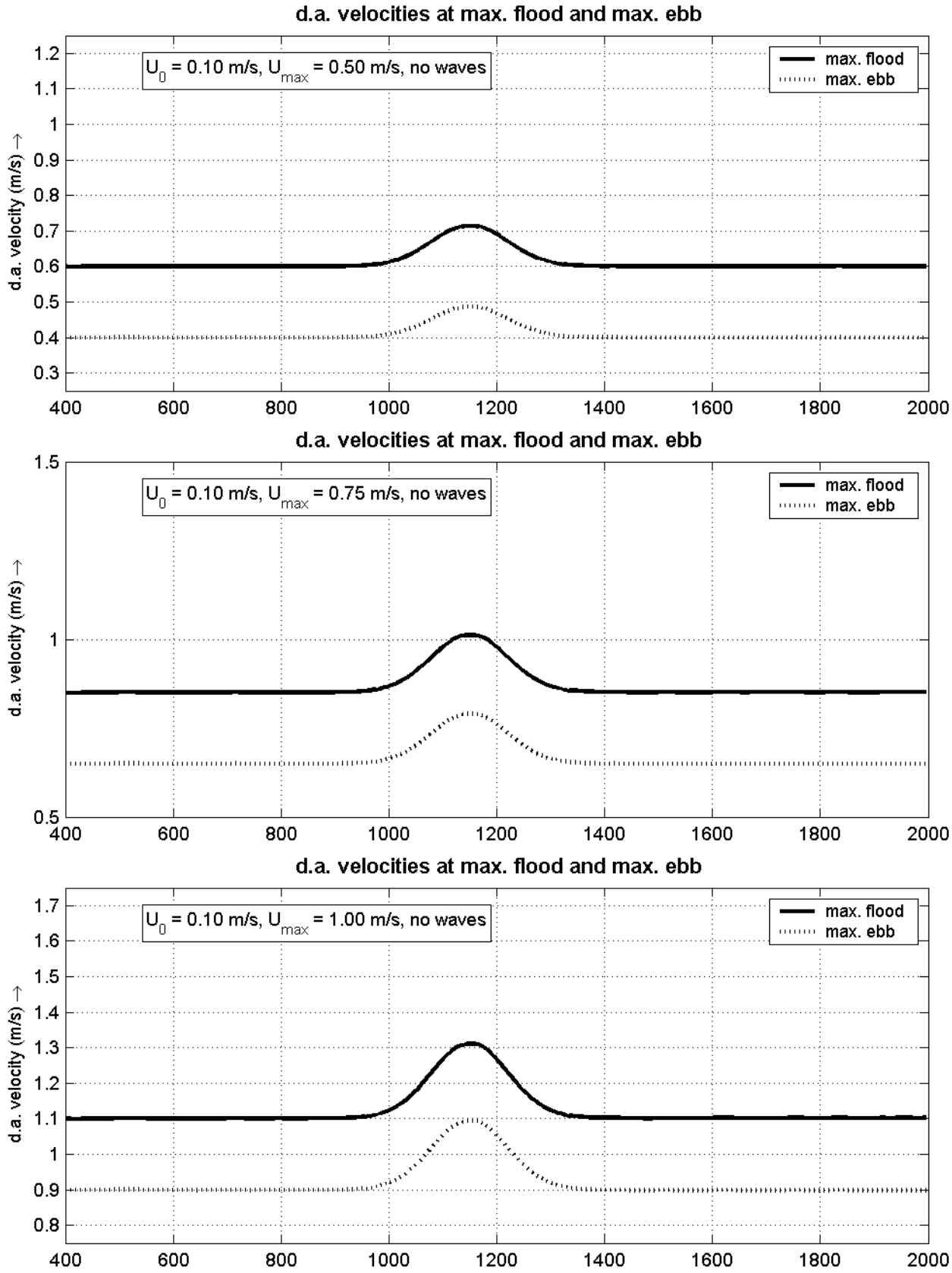

idealized sand ridge model effect of tides with net current (drift) d.a. velocities at max. flood and max. ebb U_0 = 0.10m/s, U_1 = 0.50/0.75/1.00m/s. no waves		2005
	idealized sand ridge	
WL | Delft Hydraulics	Z3079.40	Figure C.24

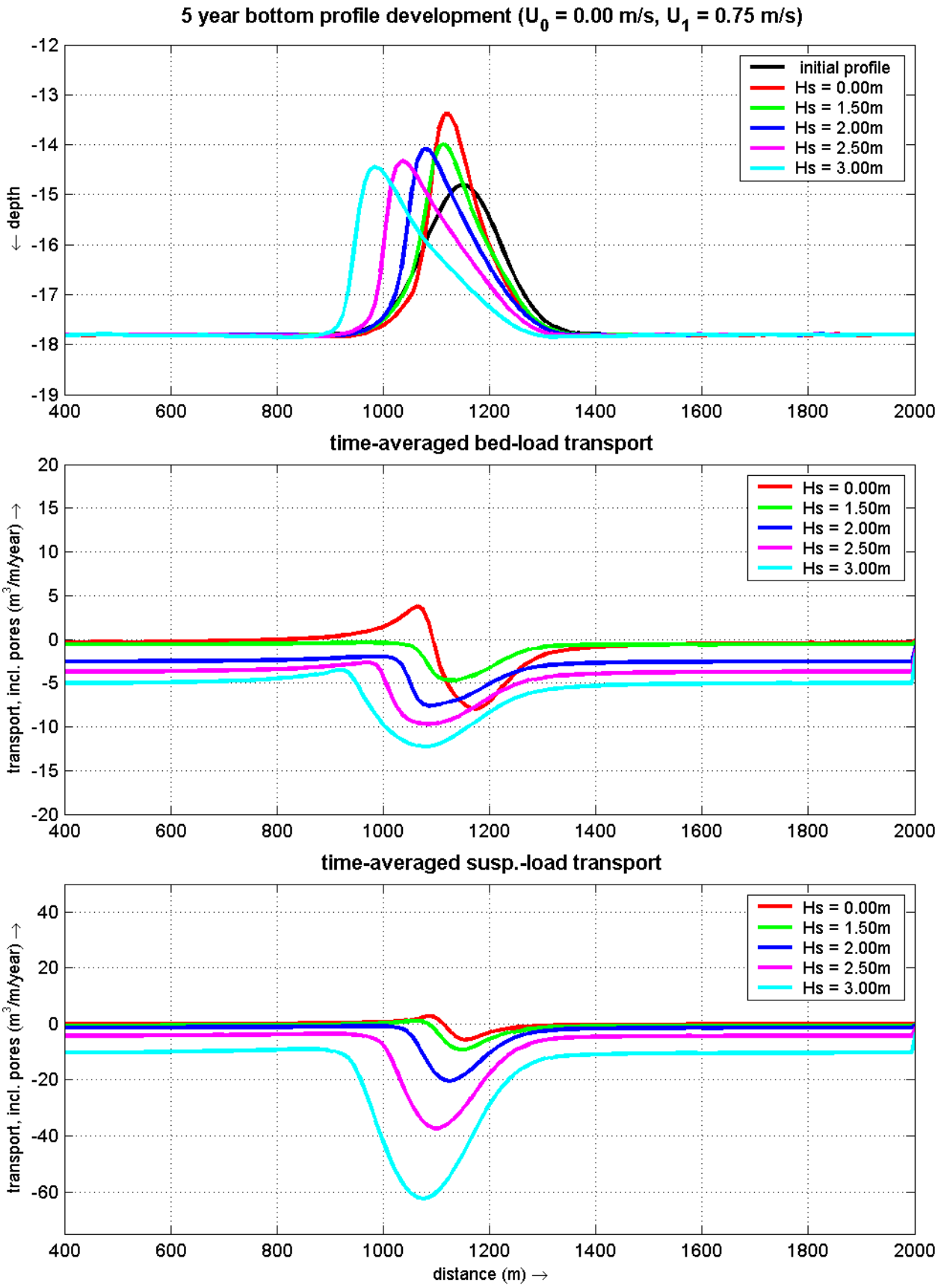

idealized sand ridge model: effect of waves
bottom profile development, time-averaged bed-l. and suspended-l transport rates
tide: (U_0 = 0.00m/s, U_1 = 0.50m/s) waves: H_s = 0.00/1.50/2.00/2.50/3.00m

2005

idealized sand ridge

WL | Delft Hydraulics

Z3079.40

Figure C.25

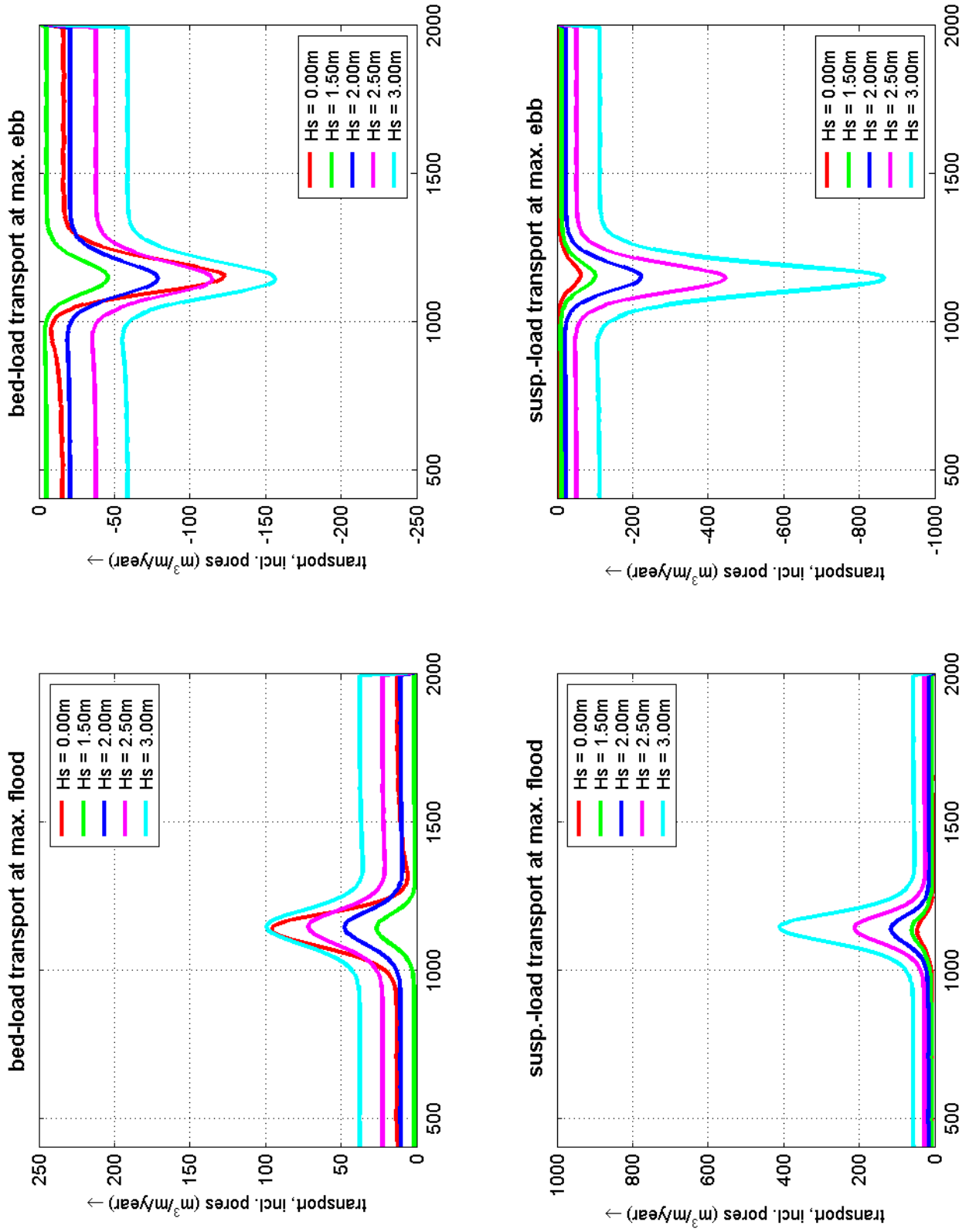

idealized sand ridge model: effect of waves
transport rates at max. flood and max. ebb over initial bottom profile
tide: (U_0 = 0.00m/s, U_1 = 0.50m/s) waves: H_s = 0.00/1.50/2.00/2.50/3.00m

2005

idealized sand ridge

WL | Delft Hydraulics

Z3079.40

Figure C.26

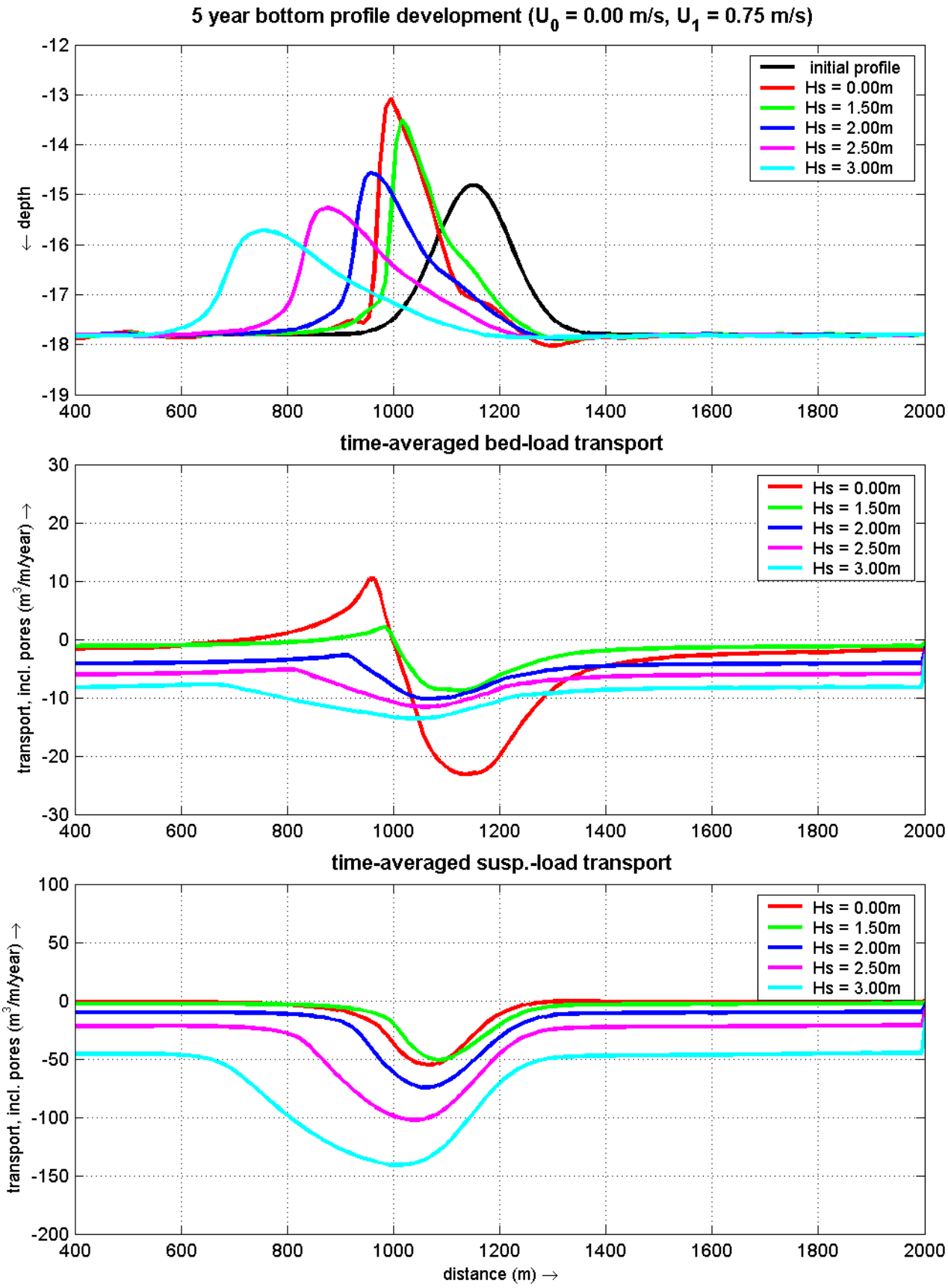

idealized sand ridge model: effect of waves bottom profile development, time-averaged bed-l. and suspended-l transport rates tide: (U_0 = 0.00m/s, U_1 = 0.75m/s) waves: H_s = 0.00/1.50/2.00/2.50/3.00m		2005
		idealized sand ridge
WL | Delft Hydraulics	Z3079.40	Figure C.27

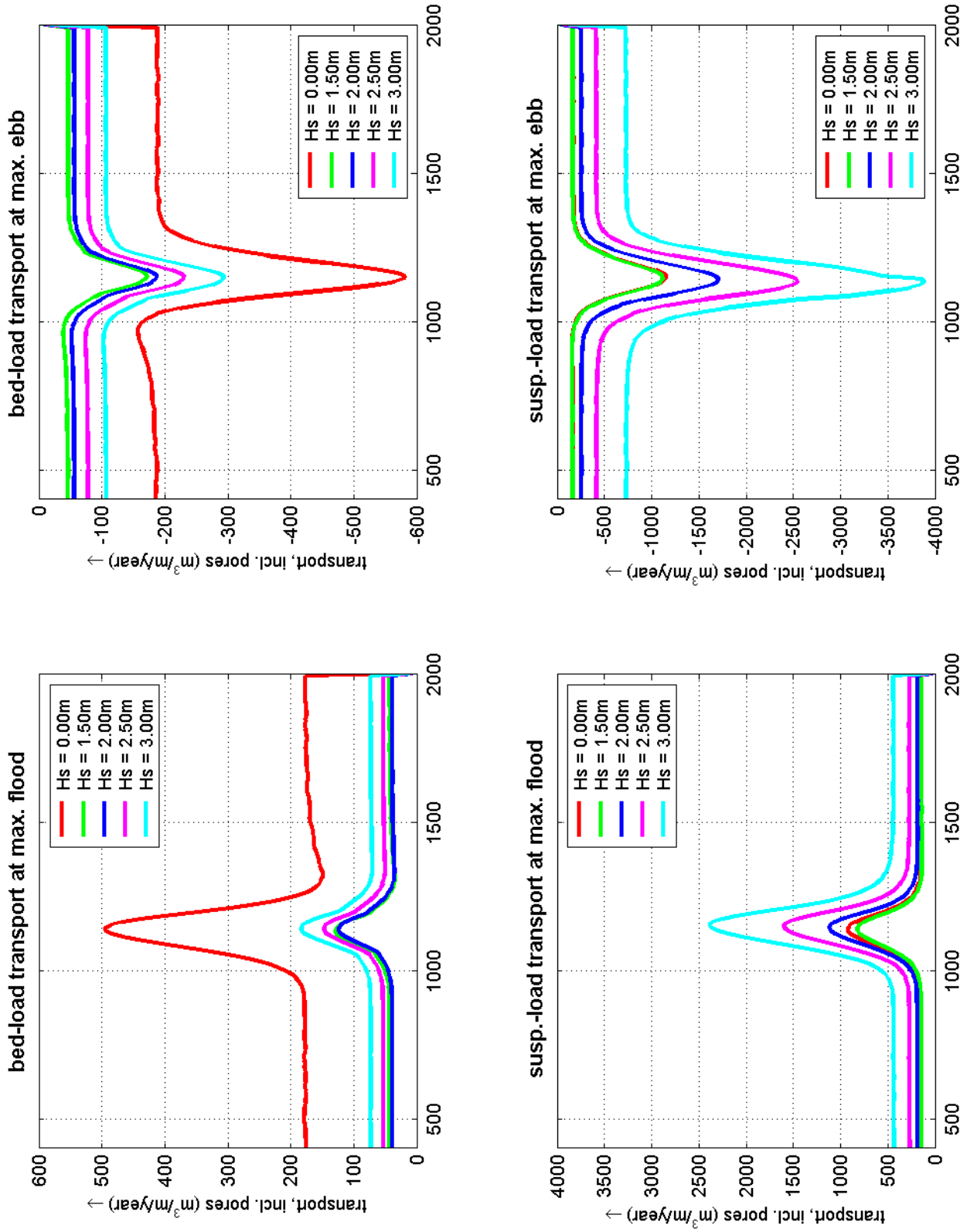

idealized sand ridge model: effect of waves transport rates at max. flood and max. ebb over initial bottom profile tide: (U_0 = 0.00m/s, U_1 = 0.75m/s) waves: H_s = 0.00/1.50/2.00/2.50/3.00m		2005
	idealized sand ridge	
WL | Delft Hydraulics	Z3079.40	Figure C.28

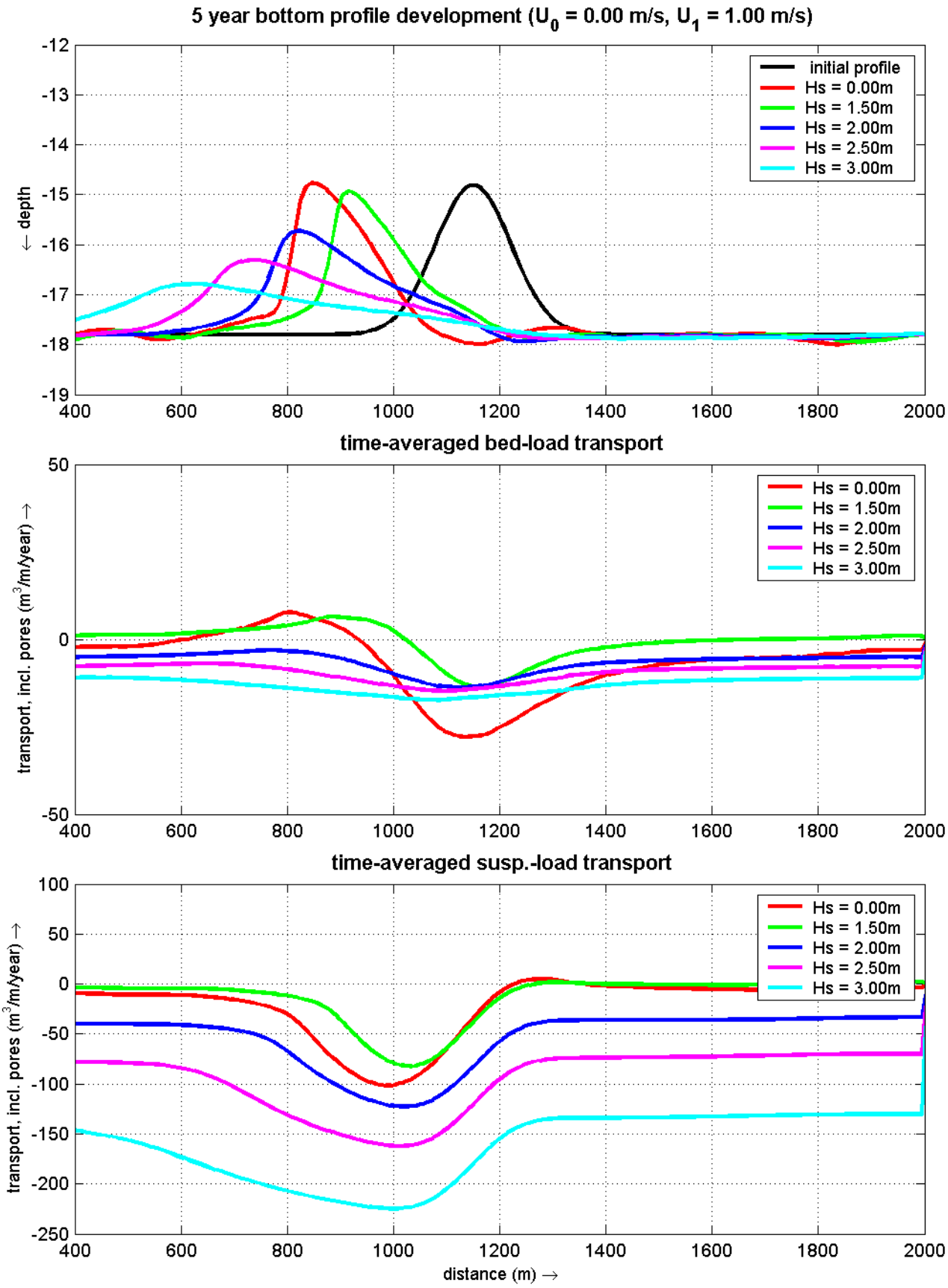

idealized sand ridge model: effect of waves
bottom profile development, time-averaged bed-l. and suspended-l transport rates
tide: (U_0 = 0.00m/s, U_1 = 1.00m/s) waves: H_s = 0.00/1.50/2.00/2.50/3.00m

2005

idealized sand ridge

WL | Delft Hydraulics

Z3079.40

Figure C.29

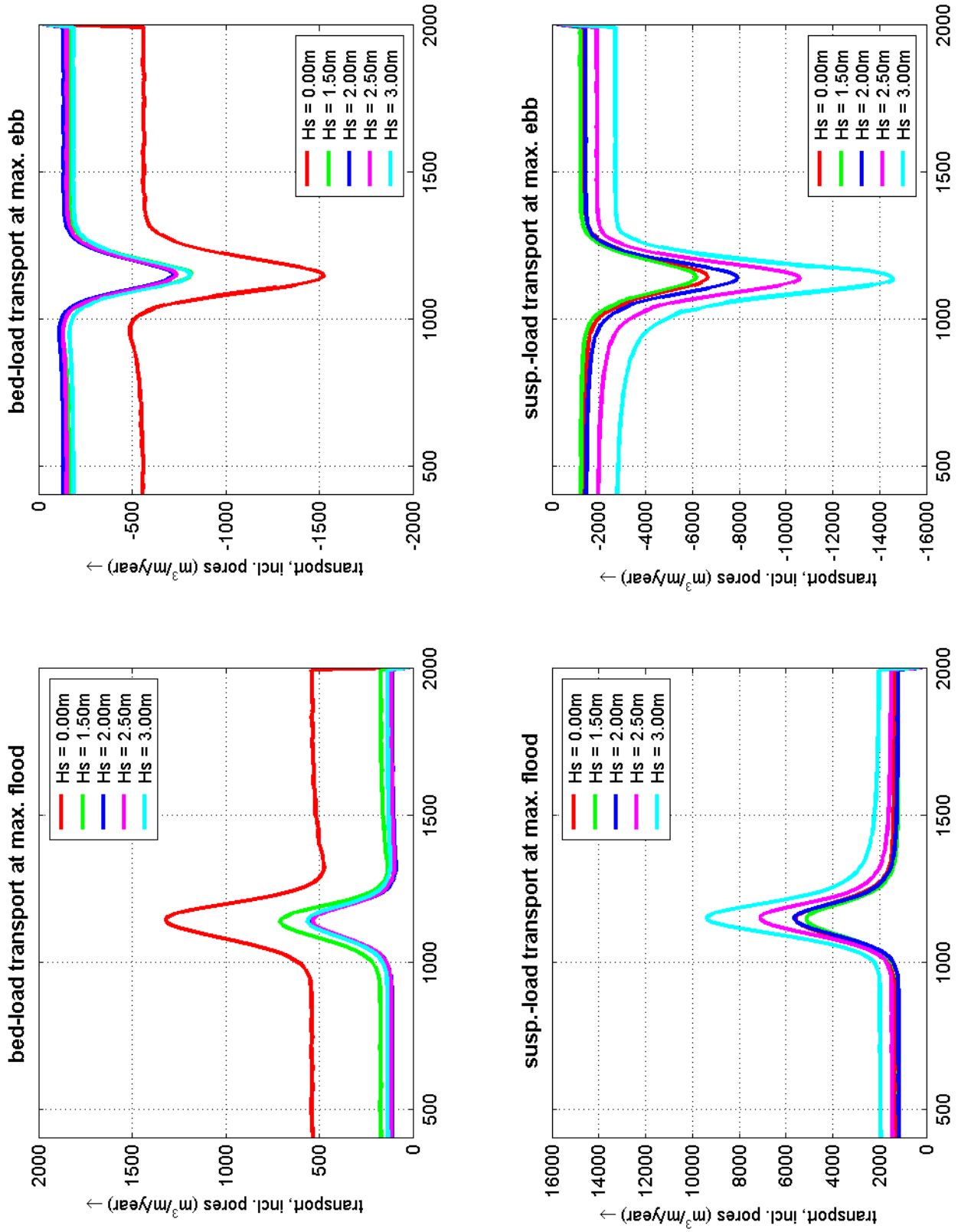

idealized sand ridge model: effect of waves
transport rates at max. flood and max. ebb over initial bottom profile
tide: (U_0 = 0.00m/s, U_1 = 1.00m/s) waves: H_s = 0.00/1.50/2.00/2.50/3.00m

2005

idealized sand ridge

WL | Delft Hydraulics

Z3079.40

Figure C.30

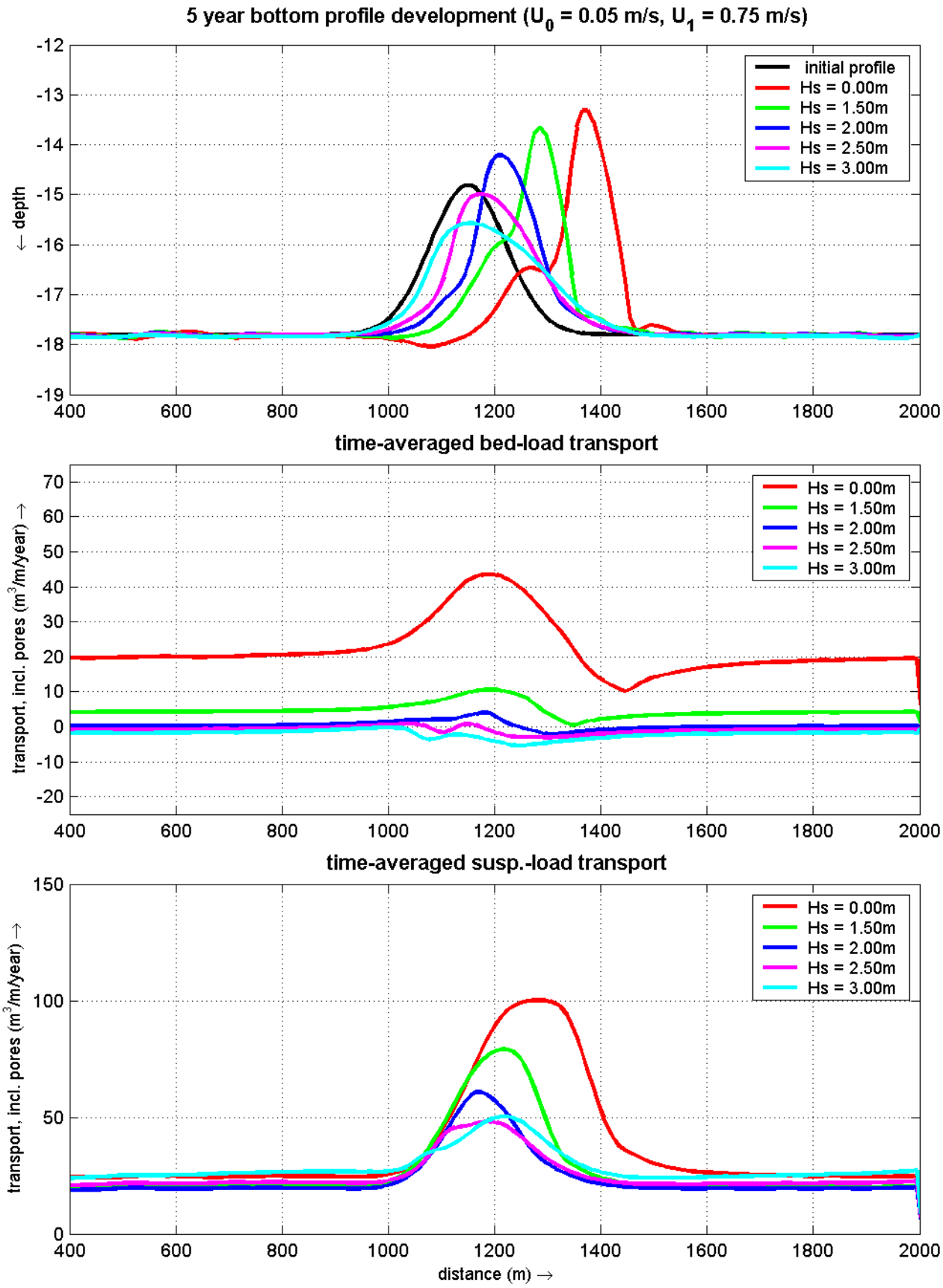

idealized sand ridge model: effect of waves bottom profile development, time-averaged bed-l. and suspended-l transport rates tide: (U_0 = 0.05m/s, U_1 = 0.75m/s) waves: H_s = 0.00/1.50/2.00/2.50/3.00m		2005
	idealized sand ridge	
WL | Delft Hydraulics	Z3079.40	Figure C.31

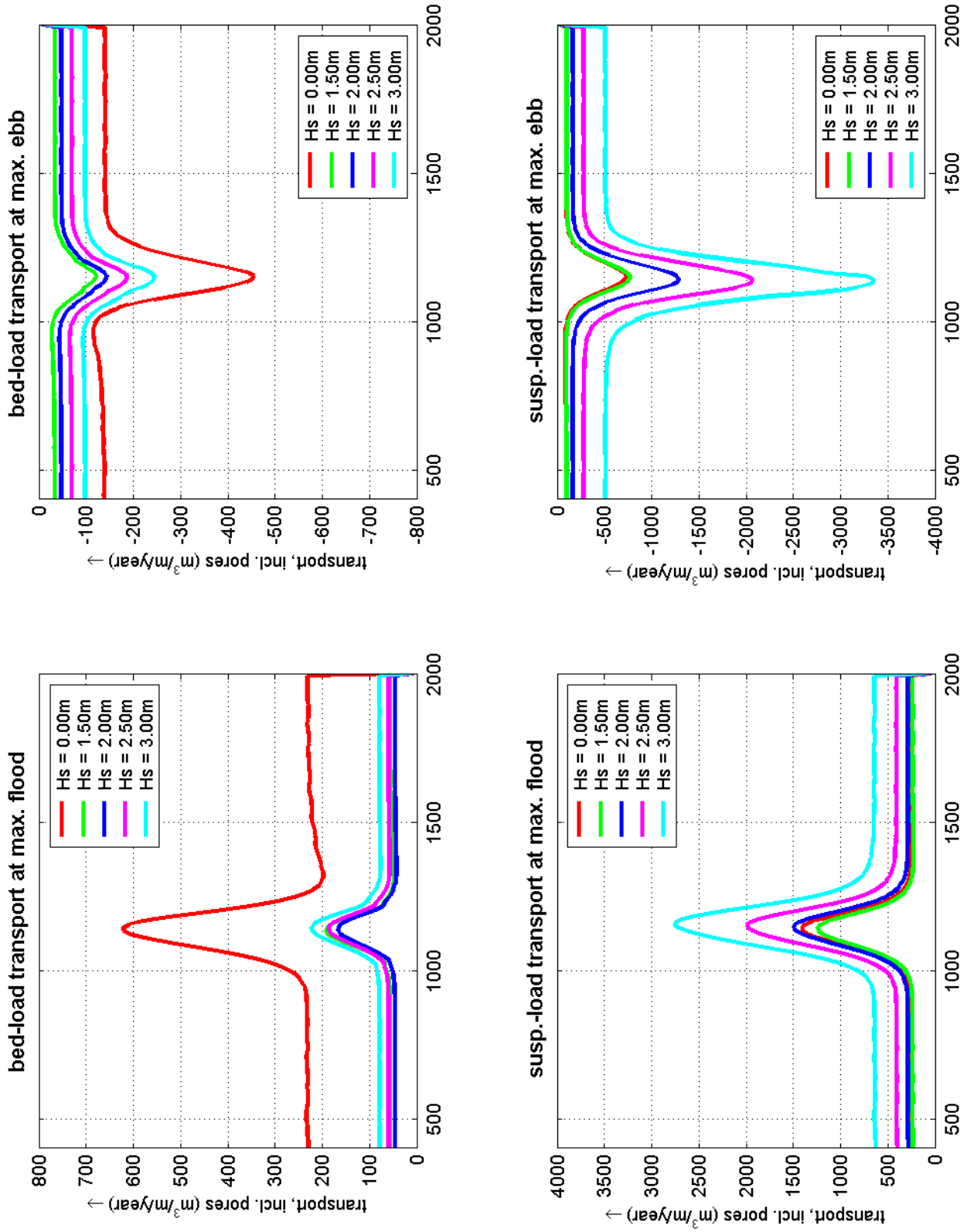

idealized sand ridge model: effect of waves
transport rates at max. flood and max. ebb over initial bottom profile
tide: (U_0 = 0.05m/s, U_1 = 0.75m/s) waves: H_s = 0.00/1.50/2.00/2.50/3.00m

	2005
idealized sand ridge	
WL | Delft Hydraulics	Z3079.40 Figure C.32

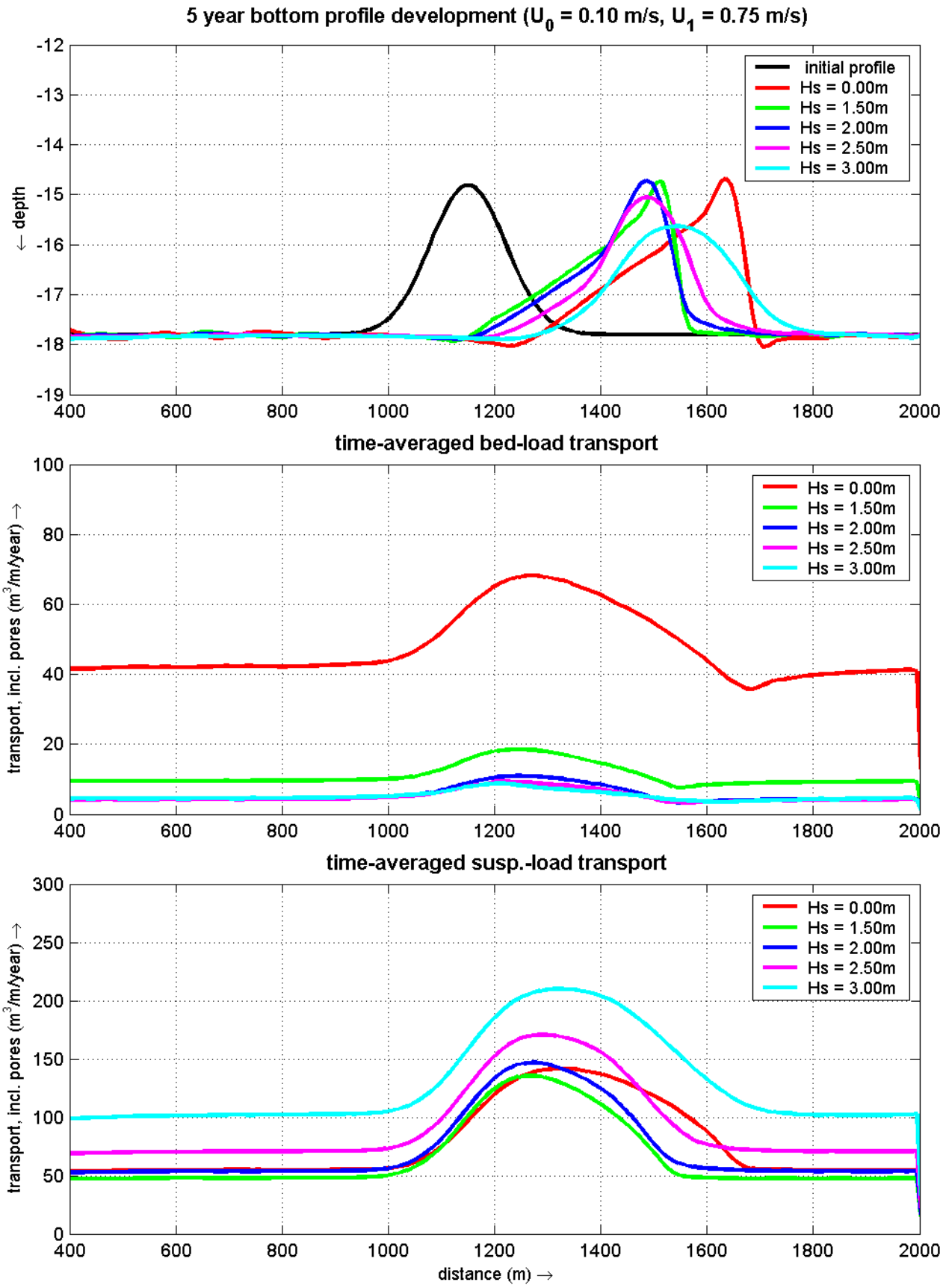

idealized sand ridge model: effect of waves bottom profile development, time-averaged bed-l. and suspended-l transport rates tide: (U_0 = 0.10m/s, U_1 = 0.75m/s) waves: H_s = 0.00/1.50/2.00/2.50/3.00m		2005
	idealized sand ridge	
WL | Delft Hydraulics	Z3079.40	Figure C.33

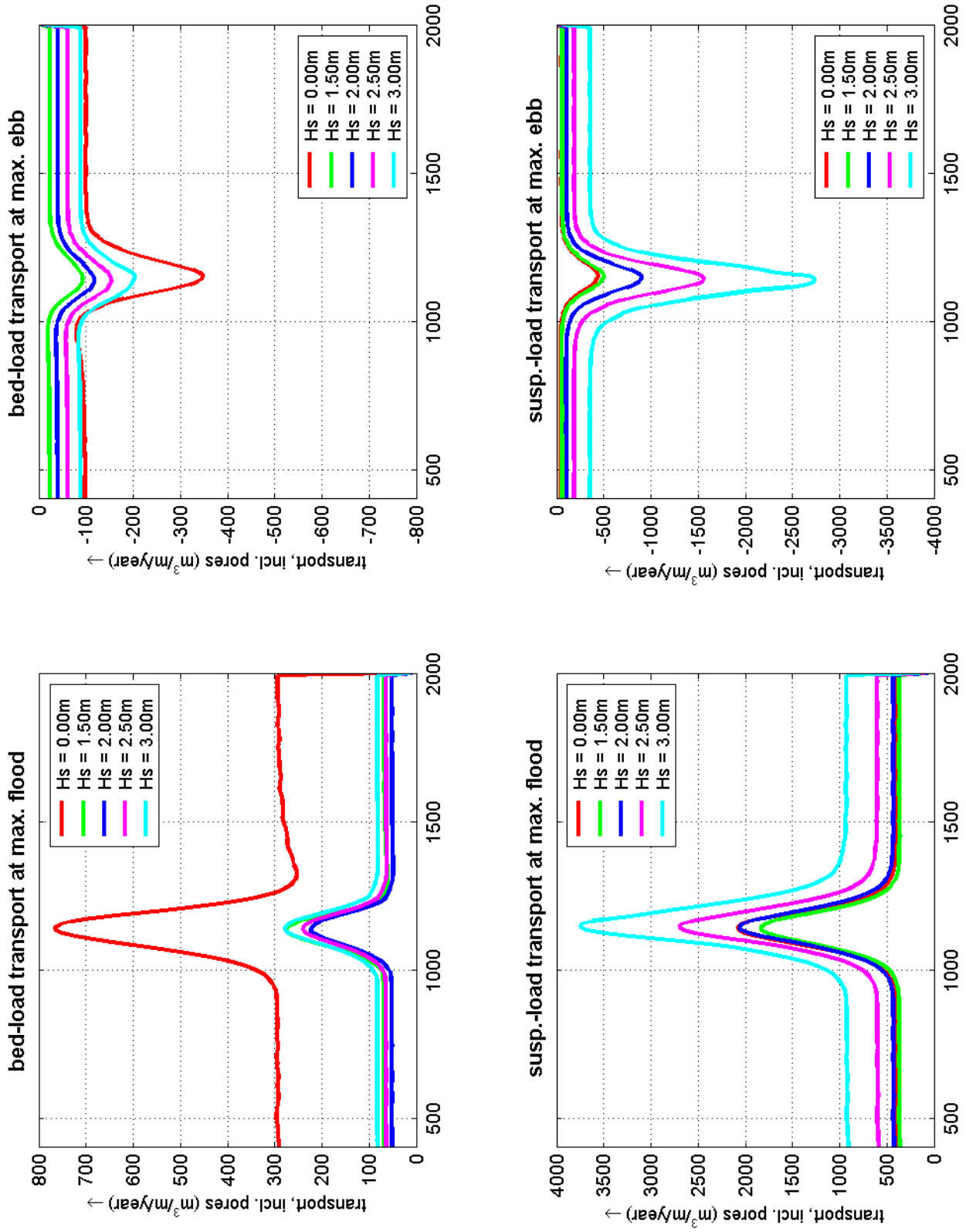

idealized sand ridge model: effect of waves
transport rates at max. flood and max. ebb over initial bottom profile
tide: (U_0 = 0.10m/s, U_1 = 0.75m/s) waves: H_s = 0.00/1.50/2.00/2.50/3.00m

2005

idealized sand ridge

WL | Delft Hydraulics

Z3079.40

Figure C.34

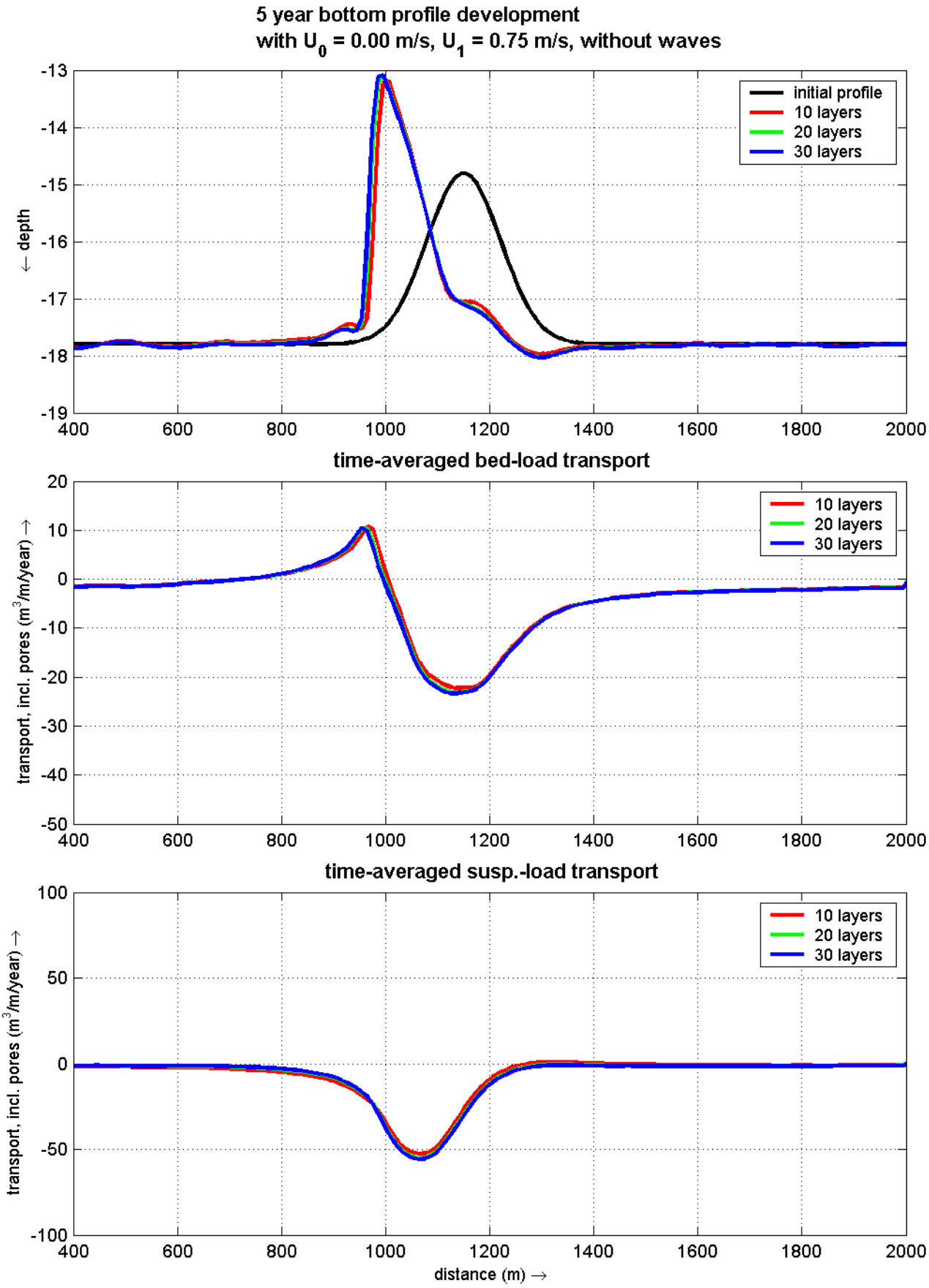

idealized sand ridge model set-up: number of vertical layers bottom profile development, time-averaged bed-l. and suspended-l. transport rates tide: (U_0 = 0.00m/s, U_1 = 0.75m/s) without waves		2005
	idealized sand ridge	
WL | Delft Hydraulics	Z3079.40	Figure C.35

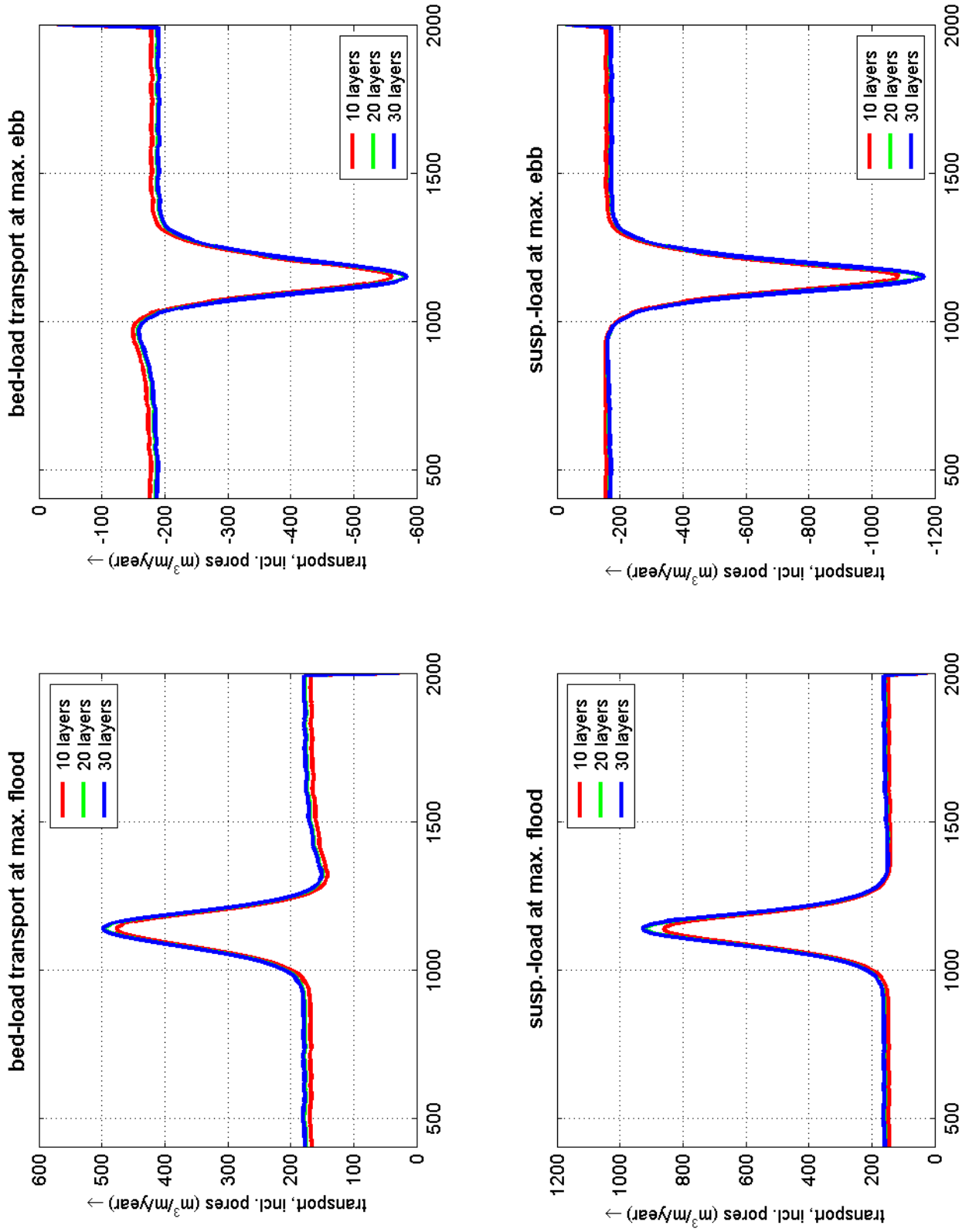

idealized sand ridge model set-up: number of vertical layers
transport rates at max. flood and max. ebb over initial bottom profile
tide: (U_0 = 0.00m/s, U_1 = 0.75m/s) without waves

2005

idealized sand ridge

WL | Delft Hydraulics

Z3079.40

Figure C.36

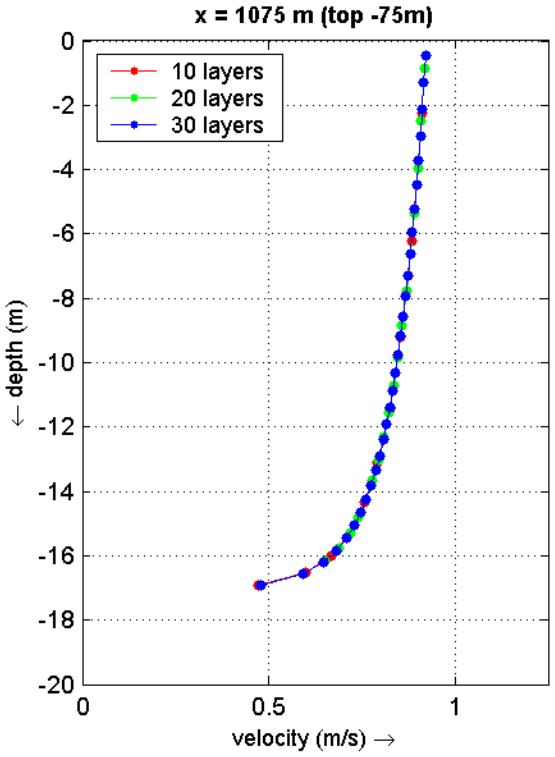

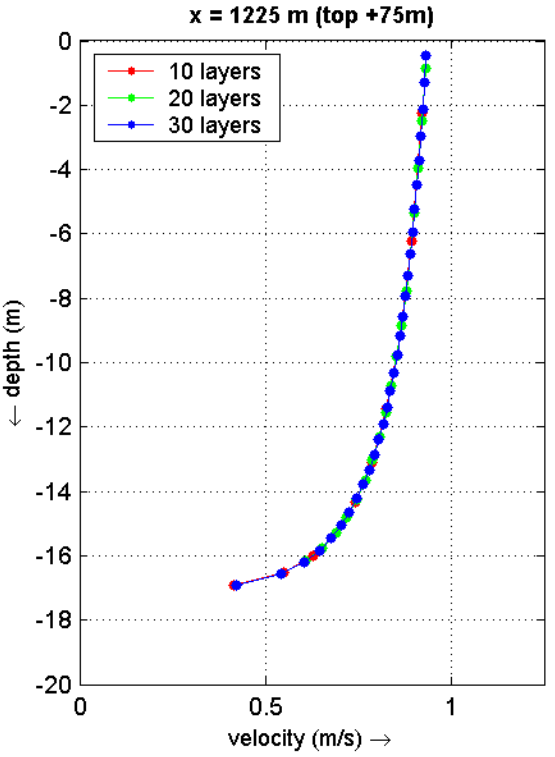

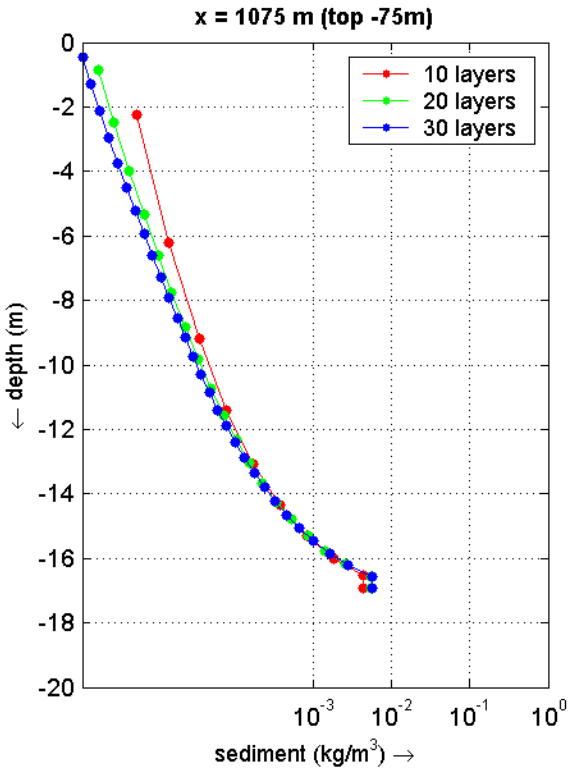

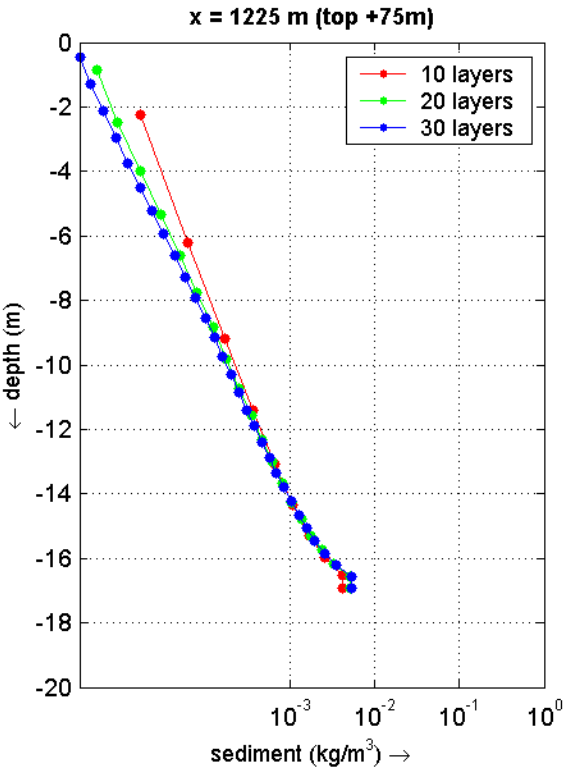

idealized sand ridge model set-up: number of vertical layers
velocity and concentration profiles at max. flood for 10,20 and 30 layers
tide:(U_0 = 0.00 m/s, U_1 = 0.75 m/s) no waves

2005

idealized sand ridge model

WL | Delft Hydraulics

Z3079.40

Figure C.37

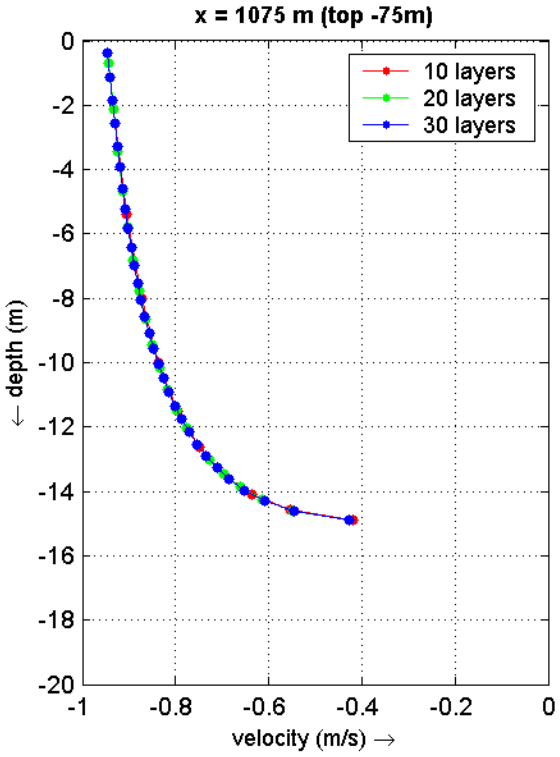

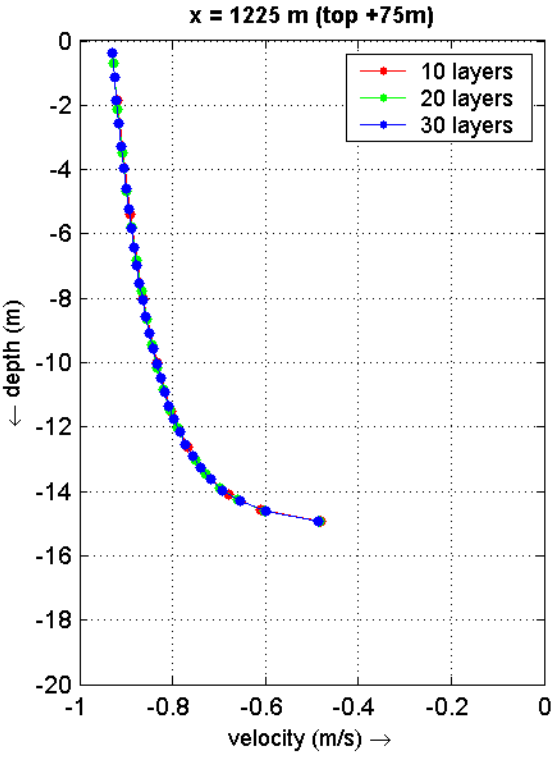

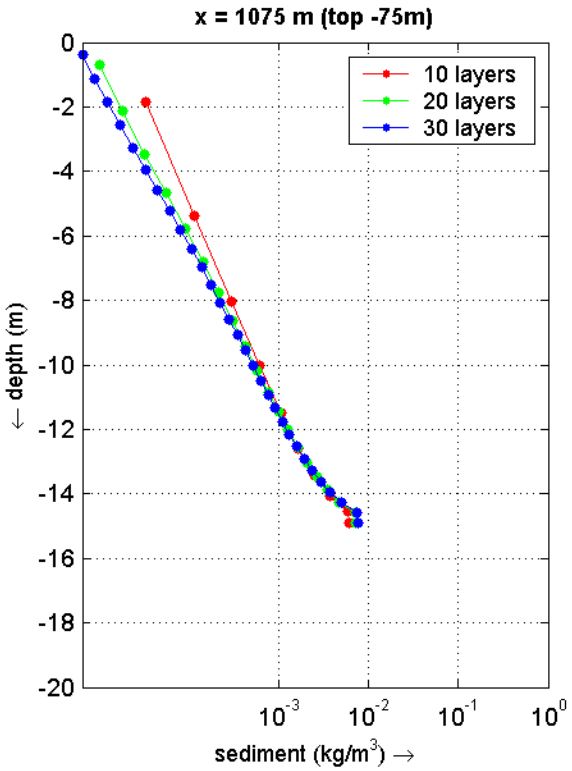

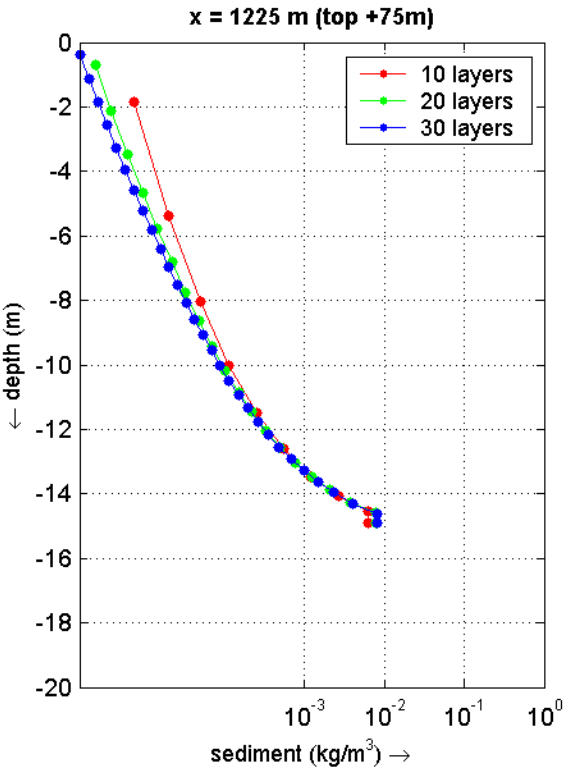

idealized sand ridge model set-up: number of vertical layers
velocity and concentration profiles at max. ebb for 10,20 and 30 layers
tide:(U_0 = 0.00 m/s, U_1 = 0.75 m/s) no waves

2005

idealized sand ridge model

WL | Delft Hydraulics

Z3079.40

Figure C.38

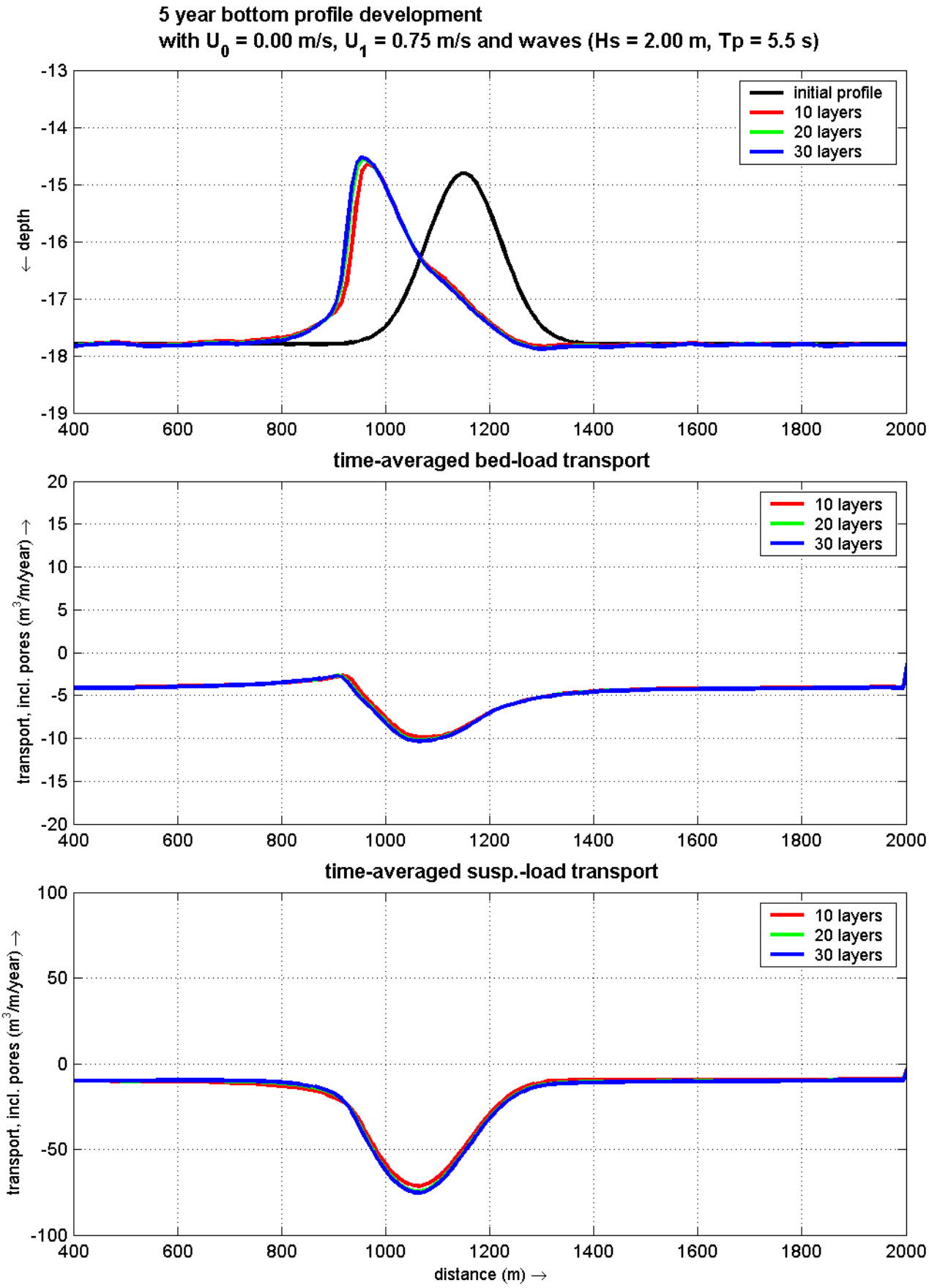

idealized sand ridge model set-up: number of vertical layers
bottom profile development, time-averaged bed-l. and suspended-l. transport rates
tide: (U_0 = 0.00m/s, U_1 = 0.75m/s) waves: (Hs = 2.00m, Tp = 5.5s)

2005

idealized sand ridge

WL | Delft Hydraulics

Z3079.40

Figure C.39

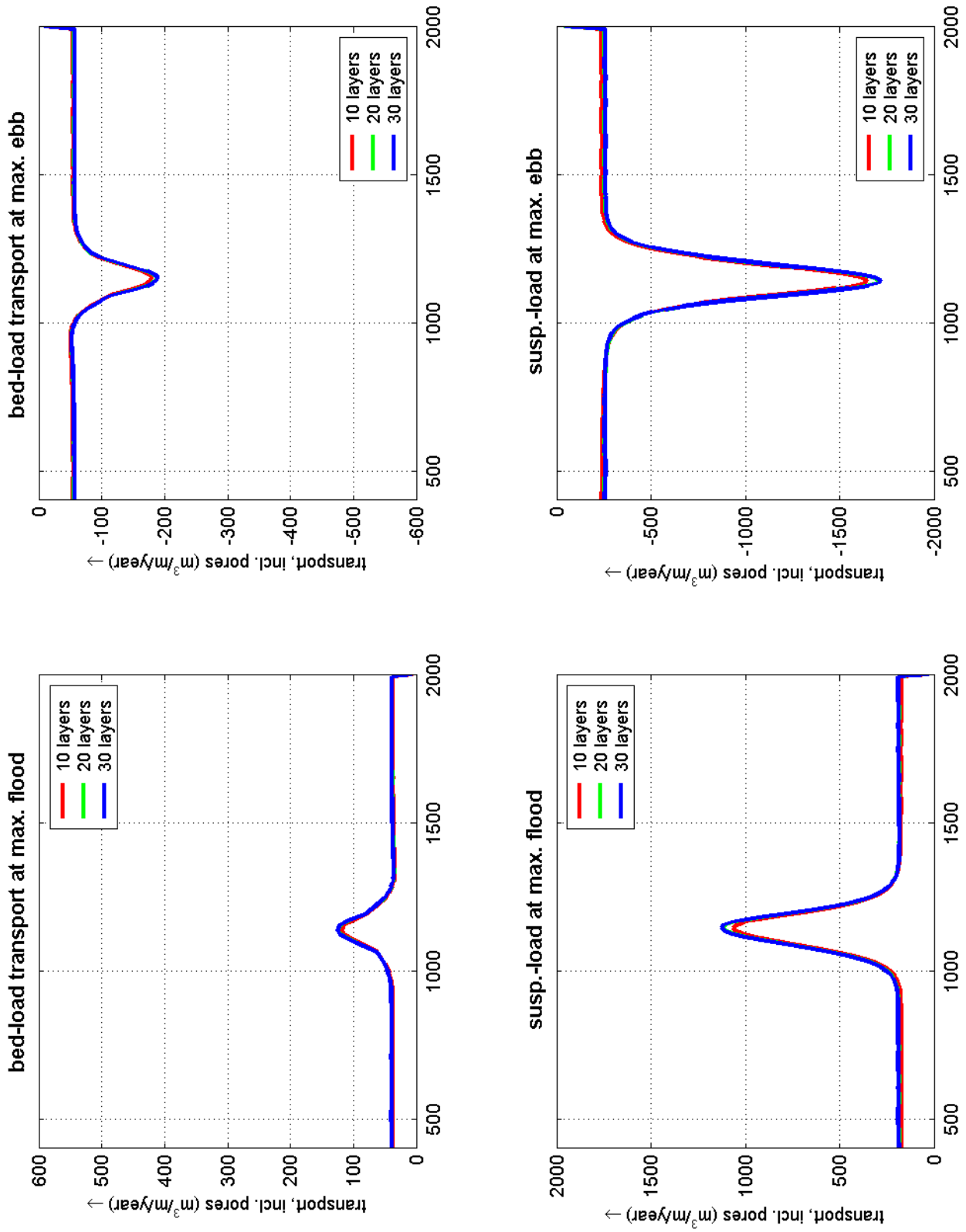

idealized sand ridge model set-up: number of vertical layers
transport rates at max. flood and max. ebb over initial bottom profile
tide: (U_0 = 0.00m/s, U_1 = 0.75m/s) waves: (Hs = 2.00m, Tp = 5.5s)

2005

idealized sand ridge

WL | Delft Hydraulics

Z3079.40

Figure C.40

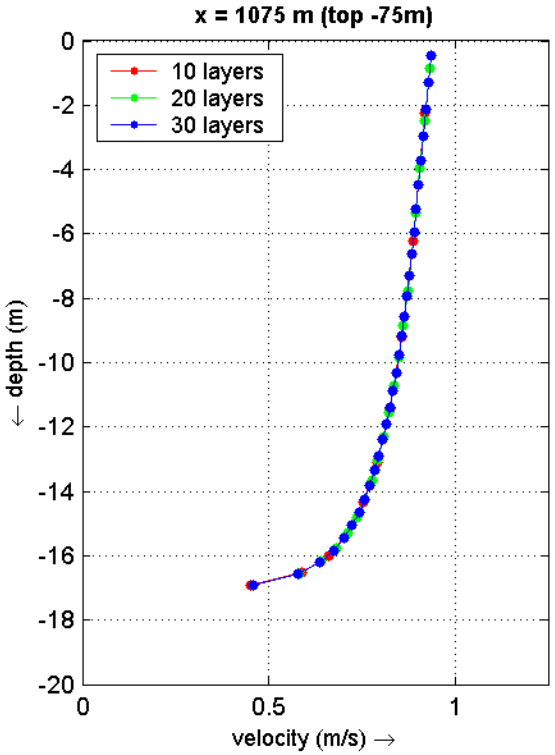

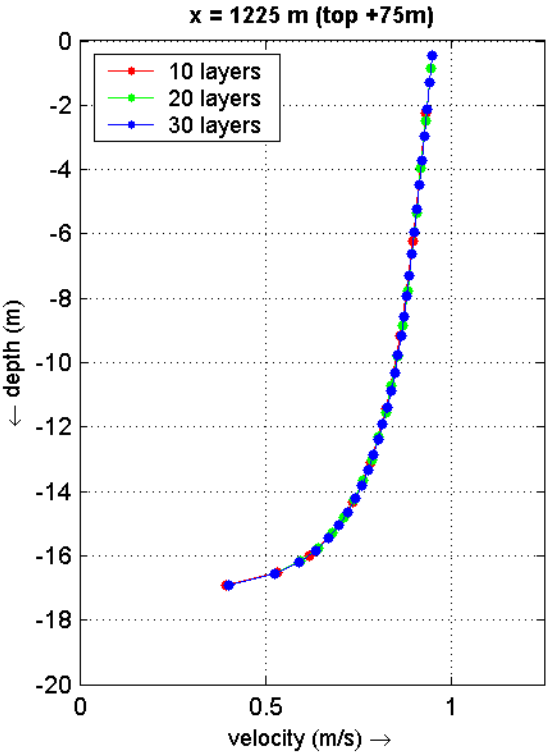

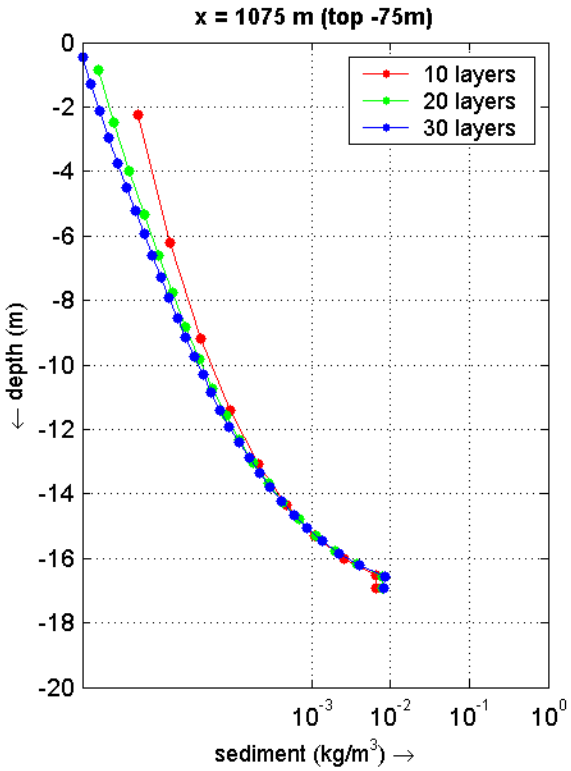

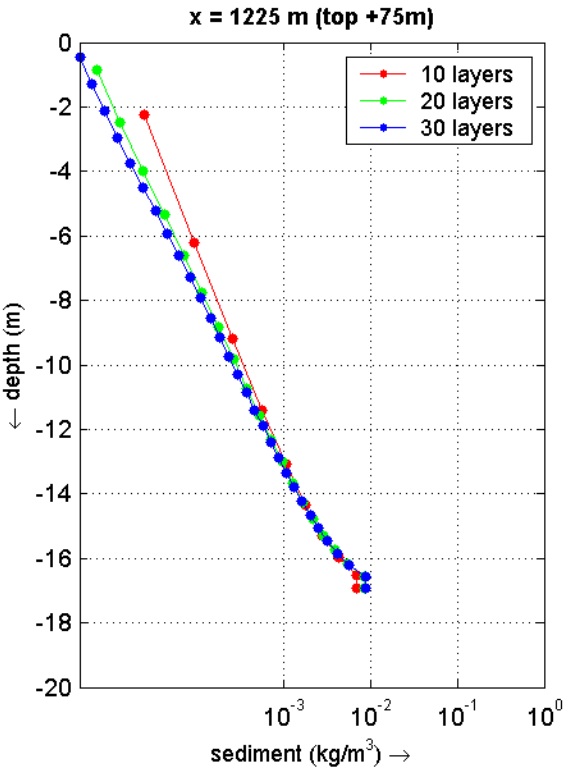

idealized sand ridge model set-up: number of vertical layers
velocity and concentration profiles at max. flood for 10,20 and 30 layers
tide:(U_0 = 0.00 m/s, U_1 = 0.75 m/s) waves: (Hs = 2.00m, Tp = 5.5s)

2005

idealized sand ridge model

WL | Delft Hydraulics

Z3079.40

Figure C.41

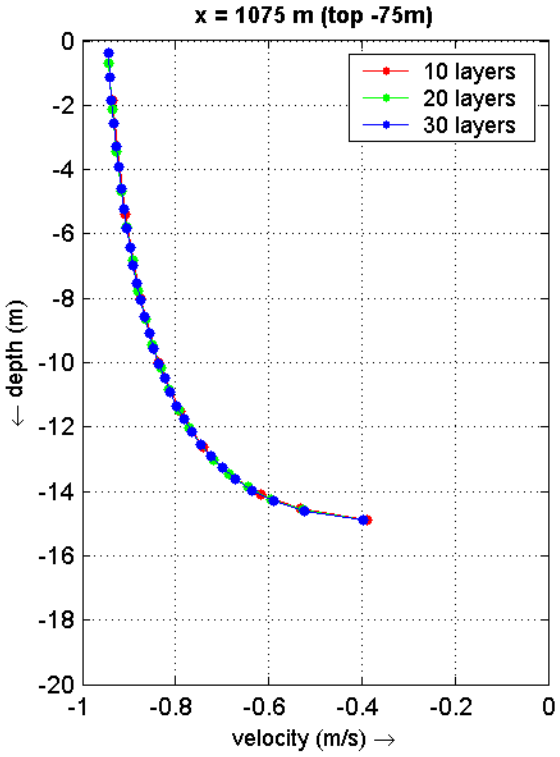

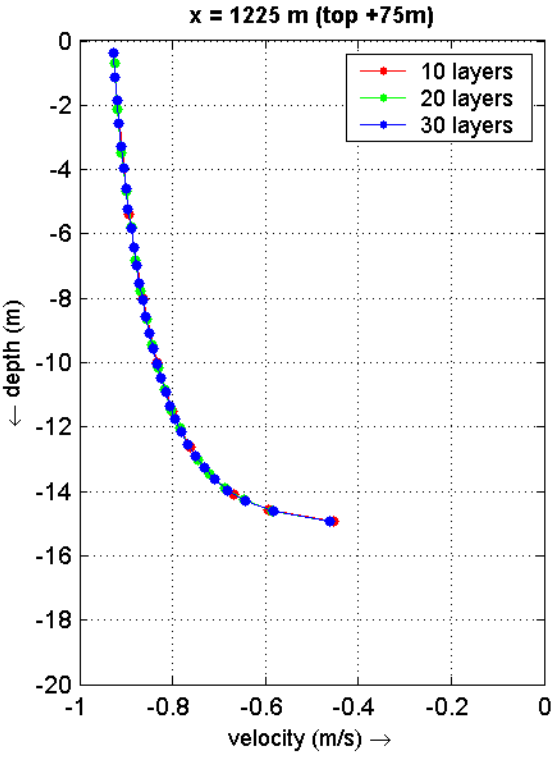

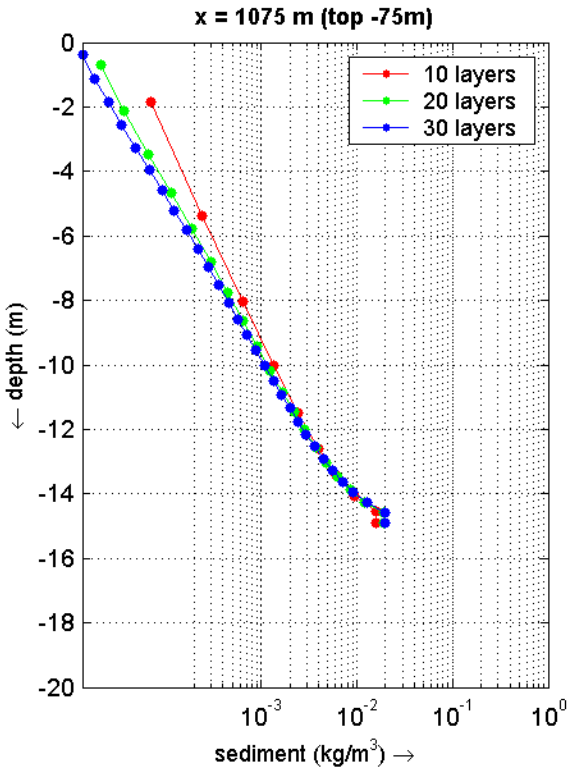

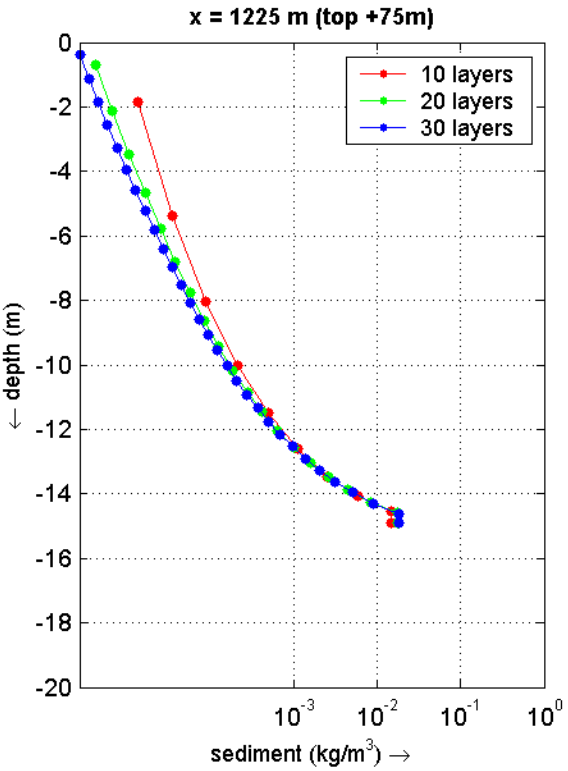

idealized sand ridge model set-up: number of vertical layers velocity and concentration profiles at max. ebb for 10,20 and 30 layers tide:(U_0 = 0.00 m/s, U_1 = 0.75 m/s) waves: (Hs = 2.00m, Tp = 5.5s)		2005
		idealized sand ridge model
WL | Delft Hydraulics	Z3079.40	Figure C.42

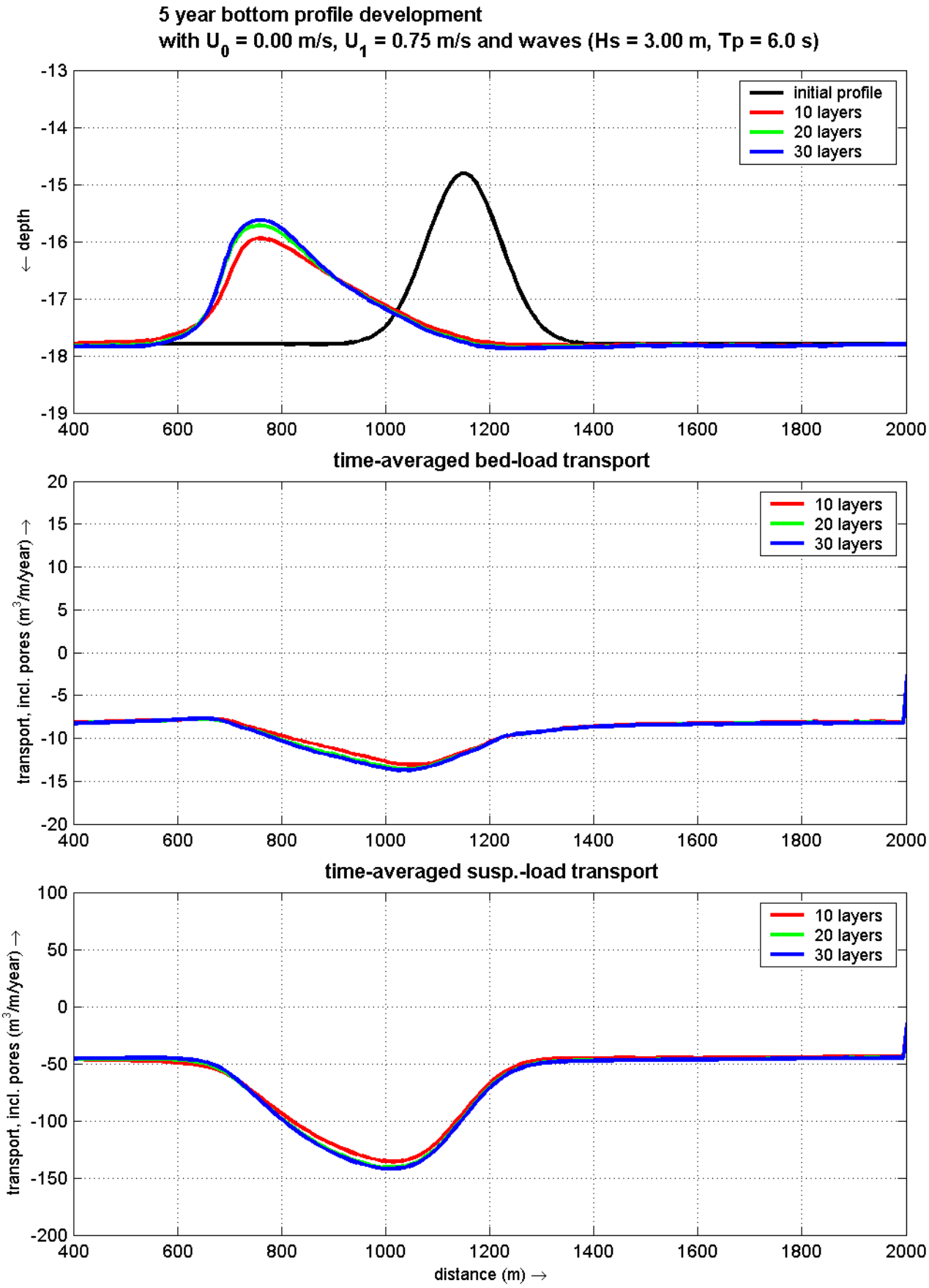

idealized sand ridge model set-up: number of vertical layers
bottom profile development, time-averaged bed-l. and suspended-l. transport rates
tide: (U_0 = 0.00m/s, U_1 = 0.75m/s) waves: (Hs = 3.00m, Tp = 6.0s)

2005

idealized sand ridge

WL | Delft Hydraulics

Z3079.40

Figure C.43

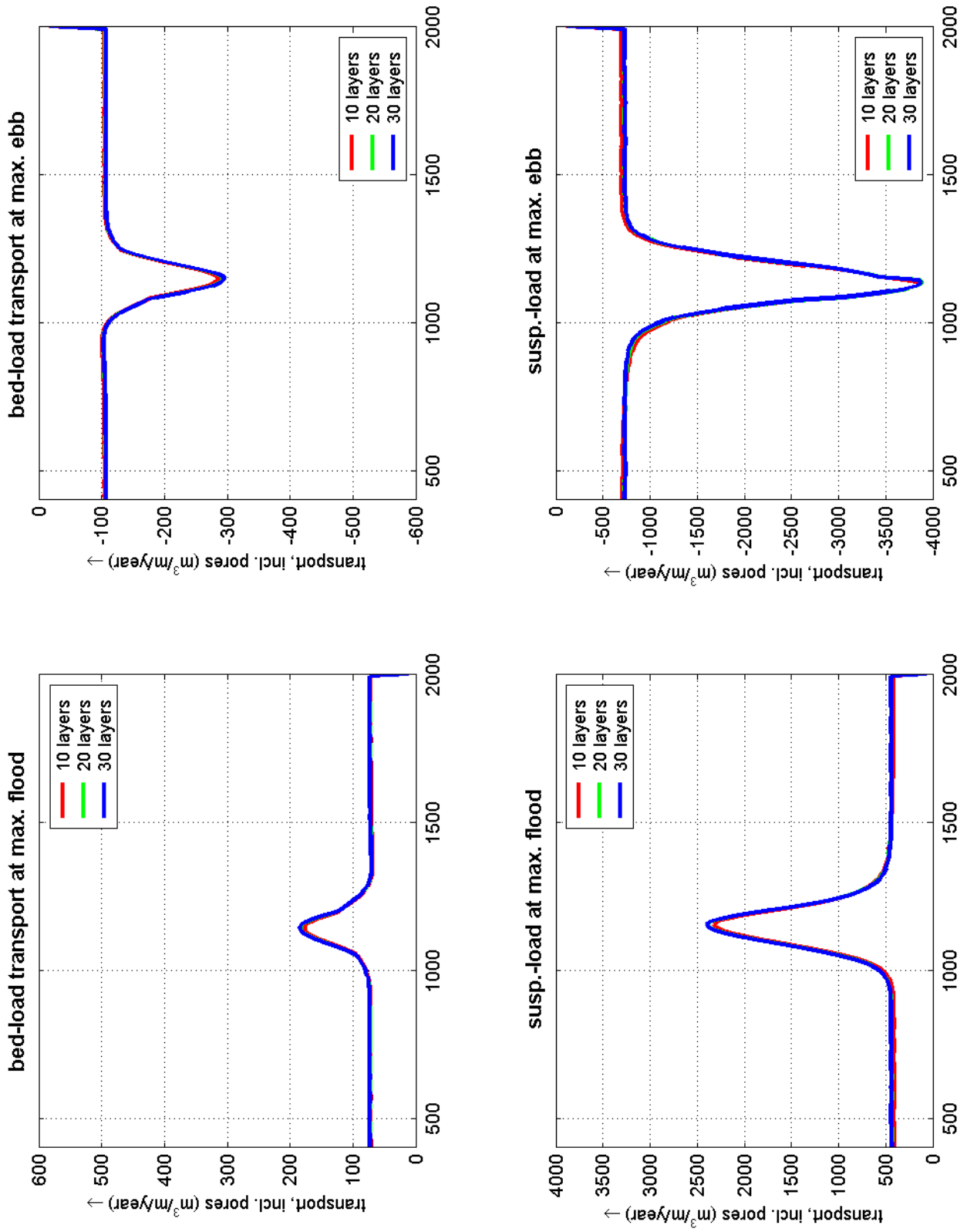

idealized sand ridge model set-up: number of vertical layers
transport rates at max. flood and max. ebb over initial bottom profile
tide: (U_0 = 0.00m/s, U_1 = 0.75m/s) waves: (Hs = 3.00m, Tp = 6.0s)

2005

idealized sand ridge

WL | Delft Hydraulics

Z3079.40

Figure C.44

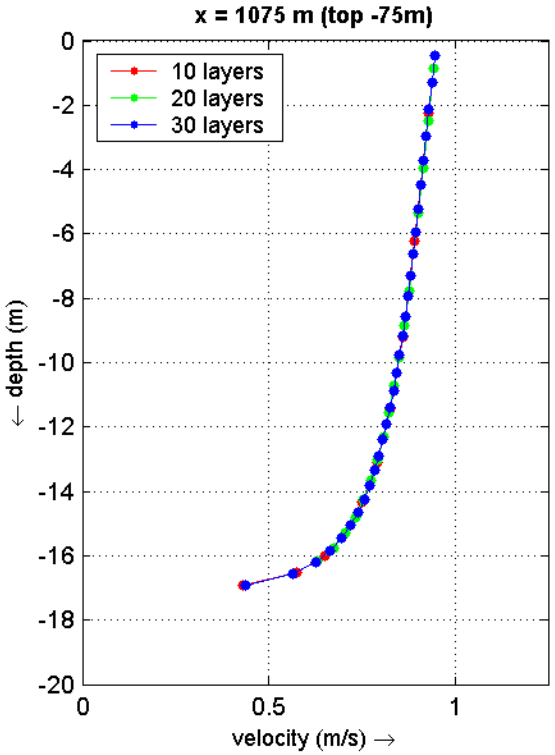

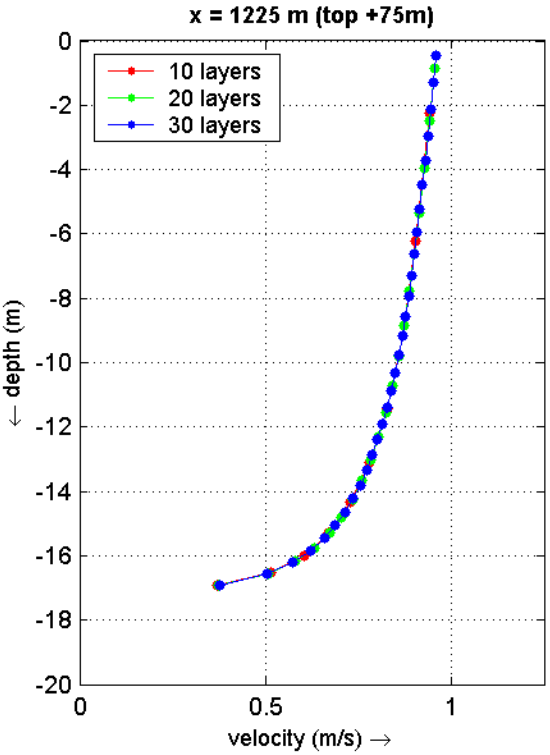

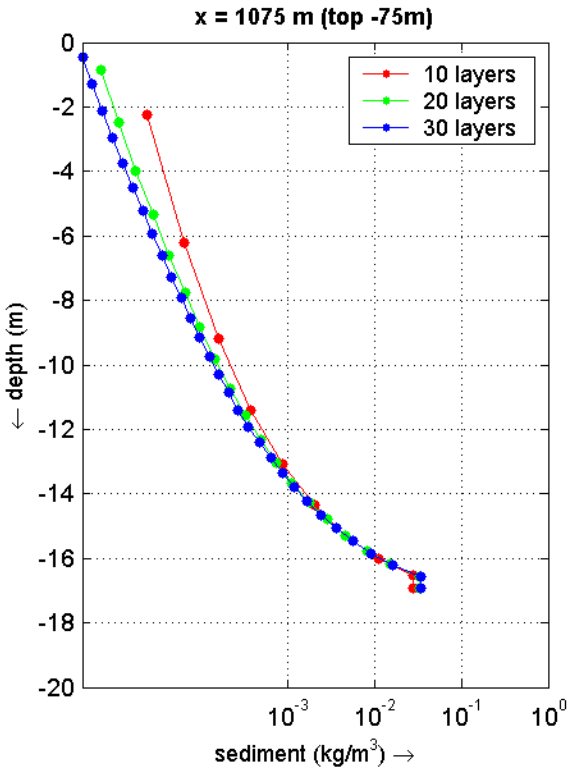

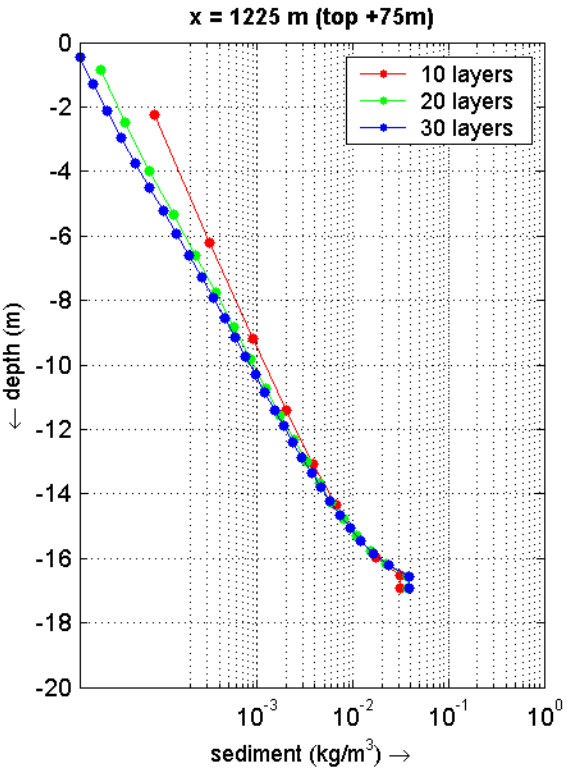

idealized sand ridge model set-up: number of vertical layers
velocity and concentration profiles at max. flood for 10,20 and 30 layers
tide:(U_0 = 0.00 m/s, U_1 = 0.75 m/s) waves: (Hs = 3.00m, Tp = 6.0s)

2005

idealized sand ridge model

WL | Delft Hydraulics

Z3079.40

Figure C.45

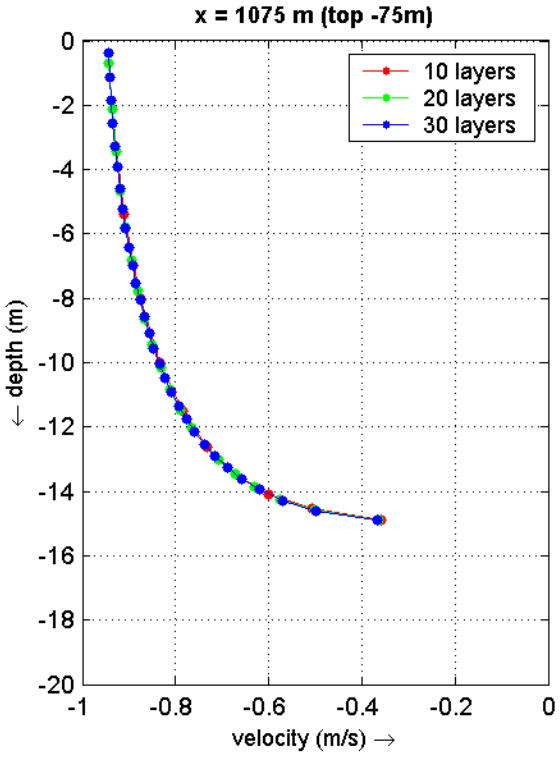

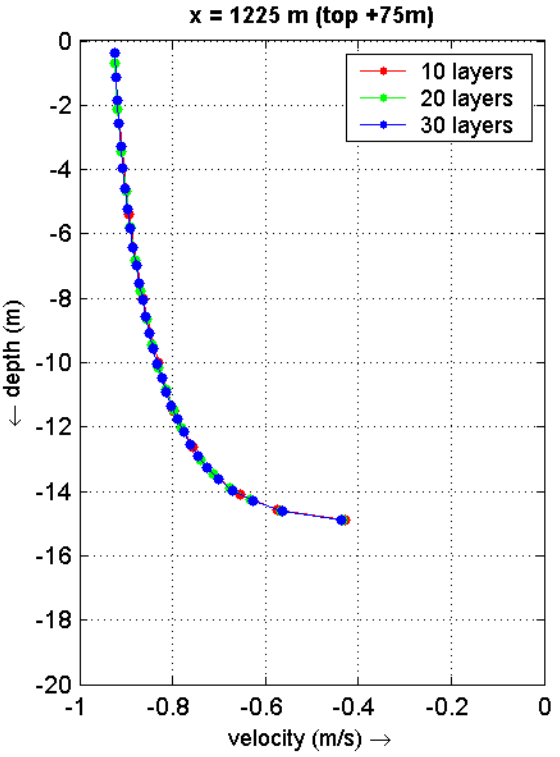

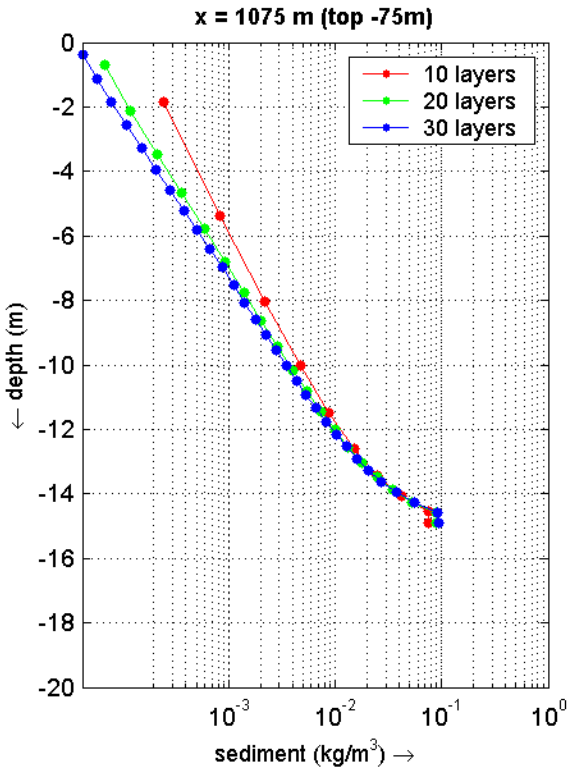

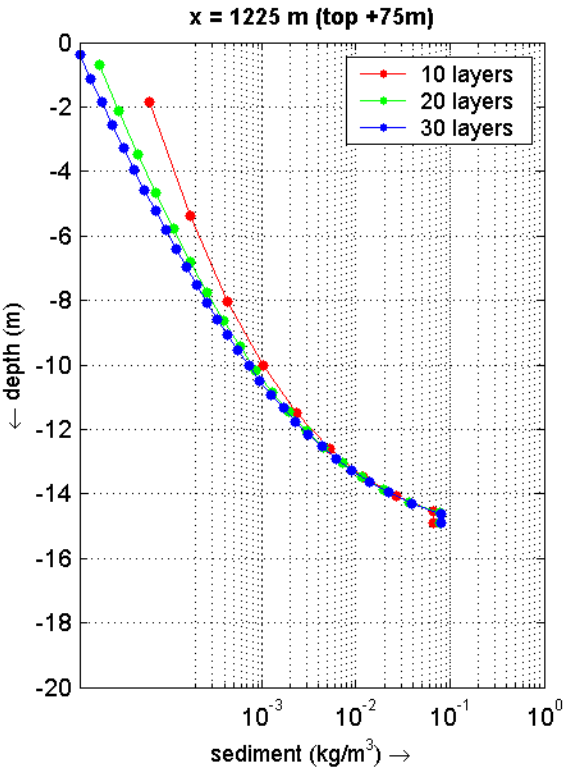

idealized sand ridge model set-up: number of vertical layers velocity and concentration profiles at max. ebb for 10,20 and 30 layers tide:(U_0 = 0.00 m/s, U_1 = 0.75 m/s) waves: (Hs = 3.00m, Tp = 6.0s)		2005
		idealized sand ridge model
WL | Delft Hydraulics	Z3079.40	Figure C.46

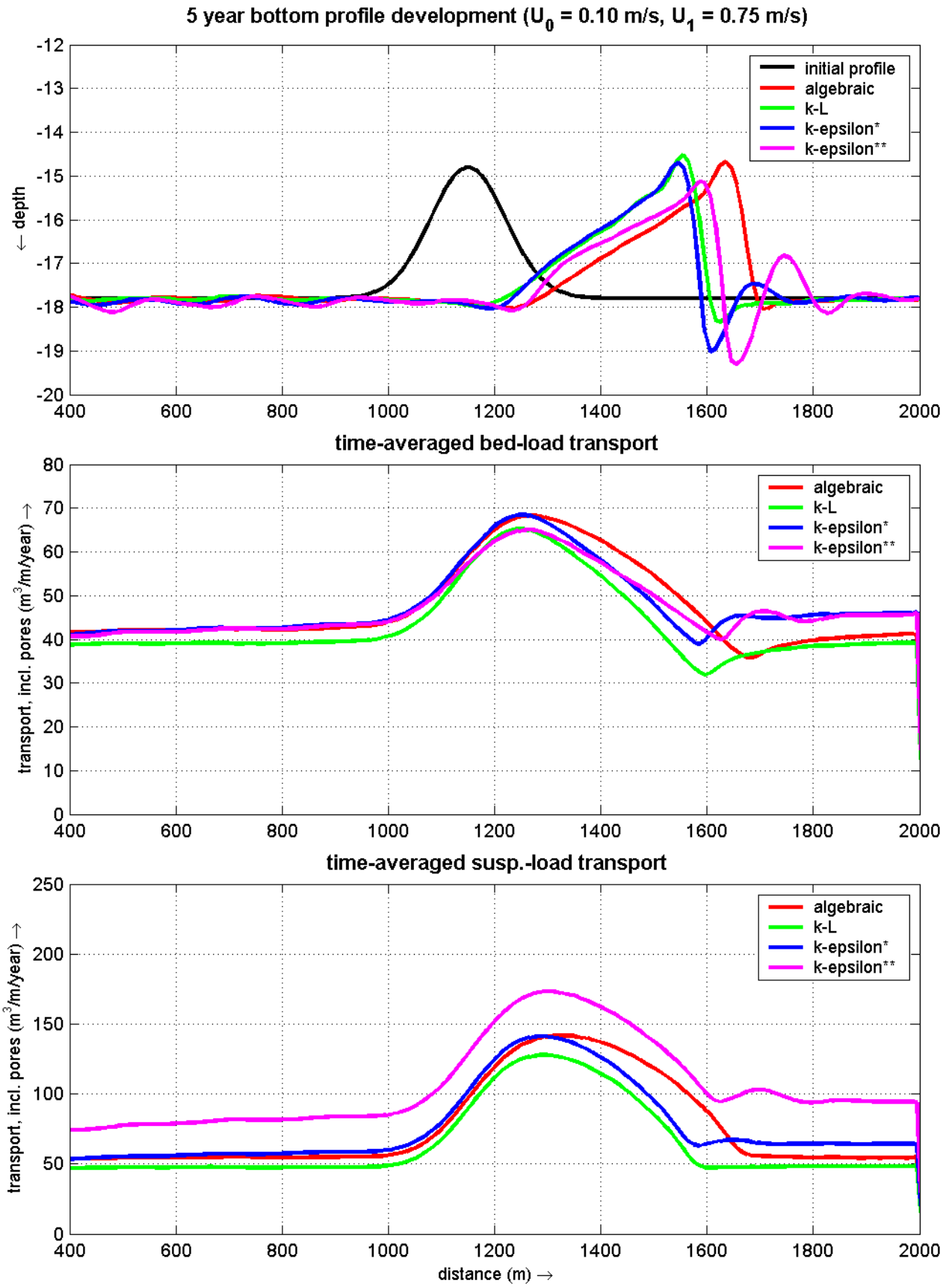

idealized sand ridge model: effect of turbulence model
bottom profile development, time-averaged bed-l. and suspended-l transport rates
tide: (U_0 = 0.10m/s, U_1 = 0.75m/s) no waves

2005

idealized sand ridge

WL | Delft Hydraulics

Z3079.40

Figure C.47

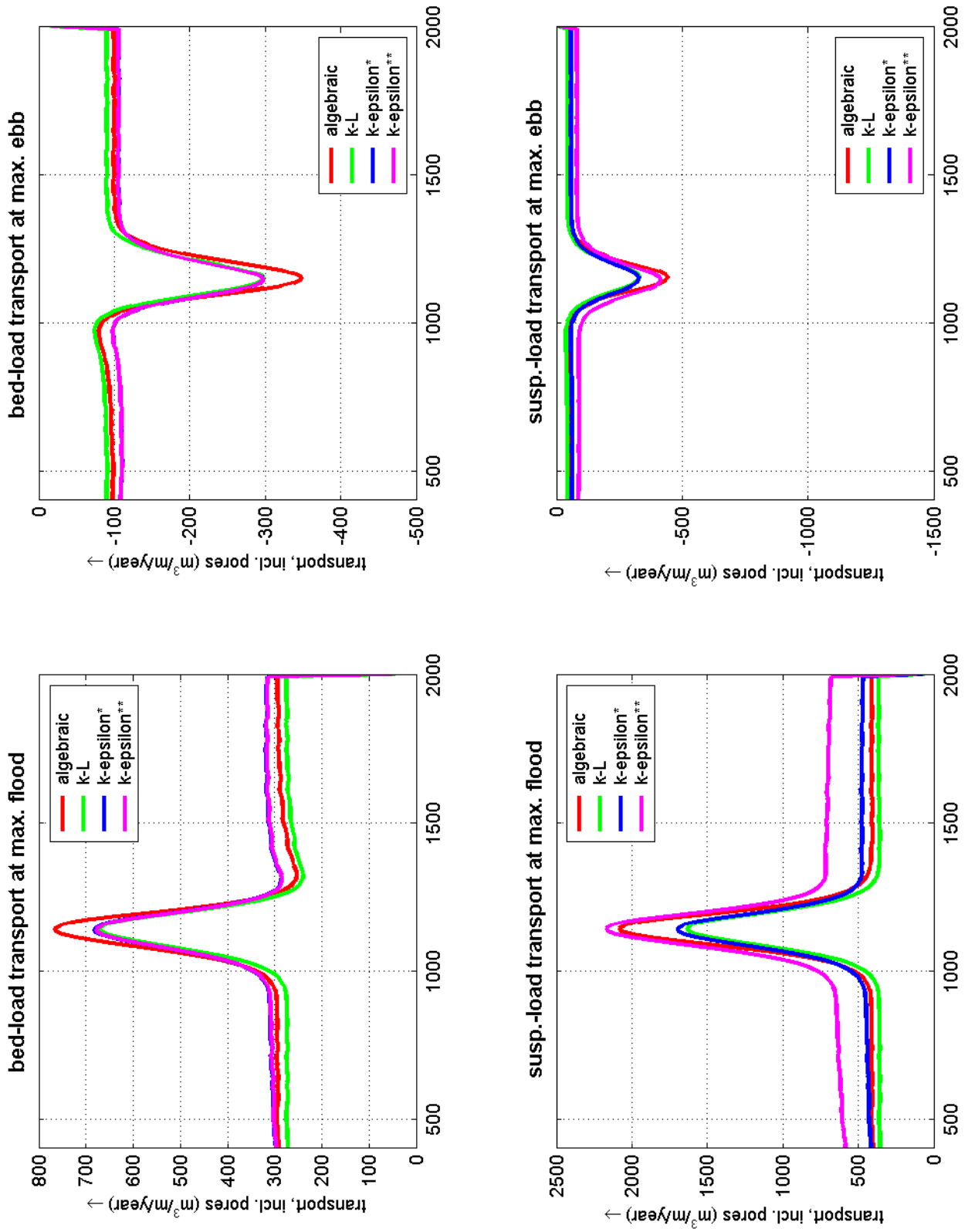

idealized sand ridge model: effect of turbulence model
transport rates at max. flood and max. ebb over initial bottom profile
tide: (U_0 = 0.10m/s, U_1 = 0.75m/s) waves: H_s = 2.50m, T_p = 5.75s

2005

idealized sand ridge

WL | Delft Hydraulics

Z3079.40

Figure C.48

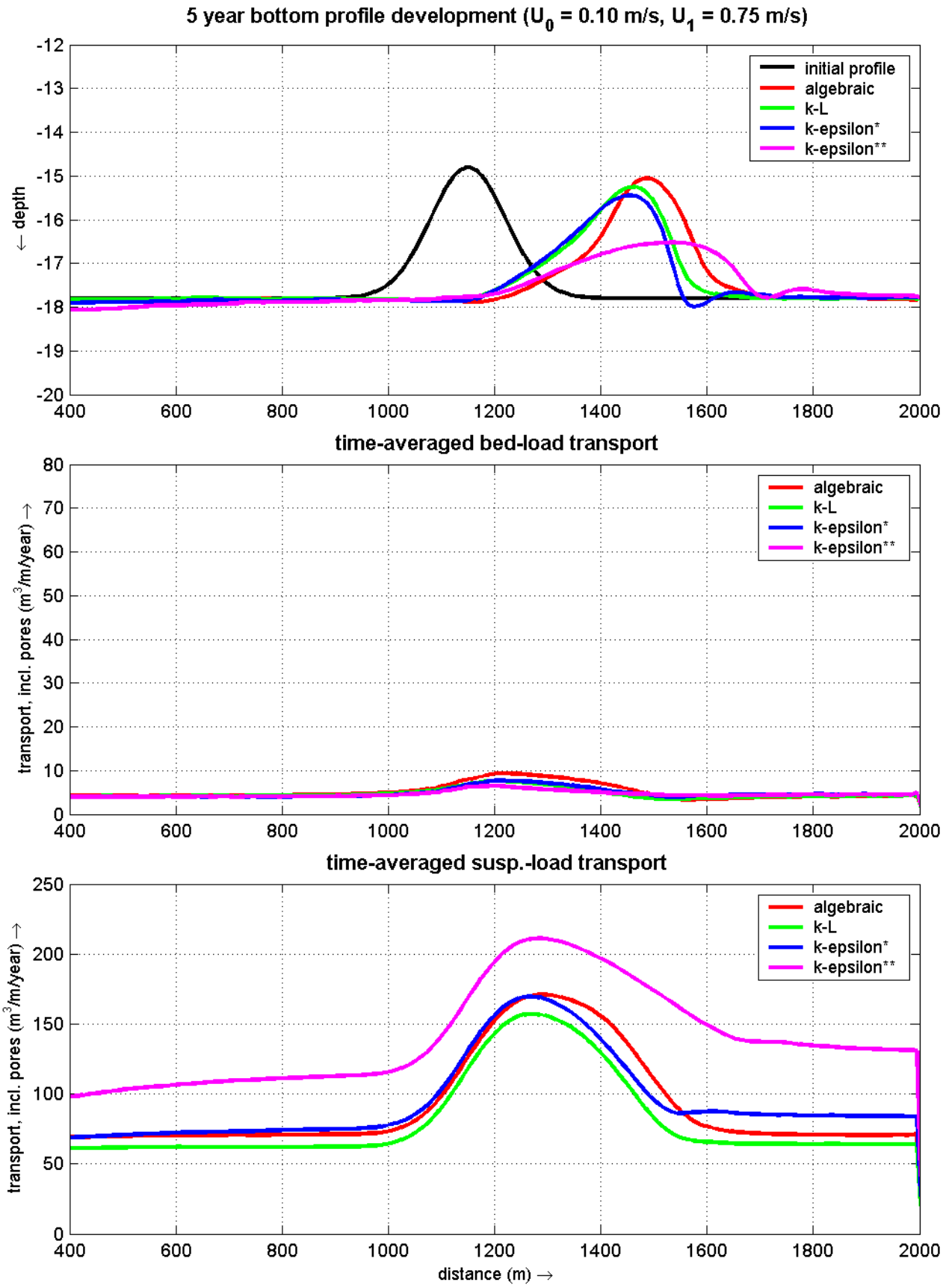

idealized sand ridge model: effect of turbulence model
bottom profile development, time-averaged bed-l. and suspended-l transport rates
tide: (U_0 = 0.10m/s, U_1 = 0.75m/s) waves: (Hs = 2.50m, Tp = 5.75s)

2005

idealized sand ridge

WL | Delft Hydraulics

Z3079.40

Figure C.49

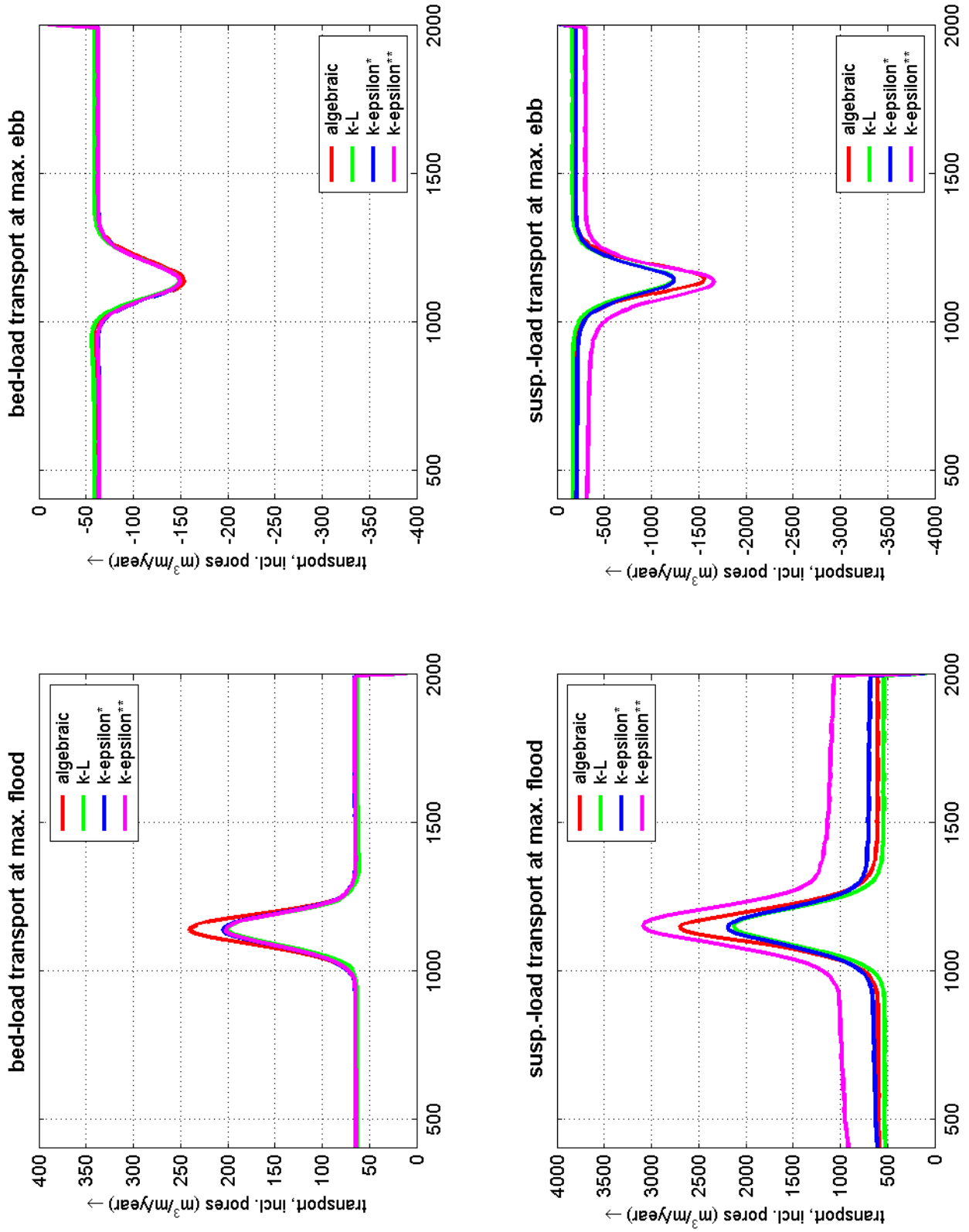

idealized sand ridge model: effect of turbulence model
transport rates at max. flood and max. ebb over initial bottom profile
tide: (U_0 = 0.10m/s, U_1 = 0.75m/s) waves: H_s = 2.50m, T_p = 5.75s

2005

idealized sand ridge

WL | Delft Hydraulics

Z3079.40

Figure C.50

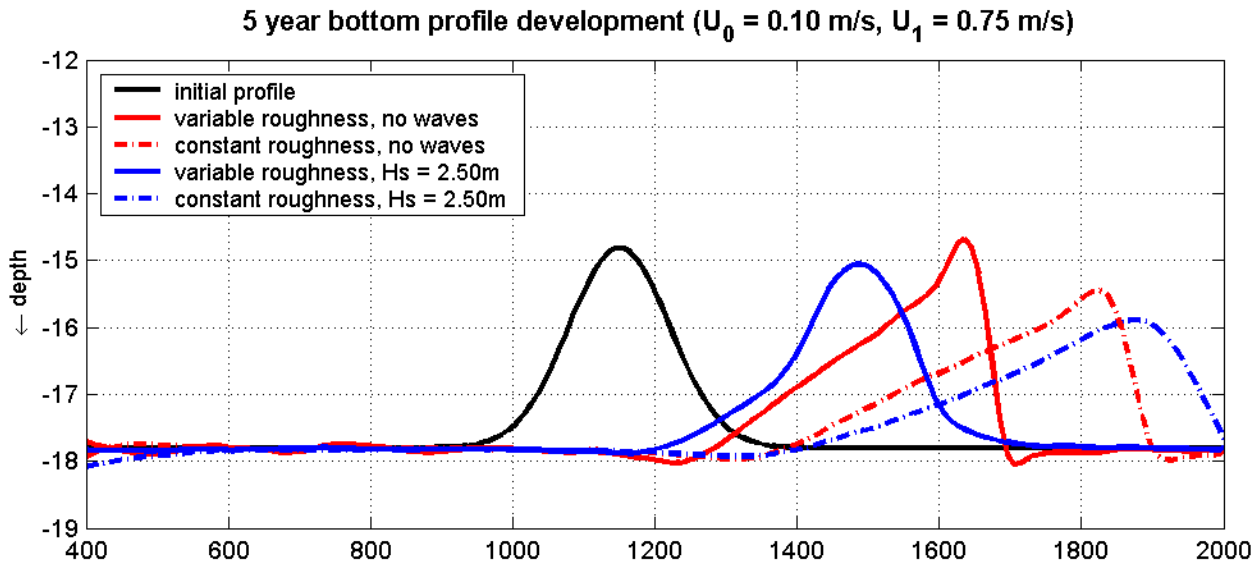

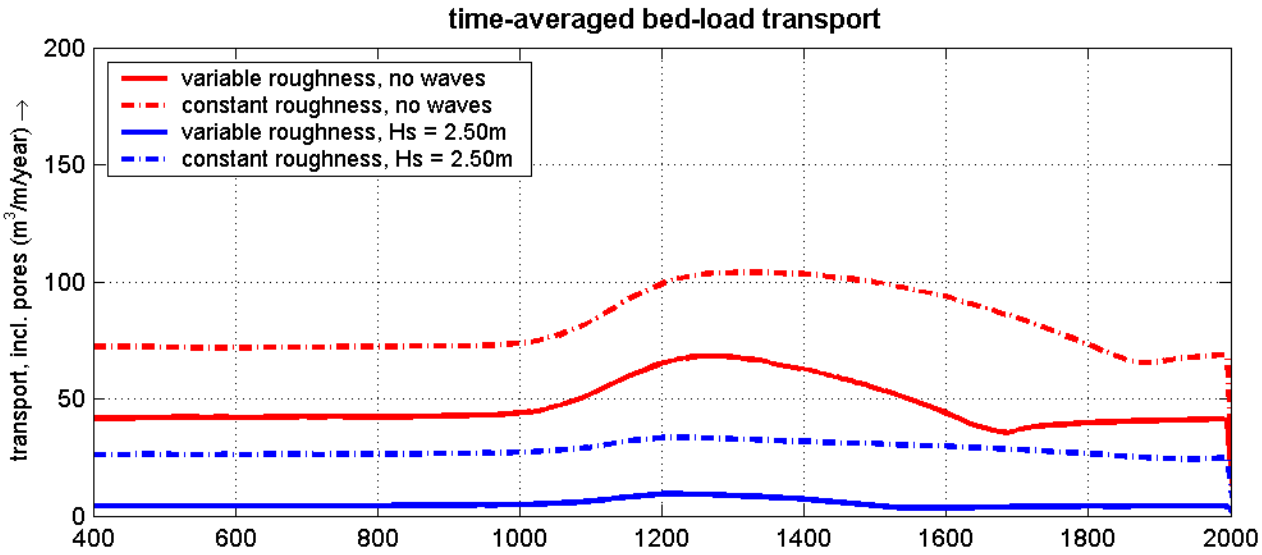

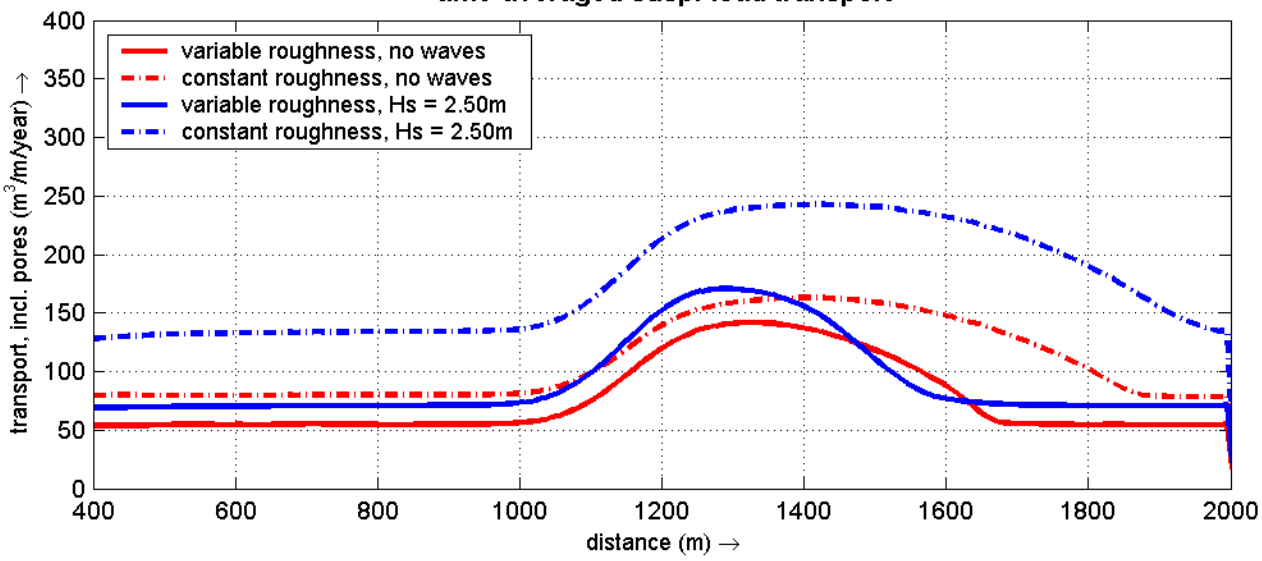

idealized sand ridge model: effect of bed roughness

bottom profile development, time-averaged transport rates with constant (C=65 $m^{1/2}$/s) and variable bed roughness. tide: (U_0=0.10m/s, U_1=0.75m/s) waves: H_s=0.00/2.50m

2005

idealized sand ridge

WL | Delft Hydraulics

Z3079.40

Figure C.51

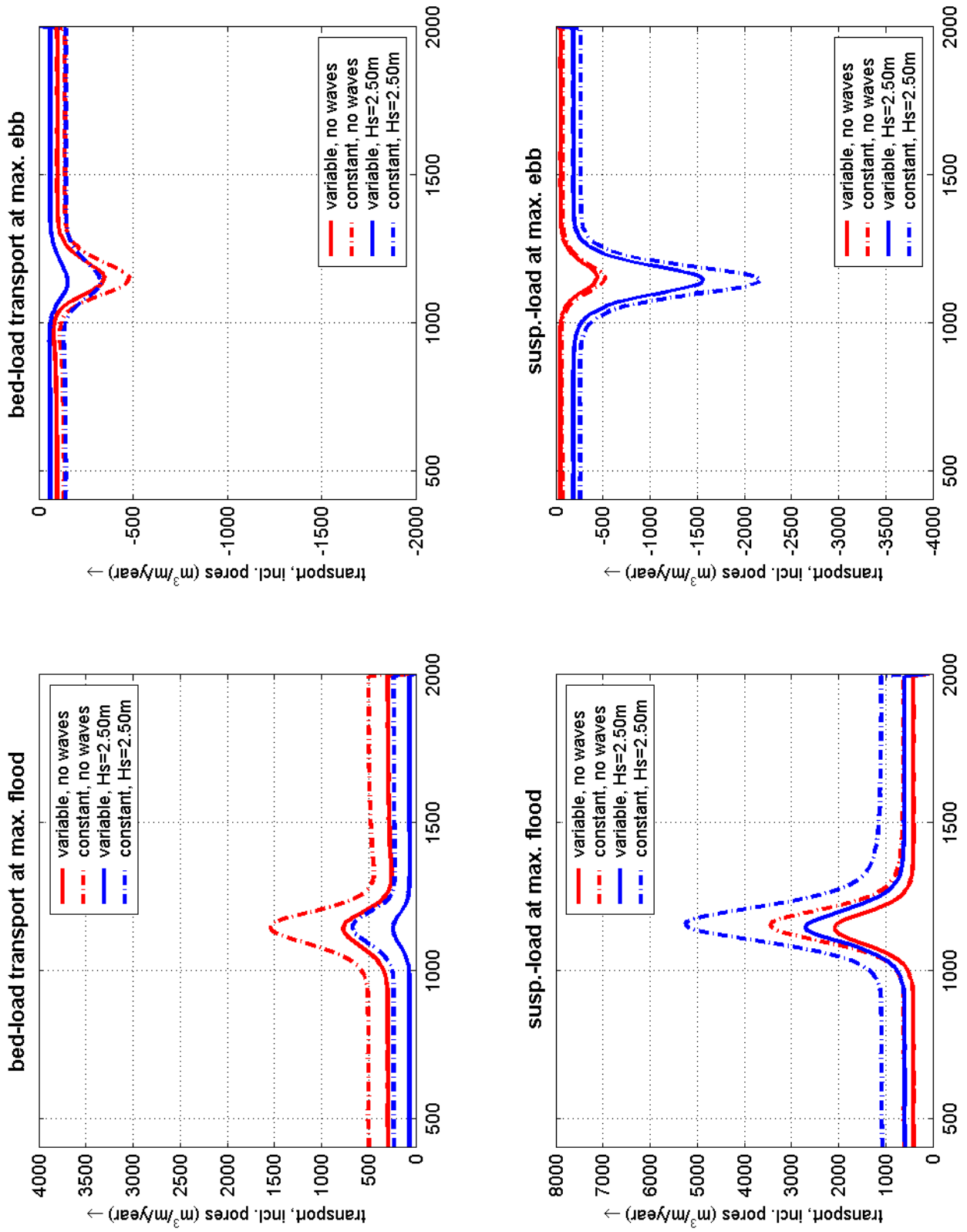

idealized sand ridge model: effect of bed roughness

transport rates at max. flood and max. ebb with constant ($C=65 m^{1/2}/s$) and variable bed roughness. tide: (U_0=0.10m/s, U_1=0.75m/s) waves: H_s=0.00/2.50m

2005

idealized sand ridge

WL | Delft Hydraulics

Z3079.40

Figure C.52

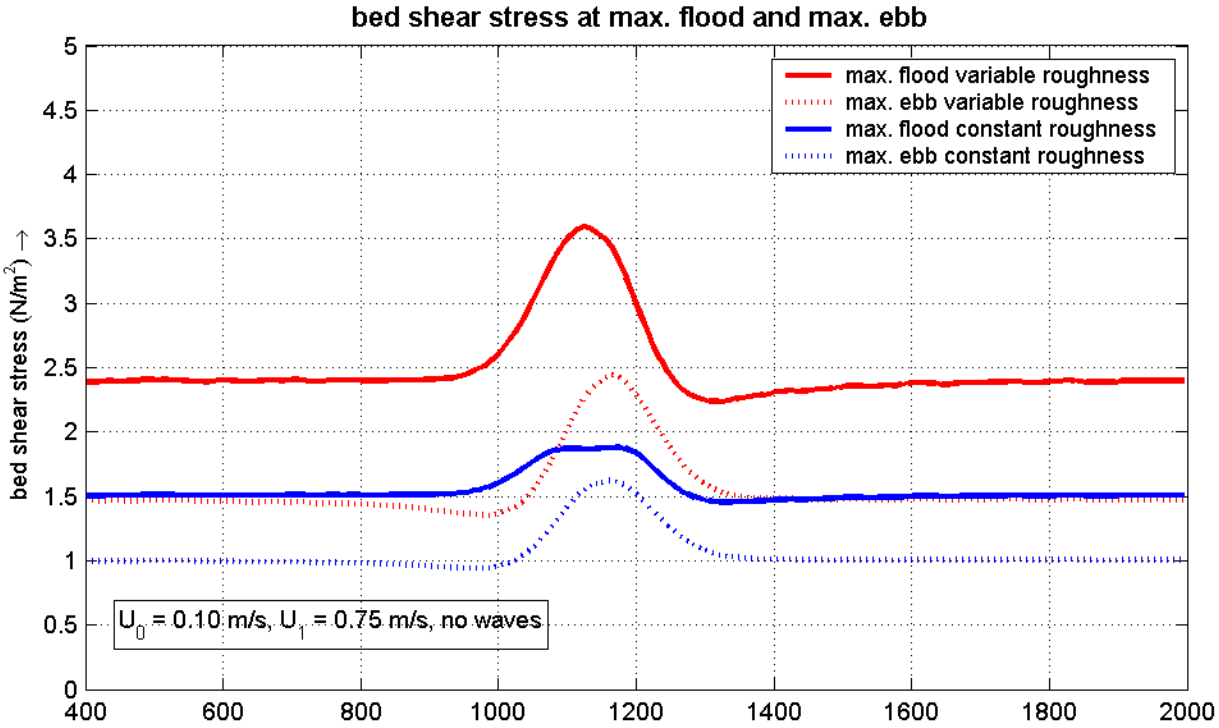

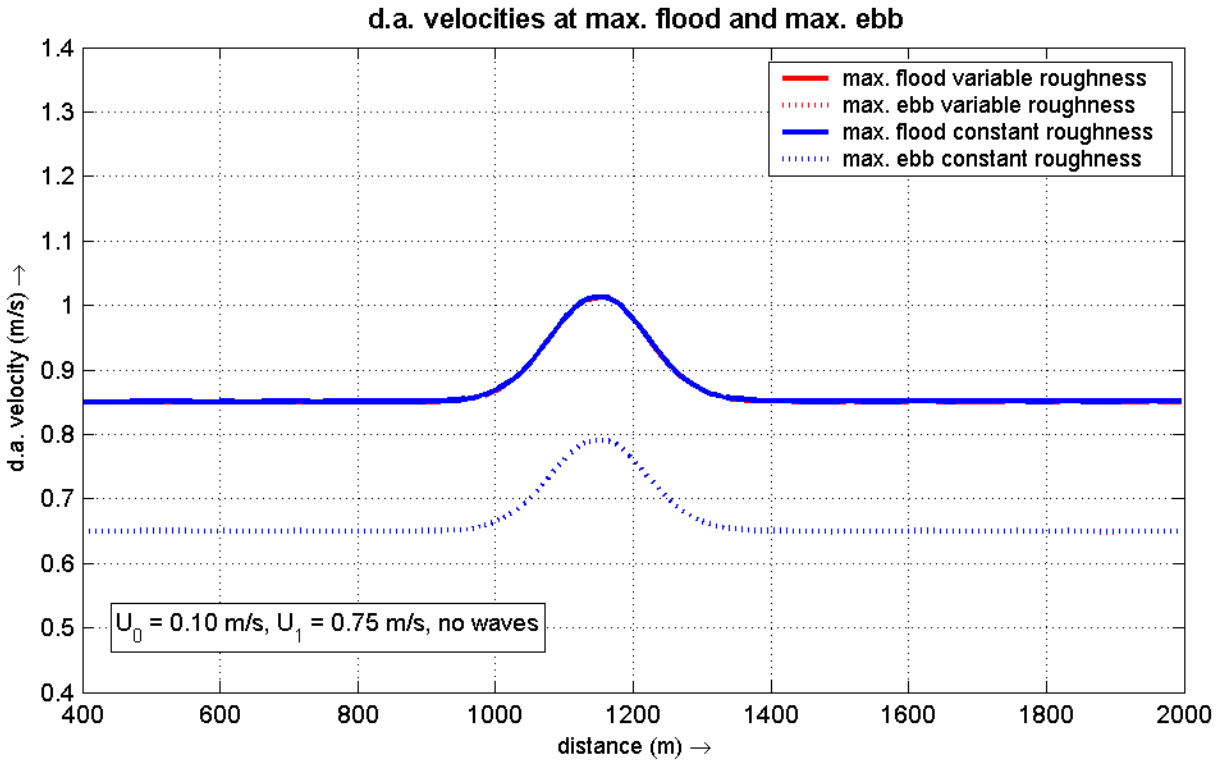

idealized sand ridge model: effect of bed roughness
bed shear stress and d.a. velocities at max. flood and max. ebb
tide: (U_0 = 0.10m/s, U_1 = 0.75m/s) without waves

2005

idealized sand ridge

WL | Delft Hydraulics

Z3079.40

Figure C.53

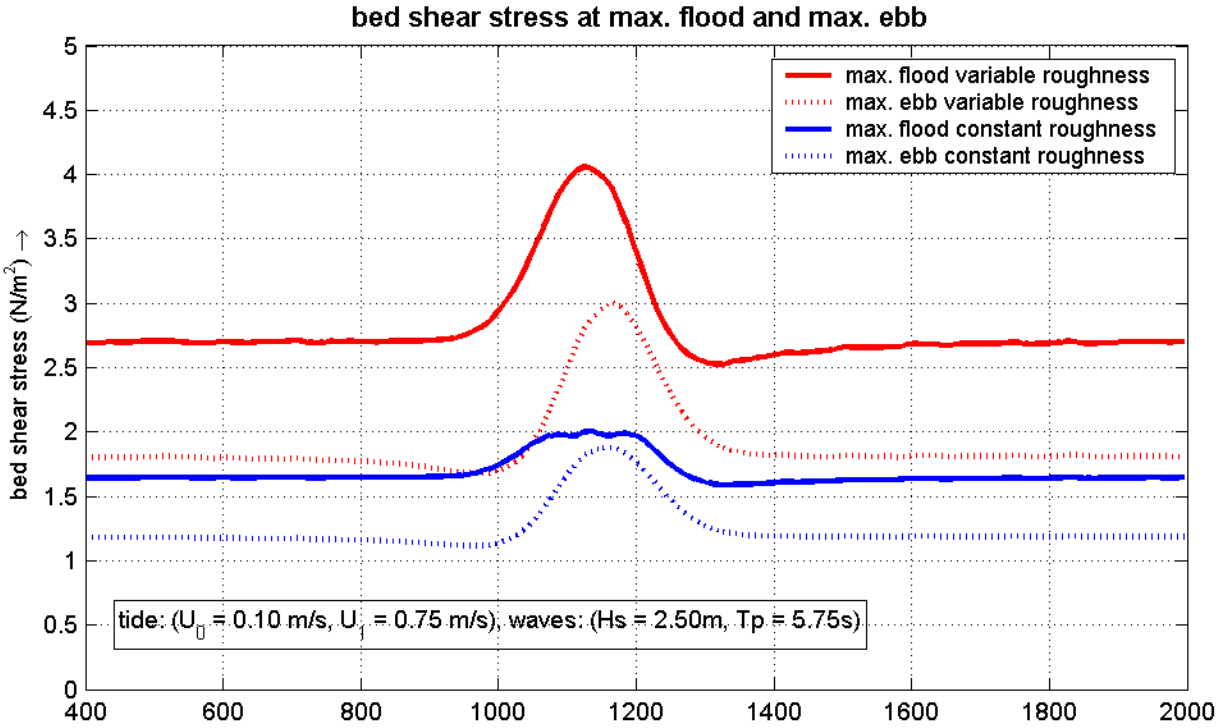

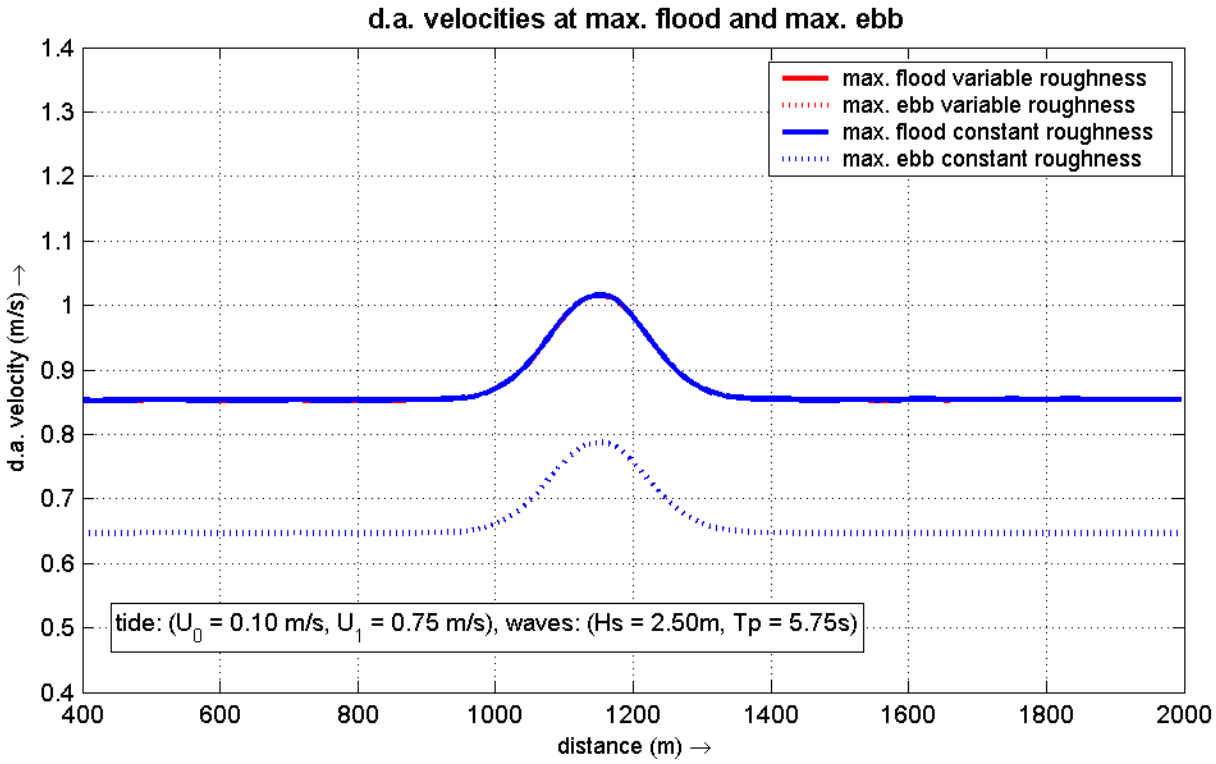

idealized sand ridge model: effect of bed roughness
bed shear stress and d.a. velocities at max. flood and max. ebb
tide: (U_0 = 0.10m/s, U_1 = 0.75m/s) waves: (Hs = 2.50m, Tp = 5.75s)

2005

idealized sand ridge

WL | Delft Hydraulics

Z3079.40

Figure C.54

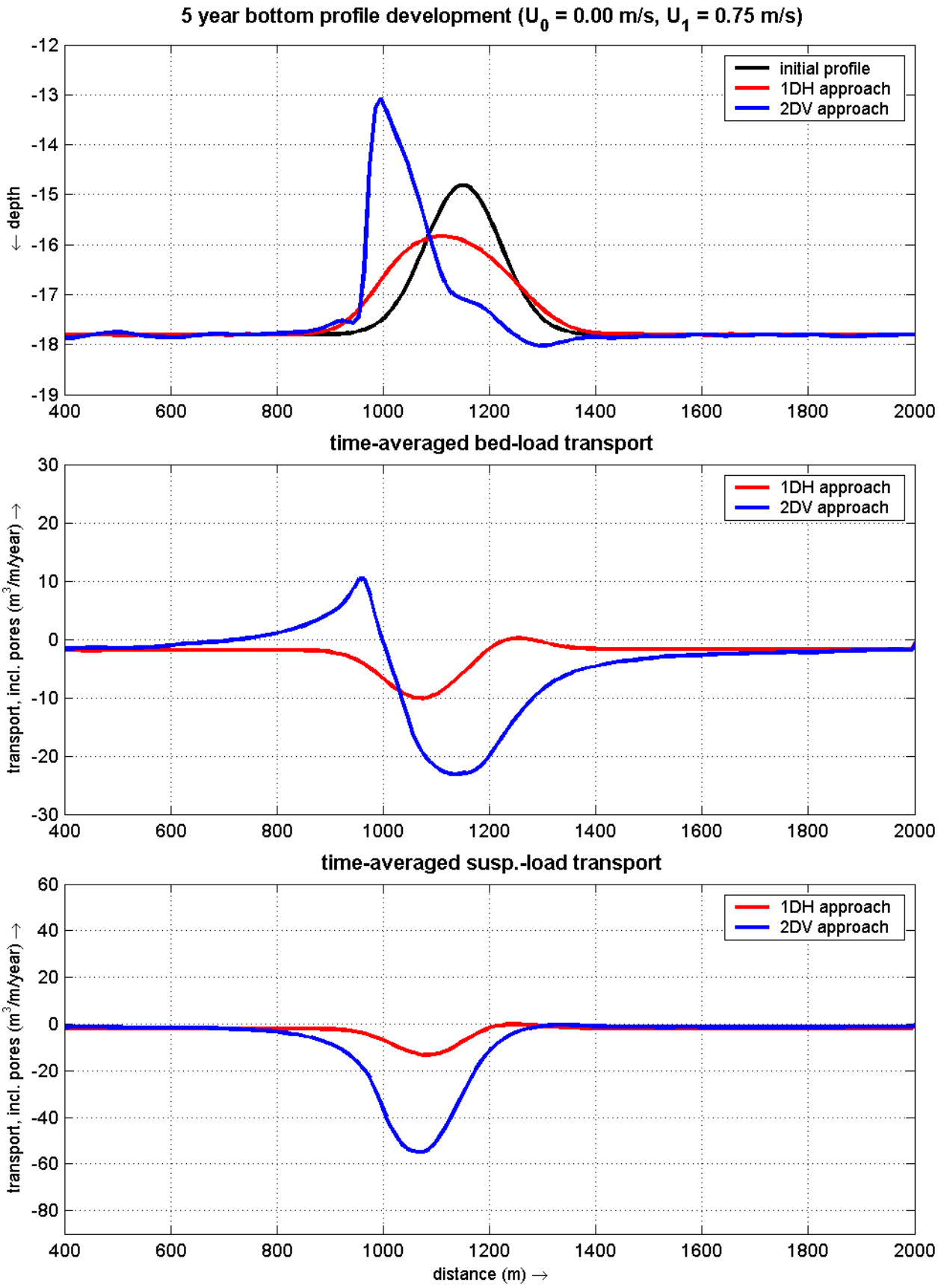

idealized sand ridge model: comparison of 1DH and 2DV model approach
bottom profile development, time-averaged bed-l. and suspended-l transport rates
tide: (U_0 = 0.00m/s, U_1 = 0.75m/s) no waves

2005

idealized sand ridge

WL | Delft Hydraulics

Z3079.40

Figure C.55

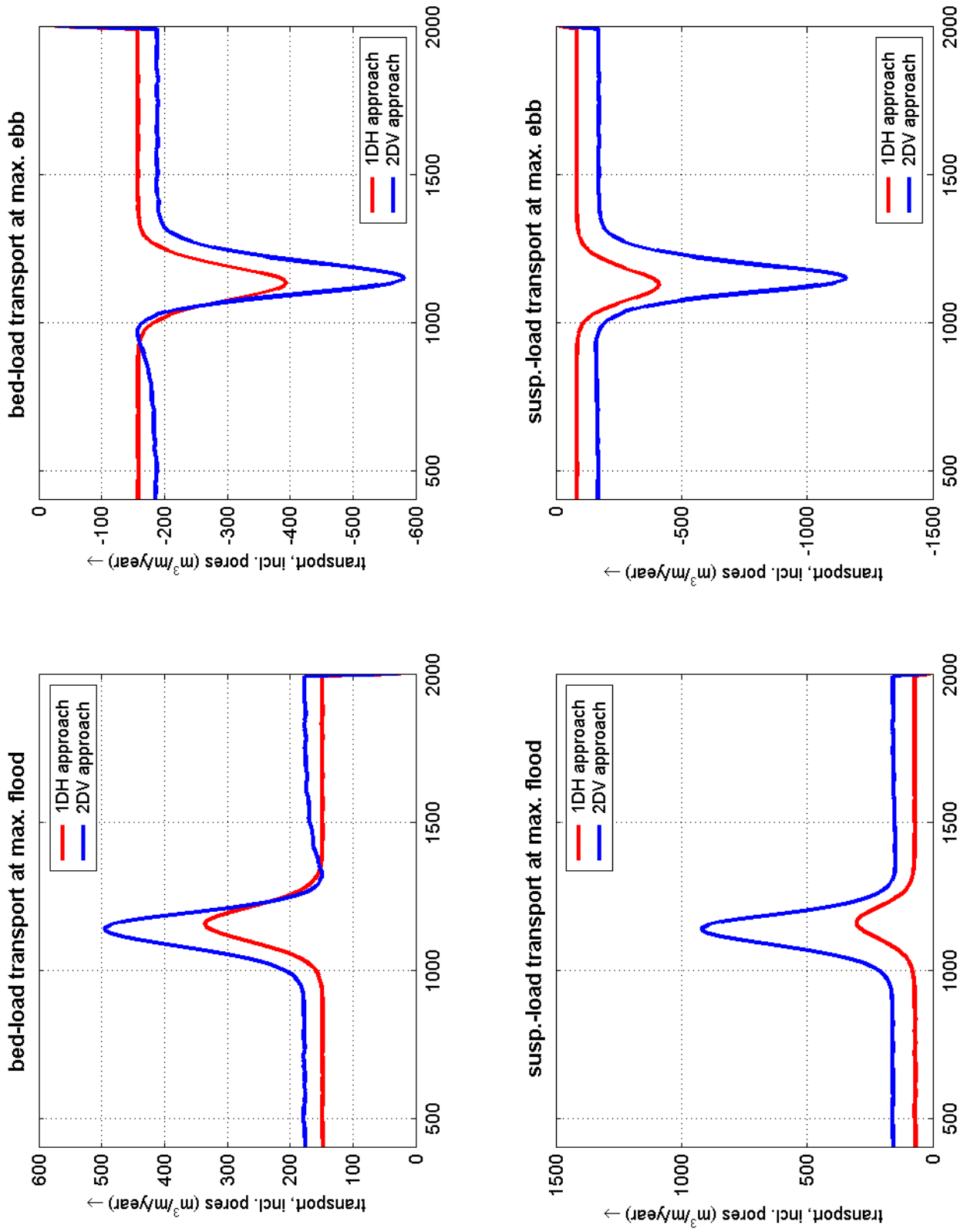

idealized sand ridge model: comparison of 1DH and 2DV model approach
transport rates at max. flood and max. ebb over initial bottom profile
tide: (U_0 = 0.00m/s, U_1 = 0.75m/s) no waves

2005

idealized sand ridge

WL | Delft Hydraulics

Z3079.40

Figure C.56

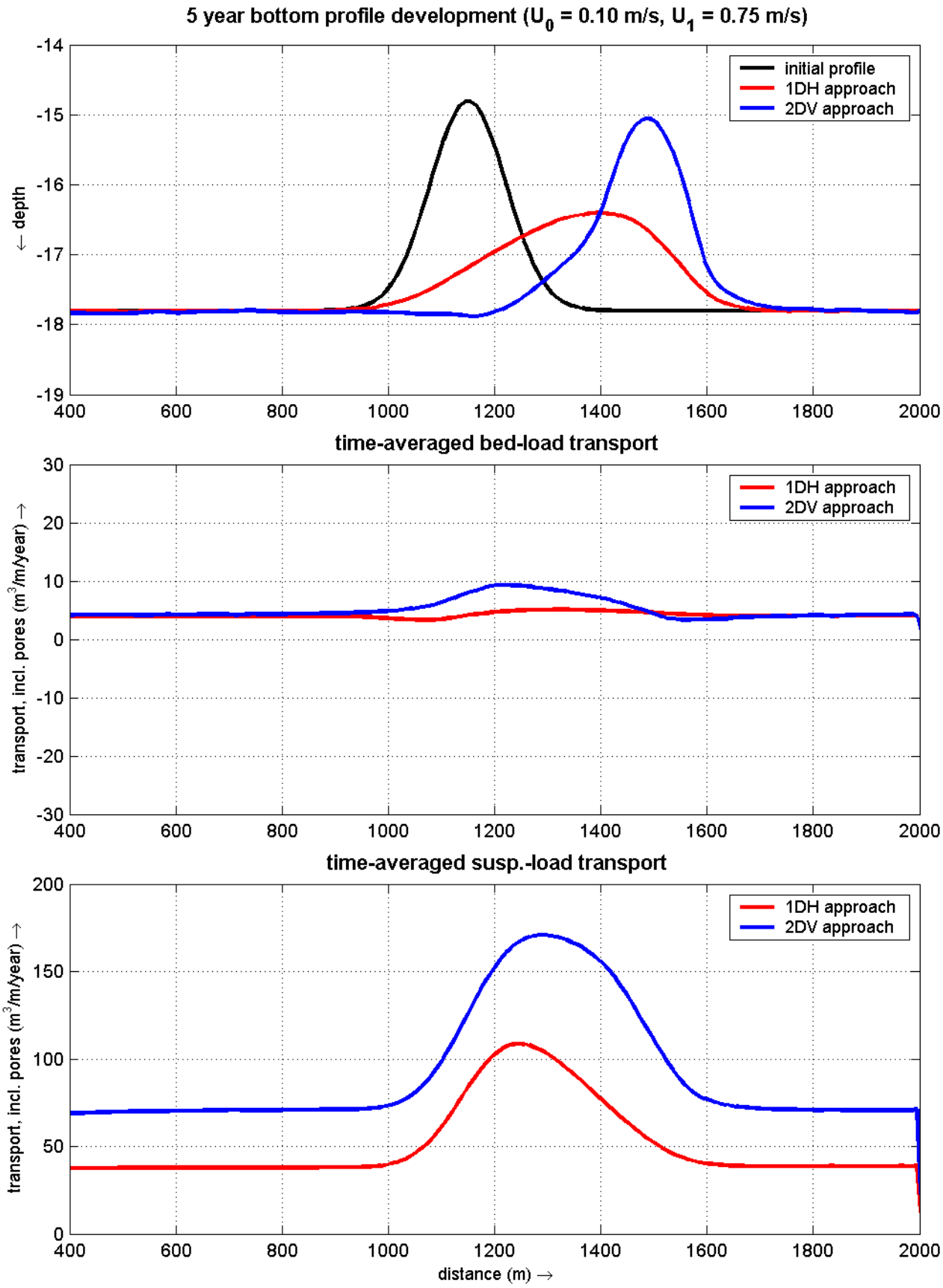

idealized sand ridge model: comparison of 1DH and 2DV model approach
bottom profile development, time-averaged bed-l. and suspended-l transport rates
tide: (U_0 = 0.10m/s, U_1 = 0.75m/s) waves: (Hs = 2.50m, Tp = 5.75s)

2005

idealized sand ridge

WL | Delft Hydraulics

Z3079.40

Figure C.57

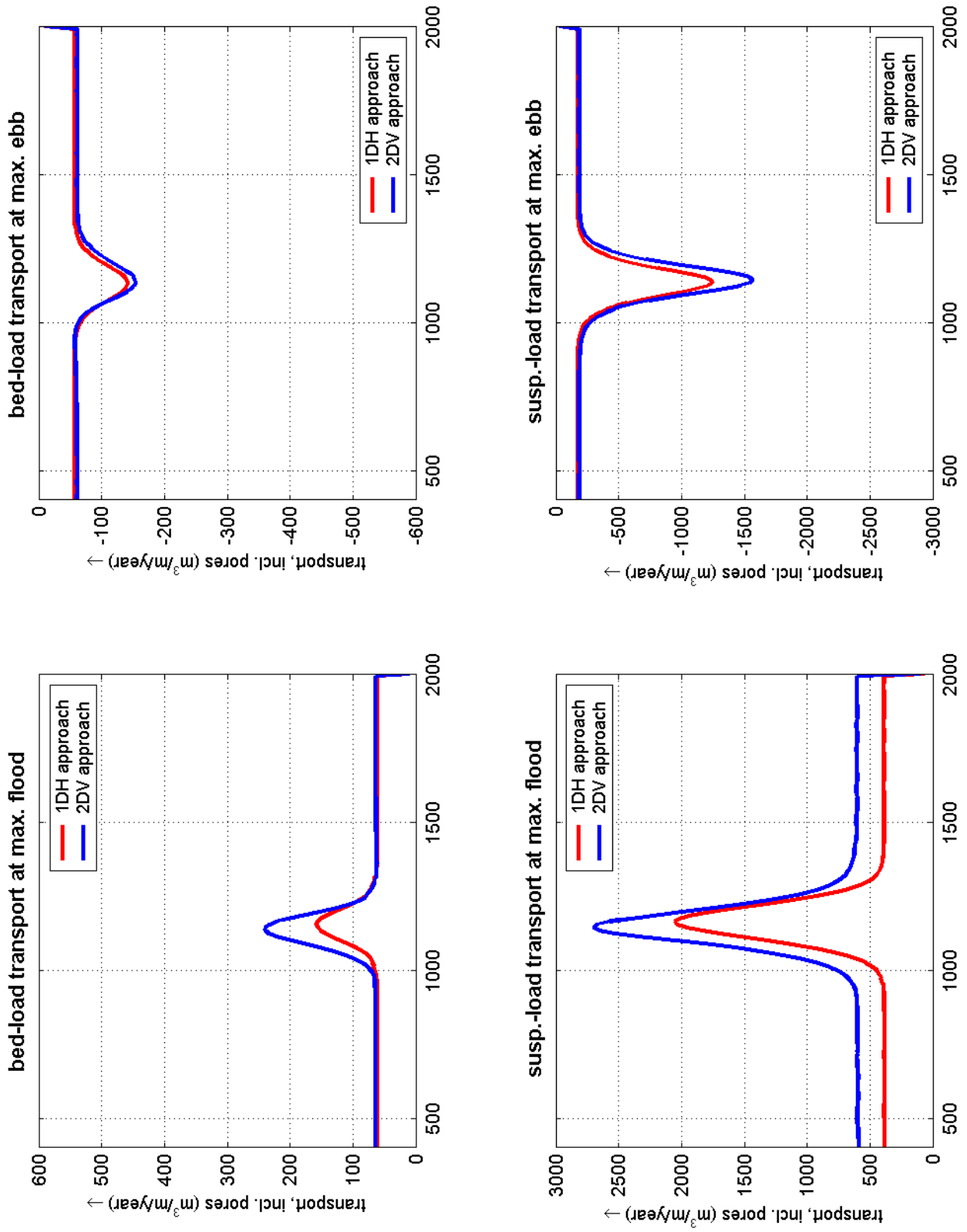

idealized sand ridge model: comparison of 1DH and 2DV model approach
transport rates at max. flood and max. ebb over initial bottom profile
tide: (U_0 = 0.10m/s, U_1 = 0.75m/s) waves: (Hs = 2.50m, Tp = 5.75s)

2005

idealized sand ridge

WL | Delft Hydraulics

Z3079.40

Figure C.58

D Nesting procedure

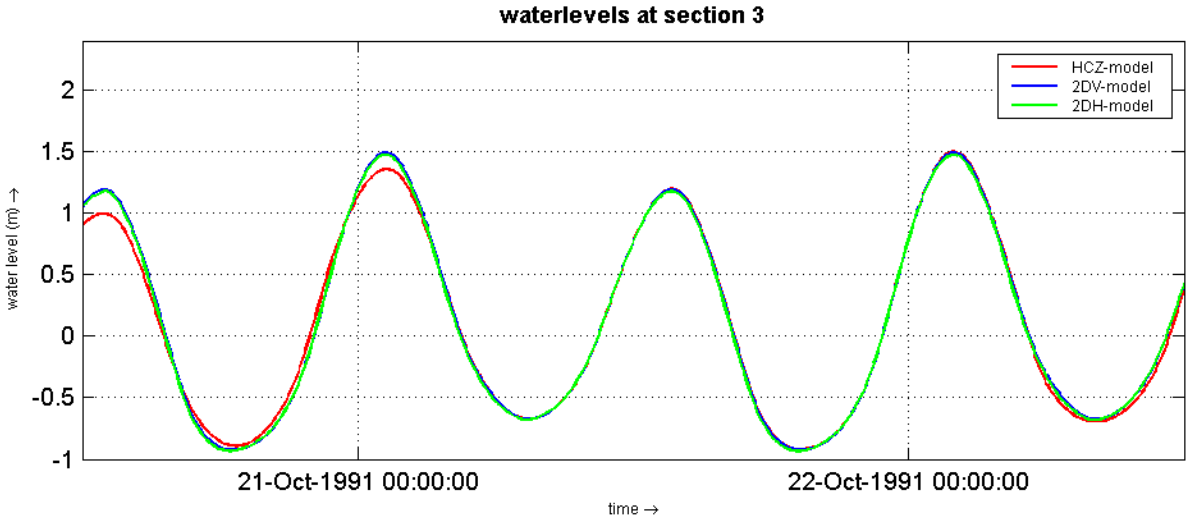

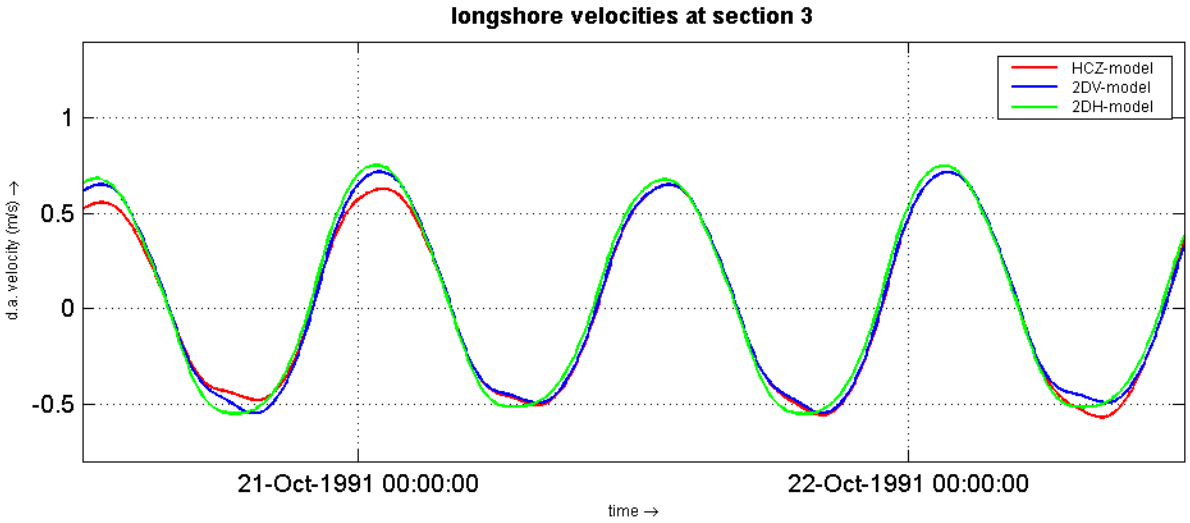

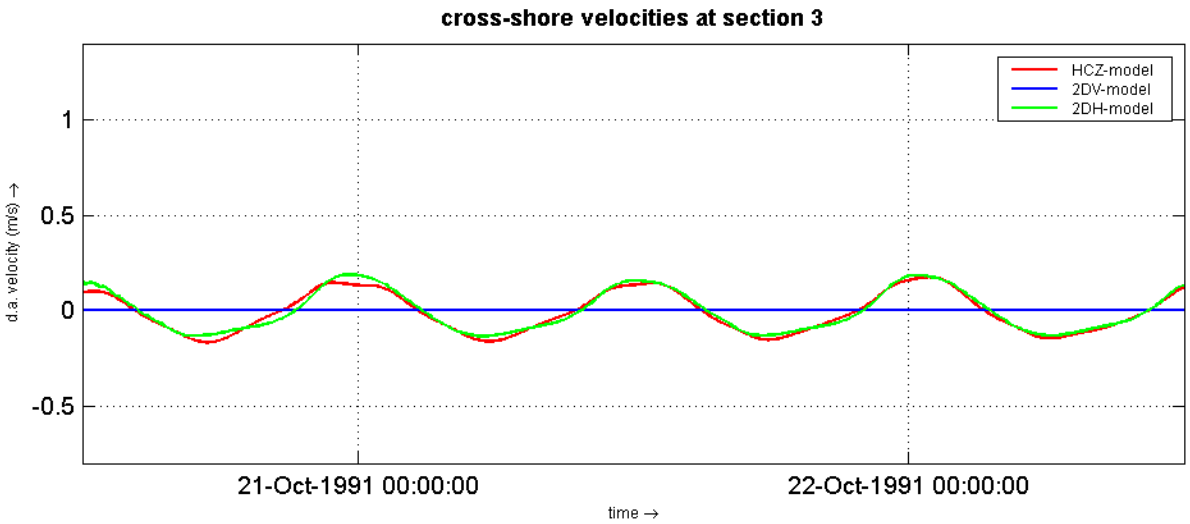

nesting procedure: comparison of waterlevels and velocities at section 3		2005
	nesting	
WL | Delft Hydraulics	Z3079.40	Figure D.01

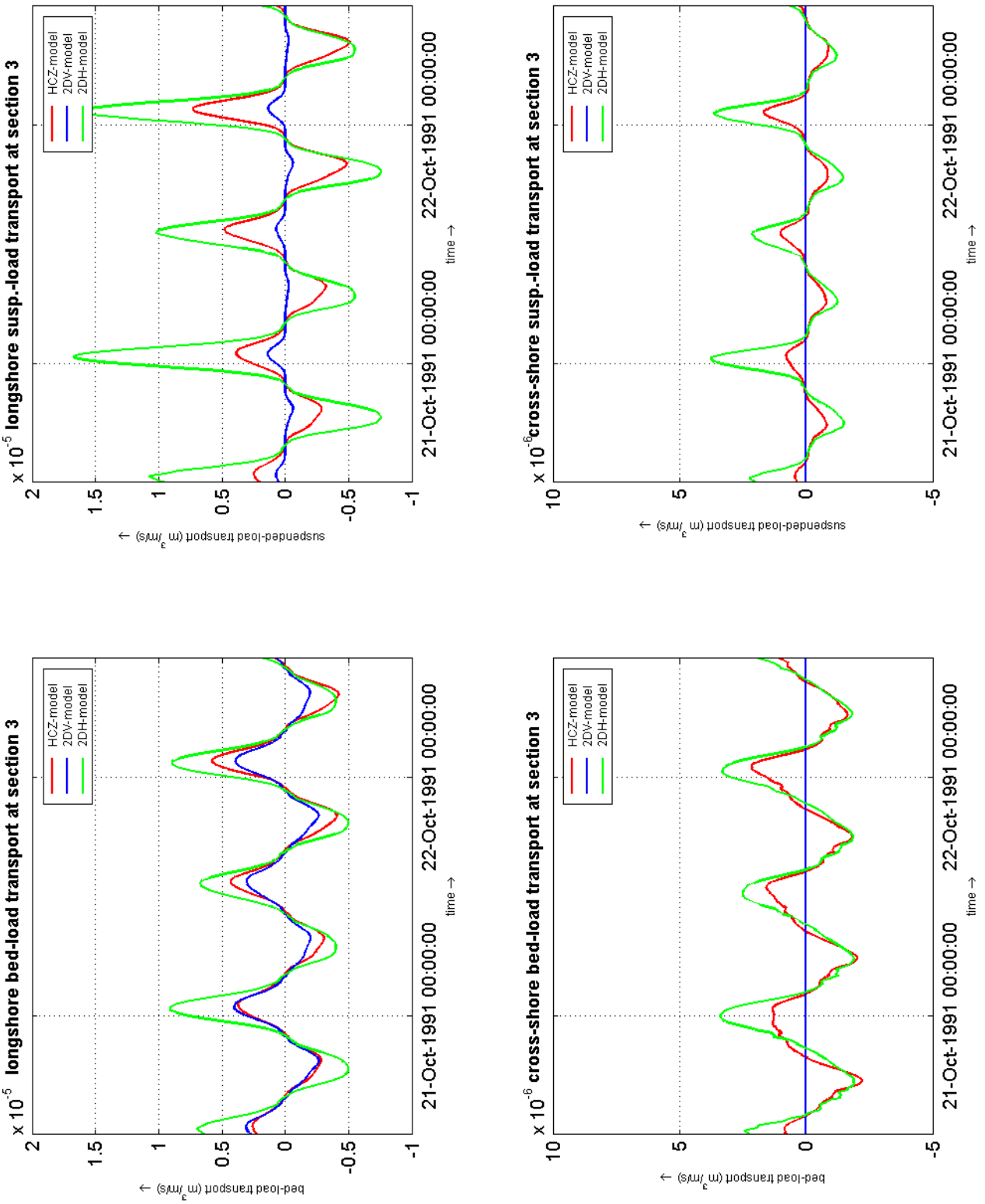

nesting procedure: comparison of bed-load and suspended-load transport rates at section 3		2005
	nesting	
WL | Delft Hydraulics	Z3079.40	Figure D.02

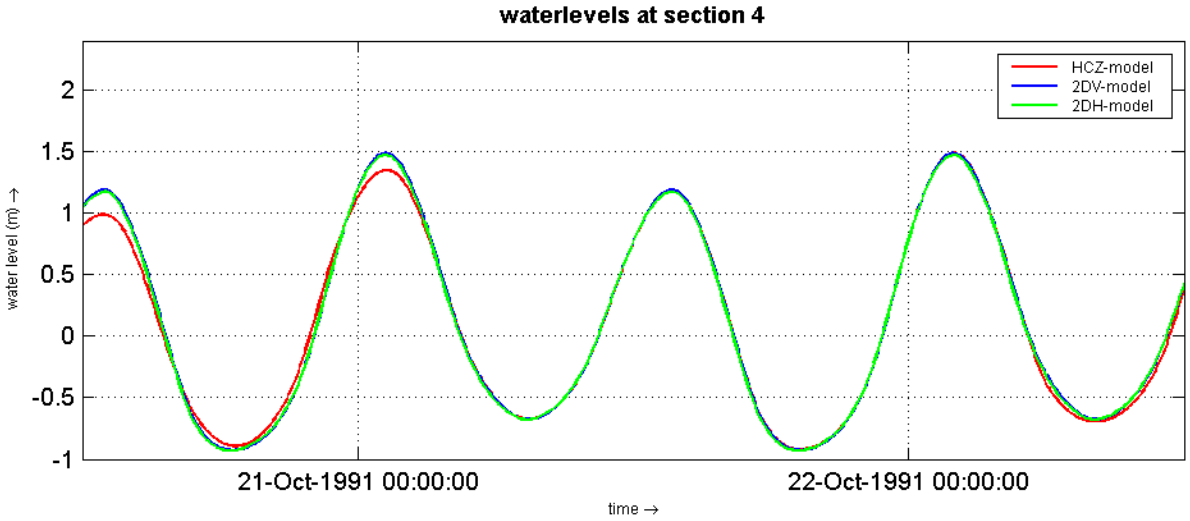

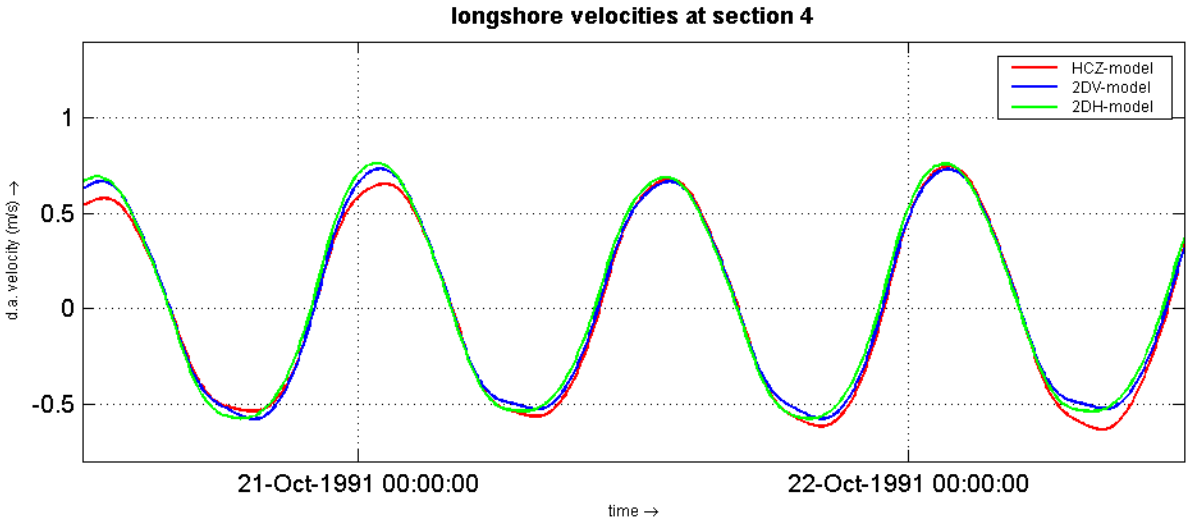

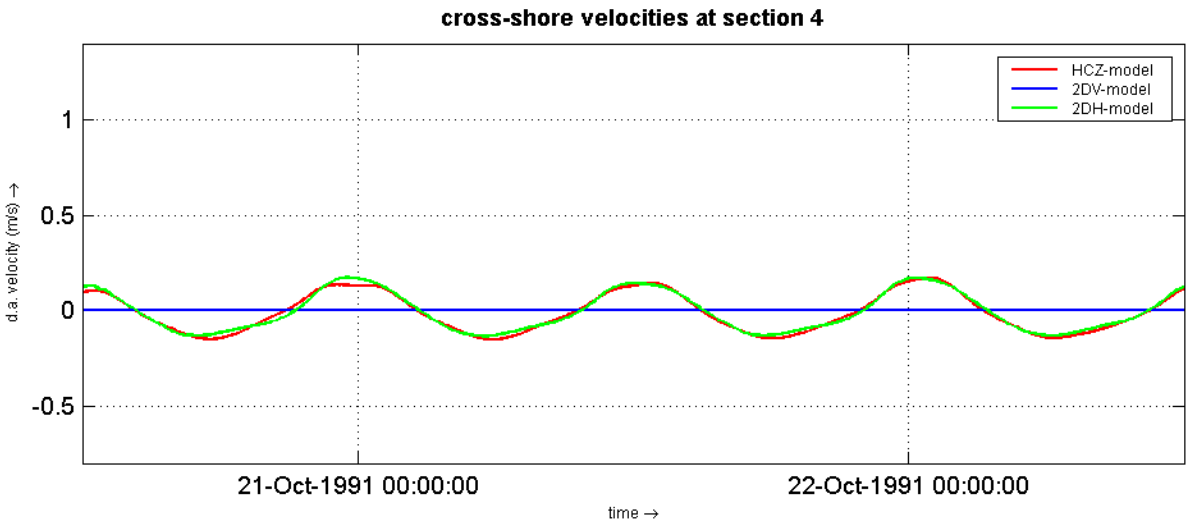

nesting procedure comparison of waterlevels and velocities at section 4		2005
	nesting	
WL | Delft Hydraulics	Z3079.40	Figure D.03

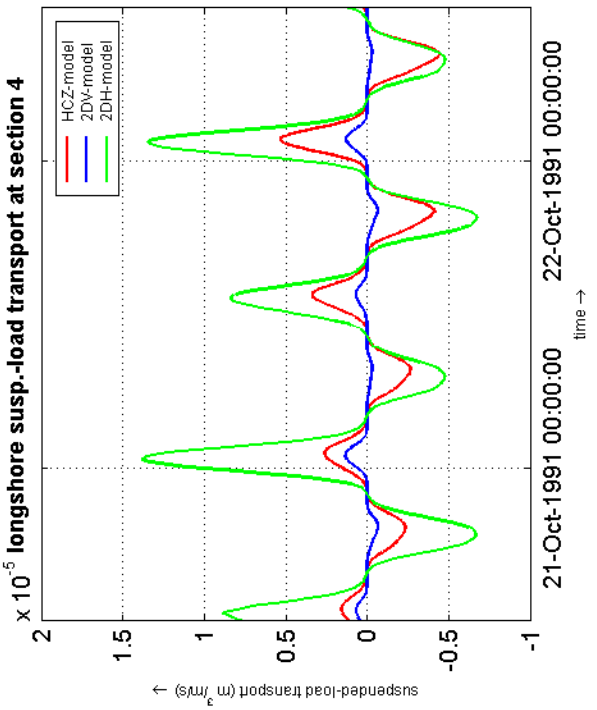

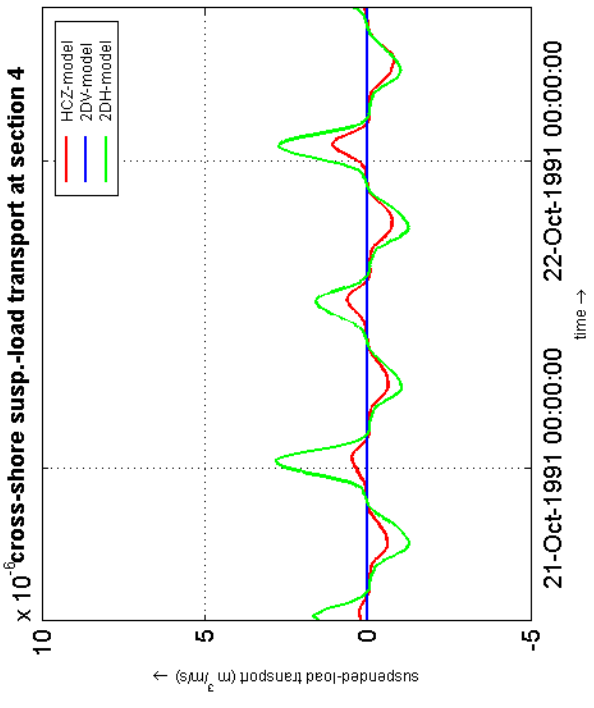

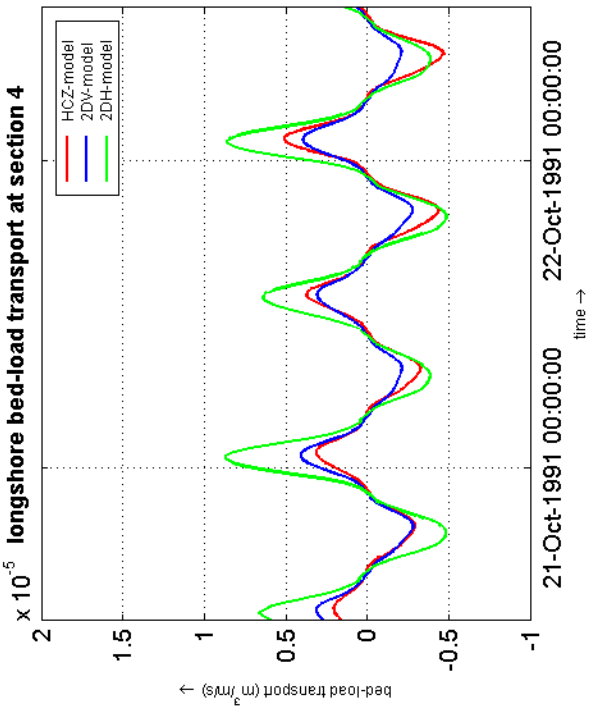

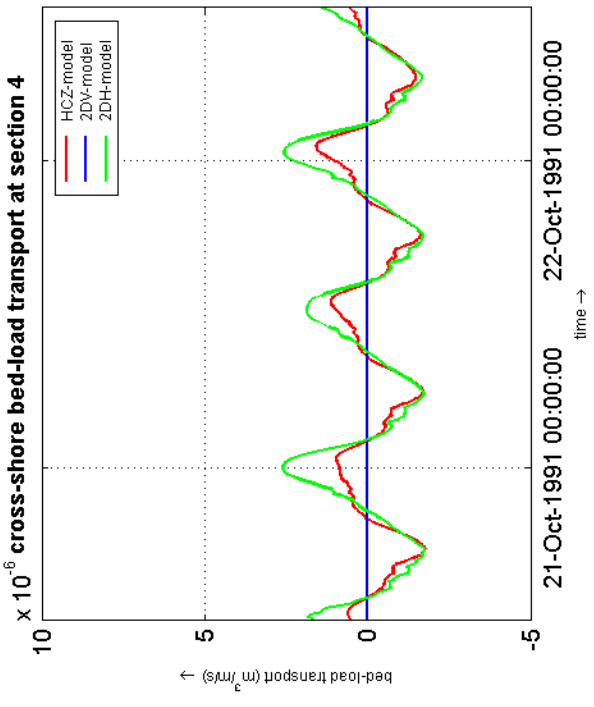

nesting procedure: comparison of bed-load and suspended-load transport rates at section 4		2005
	nesting	
WL | Delft Hydraulics	Z3079.40	Figure D.04

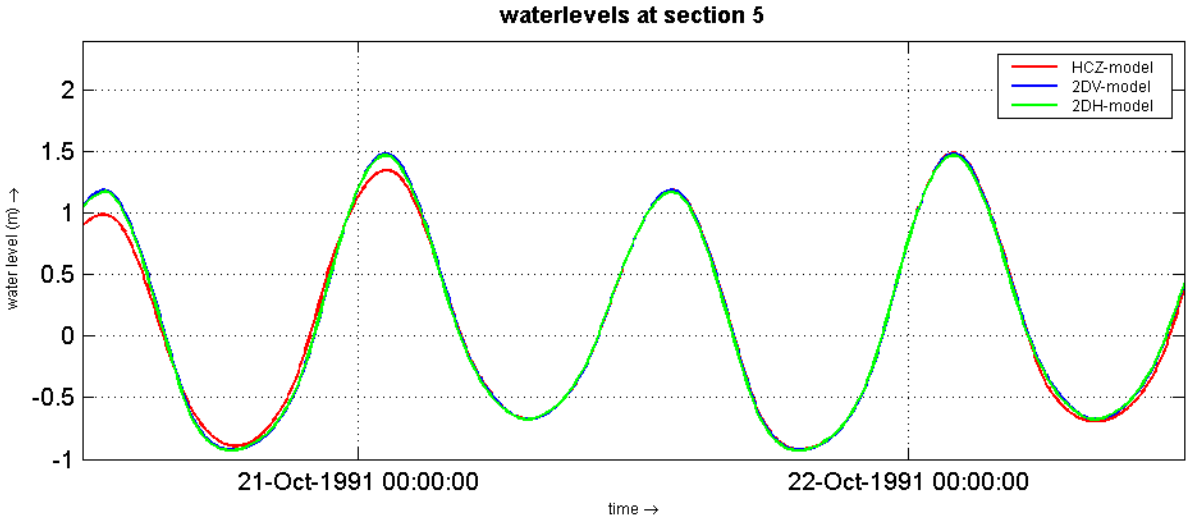

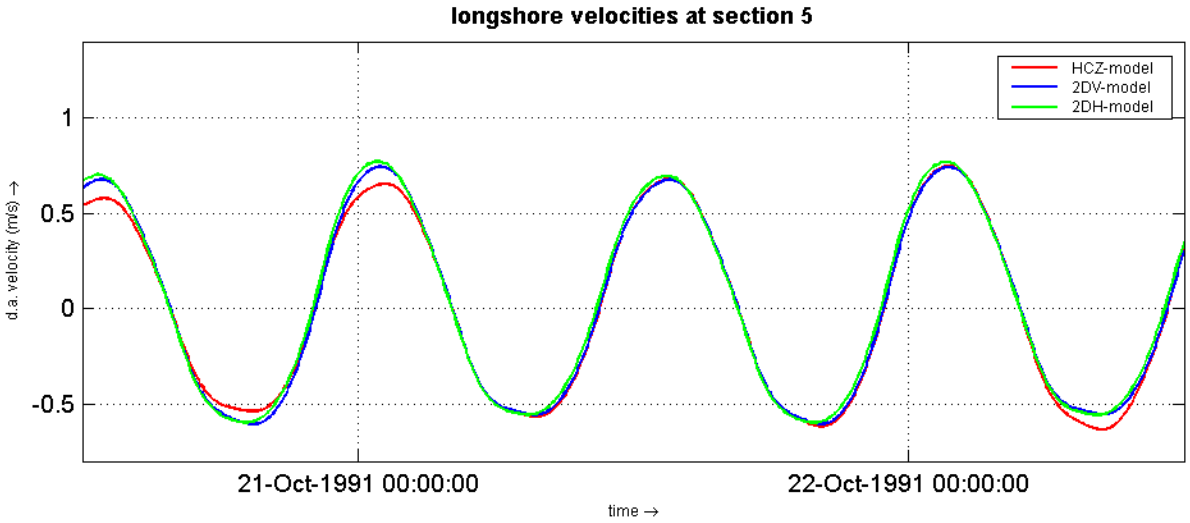

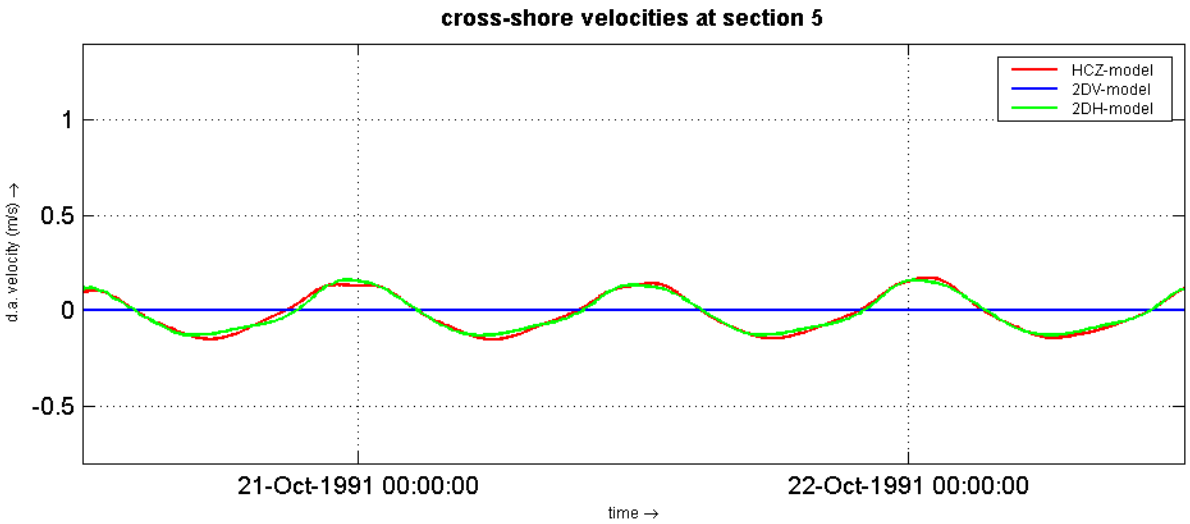

nesting procedure: comparison of waterlevels and velocities at section 5		2005
	nesting	
WL | Delft Hydraulics	Z3079.XX	Figure X.XX

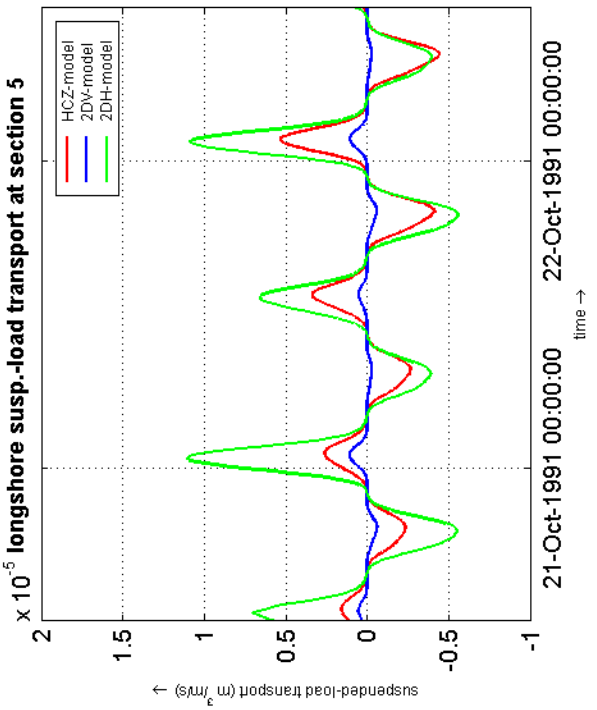

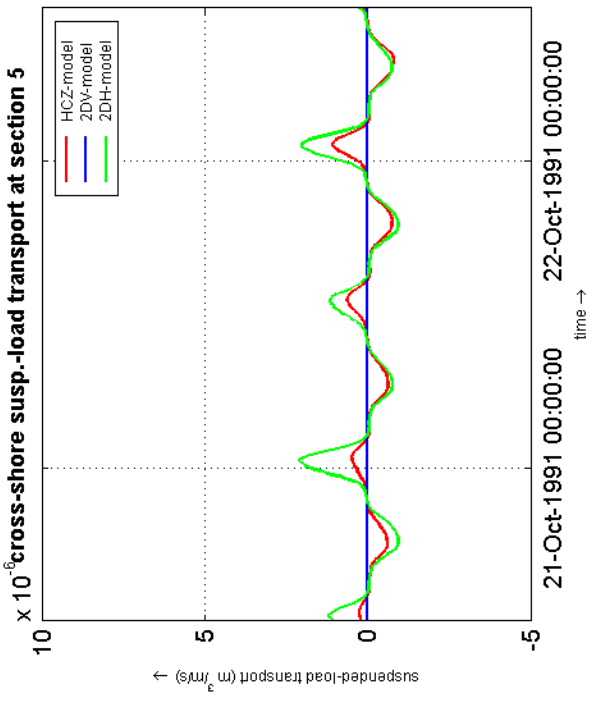

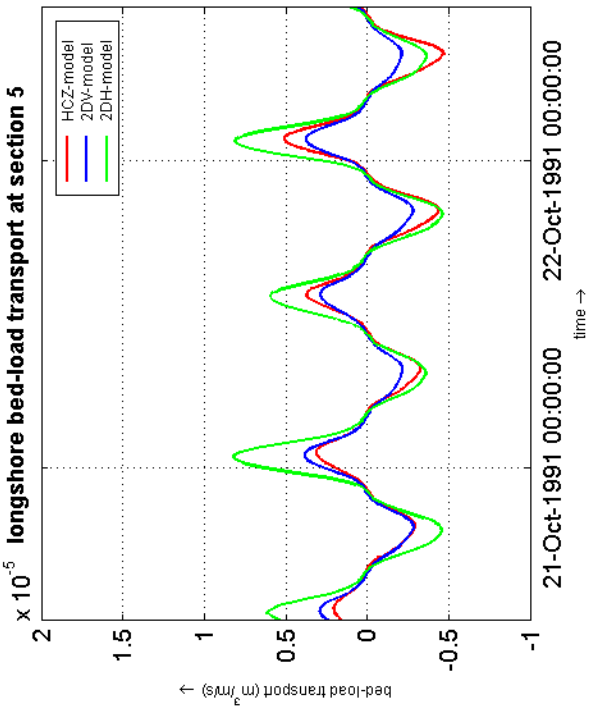

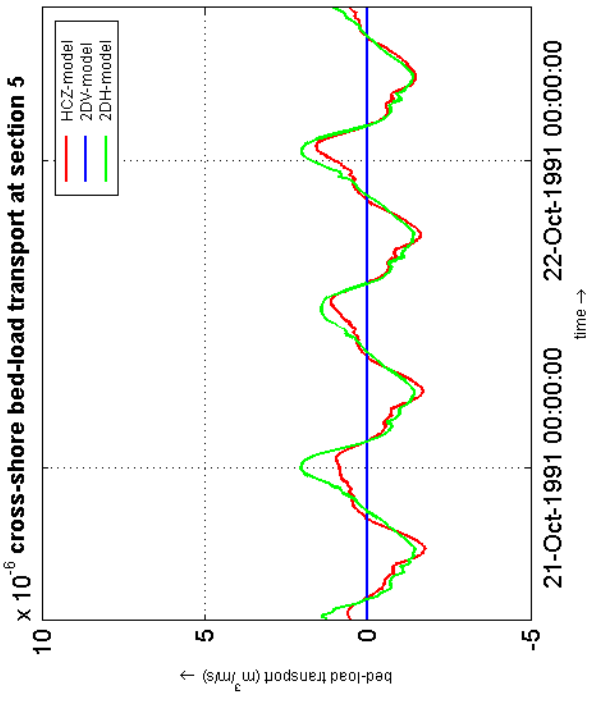

nesting procedur: comparison of bed-load and suspended-load transport rates at section 5		2005
	nesting	
WL | Delft Hydraulics	Z3079.40	Figure D.06

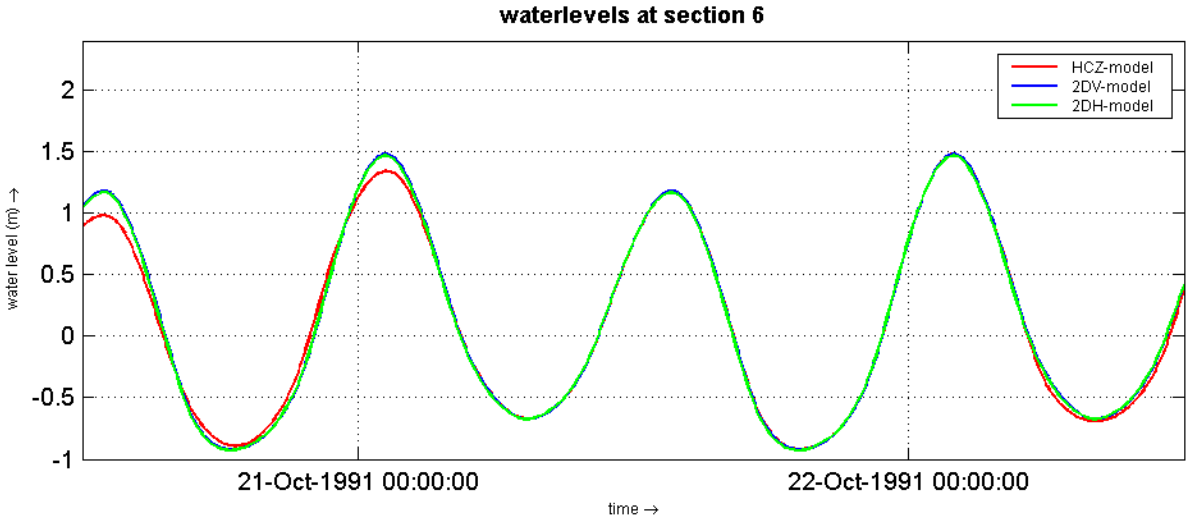

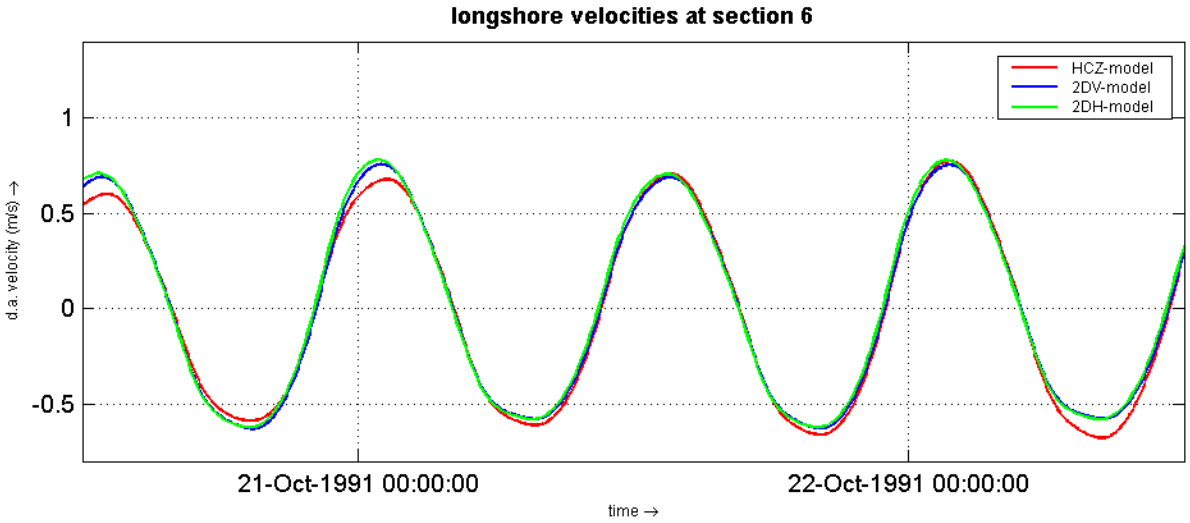

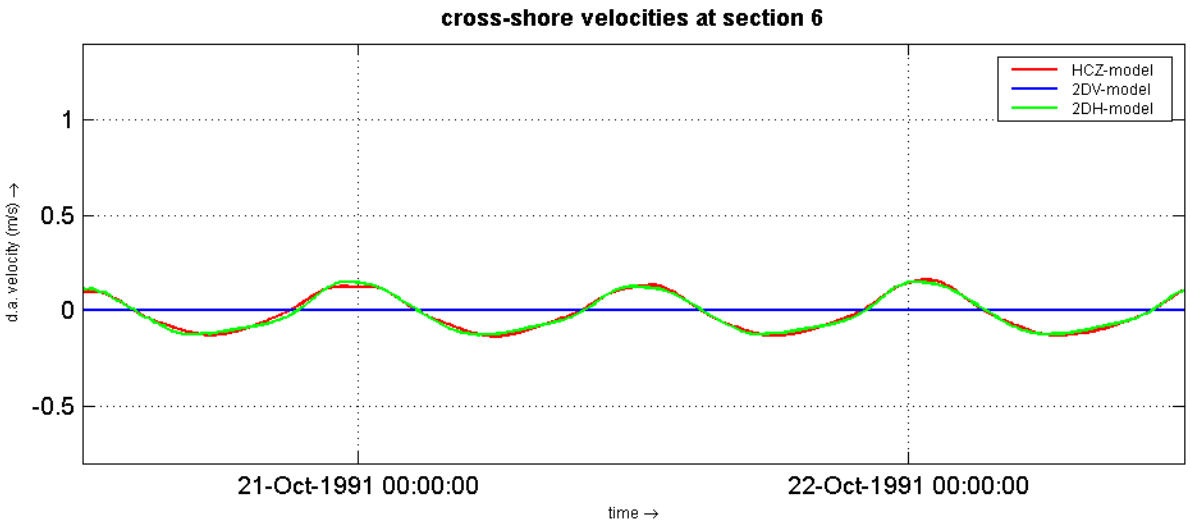

nesting procedure: comparison of waterlevels and velocities at section 6		2005
	nesting	
WL | Delft Hydraulics	Z3079.40	Figure D.07

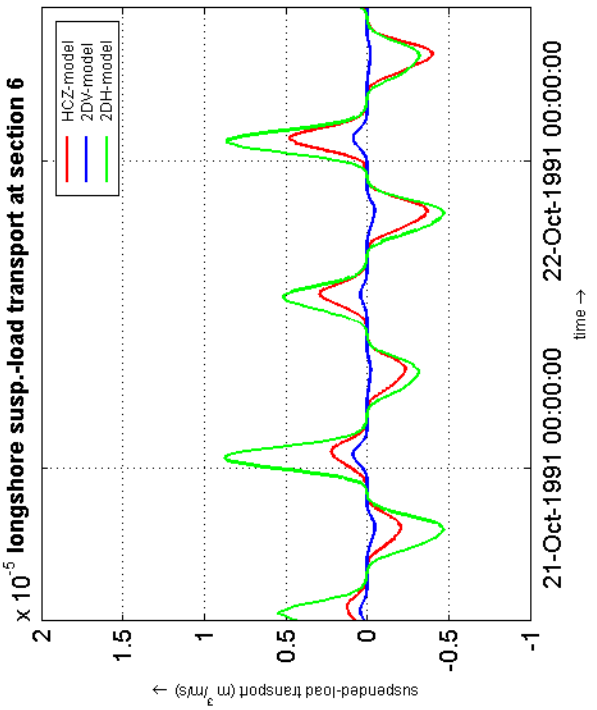

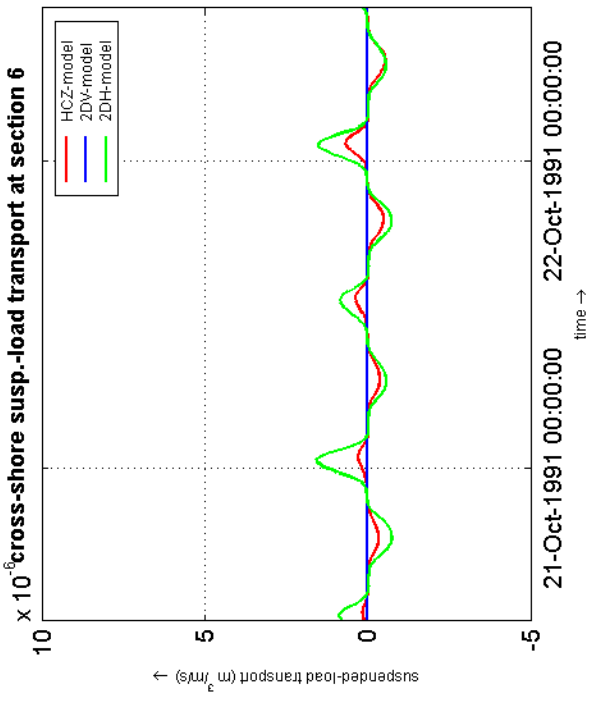

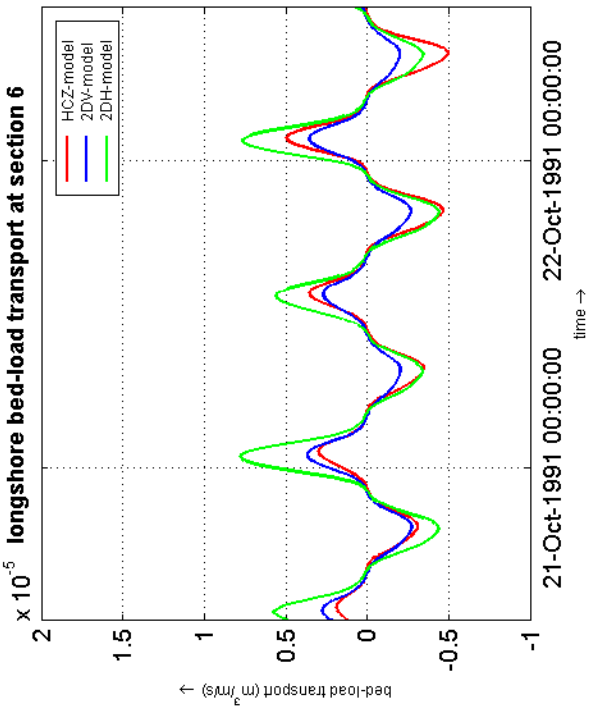

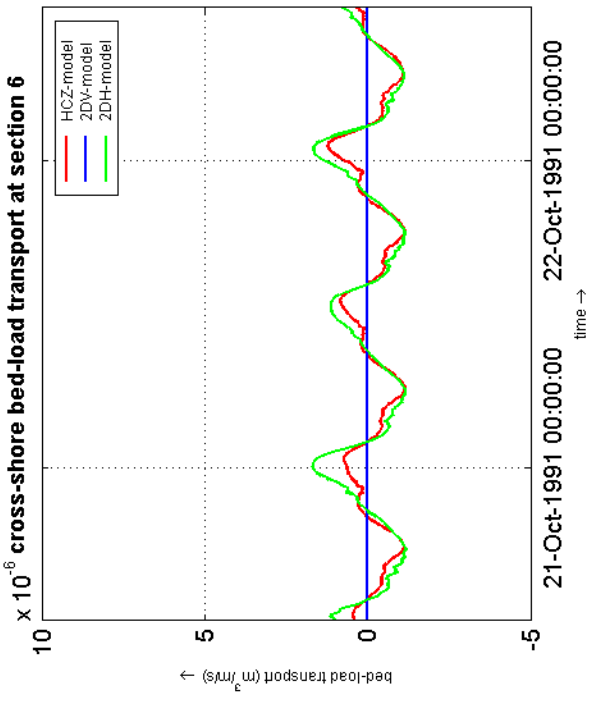

nesting procedure: comparison of bed-load and suspended-load transport rates at section 6		2005
	nesting	
WL | Delft Hydraulics	Z3079.40	Figure D.08

E Boundary conditions

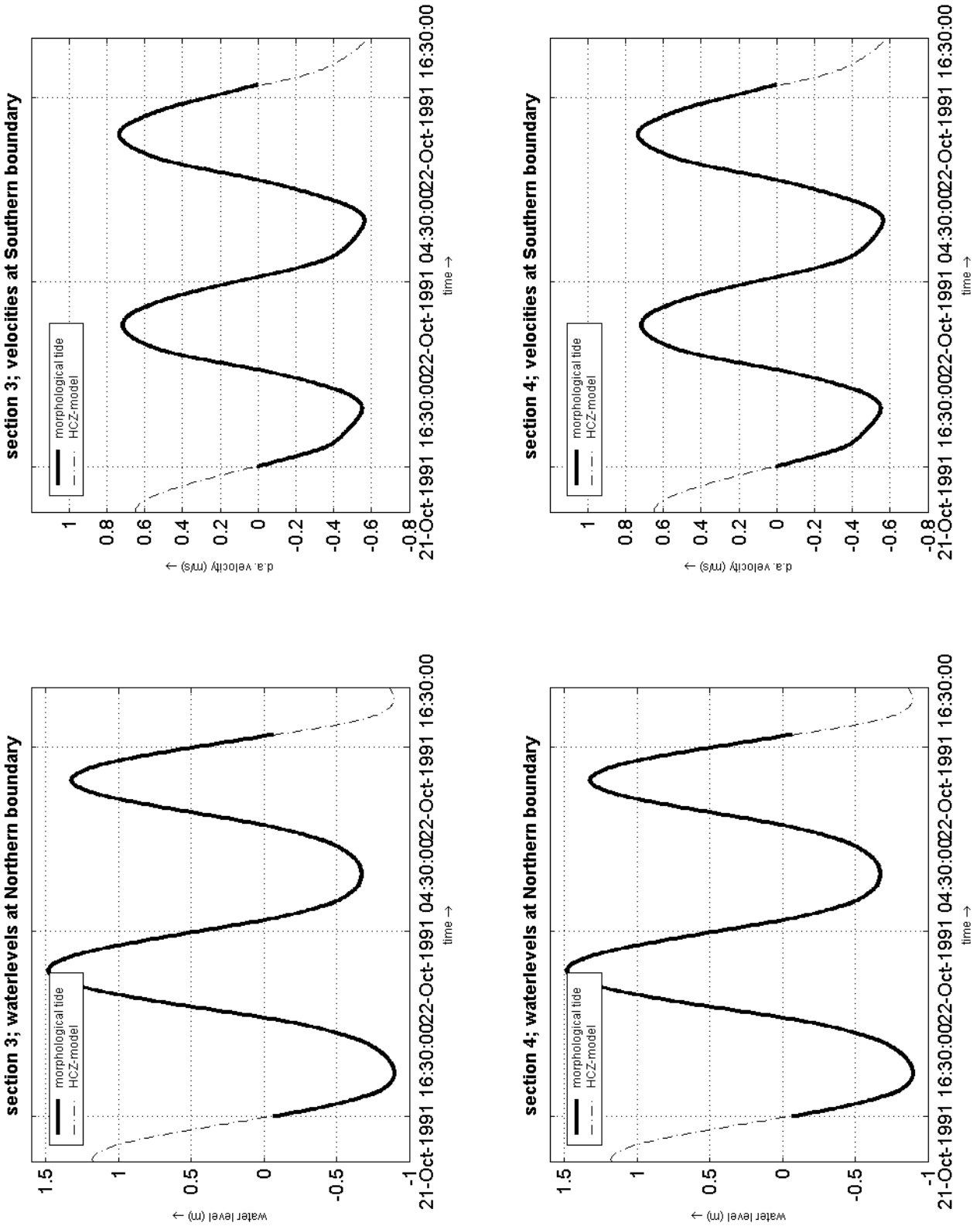

boundary conditions boundary conditions for section 3 and 4; morphological tide = basic a		2005
	boundary conditions	
WL | Delft Hydraulics	Z3079.40	Figure E.01

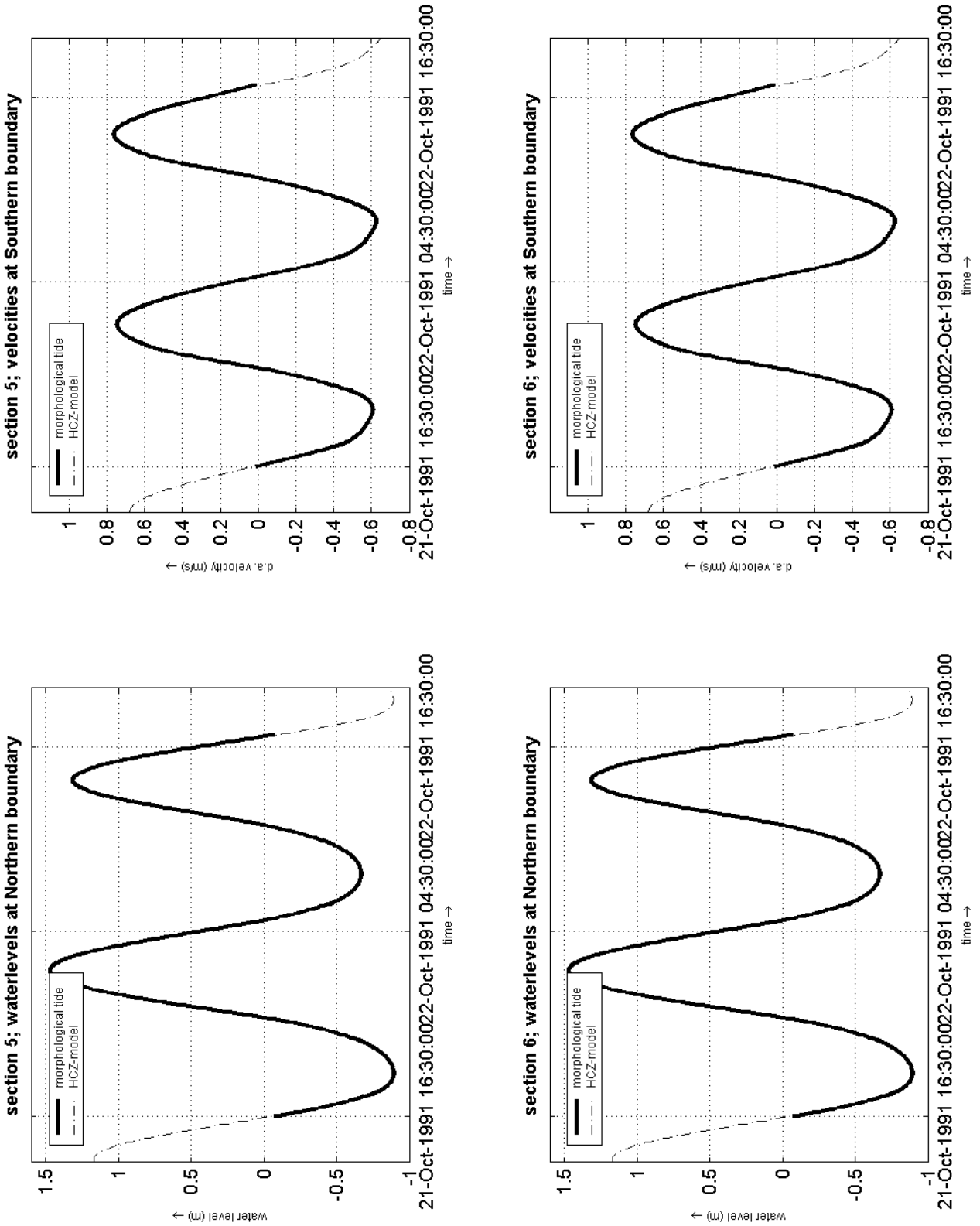

boundary conditions: boundary conditions for section 5 and 6; morphological tide = basic a		2005
	boundary conditions	
WL | Delft Hydraulics	Z3079.40	Figure E.02

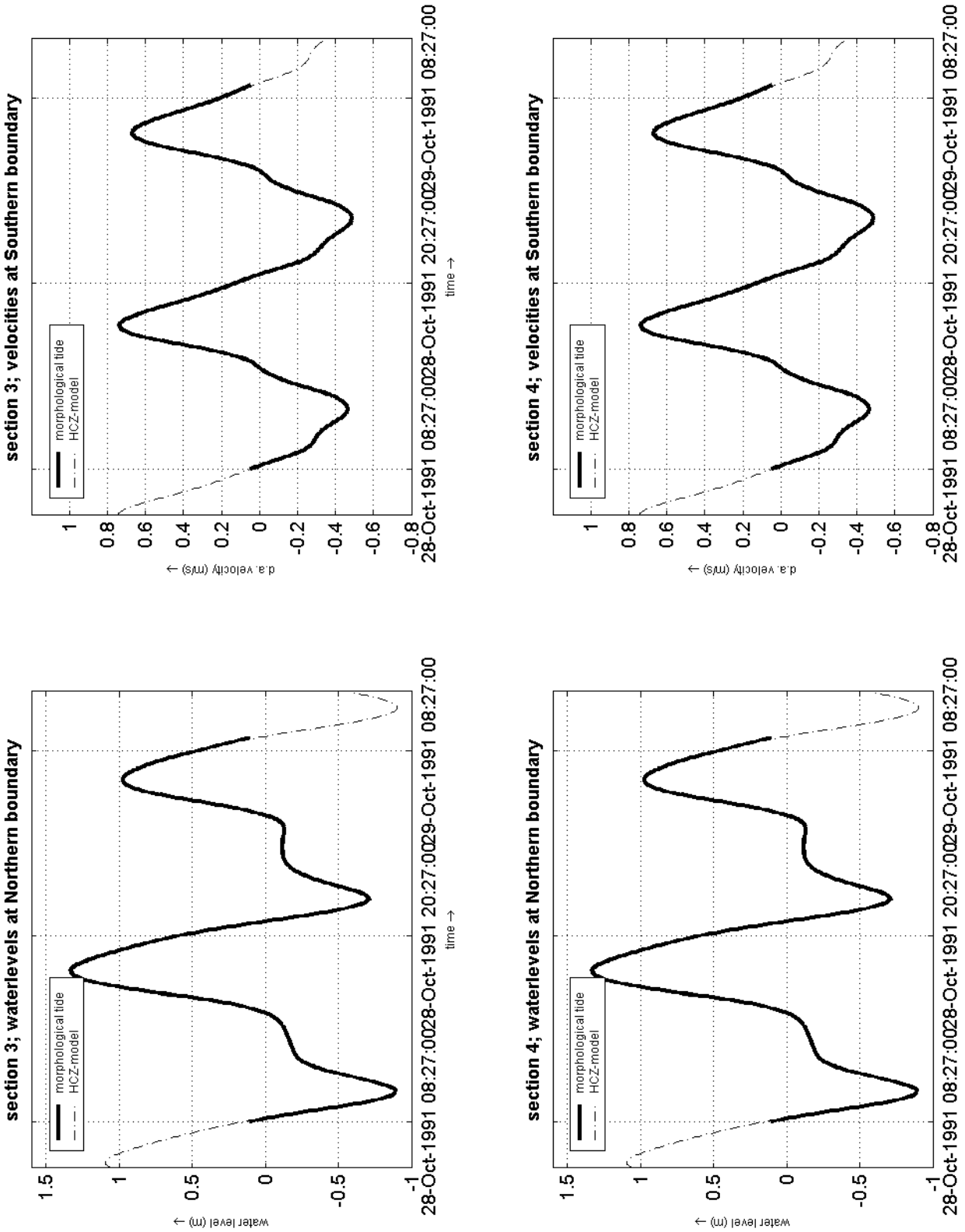

boundary conditions
boundary conditions for section 3 and 4; morphological tide = basic b

boundary conditions

WL | Delft Hydraulics

Z3079.40

Figure E.03

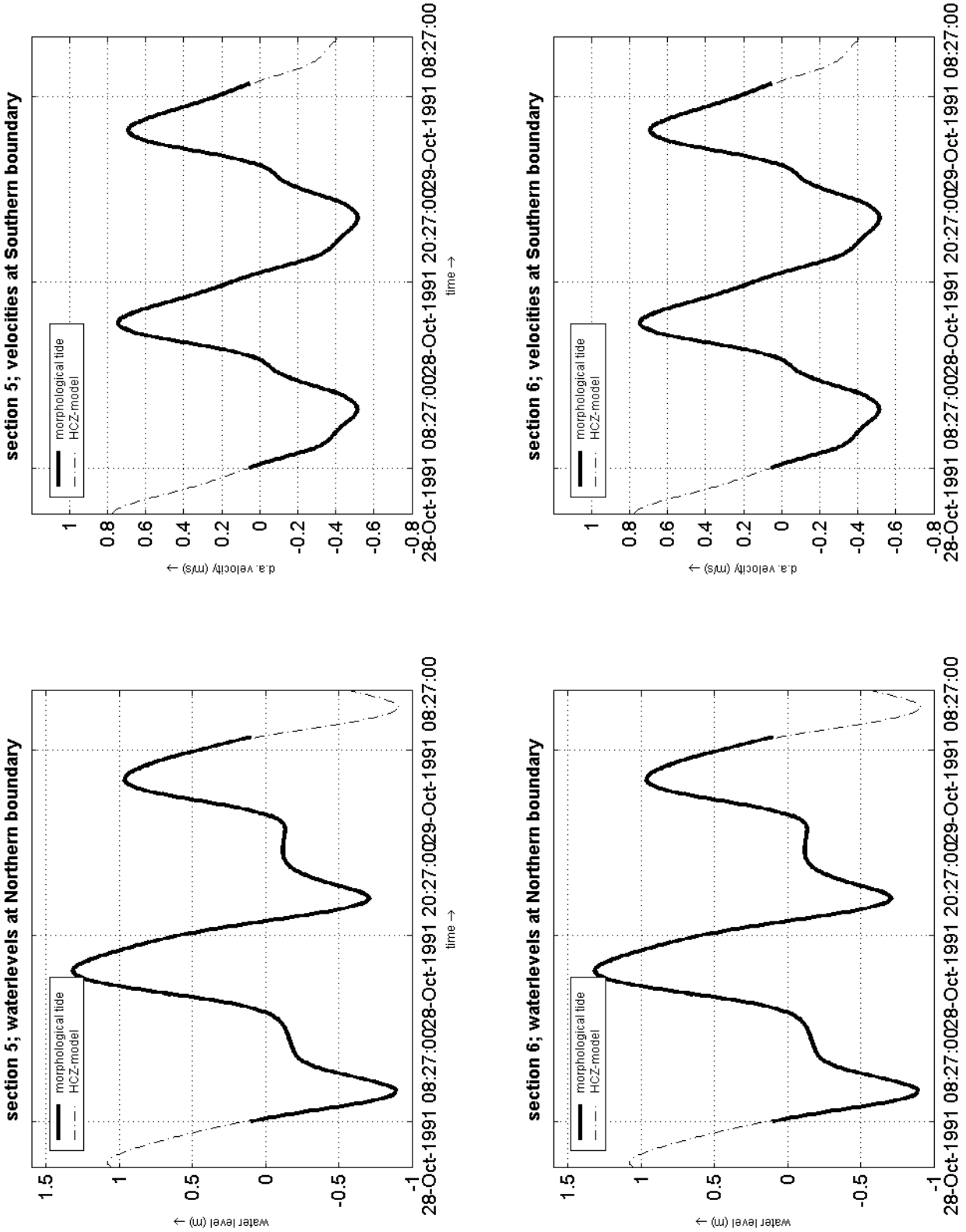

boundary conditions boundary conditions for section 5 and 6; morphological tide = basic b		2005
	boundary conditions	
WL | Delft Hydraulics	Z3079.40	Figure E.04

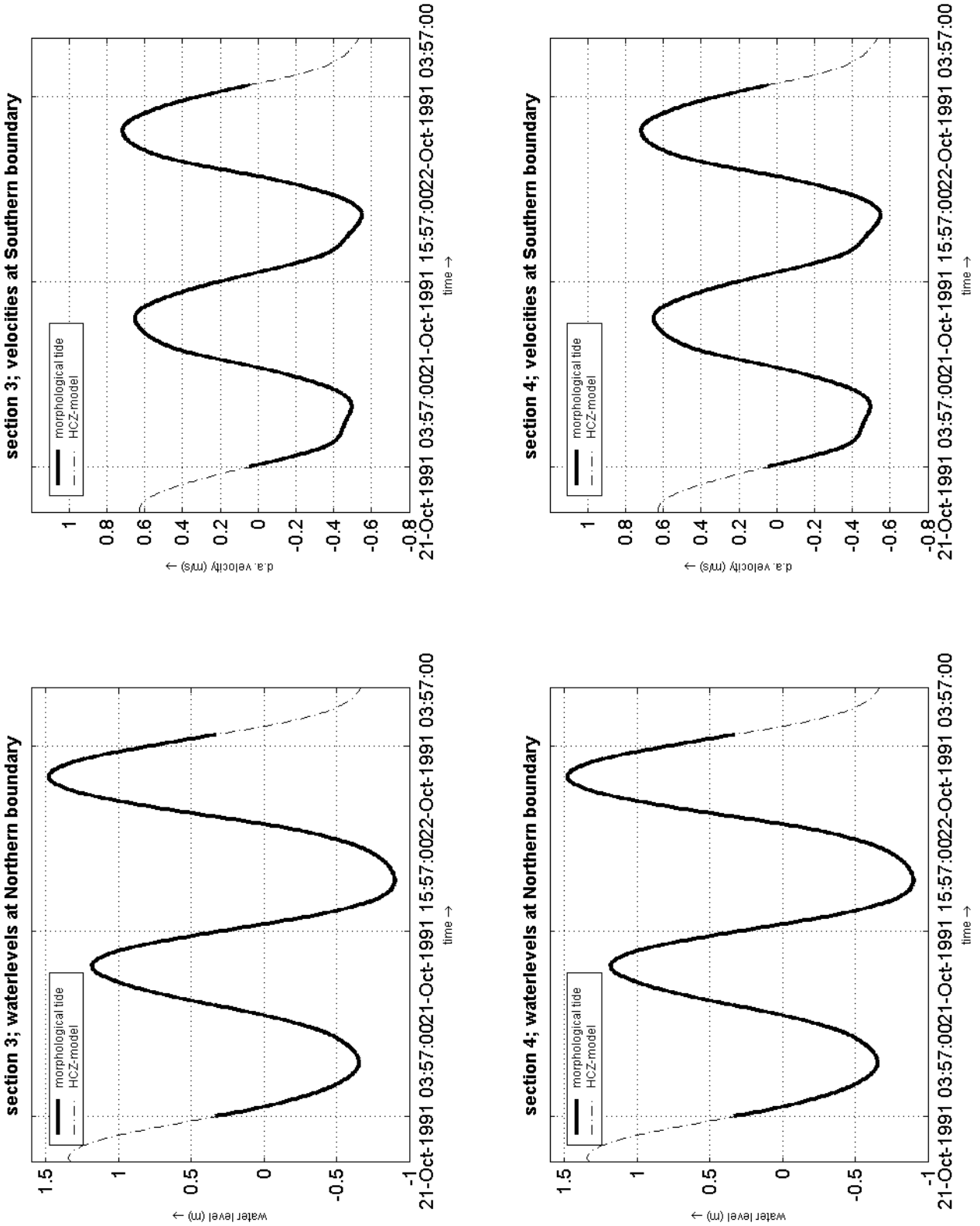

boundary conditions boundary conditions for section 3 and 4; morphological tide = mt2		2005
	boundary conditions	
WL | Delft Hydraulics	Z3079.40	Figure E.05

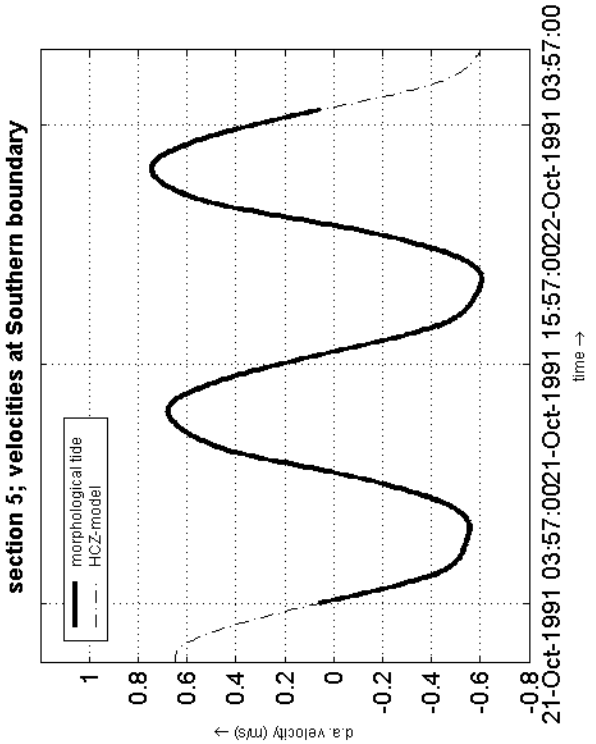

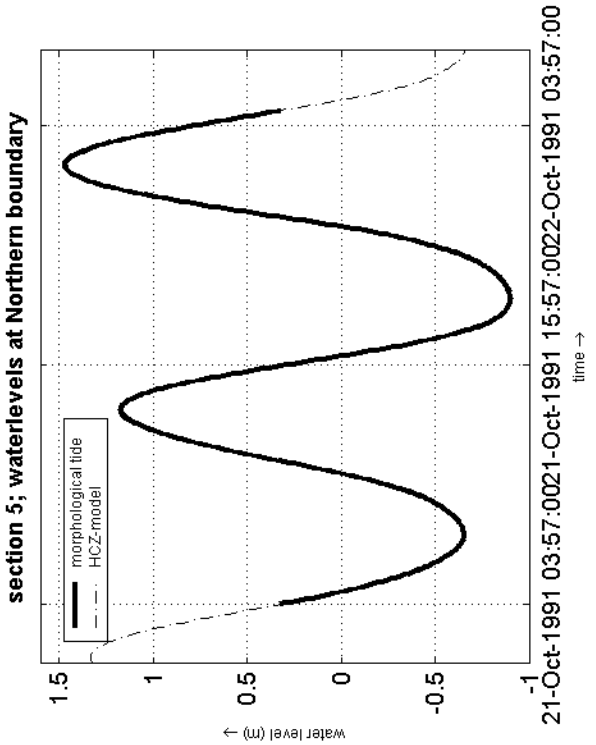

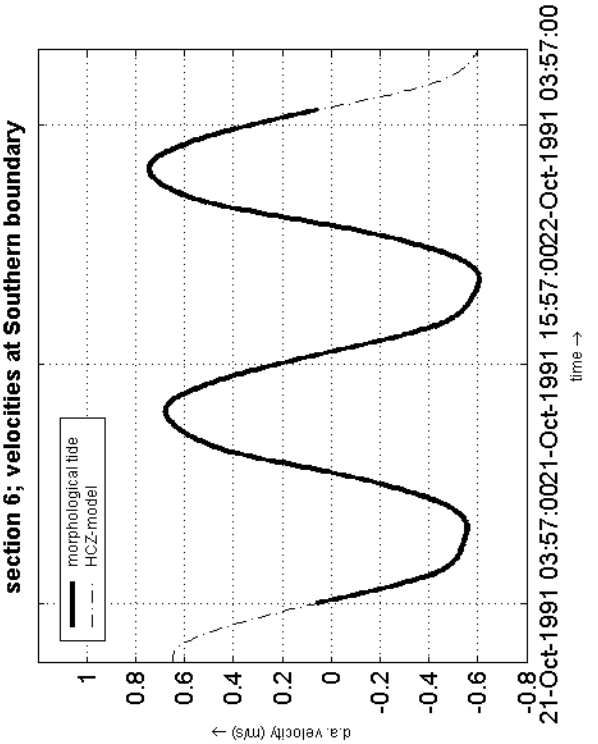

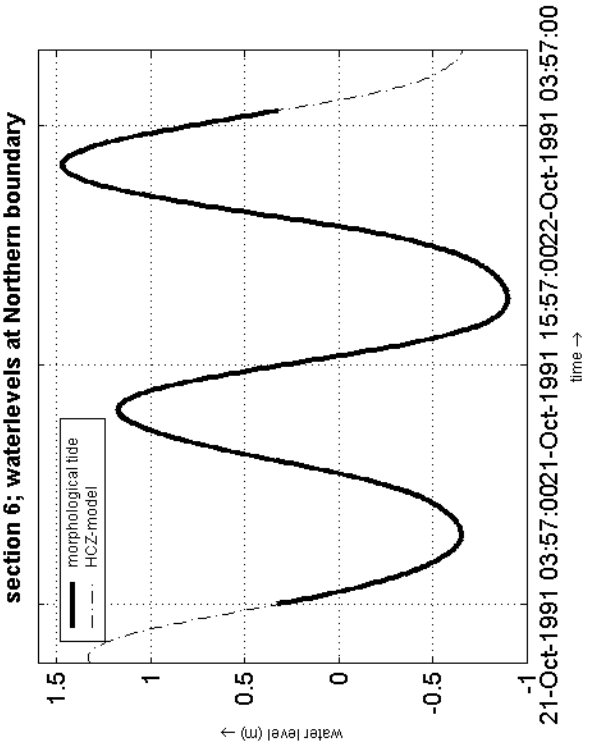

boundary conditions
boundary conditions for section 5 and 6; morphological tide = mt2

2005

boundary conditions

WL | Delft Hydraulics

Z3079.40

Figure E.06

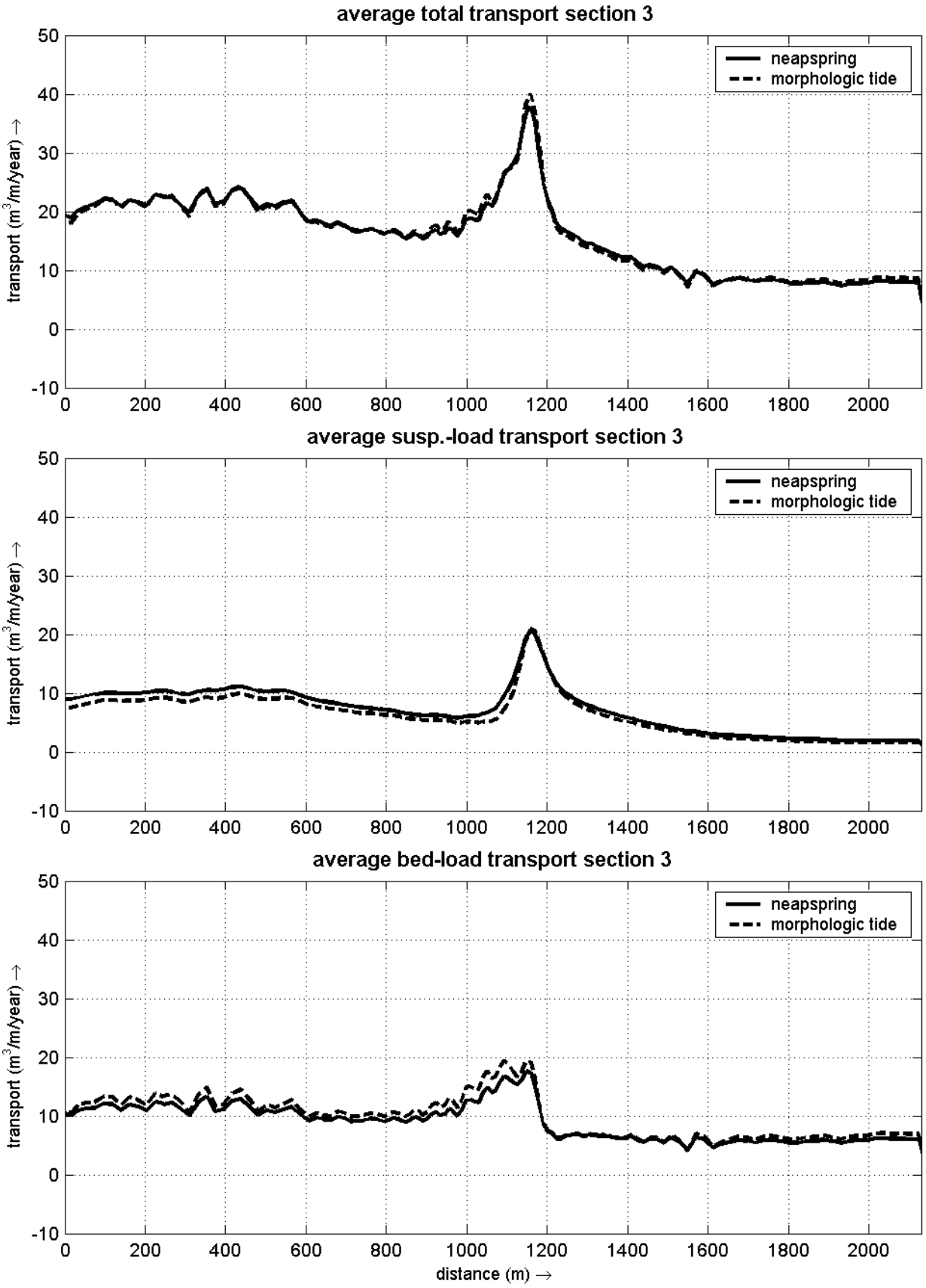

morphological tide: basic a (from single observation point)
section 3: average transports over 1986 bathymetry

2005

morphological tide

WL | Delft Hydraulics

Z3079.40

Figure E.07

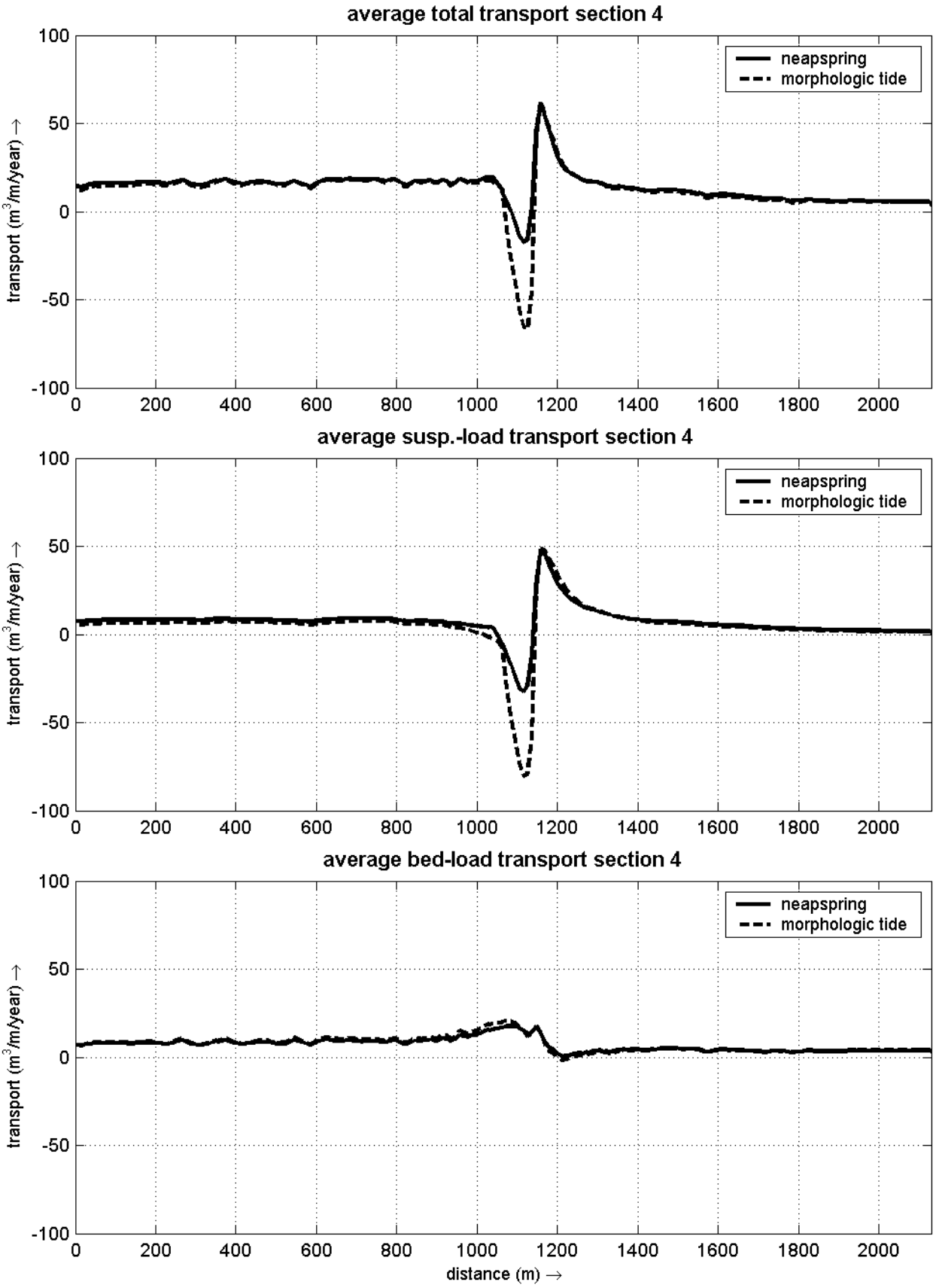

morphological tide: basic a (from single observation point)
section 4: average transports over 1986 bathymetry

2005

morphological tide

WL | Delft Hydraulics

Z3079.40

Figure E.08

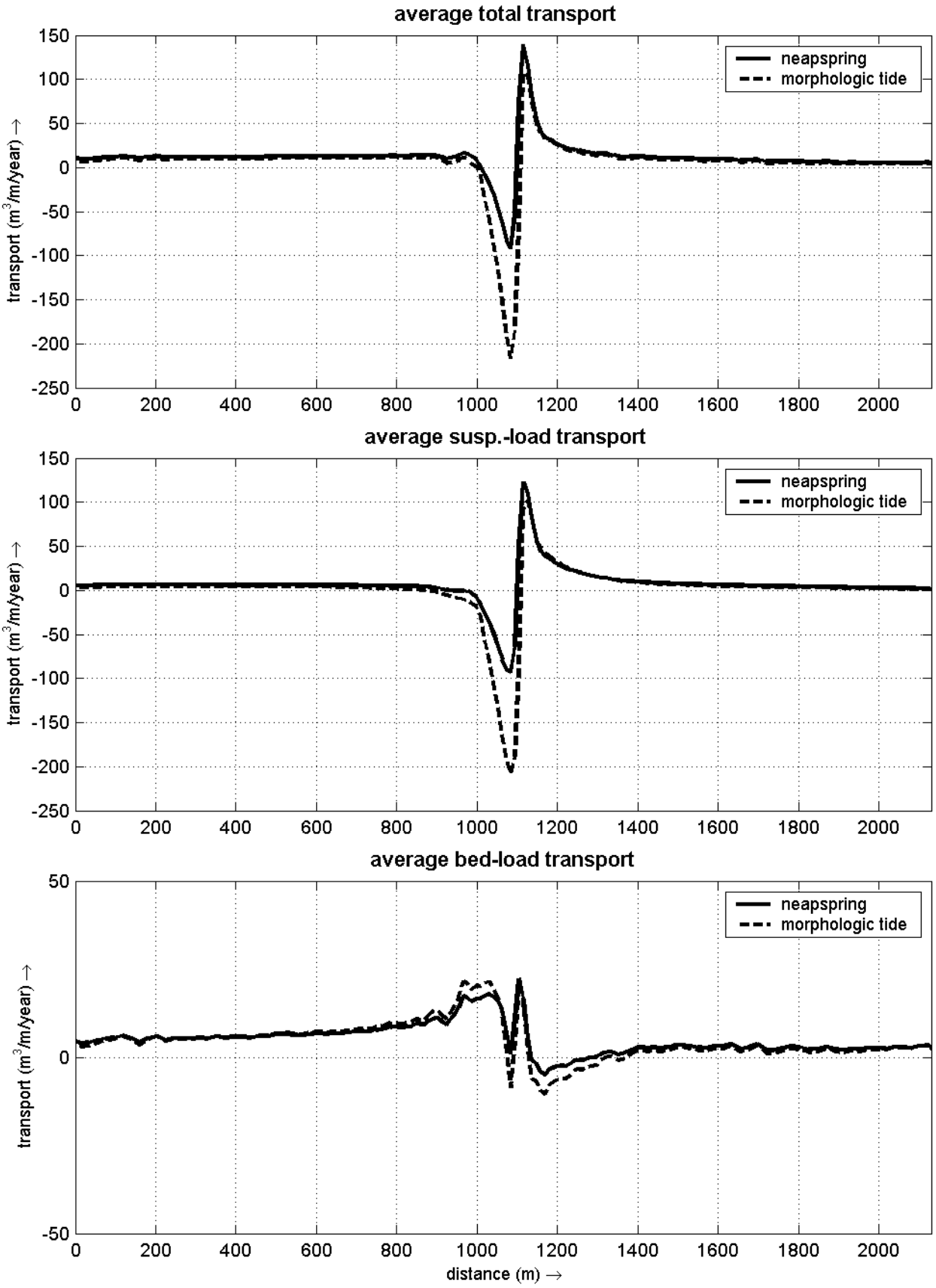

morphological tide: basic a (from single observation point)
section 5: average transports over 1986 bathymetry, no updating

2005

morphological tide

WL | Delft Hydraulics

Z3079.40

Figure E.09

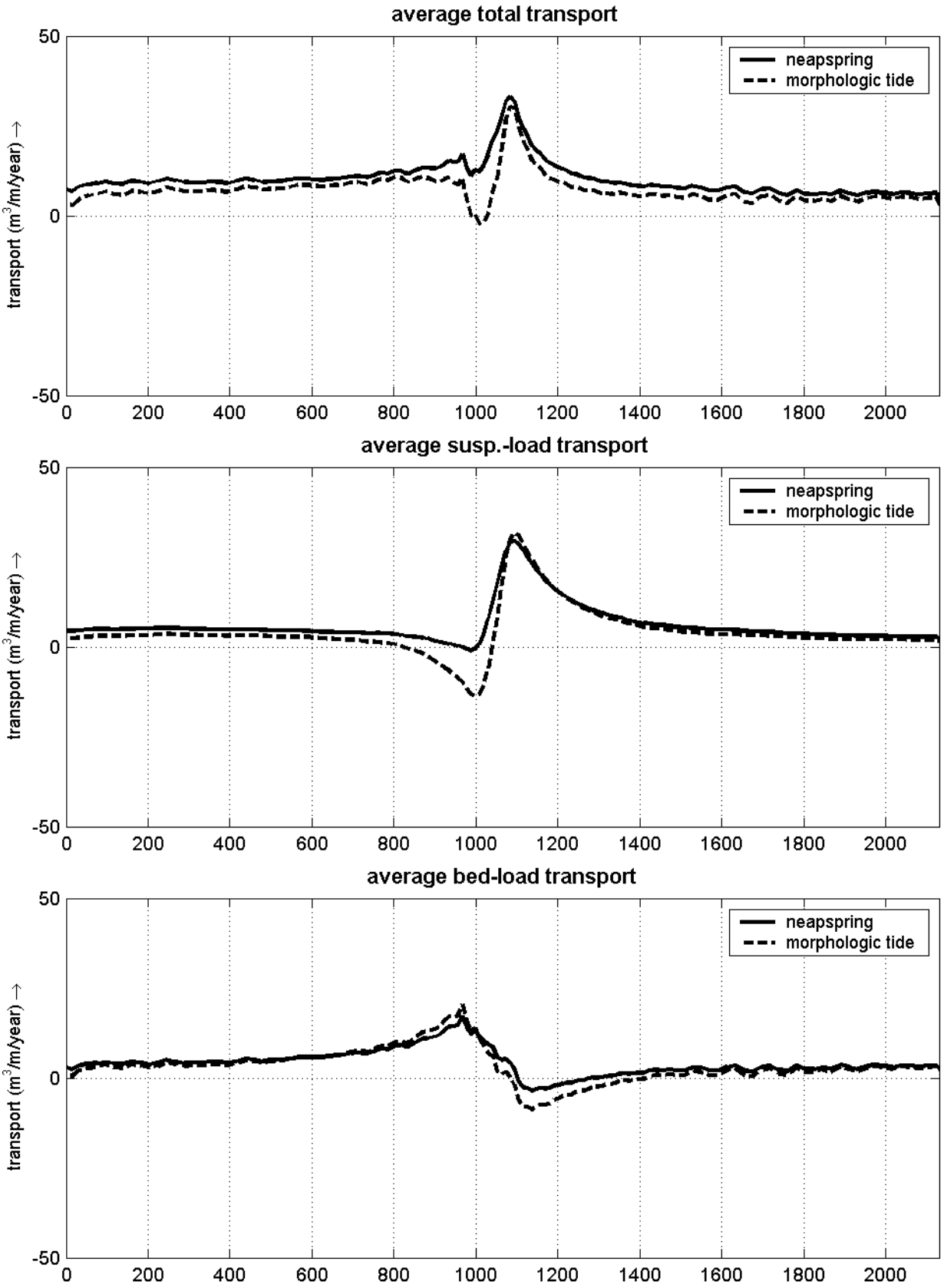

morphological tide: basic a (from single observation point) section 6: average transports over 1986 bathymetry, no updating		2005
	morphological tide	
WL | Delft Hydraulics	Z3079.40	Figure E.10

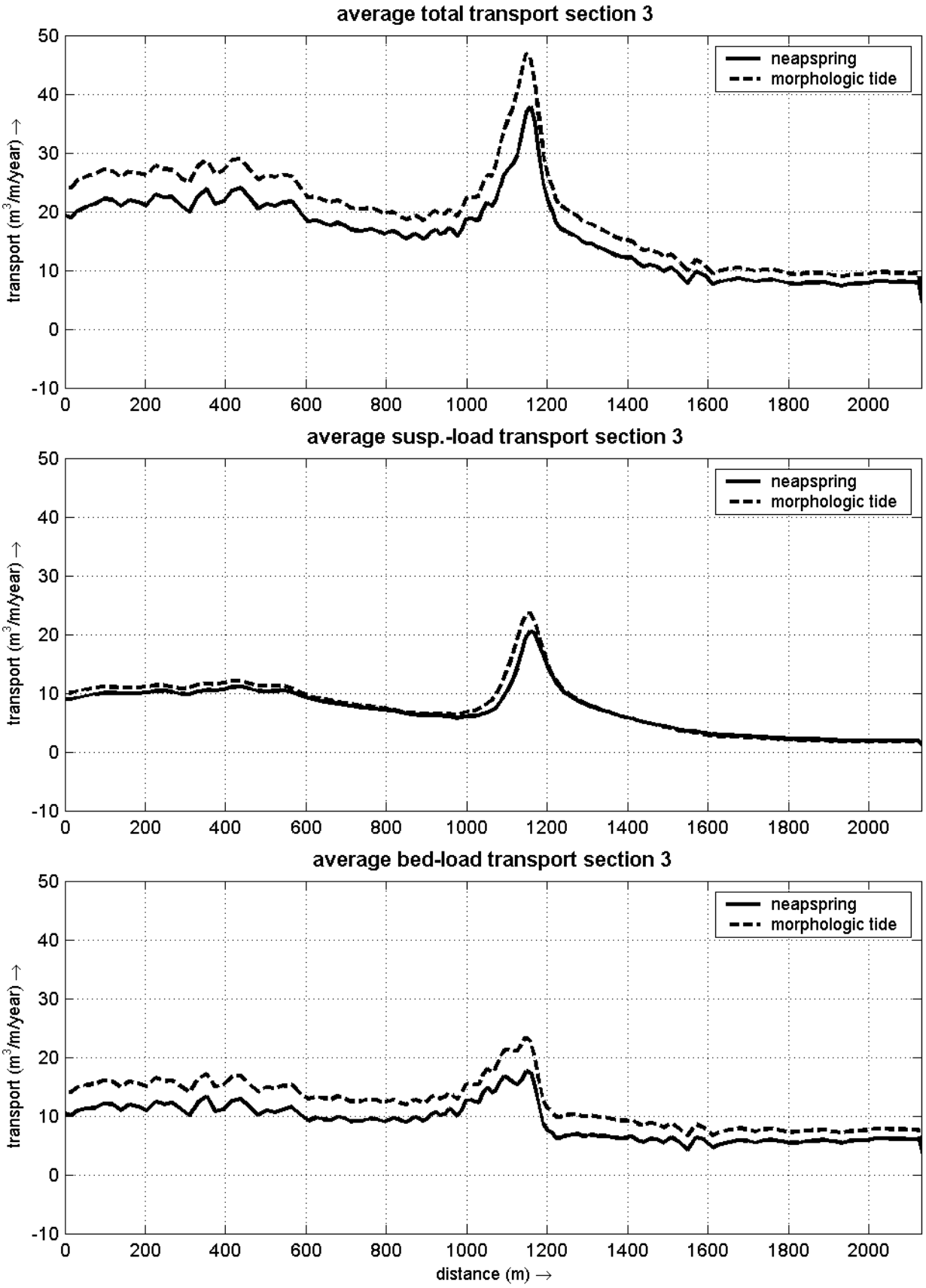

morphological tide: basic b (from single observation point)
section 3: average transports over 1986 bathymetry, no updating

2005

morphological tide

WL | Delft Hydraulics

Z3079.40

Figure E.11

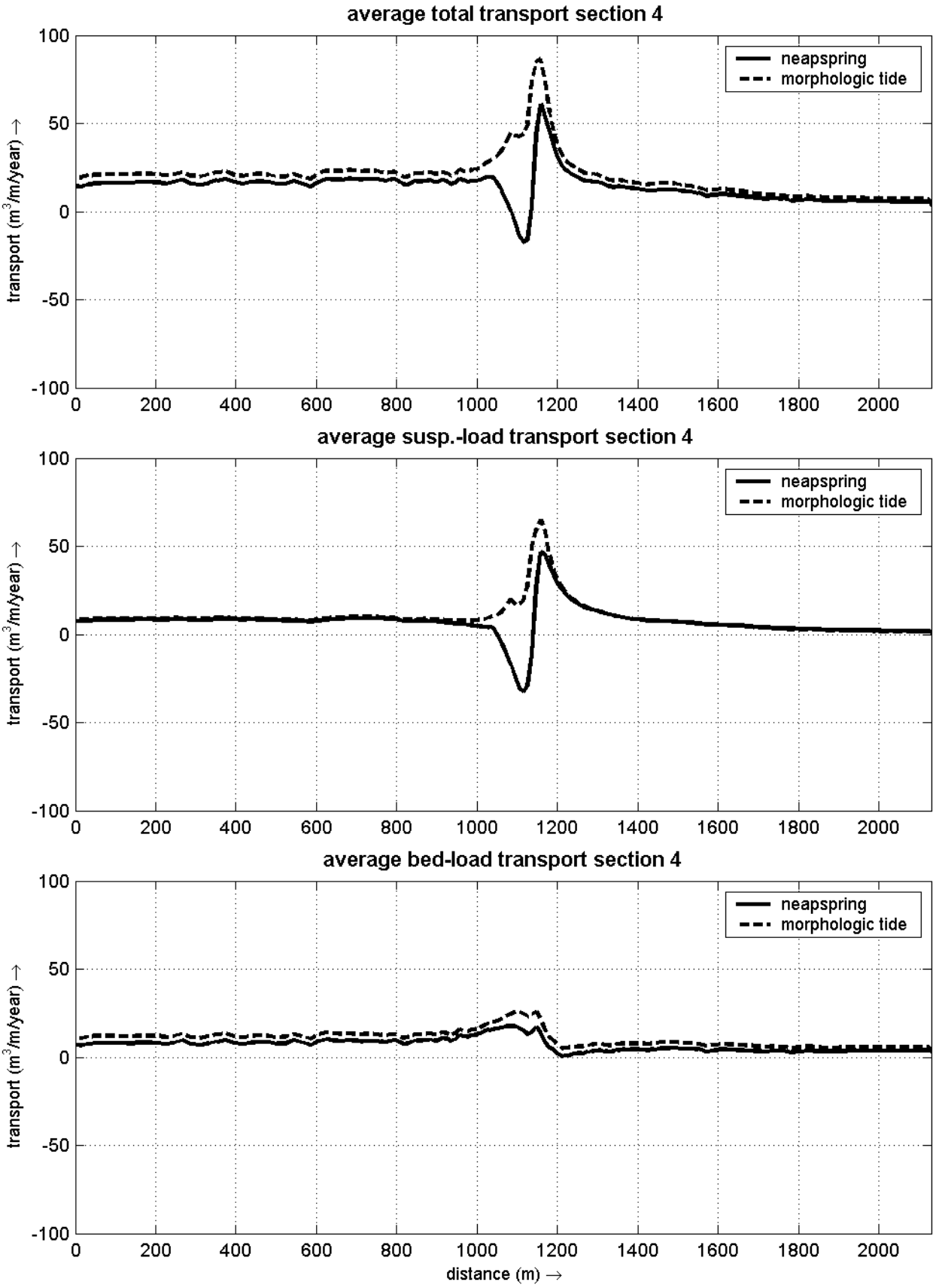

morphological tide: basic b (from single observation point)
section 4: average transports over 1986 bathymetry, no updating

2005

morphological tide

WL | Delft Hydraulics

Z3079.40

Figure E.12

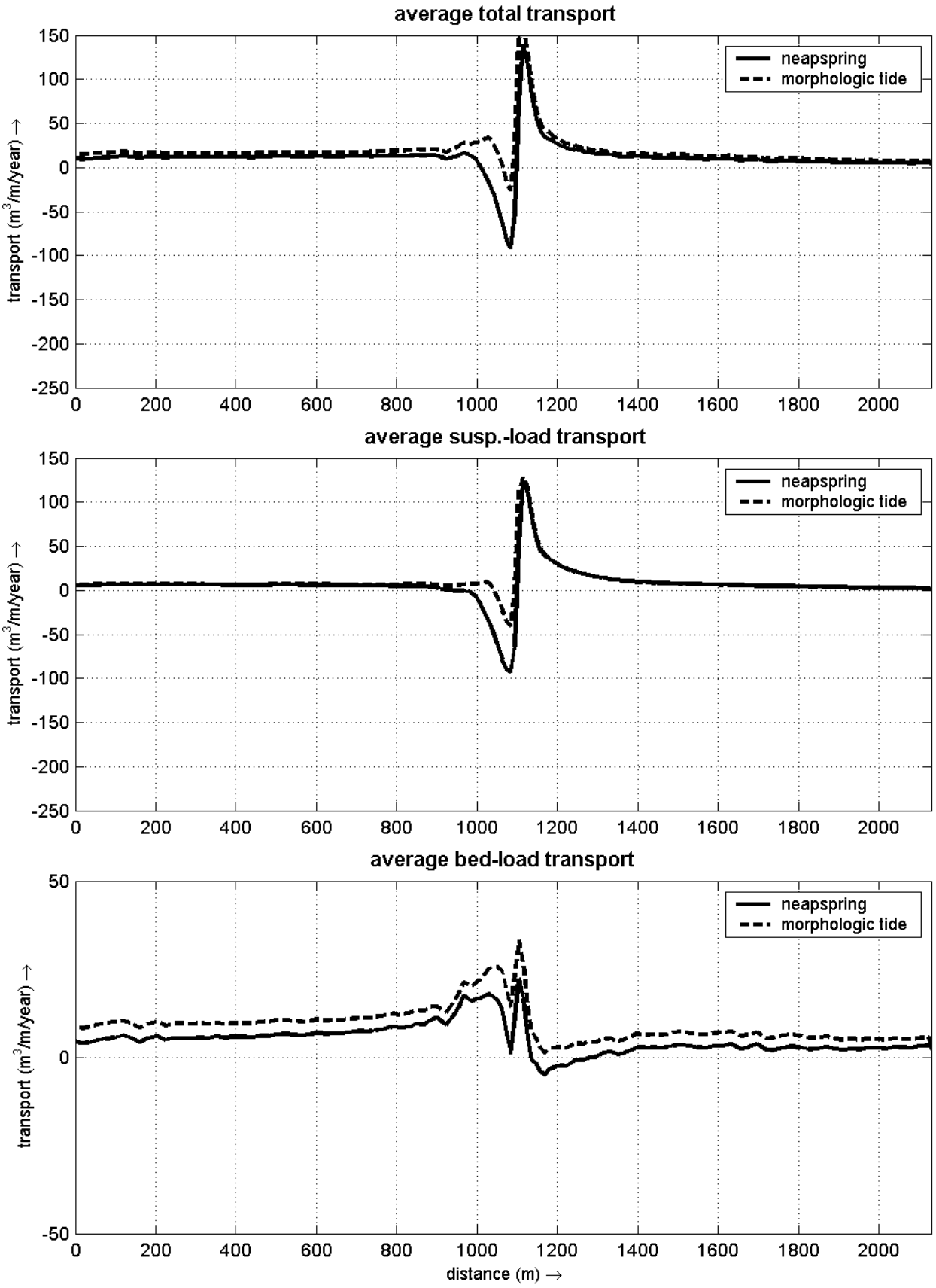

morphological tide: basic b (from single observation point) section 5: average transports over 1986 bathymetry, no updating		2005
	morphological tide	
WL | Delft Hydraulics	Z3079.40	Figure E.13

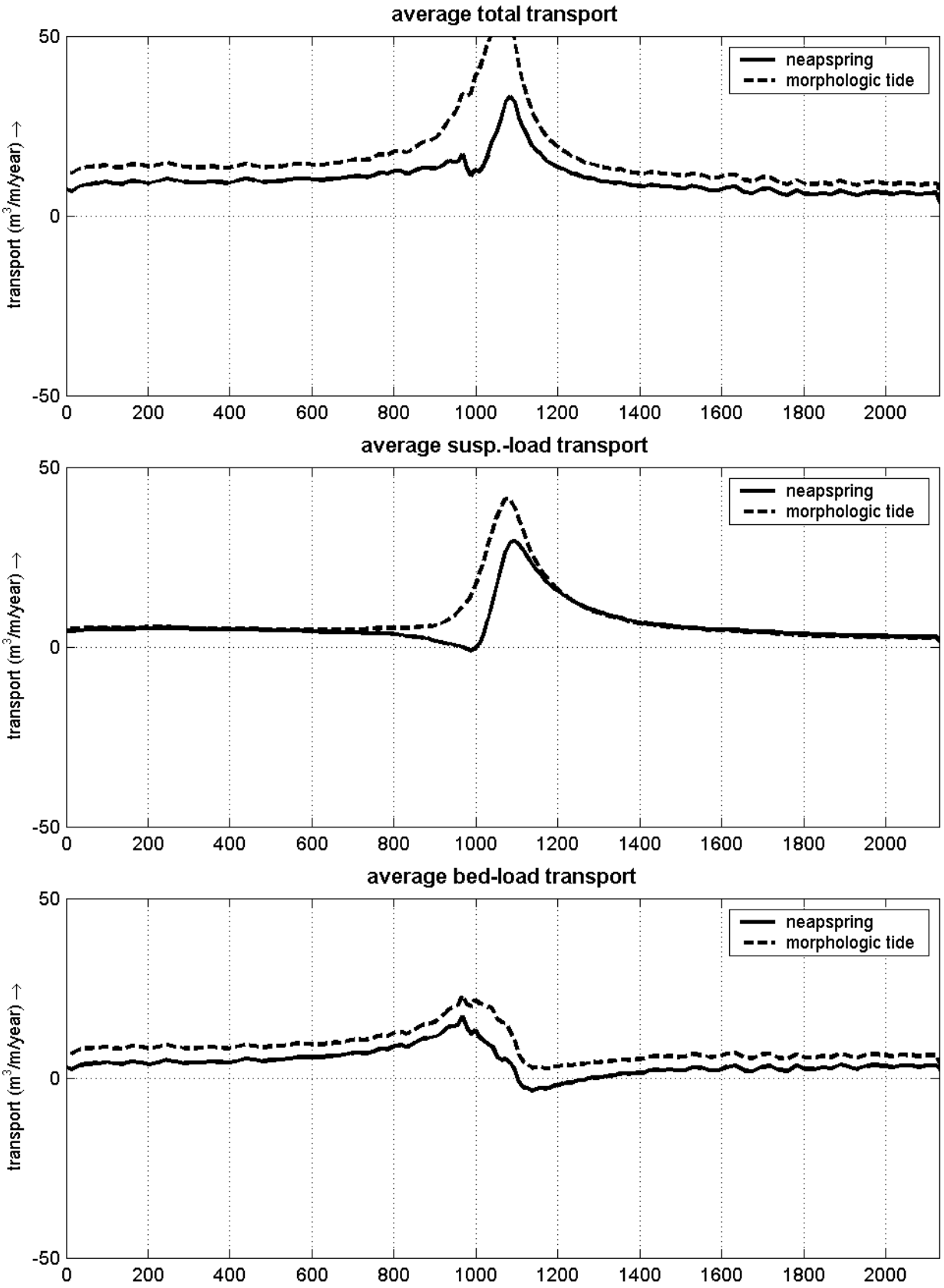

morphological tide: basic b (from single observation point)
section 6: average transports over 1986 bathymetry, no updating

2005

morphological tide

WL | Delft Hydraulics

Z3079.40

Figure E.14

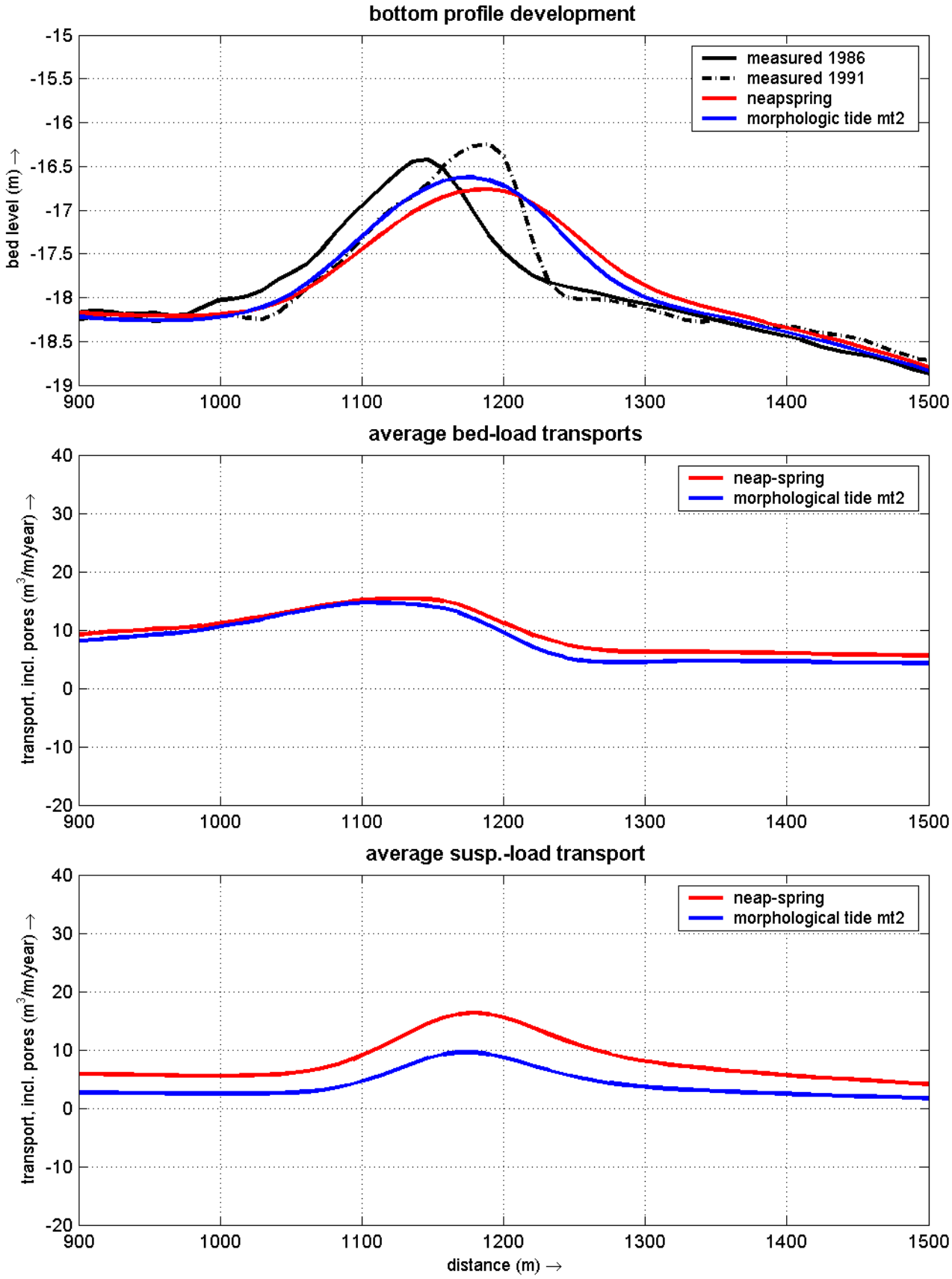

morphological tide: mt2 bottom profile development and average bed-load and susp.-load transports for complete neap-spring tidal cycle and morphological tide mt2 for section 3.		2005
	morphological tide	
WL | Delft Hydraulics	Z3079.40	Figure E.15

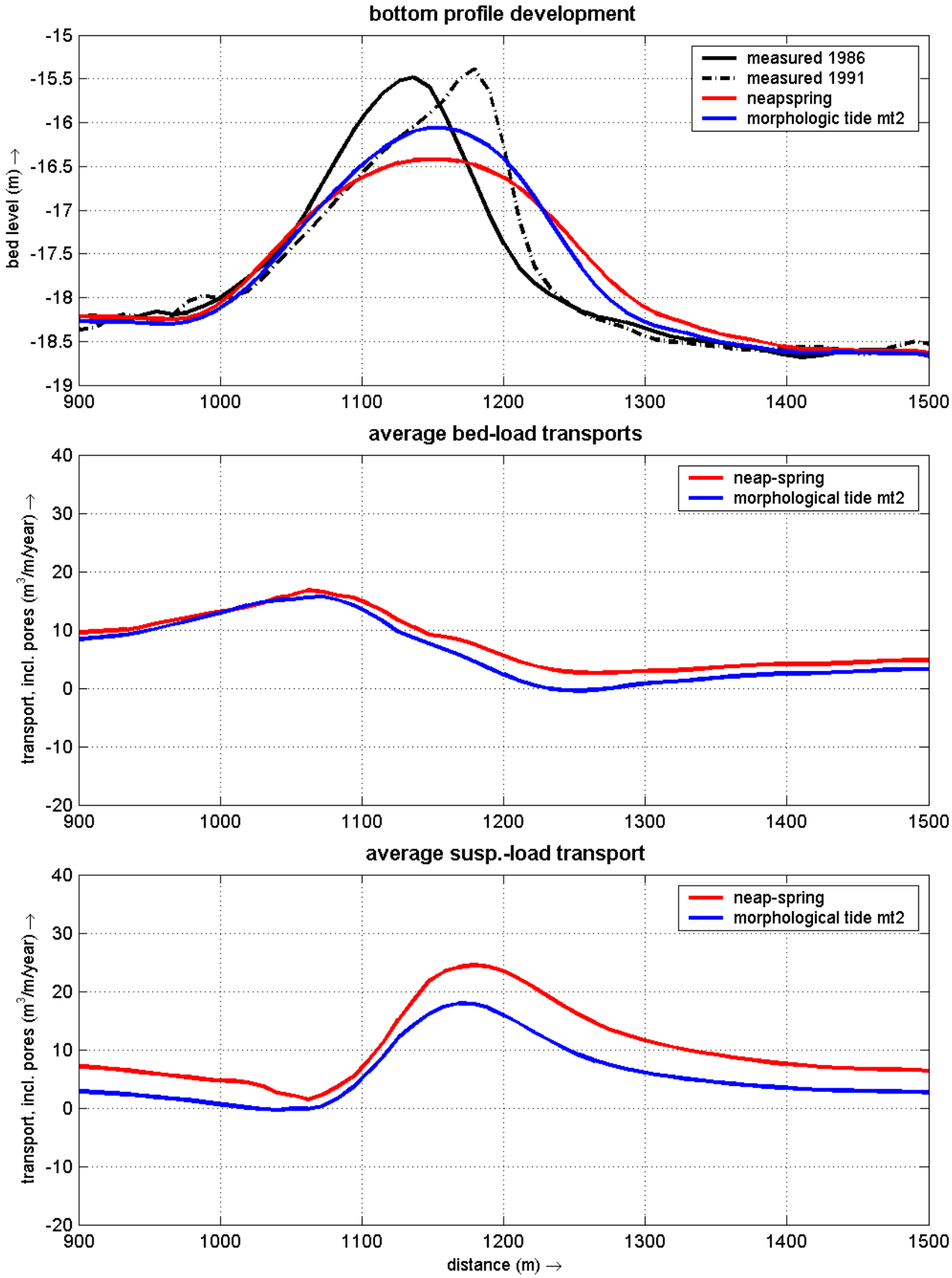

morphological tide: mt2 bottom profile development and average bed-load and susp.-load transports for complete neap-spring tidal cycle and morphological tide mt2 for section 4.

2005

morphological tide

WL | Delft Hydraulics

Z3079.40

Figure E.16

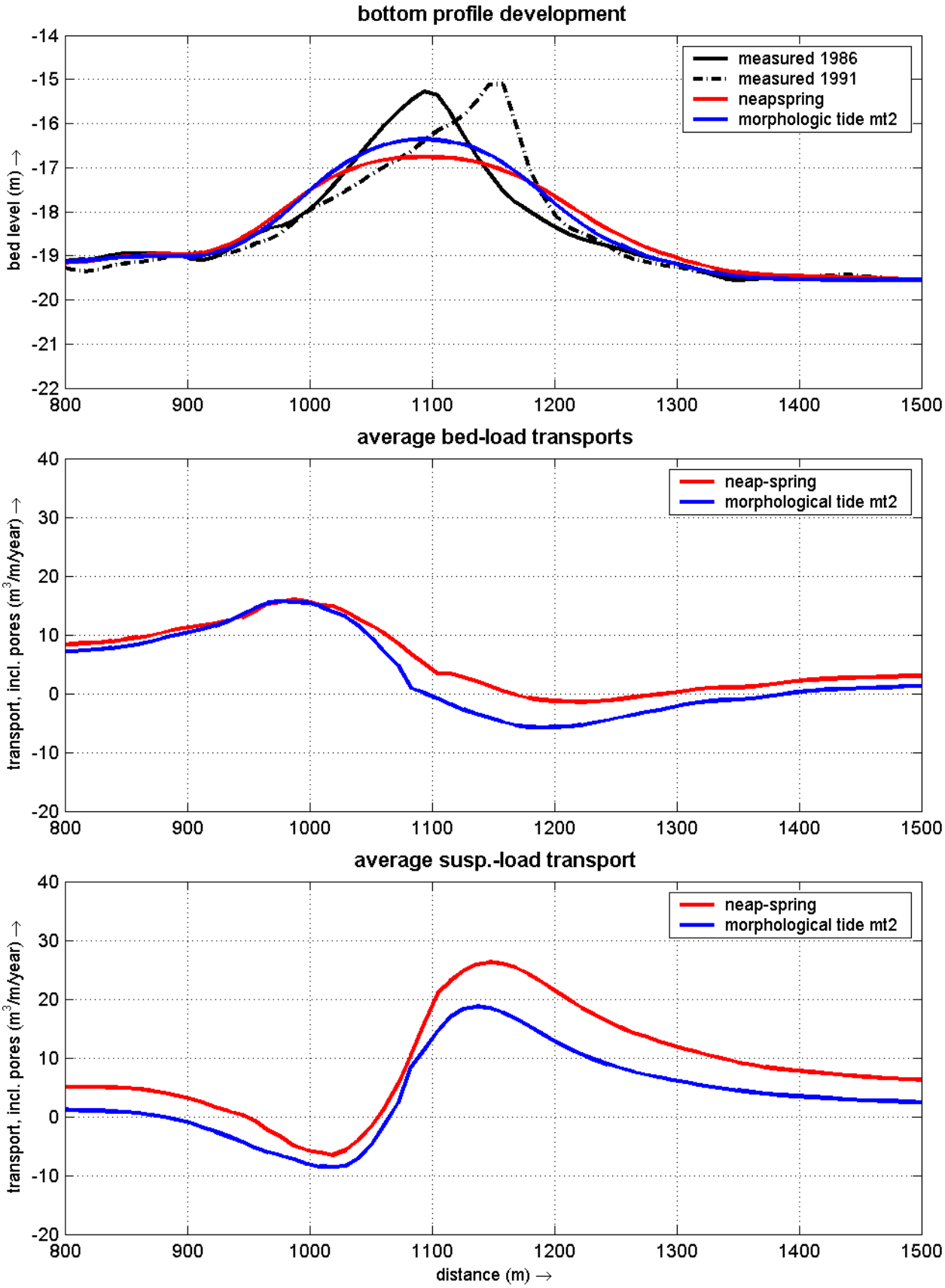

morphological tide: mt2 bottom profile development and average bed-load and susp.-load transports for complete neap-spring tidal cycle and morphological tide mt2 for section 5.

2005

morphological tide

WL | Delft Hydraulics

Z3079.40

Figure E.17

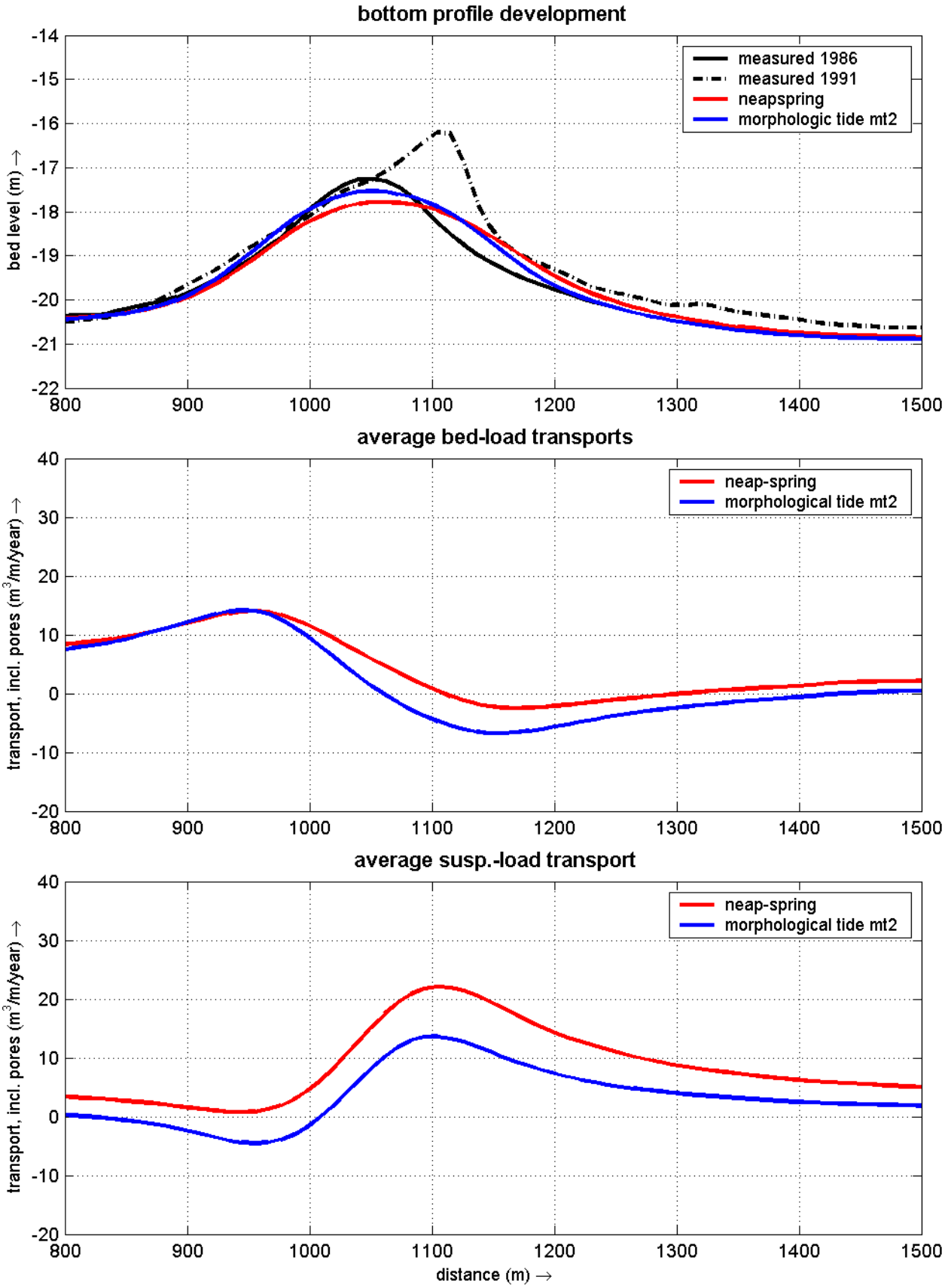

morphological tide: mt2 bottom profile development and average bed-load and susp.-load transports for complete neap-spring tidal cycle and morphological tide mt2 for section 6.

2005

morphological tide

WL | Delft Hydraulics

Z3079.40

Figure E.18

F 2DV sensitivity analysis

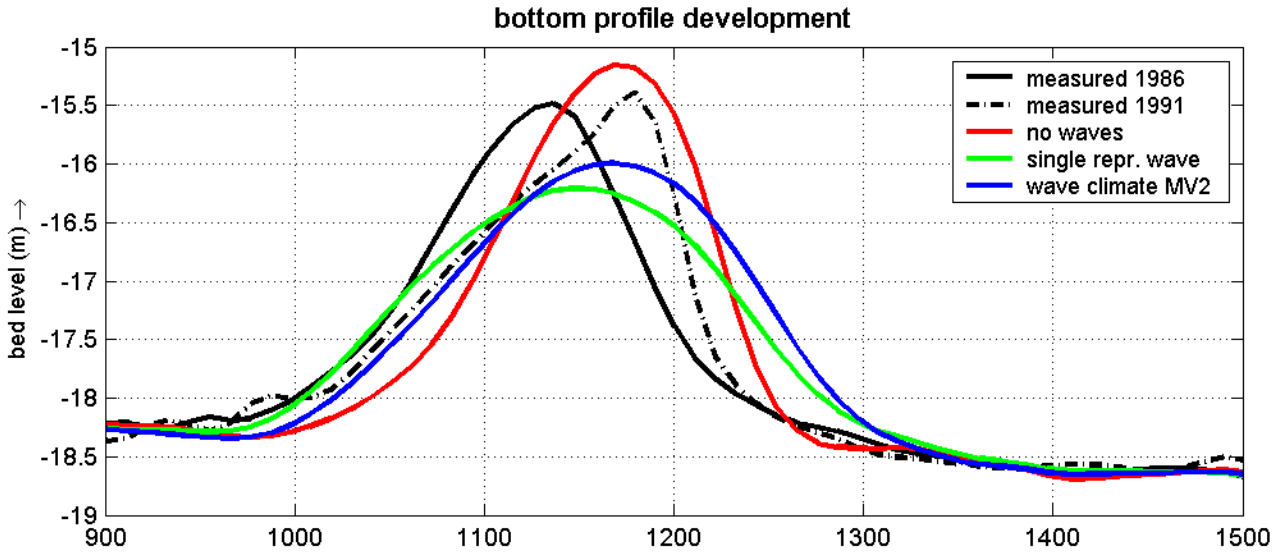

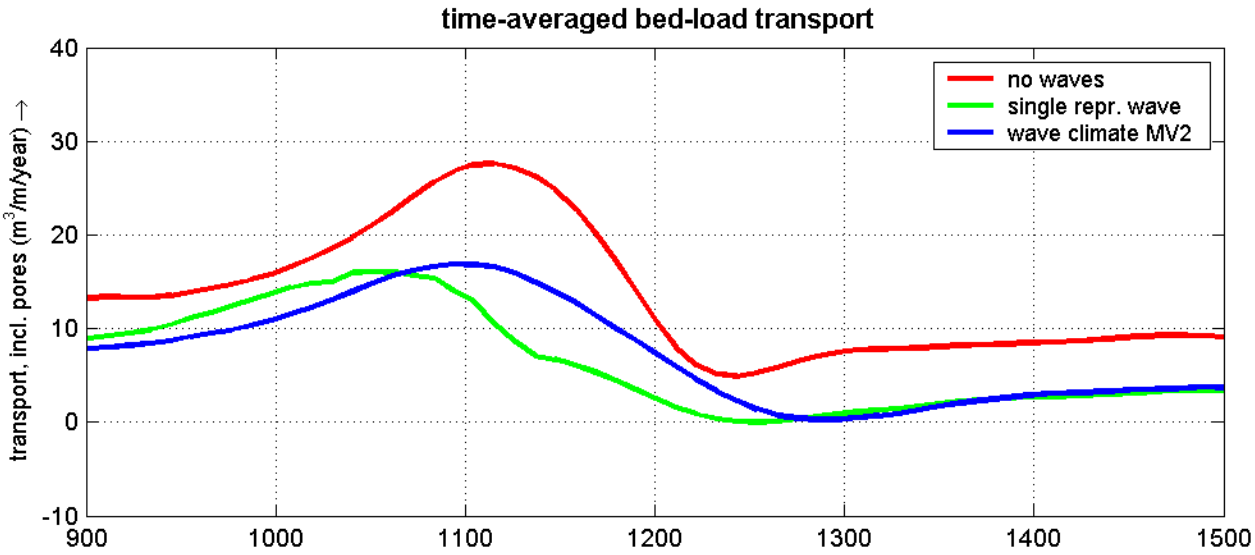

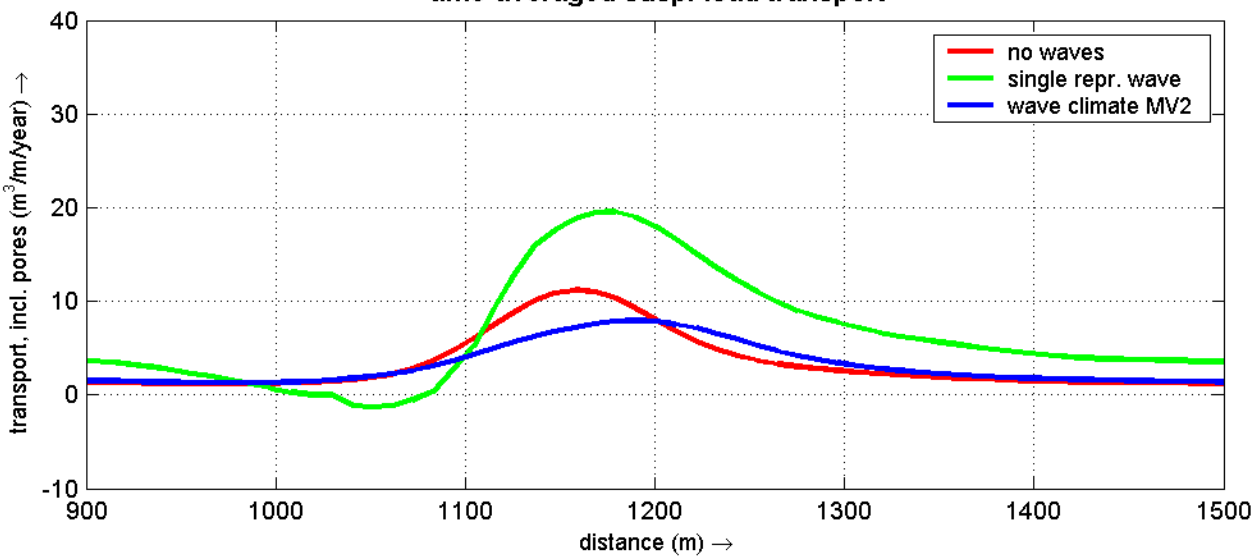

sensitivity: wave schematization bed level development,time-averaged susp.-load and bed-load transport rates		2005
		sensitivity
WL | Delft Hydraulics	Z3079.40	Figure F.01

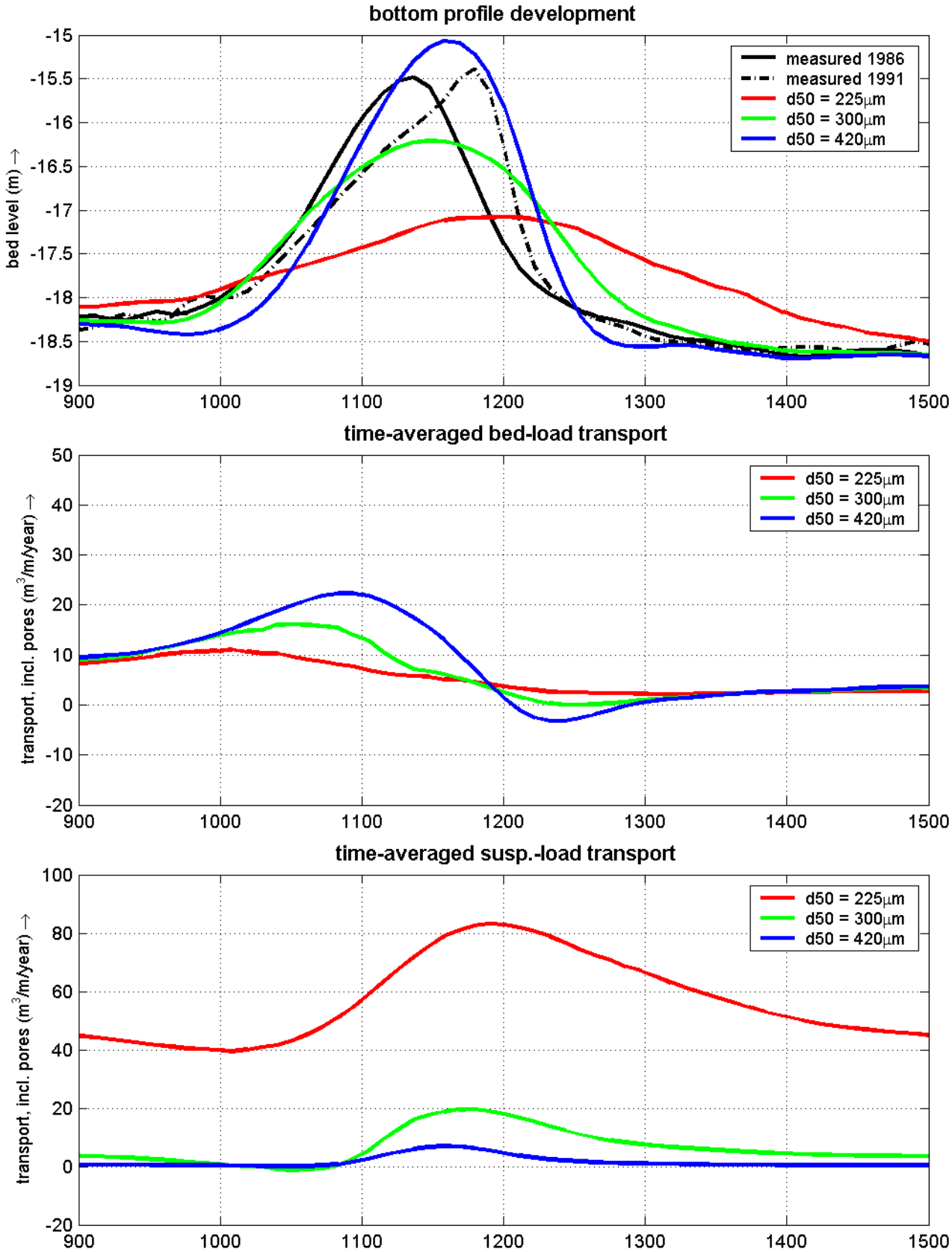

sensitivity: mean sediment diameter
bed level development,time-averaged susp.-load and bed-load transport rates

2005

sensitivity

WL | Delft Hydraulics

Z3079.40

Figure F.02

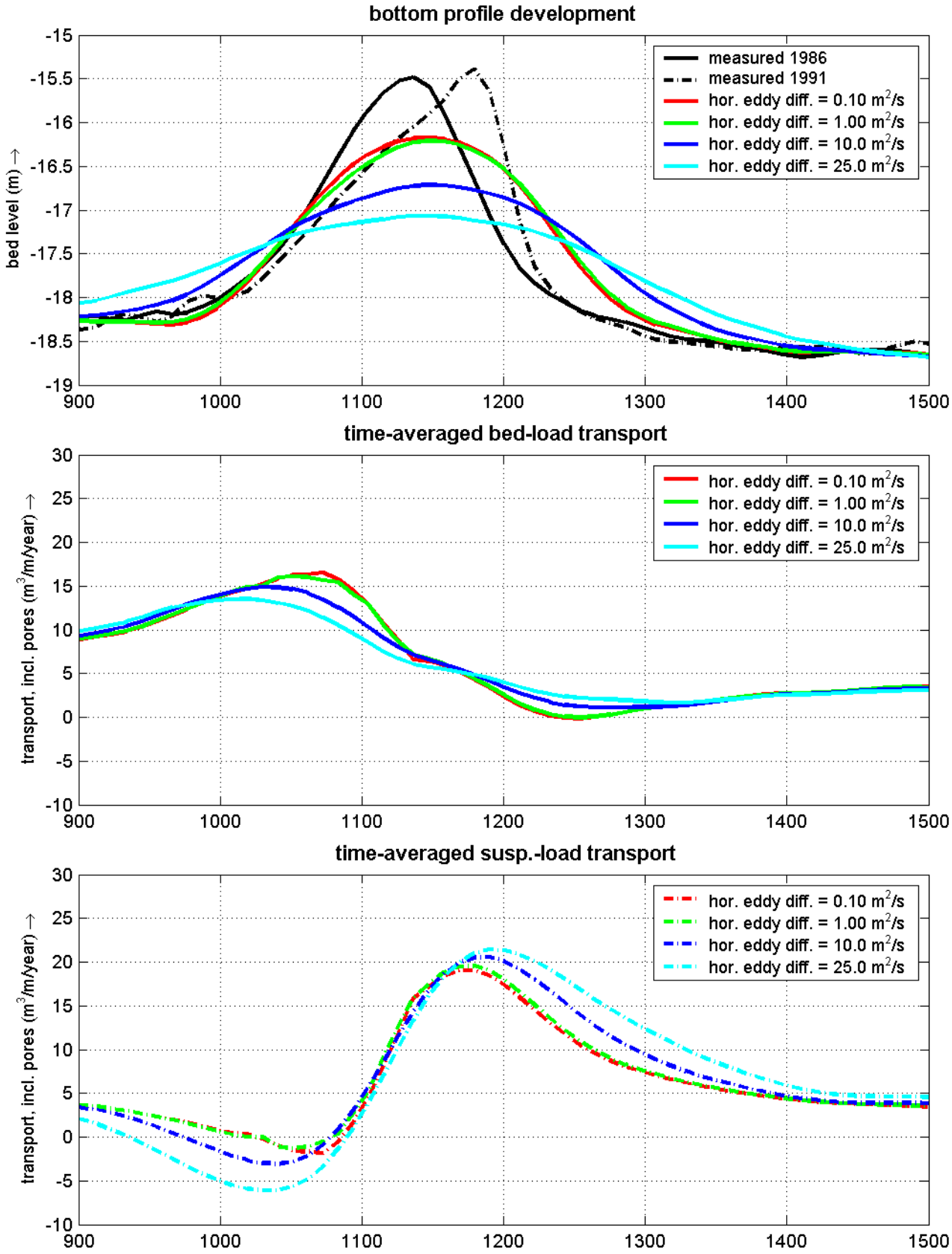

sensitivity: horizontal eddy diffusivity
bed level development,time-averaged susp.-load and bed-load transport rates

2005

sensitivity

WL | Delft Hydraulics

Z3079.40

Figure F.03

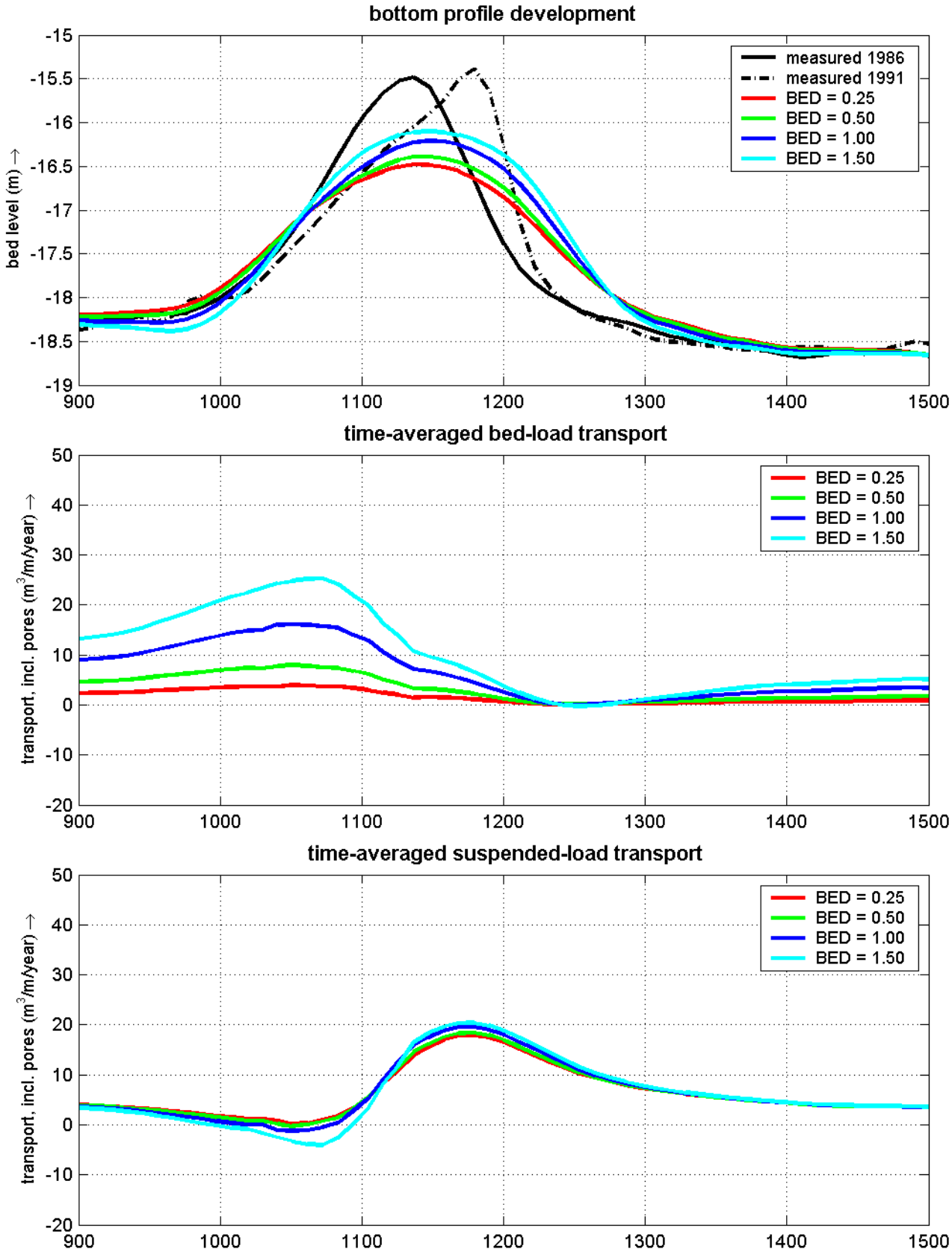

sensitivity: bed-load transport factor
bed level development,time-averaged susp.-load and bed-load transport rates

2005

sensitivity

WL | Delft Hydraulics

Z3079.40

Figure F.04

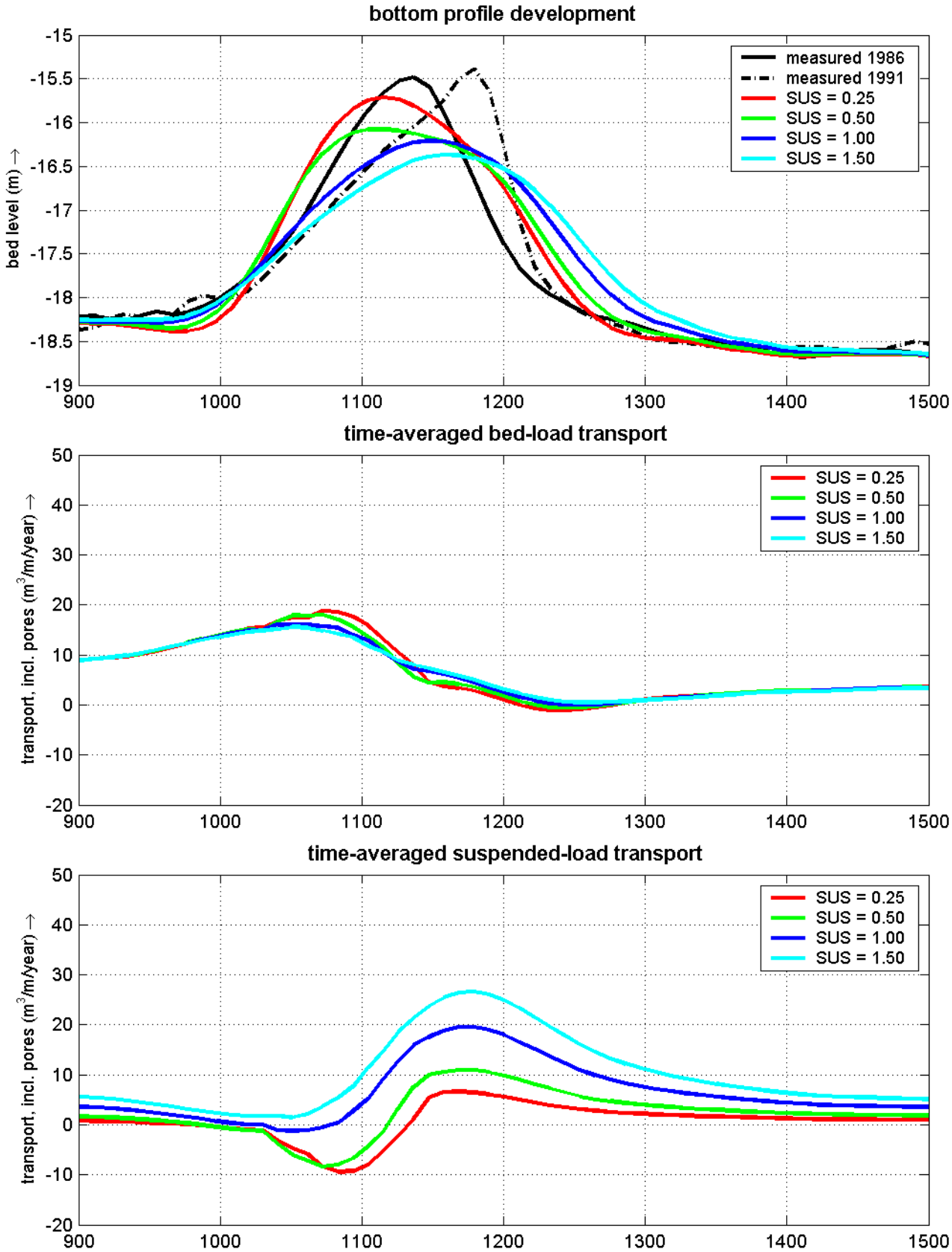

sensitivity: suspended-load transport factor
bed level development,time-averaged susp.-load and bed-load transport rates

2005

sensitivity

WL | Delft Hydraulics

Z3079.40

Figure F.05

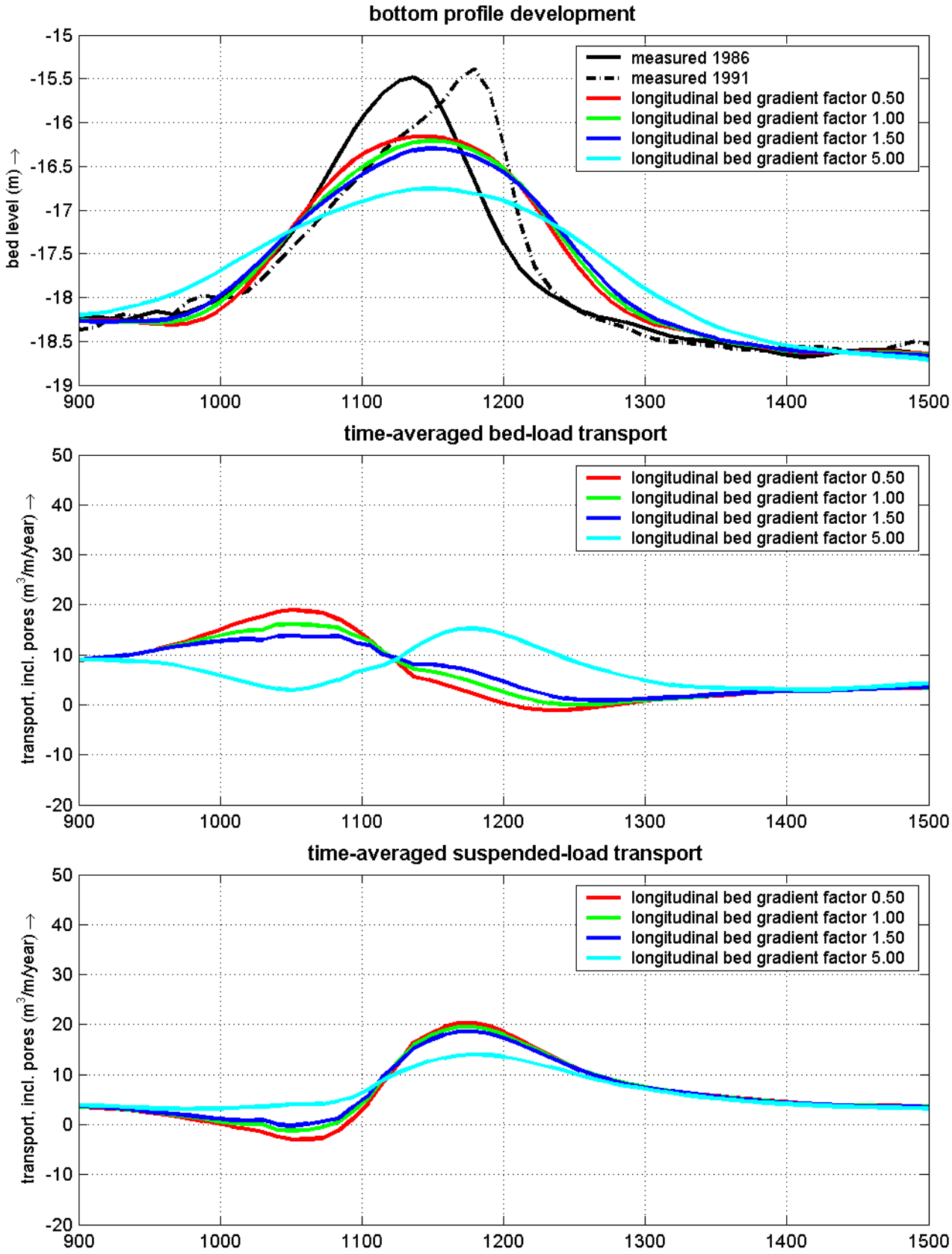

sensitivity: longitudinal bed gradient factor
bed level development,time-averaged susp.-load and bed-load transport rates

2005

sensitivity

WL | Delft Hydraulics

Z3079.40

Figure F.06

G Model results

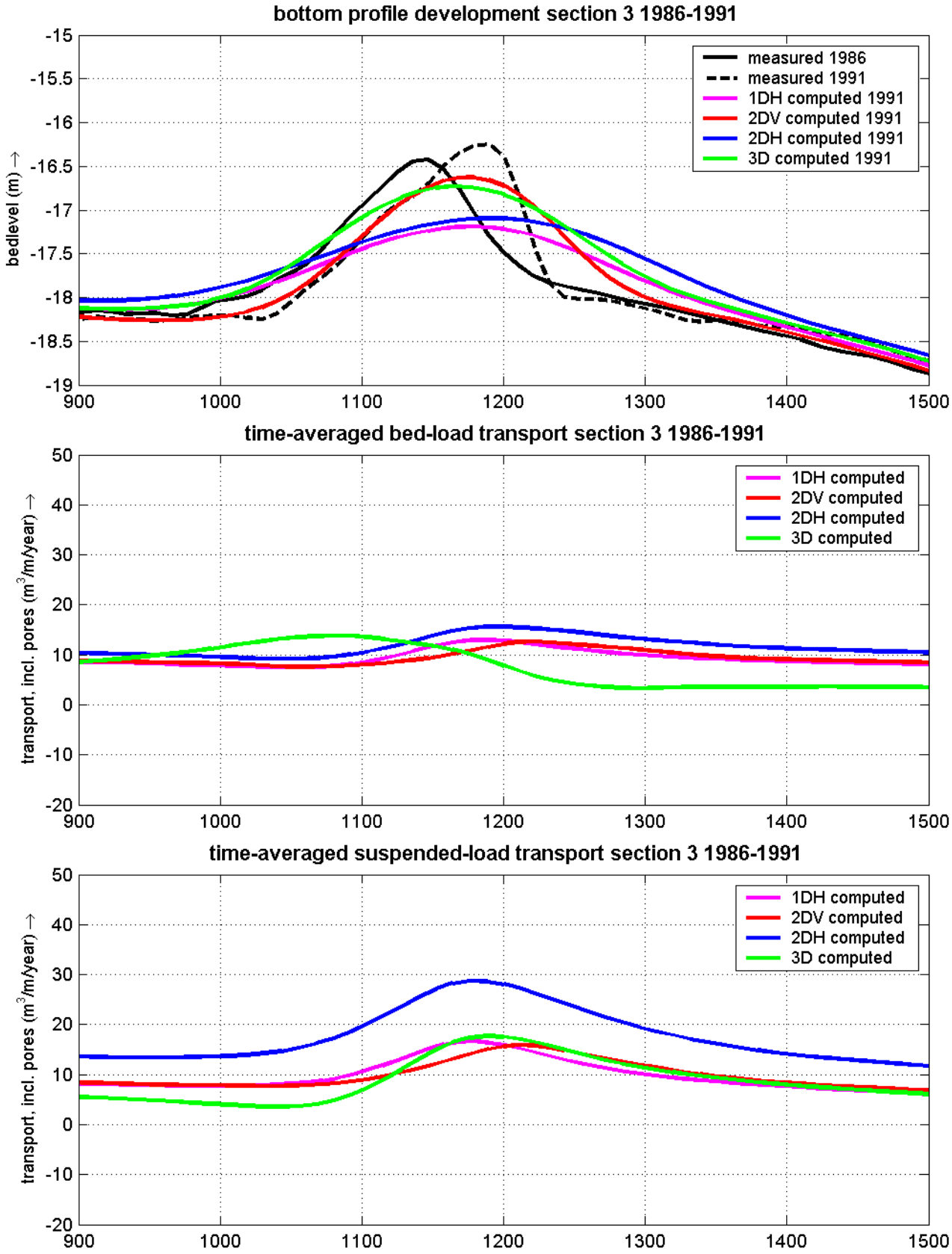

bed level development, time-averaged bed-load transport rates and time-averaged suspended-load transport rates for section 3 using 1DH, 2DV, 2DH and 3D model approach in Delft3D for the period 1986-1991		2005
	artificial sand ridge HvH, NL	
WL | Delft Hydraulics	Z3079.40	Figure G.01

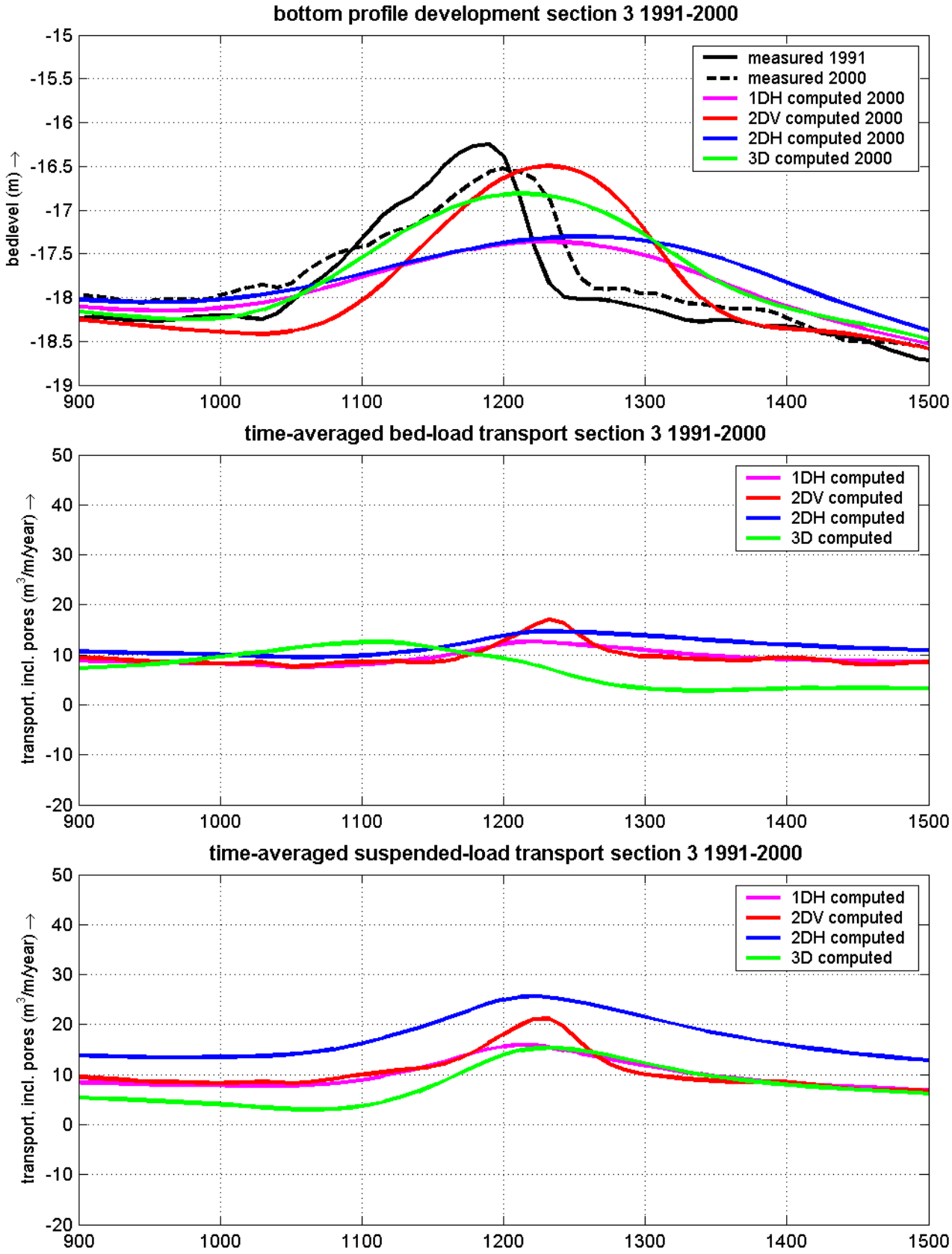

bed level development, time-averaged bed-load transport rates and time-averaged suspended-load transport rates for section 3 using 1DH, 2DV, 2DH and 3D model approach in Delft3D for the period 1991-2000		2005
	artificial sand ridge HvH, NL	
WL | Delft Hydraulics	Z3079.40	Figure G.02

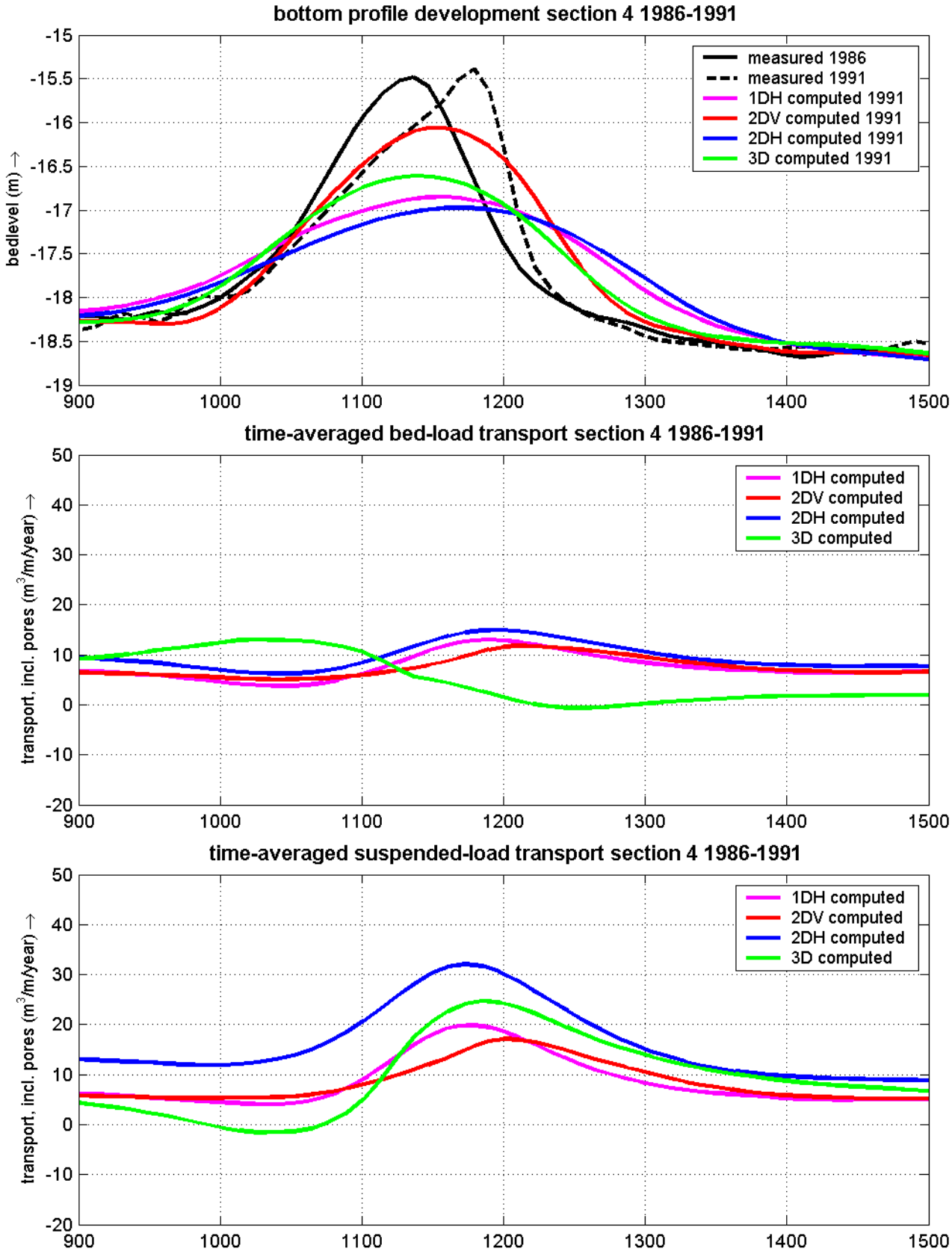

bed level development, time-averaged bed-load transport rates and time-averaged suspended-load transport rates for section 4 using 1DH, 2DV, 2DH and 3D model approach in Delft3D for the period 1986-1991		2005
	artificial sand ridge HvH, NL	
WL | Delft Hydraulics	Z3079.40	Figure G.03

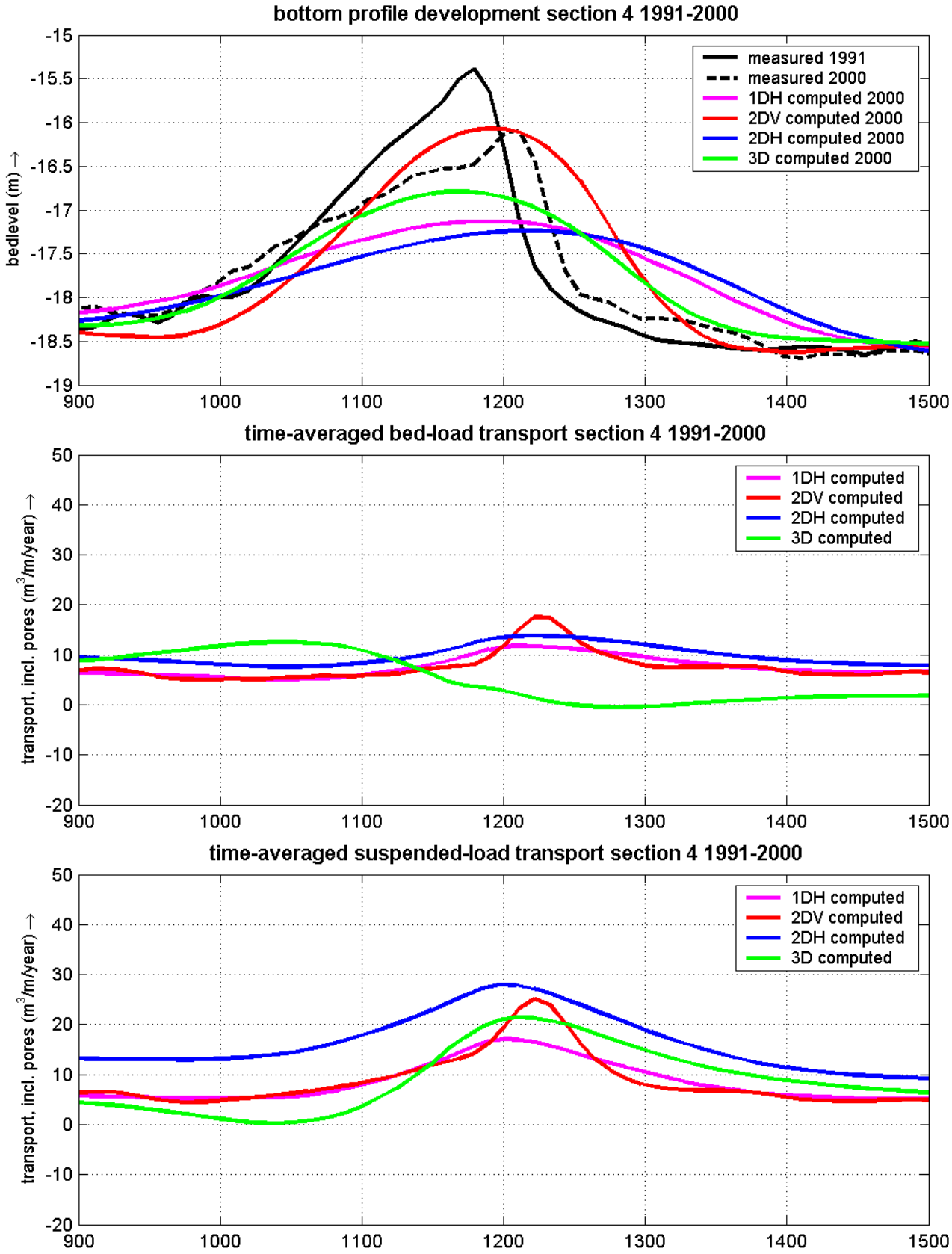

bed level development, time-averaged bed-load transport rates and time-averaged suspended-load transport rates for section 4 using 1DH, 2DV, 2DH and 3D model approach in Delft3D for the period 1991-2000		2005
	artificial sand ridge HvH, NL	
WL | Delft Hydraulics	Z3079.40	Figure G.04

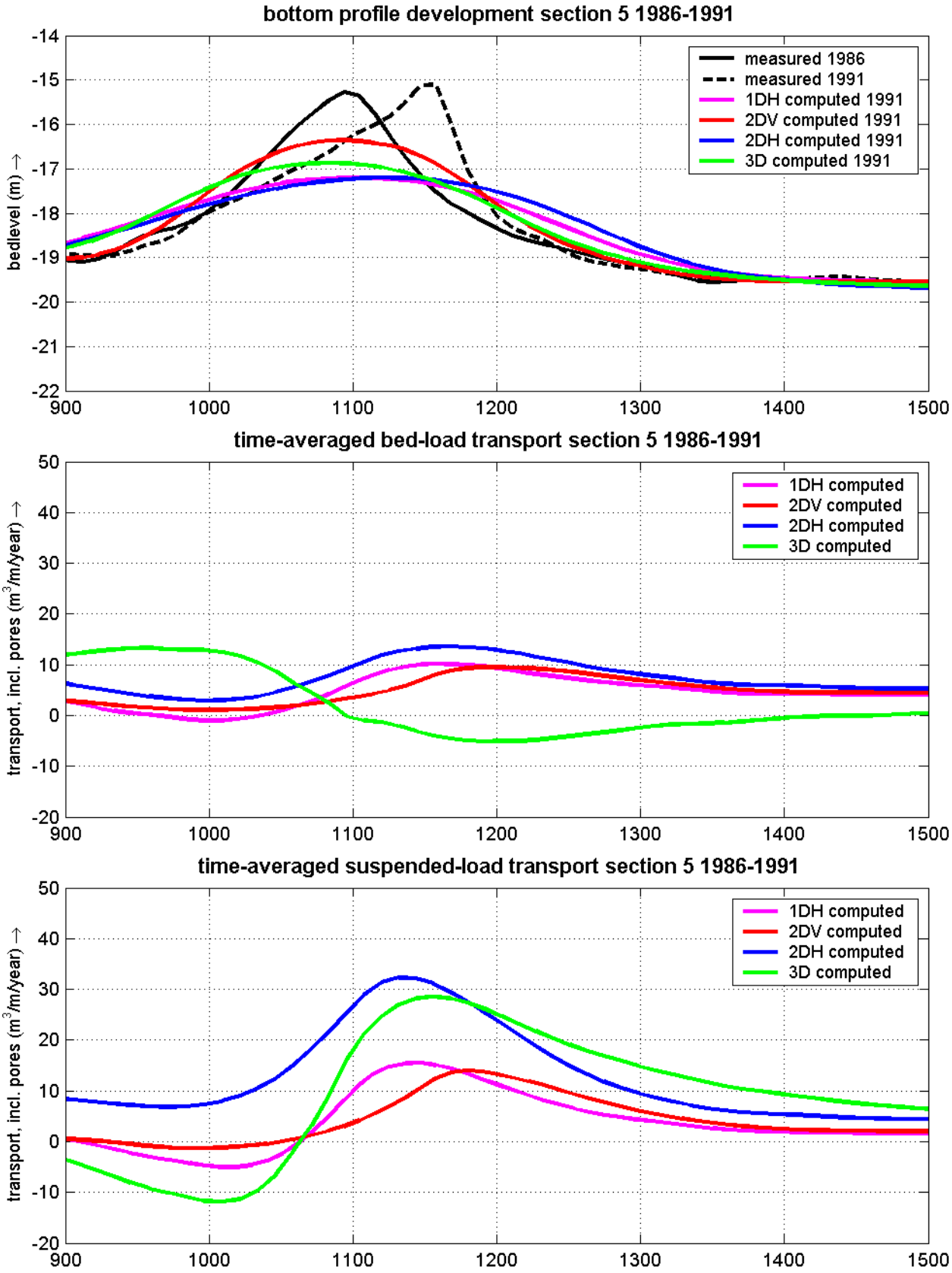

bed level development, time-averaged bed-load transport rates and time-averaged suspended-load transport rates for section 5 using 1DH, 2DV, 2DH and 3D model approach in Delft3D for the period 1986-1991		2005
	artificial sand ridge HvH, NL	
WL | Delft Hydraulics	Z3079.40	Figure G.05

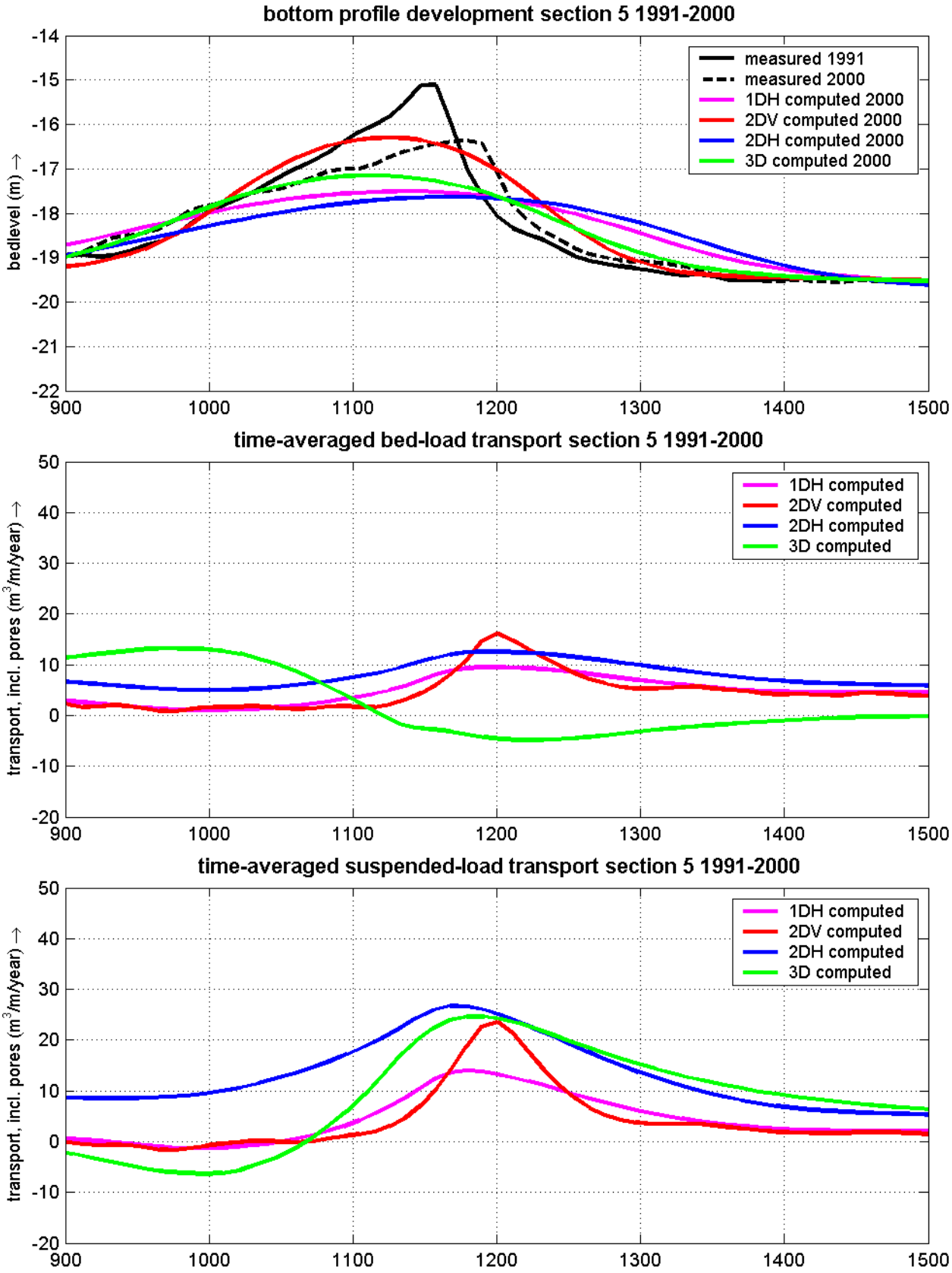

bed level development, time-averaged bed-load transport rates and time-averaged suspended-load transport rates for section 5 using 1DH, 2DV, 2DH and 3D model approach in Delft3D for the period 1991-2000

2005

artificial sand ridge HvH, NL

WL | Delft Hydraulics

Z3079.40

Figure G.06

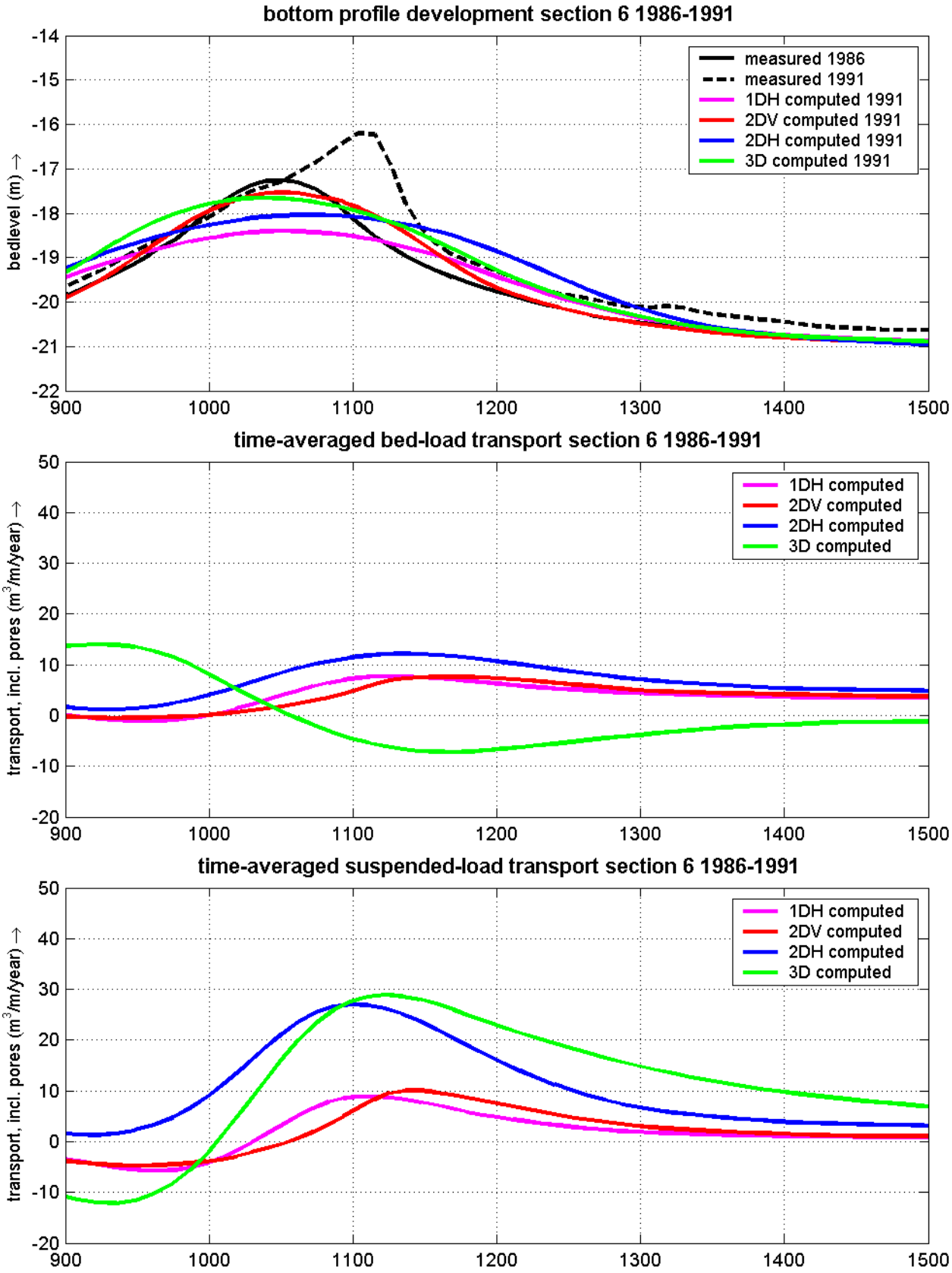

bed level development, time-averaged bed-load transport rates and time-averaged suspended-load transport rates for section 6 using 1DH, 2DV, 2DH and 3D model approach in Delft3D for the period 1986-1991		2005
	artificial sand ridge HvH, NL	
WL | Delft Hydraulics	Z3079.40	Figure G.07

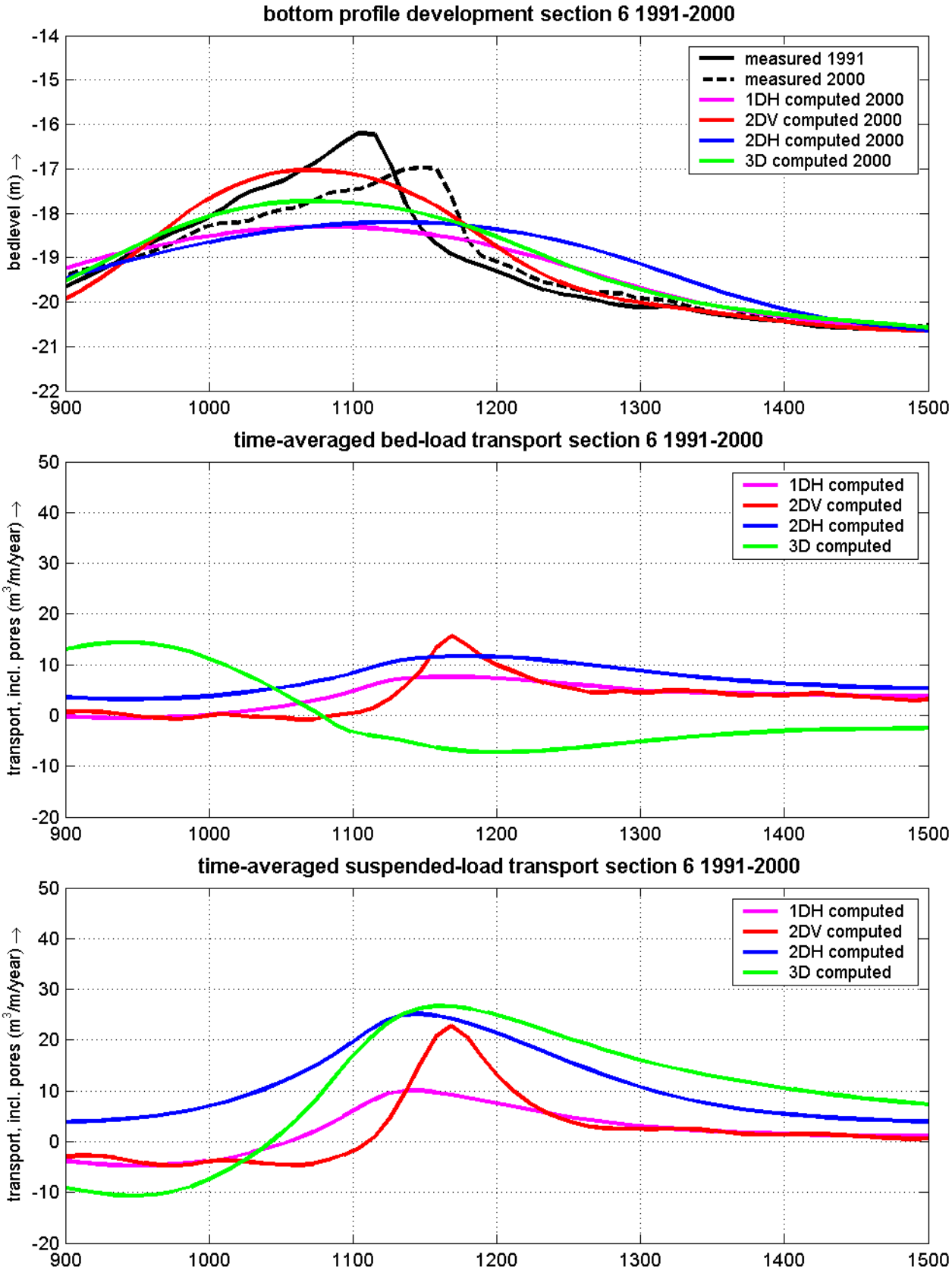

bed level development, time-averaged bed-load transport rates and time-averaged suspended-load transport rates for section 6 using 1DH, 2DV, 2DH and 3D model approach in Delft3D for the period 1991-2000		2005
	artificial sand ridge HvH, NL	
WL | Delft Hydraulics	Z3079.40	Figure G.08

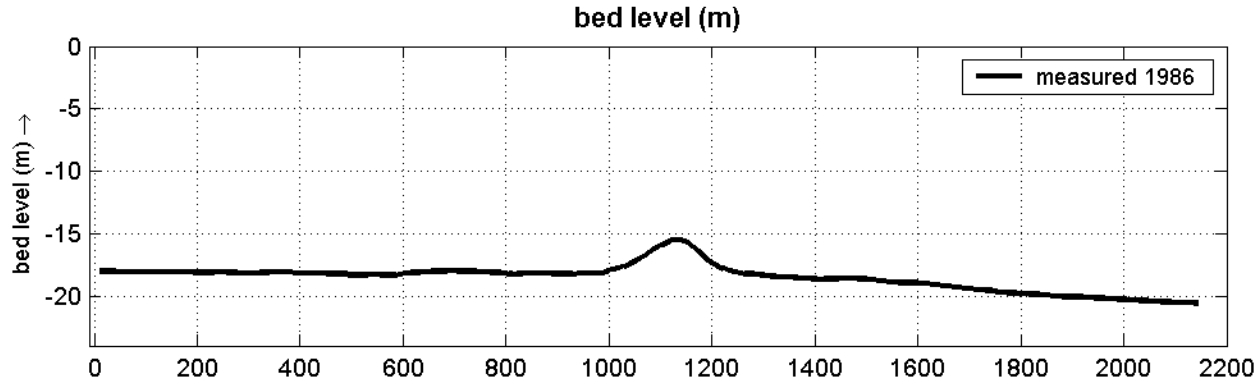

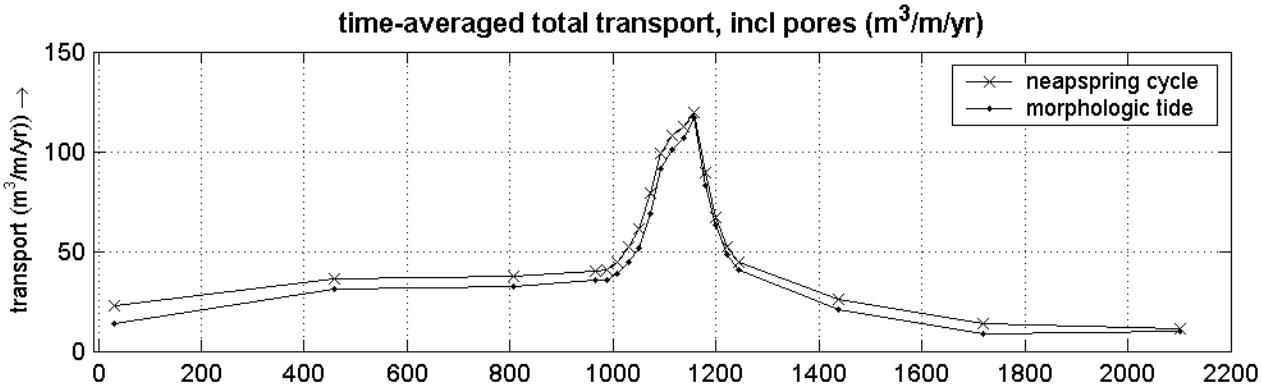

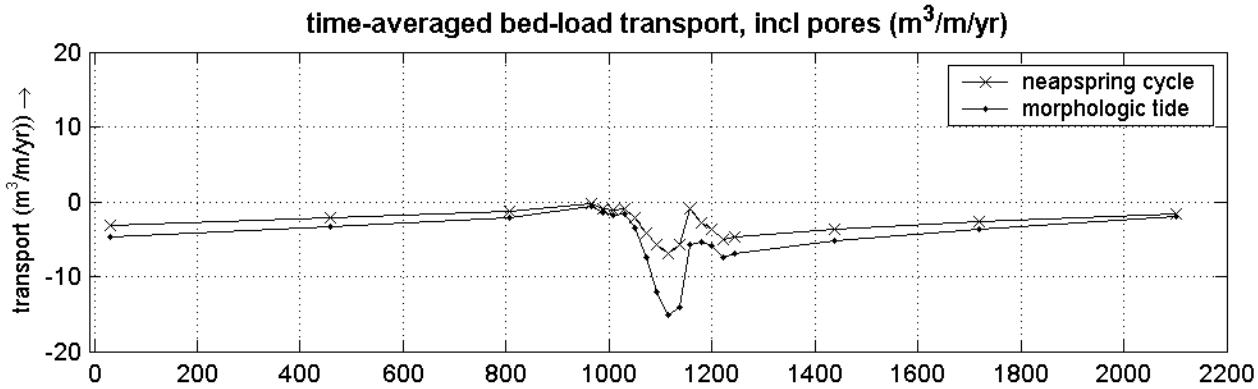

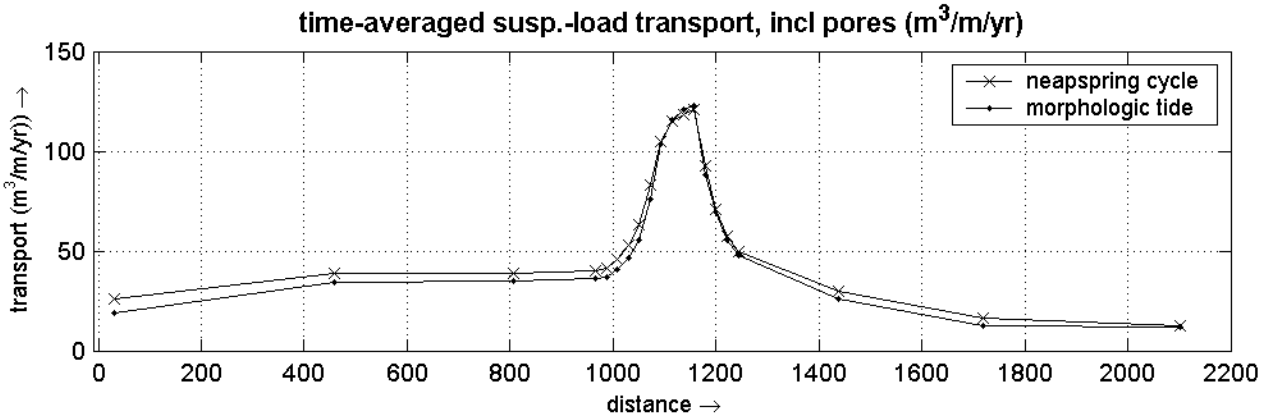

sand ridge Hoek van Holland: comparison Delft3D versions evaluation of morphological tide derived with most recent Delft3D version		2005
	artificial sand ridge HvH, NL	
WL | Delft Hydraulics	Z3079.40	Figure G.09

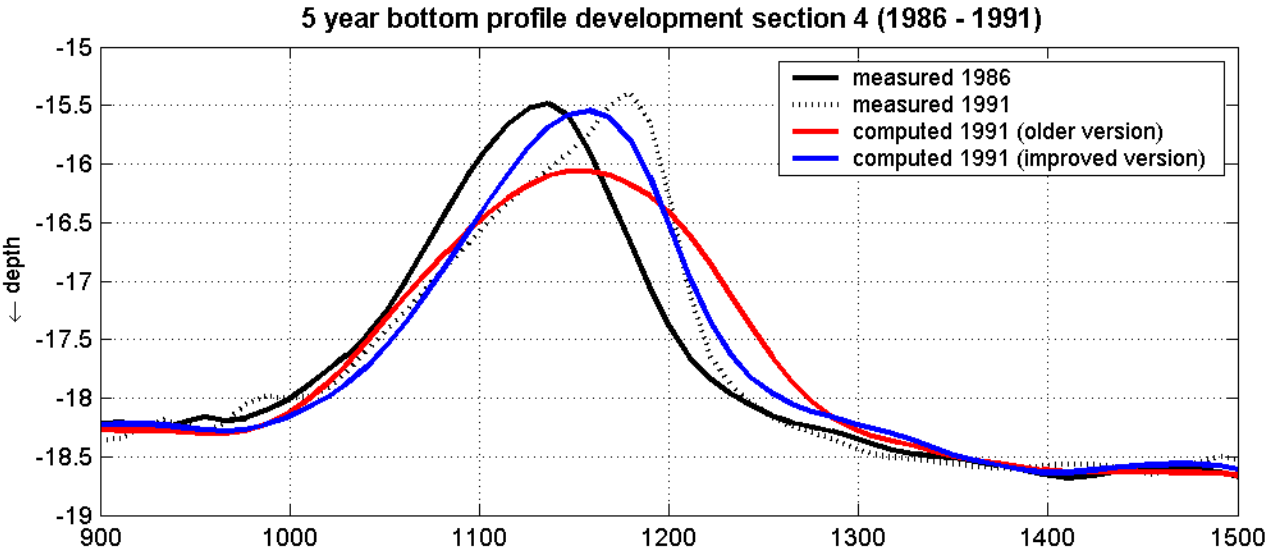

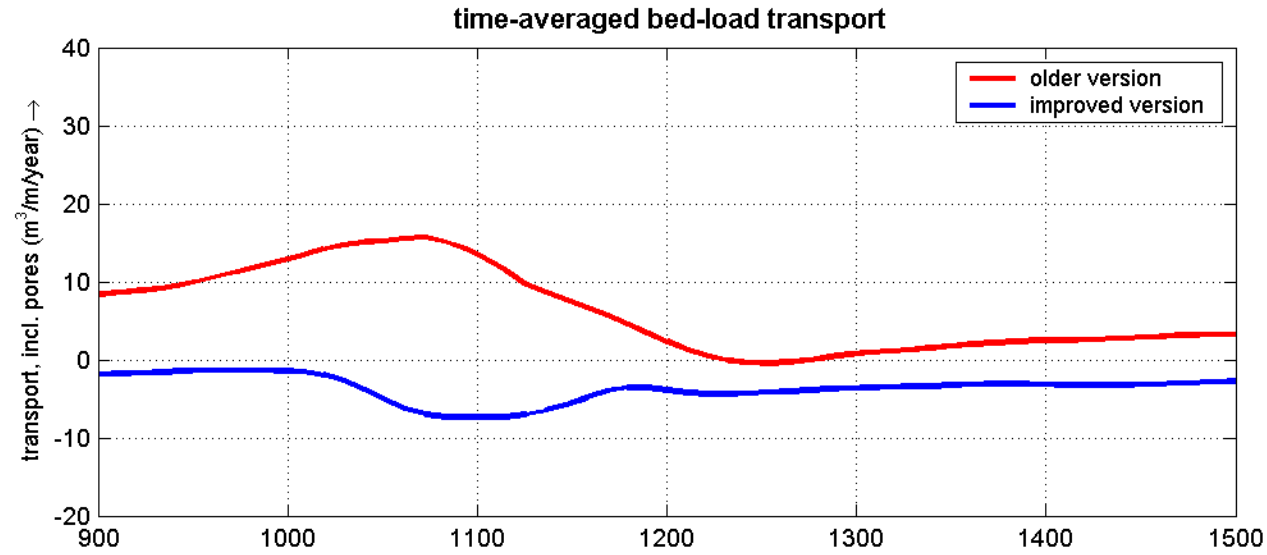

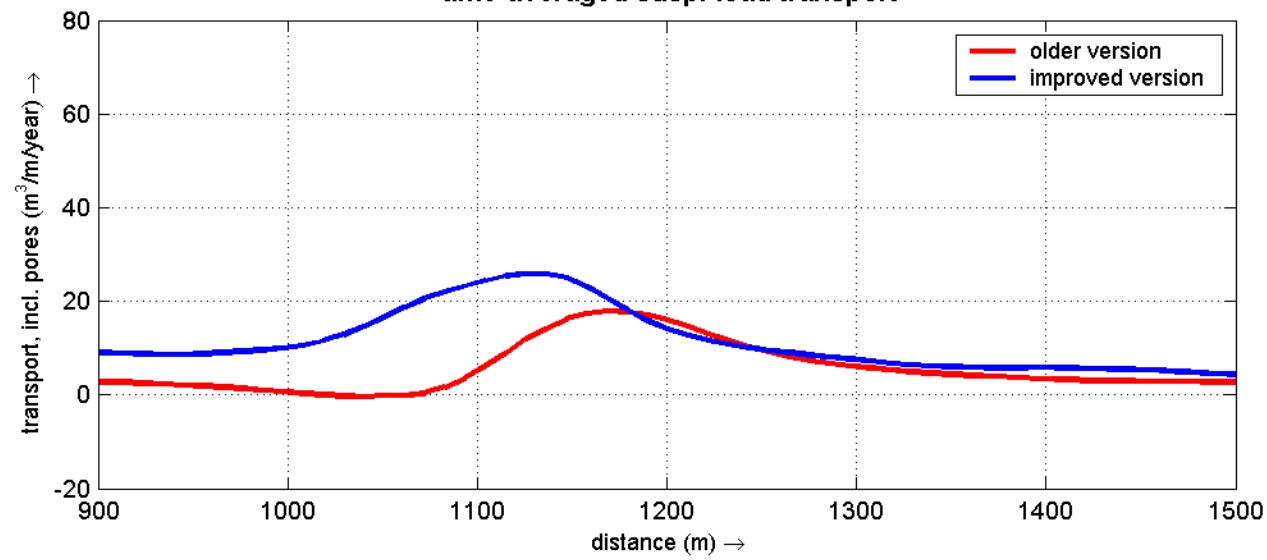

sand ridge Hoek van Holland: comparison older and improved Delft3D versions bottom profile development, time-averaged bed-l. and suspended-l transport rates between 1986 and 1991. old version = dd 11-11-2004, new version = dd 01-04-2005		2005
		artificial sand ridge HvH, NL
WL | Delft Hydraulics	Z3079.40	Figure G.10

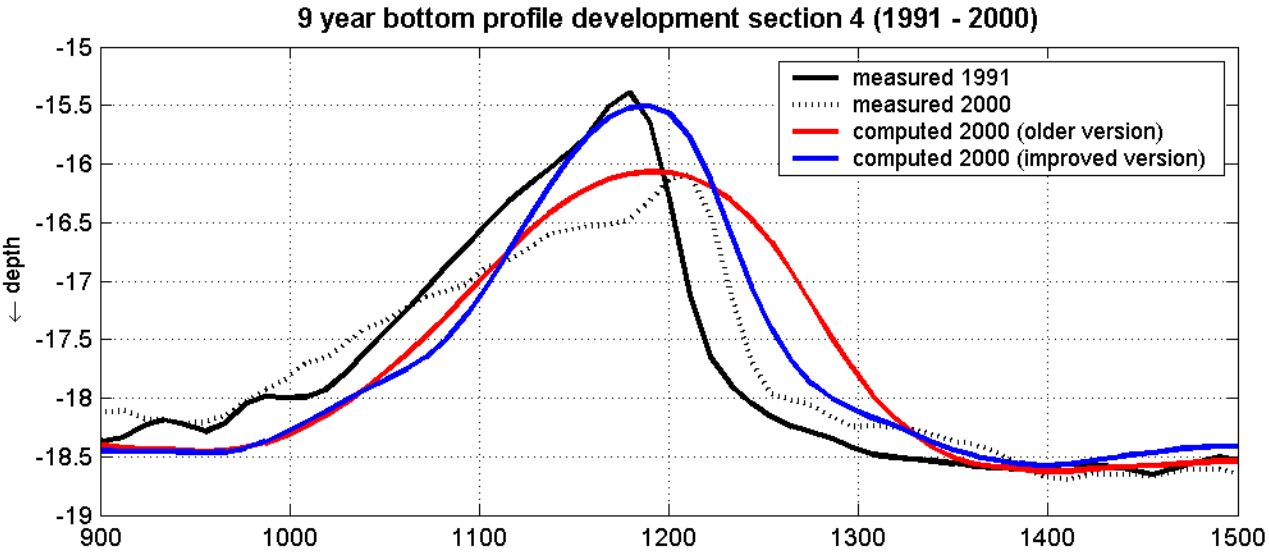

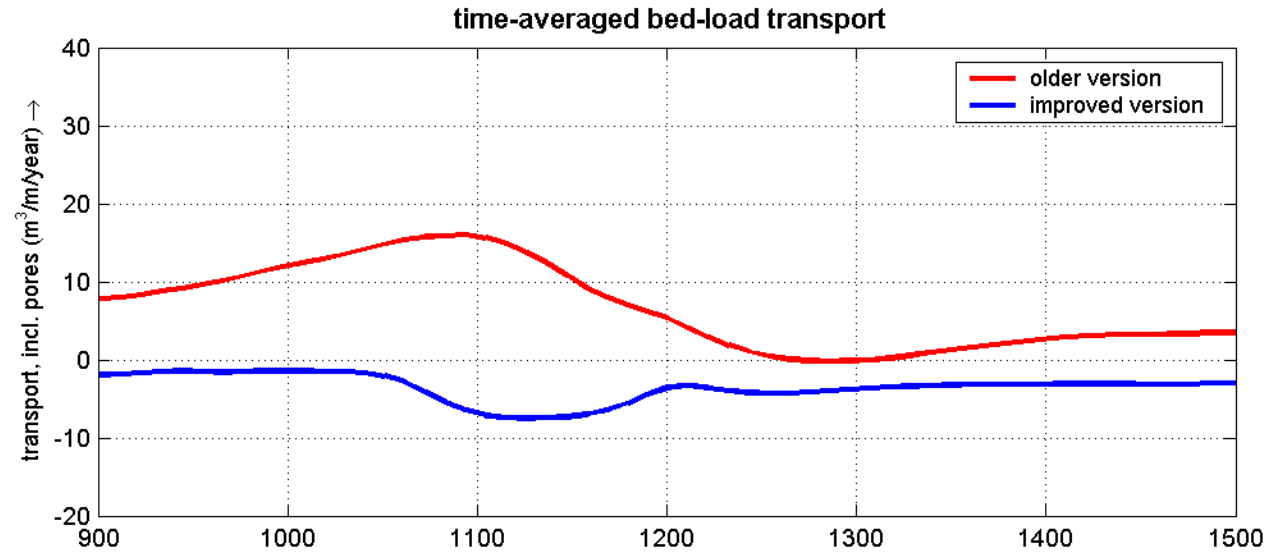

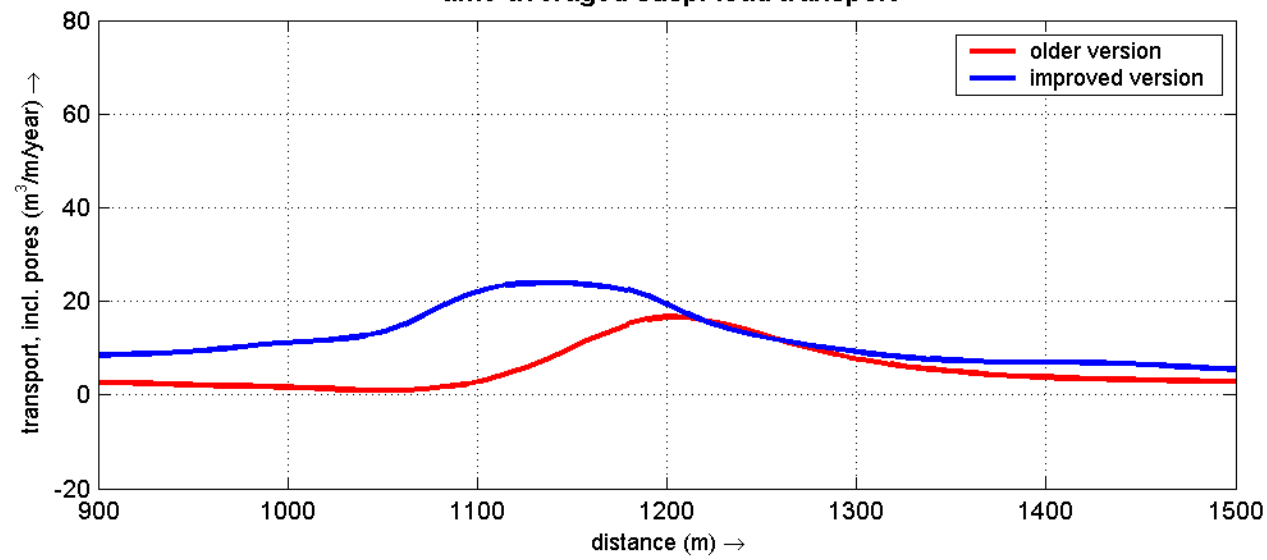

sand ridge Hoek van Holland: comparison older and improved Delft3D versions profile development, time-averaged bed-l. and suspended-l transport rates between 1991 and 2000. old version = dd 11-11-2004, new version = dd 01-04-2005		2005
		artificial sand ridge HvH, NL
WL | Delft Hydraulics	Z3079.40	Figure G.11

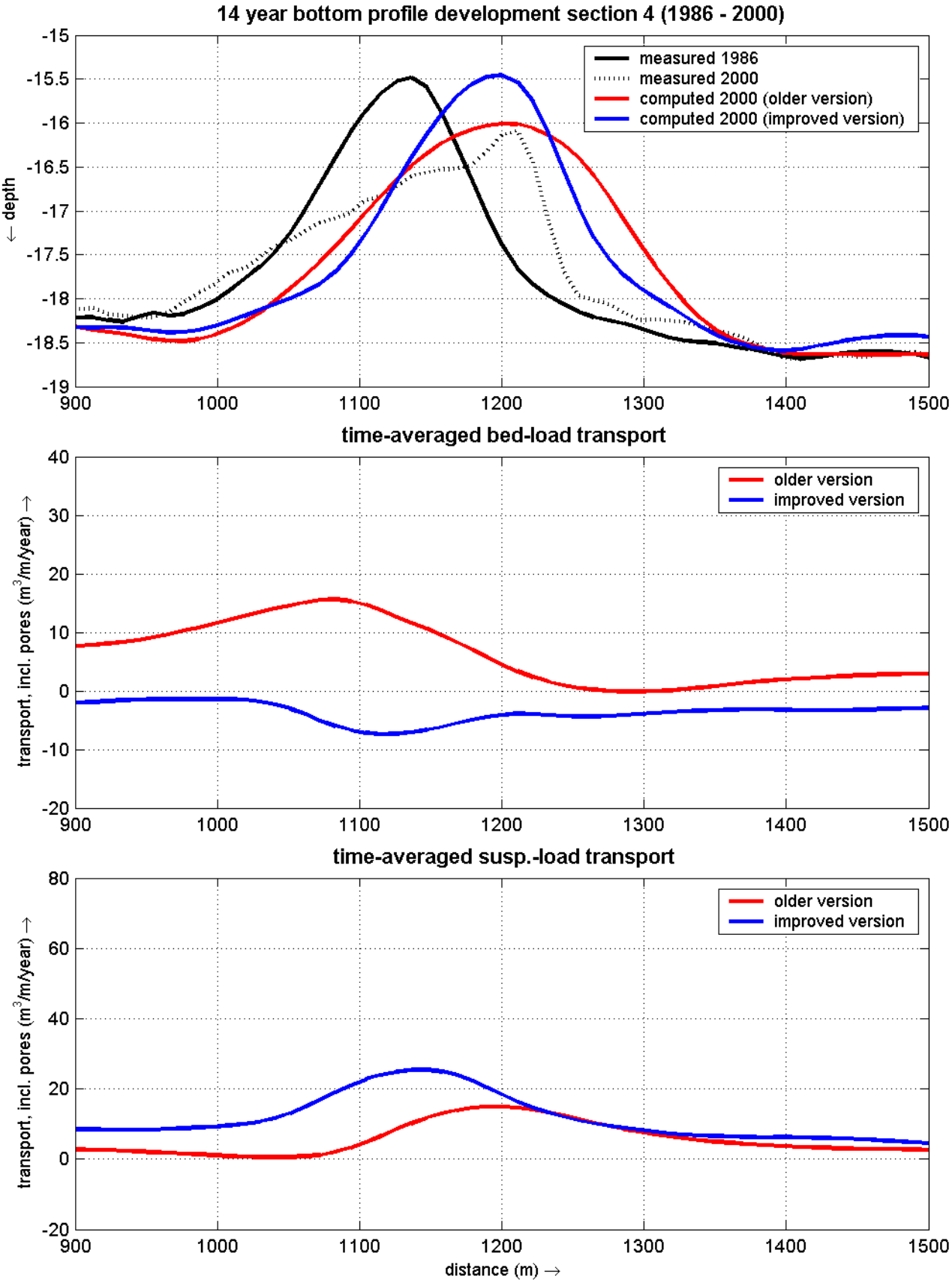

sand ridge Hoek van Holland: comparison older and improved Delft3D versions
bottom profile development, time-averaged bed-l. and suspended-l transport rates between 1986 and 1991. old version = dd 11-11-2004, new version = dd 01-04-2005

2005

artificial sand ridge HvH, NL

WL | Delft Hydraulics

Z3079.40

Figure G.12

References

Capobianco, M., 1998. Predictability for long-term coastal evolution-handling the limiting factors. Keynote speech to the third European Marine Science and Technology Conference – Scientific Colloquium: predictability for long-term Coastal Evolution – Is it feasible?, Lisbon, Portugal 23-27 May 1998, pp 277-288

Heuvel, Tj. van., 1988. Verspreiding van baggerspecie tijdens en na storten vanuit een baggerschip. RWS Dienst Getijdewateren, nota GWAO 88.034

Klein, J.A., 2003. Verification of morphodynamic models on channels and trenches. MSc Thesis/Report Z3079.40, Delft Hydraulics, Delft, The Netherlands.

Koelwijn, H. and Ribberink, J.S., 1994. Sediment transport under sheetflow conditions. WL | Delft Hydraulics, TU Delft and NCK.

Latteux, B., 1995. Techniques for long-term morphological simulation under tidal action, Marine Geology 126, 129-141

Lesser, G., Roelvink, J.A.,Van Kester, J. and Stelling, G.S., 2004. Development and validation of a three-dimensional morphological model (Delft3D-FLOW). Coastal engineering. - Vol. 51 (2004), no. 8-9 (October), p. 883-915.

Redeker, F.R., and Kollen, J., 1983. De vorm en vormveranderingen van een onderwater-zanddam in de Noordzee nabij Hoek van Holland loodrecht op de getijstroom. MSc Thesis/report. NZ-N-83.05, RWS Dir Noordzee, The Hague, The Netherlands

Rijn, L.C. van, 1993. Principles of sediment transport in rivers, estuaries and coastal seas. Aqua Publications., Amsterdam, 673 pp.

Rijn, L.C. van and Walstra, D.J.R., 2002. Morphology of mining areas (pits, channels and trenches, shoals and banks) and effect on coast; Literature review. WL | Delft Hydraulics report no. Z3079.01, Delft, The Netherlands

Rijn, L.C. van, Walstra, D.J.R., Ormondt, van M., 2004. Description of TRANSPOR2004 and implementation in Delft3D-ONLINE: final report. WL | Delft Hydraulics report no. Z3748.10.

Roelvink J.A., Van Holland, G. and Bosboom, J., 1998. Kleinschalig morfologisch onderzoek MV2, Fase 1. Validatie morfologische modellering Haringvlietmonding, WL | Delft Hydraulics, report Z2428

Roelvink, J.A., van der Kaaij, T., Ruessink, B.G., 2001b. Calibration and verification of

large-scale 2D/3D flow models. Phase 1, Parcel 2, Subproduct 2, ONL FLYLAND report.

Tobias, F.C., 1989. Morphology of sandwaves in relation to current, sediment, and wave data along the Eurogeul, North Sea. University of Utrecht, report GEOPRO 1989.01

Verhagen, W. and Wiersma, J., 1992. Zandstort voor de kust van Wijk aan zee. rapport NZ-N-92.02, RWS Dir. Noordzee, The Hague, The Netherlands

De Vriend, H.J., Capobianco, M., Chester, T., De Swart, H.E., Latteux, B. and Stive, M.J.F.,1993. Approaches to long-term modelling of coastal morphology; A review. J.Coastal Engineering, 21, 225-269.

Walstra, D.J.R., Renier, A.J.H.M., Roelvink, J.A., Wang, Z.B., Steetzel, H.J., aarninkhof, S.G.J., van Holland, G. and Stive, M.J.F., 1997. Morphological impact of large-scale marine sand extraction (in Dutch). WL | Delft Hydraulics report Z2255, Delft, The Netherlands.

Walstra, D.J.R., Van Rijn, L.C. and Aarninkhof, S.G.J., 1998. Sand transport at the middle and lower shoreface of the Dutch coast; simulations of SUTRENCH-model and proposal for large-scale laboratory tests. Report Z2378, Delft Hydraulics, Delft, The Netherlands.

Westlake, S.J., Heinen, P.F., Knudsen, S. and Heddinga, P., 1996. Accuracy of NOURTEC bathymetric surveys. RWS RIKZ, The Hague, The Netherlands.

Woudenberg, C.C. van, 1996. De onderwater zanddam bij loswal Noord: gedrag en zandtransport. MSc Thesis/report NZ-N-92.02, RWS Dir. Noordzee, The Hague, The Netherlands.

WL | Delft Hydraulics, March 2003. Delft3D-FLOW, User Manual version 3.10.

WL | Delft Hydraulics, January 2005. Delft3D-FLOW, User Manual version 3.11 Daft.